



1303

Structural Studies of Polynuclear
Metal Carbonyl Derivatives.

A thesis submitted to the Council for
National Academic Awards in partial
fulfilment of the requirements for
the Degree of Doctor of Philosophy.

LIBRARY AND INFORMATION SERVICE
POLYTECHNIC OF NORTH LONDON
HOLLOWAY ROAD
LONDON N7 8DB

by

Gráinne Conole

BEST COPY AVAILABLE.

VARIABLE PRINT QUALITY

DECLARATION

Whilst registered as a candidate for this degree, the author has not been registered as a candidate for any other award.

Gráinne Conole

DEDICATED TO MUM, DAD, and MOYA

The truth is rarely pure and never simple. Modern life would be very tedious if it were either.

-Algernon, The importance of being earnest by Oscar Wilde.

'What is the use of a book,' thought Alice, 'without pictures or conversation?'

Alice's Adventures in Wonderland by Lewis Carroll.

ACKNOWLEDGEMENTS

I would first and foremost like to thank my Supervisor Prof. M. McPartlin for her help, enthusiasm, and constant encouragement (not to mention all the memorable long discussions!) during this project.

Thanks to everyone in the lab and the department for making it all bearable, especially Trusha Adatia, Alan Bashall, Barbara Page, and Harry Powell.

Thanks for the crystals, from Phil Bailey, Simon Drake, Tom Dutton, and Julie Lunniss at Cambridge University, without which this thesis could never have been written!

For totally ruthless editing - thanks Mike!

The award of an S.E.R.C. Research Studentship for the duration of my studies is gratefully acknowledged.

ABBREVIATIONS.

Me	Methyl, CH_3
Et	Ethyl, C_2H_5
Pr	Propyl, C_3H_7
Pr ⁱ	iso-propyl, $\text{C}(\text{H})(\text{CH}_3)_2$
Bu ^t	Tertiary butyl, $\text{C}(\text{CH}_3)_3$
Ph	Phenyl, C_6H_5
Cp	C_5H_5 , in and η^5 -bonding mode, unless otherwise stated.
Tol	Tolyl, $\text{C}_6\text{H}_4\text{CH}_3$
Hal	Halogen
dppm	$\text{P}(\text{C}_6\text{H}_5)_2-\text{CH}_2-\text{P}(\text{C}_6\text{H}_5)_2$
dppe	$\text{P}(\text{C}_6\text{H}_5)_2-(\text{CH}_2)_2-\text{P}(\text{C}_6\text{H}_5)_2$
dppb	$\text{P}(\text{C}_6\text{H}_5)_2-(\text{CH}_2)_4-\text{P}(\text{C}_6\text{H}_5)_2$
PPN	$\text{N}(\text{PPH}_3)_2$
i.r.	Infrared
n.m.r.	Nuclear magnetic resonance
M	Metal
L	Ligand
AO	Atomic orbital
MO	Molecular orbital
P.E.	Potential energy
CVE	Number of cluster valence electrons
U	Temperature factor

G. Conole

Abstract

X-Ray structure analysis of fifteen metal carbonyl cluster compounds of nuclearity three to seven have been carried out to investigate the effect organo-fragments have on metal core geometry.

An orthometallated pyridyl ligand, bridges two non-bonded metal atoms in each of the 'bridged-butterfly' clusters $\text{HRu}_5\text{C}(\text{CO})_{14}(\text{C}_5\text{H}_4\text{N})$ [Isomer A (XR1), Isomer B (XR2)], and $\text{HRu}_5\text{C}(\text{CO})_{13}(\text{C}_5\text{H}_4\text{N})(\text{C}_5\text{H}_5\text{N})$ (XR3), with the hydrogen ligand bridging the hinge M-M bond. In addition, for (XR3), a second pyridine ligand bonds terminally to the bridging metal atom. A bridging pyridyl group is also observed along an axial edge in both the square pyramidal clusters $\text{HRu}_5\text{C}(\text{CO})_{13}(\text{C}_5\text{H}_4\text{N})$ [Isomer A and B (XR4)]. The two pairs of isomers are the first examples of clusters differing only in the orientation of a pyridyl ligand to be fully characterised.

The cyclohexadiene derivative $\text{Ru}_6\text{C}(\text{CO})_{15}(\eta^4\text{-C}_6\text{H}_8)$ (XR5) is an octahedral cluster with the cyclohexadiene group forming two π -bonds to two adjacent metal atoms. This is compared to the structure of the linear hexadiene analogue $\text{Ru}_6\text{C}(\text{CO})_{15}(\eta^4\text{-C}_6\text{H}_{10})$ reported earlier.

The $\mu_3\eta^2$ -bonding mode commonly adopted by alkyne fragments is observed for both mono- and disubstituted alkynes in the hexaruthenium clusters $\text{Ru}_6\text{C}(\text{CO})_{15}(\text{PhCCH})$ (XR6) and $\text{Ru}_6\text{C}(\text{CO})_{15}(\text{MeCCMe})$ (XR7), and in the heterometallic cluster $\text{Ru}_6\text{C}(\text{CO})_{14}(\text{PhCCH})(\text{AuPEt}_3)_2$ (XR8), in all of which the octahedral metal framework is maintained.

$\text{Ru}_6(\text{CO})_{13}(\eta^2\text{-CO})_2(\eta^6\text{-C}_6\text{H}_3\text{Me}_3)$ (XR10) is isolated as an intermediate in cluster build-up from $\text{Ru}_3(\text{CO})_{12}$ and yields $\text{Ru}_6\text{C}(\text{CO})_{15}(\eta^6\text{-C}_6\text{H}_3\text{Me}_3)$ (XR9) and $\text{HRu}_6(\text{CO})_{13}(\eta^2\text{-CO})(\eta^7\text{-C}_6\text{H}_3\text{Me}_2\text{CH}_2)$ (XR11) in equal amounts. The structures of these three hexanuclear clusters (XR9), (XR10), and (XR11) give an insight into the mechanism of formation of octahedral carbido-species. Also produced from this reaction is the decanuclear carbido-cluster $[\text{HRu}_{10}\text{C}(\text{CO})_{24}]^-$, and a product from a related reaction is the decanuclear nitrido-cluster $[\text{Ru}_{10}\text{N}(\text{CO})_{24}]^-$ (XR12), which has been shown to have a tetracapped octahedral framework and is isostructural with the hydrido-cluster $[\text{HRu}_{10}\text{C}(\text{CO})_{24}]^-$.

The interaction of alkyne fragments and some metal frameworks has been investigated. The reaction of $[\text{HOs}_3(\text{CO})_{11}]^-$ with mono-substituted alkynes, followed by $[\text{AuPR}_3]^+$, gives the alkenylidene cluster $\text{Os}_3(\text{CO})_{10}(\text{PhCCH}_2)(\text{AuPMe}_3)$ (XR13), whereas in its reaction with disubstituted alkynes the alkyne remains intact to give $\text{HOs}_3(\text{CO})_9(\text{MeCCMe})(\text{AuPPh}_3)$ (XR14). Finally, a unique example of a high nuclearity cluster with three intact alkynes on the cluster surface has been characterised; the heptanuclear cluster $\text{Os}_7(\text{CO})_{16}(\text{MeCCMe})_3$ (XR15), has a previously unobserved metal framework and two different alkyne bonding modes are present.

Contents

Title	(i)
Declaration	(ii)
Dedication	(iii)
Acknowledgements	(iv)
Abbreviations	(v)
Abstract	(vi)
Chapter 1 Introduction.	1
1.1 Preliminary Results.	1
1.2 Theoretical Aspects of cluster chemistry.	2
1.2.1 The eighteen electron rule.	3
1.2.2 The polyhedral skeletal electron pair theory.	6
1.2.3 The capping principle.	9
1.2.4 Polyhedral fusion.	11
1.2.5 The isolobal analogy- $M(CO)_3$ and $M(CO)_4$ fragments.	12
1.2.6 The isolobal connection between H and $Au(PR_3)$.	14
1.2.7 Alternative electron counting schemes.	16
1.3 A rationale for geometric flexibility.	18
1.4 M-L bonding modes for organo-ligands on cluster surfaces.	25
1.4.1 Naming of fragments.	26
1.4.2 Structural review of dicarbon fragments.	29
1.5 Conclusion.	36
Chapter 2 Organo-fragments on pentanuclear clusters.	37
2.1 Routes reported for the formation of pentanuclear complexes.	
2.1.1 Build-up synthesis.	37
2.1.2 Cluster degradation.	38
2.2 Cluster reactivity.	38

2.2.1 Nucleophilic attack on clusters.	39
2.2.2 Electrophilic attack on pentanuclear clusters.	45
2.2.3 Organic reactions of pentanuclear clusters.	46
2.3 Interaction of $\text{Ru}_5\text{C}(\text{CO})_{15}$ (1a) with pyridine.	51
2.3.1 Synthesis.	51
2.3.2 Overall description of the molecular structures.	52
2.3.3 Structural comparison of the bridged butterflies.	56
a) The effect of a terminal ligand on the bridging metal atom.	56
b) The effect of a bridging ligand (on the hinge bond).	58
c) The effect of a bridging ligand between two non-bonding metal atoms.	59
2.3.4 Structural comparison for the clusters with square pyramidal cores.	60
2.4 Mechanistic Analysis.	62
2.5 A reaction pathway for pyridyl addition to pentanuclear clusters.	64
2.5.1 Proposed mechanism.	64
a) Axial-basal bond cleavage.	65
b) Basal-basal bond cleavage.	66
2.6 Conclusion and summary.	67
 Chapter 3 Derivatives of octahedral hexaruthenium clusters.	 69
3.1 Historical review.	69
3.2 X-Ray structure analysis of $\text{Ru}_6\text{C}(\text{CO})_{15}(\text{C}_6\text{H}_8)$ (XR5) and a comparison with the linear analogue $\text{Ru}_6\text{C}(\text{CO})_{15}(\text{C}_6\text{H}_{10})$ (17).	89
3.2.1 Surface competition.	89
3.2.2 Structural description.	90

3.2.3 Discussion.	90
3.2.4 Conclusion.	95
3.3 X-Ray structure analysis of $\text{Ru}_6\text{C}(\text{CO})_{15}(\text{PhCCH})$ (XR6) and $\text{Ru}_6\text{C}(\text{CO})_{15}(\text{PhCCMe})$ (XR7).	96
3.3.1 Introduction.	96
3.3.2 Preparation.	97
3.3.3 Structural description.	97
3.3.4 Conclusion.	100
3.4 X-Ray structure analysis of $\text{Ru}_6\text{C}(\text{CO})_{14}(\text{PhCCH})(\text{AuPMe}_3)_2$ (XR8).	100
3.4.1 Synthesis.	101
3.4.2 Structural description.	101
3.4.3 Discussion.	101
3.4.4 Mechanism.	
3.4.5 Conclusion.	107
3.5 Overall Summary.	108
Chapter 4 A key to interstitial carbide formation.	109
4.1 Cluster catalysis.	109
4.1.1 Fischer-Tropsch synthesis.	110
4.2 An early investigation of the process involved in carbido-cluster formation.	111
4.3 X-Ray structure analysis of $\text{Ru}_6\text{C}(\text{CO})_{14}(\eta^6\text{-C}_6\text{H}_3\text{Me}_3)$ (XR9), $\text{Ru}_6(\text{CO})_{13}(\mu_4\eta^2\text{-CO})_2(\eta^6\text{-C}_6\text{H}_3\text{Me}_3)$ (XR10), and $\text{HRu}_6(\text{CO})_{13}(\mu_4\eta^2\text{-CO})(\eta^7\text{-C}_6\text{H}_3\text{Me}_2\text{CH}_2)$ (XR11).	112
4.3.1 Synthesis.	112
4.3.2 Structural description.	114
a) $\text{Ru}_6\text{C}(\text{CO})_{14}(\eta^6\text{-C}_6\text{H}_3\text{Me}_3)$ (XR9).	114
b) $\text{Ru}_6(\text{CO})_{13}(\mu_4\eta^2\text{-CO})(\eta^6\text{-C}_6\text{H}_3\text{Me}_3)$ (XR10).	114
c) $\text{HRu}_6(\text{CO})_{13}(\mu_4\eta^2\text{-CO})(\eta^7\text{-C}_6\text{H}_3\text{Me}_2\text{CH}_2)$ (XR11).	115

4.3.3 Discussion.	116
4.3.4 A structural pathway for the generation of interstitial C-atoms.	121
4.4 The formation of a nitrido decanuclear cluster.	124
4.4.1 The predominant decanuclear cluster core.	124
4.4.2 X-Ray structure analysis of the nitrido-anion $[\text{Ru}_{10}\text{N}(\text{CO})_{24}]^-$ (XR12).	130
a) Synthesis.	130
b) Structural description.	130
c) Discussion.	131
4.5 Conclusion.	133
 Chapter 5 Osmium clusters with alkyne fragments.	 135
5.1 The reactivity of trinuclear clusters with alkenes and alkynes.	135
5.1.1 Trinuclear clusters with alkene ligands.	135
5.1.2 Reaction of $\text{H}_2\text{Os}_3(\text{CO})_{10}$ (8) with alkynes.	139
5.2 X-Ray structure analysis of	143
$\text{Os}_3(\text{CO})_{10}(\text{PhCCH}_2)(\text{AuPEt}_3)$ (XR13).	
5.2.1 Synthesis.	143
5.2.2 Structural description.	144
5.2.3 Discussion.	145
5.2.4 Mechanism for the formation of	146
$\text{Os}_3(\text{CO})_{10}(\text{PhCCH}_2)(\text{AuPEt}_3)$ (XR13).	
5.2.5 Conclusion.	147
5.3 X-Ray structural analysis of $\text{HOs}_3(\text{CO})_9(\text{AuPPH}_3)$ (XR14).	148
5.3.1 Synthesis.	148
5.3.2 Structural description.	148
5.3.3 Discussion.	149
5.3.4 Mechanism.	150
5.3.5 Conclusion.	151

5.4 Interaction of heptanuclear clusters with mono- and disubstituted alkynes.	152
5.4.1 Heptanuclear metal core geometries.	152
5.4.2 The reactions of heptanuclear clusters with mono-substituted alkynes.	156
5.5 X-Ray structure analysis of $\text{Os}_7(\text{CO})_{16}(\text{MeCCMe})_3$ (XR15).	163
5.5.1 Synthesis.	163
5.5.2 Structural description.	163
5.5.3 Discussion.	164
5.5.4 Proposed mechanism for the formation of (XR15).	167
5.5.5 Conclusion.	168
Chapter 6 Background crystallography and experimental details.	169
6.1 Conditions for X-ray diffraction and fundamental symmetry concepts.	169
6.1.1 Geometry of X-ray diffraction by crystals.	169
6.1.2 The reciprocal lattice.	171
6.1.3 Symmetry elements.	173
a) Point group symmetry.	174
b) Translational symmetry.	174
6.1.4 Crystal systems.	175
6.2 Intensity of X-ray diffraction.	176
6.2.1 The atomic scattering factor.	176
6.2.2 The structure factor.	177
6.3 The use of the diffractometer.	177
6.3.1 Selection and mounting of a crystal.	177
6.3.2 Mounting and centring the crystal.	178
6.3.3 Peak hunting.	179
6.3.4 Automatic data collection.	182
6.3.5 Data reduction.	182

b) Data collection.	201
c) Structural solution and refinement.	201
6.5.6 X-Ray structure analysis of	202
$\text{Ru}_6(\text{CO})_{13}(\text{2-CO})_2(\text{C}_6\text{H}_3\text{Me}_3)$ (XR10).	
a) Crystal data.	202
b) Data collection.	202
c) Structural solution and refinement.	203
6.5.7 X-Ray structure analysis of	204
$\text{HRu}_6(\text{CO})_{13}(\mu_4\text{-CO})(\text{C}_6\text{H}_3\text{Me}_2\text{CH}_2)$ (XR11).	
a) Crystal data.	204
b) Data collection.	205
c) Structural solution and refinement.	205
6.5.8 X-Ray structure analysis of	205
$[\text{Ru}_{10}\text{N}(\text{CO})_{24}]^-$ (XR12).	
a) Crystal data.	206
b) Data collection.	206
c) Structural solution and refinement.	206
6.5.9 X-Ray structure analysis of $\text{Os}_3(\text{CO})_{10}(\text{AuPEt}_3)$ (XR13).	207
a) Crystal data.	207
b) Data collection.	207
c) Structural solution and refinement.	208
6.5.10 X-Ray structure analysis of $\text{HOs}_3(\text{CO})_9(\text{AuPPH}_3)$ (XR14).	208
a) Crystal data.	209
b) Data collection.	209
c) Structural solution and refinement.	209
6.5.11 X-Ray structure analysis of	210
$\text{Os}_7(\text{CO})_{16}(\text{MeCCMe})_3$ (XR15).	
a) Crystal data.	210
b) Data collection.	211
c) Structural solution and refinement.	211

Appendix A Selected bond lengths (Å) and angles(°).

A1	$\text{HRu}_5\text{C}(\text{CO})_{14}(\text{C}_5\text{H}_4\text{N})$ Isomer A (XR1)	A1
A2	$\text{HRu}_5\text{C}(\text{CO})_{14}(\text{C}_5\text{H}_4\text{N})$ Isomer B (XR2)	A7
A3	$\text{HRu}_5\text{C}(\text{CO})_{13}(\text{C}_5\text{H}_4\text{N})(\text{C}_5\text{H}_5\text{N})$ (XR3)	A14
A4	$\text{HRu}_5\text{C}(\text{CO})_{13}(\text{C}_5\text{H}_4\text{N})$ (XR4)	A18
A5	$\text{Ru}_6\text{C}(\text{CO})_{15}(\text{C}_6\text{H}_8)$ (XR5)	A24
A6	$\text{Ru}_6\text{C}(\text{CO})_{15}(\text{PhCCH})$ (XR6)	A30
A7	$\text{Ru}_6\text{C}(\text{CO})_{15}(\text{MeCCMe})$ (XR7)	A36
A8	$\text{Ru}_6\text{C}(\text{CO})_{14}(\text{PhCCH})(\text{AuPMe}_3)_2$ (XR8)	A42
A9	$\text{Ru}_6\text{C}(\text{CO})_{14}(\eta^6\text{-C}_6\text{H}_3\text{Me}_3)$ (XR9)	A47
A10	$\text{Ru}_6(\text{CO})_{15}(\eta^6\text{-C}_6\text{H}_3\text{Me}_3)$ (XR10)	A51
A11	$\text{HRu}_6(\text{CO})_{14}(\eta^7\text{-C}_6\text{H}_3\text{Me}_2\text{CH}_2)$ (XR11)	A58
A12	$[\text{N}(\text{PPH}_3)_2]^-[\text{Ru}_{10}\text{N}(\text{CO})_{24}]^-$ (XR12)	A65
A13	$\text{Os}_3(\text{CO})_{10}(\text{PhC=CH}_2)(\text{AuPEt}_3)$ (XR13)	A72
A14	$\text{HOs}_3(\text{CO})_9(\text{MeCCMe})(\text{AuPPH}_3)$ (XR14)	A77
A15	$\text{Os}_7(\text{CO})_{16}(\text{MeCCMe})_3$ (XR15)	A82

Appendix B Patterson solutions.

B1

B.1 Location of the six ruthenium atoms in

$\text{Ru}_6\text{C}(\text{CO})_{15}(\text{PhCCH})$ (XR6) By use of Patterson synthesis. B1

B.2 The transformed vectors of the Patterson synthesis used to B5

solve $\text{HRu}_5\text{C}(\text{CO})_{14}(\text{C}_5\text{H}_4\text{N})$ Isomer A (XR1).

B.3 Patterson solution for $\text{HRu}_5\text{C}(\text{CO})_{14}(\text{C}_5\text{H}_4\text{N})(\text{C}_5\text{H}_5\text{N})$ (XR3). B6B.4 Patterson solution for $\text{Ru}_6\text{C}(\text{CO})_{15}(\text{C}_6\text{H}_8)$ (XR5). B8B.5 Patterson solution for $\text{Ru}_6\text{C}(\text{CO})_{15}(\text{PhCCMe})$ (XR7). B10B.6 Patterson solution for $\text{Ru}_6\text{C}(\text{CO})_{14}(\text{PhCCH})(\text{AuPEt}_3)_2$ (XR8). B11B.7 Patterson solution for $\text{Ru}_6\text{C}(\text{CO})_{14}(\text{C}_6\text{H}_3\text{Me}_3)$ (XR9). B13B.8 Patterson solution for $\text{Ru}_6(\text{CO})_{15}(\text{C}_6\text{H}_3\text{Me}_3)$ (XR10). B14

- B.9 Patterson solution for $\text{Os}_3(\text{CO})_{10}(\text{PhCCH}_2)(\text{AuPEt}_3)$ (XR13). B15
- B.10 Patterson solution for $\text{HOs}_3(\text{CO})_9(\text{MeCCMe})(\text{AuPPH}_3)$ (XR14). B16
- B.11 Patterson solution for $\text{Os}_7(\text{CO})_{16}(\text{MeCCMe})_3$ (XR15). B17

Publications - arising from this thesis are included in the back.

CHAPTER ONE

An overview of organo-cluster chemistry.

Chapter 1 - An overview of organo-cluster chemistry.

Since the early sixties cluster chemistry, like organometallic chemistry, has been rapidly developing. The aim of this research was to characterise new organo-derivatives of metal carbonyl clusters by use of X-ray structural analysis and to study the effect organo-fragments have on metal core geometries.

This introductory chapter outlines the theoretical background to cluster compounds and considers both the range of hypothetical metal core frameworks and the types of organic fragments, in terms of their potential bonding modes. In Chapter 2 a review of pentanuclear clusters of ruthenium and osmium is given and the X-ray structural analyses of five pyridyl derivatives are reported. A possible mechanistic pathway is proposed for the formation of these compounds from $\text{Ru}_5\text{C}(\text{CO})_{15}$. Chapter 3 begins with a historical review of hexanuclear clusters and the X-ray structural analyses of five compounds of this class of clusters are reported, including a heteronuclear digold hexaruthenium derivative. The importance of cluster compounds with respect to the Fischer-Tropsch synthesis is stressed in Chapter 4, and the four structures reported there are believed to offer an important insight into this area of catalytic chemistry. Two trinuclear and one heptanuclear cluster are reported in Chapter 5, along with possible mechanistic pathways for a number of heptanuclear reactions. Finally, background crystallography and experimental details are presented in Chapter 6 and the Appendices (A and B) list fractional atomic coordinates, essential bond lengths, angles, and interpretations of the Patterson syntheses.

1.1 Preliminary results.

In order to gain some insight into the reactivity of organo-fragments with clusters, dinuclear species were studied in the early stages of the

project. These compounds are characterised by a constant metal core geometry and so variation in hydrocarbon ligand bonding modes alone can be analysed. A correlation of these dinuclear species was attempted to obtain an insight into the effect dinuclear metal cores have on organic fragments, before investigation of larger clusters. Related structures previously reported had shown that unusual modes of bonding of organic fragments can arise in such clusters,[1-4] and many of the fragments identified for dinuclear complexes have not been reported for mononuclear compounds.

All the dimolybdenum compounds characterised by X-ray structural analysis have some form of organo-fragment bonded to the dimetal centre, and range from relatively simple organo-derivatives, as found in $\text{Mo}_2(\eta^5\text{-Cp})_2(\text{CO})(\mu\text{-PPh}_2)_2(\eta^2\text{-MeCCMe})$ to more complicated structures such as $\text{Mo}_2(\eta^5\text{-Cp})_2(\mu\text{-PPh}_2)(\mu_2\text{-}\eta^6\text{-MeO}_2\text{CC}_2\text{CO}_2\text{Me})$. Most of these structural results have already been published,[5-8] and will not be discussed further here. The main part of the project involved higher nuclearity clusters where a variety of metal frameworks are possible for any given number of metal atoms and these form the basis of this thesis.

1.2 Theoretical aspects of cluster chemistry.

An understanding of the theoretical aspects of chemistry has usually developed in parallel to synthetic discoveries. Some theoretical insights arise from detailed quantum analysis, but quite often simple empirical rules can be used to explain observed results and can often predict new features. Examples of empirical rules that have proved particularly useful include the concept of atomic orbital hybridisation,[9] the Octet Law and the Woodward-Hoffmann rules.[10]

The interest in the theoretical aspects of the enormous array of geometries observed for cluster species is almost as diverse as the range of products now known. A number of reviews have appeared, the most recent of which are those by Mingos[11] and Owen.[12]

1.2.1 The Eighteen Electron Rule.

For any new class of molecule it is helpful to develop simple empirical bonding concepts, or rules, that rationalise and predict which molecular geometries represent realistic structures for members of the group. The effective atomic number or eighteen-electron rule, revolutionised both formal electron bookkeeping and understanding of the intermediate steps involved in mononuclear organometallic reaction processes.[13-15] It is discussed here not only because of its application to cluster electron counting but also because it is often implicit in the alternative electron counting theories discussed further on in this section. The effective atomic number rule was introduced by Sidgwick for coordination compounds but was of limited use. The modern version, frequently referred to as the eighteen electron rule, was developed for organometallic compounds and is nearly always obeyed for transition metals (particularly for those in the middle of the transition series) in compounds with strong π -acceptor ligands.

The eighteen electron rule is derived from the fact that transition metals have nine atomic orbitals [$5xnd + (n+1)s + 3x(n+1)p$, where n is the principal quantum number and d,s,p are orbitals]. In organometallic compounds these nine atomic orbitals give rise to 9 low lying molecular orbitals of bonding or non-bonding character. Maximum kinetic stability will result when 18 electrons fill these 9 low lying orbitals. The resultant separation between these orbitals and the associated antibonding orbitals is large and therefore the eighteen electron rule is not usually

broken and is associated with kinetic stability. Thus maximum kinetic stability is associated with all bonding and non-bonding orbitals being filled and all anti-bonding orbitals being empty.

The application of the eighteen electron rule assumes that clusters are held together by a network of (2c-2e) M-M bonds and is successful for transition metal clusters containing up to, and including, five metal atoms. This therefore determines the number of cluster valence electrons (CVE) and can be expressed by the following formula,

$$\text{CVE} = 18M - 2E \quad \text{or} \quad E = (18M - \text{CVE})/2 \quad (1)$$

where E is the number of edges in the cluster polyhedron and M denotes the number of metal atoms.

In rare cases, multiple bonds are necessary to satisfy the 18e rule. For example, the trinuclear cluster $\text{H}_2\text{Os}_3(\text{CO})_{10}$ has 46 CVE's and therefore four M-M bonds are expected, and achieved by one double Os-Os bond. This is reflected both by a shortened bonding distance for the hydrido bridged Os-Os bond and by the cluster's reactivity, with the observed addition reactions across the M-M double bond being reminiscent of alkene chemistry.[16]

An interesting consequence of the eighteen electron rule, of fundamental importance in cluster reactivity, is that addition of two electrons to a cluster results in M-M bond cleavage. This feature can be illustrated for M_4 and M_5 cluster cores. The anion, $[\text{H}_3\text{Ru}_4(\text{CO})_{12}]^-$, [17] has 60 CVE's which gives the correct six edges required for the observed tetrahedral geometry. Formally, the more open butterfly in $\text{Ru}_4(\text{CO})_{12}(\text{PhCCPh})$, [18] with 62 CVE's has only five edges and may be regarded as an 'opened up' tetrahedron. Two additional electrons results in the square geometry found in $\text{Ir}_4(\text{CO})_8(\text{MeCO}_2\text{CCCO}_2\text{Me})_4$, [19] with 64 CVE's. This formal metal core opening process is schematically illustrated in Figure 1.2/1.

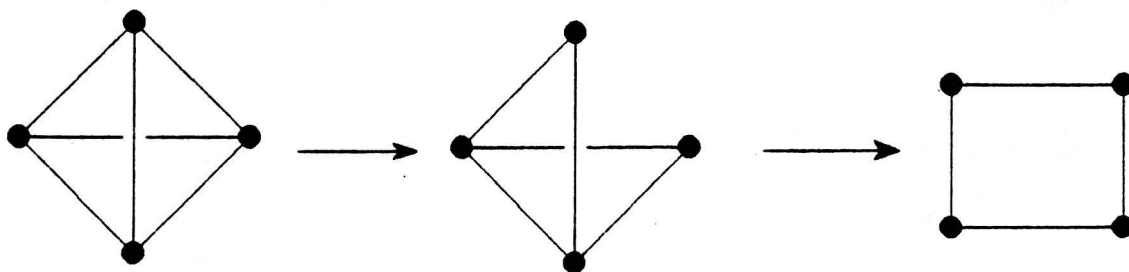


Figure 1.2/1 Progressive M-M cleavage for an M_4 core.

Similar relationships occur for pentanuclear species. The trigonal bipyramidal cluster $[Os_5(CO)_{15}]^{2-}$, [20] has 72 CVE's and the correct nine edges predicted by equation (1) (Figure 1.2/2). Addition of $2e$ causes opening of the metal framework and the $74e$ cluster $Os_5C(CO)_{15}$, [21-22] has a square pyramidal core. Attack by a $2e$ donor to this cluster breaks another M-M bond to give a 'bridged butterfly' as in, for example, $Os_5C(CO)_{16}$ (Figure 1.2/2). [23]

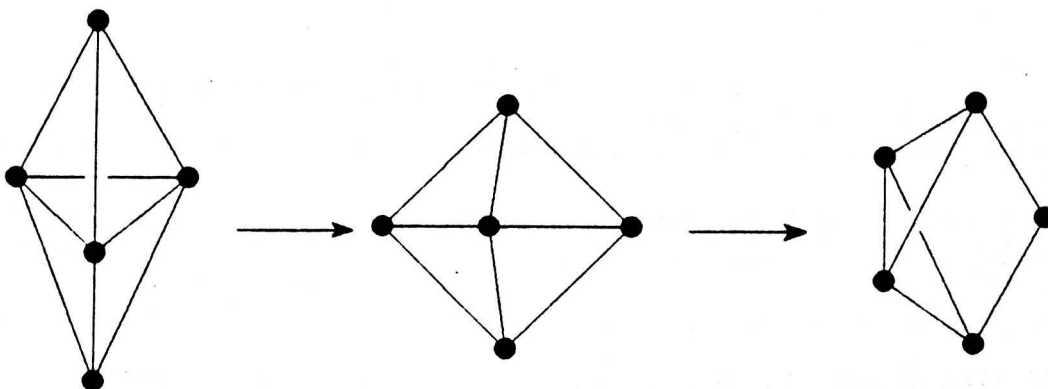


Figure 1.2/2 Progressive cleavage for an M_5 core.

The eighteen electron rule breaks down for the most widely observed type of hexanuclear cluster core, the octahedron. This has twelve edges and, by the $18e$ rule, should have 84 electrons but metal carbonyl clusters are almost invariably associated with 86 electrons. When $Os_6(CO)_{18}$, which has 84 electrons, was first synthesised an octahedral geometry was assumed. X-Ray structural analysis showed that this compound was not octahedral but capped trigonal bipyramidal. [24] Significantly, on reduction with iodide an octahedral metal framework was obtained in the dianion $[Os_6(CO)_{18}]^{2-}$, which has 86 electrons (Figure 1.2/3). [25-27]

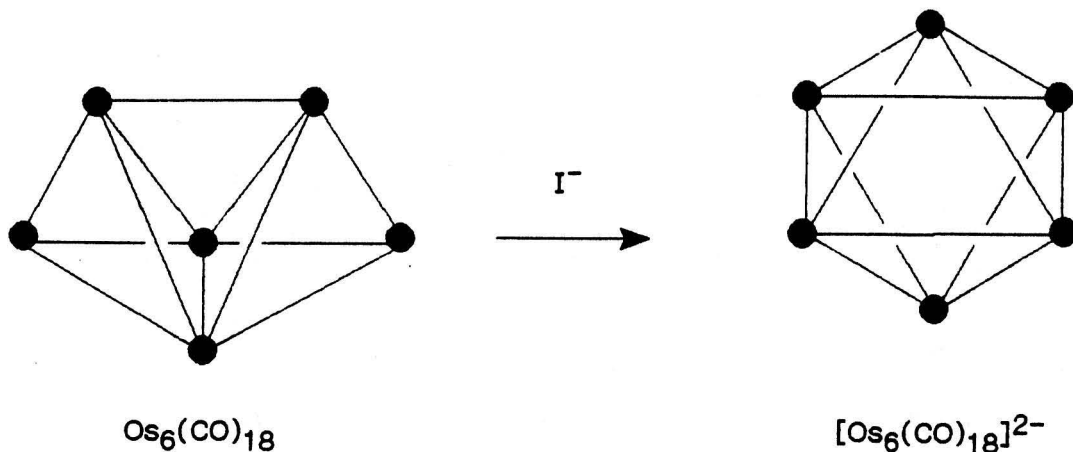


Figure 1.2/3 Reduction of $\text{Os}_6(\text{CO})_{18}$ to $[\text{Os}_6(\text{CO})_{18}]^{2-}$.

In terms of the eighteen electron rule this was surprising because instead of the extra two electrons causing bond rupture, a core rearrangement had occurred but the number of M-M bonds (12) had remained the same. Adequate explanation of this phenomenon and rationalisation of the stability of 86 electron octahedral species was provided by the polyhedral skeletal electron pair theory (PSEPT).

1.2.2 The Polyhedral Skeletal Electron Pair Theory.

A quirk of chemistry is that the seemingly diverse areas of borane and transition metal clusters should have amalgamated to produce a unifying electron counting formalism.

The PSEPT states that a cluster polyhedron with n vertices is held together by $(n+1)$ skeletal electron pairs (S) [where $S=(n+1)$] and this theory was first developed for boranes.[28-33] The simplest boranes of the general formula $[\text{B}_n\text{H}_n]^{2-}$ form a series of polyhedral structures with n vertices. Each boron atom uses 1e to form a bond to its hydrogen atom, leaving two electrons available for cluster bonding. Overall these dianionic species are observed to have $(n+1)$ skeletal electron pairs with the nido- and arachno-polyhedra requiring the same number of skeletal electron pairs as the parent closo-polyhedron.[29] This conversion process is illustrated in Figure 1.2/4 for the closo-species $[\text{B}_7\text{H}_7]^{2-}$.

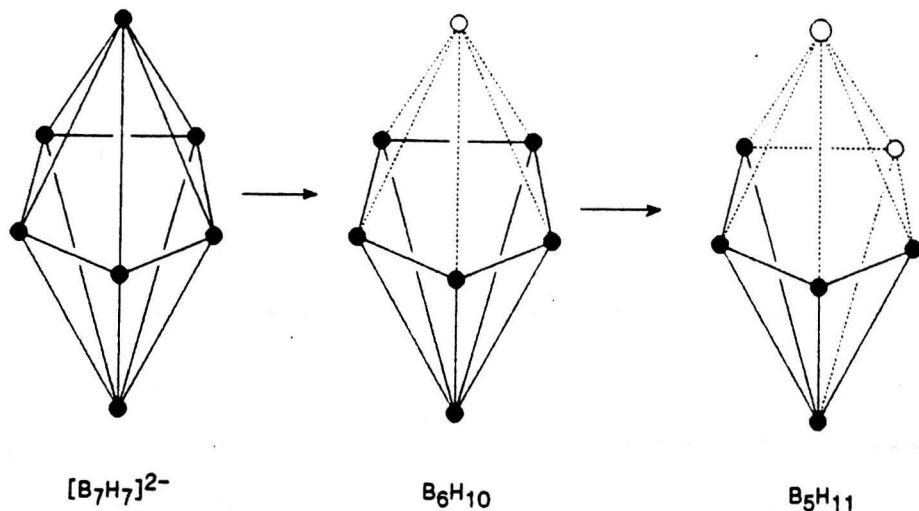


Figure 1.2/4 Conversion of a closo-core to nido- and arachno-cores.

Wade made the perceptive analogy between the isostructural borane and transition metal compounds, recognising that the bonding pattern observed in boranes was reproduced by metal carbonyl clusters, i.e., that n vertex polyhedra require $(n+1)$ skeletal electron pairs.[29]

For transition metal clusters this may be illustrated with the octahedral dianion $[Os_6(CO)_{18}]^{2-}$, [25-27] which has $Os(CO)_3$ groups at each vertex of the fundamental polyhedron. Wade considered that each of these groups contributes two electrons to the skeletal electron bonding, as each skeletal metal uses 12 electrons for M-L bonding or housing of non-bonding electrons. Therefore this dianionic species has the required 7 skeletal electron pairs (S.E.P.) which explains the generally derived 86 polyhedral electron count (PEC) for octahedral species. As with boranes, nido- and arachno- transition metal clusters require the same number of skeletal electron pairs as the closo-species.

In summary, the skeletal electron pairs (S) are those left over after 12e have been assigned to each metal atom, and the number of vertices in the fundamental polyhedron (n) will be one less than this, i.e. $S-1$. Removal of either one or two metal atoms produces the corresponding nido- or arachno-polyhedron respectively, whereas if extra metal atoms are present these must occupy capping positions. Thus for $H_2Ru_6(CO)_{18}$, [34-35] the number of CVE's is 86e ($6 \times 8 + 18 + 2 + 2$) minus 12×6 , giving 14e or 7 skeletal

electron pairs (S.E.P.) and therefore the fundamental polyhedron has six vertices and is octahedral.

The first theoretical justification of Wade's theory came from molecular orbital calculations by Mingos on the 86 electron octahedral cluster $[\text{Co}_6(\text{CO})_{14}]^{4-}$. [36] Further research was carried out by Lauher, who performed extended Huckel calculations on a wide range of bare n-atom close transition metal clusters. [37] The results indicated that for an M_6 cluster, of the 54 metal molecular orbitals (9 atomic orbitals from each M) 11 are highly antibonding in character, leaving 43 cluster valence molecular orbitals (CVMO) and it is in these CVMO's that the 86 electrons observed for an octahedral geometry are accommodated. For example, in the dihydro cluster $\text{H}_2\text{Ru}_6(\text{CO})_{18}$, [34-35] 19 of the 43 CVMO's are used to accommodate the ligand electrons ($2 \times 18 + 2 = 38$ electrons in 19 electron pairs), leaving 24 CVMO's to house the 48e from the d orbitals of the 6 ruthenium atoms. Amongst the conclusions reached by Lauher was the fact that the principal acceptor orbitals in transition metals are of s and p character. [37]

For a general case, a polyhedron of n metal atoms has $(2n-1)$ inaccessible high-lying antibonding orbitals, leaving a total of $[9n - (2n-1)]$ or $(7n+1)$ occupied cluster valence MO's and thus a CVE of $(14n+2)$. This is exactly what Wade had deduced on empirical grounds, i.e., $12n$ electrons are used for M-L bonding leaving $(n+1)$ S.E.P. or $[6n + (n+1)]$ occupied molecular orbitals. Further calculations on nido- and arachno-clusters showed that they are characterised by $(14n+4)$ and $(14n+6)$ valence electrons respectively, i.e. an additional two or four electrons, exactly the conclusion of the Wade empirical approach. Further theoretical calculations in general agreed with these conclusions. [38-40]

1.2.3 The Capping Principle.

The arguments outlined above explain the 86 electrons observed for all octahedral cluster compounds, but they do not explain the capped trigonal bipyramidal structure of the 84 electron compound $\text{Os}_6(\text{CO})_{18}$. [24] Mingos introduced the capping theory to explain this and other apparently anomalous structures. [38, 41, 42]

The capping principle has proved to be invaluable in clusters of the iron triad which are dominated by capped octahedral structures. It states that capping a face of a polyhedron leads to no change in the number of skeletal bonding MO's. This is because the frontier orbitals of the capping fragment are matched in symmetry by orbitals of the parent cluster which are already bonding. [38] Capping with a conical $\text{M}(\text{CO})_3$ fragment, therefore, leads to an increase in the cluster valence electron count of 12 (since the fragment has 12 electrons in non-bonding and metal-ligand bonding orbitals). Thus, capped clusters are characterised by $[(14n+2)+12m]$ valence electrons, where n is the number of metal atoms defining the parent core and m is the number of capping metal fragments. [11,42]

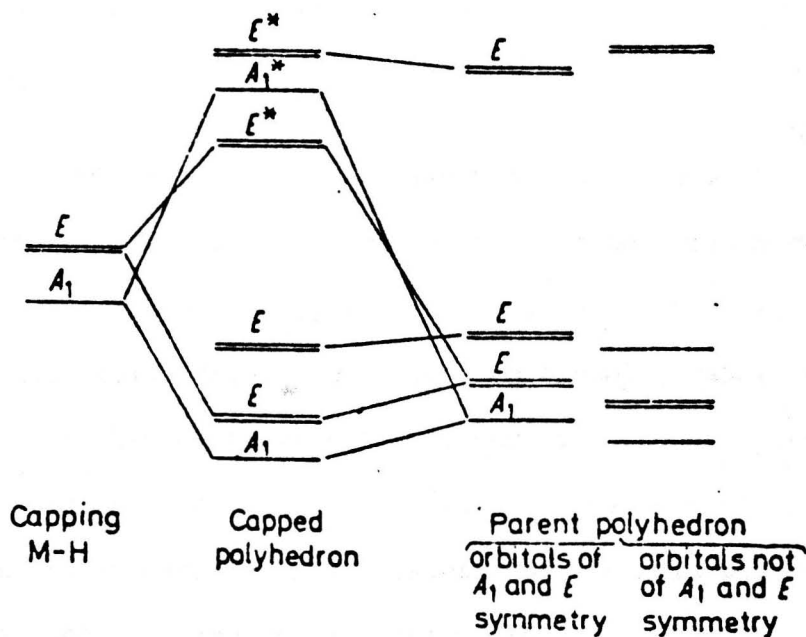


Figure 1.2/5 Molecular orbital diagram for the capping process. [38]

Figure 1.2/5 is the interaction diagram for the capping process.[38] The strongest interaction is between the A_1 and E orbitals on the capping fragment and the parent polyhedron. In each case a filled bonding orbital of lower energy and an empty antibonding orbital of higher energy are produced. The remaining 6 orbitals of the $M(CO)_3$ fragment are involved in ligand bonding and holding of non-bonding electrons, and do not participate in bonding to the parent cluster. In all, as six orbitals have been added, the CVMO increases by six. This justifies the fact that a capping group adds twelve electrons to the cluster valence electron count.

McPartlin added two useful concepts in correlating the observed structures of the iron triad. Firstly, that incomplete polyhedra could be capped and secondly, that capping could occur on already existing caps rather than on the fundamental polyhedron.[43-44] These additional concepts allowed a correlation of all the known structures for osmium with $S=7$; addition, or loss, of a vertex results in gain, or loss, of 12e. The correlation matrix for structures based on $S=7$ emphasises this connection and is illustrated in Figure 1.2/6.[43] The beauty of this matrix lies in connecting the multitude of possible geometries, and in showing the way different cores are related.

Because pentanuclear clusters were important in this work (Chapter 2), a corresponding matrix for structures with $S = 6$ was considered. This matrix gives the same polyhedra along all the diagonals (Figure 1.2/7), because the fundamental polyhedron, the trigonal bipyramid, has a central triangle. The possible structural isomers that occur for clusters derived from the octahedron (which contains a central square plane) are precluded. Of interest in the appearance of the matrix for $S = 6$ is the capped trigonal bipyramidal core (84 CVE) evident for $Os_6(CO)_{18}$. [24]

Figure 1.2/6 Correlation Matrix for structures with S = 7.[43]

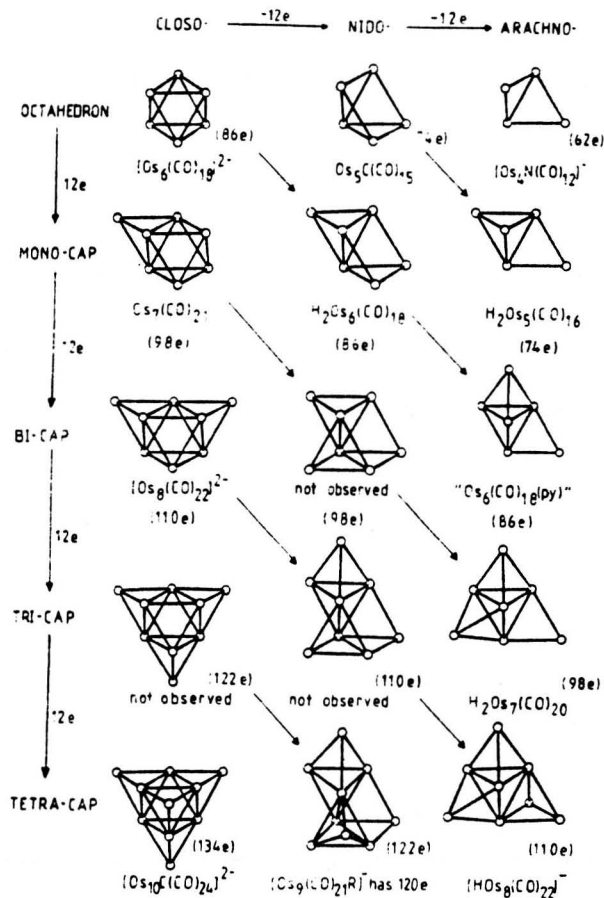
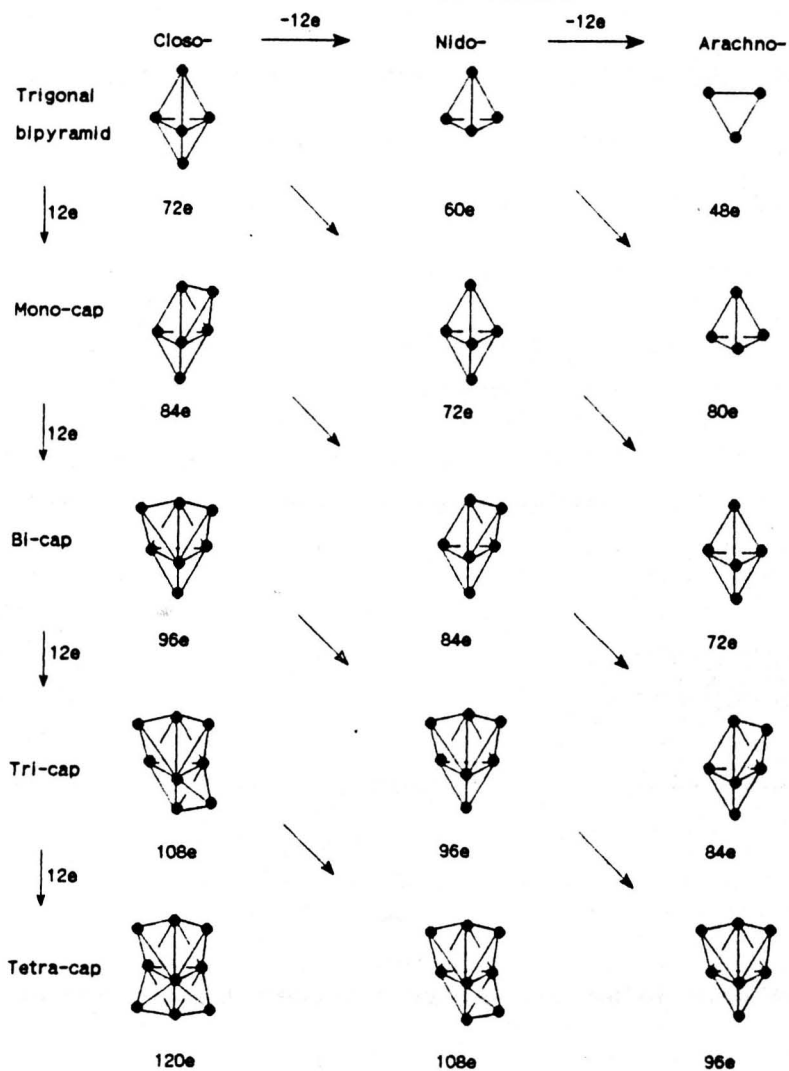
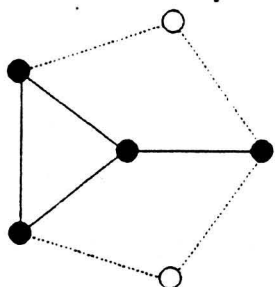


Figure 1.2/7 Correlation matrix for structures with S = 6.



By analogy, the next matrix up (with a CVE of 100e and therefore 8 S.E.P.) could be considered to be based on a fundamental polyhedron which would contain a central pentanuclear planar ring. Although this is observed for boranes it has not so far been observed for transition metal clusters. However, one important geometry in this matrix is the arachno-version of this polyhedron which has 5 metal atoms (Figure 1.2/8). The pyridyl clusters $\text{HRu}_5\text{C}(\text{CO})_{13}(\text{C}_5\text{H}_4\text{N})\text{L}$ [$\text{L}=(\text{CO})$ for (XR1) and (XR2) and $\text{L}=(\text{C}_5\text{H}_5\text{N})$ for (XR3)] discussed in Chapter 2 have this metal core framework.



View on to the equatorial plane of an arachno-core with 8 SEP.

Figure 1.2/8 The arachno-core for 8 skeletal electron pairs.

1.2.4 Polyhedral fusion.

The discovery of more complicated clusters with geometries consisting of fused polyhedra prompted Mingos to devise a formalism that these cores contain fused geometries sharing vertices, edges, or triangular faces. [45-46]

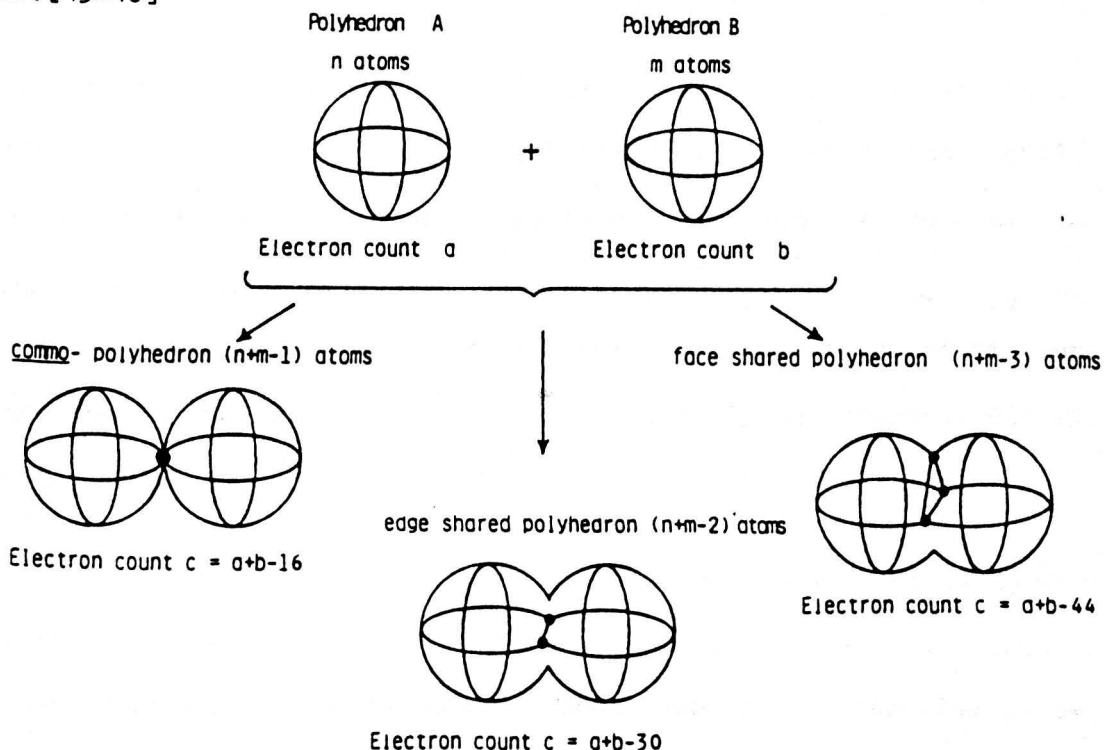


Figure 1.2/9 The condensation processes possible for metal clusters. [45]

Figure 1.2/9 illustrates the three fundamental condensation processes. In the first, the parent polyhedra (A) and (B) are linked through a common vertex, whereas in the second and third cores the polyhedra are condensed through either an edge or a triangular face.

"The total electron count in a condensed polyhedron is equal to the sum of the characteristic electron counts for the parent polyhedra (A) and (B), minus the electron count characteristic[†] for the atom, pair of atoms, or face of atoms common to both polyhedra." [46]

1.2.5 The isolobal analogy for $M(CO)_3$ and $M(CO)_4$ fragments.

The term 'isolobal' was first introduced by Hoffmann. [47] Two molecular orbital fragments are termed isolobal if the number, symmetry properties, approximate energy, shape of the frontier orbitals, and the number of electrons in them are similar. [48] This is in part based on viewing the frontier orbitals of the M.O. fragments; the highest occupied and lowest unoccupied levels, i.e., the valence active orbitals. [49-50] Hoffmann and co-workers analysed a set of $M(CO)_n$ fragments ($n=3-5$), the most important of which in the context of this work are $M(CO)_3$ and $M(CO)_4$. [48,51]

The initial starting point is to consider the metal in an octahedral environment. Of the 9 atomic orbitals of a transition metal, six equivalent hybrid orbitals are formed in anticipation of bonding to six ligand groups, leaving three unhybridised d orbitals (d_{xz} , d_{xy} and d_{yz}) (Figure 1.2/10). These 6 octahedral hybrids can then interact with up to 6 ligands but only interaction with 3 and 4 ligands respectively will be discussed here.

[†]The characteristic electron counts are; 18e for mononuclear, 34 for dinuclear, and 48 for triangular arrays.

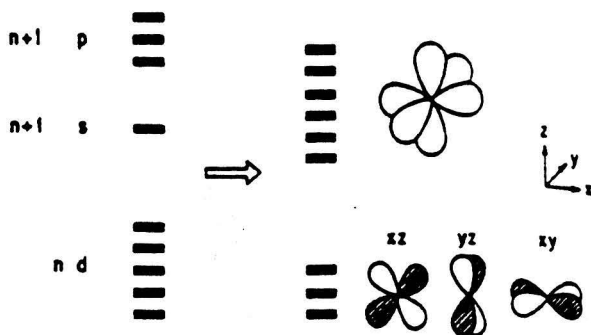


Figure 1.2/10 The formation of 6 equivalent octahedral hybrid orbitals.[48]

Introduction of three two-electron donor ligands results in the formation of 3 strong M-L bonding orbitals and three anti-bonding orbitals, leaving three of the hybrid orbitals untouched (Figure 1.2/11). Thus for an iron triad fragment such as $\text{Os}(\text{CO})_3$ there are three highest occupied molecular orbitals (HOMO's) containing two electrons. An $\text{Os}(\text{CO})_3$ fragment is therefore isolobal with a BH or a CH^+ fragment and this explains the connection between boranes and transition metal clusters.

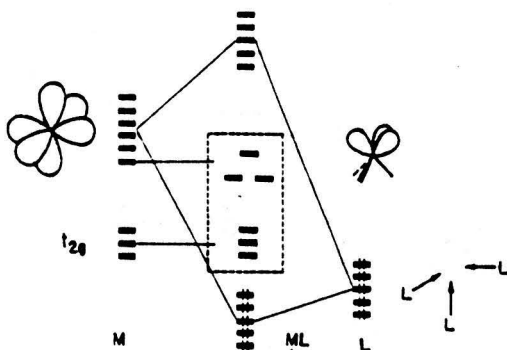


Figure 1.2/11 The MO diagram for interaction with 3 ligands.[48]

For example, the closo-octahedral anion $[\text{Os}_6(\text{CO})_{18}]^{2-}$ [25-26] possesses seven skeletal bonding molecular orbitals and is, therefore, analogous with species such as $[\text{B}_6\text{H}_6]^{2-}$. [32] For this to be true the fragments $\text{M}(\text{CO})_3$ and BH must have the same frontier orbitals, each contributing three orbitals and two electrons to skeletal bonding. Each skeletal metal atom in a transition metal cluster, uses 6 atomic orbitals for metal-ligand (M-L) bonding and housing of non-bonding electrons. This leaves three dsp hybrid orbitals for skeletal bonding. One "radial" orbital points towards the centre of the polyhedron with two "tangential" orbitals lying on the surface of the cluster (Figure 1.2/12).

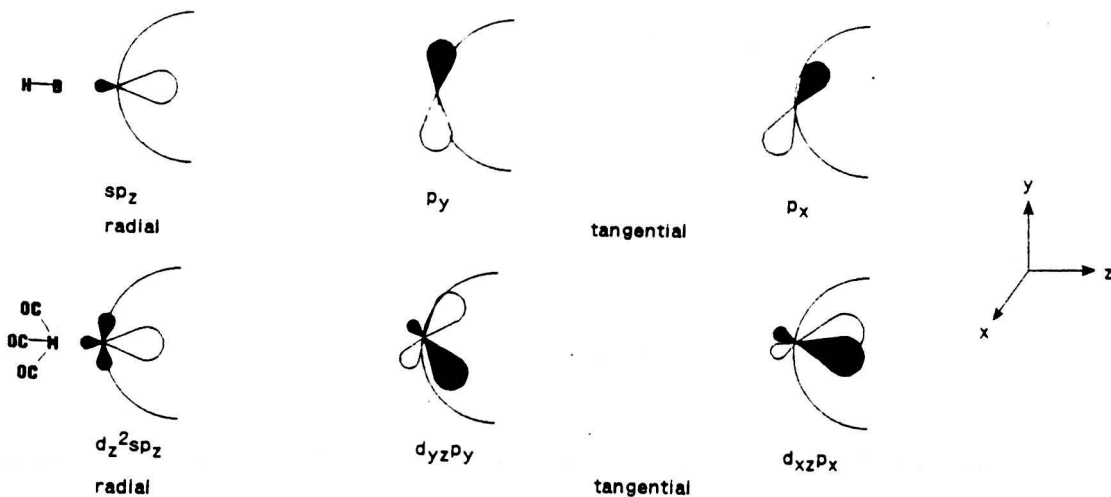


Figure 1.2/12 Comparison of $M(CO)_3$ and BH frontier orbitals.

In addition to $M(CO)_3$ fragments, one of the X-ray structures discussed in this work, $Os_3(CO)_{10}(CPh=CH_2)(AuPEt_3)$ (XR13), contains an $M(CO)_4$ fragment (Chapter 5) and so this fragment is discussed here. From the octahedral metal environment discussed above, if four ligand donors are introduced, four strong M-L bonding and antibonding M.O.'s are formed, leaving two hybrid orbitals (Figure 1.2/13). For $Os_3(CO)_4$ the lower orbital of e symmetry will contain two electrons, and as such is isolobal with CH_2 .

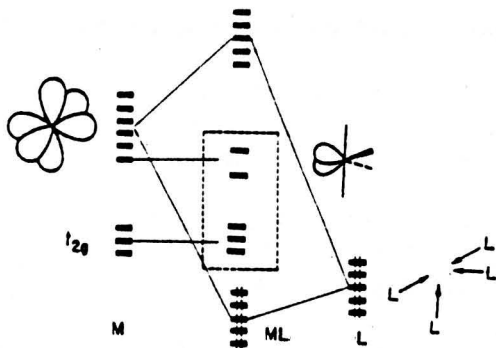


Figure 1.2/13 The MO diagram for the interaction with 4 ligands.

1.2.6 The isolobal connection between H and $Au(PR_3)_3$.

Mingos has considered both homo- and hetero-nuclear gold clusters both from a theoretical and a structural viewpoint.[52-54] On symmetry grounds alone an $Au(PR_3)_3$ fragment would be anticipated to be isolobal with a conical $M(CO)_3$ fragment, since each has an outpointing a_1 $hy(s-z)$ hybrid orbital and a degenerate set of e orbitals (Figure 1.2/14).[54] But in the case of the gold fragment, the latter are so high lying that their contribution to bonding is negligible and the bonding of the $Au(PR_3)_3$ fragment is dictated primarily by the a_1 $hy(s-z)$ orbital and is therefore isolobal with hydrogen which has a single frontier orbital.

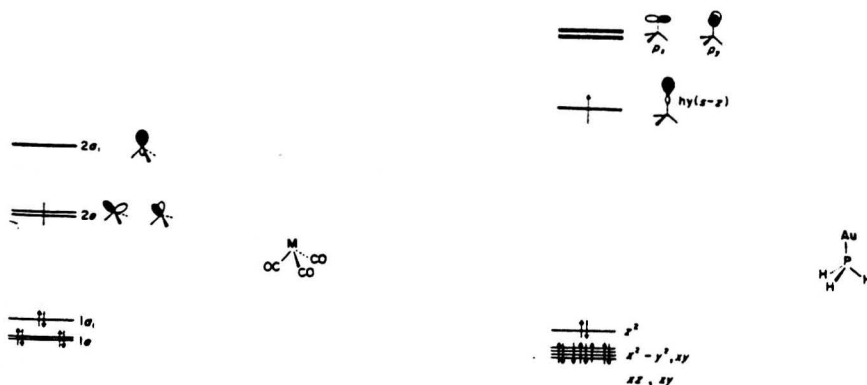


Figure 1.2/14 An MO comparison of $M(CO)_3$ and $Au(PR_3)$ fragments.

In addition to being useful in relating seemingly very different structures, Stone suggested that Hoffmann's isolobal analogy could be used as a predictive tool for the synthesis of novel clusters.[55] By the early eighties this idea was being successfully employed in producing a wider range of hetero-nuclear clusters, for example the trimetallic cluster $FeCo_3(CO)_{12}AuPPh_3$, [56] and a number of ruthenium-gold clusters.[57] As gold-phosphine groups can adopt the same types of bonding as hydride ligands (terminal, μ_2 - and μ_3 -bridging) they have been used as an indirect way of deducing hydrogen atom sites in those cases where hydrides could not be located directly by X-ray diffraction techniques. For example, bridging $Au(PR_3)$ fragments are common and the two μ_2 - $AuPPh_3$ clusters $HOs_3(CO)_{10}(AuPPh_3)$ and $Os_3(CO)_{10}(AuPPh_3)_2$, [58-59] can be directly related to the dihydride $H_2Os_3(CO)_9$. [60] Lauher and Wald illustrated the similarity between the μ_3 -H and the μ_3 - $Au(PR_3)$ units by the structural analysis of the heterometallic cluster $FeCo_3(CO)_{12}AuPPh_3$. [56] This has the $AuPPh_3$ capping a triangular face of cobalt atoms in an analogous fashion to that reported for the μ_3 -hydrido ligand in $HFeCo_3(CO)_9(P(OMe)_3)_3$. [61]

However, the simple analogy between hydrides and gold-phosphine groups often breaks down when more than one gold atom is present. For example, in the trigold clusters $Ru_3(CO)_9(COMe)(AuPPh_3)_3$, [57] and $HRu_4(CO)_{12}(AuPPh_3)_3$, [57,62] the metal core geometry consists of a triangle and tetrahedron of ruthenium atoms respectively, with one triruthenium face of the fundamental polyhedron capped by an $Au(PPh_3)$ group (which is then

further capped on adjacent faces by the remaining two gold fragments), so that these clusters contain gold-gold bonds a feature which does not occur for hydrido ligands. The X-ray structural analyses of 3 heterometallic clusters are presented in this work and will be discussed in Chapters 3 and 5, one of these clusters contains a gold-gold bond.

1.2.7 Alternative electron counting schemes.

Although the polyhedral skeletal electron pair theory (PSEPT) discussed in Section 1.2.2 is the most widely used counting method in cluster chemistry, several alternative strategies (which can be related to PSEPT) have been devised.

One of the most important of these is the topological electron counting theory (TEC), [63-68] which is derived from Euler's theorem[†] for polyhedra and the effective atomic number rule.

For a polyhedron with V vertices, F faces, and E edges, Euler's theorem states: [69]

$$E = V + F - 2 \quad (2)$$

Each metal atom is assumed to obtain the 18-electron valence shell configuration, and all metal-metal bonds are considered as (2c-2e) bonds.

The total number of cluster valence electrons (CVE) is given by:

$$\text{CVE} = 18V - 2E \quad (1)$$

The CVE will fill CVE/2 energetically low lying metal CVMO (cluster valence molecular orbitals) and so:

$$\text{CVMO} = \text{CVE}/2 = 9V - E \quad (3).$$

Substitution of equation (2) into equation (3) gives:

$$\text{CVMO} = 8V - F + 2 + X \quad (4)$$

where X is an adjustment factor accounting for delocalised systems.

[†] This is often erroneously accredited to Euler, but was in fact discovered by Descartes in 1619. [69]

One interpretation of this is that the number of extra electrons in excess of the 18e rule are characterised by X, alternatively X gives the number of false M-M bonds required if each polyhedral edge is considered as a (2c-2e) bond. Teo has defined the parameter X in terms of a set of rules,[63] however these rules are more difficult to remember than those for PSEPT.

Mingos suggested that in fact PSEPT and TEC shared a common base and has demonstrated that they can be algebraically interconverted.[65] Both Teo,[66] and Mingos,[67] have discussed the similarities and differences of the two approaches. To conclude one of the possible advantages of TEC is that it can account for double bond character which is not explicit in any of the alternative electron counting techniques.

King showed that graph theory can be applied, with some success, to the study of polyhedral boranes and transition metal clusters.[70] The chemical bonding topology in metal clusters can be represented by a graph in which the vertices correspond to the atoms or orbitals participating in bonding and the edges correspond to bonding relationships. An adjacency matrix A (where A_{ij} is an element in the i^{th} row and j^{th} column of the matrix) of such a graph can be defined as follows:

$$A_{ij} = \begin{cases} 0 & \text{if } i=j \\ 1 & \text{if } i \text{ and } j \text{ are connected by an edge} \\ 0 & \text{if } i \text{ and } j \text{ are not connected by an edge} \end{cases}$$

The method is based on the Huckel approximation and in a comparison of polygonal C_nH_n systems (such as benzene) and polyhedral boranes King stated that C_nH_n systems can be considered as two-dimensional aromatic systems, whereas the polyhedral boranes may be considered as three-dimensional aromatic systems.[70]

In the surface harmonic tensor theory, Stone provided a detailed theoretical analysis which unified previous individual calculations.[71-73] As with other theoretical and empirical methods, Stone concluded that an n

vertex system requires $(n+1)$ skeletal electron pairs. Maximisation of bond energies is achieved in polyhedra with the maximum number of triangular faces and this accounts for the general observation of mainly triangulated faces in clusters compounds.

To conclude, theoretical aspects of cluster chemistry have been, and continue to be, widely studied.[11-12] The empirical PSEPT has proved a considerable success and can be used with ease to explain observed structural geometries. However one drawback is that higher nuclearity clusters often have a number of alternative geometries with the same CVE and PSEPT can not be used to predict which of these metal frameworks will occur.

1.3 A rationale for geometric flexibility.

Clusters have been defined as molecules which contain two or more metal atoms joined together. Part of their interest is that even with low nuclearity clusters, geometrical flexibility introduces an extra dimension into the potential chemistry of these species. In order to rationalise many of the results in this project a new method of indexing geometric flexibility has been developed and will be discussed in the following pages.

For simple trinuclear compounds, very few alternative frameworks are available. Figure 1.3/1 illustrates the successive cleavage of M-M bonds, leading to cluster degradation.

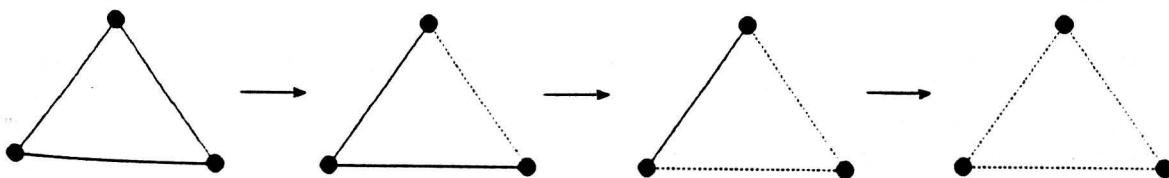


Figure 1.3/1 Trinuclear degradation.

Addition of one more metal atom to the cluster framework introduces a greater degree of flexibility and two of the most commonly encountered shapes for tetranuclear species are the butterfly and the tetrahedron. Figure 1.3/2 illustrates successive bond breaking for a tetranuclear core geometry and shows that two alternative metal cores can arise from the butterfly core.

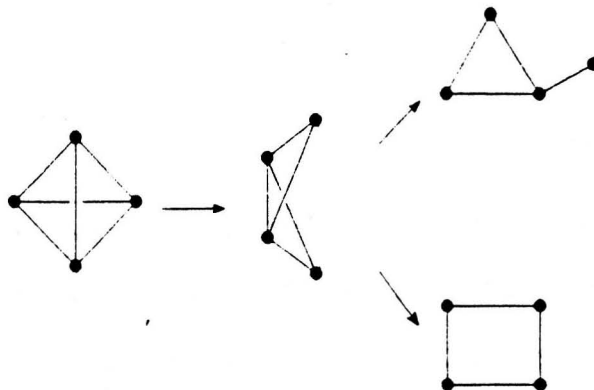


Figure 1.3/2 Metal cores available for an M_4 cluster.

Progressing to pentanuclear clusters, a surprisingly complex range of alternative geometries may be envisaged. From the most triangulated pentanuclear geometry (the trigonal bipyramid), successive cleavage of metal bonds leads to the creation (in principal) of a wide variety of metallic networks, which provide a diverse range of potential frameworks for organo-fragments to interact with. Each metal-metal bond broken is accompanied by the addition of two electrons to the total valence count. The corollary of this is that as electron count increases, due to addition of pairs of electrons, so the geometry begins to open out, with the resulting framework depending on the type and number of metal-metal bonds broken. Ultimately, this procedure would lead to five non-bonded metal atoms, linked only by ligand coordination.

In virtually all known chemical examples, the trigonal bipyramidal polyhedron has the 72 electrons predicted by PSEPT (Section 1.2). The metal bonds in a trigonal bipyramid (I) fall into two distinct categories, equatorial-axial bonds and equatorial-equatorial bonds (Figure 1.3/3).

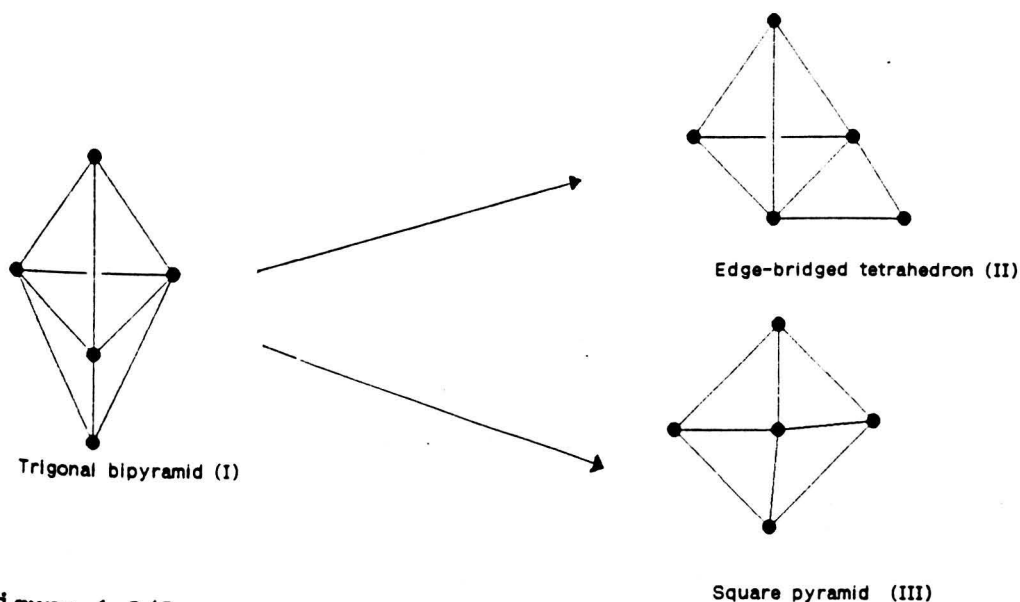
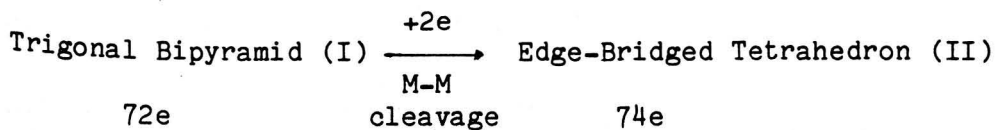
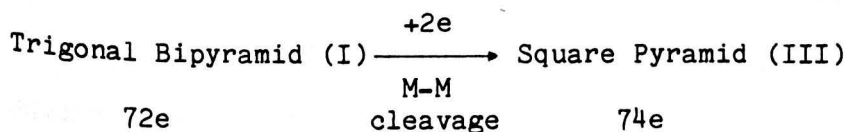


Figure 1.3/3.

Cleavage of an equatorial-axial bond, with addition of 2e, leads to a 74e edge-bridged tetrahedron (II) (Figure 1.3/3). This cluster has four distinct types of metallic bond, two more than the precursor (I) (Figure 1.3/3).



Alternatively, breaking one of the three equatorial-equatorial bonds in (I) gives a square pyramidal species (III) (Figure 1.3/3). Again one metal-metal bond is broken, so two electrons are added to the cluster, also making this a 74 electron species.



This square pyramid (III) is more symmetrical than (II), and, as such, has only two different types of M-M bond: apical-basal and basal-basal.

The process of M-M cleavage outlined for (I) can be repeated with structures (II) and (III). From the edge-bridged tetrahedron (II), cleavage of any of the three different categories of bond in the tetrahedron leads to a bridged-butterfly (Figure 1.3/4). If one M-M bond is broken, a statistical (4:1:1) ratio of hinge-wingtip (IV), wingtip (V), and hinge-bridged (VI) butterflies would be expected. Alternatively,

fission of either of the triangular edges leads to a spiked tetrahedron (VII).

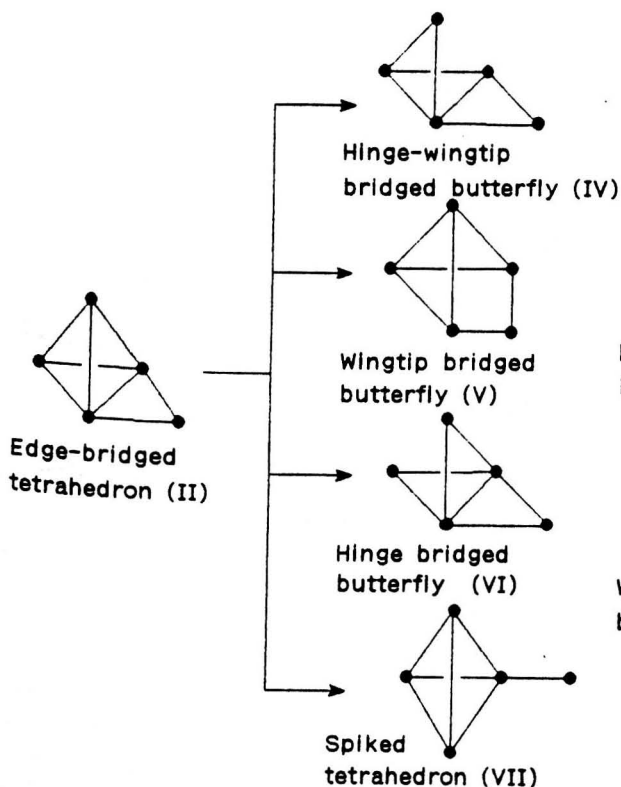


Figure 1.3/4.

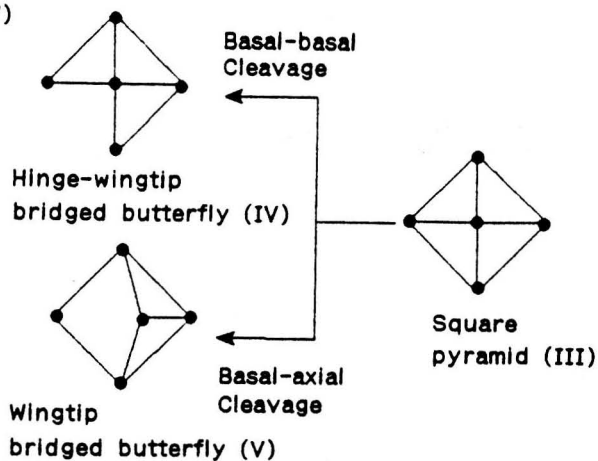


Figure 1.3/5.

The hinge-wingtip (IV) and wingtip bridged (V) butterflies can alternatively be obtained from the square pyramid (III) (Figure 1.3/5), with (IV) and (V) being obtained by cleavage of a basal-basal and a basal-axial bond respectively. As no alternative types of metallic bond are present in (III), structures (VI) and (VII) can not be obtained from a square pyramidal precursor.

The hinge-wingtip bridged butterfly (IV) [obtainable from either (II) or (III)] has, like (II), four different types of metallic bond (Figure 1.3/6). It can therefore generate four alternative new geometries by one bond cleavage, and these 78 electron species are shown in Figure 1.3/6. The bow tie geometry (X) can only be obtained if the unique hinge-tip bond of (IV) is cleaved, whereas the hinge or tip spiked butterflies, (VIII) and (IX), and the edge-bridged square (XI) can all be produced if two separate bonds are broken.

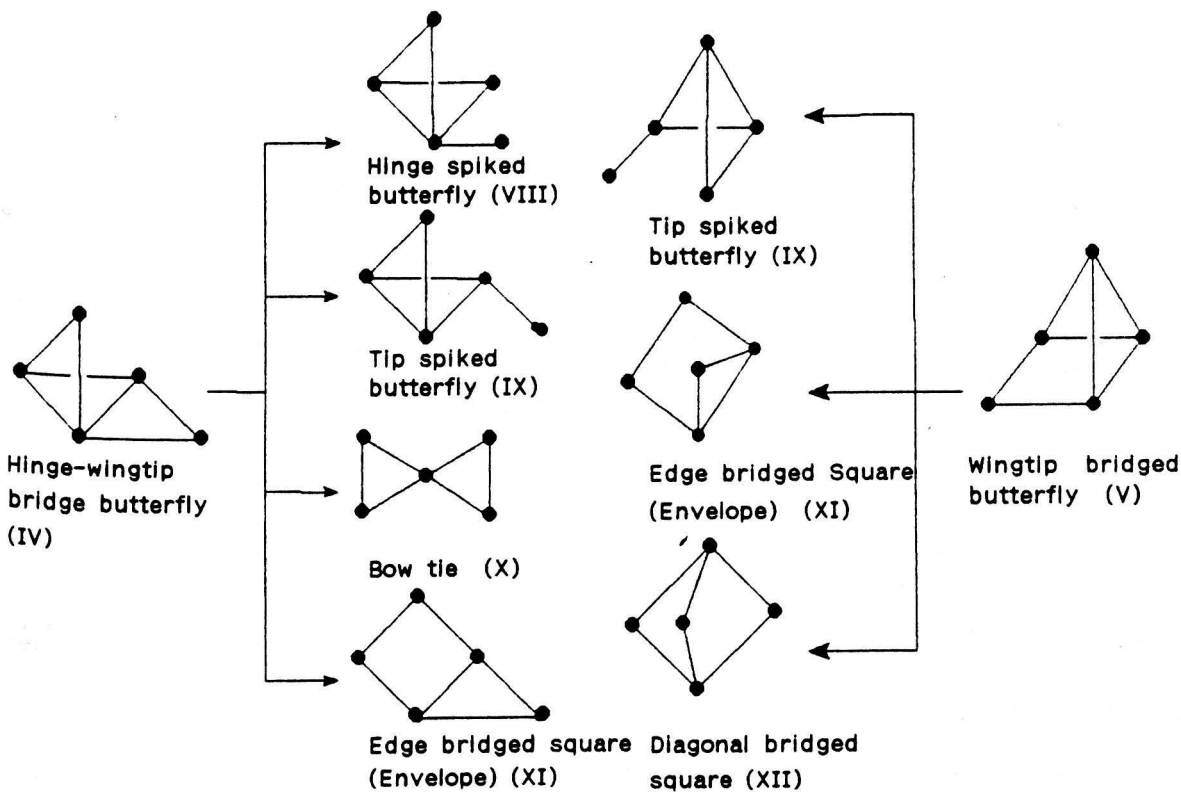


Figure 1.3/6.

Figure 1.3/7.

The wingtip-bridged butterfly (V), has three distinct type of M-M bonds, and can therefore create three 78 electron geometries (Figure 1.3/7). These are the (previously noted) spiked-butterfly (IX), and the edge-bridged square (XI) but the diagonal bridged square (XII) is new. They arise in the ratio of 2:4:1 repectively.

The hinge-bridged butterfly (VI) generates the hinge spiked butterfly (VIII) and the diagonal-bridged square (XII) in the ratio 6:1 (Figure 1.3/8) when one M-M bond is broken. Both the tip and hinge spiked butterflies (VIII and IX) can be produced from the spiked tetrahedron (VII), but alternatively a cluster of lower nuclearity (XIII) may result (Figure 1.3/9): and thus cluster degradation is beginning to occur. Such non-bonding geometries will always begin to arise once M-M bonds with a connectivity of only two are present in the precursor molecule.

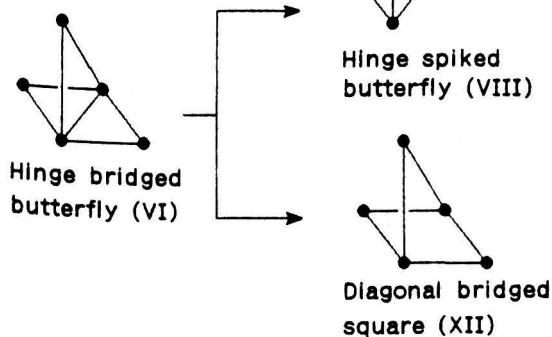


Figure 1.3/8.

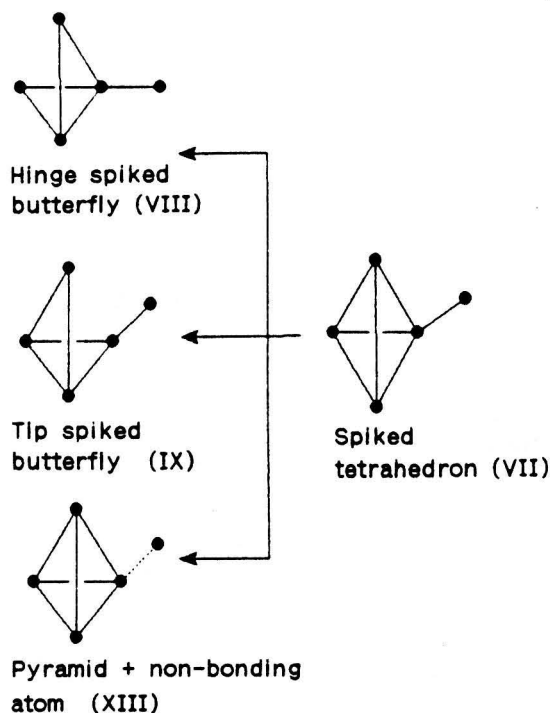


Figure 1.3/9.

Figures 1.3/10-15 show how progressive cleavage leads to further overlapping of structural types, and to a fascinating array of structures such as the n,m spiked triangle[†], the coat hanger, and the crown.

Table 1.3/1 lists reported structures for the iron triad which have the geometries discussed above. There are no known clusters with interstitial atoms which have a trigonal bipyramidal (I), an edge-bridged tetrahedral (II), or a spiked tetrahedral (VII) metal core. All three of these geometries have at least one tetrahedral fragment and the lack of interstitial atoms can be attributed to the fact that the tetrahedral cavity is not large enough to accommodate even small atoms such as carbon and nitrogen. This is because the metal-ligand(interstitial) contacts would be too close and this can be demonstrated by consideration of a known trigonal bipyramid cluster, $\text{Os}_5(\text{CO})_{16}$. [74] From the mean of the Os-Os bonds (ca. 2.8 Å), an approximate central position inside one of the tetrahedrons may be calculated, giving a mean hypothetical osmium-interstitial atom distance of 1.7 Å. As a normal osmium-carbide distance is ca. 2.0 Å, a value of 1.7 Å would be extremely unfavourable. However, hydrogen atoms in tetrahedral sites are known, particularly

[†](where n and m refer to spiked atom positions on the triangle)

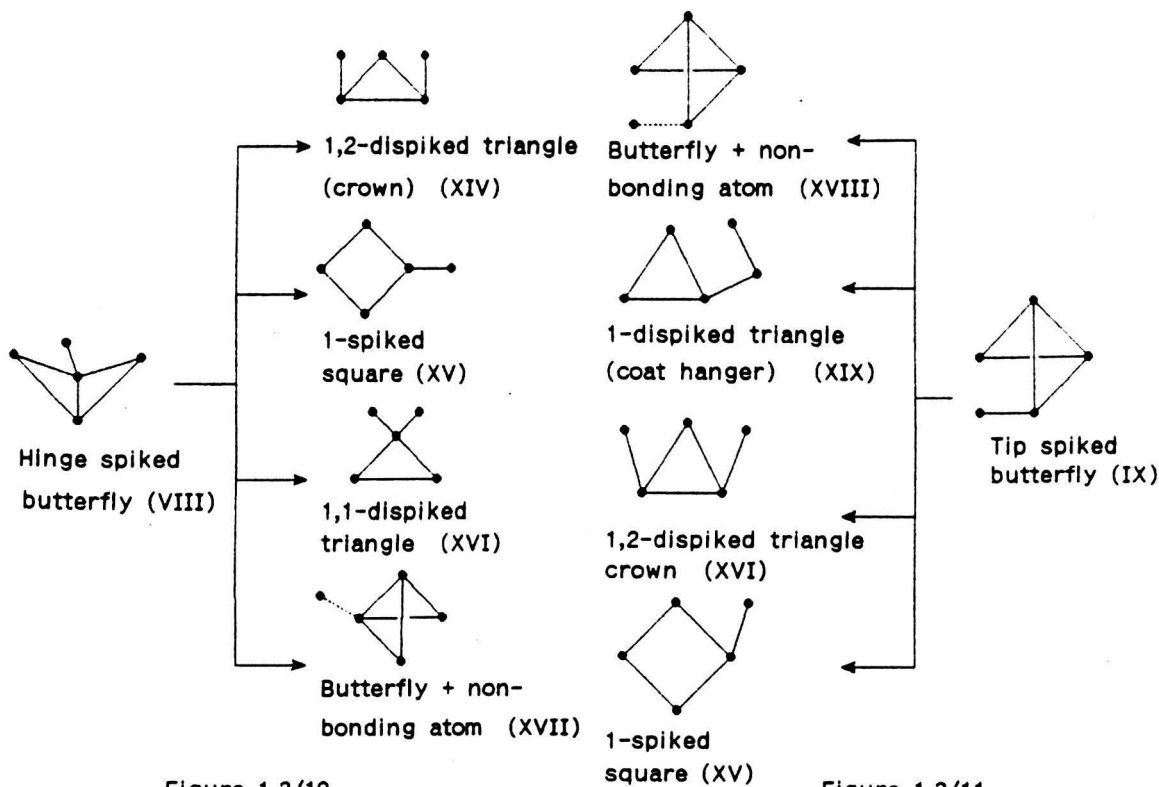


Figure 1.3/10

Figure 1.3/11

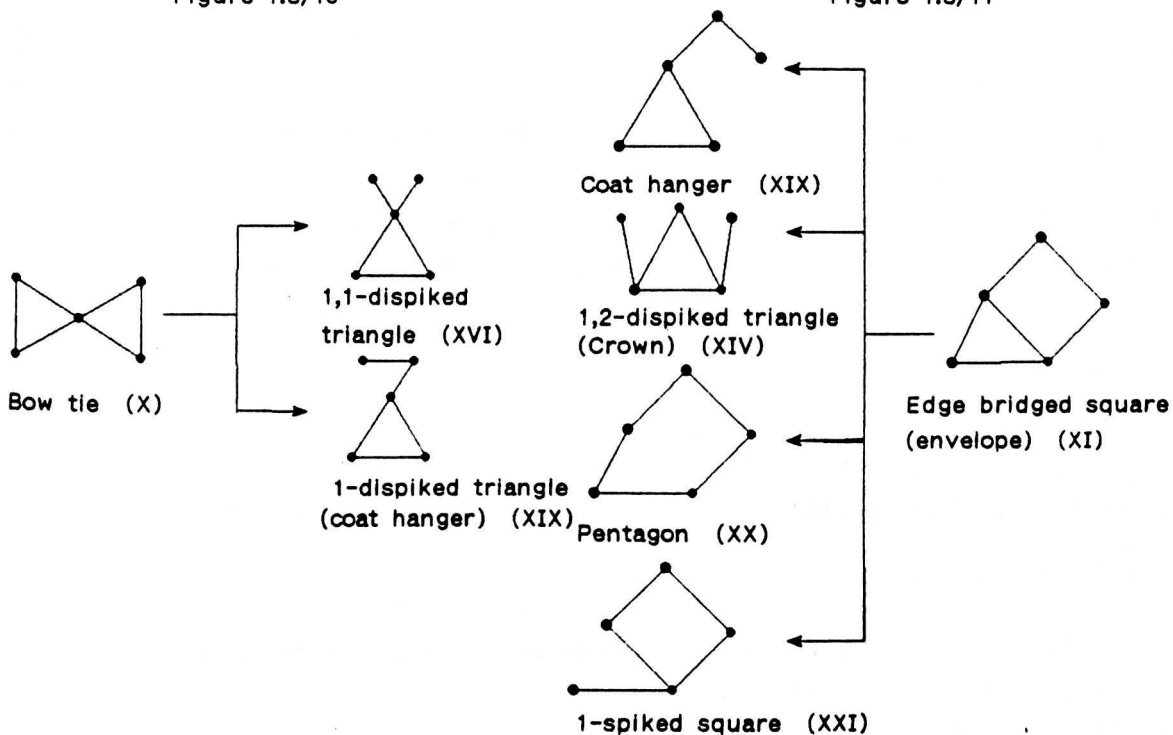


Figure 1.3/12

Figure 1.3/13

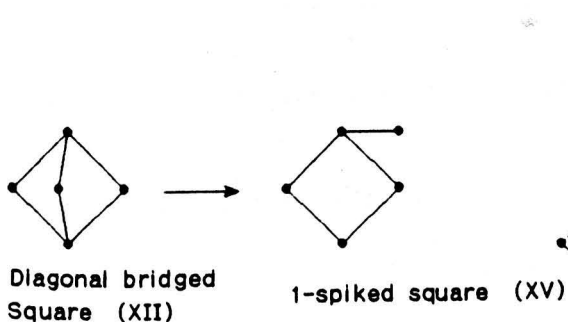


Figure 1.3/14

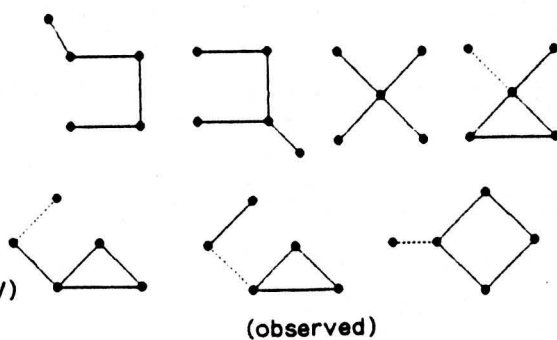


Figure 1.3/15

Table 1.3/1

Metal-core geometry	Structure	Refs.
Trigonal bipyramid (I)	$\text{Os}_5(\text{CO})_{16}$	74, 75
	$\text{H}_2\text{Os}_5(\text{CO})_{15}$	20
	$[\text{HOs}_5(\text{CO})_{15}]^-$	76, 20, 77
	$[\text{Os}_5(\text{CO})_{15}]^{2-}$	20
	$\text{H}_2\text{Os}_5(\text{CO})_{14}(\text{PEt}_3)$	78
	$\text{H}_2\text{Os}_5(\text{CO})_{13}(\text{PEt}_3)\{\text{P}(\text{OMe})_3\}$	78
	$[\text{IOs}_5(\text{CO})_{15}]^-$	79
	$\text{H}_2\text{Os}_5(\text{CO})_{14}(\text{C}_5\text{H}_5\text{N})$	80
Edge-bridged tetrahedron (II)	$\text{H}_2\text{Os}_5(\text{CO})_{16}$	31, 20
	$[\text{H}_2\text{Os}_5(\text{CO})_{15}\text{I}]^-$	20
	$\text{H}_2\text{Os}_5(\text{CO})_{15}\{\text{P}(\text{OMe})_3\}$	20
	$\text{H}_3\text{Os}_5(\text{CO})_{14}(\text{C}_5\text{H}_4\text{N})$	80
	$\text{H}_2\text{Os}_5(\text{CO})_{15}(\text{C}_5\text{H}_5\text{N})^b$	80
	$\text{HOs}_5(\text{CO})_{13}(\text{PhNC}_6\text{H}_4\text{N})(\text{PEt}_3)$	82
	$\text{Os}_5(\text{CO})_{15}\{\text{CC}(\text{H})\text{Ph}\}$	83
Square pyramid (III)	$\text{M}_5\text{C}(\text{CO})_{15}$	21, 22, 84, 85
	$\text{Ru}_5\text{C}(\text{CO})_{14}(\text{PPh}_3)$	84, 85
	$\text{HRu}_5\text{C}(\text{CO})_{13}(\text{C}_5\text{H}_4\text{N})$	This work
	$\text{Ru}_5\text{C}(\text{CO})_{13}(\text{dppb})$	86
	$\text{Ru}_5\text{C}(\text{CO})_{13}(\text{PPh}_3)_2$	85
	$\text{H}_2\text{Ru}_5\text{C}(\text{CO})_{12}\{\text{Ph}_2\text{P}(\text{CH}_2)_2\text{PPh}_2\}$	85
	$[\text{Os}_5\text{C}(\text{CO})_{14}]^{2-}$	23
	$\text{Os}_5\text{C}(\text{CO})_{14}\{\text{Au}(\text{PPh}_3)\}_2$	23
	$\text{Ru}_5\text{C}(\text{CO})_{13}(\text{NO})(\text{AuPEt}_3)$	87
	$\text{HRu}_5\text{C}(\text{CO})_{13}(\text{PPh}_2)$	88
	$\text{H}_3\text{Ru}_5\text{C}(\text{CO})_{11}(\text{PPh}_2)(\text{PMePh}_2)$	89
	$\text{HRu}_5\text{C}(\text{CO})_{12}(\text{PPh}_3)(\text{SEt})$	90
	$\text{Ru}_5(\text{CO})_{13}(-\text{CCPh})(\text{PPh}_2)$	91, 92
	$\text{H}_2\text{Ru}_5(\text{CO})_{13}(-\text{PCCH}_2\text{PPh}_2)(\text{PPh}_2)$	93
	$[\text{Ru}_5\text{N}(\text{CO})_{14}]^-$	94, 95
	$\text{Ru}_5(\text{CO})_{15}(\text{PR})^a$	96

Table 1.3/1 continued

Metal-core geometry	Structure	Refs.
Square pyramid (III)	$\text{HOs}_5\text{C}(\text{CO})_{13}\{\text{OP}(\text{OMe})\text{OP}(\text{OMe})_2\}$	97
	$\text{Os}_5(\text{CO})_{15}(\text{CH}_3\text{OP})$	98
	$\text{Ru}_5(\text{CO})_{12}(\text{PPh})(\text{CCH}_2\text{-i-Pr})(\text{PPh}_2)$	99
Hinge-wingtip bridged butterfly (IV)	$\text{Ru}_5(\text{CO})_{14}(\text{CNBu}^t)_2$	100
	$\text{Os}_5(\text{CO})_{13}(\text{PhCCPh})_2$	101
	$\text{Ru}_5(\text{CO})_{13}(\text{C}_2\text{PPh}_2)(\text{PPh}_2)$	89
	$\text{HRu}_5(\text{CO})_{13}\{\text{CC}(\text{H})\text{PPh}_2\}(\text{PPh}_2)$	89
	$\text{Ru}_5(\text{CO})_{12}(-\text{CCPh})\{\text{PhCCCCPh}\}(\text{PPh}_2)$	102
	$\text{Ru}_5(\text{CO})_{13}(-\text{C}_2\text{PPh}_2\text{P})(\text{PPh}_2)$	103
Wingtip Bridged butterfly (V)	$[\text{Os}_5\text{C}(\text{CO})_{15}\text{I}]^-$	22
	$\text{HM}_5\text{C}(\text{CO})_{14}(\text{C}_5\text{H}_4\text{N})^c$	104, This work
	$\text{HRu}_5\text{C}(\text{CO})_{13}(\text{C}_5\text{H}_4\text{N})(\text{C}_5\text{H}_5\text{N})$	This work
	$\text{Ru}_5\text{C}(\text{CO})_{15}(\text{MeCN})$	35
	$\text{Os}_5\text{C}(\text{CO})_{16}$	23
	$\text{HOs}_5\text{C}(\text{CO})_{14}(\text{CO}_2\text{Et})$	105, 106
	$\text{Os}_5\text{C}(\text{CO})_{15}(\text{dppe})$	107
	$\text{H}_2\text{Os}_5(\text{CO})_{15}(\text{CCPh})$	101
	$\text{HOs}_5\text{C}(\text{CO})_{13}\{\text{OP}(\text{OMe})_2\}\{\text{P}(\text{OMe})_3\}$	108
	$\text{Ru}_5\text{C}(\text{CO})_{15}\{\text{Au}(\text{PPh}_3)\}\text{Cl}$	109
	$\text{Ru}_5\text{C}(\text{CO})_{14}\{\text{Au}(\text{PPh}_3)\}\text{Br}$	109
	$\text{Ru}_5\text{C}(\text{CO})_{14}\{\text{Au}(\text{PPh}_3)\}(\text{MeCO})$	110
	$\text{Ru}_5\text{C}(\text{CO})_{13}\{\text{Au}(\text{PPh}_3)\}(\text{C}_5\text{H}_5)$	110
	$\text{HRu}_5\text{C}(\text{CO})_{14}(\text{SEt})$	90
	$\text{HRu}_5\text{C}(\text{CO})_{13}(\text{SEt})(\text{PPh}_3)$	90
	$\text{Ru}_5\text{C}(\text{CO})_{13}\text{I}(\text{PPh}_3)\{\text{Au}(\text{PPh}_3)\}$	90
	$\text{HRu}_5\text{C}(\text{CO})_{10}(\text{PPh}_2)(\text{PPh})_3$	99
	$\text{HOs}_5\text{C}(\text{CO})_{14}\{\text{OP}(\text{OMe})_2\}$	111
	Spiked tetrahedron (VIII)	$\text{HOs}_5(\text{CO})_{13}(\text{PhNC}_6\text{H}_4\text{N})$

Table 1.3/1 continued

Metal-core geometry	Structure	Refs.
Edge-bridged square (envelope) (XI)	$\text{Ru}_5(\text{CO})_{13}(\text{C}_6\text{H}_4)(\text{PPh})$	113
	$\text{Ru}_5(\text{CO})_{14}(\text{S})(\text{HC}_2\text{Ph})$	114
	$\text{Ru}_5(\text{CO})_{12}(\text{CCH}_2\text{R})(\text{PPh}_2)(\text{PPh})$	99
	$\text{Ru}_5(\text{CO})_{12}(\text{CCR})(\text{N}_2\text{CPh}_2)(\text{PPh}_2)^{\text{d}}$	115
	$\text{Os}_5(\text{CO})_{15}\{\text{CC}(\text{H})\text{Ph}\}$	83
	$\text{HOs}_5(\text{CO})_{13}(\text{PhNC}_6\text{H}_4\text{N})$	112
	$\text{HOs}_5(\text{CO})_{15}\{\text{PhNC}_6\text{H}_4\text{N}\}(\text{PEt}_3)$	82
Bow tie (X)	$\text{Os}_5(\text{CO})_{19}$	116, 117
	$\text{Os}_5(\text{CO})_{17}(\text{HCCH})$	118
	$\text{Os}_5(\text{CO})_{16}\{\text{P}(\text{OMe})_3\}_3$	117
	$\text{HRu}_5(\text{CO})_{13}(\text{C}_2\text{Ph})(\text{PPh}_2)_2$	119
Diagonal-bridged square (XII)	$\text{Os}_5\text{C}(\text{CO})_{14}(\text{CO}_2\text{Me})\text{I}$	105, 106
	$\text{Os}_5\text{C}(\text{CO})_{15}\text{I}_2$	105
Coat hanger (XIX)	$\text{HRu}_5\text{Cu}(\text{CO})_{13}\text{PPh}_3$	120
Spiked square (XV)	$\text{Ru}_5(\text{CO})_{13}(\text{CCR})\{\text{NC}(\text{O})\text{NCPH}_2\}(\text{PPh}_2)$	115
	$\{\text{Ru}_3(\text{CO})_3(\text{Cp})_3\}\{\text{Ru}_2(\text{CO})_3(\text{Cp})_2\}$	121
	$\text{Ru}_5(\text{CO})_{12}(\text{NPh})\{\text{N}(\text{Ph})\text{C}(\text{O})\text{C}(\text{Cp})\text{CPh}\}$	122

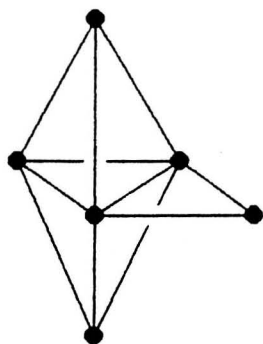
Notes:-

a; R = C_6H_5 , CH_3 , CH_2CH_3 and $\text{CH}_2\text{C}_6\text{H}_5$

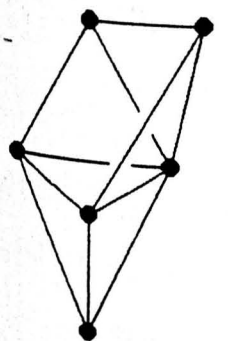
b; Proposed structure

c; M = Ru or Os

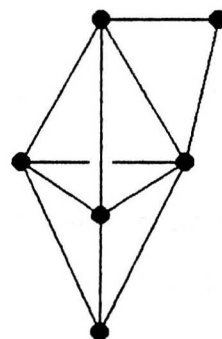
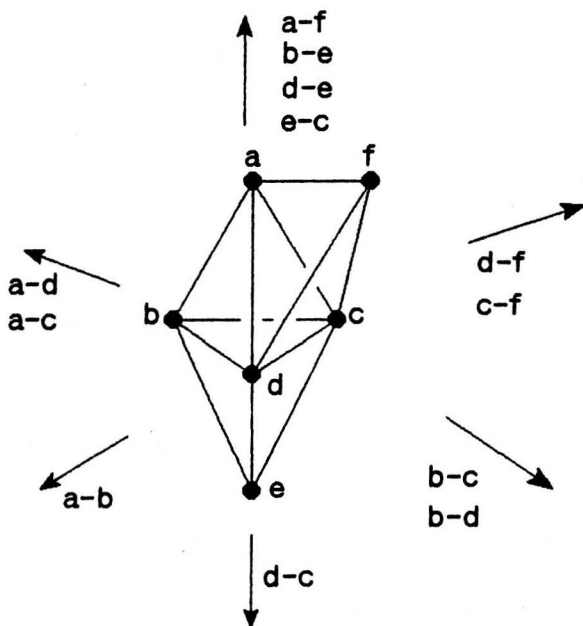
d; R = Ph, Pr^i



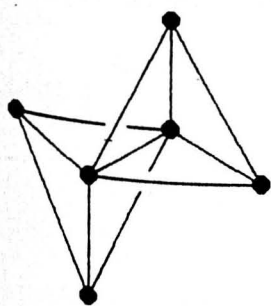
Equatorial edge-bridged trigonal bipyramid



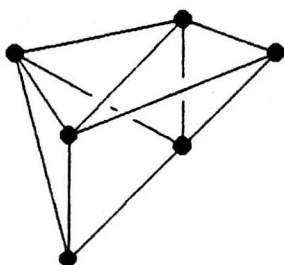
μ_3 -Bridged edge-bridged tetrahedron



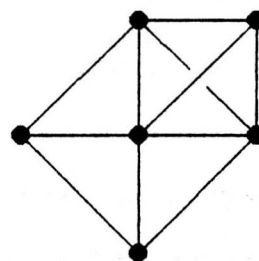
Axial edge-bridged trigonal bipyramid



Edge-fused tetrahedra

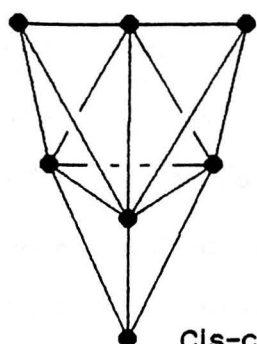


μ_3 -bridged square pyramid

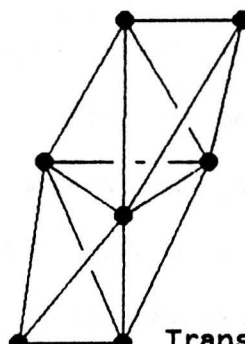


Capped square pyramid

Figure 1.3/16 Geometries available from a capped trigonal pyramid by M-M cleavage.



Cis-caps



Trans-caps

Figure 1.3/17 The 2 alternative M cores for a totally triangulated heptanuclear cluster

amongst the higher nuclearity species (some examples are discussed in Chapter 4).

In contrast to tetrahedral geometries, structures based on the square pyramidal framework (III) predominately have semi-interstitial atoms, such as the μ_5 -coordinate carbido-atom in the pentanuclear cluster $M_5C(CO)_{15}$ ($M = Fe, Ru$ or Os), [21,22,84,85] or the μ_4 -phosphorus atom in $Ru_5(CO)_{13}(\mu_4-n^2-CCPh)(\mu_4-PPh_2)$. [96] No examples of the hinge-bridged butterfly (VI) have been reported, whilst wingtip-bridged butterflies (VI) are relatively common (Table 1.3/1) and these pentanuclear clusters will form a major part of the discussion in Chapter 2. Finally, of the 76e-species a wide variety of reported clusters have a hinge-wingtip bridged butterfly geometry, and Table 1.3/1 shows that these often contain multi-coordinating organo-fragments.

Table 1.3/1 shows that of the six potential 78e-species (geometries VIII to XIII), only clusters based on the bow tie (X) and the two bridged square frameworks (XI) and XII) have been reported in the literature. Frequently these complexes contain highly coordinated organo-fragments which have both the electronic and geometric flexibility to hold such open frameworks together. It is interesting that neither of the spiked butterflies (VIII and IX), nor structure (XIII), have so far been reported. These may require unusually versatile ligands to accommodate the cluster shape.

The situation is progressively more complicated for higher nuclearity cores. Figure 1.3/16 illustrates the initial process of M-M cleavage for the M_6 triangulated cluster. The most common metal framework for M_6 clusters, the octahedron, is not included in this scheme, as cleavage of just one of the octahedral bonds leads immediately to a very open structure. Often octahedral reactions are characterised by metal core rearrangements. Similarly, for M_7 cores a totally triangulated framework

is a bicapped trigonal bipyramid. This has not so far been observed but could exist in two alternative forms (Figure 1.3/17). The most common heptanuclear cores observed are discussed in Chapter 5.

This section has shown the wide range of metal core geometries that are available even with relatively low nuclearity clusters. These metal frameworks provide a diverse and flexible range of surfaces for organo-fragments to interact with.

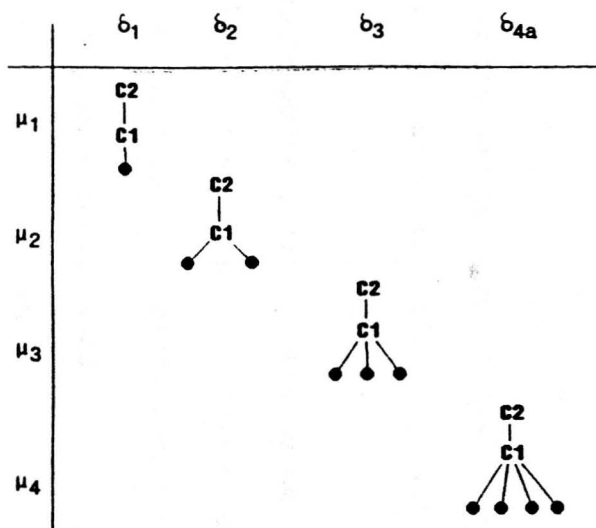
1.4 M-L bonding modes for organo-ligands on cluster surfaces.

The major area of interest in this thesis is the interaction of metallic clusters with small organic fragments. Whereas there are only a limited number of M-L bonding modes available for organo-mononuclear complexes, greater flexibility is available with multinuclear clusters. In fact dicarbon-fragments bonded to metal clusters show the most diverse range of coordination modes known for any ligands to date (Section 1.4.2).

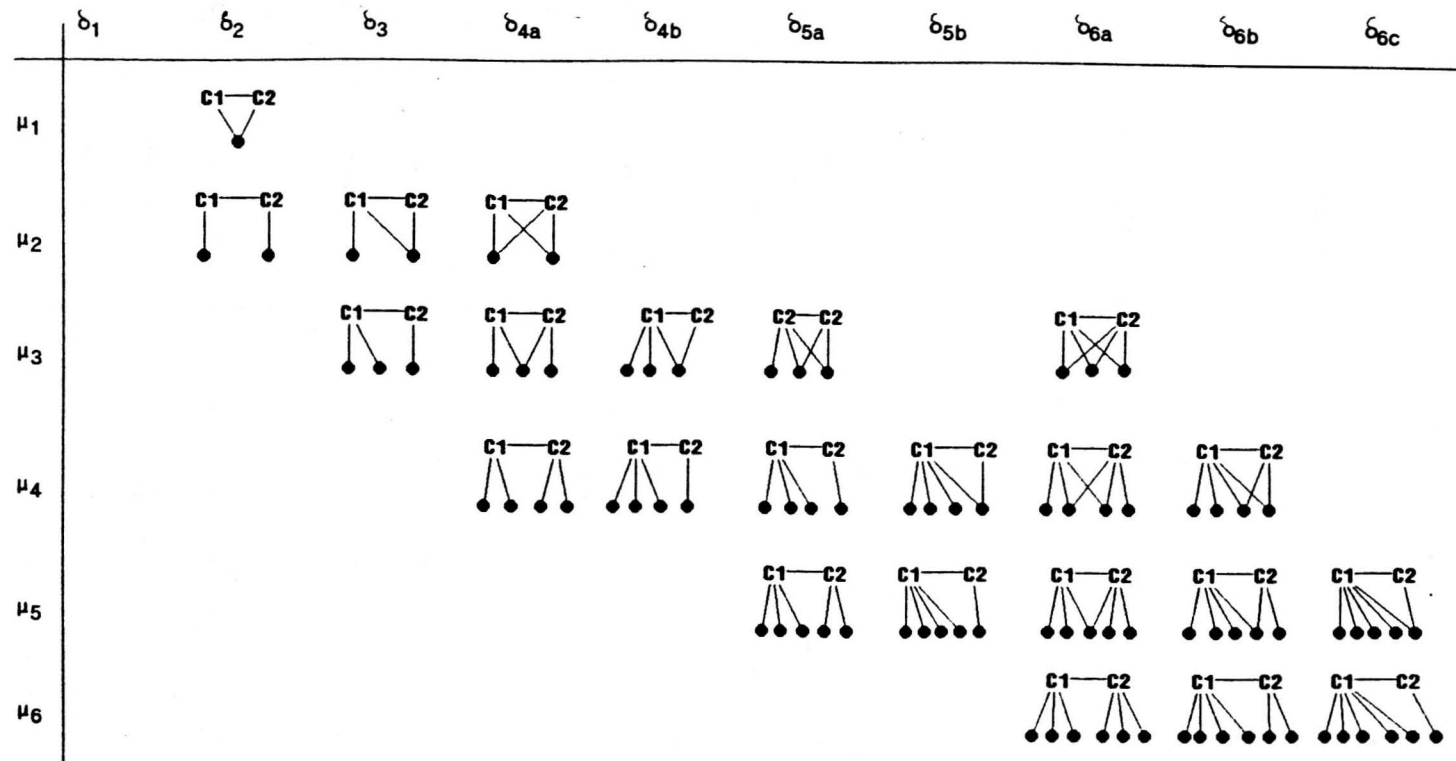
This section classifies the range of theoretically possible structural features adopted by these fragments according to ligand type and the number of metal atoms involved in coordination. Only dicarbon fragments are reviewed, but most larger organo-fragments, aromatic derivatives, and many hetero-atom species can be considered as multiple forms of these dicarbon fragments.

Interest in organo-cluster chemistry has expanded rapidly in the last decade.[123-124] Some of this can be attributed to purely academic excitement in a new class of compounds and in the bonding modes they adopt. In addition, there is an important correlation between these clusters and the modes of interaction of organic fragments with metal surfaces, so they may be used as models for the chemisorption of small molecules on metal surfaces. Clusters are more accessible to chemical scrutiny than bulk

Matrix 1.4/1 η^1 -Coordination bonding modes.



Matrix 1.4/2 η^2 -Coordination bonding modes



metals and factors such as carbon triple bond activation and reduction can be monitored more effectively on cluster surfaces. Another potential use of organo-clusters is as templates for organic synthesis and the use of metal clusters, which can 'mould' organic fragments, may ultimately yield alternative pathways for the synthesis of novel organic materials.

1.4.1 Naming of fragments.

In theory nine forms of dicarbon ligand can be envisaged for bonding to a cluster surface (Table 1.4/1).

Table 1.4/1 Prospective organic ligands.

Ligand	Name	No. of electrons donated	No. of R groups
R_2C-CR_3	Alkyl(yl)	1	5
$RC-CR_3$	Alkylidene	2	4
$C-CR_3$	Alkylidyne	3	3
$R_2C=CR_2$	Alkene	2	4
$RC=CR_2$	Alkenyl	1 or 3	3
$C=CR_2$	Alkenylidene	2 or 4	2
$RC\equiv CR$	Alkyne	2 or 4	2
$C\equiv CR$	Alkynyl	1, 3, or 5	1
$C\equiv C$	Dicarbide	2, 4, or 6	0

Saturated alkanes (C_2R_6) are not included as they have no electrons available for bonding to the metal core. The nomenclature adopted in Table 1.4/1 is dependant on the number and position of the substituent (R) groups, the degree of bond multiplicity, and the number of electrons available for cluster bonding. Matrix 1.4/1 shows the forms of η^1 -bonding possible for organic fragments, the corresponding forms for η^2 -coordination are illustrated in Matrix 1.4/2. These matrices are purely schematic and do not specify M-M linkages (a variety of frameworks are possible for clusters containing 4 or more metal atoms).

The degree and type of bonding illustrated in these matrices is specified by three prefixes.

- a) Ligands can bond to one or more metal atoms, and this is denoted by the prefix μ_n (where n is the number of metal atoms bridged).
- b) Either one (η^1 -) or both (η^2 -) carbon atoms may be coordinated to the cluster core.
- c) In this thesis the number of M-C contacts is denoted by δ_m (where m = No of M-C contacts).

It should be stressed that μ and δ are not totally independent. For example, a coordination mode such as $\mu_2\eta^1\delta_1$ is impossible since δ_1 implies only 1 M-C contact and μ_2 implies at least 2 M-C contacts. These 'impossible' forms are blocked out of Matrices 1.4/1 and 1.4/2 and, indeed, for η^1 -coordination only the diagonal elements of the matrix occur.

A full analysis of all the possible η^2 -bonding modes would be complicated and in this discussion the matrix for η^2 -coordination is only considered in a truncated form (namely that which is chemically sensible), δ -values of greater than six have not been considered. This gives a 6x6 matrix (36 structures) but, as a consequence of the dependency of μ and δ , a number of forms are precluded.

For a given number of metal atoms (M) the total number of forms is $2M$, since each metal can never be attached to more than two carbon atoms. It is evident from Matrix 2 that all elements to the left of the diagonal are zero, because a value of μ_n implies a δ -value of at least n . For μ^1 alone the 0-value is dominant and the structure on the diagonal does not occur. Because all elements to the left of the diagonal are zero ($M-1$) is subtracted from $2M$ for each row. Thus, an overall formula $[2M-(M-1)]$ or $M+1$ accounts for the total number of connection types. (For the unique case of $M=1$, only 1 structure occurs.)

The restriction of the total δ -coordination to 6 is accounted for by subtracting $(2M-6)$ (the difference between the total number of coordinations and the restriction) from metal systems containing four or more metal atoms. Thus for $M > 3$ the number of possible forms is given by $2M - (M-1) - (2M-6)$ or $7-M$.

In addition to these structures, isomers occur for o-coordination forms above 3. Figure 1.4/1 illustrates the isomeric forms for δ_{4-8} and shows there are two isomers for δ_4 and δ_5 , three for δ_6 and δ_7 , four for δ_8 , etc.

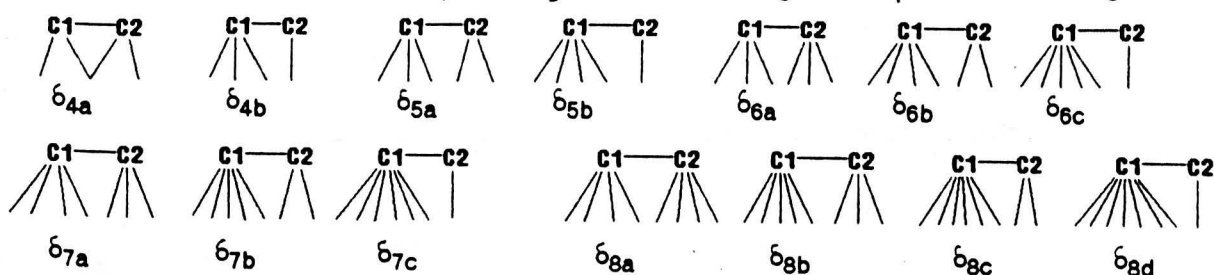


Figure 1.4/1 Dicarbon fragment isomers.

It is possible to obtain the correct number of isomers by returning only the integer part of $\delta/2$. By inspection the forms allowed for any given number of metal atoms can be determined by considering two features (Table 1.4/2). Firstly, the total number of M-C contacts (δ) must always be greater than or equal to the number of metal atoms. (For example, the isomer δ_{4a} is not allowed for metal systems with more than four metal atoms.) Secondly, the number of M-C contacts (δ) from one carbon atom must be less than or equal to the total number of metal atoms and therefore the isomer δ_{6a} is not allowed for metal systems with less than five metal atoms.

Table 1.4/2 Allowed isomeric fragments.

	δ_{4a}	δ_{4b}	δ_{5a}	δ_{5b}	δ_{6a}	δ_{6b}	δ_{6c}
M=3	yes	yes	yes				
M=4	yes	yes	yes	yes	yes	yes	
M=5			yes	yes	yes	yes	yes
M=6					yes	yes	yes

M = No. of metal atoms

δ_n = No. of M-C contacts

Thus the general formula on simplification becomes:

Total number of structures = $(7-M)+i$

M = No. of metal atoms ($M > 3$)

i = No. of additional isomers

1.4.2 Structural Review of dicarbon fragments.

The simplest form of bonding, the $\mu_1 \eta^1 \delta_1$ mode, has only been observed in the dinuclear compound $\text{Pt}_2(\text{C}_2\text{Ph})_2(\text{SiMe})_2(\text{PR}_3)_2$ (1) (Figure 1.4/2). [125] Of the two alkynyl ligands in (1), one bridges the Pt bond in a δ, π -fashion, whilst the second donates to only one Pt atom, through a σ -bond.

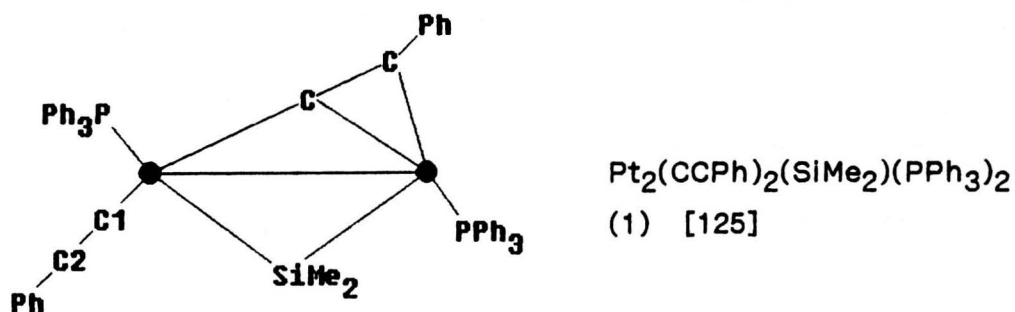


Figure 1.4/2 The $\mu_1 \eta^1 \delta_1$ bonding mode.

The terminal bonding mode adopted by the alkynyl ligand in (1) is probably due to the steric hindrance by the remaining substituents in this complex. [125] In contrast, this terminal mode is the standard form of bonding for the carbonyl ligand. The rarity of this type of bonding for dicarbon fragments is probably a consequence of the ease with which an unsaturated C=C bond can interact with other metal atoms in the cluster.

The $\mu_2 \eta^1 \delta_2$ bonding mode is relatively common for dinuclear and trinuclear species; the latter are illustrated in Figure 1.4/3. The alkynyl cluster $\text{Os}_3(\text{CO})_9(\text{CCPh})_2$ (4) merits further comment. The two alkynyl groups bond differently, the first acts as a 5e donor, bonding to all three osmium atoms in a $\mu_3 \eta^2 \delta_{5a}$ fashion, whereas the second alkynyl group bridges an Os-Os bond ($\mu_2 \eta^1 \delta_2$) and although normally this bonding mode would be considered as a 2e in this cluster the authors assigned it as a 3e donor. [128] This gives a C.V.E. of 50 and as such only two Os-Os bonds are present. In comparison CO ligands are also often found bridging M-M bonds.

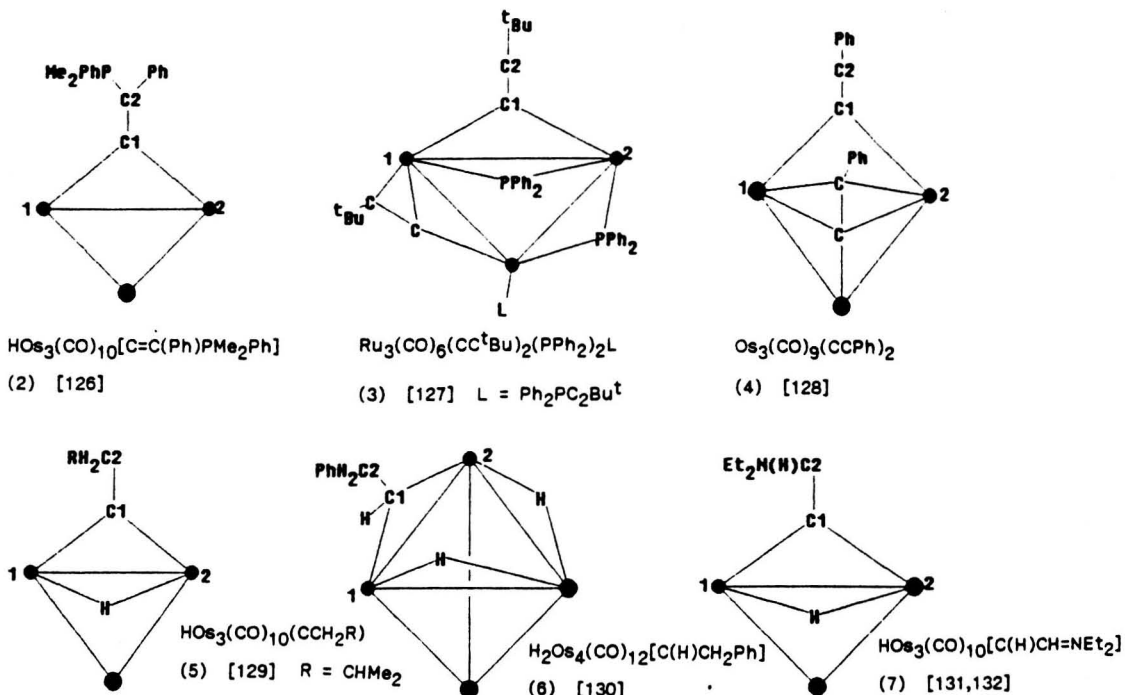


Figure 1.4/3 The $\mu_3\eta^1\delta_2$ bonding mode.

The only type of ligand which has been observed to cap a triangular face of a cluster ($\mu_3\eta^1\delta_3$) is the alkyldiyne group (Figure 1.4/4). This suggests that the presence of R groups on the α -carbon atom would be sterically unfavourable. The μ_3 -capping mode has been reported for a number of carbonyl clusters, but is less common than the terminal or μ_2 -bridging modes discussed above.

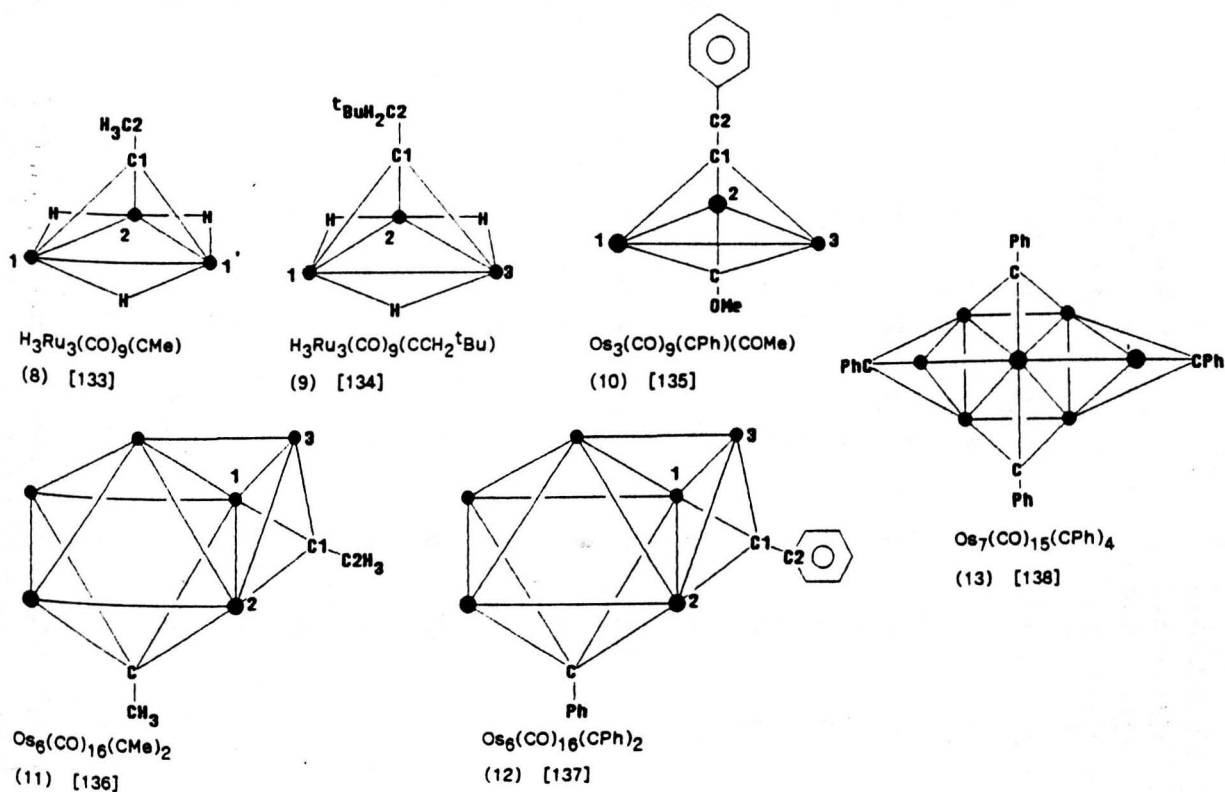


Figure 1.4/4 The $\mu_3\eta^1\delta_3$ bonding mode.

Table 1.4/3 bond lengths for η^1 -coordination (Å).

Cmpd.	Ref.	Ligand	Mode	M1-C1	M1-C2	M2-C1	M1-C2	M3-C1	M3-C2	M4-C1	M4-C2	C1-C2
(1)	125	i	$\mu_1\eta^1\delta_1$	2.01(1)								1.20
(2)	126	g	$\mu_2\eta^1\delta_2$	2.096(10)		2.103(10)						1.356
(3)	127	i	$\mu_2\eta^1\delta_2$	2.22(1)		2.185(9)						1.19(1)
(4)	128	i	$\mu_2\eta^1\delta_2$	2.113(15)		2.251(17)						1.198(19)
(5)	129	c	$\mu_2\eta^1\delta_2$	1.966(22)		2.020(24)						1.528(28)
(6)	130	b	$\mu_2\eta^1\delta_2$	2.11(2)		2.15(2)						1.60(3)
(7)	131, 132	g	$\mu_2\eta^1\delta_2$	2.15(3)		2.16(3)						1.42(3)
(8)	133	c	$\mu_3\eta^1\delta_3$	2.086(10)		2.078(12)		2.086(10)				1.511(20)
(9)	134	c	$\mu_3\eta^1\delta_3$	2.116(5)		2.098(5)		2.091(5)				1.525(9)
(10)	135	d	$\mu_3\eta^1\delta_3$	2.120(12)		2.126(13)		2.139(13)				1.458(18)
(11)	136	c	$\mu_3\eta^1\delta_3$	2.10(7)		1.95(7)		2.14(7)				-
(12)	137	d	$\mu_3\eta^1\delta_3$	2.025(40)		2.069(37)		2.165(36)				1.470(42)
(13)	138	d	$\mu_3\eta^1\delta_3$	2.12(1)i								1.45(1)i
(11)	136	c	$\mu_4\eta^1\delta_4$	2.24(7)		2.17(7)		2.13(7)		2.19(7)		-
(12)	137	d	$\mu_4\eta^1\delta_4$	2.120(32)		2.242(35)		2.185(37)		2.195(37)		1.535(38)

a alkyl(yl)
 b alkylidene
 c alkylidyne
 i) Mean value

d benzylidyne
 e alkene
 f alkenyl

g alkenylidene
 h alkyne
 i alkynyl

Alkynyl ligands can bond in a $\mu_4\eta^1\delta_4$ bonding mode and this frequently occurs with square pyramidal metal frameworks. Examples are found in the hexanuclear clusters $\text{Os}_6(\text{CO})_{16}(\text{CR})_2$ (where R = Me (11)[136] and R = Ph (12)[137]) (Figure 1.4/5).

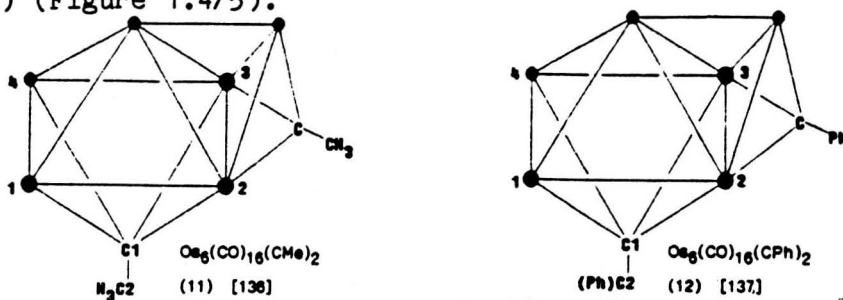


Figure 1.4/5 The $\mu_4\eta^1\delta_4$ bonding mode.

Thus for the η^1 -bonding mode, fragments without any substituents on the α -carbon atom are prevalent namely; alkynyls ($-\text{CCR}$), alkenylidenes ($:\text{C}=\text{CR}_2$), and alkylidyne ($:\text{C}-\text{CR}_3$). This suggests that for η^1 -coordination substituents on the α -carbon atom are sterically unfavourable. Important structural parameters for compounds (1)-(13) are tabulated in Table 1.4/3. This shows that the C1-C2 bond length in these ligands increases in the order alkynyl (ca. 1.20 Å), alkenylidene (1.356 Å), benzylidene (range 1.45(1)-1.470(42) Å), and alkylidyne (range 1.511(20)-1.60(3) Å).

Whereas most dicarbon fragments on cluster surfaces adopt η^2 -coordination, carbonyl ligands rarely adopt bonding modes which involve coordination of the oxygen atom. The simplest example of η^2 -bonding for dicarbon fragments, in which both carbon atoms are bonded to one metal atom ($\mu_1\eta^2\delta_2$), has been reported for the alkene clusters $\text{HOs}_3(\text{CO})_9(\text{H}_2\text{C}=\text{CH}_2)(\text{SMe})$ (14), [139] and $\text{Ru}_6\text{C}(\text{CO})_{15}(\text{MeHC}=\text{C}(\text{H})\text{C}(\text{H})=\text{CHMe})$ (15) (Figure 1.4/6). [140]

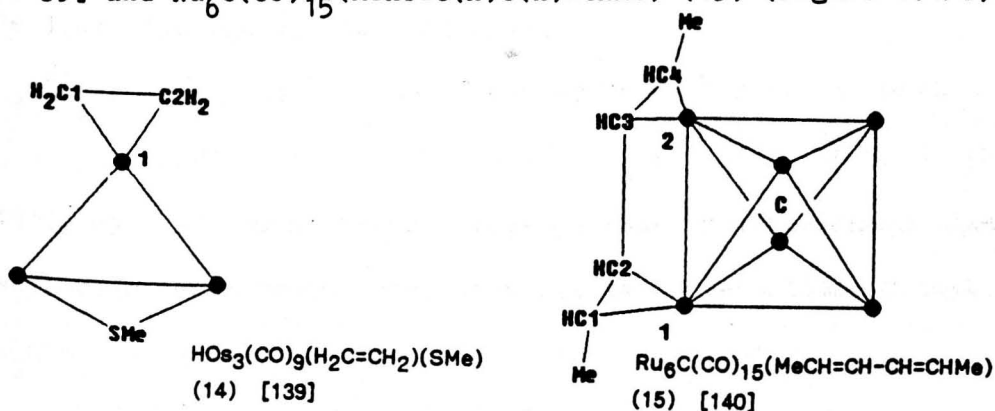


Figure 1.4/6 The $\mu_1\eta^2\delta_2$ bonding mode.

The only known example of the $\mu_2 n^2 \delta_2$ coordination is observed for two of the substituted alkynes in $\text{Ir}_4(\text{CO})_8(\text{CO}_2\text{MeCCCO}_2\text{Me})_4$ (16) (Figure 1.4/7).[19] The remaining substituted alkynes are discussed further on in this section.

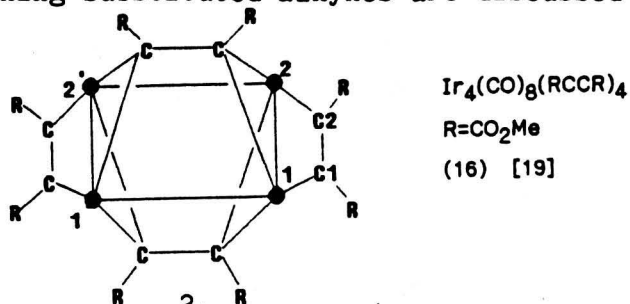


Figure 1.4/7 The $\mu_2 n^2 \delta_2$ bonding mode.

Both alkenyl and alkynyl ligands display $\mu_2 n^2 \delta_3$ bonding, as reported for both trinuclear and tetranuclear cluster species (Figure 1.4/8).

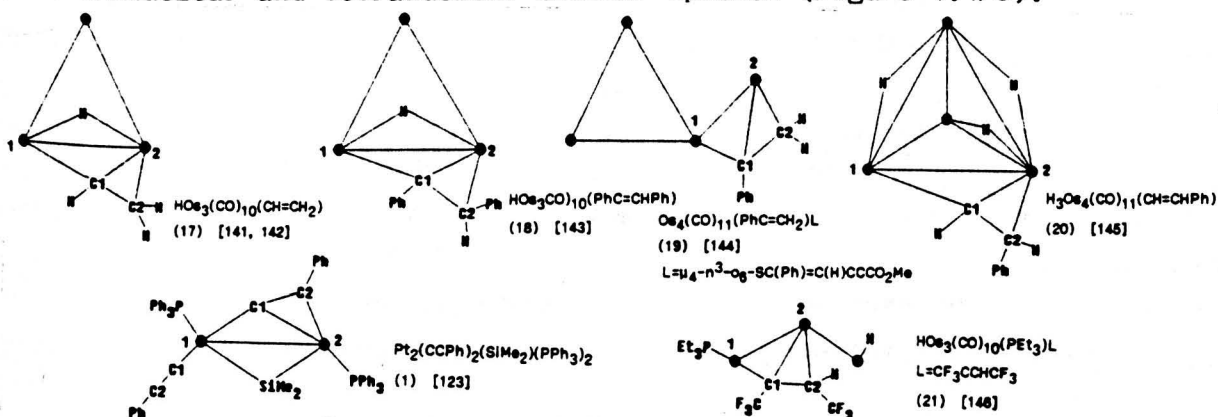


Figure 1.4/8 The $\mu_2 n^2 \delta_3$ bonding mode.

There are no examples of the $\mu_2 n^2 \delta_{4a}$ bonding mode for the iron triad but both of the alkyne ligands in the platinum cluster $\text{Pt}_3(\text{PET}_3)_4(\text{PhCCPh})_2$ (22) adopt this bonding mode (Figure 1.4/9).[147]

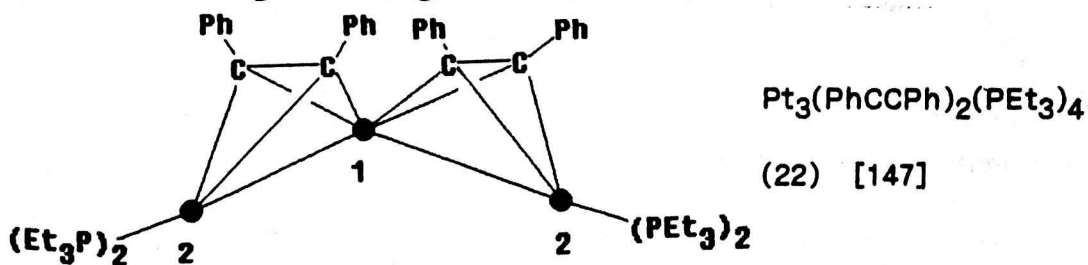


Figure 1.4/9 The $\mu_2 n^2 \delta_{4a}$ bonding mode.

The $\mu_3 n^2 \delta_3$ bonding mode has only been reported for two triosmium clusters, $\text{H}_2\text{Os}_3(\text{CO})_9(\text{HC}=\text{CNEt}_2)$ (23), [148] and $\text{HOs}_3(\text{CO})_{10}(\text{CF}_3\text{C}=\text{CHCF}_3)$ (24) (Figure 1.4/10).[149] In both these clusters the organo-ligand lies almost perpendicular to an Os-Os bond, in a similar orientation to that adopted by the $\mu_3 n^2 \delta_{5a}$ bonding mode discussed below.

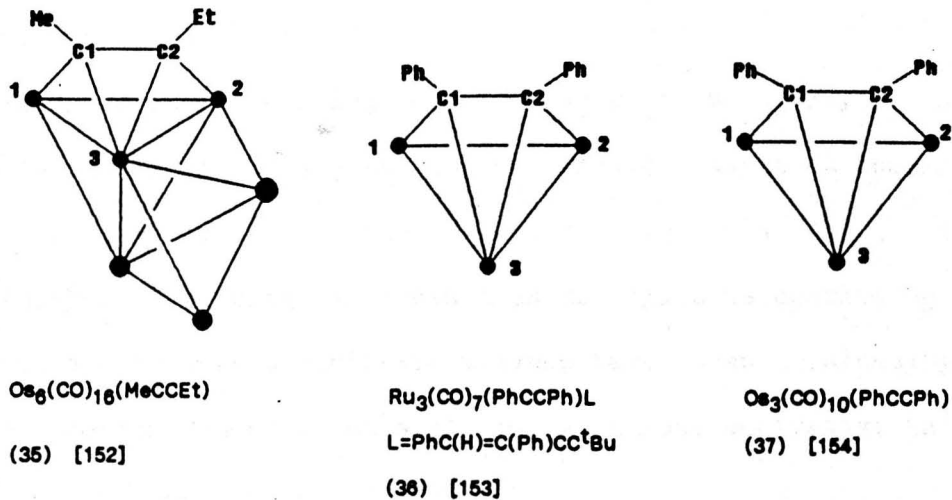
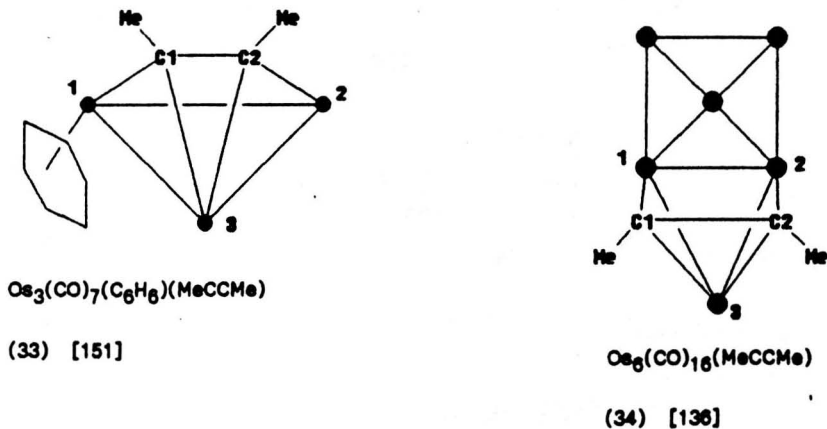
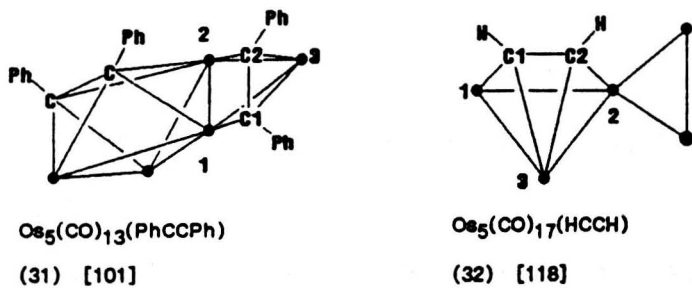
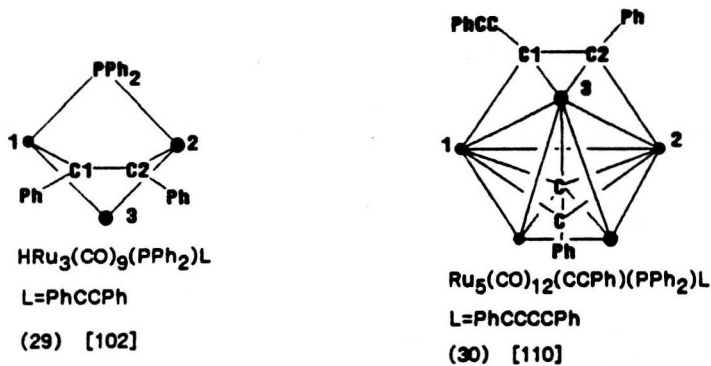
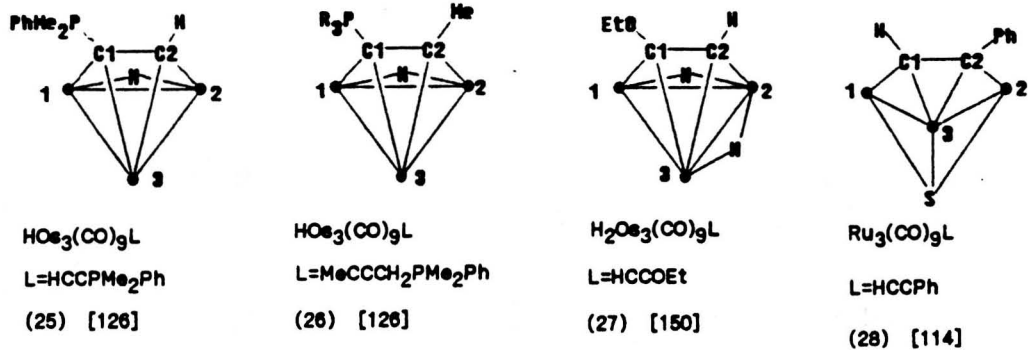
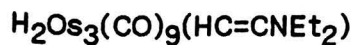
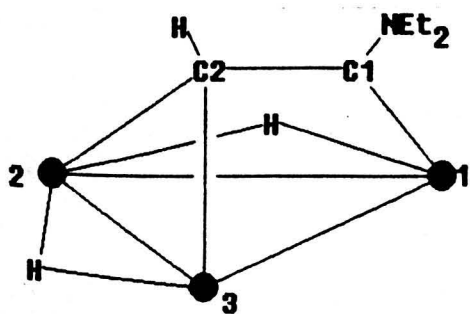
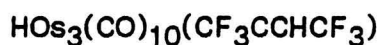
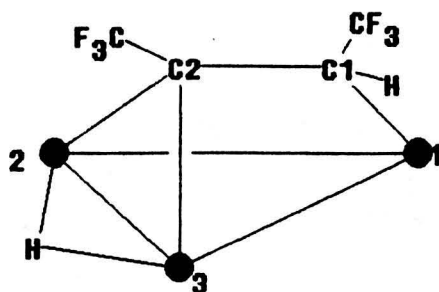


Figure 1.4/11 The $\mu_3\eta^2\delta_{4a}$ bonding mode



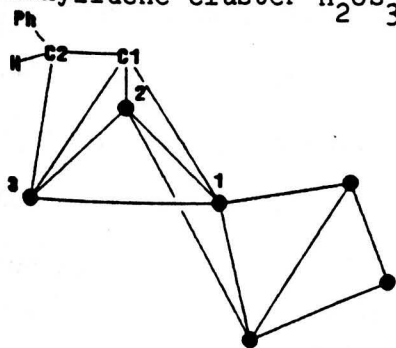
(23) [148]



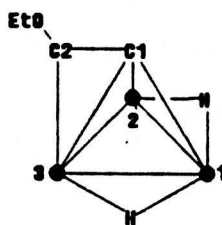
(24) [149]

Figure 1.4/10 The $\mu_3\eta^2\delta_3$ bonding mode.

The most common of all the bonding modes for dicarbon fragments ($\mu_3\eta^2\delta_{4a}$) is adopted by a variety of alkyne clusters (Figure 1.4/11). This is often referred to as the 'parallel' bonding mode as a result of the orientation of the organo-group to the cluster core. In contrast, the alternative $\mu_3\eta^2\delta_{4b}$ bonding is relatively rare, but has been reported for the alkenylidene cluster $\text{Os}_6(\text{CO})_{20}(\text{C}=\text{CHPh})$ (38) and for the substituted alkenylidene cluster $\text{H}_2\text{Os}_3(\text{CO})_9(\text{C}=\text{CHOEt})$ (39) (Figure 1.4/12).



(38) [83]



(39) [150]

Figure 1.4/12 The $\mu_3\eta^2\delta_{4b}$ bonding mode.

The $\mu_3\eta^2\delta_{5a}$ or 'perpendicular' bonding mode is adopted by both alkynyl and alkyne ligands (which donate 5e and 4e respectively) and has been compared to the parallel bonding mode discussed above (Figure 1.4/13). The perpendicular ($\mu_3\eta^2\delta_{5a}$) bonding mode has been described as consisting of 1σ - and 2π -bonds, and by this description alkynes have been misleadingly assigned as five electron donors (impossible for an alkyne derivative which may donate only two or four electrons).[124]

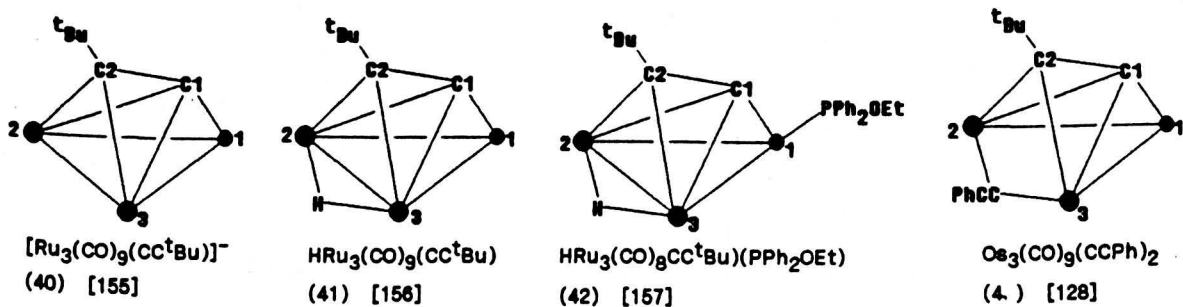


Figure 1.4/13 The $\mu_3\eta^2\delta_{5a}$ bonding mode.

There are no known organo-clusters which contain the $\mu_3\eta^2\delta_6$ coordination mode. Geometrically the 3 M-C contacts from each carbon atom can not be symmetrical - at least one weaker interaction to one of the metals will result. An alternative form would be for the fragment to cut perpendicularly through the M_3 triangle, enabling symmetrical $\mu_3\eta^2\delta_6$ coordination (effectively two joined μ_3 -capping carbon atoms).

The two remaining substituted alkynes in the square planar cluster (16) cap the open square face of the metal core in a $\mu_4\eta^2\delta_{4a}$ bonding mode (Figure 1.4/14). This is the only known example of this type of bonding and thus in (16) the 4 substituted alkyne groups adopt two unique bonding modes. Interestingly, as yet there are no examples of the alternative $\mu_4\eta^2\delta_{4b}$ bonding mode.

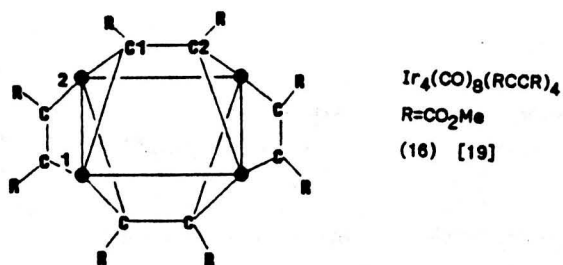
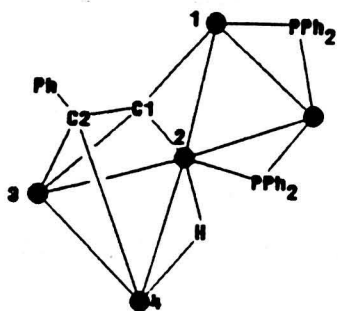


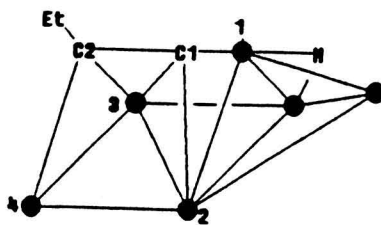
Figure 1.4/14 The $\mu_4\eta^2\delta_{4a}$ bonding mode.

Two alkynyl clusters with very different metal core geometries have been reported which exhibit $\mu_4\eta^2\delta_{5a}$ bonding, the pentaruthenium cluster $\text{HRu}_5(\text{CO})_{13}(\text{CCPh})(\text{PPh}_2)_2$ (43), [119] and the hexaosmium cluster $\text{HOs}_6(\text{CO})_{17}(\text{CCEt})$ (44), [152] (Figure 1.4/15).



$\text{HRu}_5\text{CO}_{13}(\text{CCPh})(\text{PPh}_2)_2$

(43) [119]

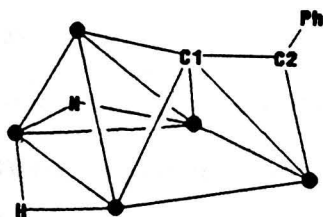


$\text{HOs}_6(\text{CO})_{17}(\text{CCEt})$

(44) [152]

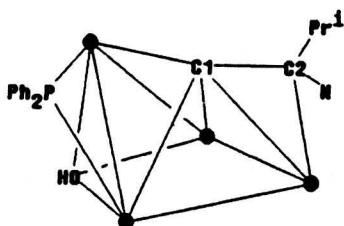
Figure 1.4/15 The $\mu_4\eta^2\delta_{5a}$ bonding mode.

The alternative $\mu_4\eta^2\delta_{5b}$ isomeric form appears to be more common and is adopted by a number of clusters (Figure 1.4/16).



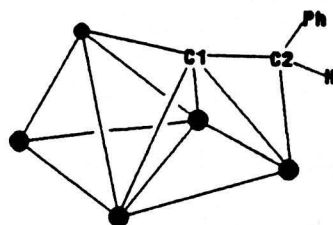
$\text{H}_2\text{Os}_5(\text{CO})_{15}(\text{CCPh})$

(45) [101]



$\text{Ru}_4(\text{CO})_{10}(\text{C}=\text{CHPr}^1)(\text{OH})(\text{PPh}_2)$

(46) [158]

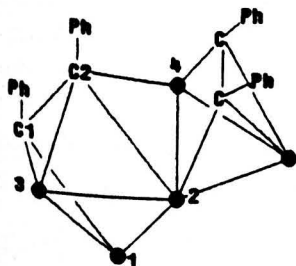


$\text{Os}_5(\text{CO})_{15}(\text{C}=\text{C}(\text{H})\text{Ph})$

(47) [83]

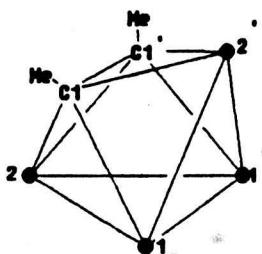
Figure 1.4/16 The $\mu_4\eta^2\delta_{5b}$ bonding mode.

The $\mu_4\eta^2\delta_{6a}$ bonding mode is adopted by alkyne or alkynyl organo-clusters and is frequently observed in the cleft of an M_4 butterfly arrangement (Figure 1.4/17), whereas the alternative $\mu_4\eta^2\delta_{6b}$ bonding mode has not so far been observed.



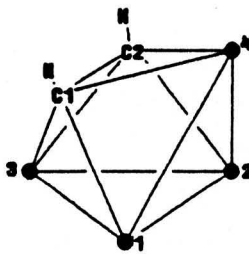
$\text{Os}_5(\text{CO})_{13}(\text{PhCCPh})_2$

(31) [101]



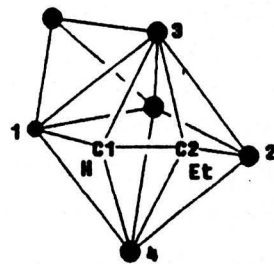
$\text{Ru}_4(\text{CO})_{12}(\text{MeCCMe})$

(48) [140]



$\text{Os}_4(\text{CO})_{12}(\text{HCCH})$

(49) [159]



$\text{Os}_6(\text{CO})_{17}(\text{HCCEt})$

(50) [152]

Figure 1.4/17 The $\mu_4\eta^2\delta_{6a}$ bonding mode.

To date the μ_5 - or μ_6 - bonding modes have only been observed for the dicarbide (CC) fragment, in a semi- or totally encapsulated form. This is more common for higher nuclearity cobalt and rhodium clusters. [160]

1.5 Conclusion.

This chapter has reviewed three major aspects of cluster chemistry;

- a) electron counting procedures and the effect the number of skeletal electron pairs have on the metal core framework,
- b) the variety of metal core frameworks observed,
- c) the types of organic ligands and bonding modes possible.

It is evident that these three features are inextricably entwined. The study of metal core frameworks (Section 1.3) has shown that even with relatively low nuclearity clusters ($M = 5$ to 7) an enormous array of geometries are available and that very open clusters can be held together by organo-fragments (Table 1.3/1). Section 1.4 illustrates that these organo-fragments can bond to cluster surfaces in a large number of different ways but (surprisingly) so far bonding is restricted to 4 or less metal atoms. The X-ray structures reported in this work provide an opportunity to see if the trends discussed in this chapter are continued.

Table 1.4/4 Bond lengths for n^2 -coordination (Å).

Cmpd.	Ref.	Ligand Mode	M1-C1	M1-C2	M2-C1	M2-C2	M3-C1	M3-C2	M4-C1	M4-C2	C1-C2
(14)	139	e $\mu_1 n^2 \delta_2$	2.23(4)	2.23(4)							1.42
(15)	140	e $\mu_1 n^2 \delta_2$	2.30(1)	2.27(1)							1.37(2)
			2.31(1)	2.31(1)							1.42(2)
(16)	19	h $\mu_2 n^2 \delta_2$	2.127(9)			2.095(7)					1.278(11)
(17)	141, 142	f $\mu_2 n^2 \delta_3$	2.107(3)		2.273(3)	2.362(3)					1.396(3)
(18)	143	f $\mu_2 n^2 \delta_3$	2.11(4)		2.34(4)	2.44(4)					1.40(5)
(19)	144	f $\mu_2 n^2 \delta_3$	2.16(2)		2.29(2)	2.29(2)					1.42(2)
(20)	145	f $\mu_2 n^2 \delta_3$	2.154(10)		2.151(13)	2.299(13)					1.356(13)
(1)	125	i $\mu_2 n^2 \delta_3$	1.96(1)		2.14(1)	2.47(1)					1.26(1)
(21)	146	f $\mu_2 n^2 \delta_3$	2.16(3)		2.24(3)	2.20(3)					1.41(4)
(22)	147	h $\mu_2 n^2 \delta_{4a}$	2.07(2)i)								1.34(3)
(23)	148	h $\mu_3 n^2 \delta_3$									
(24)	149	f $\mu_3 n^2 \delta_3$	2.11		2.06			2.19			1.54
(25)	126	h $\mu_3 n^2 \delta_{4a}$	2.127(18)			2.064(17)	2.226(15)	2.252(16)			1.411(23)
(26)	126	h $\mu_3 n^2 \delta_{4a}$	2.132(19)			2.127(19)	2.247(20)	2.293(19)			1.423(28)

Table 1.4/4 (continued) Bond lengths for η^2 -coordination (Å).

Compd.	Ref.	Ligand Mode	M1-C1	M1-C2	M2-C1	M2-C2	M3-C1	M3-C2	M4-C1	M4-C2	C1-C2
(27)	150	h $\mu_3\eta^2\delta_{4a}$	1.86(5)			2.08(3)	2.32(4)	2.45(5)			1.40(5)
(28)	114	h $\mu_3\eta^2\delta_{4a}$	2.04(1)			2.07(1)	2.29(1)	2.31(1)			1.43(2)
(29)	102	h $\mu_3\eta^2\delta_{4a}$	2.168(7)			2.118(8)	2.118(8)	2.274(7)			1.415(11)
(30)	102	h $\mu_3\eta^2\delta_{4a}$	2.138(7)			2.159(6)	2.192(6)	2.202(6)			1.397(9)
(31)	101	h $\mu_3\eta^2\delta_{4a}$	2.09(2)			2.15(2)	2.21(2)	2.24(2)			1.39(4)
(32)	118	h $\mu_3\eta^2\delta_{4a}$	2.10			2.21	2.30	2.17			1.36
(33)	151	h $\mu_3\eta^2\delta_{4a}$	2.14(1)			2.09(1)	2.18(1)	2.27(1)			1.44(2)
(34)	136	h $\mu_3\eta^2\delta_{4a}$	2.13(2)			2.13(2)	2.18(2)	2.20(2)			1.36(2)
(35)	152	h $\mu_3\eta^2\delta_{4a}$	2.25(4)			2.16(4)	2.25(4)	2.09(5)			1.35(6)
(36)	153	h $\mu_3\eta^2\delta_{4a}$	2.33(2)			2.07(2)	2.10(2)	2.21(2)			1.37(2)
(37)	154	h $\mu_3\eta^2\delta_{4a}$	2.182(8)			2.070(9)	2.293(9)	2.188(8)			1.439(10)
(38)	83	g $\mu_3\eta^2\delta_{4b}$	2.161(3)		1.95(3)		2.09(3)	2.34(3)			1.42(4)
(39)	150	i $\mu_3\eta^2\delta_{4b}$	2.06(2)		2.01(2)		2.21(2)	2.43(2)			1.39(2)
(40)	155	i $\mu_3\eta^2\delta_{5a}$	1.95(2)		2.18(2)	2.24(2)	2.16(2)	2.24(2)			1.27(3)
(41)	156	i $\mu_3\eta^2\delta_{5a}$	1.947(3)		2.207(3)	2.268(3)	2.214(3)	2.271(3)			1.315(3)

Table 1.4/4 (continued) Bond lengths for n^2 -coordination (Å).

Cmpd.	Ref.	Ligand Mode	M1-C1	M1-C2	M2-C1	M2-C2	M3-C1	M3-C2	M4-C1	M4-C2	C1-C2
(42)	157	i $\mu_3 n^2 \delta_{5a}$	1.946(4)		1.194(4)	2.252(4)	2.209(4)	2.243(4)			1.320(6)
(4)	128	i $\mu_3 n^2 \delta_{5a}$	1.922(18)		2.240(17)	2.297(17)	2.235(17)	2.283(19)			1.333(22)
(16)	19	h $\mu_4 n^2 \delta_{4a}$	2.136(7)		2.117(8)			2.161(7)		2.120(7)	1.446(9)
(43)	119	i $\mu_4 n^2 \delta_{5a}$	1.985(4)	2.296(4)	2.168(4)		-			2.096(4)	1.367(6)
(44)	152	i $\mu_4 n^2 \delta_{5a}$	2.09(2)		2.04(2)		2.35(2)	2.28(3)		2.11(2)	-
(45)	101	i $\mu_4 n^2 \delta_{5b}$	2.11(3)		2.21(3)		2.22(3)		2.12(3)	2.20(3)	1.49(3)
(46)	158	g $\mu_4 n^2 \delta_{5b}$	2.237		2.183		2.178		2.105	2.267	1.415
(47)	83	g $\mu_4 n^2 \delta_{5b}$	2.033(1)		2.081(2)		2.171(2)		2.415(2)	2.265(2)	1.51(3)
(31)	101	h $\mu_4 n^2 \delta_{6a}$	2.17(2)			2.22(2)	2.27(2)	2.22(2)	2.30(2)	2.23(2)	1.46(3)
(48)	140	h $\mu_4 n^2 \delta_{6a}$	2.16(1)			2.24(1)	2.27(1)				1.45(1)
(49)	159	h $\mu_4 n^2 \delta_{6a}$	2.19(3)			2.22(3)	2.16(3)	2.22(3)	2.24(3)	2.11(3)	1.55(4)
(50)	152	h $\mu_4 n^2 \delta_{6a}$	2.16(2)			2.15(2)	2.23(1)	2.43(1)	2.34(2)	2.32(2)	1.45(2)

a alkyl(yl)
 b alkylidene
 c alkylidyne
 i) Mean value

d benzylidyne
 e alkene
 f alkenyl

g alkenylidene
 h alkyne
 i alkynyl

CHAPTER TWO

Organo-fragments on pentanuclear clusters.

Chapter 2- Organo-fragments on pentanuclear clusters.

There is currently much interest in the rearrangement reactions of metal clusters, and in the extended interactions that are possible between unsaturated ligands and arrays of metal atoms.[91,161,162,163] Clusters may prove useful in interpreting modes of interaction between small molecules and metal surfaces, and hence lead ultimately to a better understanding of heterogeneously catalysed reactions. Pentanuclear clusters are large enough to exhibit a wide range of core geometries, but, at the same time, small enough in cluster terms to be amenable to planned synthesis.

This chapter begins with a review of pentanuclear clusters, their synthesis and reactivity. In Section 2.3 the X-ray structural analyses of 5 clusters containing pyridyl ligands are reported and a structural comparison is made to related pentanuclear clusters. A mechanism for the formation of these 5 structures from $\text{Ru}_5\text{C}(\text{CO})_{15}$ is proposed.

2.1 Routes reported for the formation of pentanuclear clusters.

Numerous techniques have been used to prepare pentanuclear clusters, some more fortuitous than others. Historically the most important method was by build up synthesis, but recently routes to pentanuclear clusters by degradation of higher nuclearity clusters have been reported.

2.1.1 Build-up synthesis.

Trinuclear complexes can serve as precursors, not only to pentanuclear clusters, but to a range of high nuclearity clusters and metal core geometries containing from 4 up to 20 metal atoms have so far been reported.[164] Table 2.1/1 illustrates a selection of pentanuclear clusters that have been synthesised from trinuclear precursors. One of the earliest strategies used in cluster synthesis was pyrolysis and although pentanuclear derivatives have been obtained from $\text{Os}_3(\text{CO})_{12}$, [165,166] the

Table 2.1/1 Pentanuclear clusters from trinuclear precursors.

Reactant	Product	Synthesis	Refs.
$\text{Os}_3(\text{CO})_{12}$	$\text{Os}_5\text{C}(\text{CO})_{15}$	a	22, 161
	$\text{Os}_5(\text{CO})_{16}$	a	74, 165
	$\text{H}_2\text{Os}_5(\text{CO})_{15}$	b	166
	$\text{H}_2\text{Os}_5(\text{CO})_{16}$	b	166
	$\text{Os}_5\text{S}(\text{CO})_{15}$	c	168
$\text{Os}_3(\text{CO})_{11}\text{P}(\text{OMe})_3$	$\text{Os}_5(\text{CO})_{15}\{\text{POMe}\}$	a	98, 108
	$\text{HOs}_5\text{C}(\text{CO})_{14}\{\text{OP}(\text{OMe})_2\}$	a	108, 111
	$\text{HOs}_5\text{C}(\text{CO})_{13}\{\text{OP}(\text{OMe})\text{OP}(\text{OMe})_2\}$	a	97, 108
	$\text{HOs}_5\text{C}(\text{CO})_{13}\{\text{OP}(\text{OMe})_2\}\{\text{P}(\text{OMe})_3\}$	a	108
$\text{Os}_3(\text{CO})_{11}(\text{C}_5\text{H}_4\text{N})$	$\text{HOs}_5\text{C}(\text{CO})_{14}(\text{C}_5\text{H}_4\text{N})$	a	104
	$[\text{HOs}_5(\text{CO})_{15}]^-$	a	104
$\text{HOs}_3(\text{CO})_{10}(\text{SC}_6\text{H}_5)$	$\text{Os}_5\text{S}(\text{CO})_{15}$	d	169
$\text{Ru}_3(\text{CO})_{11}(\text{CNBu}^t)$	$\text{Ru}_5(\text{CO})_{14}(\text{CNBu}^t)_2$	e	100
$\text{Ru}_3(\text{CO})_{11}(\text{Ph}_2\text{PCCP})$	$\text{Ru}_5(\text{CO})_{13}(\text{CCPh})(\text{PPh}_2)$	f	92
$\text{HRu}_3(\text{CO})_9(\text{PPh}_2)$	$\text{Ru}_5\text{P}(\text{CO})_{16}(\text{PPh}_2)$	f	170
$\text{Ru}_3(\text{CO})_{11}(\text{PPh}_3)$	$\text{Ru}_5(\text{CO})_{13}(\text{PPh})(\text{C}_6\text{H}_4)$	g	113
$\text{Ru}_3(\text{CO})_9(\text{HC}_2\text{Ph})(\text{S})$	$\text{Ru}_5\text{S}(\text{CO})_{14}(\text{HC}_2\text{Ph})$	h	114
$\text{H}_2\text{Os}_3(\text{CO})_{10}$	$\text{HOs}_5(\text{CO})_{13}(\text{PhNC}_6\text{H}_4\text{N})$	i	112

- a: Pyrolysis
- b: $\text{H}_2\text{O}/\text{Vacuum}$
- c: S_8/Vacuum
- d: CO/Heat
- e: N_2/Heat
- f: Heptane/Heat
- g: Toluene/Heat
- h: $\text{Ru}(\text{CO})_5/\text{Heat}$
- i: $\text{Ph-NHNH-Ph}/\text{Heat}$

ruthenium analogue $\text{Ru}_3(\text{CO})_{12}$ gives only hexanuclear derivatives (these are discussed in Chapter 3).[167] However, it can be seen from Table 2.2/1 that pentaruthenium clusters can be produced from activated triruthenium clusters such as $\text{Ru}_3(\text{CO})_{11}(\text{CNBu}^t)$.[100]

2.1.2 Cluster degradation.

An alternative route to M_5 clusters involves degradation of higher nuclearity clusters. Carbonylation, vacuum pyrolysis, or treatment with base can yield pentanuclear derivatives from hexanuclear precursors (Table 2.1/2). For example, the interstitial nitrido-compound $[\text{Ru}_6\text{N}(\text{CO})_{16}]^-$ gives the square pyramidal cluster $[\text{Ru}_5\text{N}(\text{CO})_{14}]^-$, a route which is, as yet, not available to pentanuclear osmium clusters since no hexaosmium nitrido-species have been isolated.[95]

Table 2.1/2 Cluster degradation.

Reactant	Product	Synthesis	Refs.
$\text{Ru}_6(\text{CO})_{17}$	$\text{Ru}_5\text{C}(\text{CO})_{15}$	a	84, 85
$[\text{Ru}_6\text{N}(\text{CO})_{16}]^-$	$[\text{Ru}_5\text{N}(\text{CO})_{14}]^-$	a	95
$\text{Os}_6(\text{CO})_{18}$	$\text{Os}_5(\text{CO})_{19}$	a	116
	$[\text{Os}_5(\text{CO})_{15}]^{2-}$	b	76
	$\text{Os}_5\text{C}(\text{CO})_{15}$	c	21

a; CO

b; KOH/MeOH

c; Vacuum pyrolysis

2.2 Cluster reactivity.

The chemical behaviour of pentanuclear clusters can be broadly classified as either involving nucleophilic or electrophilic attack by an incoming ligand.

2.2.1 Nucleophilic attack on clusters.

Ligands such as CO, PR_3 , alkenes, alkynes, iodide, pyridine (and its derivatives) may be regarded as soft nucleophiles. The reaction of these types of ligands with pentanuclear clusters have been widely studied and usually give addition or substitution products.[162] Reactions pathways which result in cluster breakdown are less common, and will not be discussed.

The bridging properties of ligands are of particular importance in the control of metal core geometry. Halides, for example, may coordinate as terminal 1e donors or bridge two metal atoms as 3e donors. Similarly, pyridine is a 2e donor when terminal, but orthometallation of its α -carbon (with transfer of hydrogen to the metal core) creates a 3e bridging pyridyl ligand, along with a 1e donation from the generated hydrogen atom, which adopts a bridging site.

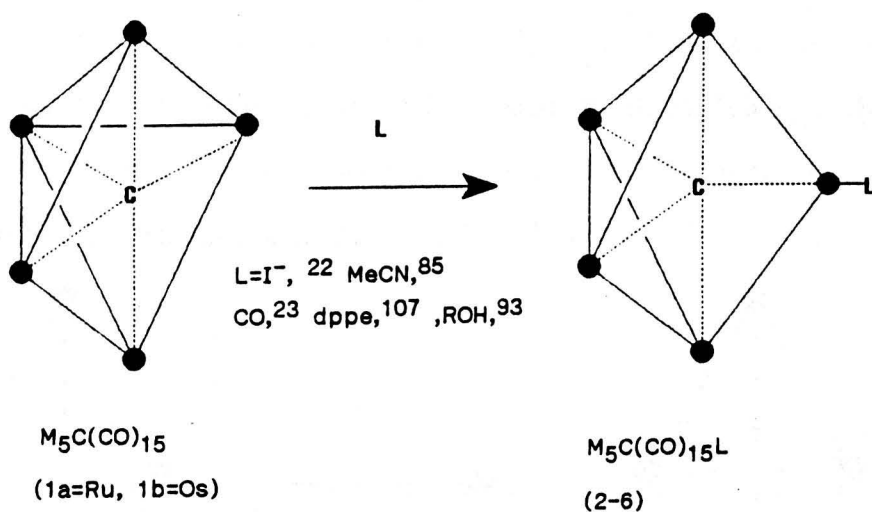


Figure 2.2/1 Cluster opening on addition of nucleophiles.

One of the simplest types of nucleophilic reaction is addition. This results in an increase in the number of cluster valence electrons (CVE), and for each pair of electrons added cleavage of an M-M bond occurs. Addition reactions therefore result in opening of the cluster framework, and in some cases may ultimately lead to cluster breakdown (Section 1.3). For example, the 74e square pyramidal clusters $M_5C(CO)_{15}$ [M=Ru (1a) or Os

(1b)] undergo a range of addition reactions, which lead to opening of the cluster framework. In the parent species, cleavage of one axial bond leads to the 76e bridged butterfly derivatives (2-6) (Figure 2.2/1). Structures of this type are discussed in more detail in Section 2.3, where the results of the present work are reported.

Another example of nucleophilic addition occurs when the dihydride $\text{H}_2\text{Os}_5(\text{CO})_{15}$ (7), which has a trigonal bipyramidal framework, reacts with nucleophiles such as I^- , $\text{P}(\text{OMe})_3$, CO , and pyridine to give adducts of the form $\text{H}_2\text{Os}_5(\text{CO})_{15}\text{L}$ (8-12) (Figure 2.2/2).[20] Cleavage of an axial-equatorial bond in the trigonal bipyramid (7) gives the observed edge-bridged tetrahedral metal framework. The iodine atom in $[\text{H}_2\text{Os}_5(\text{CO})_{15}\text{I}]^-$ (9) adopts an axial position on the bridging osmium, whereas the trimethylphosphite group in complex (12) adopts an equatorial position. This difference in site preference can be attributed to the greater steric bulk of the phosphite ligand. Pyridine is intermediate in size between I^- and $\text{P}(\text{OMe})_3$, and the complex $\text{H}_2\text{Os}_5(\text{CO})_{15}(\text{C}_5\text{H}_5\text{N})$ (11) is believed to exist in two isomeric forms, with the pyridine either axially or equatorially coordinated.[80]

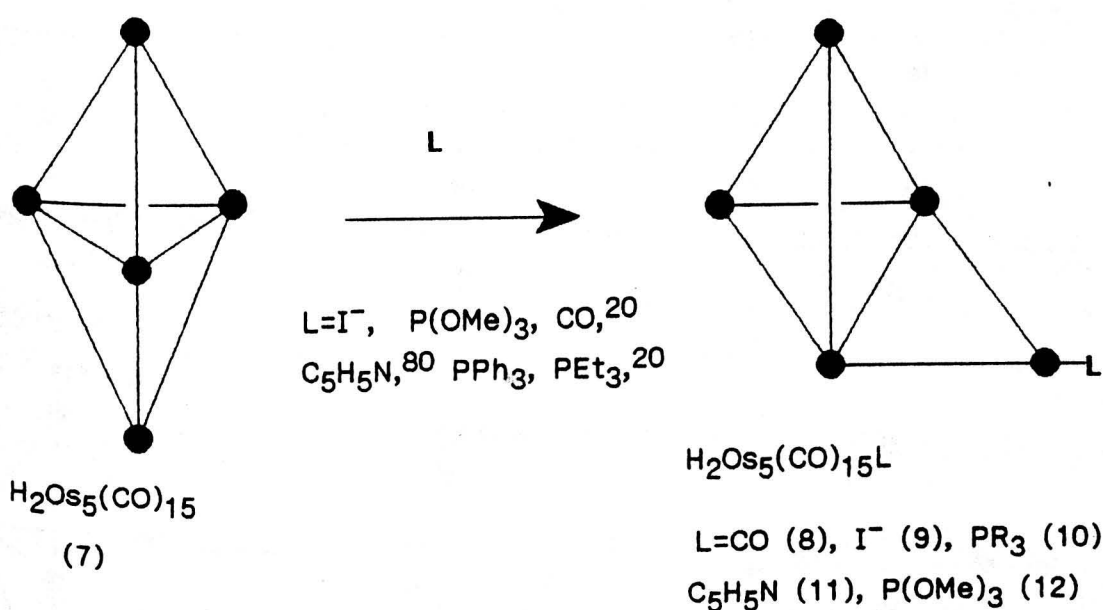
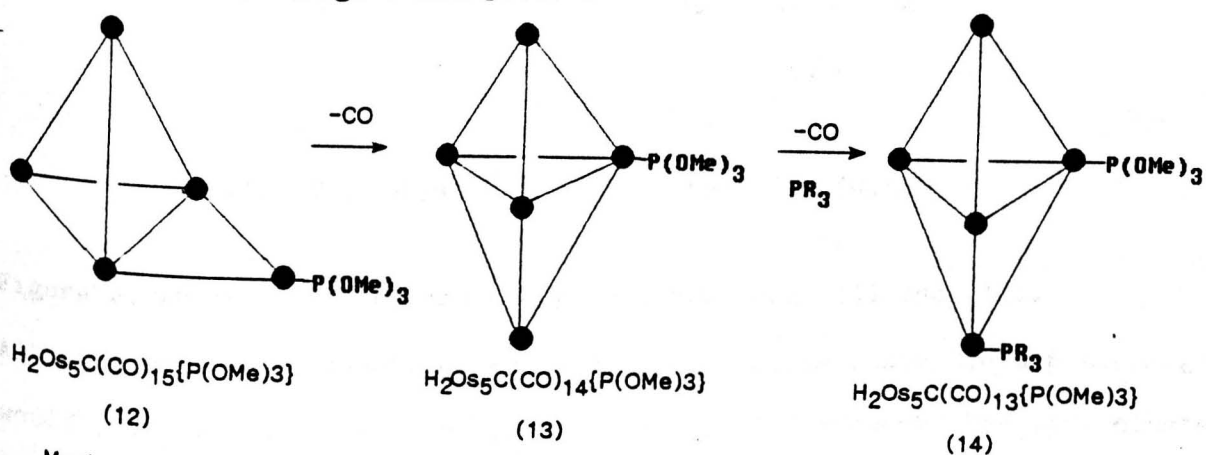


Figure 2.2/2 The reaction of $\text{H}_2\text{Os}_5(\text{CO})_{15}$ (7) with nucleophiles.

One of the products of this reaction, the phosphite derivative (12), can undergo subsequent elimination of a carbonyl ligand. This reduces the CVE and has the reverse effect on the polyhedron, resulting in framework closure.[78] Effectively, the edge-bridged tetrahedral cluster (12) decarbonylates yielding the trigonal bipyramidal cluster $H_2Os_5(CO)_{14}\{P(OMe)_3\}$ (13) (Figure 2.2/3). In this process of metal core geometry closure the phosphite has been retained in preference to a carbonyl ligand. An axially coordinated $P(OMe)_3$ would be expected from a simple closure process, whereas in fact the phosphite ligand in (13) bonds to an equatorial metal atom. Thus, the mechanism appears to proceed by rearrangement of the metal core to an intermediate square pyramidal geometry with the phosphite on a basal site, which can then close to give the observed product. The phosphite cluster (13) can be subsequently substituted by a second phosphorus ligand PR_3 ($R = Et, OMe$) to give $H_2Os_5(CO)_{13}\{P(OMe)_3\}(PR_3)$ (14), in which the added ligand is bonded to an axial osmium atom (Figure 2.2/3).[78]



Mechanism

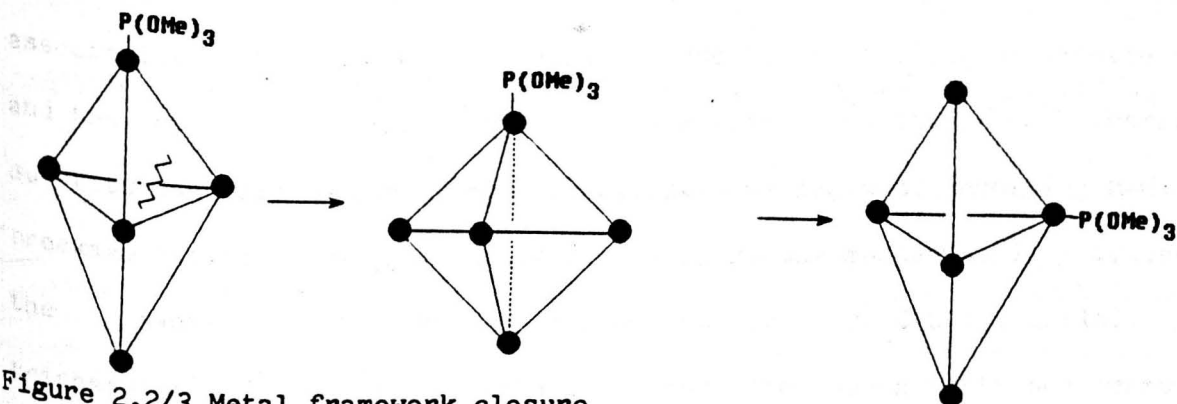


Figure 2.2/3 Metal framework closure.

The reaction of the trigonal bipyramidal cluster $\text{H}_2\text{Os}_5(\text{CO})_{15}$ (7) with pyridine merits further comment, as a total of 4 products have been characterised from it. In addition to the two isomeric products referred to above, a substituted product $\text{H}_2\text{Os}_5(\text{CO})_{14}(\text{C}_5\text{H}_5\text{N})$ (15) and an adduct with a bridging pyridyl ligand $\text{H}_3\text{Os}_5(\text{CO})_{14}(\text{C}_5\text{H}_4\text{N})$ (16) are formed (Figure 2.2/4). The substituted product $\text{H}_2\text{Os}_5(\text{CO})_{14}(\text{C}_5\text{H}_5\text{N})$ (15) retains the trigonal pyramidal metal core of the parent dihydride (so the CVE is unchanged), with one of the equatorial carbonyl ligands having been directly replaced by a terminally bonding pyridyl ligand.[80] In the second product $\text{H}_3\text{Os}_5(\text{CO})_{14}(\text{C}_5\text{H}_4\text{N})$ (16), the μ^2 -pyridyl is bonded through the nitrogen atom to the edge-bridging osmium, with the α -carbon atom bonded to the apex of the tetrahedron (Figure 2.2/4). All three hydrides in (16) bridge axial M-M bonds of the tetrahedral core.

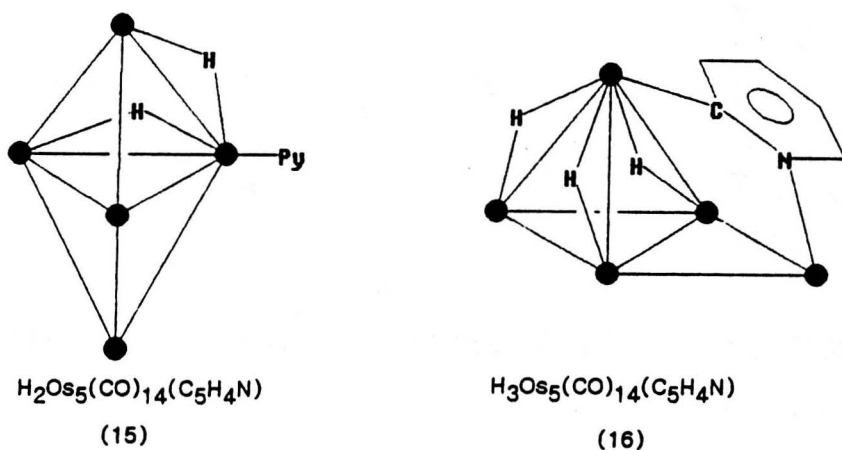


Figure 2.2/4 The pyridine and μ_2 -pyridyl clusters (15) and (16).

Although reactions classified as substitution which leave the CVE unchanged would not be expected to effect the metal framework, for many cluster reactions it is difficult to establish whether substitution occurs via an associative or dissociative mechanism due to the absence of kinetic data and the infrequent isolation of any intermediate products.[162] Therefore substitution may occur by more complicated mechanisms, involving M-M bond breakage and re-formation. A superficially simple mechanism is provided by the reaction of the carbido-cluster $\text{Ru}_5\text{C}(\text{CO})_{15}$ (1a) with triphenylphosphine. This initially gives the monosubstituted compound

$\text{Ru}_5\text{C}(\text{CO})_{14}(\text{PPh}_3)$ (17) and subsequently the disubstituted product $\text{Ru}_5\text{C}(\text{CO})_{13}(\text{PPh}_3)_2$ (18) (Figure 2.2/5).[85] Although the square pyramidal geometry of the parent compound is retained, and these reactions could be seen simplistically as direct carbonyl substitution, by analogy with $\text{Os}_5\text{C}(\text{CO})_{15}$ (1b), $\text{Ru}_5\text{C}(\text{CO})_{15}$ (1a) is thought to react via an associative mechanism. The reaction process proceeds by addition of the PPh_3 accompanied by M-M bond cleavage, followed by loss of a carbonyl ligand with re-formation of an M-M bond.[85] Much clearer evidence for this type of mechanistic pathway has been found from the present work and will be discussed in Section 2.4.

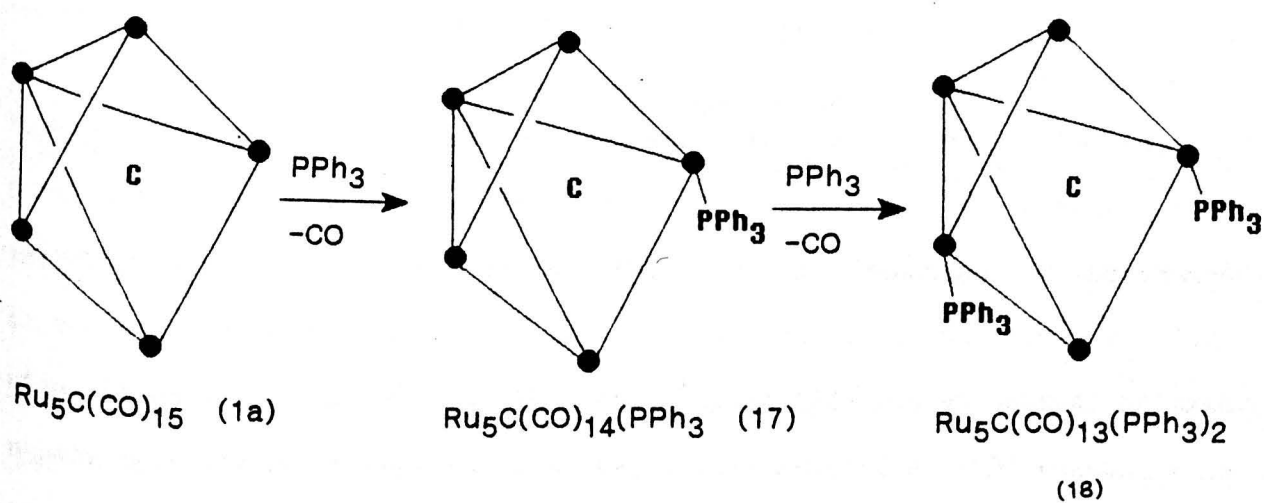


Figure 2.2/5 The mono- and disubstituted phosphine clusters (17) and (18). Direct substitution of carbonyl ligands is often difficult, so activation of trinuclear clusters with labile ligands (such as acetonitrile) is now a well established synthetic strategy.[171] Similarly, the pentanuclear cluster $\text{Os}_5(\text{CO})_{15}(\text{MeCN})$ (19) undergoes a series of nucleophilic displacement reactions with a variety of alkynes and phospho-derivatives (Figure 2.2/6), which could not be obtained directly from the binary carbonyl cluster.[162]

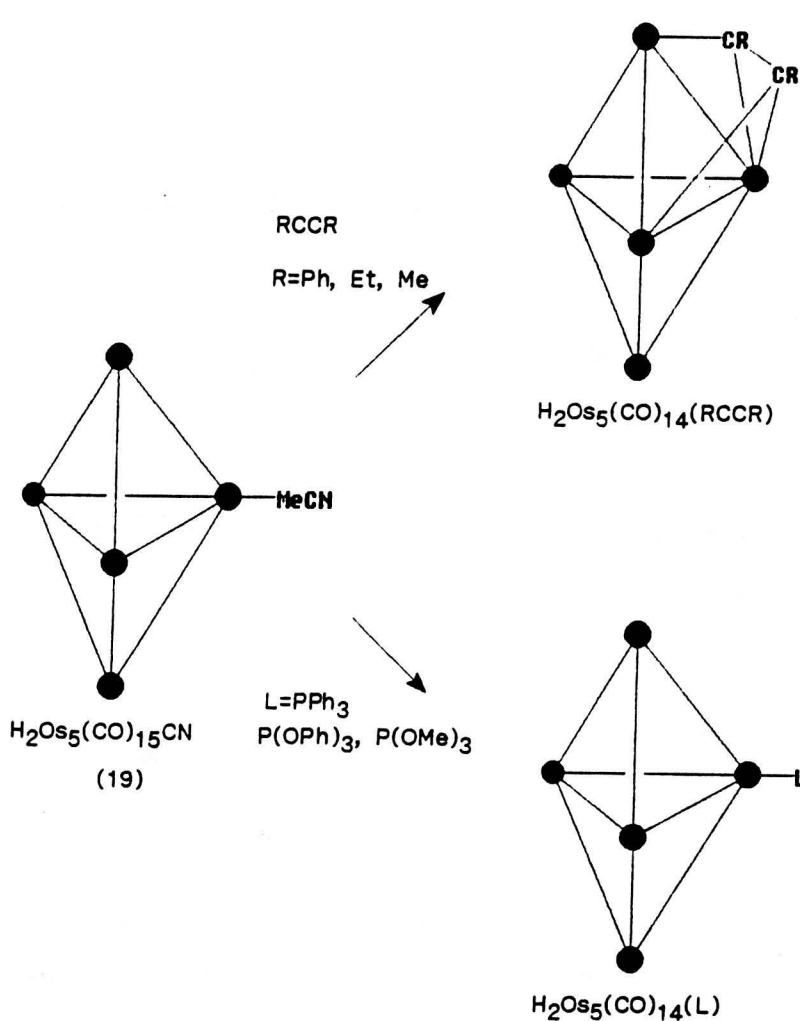


Figure 2.2/6 The reactions of the activated cluster $\text{Os}_5(\text{CO})_{15}(\text{MeCN})$ (19). Substitution reactions can also occur after nucleophilic attack at a carbonyl ligand. An example of this is the reaction of the square pyramidal cluster $\text{Os}_5\text{C}(\text{CO})_{15}$ (1b) and its iodo-analogue $\text{Os}_5\text{C}(\text{CO})_{15}\text{I}_2$ (20) with alcohol (Figure 2.2/7).[105] The complex (20) has an unusual bridged square geometry which appears to activate the cluster, as (20) reacts with alcohols under milder reaction conditions than (19). It has been proposed that in both of these reactions initial nucleophilic attack by RO^- occurs at the C-atom of one of the carbonyl ligands attached to the bridging osmium, followed by 2e donation from the carbonyl O-atom to an adjacent osmium atom.[105]

Finally, in some cases, reaction with nucleophiles does not result in addition or substitution but leads to cluster reduction. For example, the treatment of $\text{Os}_5(\text{CO})_{16}$ with potassium hydroxide does not lead to hydroxy coordination but gives the dianion $[\text{Os}_5(\text{CO})_{15}]^{2-}$.[162]

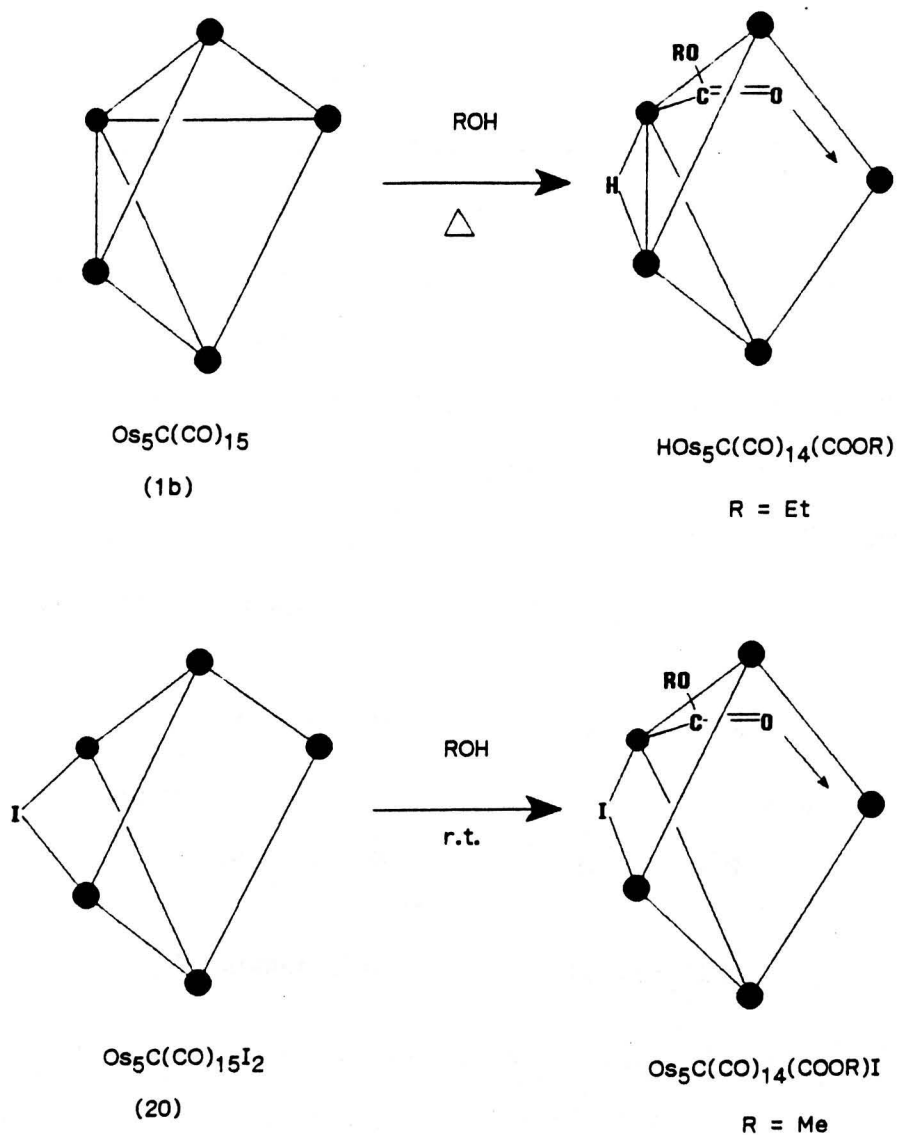


Figure 2.2/7 Comparison of the reaction of (1b) and (20) with ROH.

2.2.2 Electrophilic attack on pentanuclear clusters.

One of the most important types of electrophilic reaction is protonation. An example of simple addition, without change in metal core geometry, is the protonation of the dianion $[\text{Os}_5(\text{CO})_{15}]^{2-}$, which gives the mono-hydride $[\text{HOs}_5(\text{CO})_{15}]^-$ and the dihydride $\text{H}_2\text{Os}_5(\text{CO})_{15}$ respectively.[76] The dihydride is not deprotonated by I^- , whereas the higher nuclear analogues are readily deprotonated under such conditions. This fact can be attributed to the increase of Lewis acidity with cluster size. Protonation does not increase the electron density of the cluster and so, on these grounds, would not be expected to undergo metal core transformation. Despite this, many higher nuclearity clusters (where alternative geometries of the same electron count are of comparable energy) undergo cluster core rearrangement on protonation.[162]

The most widely studied group of electrophilic reagents are cationic heterometallic species $[MR_n]^+$, where M is typically gold, silver, or copper and R is an alkyl or aryl group. One important example, which involves solid state isomerism, is the reaction of the nitrosyl anion $[Ru_5C(CO)_{13}(NO)]^-$ with $[AuPET_3]^+$, which gives isomers of $Ru_5C(CO)_{13}(NO)(AuPET_3)$ (21) (Figure 2.2/8).[87] In the first isomer the gold triphenylphosphine ligand asymmetrically caps one face of the Ru_5 square pyramid, whilst in the second isomer the $AuPET_3$ group bridges an edge of the pyramid (Figure 2.2/8).[87]

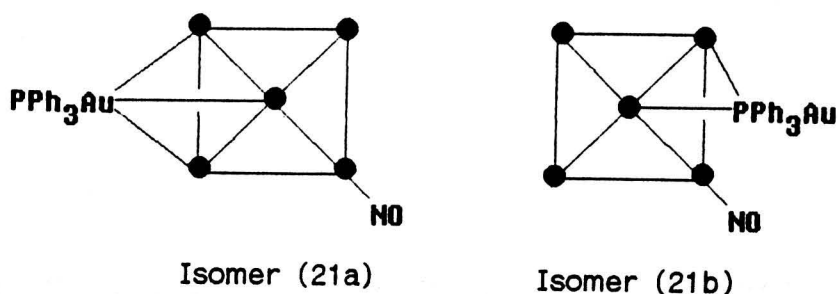


Figure 2.2/8 Solid state isomers of $Ru_5C(CO)_{13}(NO)(AuPET_3)$ (21).

2.2.3 Organic reactions of pentanuclear clusters.

The behaviour of polynuclear clusters towards organic reagents is particularly interesting but, in comparison with simple inorganic species, reaction pathways are generally more complex. As such, the division of these reactions as nucleophilic or electrophilic is too simplistic, so the reaction of pentanuclear clusters with organo-groups is considered here as a separate classification.

The reaction of the bow-tie cluster $Os_5(CO)_{19}$ (22) with mono-substituted alkynes gives an organo-cluster $Os_5(CO)_{17}(HCCR)$ (23) (Figure 2.2/9).[118]

The bonding mode adopted by the alkyne ligand in this cluster ($\mu_3\eta^2\epsilon_{4a}$) is the most commonly reported form of bonding for dicarbon fragments (Section 1.4). The reaction of (22) with ethyne gives an additional product, the tetranuclear cluster $Os_4(CO)_{12}(HCCH)$ (24), in which the alkyne interacts

with the cleft of the metal core butterfly, π -donating to the wingtip metal atoms and σ -bonding to the hinge bond atoms ($\mu_4 \eta^2 \sigma_{6a}$). [159] This mode of bonding is also relatively common and has been established for a number of tetranuclear butterfly complexes (Section 1.4). [172]

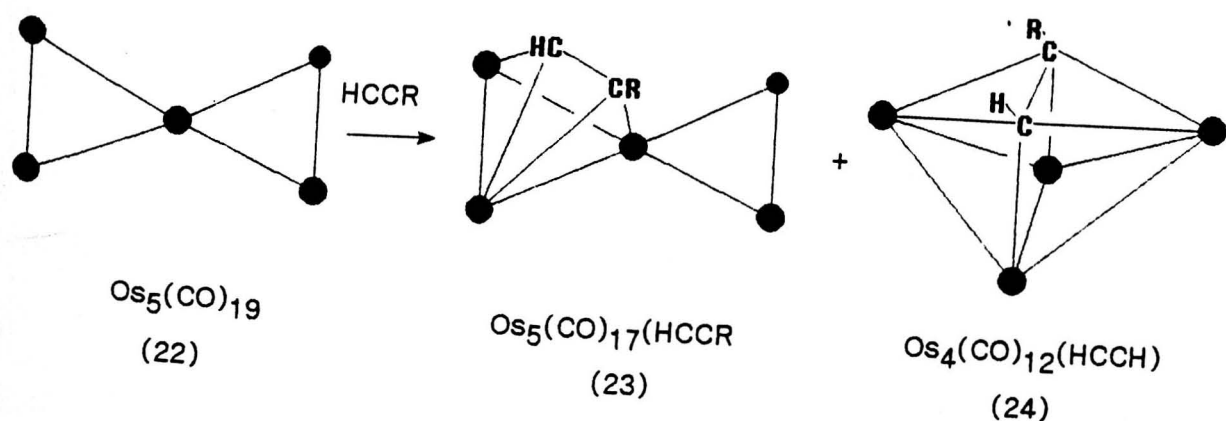


Figure 2.2/9 The reaction of $\text{Os}_5(\text{CO})_{19}$ (22) with alkynes.

Both these forms of alkyne interaction are observed in the product from the reaction of the trigonal bipyramid $\text{H}_2\text{Os}_5(\text{CO})_{15}$ (7) with disubstituted alkynes. [101] Treatment of (7) with PhCCPh gives the disubstituted product $\text{Os}_5(\text{CO})_{13}(\text{PhCCPh})_2$ (25) (Figure 2.2/10). This 76e-species is illustrated in Figure 2.2/11 and has the relatively unusual hinge-wingtip bridged butterfly arrangement of metal atoms (Section 1.3). [101]

In contrast, the reaction of (7) with the monosubstituted acetylene PhCCH gives $\text{H}_2\text{Os}_5(\text{CO})_{15}\{\text{CC}(\text{H})\text{Ph}\}$ (26), in which the metal core has the more common wingtip-bridged butterfly geometry (Figure 2.2/10). [101] Thus with mono-substituted alkynes a 1,2-hydrogen shift has occurred, which is accompanied by M-core rearrangement. The bonding mode adopted by the acetylene ligand ($\mu_4 \eta^2 \sigma_{5b}$) is relatively unusual (Section 1.4) and can be described as involving π -donation to the bridging osmium atom with the two remaining electrons being involved in a (4-c,2-e) bond to three other M atoms.

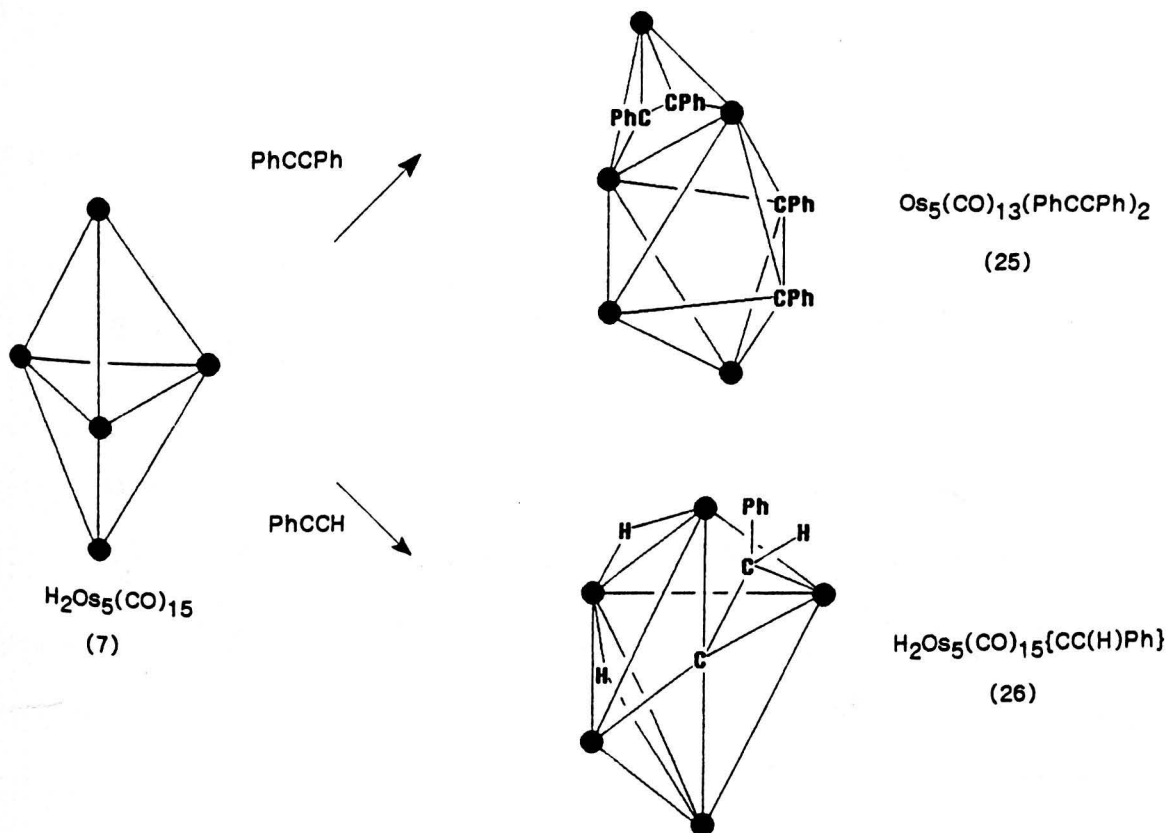


Figure 2.2/10 The reaction of $\text{H}_2\text{Os}_5(\text{CO})_{15}$ (7) with alkynes.

This mode of interaction is also observed for the alkenylidene fragment in $\text{Os}_5(\text{CO})_{15}\{\text{CC}(\text{H})\text{Ph}\}$ (27) and occurs in the cleft of the 'butterfly' segment of the edge-bridged tetrahedral metal core (Figure 2.2/11).[83]

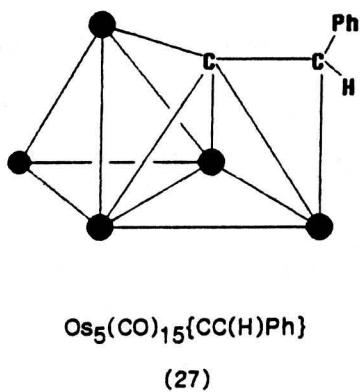


Figure 2.2/11 $\text{Os}_5(\text{CO})_{15}\{\text{CC}(\text{H})\text{Ph}\}$ (27).

Addition of the 3e donor diphenylphosphine to the (74e) square pyramidal complex $\text{Ru}_5(\text{CO})_{13}(\mu_4\eta^2\delta_{6b}\text{-C}_2\text{Ph})(\mu\text{-PPh}_2)$ (28) gives the 78e bow tie cluster $\text{HRu}_5(\text{CO})_{13}(\mu_4\eta^2\delta_{6a}\text{-C}_2\text{Ph})(\text{PPh}_2)_2$ (29) (Figure 2.2/12).[119] Although the metal core has been transformed, the alkenyl group still adopts a $\mu_4\eta^2\delta_6$ bonding mode. The complex (28) can also react with diphenylbutadiyne, with the acetylene ligand in (30) contributing 4e in a pseudo-parallel mode of bonding ($\mu_3\eta^2\delta_{4a}$) and the alkyne carbons lying almost parallel to a non-bonding edge of an open triangle.

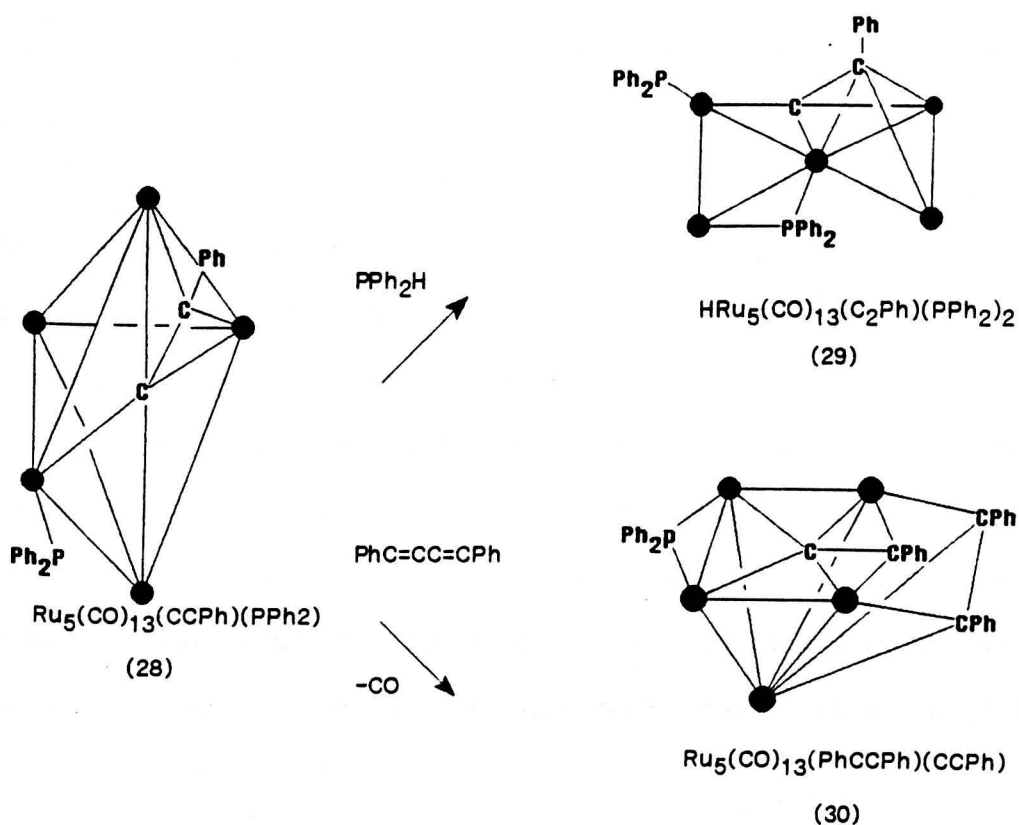
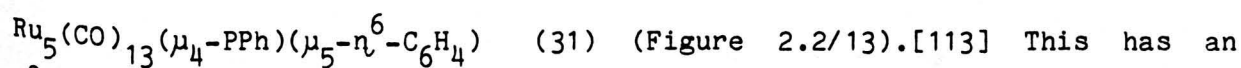


Figure 2.2/12 The bow tie and hinge-wingtip bridged clusters (29) and (30).

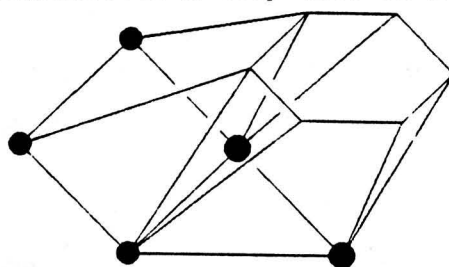
An unusual edge-bridged square geometry is exhibited by the organo-cluster



η^8 -benzyne ligand bonded in a $\mu_5\eta^8\sigma_8$ bonding mode by forming 3 π -bonds to

the metal triangle and 2 σ -bonds to the remaining 2 M atoms. Muetterties

has compared this molecule to a step-site on a (111) metal surface. [173]



(31)

Figure 2.2/13 The edge-bridged square cluster $\text{Ru}_5(\text{CO})_{13}(\text{PPh})(\text{C}_6\text{H}_4)$ (31).

The substituted alkenyl cluster $\text{Ru}_5(\text{CO})_{13}(\mu_5\text{-C}_2\text{PPh}_2\text{-P})(\mu\text{-PPh}_2)$ (32), [103]

also shows an interesting mode of ligand interaction (Figure 2.2/14). The

C_2PPh_2 group contributes seven electrons to the electron count of the

hinge-wingtip bridged butterfly- two via the phosphorus atom, and five via

the C_2 unit. This C_2 fragment may be considered as σ -donating to three

metal atoms, and asymmetrically π -donating to a fourth. Hydrogenation of

the substituted alkenyl ligand in (32) results in the stepwise absorption

of three molecules of hydrogen, with transfer of one hydrogen to the cluster framework and one to the α -carbon at each stage (Figure 2.2/14). This leads to the formation of clusters containing μ_5 -vinylidene (33), methylidene (34), and carbide (35) ligands. Overall, the coordinated μ_5 -CCPh₂ ligand is converted into a carbide and a MePPh₂ group. The metal core geometry is maintained throughout hydrogenation, until absorption of the third and final molecule of hydrogen causes closure to a square pyramidal core. This sequential process illustrates the potential metal cluster cores have in activating organo-fragments. In contrast, the same cluster undergoes extensive rearrangement on reaction with carbon monoxide, resulting in the formation of the more open 'coat-hanger' metal core geometry (Section 1.3).[174]

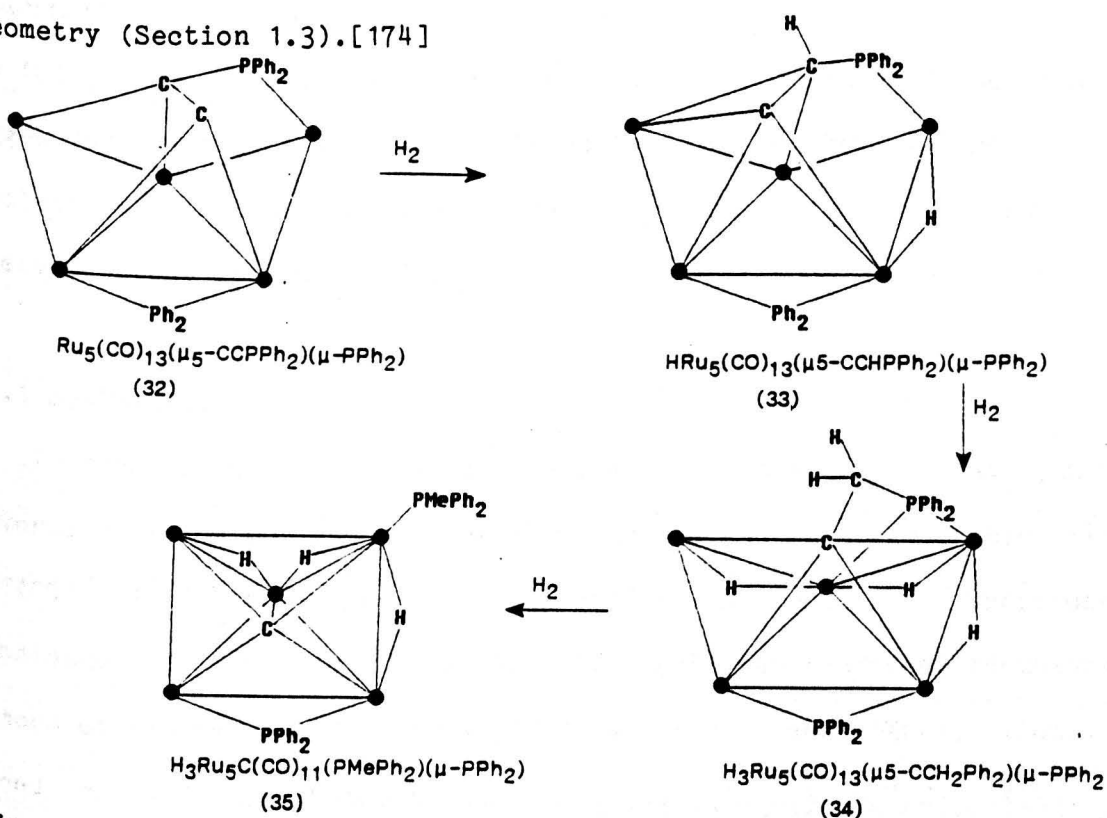


Figure 2.2/14 Hydrogenation of $\text{Ru}_5(\text{CO})_{13}(\text{C}_2\text{PPh}_2\text{P})(\mu\text{-PPh}_2)$ (32).

2.2.4 Conclusion.

This section has reviewed a variety of pentanuclear reactions and shows that many of the organo-fragments and metal core frameworks discussed in Chapter 1 have been reported. It also highlights the lack of mechanistic data available for reaction pathways. In subsequent sections, 5 X-ray structures are reported which are believed to offer an insight into one particular reaction pathway.

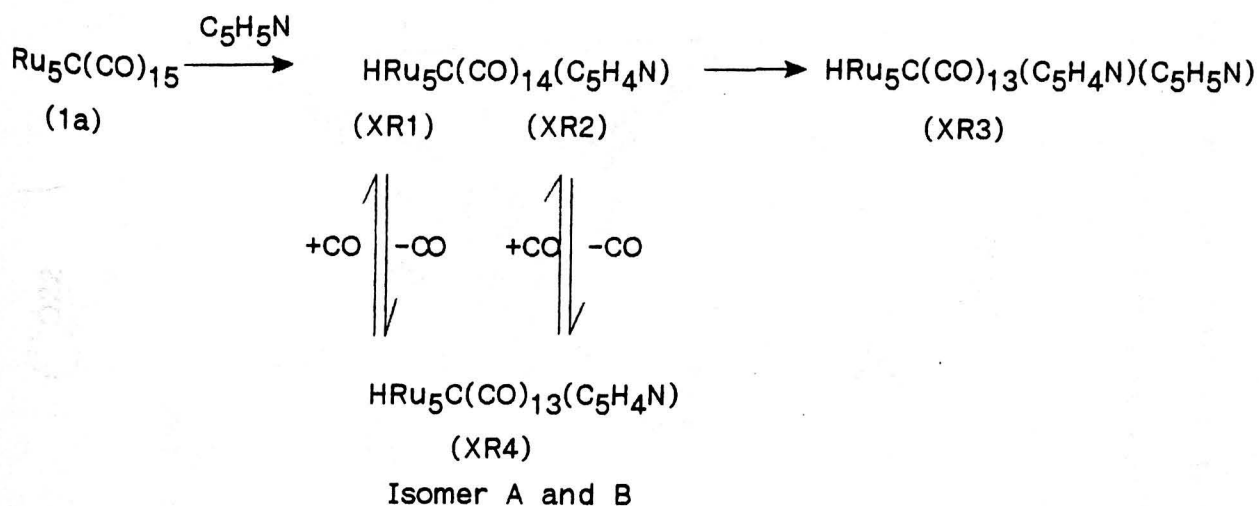
2.3 The interaction of $\text{Ru}_5\text{C}(\text{CO})_{15}$ (1a) with pyridine.

Metal cluster isomers are relatively rare in the solid state but several have now been structurally characterised. These have previously involved different sites for hydride or other monodentate ligands, [17,87,175] alternative metal framework polyhedra, [87] or isomerism of an organo-ligand. [150] An example closer to the structures discussed in this section is provided by the capped trigonal bipyramidal cluster $\text{HOs}_6(\text{CO})_{16}(\mu_2\text{-C}_5\text{H}_4\text{N})$, which has a μ_2 -pyridyl ligand bridging an Os-Os edge. [176] As there was evidence of disorder of the site of pyridyl attachment, Pearsall synthesised the related cluster $\text{HOs}_6(\text{CO})_{16}(\mu_2\text{-C}_5\text{H}_4\text{NMe})$. [176] However, this too appeared to be disordered suggesting the possibility of two isomeric forms for both clusters. More conclusive evidence for the presence of solid state isomerism has been achieved in the present study.

2.3.1 Synthesis.

The clusters discussed in this section were synthesised at Cambridge University by Tom Dutton. The reaction of the pentanuclear carbido cluster $\text{Ru}_5\text{C}(\text{CO})_{15}$ (1a) with an excess of pyridine was shown by spectroscopic techniques to give an equimolar mixture of two compounds formulated as isomers of the hydride $\text{HRu}_5\text{C}(\text{CO})_{14}(\text{C}_5\text{H}_4\text{N})$, (XR1) and (XR2), along with traces of a disubstituted product $\text{HRu}_5\text{C}(\text{CO})_{13}(\text{C}_5\text{H}_4\text{N})(\text{C}_5\text{H}_5\text{N})$, (XR3). Both isomers (XR1) and (XR2) were shown to undergo quantitative thermal decarbonylation to give the same product, $\text{HRu}_5\text{C}(\text{CO})_{13}(\text{C}_5\text{H}_4\text{N})$ (XR4). This was recarbonylated quantitatively under mild conditions, to regenerate equal proportions of (XR1) and (XR2) (Scheme 2.3/1). The X-ray structural analyses carried out in this project characterised five different products, demonstrating that $\text{HRu}_5\text{C}(\text{CO})_{13}(\text{C}_5\text{H}_4\text{N})$ (XR4) consisted of two isomers, a result not predicted by spectroscopy. Interestingly, these isomers were characterised in one crystal in a 3:1 ratio. The overall molecular

geometry of all five clusters characterised will be discussed, and then compared to similar structures described in the literature. From consideration of the structural results a mechanism is proposed for the reaction pathway. Preliminary results of this reaction have already been published.[177]



Scheme 2.3/1.

2.3.2 Overall description of the molecular structures.

The molecular structures of all the products identified from the reaction of pyridine with $\text{Ru}_5\text{C(CO)}_{15}$ (1a) are illustrated in Figures 2.3/1-3.

In both isomers of $\text{HRu}_5\text{C(CO)}_{14}(\text{C}_5\text{H}_4\text{N})$ (XR1) and (XR2), and in the disubstituted cluster $\text{HRu}_5\text{C(CO)}_{13}(\text{C}_5\text{H}_4\text{N})(\text{C}_5\text{H}_5\text{N})$ (XR3), the metal core has opened out to give a wingtip bridged butterfly arrangement (Figures 2.3/1 and 2.3/2 respectively), whereas both Isomer A and B of $\text{HRu}_5\text{C(CO)}_{13}(\text{C}_5\text{H}_4\text{N})$ (XR4) have maintained the square pyramidal geometry of the precursor (Figure 2.3/3). The wingtip atoms of the butterfly unit in (XR1), (XR2), and (XR3) are bridged by the fifth ruthenium Ru(5), which is connected to the hinge atom Ru(4) via a bridging pyridyl ligand, which results from an orthometallation reaction. In these three structures the hydride bridges the hinge bond Ru(1)-Ru(4); the hydride ligand in both isomers of (XR4) lies along an axial bond of the square pyramid.

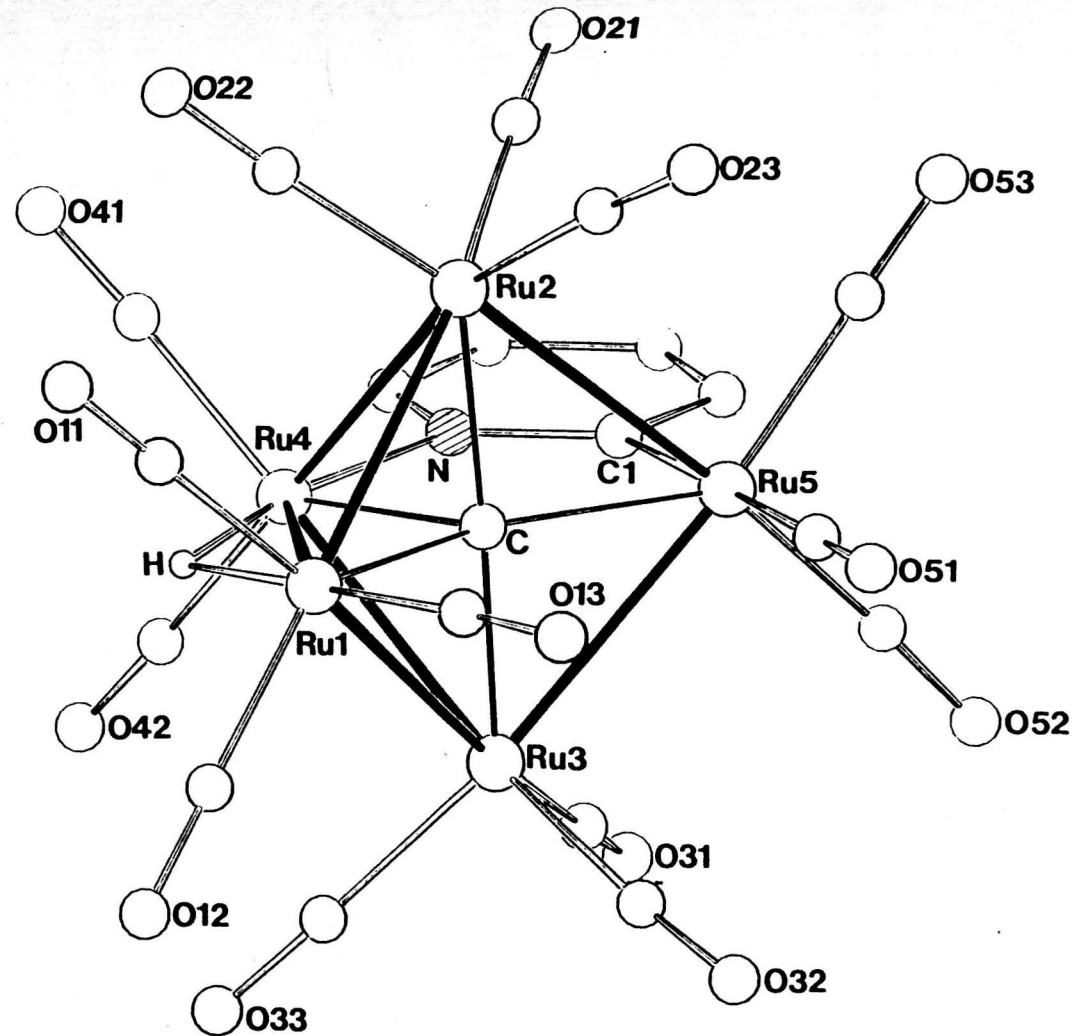
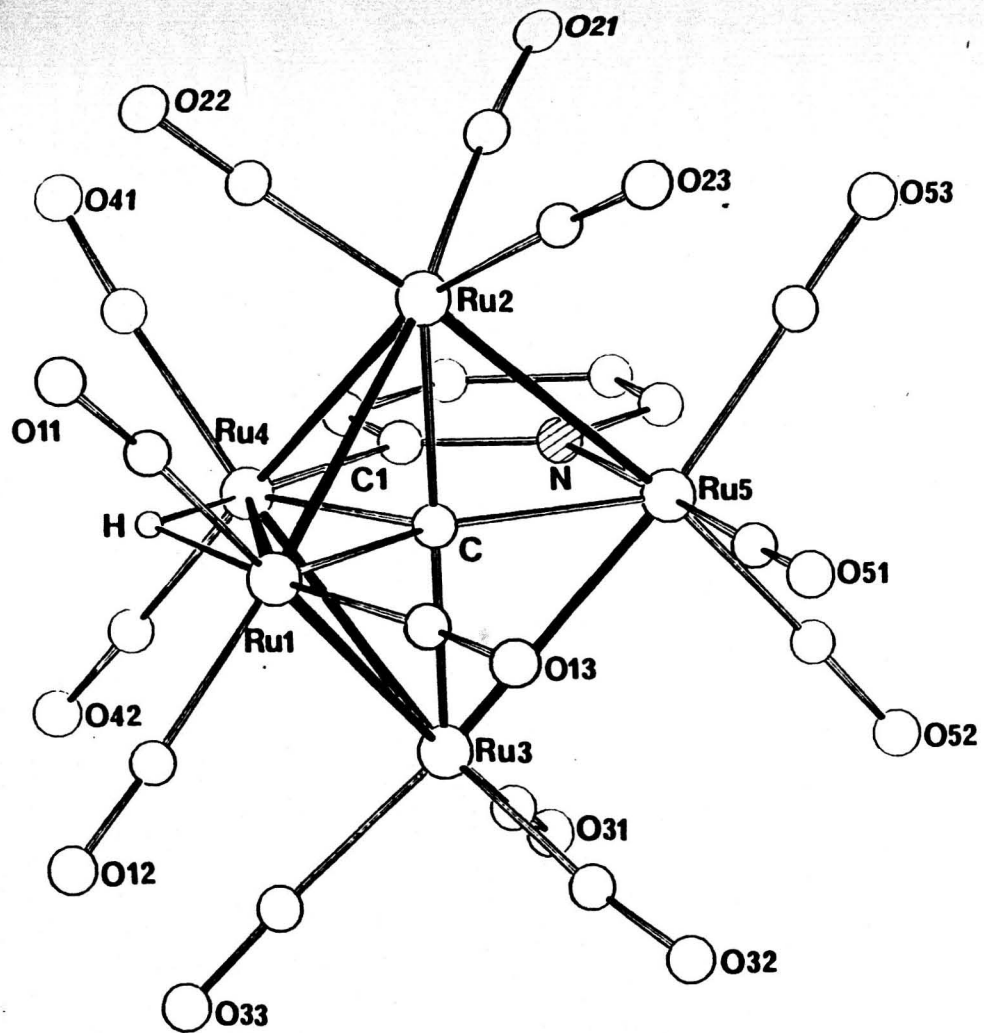


Figure 2.3/1 The molecular structure of $\text{HRu}_5\text{C}(\text{CO})_{14}(\text{C}_5\text{H}_4\text{N})$ Isomer A (XR1) and Isomer B (XR2).

Only the O-atoms of the carbonyl ligands have been labelled for clarity.

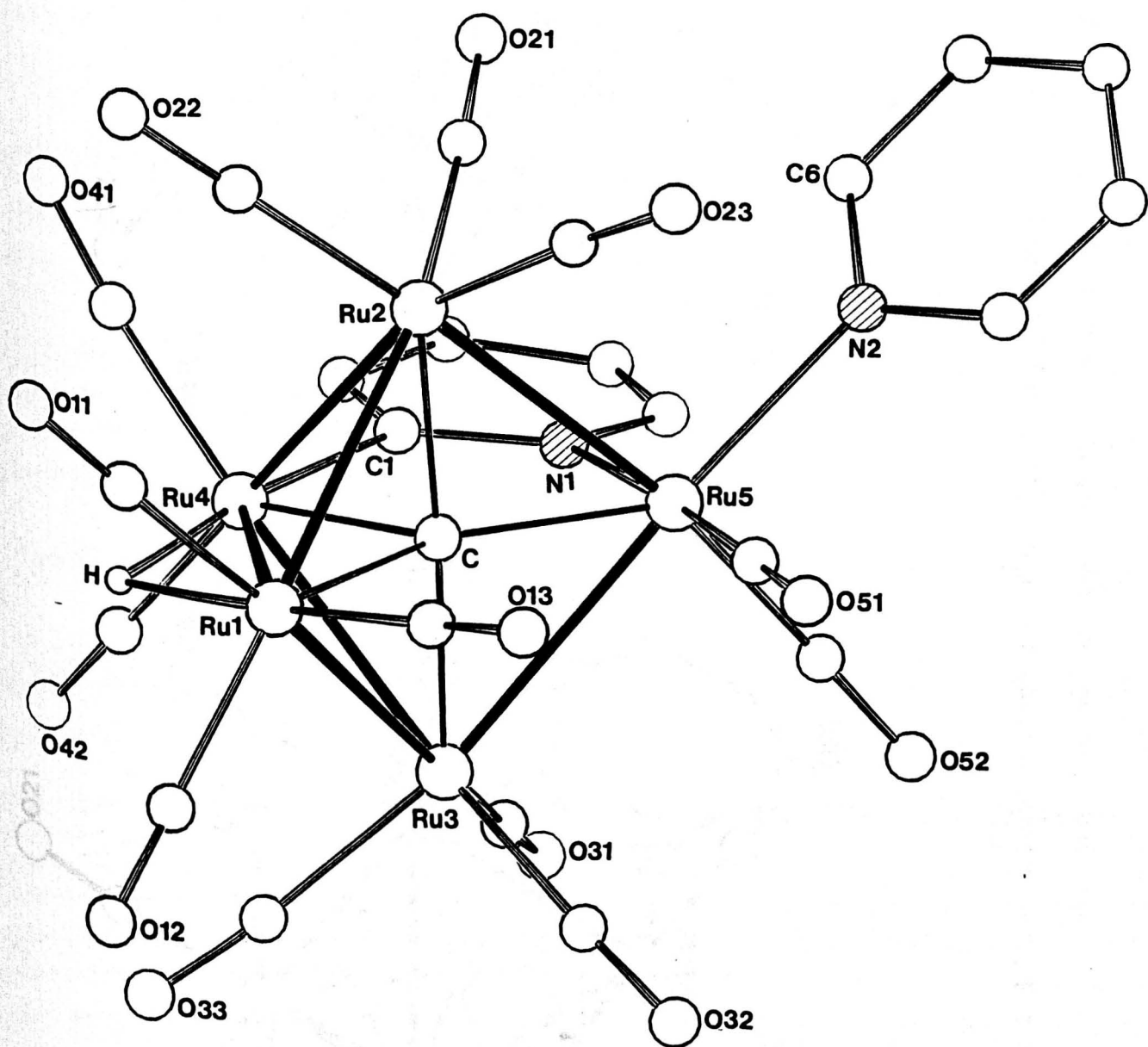


Figure 2.3/2 The molecular structure of $\text{HRu}_5\text{C}(\text{CO})_{13}(\text{C}_5\text{H}_4\text{N})(\text{C}_5\text{H}_5)$ (XR3).
 Only the O-atoms of the carbonyl ligands have been labelled
 for clarity.

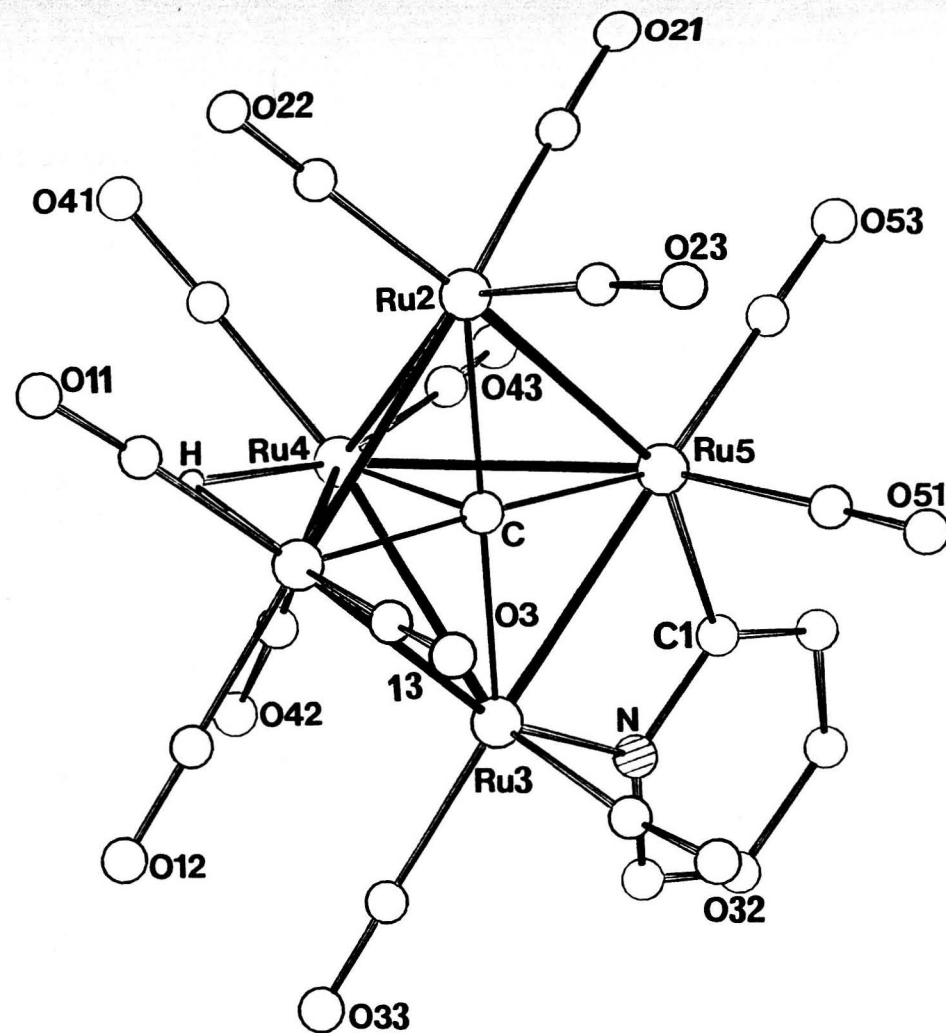
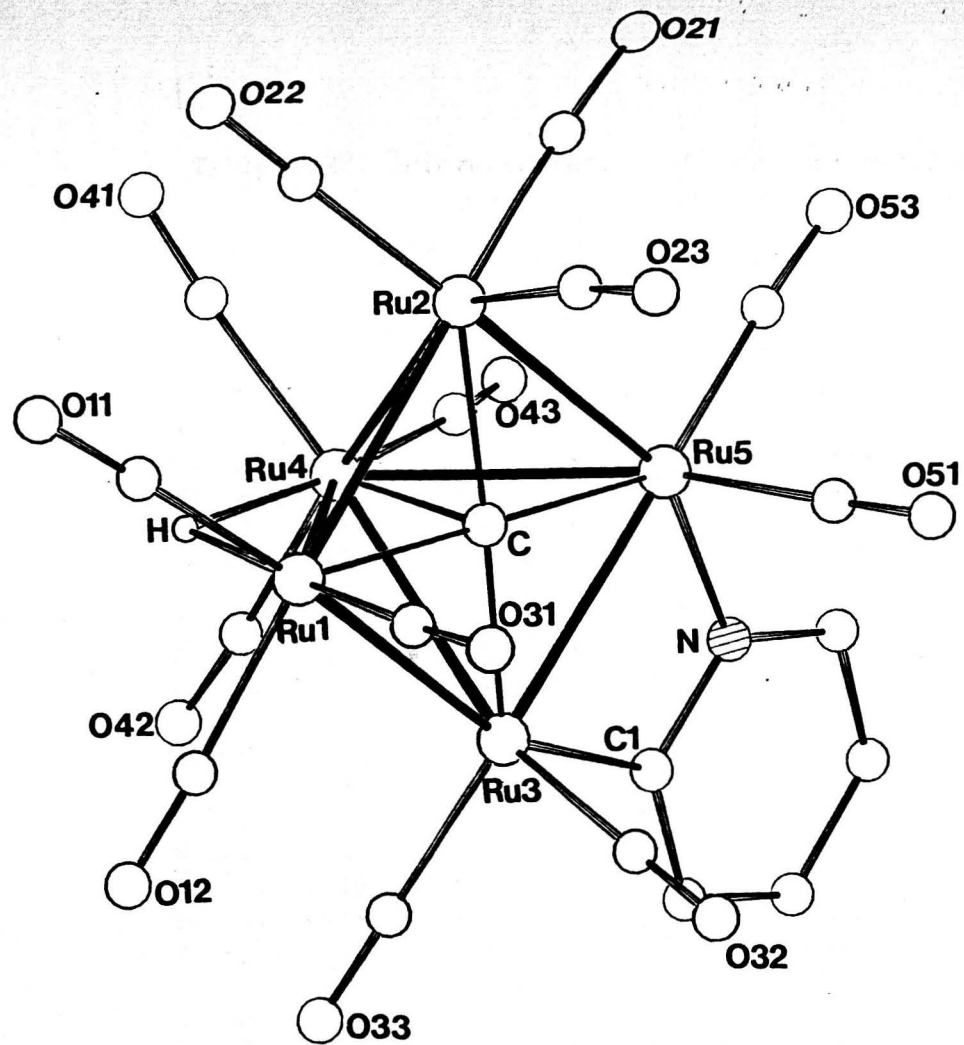


Figure 2.3/3 The molecular structure of $\text{HRu}_5\text{C}(\text{CO})_{13}(\text{C}_5\text{H}_4\text{N})$ Isomer A and Isomer B (XR4).

Only the O-atoms of the carbonyl ligands have been labelled for clarity.

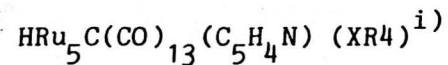
Table 2.3/1 Bridge-butterfly structures; metal-metal bond lengths (Å).

HRu ₅ C(CO) ₁₃ (X) [X=CO (XR1) Isomer A, (XR2) Isomer B, or Py (XR3)]								
	(XR1)		(XR2) ^(a)				(XR3)	
		Mean ^(b)	Molecule 1	Molecule 2	Ave. ^(c)	Mean ^(b)		Mean ^(b)
<u>HINGE-TIP</u>								
Ru(1)-Ru(2)	2.877(1)	2.880	2.853(2)	2.866(1)	2.860	2.859	2.870(1)	2.873
Ru(1)-Ru(3)	2.882(1)		2.864(1)	2.853(1)	2.859		2.876(1)	
Ru(2)-Ru(4)	2.833(1)	2.828	2.824(2)	2.814(2)	2.819	2.814	2.807(1)	2.813
Ru(3)-Ru(4)	2.823(1)		2.803(1)	2.815(1)	2.809		2.818(1)	
<u>TIP-BRIDGE</u>								
Ru(2)-Ru(5)	2.876(1)	2.876	2.894(2)	2.899(2)	2.897	2.898	2.903(1)	2.889
Ru(3)-Ru(5)	2.876(1)		2.899(1)	2.898(1)	2.899		2.875(1)	
<u>HINGE</u>								
Ru(1)-Ru(4)	2.895(1)		2.830(1)	2.838(2)	2.834	2.834	2.886(1)	
<u>NON-BONDING</u>								
Ru(1)...Ru(5)	4.055		4.050	4.046	4.048		4.010	
Ru(2)...Ru(3)	3.944		3.949	3.953	3.951		3.972	
Ru(4)...Ru(5)	3.572		3.593	3.599	3.596		3.575	

Notes

- (a) Isomer B (XR2), consist of 2 independent molecules in the asymmetric unit.
 (b) Mean values, taken for similar bond distances.
 (c) Average bond lengths for the 2 independent molecules of Isomer B₀(XR2).
 (d) Standard deviations on all metal-metal bond distances is 0.001 Å.

Table 2.3/2 Square pyramids; metal-metal bond lengths (Å).



BASAL-BASAL

	(XR4a)	(XR4a/b)	Mean	
Ru(1)-Ru(2)	2.864(1)	2.888(1)	2.876	
Ru(1)-Ru(3)	2.904(1)	2.870(1)	2.888	2.874 ⁱⁱ⁾
Ru(2)-Ru(5)	2.846(1)	2.867(1)	2.857	
Ru(3)-Ru(5)	2.747(1)	2.725(1)	2.736	

BASAL-APICAL

Ru(1)-Ru(4)	2.892(1)	2.875(1)	2.884	
Ru(2)-Ru(4)	2.811(1)	2.830(1)	2.821	
Ru(3)-Ru(4)	2.863(1)	2.875(1)	2.869	2.862 ⁱⁱ⁾
Ru(5)-Ru(4)	2.894(1)	2.898(1)	2.896	

DIAGONAL

Ru(1).Ru(5)	4.02	4.02	4.02	4.01 ⁱⁱⁱ⁾
Ru(2).Ru(3)	4.01	4.00	4.01	

Notes

- i) (XR4) consists of two independent molecules in the asymmetric unit, the second molecule is a mixture of two isomers. All bond lengths this molecule represent averages between Isomers A and B. These isomers differ only in the orientation of the bridging pyridine ligand.
- ii) Mean value of three similar basal-basal or basal-apical bonds.
- iii) Mean value for non-bonding diagonal lengths.

The type of isomerism identified in these compounds results from two different orientations of the bridging pyridyl ligand (Figures 2.3/1 and 2.3/3) and is a new type of isomerism not previously confirmed by X-ray structural analysis. In $\text{HRu}_5\text{C}(\text{CO})_{14}(\text{C}_5\text{H}_4\text{N})$ the nitrogen atom coordinates to the bridging ruthenium Ru(5) in Isomer A (XR1) but to one of the hinge ruthenium atoms Ru(4) in Isomer B (XR2) (Figure 2.3/1). For the second isomeric pair, Isomer A and B of $\text{HRu}_5\text{C}(\text{CO})_{13}(\text{C}_5\text{H}_4\text{N})$ of (XR4), it is the orientation of the pyridyl ligand relative to the μ_2 -hydride which differs. In both these isomers the hydride ligand bridges an axial edge on the far-side of the pyramid from the pyridyl ligand, with the nitrogen atom lying either 'trans' in Isomer A or 'cis' in Isomer B to this hydride (Figure 2.3/3).

Essential bond lengths for the bridged butterflies (XR1), (XR2), and (XR3) are presented in Table 2.3/1, with the bond lengths for the square pyramidal isomers of (XR4) in Table 2.3/2. The Ru-Ru bond lengths for all three bridged butterfly structures are comparable, lying in the range 2.823(1)-2.895(1) Å for (XR1), 2.803(1)-2.899(1) Å for (XR2) and 2.807(1)-2.903(1) Å for (XR3) (Table 2.3/1). The two M(hinge)-M(bridge) non-bonding distances might be expected to be similar, but the presence of the μ_2 -pyridyl ligand causes marked shortening and in all three clusters the Ru(4)...Ru(5) distance is ca. 0.05 Å shorter than Ru(1)...Ru(5) (Table 2.3/1). Table 2.3/2 compares the M-M bond lengths for the two molecules in the asymmetric unit of $\text{HRu}_5\text{C}(\text{CO})_{13}(\text{C}_5\text{H}_4\text{N})$ (XR4) and shows a wider range of Ru-Ru bond lengths [2.725(1)-2.904(1) Å] than found for the three bridged butterflies discussed above. The diagonal bond lengths for the square pyramidal cluster isomers in (XR4) are all comparable (Table 2.3/2).

In Isomer A of $\text{HRu}_5\text{C}(\text{CO})_{14}(\text{C}_5\text{H}_4\text{N})$ (XR1) the C-atom of the pyridyl ligand is bonded to one of the metal atoms of the hinge bond [$\text{Ru}(4)\text{-C}(1)$ 2.080(5) Å] with the N-atom attached to the bridging metal atom Ru(5) [$\text{Ru}(5)\text{-N}$ 2.169(4) Å]. The site of the C- and N-atoms are reversed in the two independent molecules in the asymmetric unit of the second isomer of $\text{HRu}_5\text{C}(\text{CO})_{14}(\text{C}_5\text{H}_4\text{N})$ (XR2) [mean values for the two molecules in the asymmetric unit, which are chemically equivalent, are given]; $\text{Ru}(4)\text{-N}$ 2.135(12) Å and $\text{Ru}(5)\text{-C}(1)$ 2.112(11) Å]. The μ_2 -pyridyl in the disubstituted cluster $\text{HRu}_5\text{C}(\text{CO})_{13}(\text{C}_5\text{H}_4\text{N})(\text{C}_5\text{H}_5\text{N})$ (XR3) adopts the same mode of bonding as seen for Isomer A (XR1) and has very similar metal-ligand bond distances $\text{Ru}(4)\text{-C}(1)$ 2.083(8) Å and $\text{Ru}(5)\text{-N}(1)$ 2.168(6) Å. In (XR1) and (XR3) the Ru-C bonding distance is shorter than the Ru-N distance, whereas for the second isomer of $\text{HRu}_5\text{C}(\text{CO})_{14}(\text{C}_5\text{H}_4\text{N})$ (XR2), where relatively poor data results in high e.s.d.'s, these two bond lengths are not significantly different. The second pyridyl ligand in (XR3) bonds terminally through the nitrogen atom $\text{Ru}(5)\text{-N}(2)$ 2.212(7) Å, a distance which is ca. 0.1 Å longer than any of the Ru-N distances for the μ_2 -pyridyl ligand discussed above. This is perhaps surprising as a terminally bonded pyridyl ligand might have been expected to have a shorter M-N bond length than a μ_2 -pyridyl M-N bond length.

The pyridyl ligand lies along an axial edge in both isomers of $\text{HRu}_5\text{C}(\text{CO})_{13}(\text{C}_5\text{H}_4\text{N})$ (XR4), lying 'trans' in Isomer A and 'cis' in Isomer B with respect to the μ_2 -H ligand (Figure 2.3/2). Values for molecule (a) in the asymmetric unit refer to Isomer A, whereas molecule (b) is a 50/50 mixture of Isomer A and B. Due to the large e.s.d.'s in this determination the difference between the metal-carbon and metal-nitrogen bond lengths, $\text{Ru}(3a)\text{-C}(1a)$ 2.100(11) Å, $\text{Ru}(5a)\text{-N}(a)$ 2.117(9) Å respectively, is not significant. Not surprisingly, there is no significant difference evident for these bonds in the second "molecule" of the asymmetric unit which

contains a 50/50 mixture of both isomers, Ru(3b)-C(1b)/N(b) 2.083(10) Å and Ru(5b)-N(b)/C1b) 2.102(10) Å.

The dihedral angle between the 'wings' of the butterflies [Ru(1)-Ru(2)-Ru(4) and Ru(1)-Ru(3)-Ru(4)] in all 3 bridged butterflies were found to be very similar, 106.6° for (XR1), 107.0° (mean value) for (XR2), and 108.4° for (XR3). This might have been expected for the isomeric pair (XR1) and (XR2) and its observation for (XR3) is further evidence for the similarity of all three structures. Table 2.3/3 compares the M-C(carbide) distances for the three bridged butterfly clusters and shows that a similar trend is adhered to by all three.

Table 2.3/3 M-C(carbide) distances for (XR1), (XR2), and (XR3) (Å).

	(XR1)	(XR2) ⁱ⁾	(XR3)
Ru(1)-C	2.102(5)	2.085(14)	2.113(8)
Ru(2)-C	1.975(5)	1.982(12)	1.978(8)
Ru(3)-C	1.969(5)	1.970(13)	1.995(8)
Ru(4)-C	2.030(5)	2.034(14)	2.023(7)
Ru(5)-C	2.089(5)	2.091(16)	2.050(8)

i) Mean value of the 2 independent molecules in the asymmetric unit.

All five structures retain the interstitial carbido-atom, an indication of the importance this central atom plays in the reaction pathway.

The distribution of the carbonyl ligands is the same in both isomers of HRu₅C(CO)₁₄(C₅H₄N) (XR1) and (XR2). The disubstituted product

HRu₅C(CO)₁₃(C₅H₄N)(C₅H₅) (XR3) has a similar coordination sphere except that one of the carbonyl groups on the bridging ruthenium atom is replaced

by a terminal pyridyl ligand (Figure 2.3/2). The distribution of CO-groups in both isomers of (XR4) is the same, a fact that allows the two isomers to

occupy the same site in the unit cell in a 50:50 ratio. For all five structures, the M-(carbonyl) bond lengths lie in the range [M-C(carbonyl)

1.849(19)-1.972(14) Å and C-O(carbonyl) 1.12(3)-1.178(18) Å] and all M-C-O bond angles are in the range [M-C-O 174.2(8)-179.7(5)°], values

deviating from 180° being normal for cluster compounds.[178] These values are listed in Appendix A.

The shortest intramolecular distance in (XR1) is between the μ_2 -hydride ligand and the carbido-atom [H...C 2.41 Å], and in (XR2) it is between the μ_2 -hydride ligand and a neighbouring carbonyl group [Ha...C(11a) 2.47 Å]. In contrast one of the H-atoms of the terminal pyridyl ligand is the shortest intramolecular distance in (XR3) [H(6)...O(21) 2.48 Å]. For the square pyramidal cluster (XR4) the shortest intramolecular contact is between the hydride ligand and a neighbouring carbonyl group [Ha...C(41) 2.49 Å].

2.3.3 Structural comparison of the bridged butterflies.

To interpret the effect that different ligand spheres have on the bridged butterfly metal framework, $\text{HRu}_5\text{C}(\text{CO})_{14}(\text{C}_5\text{H}_4\text{N})$ Isomer A (XR1) and Isomer B (XR2), and the disubstituted cluster $\text{HRu}_5\text{C}(\text{CO})_{13}(\text{C}_5\text{H}_4\text{N})(\text{C}_5\text{H}_5\text{N})$ (XR3) will be compared to thirteen clusters with related cores (Table 2.3/4). The M-M bond lengths of the reported structures are listed in Table 2.3/5 and these are classified as 'hinge', 'hinge-wingtip', and 'wingtip-to-bridge' bonds. The clusters have been grouped in Table 2.3/4 according to three structural features described below and are illustrated in Figure 2.3/4. The effect of these three factors on M-M bond lengths will be discussed.

a) The effect of a terminal ligand on the bridging metal atom.

The simplest examples of bridged butterflies are the derivatives of the type $\text{M}_5\text{C}(\text{CO})_{15}\text{L}$, where L is a terminal ligand coordinated to the bridging metal atom. (In Figure 2.3/4 L is denoted by R for a ligand that lies trans to a carbonyl ligand and R' when it lies trans to an M-M bond.) These are the osmium derivative $\text{Os}_5(\text{CO})_{16}[\text{L}=\text{CO}]$ (2), [23] the acetonitrile complex $\text{Ru}_5\text{C}(\text{CO})_{15}(\text{MeCN})$ (3), [85] the iodide anion $[\text{Os}_5\text{C}(\text{CO})_{15}\text{I}]^-$ (4), [22] and the diphenylphosphine (dppe) cluster $\text{Os}_5\text{C}(\text{CO})_{15}(\text{dppe})$ (5). [107] Despite the differences in L a similar pattern for the M-M bond lengths can be seen for all four derivatives (Table 2.3/5), with the hinge bonds [M(1)-M(4)] being

Table 2.3/4 Bridged butterfly clusters.

Cluster	Categories	References
$\text{Os}_5\text{C}(\text{CO})_{16}$ (2)	a	23
$\text{Ru}_5\text{C}(\text{CO})_{15}(\text{MeCN})$ (3)	a	85
$[\text{Os}_5\text{C}(\text{CO})_{15}\text{I}]^-$ (4)	a	22
$\text{Os}_5\text{C}(\text{CO})_{15}(\text{dppe})$ (5)	a	107
$\text{Ru}_5\text{C}(\text{CO})_{15}\text{Cl}(\text{AuPPh}_3)$ (36)	a, b	109
$\text{HRu}_5\text{C}(\text{CO})_{13}(\text{PPh}_3)(\text{SEt})$ (37)	a, b, c	90
$\text{HOs}_5\text{C}(\text{CO})_{13}\{\text{OP}(\text{OMe})_2\}\{\text{P}(\text{OMe})_3\}$ (38)	a, b, c	108
$\text{Ru}_5\text{C}(\text{CO})_{13}(\text{C}_5\text{H}_5)(\text{AuPPh}_3)$ (39)	a, b	110
$\text{HOs}_5\text{C}(\text{CO})_{14}(\text{C}_5\text{H}_4\text{N})$ (40)	b, c	104
$\text{HOs}_5\text{C}(\text{CO})_{14}(\text{CO}_2\text{Et})$ (41)	b, c	105, 106
$\text{HRu}_5\text{C}(\text{CO})_{14}(\text{SEt})$ (42)	b, c	90
$\text{Ru}_5\text{C}(\text{CO})_{14}(\text{MeCO})(\text{AuPPh}_3)$ (43)	b, c	110
$\text{Ru}_5\text{C}(\text{CO})_{14}\text{Br}(\text{AuPPh}_3)$ (44)	b, c	109

The atomic numbering of all reported complexes in this section have been reassigned for ease of comparison.

Categories: a) Additional ligand on bridging metal atoms.
 b) Bridging group on hinge M-M bond.
 c) Bridging group across non-bonding metallic contact.

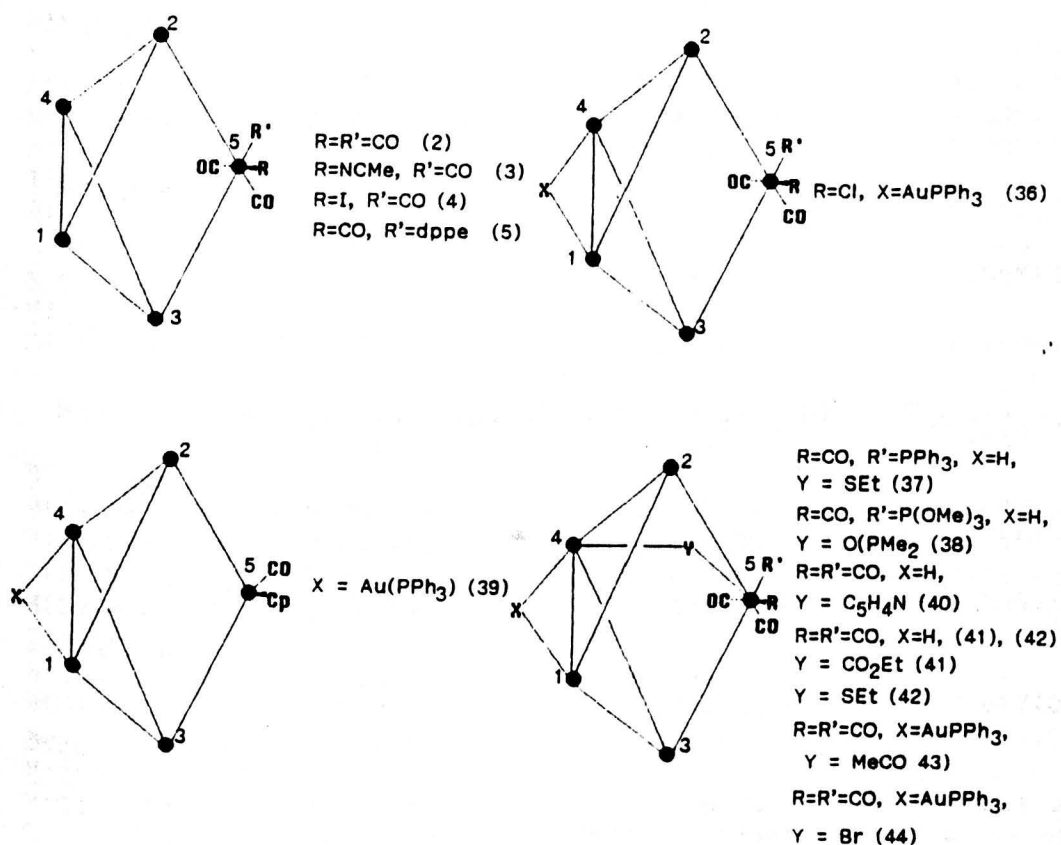


Figure 2.3/4 Clusters with bridged butterfly M-cores.

Table 2.3/5 Bond lengths (A) for the clusters listed in Table 2.3/4.

M-M	Os ₅ C(CO) ₁₆ ⁱ (2)	Ru ₅ C(CO) ₁₅ (L) (3)	[Os ₅ C(CO) ₁₅ I] ⁻ (4)	Os ₅ C(CO) ₁₅ (L) (5)
<u>Hinge-tip</u>				
M(1)-M(2)	2.901(2)	2.873(3)	2.921(1)	2.909(1)
M(1)-M(3)	2.194(2)	2.886(3)	2.903(1)	2.897(1)
M(2)-M(4)	2.913(2)	2.887(3)	2.896(1)	2.897(1)
M(3)-M(4)	2.914(1)	2.888(3)	2.899(1)	2.884(1)
<u>Tip-bridge</u>				
M(2)-M(5)	2.916(1)	2.886(3)	2.934(1)	2.947(1)
M(3)-M(5)	2.917(2)	2.873(3)	2.933(1)	2.996(1)
<u>Mean</u>	2.913(2)	2.882(3)	2.914(1)	2.922(1)
<u>Hinge</u>				
M(1)-M(4)	2.752(1)	2.720(3)	2.748(1)	2.761(1)

M-M	HRu ₅ C(CO) ₁₃ (L)(L') (37)	HOs ₅ C(CO) ₁₃ (L)(L') ⁱ (38)	HOs ₅ C(CO) ₁₄ (Py) (40)
<u>Hinge-Tip</u>			
M(1)-M(2)	2.843(1)	2.870(2)	2.896(1)
M(1)-M(3)	2.830(1)	2.876(2)	2.902(1)
M(2)-M(4)	2.818(1)	2.884(2)	2.860(1)
M(3)-M(4)	2.821(1)	2.874(2)	2.853(1)
<u>Tip-bridge</u>			
M(2)-M(5)	2.921(1)	2.965(2)	2.912(1)
M(3)-M(5)	2.972(1)	2.943(2)	2.908(1)
<u>Mean</u>	2.868(1)	2.901(2)	2.889(1)
<u>Hinge</u>			
M(1)-M(4)	2.864(1)	2.898(2)	2.927(1)

M-M	HOs ₅ C(CO) ₁₄ (CO ₂ Et) (41)	HRu ₅ C(CO) ₁₄ (SEt) (42)	Ru ₅ C(CO) ₁₅ {X} ⁱ (36)
<u>Hinge-tip</u>			
M(1)-M(2)	2.889(1)	2.852(1)	2.928(4)
M(1)-M(3)	2.885(1)	2.858(1)	2.820(4)
M(2)-M(4)	2.857(1)	2.851(1)	2.847(5)
M(3)-M(4)	2.865(1)	2.813(1)	2.826(4)
<u>Tip-bridge</u>			
M(2)-M(5)	2.916(1)	2.916(1)	2.815(4)
M(3)-M(5)	2.931(1)	2.902(1)	2.903(4)
<u>Mean</u>	2.891(1)	2.865(1)	2.857(5)
<u>Hinge</u>			
M(1)-M(4)	2.921(1)	2.853(1)	2.968(4)

M-M	Ru ₅ C(CO) ₁₃ (C ₅ H ₅){X} (39)	Ru ₅ C(CO) ₁₄ (MeCO){X} (43)	Ru ₅ C(CO) ₁₄ Br{X} (44)
<u>Hinge-tip</u>			
M(1)-M(2)	2.880(1)	2.867(3)	2.849(3)
M(1)-M(3)	2.844(1)	2.879(3)	2.866(3)
M(2)-M(4)	2.839(1)	2.817(3)	2.826(3)
M(3)-M(4)	2.867(1)	2.822(3)	2.829(3)
<u>Tip-bridge</u>			
M(2)-M(5)	2.905(1)	2.881(3)	2.892(3)
M(3)-M(5)	2.890(1)	2.880(3)	2.877(3)
<u>Mean</u>	2.871(1)	2.858(3)	2.857(3)
<u>Hinge</u>			
M(1)-M(4)	2.894(1)	2.989(3)	2.951(3)

L = MeCN (3), dppe (5), PPh₃ (37), OP(OMe)₂ (38); L' = SEt (37), P(OMe)₃ (38); X = Au(PPh₃); i) Mean of 2 molecules in asymmetric unit.

ca. 0.2 Å shorter [2.752(1) (2), 2.720(3) (3), 2.748(1) (4), and 2.761(1) Å (5)] than the mean of the remaining 6 M-M bonds [2.913(1) (2), 2.882(1) (3), 2.914(1) (4) and 2.922(1) Å (5)].

The ligand orientation at the bridging metal atom in these complexes is of importance, since it causes variation of M-M bond lengths in the framework. The terminal ligand L can either lie cis or trans to an M-M bond at the bridging atom, a factor that can be related to their π -acid character. If contact to the carbide atom is ignored, the bridging metal atom has a distorted octahedral environment (Figure 2.3/4). In both clusters (3) and (4) the ligand L (MeCN and I⁻ respectively) lies trans to a carbonyl group, whereas in (5) the diphenylphosphine ligand is trans to an Os-Os bond (Figure 2.3/4). The result of this is that M(wingtip)-M(bridge) distances in (3) and (4), are equal within experimental error, whereas, in contrast, the diphenylphosphine cluster (5) has the M(wingtip)-M(bridge) distance trans to it 0.049 Å longer ($>35\sigma$), at 2.996(1) Å, than the other (2.947(1) Å) (Table 2.3/5), indicating a trans influence for the phosphorus ligand.[179] The site preference arises from the strong π -acid nature of the dppe ligand, which renders a site trans to a carbonyl ligand unfavourable.

The hinge-bridged clusters (36), (37), and (38) also have an additional bridging ligand on the hinge bond (Figure 2.3/4). Significantly, only the complex of the chloro-ligand (36), which cannot act as a π -acceptor, has this ligand lying trans to a carbonyl. Both the derivatives (37) and (38), which contain strong π -acceptors, have phosphorus ligands trans to one of the metallic bonds (Figure 2.3/4). As the cyclopentadiene ligand in the derivative (39) replaces all three of the facial-type carbonyls, this cluster is not considered in this category. It is of significance that in the present study this pattern of π -acceptor ligands lying trans to a metallic bond in preference to one of the carbonyl ligands is also seen for

$\text{HRu}_5\text{C}(\text{CO})_{13}(\text{C}_5\text{H}_4\text{N})(\text{C}_5\text{H}_5\text{N})$ (XR3), which has a terminally coordinated pyridine ligand on the bridging ruthenium atom (Figure 2.3/3) and this is therefore consistent with pyridine having some π -acceptor character.

b) The effect of a bridging ligand (on the hinge bond).

Only 1e-donor ligands such as H and AuPR_3 have been found bridging the hinge bond of a butterfly metal core framework (clusters (36)-(44) -Figure 2.2/4). A μ_2 -hydride is known to cause M-M bond lengthening and in clusters is often cited as evidence for the presence of this ligand (which can not readily be located directly by X-ray structural analysis). [180-182] For example in the osmium derivative (40) the hydride-bridged hinge bond is 0.038 Å ($>27\sigma$) longer than the mean (2.889(1) Å) of the remaining six metallic bonds (Table 2.3/5). In the carboxy-derivative (41) the μ_2 -H bridged hinge bond [M(1)-M(4) 2.921(1) Å] is 0.01 Å ($>7\sigma$) shorter than one of the M(wingtip)-M(bridge) bonds [M(3)-M(5) 2.931(1) Å]. For the bridging thiol complexes (37) and (42), and in the phosphite derivative (38), the mean of the two M(wingtip)-M(bridge) bonds [2.947(1) (37), 2.954(1) (38) and 2.909(1) Å (42)] is longer than the μ_2 -hydride bridged hinge bond [0.083 for (37), 0.061 for (38), and 0.056 Å for (42)].

In the present work Isomer A $\text{HRu}_5\text{C}(\text{CO})_{14}(\text{C}_5\text{H}_4\text{N})$ (XR1), like its osmium analogue (40), has the H-ligand bridged hinge bond 0.034 Å ($>24\sigma$) longer than the mean of the remaining six M-M bonds (2.861(1) Å) (Table 2.3/1). The hinge bond in its isomer (XR2), which is also H-bridged, is somewhat incongruous, being one of the shortest metal bonds in the structure Ru(1)-Ru(4) 2.834(2) Å (Table 2.3/1). It is 0.061 Å ($>27\sigma$) shorter than the comparative bond in isomer (XR1) (2.895(1) Å) (Table 2.3/1). Finally, in the disubstituted cluster (XR3) the H-bridged hinge bond is 0.017 Å ($>12\sigma$) longer than all M-M bonds except one of the M(wingtip)-M(bridge) bonds (Ru(2)-Ru(5) 2.903(1) Å) (Table 2.3/1).

In the Au(PPh₃) bridged compounds (36), (43), and (44) the hinge bond is longer [by 0.11 (36), 0.13 (43), and 0.09 Å (43) (Table 2.3/5)] than the mean of the other six bonds. In contrast in the unusual cyclopentadienyl derivative (39), the AuPPh₃ bridged hinge bond [M(1)-M(4) 2.894(1) Å] is longer than all other bonds except both of the M(wingtip)-M(bridge) bonds [mean 2.898(1) Å] to which it is comparable. In μ₂-AuPPh₃ clusters (36), (43) and (44), the hinge bond is significantly longer than the H-bridged bond in the hydrido compounds, which may be a consequence of the steric bulk of the gold triphenylphosphine group.

Table 2.3/6 Ru-Au bond lengths (Å).

	(36) ⁱ	(39)	(43)	(44)
Ru(1)-Au	2.769(4)	2.750(1)	2.764(3)	2.850(2)
Ru(4)-Au	2.826(3)	2.780(1)	2.721(3)	2.633(2)

i) Mean of the 2 independent molecules in the asymmetric unit.

Table 2.3/6 shows the ruthenium-gold distances for the gold-bridged derivatives. In the cyclopentadienyl complex (39) the Ru-Au bonds are comparable in length, whereas for the other three clusters a marked asymmetry is evident. Comparisons of this type are not possible for hydrido clusters where H-atom sites are often inferred by indirect methods.

c) The effect of a bridging ligand spanning two non-bonding metal atoms.

The third and possibly most significant factor effecting metallic bond lengths in these bridged butterflies is the presence of a bridging group or ligand across one of the non-bonding M-M distances. These metal atoms can either be linked by one atom of the bridging group [clusters (37), (42) and (44)] or two [clusters (38), (40), (41), and (43)].

Figure 2.3/7 is a view on to the equatorial plane of the bridged butterfly metal core. When no bridging ligand is present [(2), (3), (4), (5), (36), and (39)], the two hinge-bridging atom M-M distances [M(1)-M(5) and M(4)-M(5)] are virtually identical (Table 2.3/7). The presence of a

Table 2.3/7 The effect of a bridging group on M(hinge)-M(bridge).

No bridging groups.

	(2) ⁱ	(3)	(4)	(5)	(36) ⁱ	(39)
M(1)-M(5)	3.999	3.967	4.022	4.021	3.900	3.877
M(4)-M(5)	4.029	3.957	4.007	4.064	3.971	3.312
α	139.5(12)	138.3(9)	139.9	135.7(7)	135	134
β	140.5(14)	139.6(9)	138.7	142.8(7)	135.5	139
γ	80.9(9)	82.0(7)	81.4	81.5(5)	89.8	87

One atom spanning M(4)-M(5).

	(37)	(42)	(44)
M(1)-M(5)	4.109	4.132	4.055
M(4)-M(5)	3.438	3.410	3.403
α	112.8(2)	110.2	111.7
β	159.3(3)	162.2	155.7
γ	87.8(2)	87.5	92.5

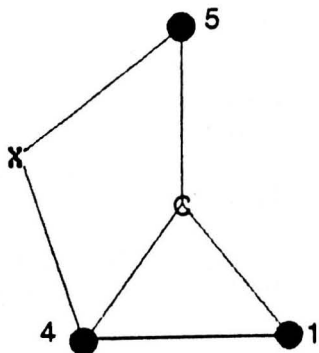
Two atoms spanning M(4)-M(5).

	(38) ⁱ	(4)	(41)	(43)
M(1)-M(5)	4.044	4.080	4.101	4.012
M(4)-M(5)	3.757	3.626	3.604	3.537
α	126.2(10)	120.6(13)	119.0	118
β	148.1(10)	150.2(13)	152.4	148
γ	85.7(6)	89.4(10)	88.5	93

Isomer A (XR1), Isomer B (XR2), and (XR3).

	(XR1)	(XR2) ⁱ	(XR3)
M(1)-M(5)	4.05	4.05	4.01
M(4)-M(5)	3.57	3.60	3.58
α	120.3(2)	121.4(7)	122.7(4)
β	150.8(3)	151.7(8)	148.8(4)
γ	89.0(2)	87.0(2)	88.5(3)

a) Mean of 2 independent molecules in the asymmetric unit.



View on to the equatorial plane
of an arachno-core with 8 SEP.

Figure 2.3/7 View onto equatorial plane.

Table 2.3/8 M-C(Carbide) bond lengths (Å).

M-M	Os ₅ C(CO) ₁₆ (2) ⁱ	Ru ₅ C(CO) ₁₅ (L) (3)	[Os ₅ C(CO) ₁₅ I] ⁻ (4)	Os ₅ C(CO) ₁₅ (L) (5)
<u>M(Wingtip)-C</u>				
M(2)-C	1.95(2)	1.961(17)	1.995(12)	1.99(1)
M(3)-C	2.02(2)	1.968(17)	1.978(12)	1.97(1)
<u>M(Hinge)-C</u>				
M(1)-C	2.13(2)	2.076(18)	2.108(12)	2.14(1)
M(4)-C	2.12(3)	2.068(18)	2.108(12)	2.09(1)
<u>M(Bridge)-C</u>				
M(5)-C	2.16(2)	2.158(18)	2.174(12)	2.20(1)

M-M	Ru ₅ C(CO) ₁₅ {X} (36) ⁱ	HRu ₅ C(CO) ₁₃ (L)(L') (37)	HOs ₅ C(CO) ₁₃ (L)(L') (38) ⁱ
<u>M(Wingtip)-C</u>			
M(2)-C	1.93(3)	2.011(5)	2.009(19)
M(3)-C	1.91(3)	1.979(5)	1.980(19)
<u>M(Hinge)-C</u>			
M(1)-C	2.14(2)	2.091(5)	2.148(19)
M(4)-C	2.08(3)	2.041(5)	2.114(18)
<u>M(Bridge)-C</u>			
M(5)-C	2.14(2)	2.086(5)	2.099(18)
M-M	HOs ₅ C(CO) ₁₃ (C ₅ H ₅){X} (39)	HOs ₅ C(CO) ₁₄ (Py){X} (40)	HOs ₅ (CO) ₁₄ (CO ₂ Et) (41)
<u>M(Wingtip)-C</u>			
M(2)-C	2.001(5)	1.97(3)	
M(3)-C	1.980(5)	2.01(3)	Range:
<u>M(Hinge)-C</u>			
M(1)-C	2.111(6)	2.11(3)	1.959-
M(4)-C	2.115(6)	2.06(3)	2.112(16)
<u>M(Bridge)-C</u>			
M(5)-C	2.023(6)	2.12(3)	

M-M	HRu ₅ C(CO) ₁₄ (SEt) (42)	Ru ₅ C(CO) ₁₄ (MeCO){X} (43)	Ru ₅ C(CO) ₁₄ Br{X} (44)
<u>M(Wingtip)-C</u>			
M(2)-C	1.969(5)	1.906(24)	1.99(1)
M(3)-C	1.990(5)	1.977(18)	1.98(1)
<u>M(Hinge)-C</u>			
M(1)-C	2.075(5)	2.080(18)	2.06(1)
M(4)-C	2.049(5)	2.035(19)	2.02(1)
<u>M(Bridge)-C</u>			
M(5)-C	2.108(5)	2.087(18)	2.09(1)

L = MeCN (3), dppe (5), PPh₃ (37), OP(OMe)₂ (38); L' = SEt (37) P(OMe)₃ (38); X = Au(PPh₃); i) Mean of 2 molecules in asymmetric unit.

bridging group significantly shortens the distance between the non-bonding metal atoms which it spans. This is corroborated by the angles at the central carbido atom. The δ -angle (which subtends to the hinge bond) is, as expected, the smallest angle, the two other angles α and β are unequal with the α -angle on the side of the bridging group markedly reduced as a direct consequence of the presence of this ligand (Table 2.3/7). The difference is heightened when only one atom links the two metal atoms. These trends are also observed in the present work in Isomer A (XR1) and Isomer B (XR2) of $\text{HRu}_5\text{C}(\text{CO})_{14}(\text{C}_5\text{H}_4\text{N})$, and in the disubstituted cluster $\text{HRu}_5\text{C}(\text{CO})_{13}(\text{C}_5\text{H}_4\text{N})(\text{C}_5\text{H}_5\text{N})$ (XR3) (Table 2.3/7).

A trend is also apparent in the M-C(carbide) distances of these structures. In all of the reported compounds described here, the M(wingtip)-carbide distances are the shortest (Table 2.3/8). This trend is also followed by the three structures reported here (XR1), (XR2), and (XR3) (Table 2.3/3).

It is perhaps surprising that this trend is adhered to by all of the complexes, considering the differences in the ligand spheres of the compounds. This suggests that the M-carbide contact is essential to the integrity of the bridged butterfly structure and thus the M-carbide distances tend to remain constant, leaving ligand differences to distort other bond parameters in the structures. Indeed, to date no non-carbido wingtip bridged butterflies have been reported.

2.3.4 Structural comparison for the clusters with square pyramidal cores.

The square pyramidal geometry observed in the isomers of $\text{HRu}_5\text{C}(\text{CO})_{13}(\text{C}_5\text{H}_4\text{N})$ (XR4) is the more commonly found of the two possible metal cores for a 74e species (Table 1.3/1). Figure 2.3/2 illustrates Isomer A and Isomer B of $\text{HRu}_5\text{C}(\text{CO})_{13}(\text{C}_5\text{H}_4\text{N})$ (XR4). Here, these isomers are compared to three clusters which have similar structural features, i.e., a bridging ligand along one of the metal-metal bonds and at least one bridging hydride along one of the metallic edges (Figure 2.3/5).

Table 2.3/9 Square pyramidal clusters.

Cluster	Categories	References
$H_3Ru_5C(CO)_{11}(PPh_2)(PMePh_2)$ (34)	a,b	89
$HRu_5C(CO)_{13}(PPh_2)$ (45)	a,b	88
$HRu_5C(CO)_{12}(PPh_3)(SEt)$ (46)	a,b	90

The atomic numbering of all reported complexes in this section have been reassigned for ease of comparison.

Categories: a) Bridging ligand along one of the M-M bonds.

b) μ_2 -H along an M-M bond.

Figure 2.3/5 Clusters with square pyramidal M-cores.

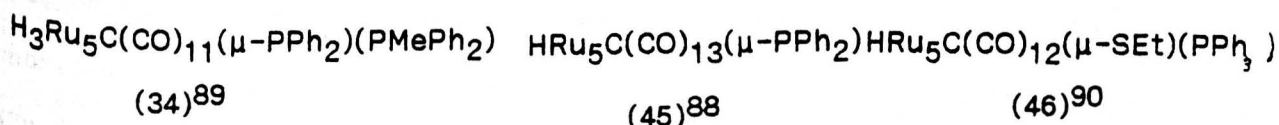
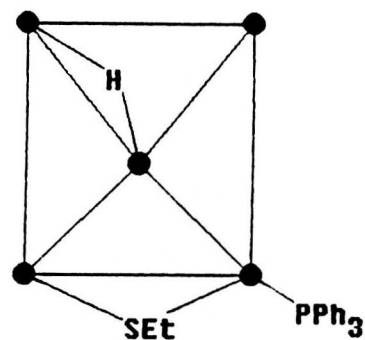
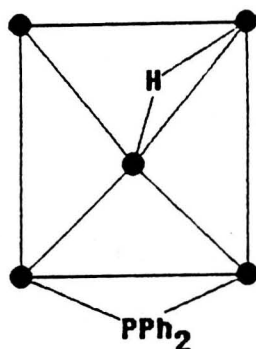
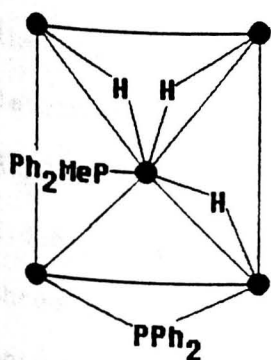


Table 2.3/10 Bond lengths (Å) for square pyramidal clusters.

	(1) ⁱ	(34)	(45)	(46)
Basal-Basal				
M(1)-M(2)	2.832(2)	2.9014(7)	2.878(1)	2.882(1)
M(1)-M(3)	2.851(2)	2.8948(7)	2.873(1)	2.945(1)
M(2)-M(5)	2.802(2)	2.8347(5)	2.886(1)	2.858(1)
M(3)-M(5)	2.819(2)	2.8391(6)	2.721(1)	2.698(1)
Basal-Apical				
M(2)-M(3)	2.837(2)	2.8391(6)	2.866(1)	2.791(1)
M(2)-M(5)	2.846(2)	2.8934(6)	2.786(1)	2.851(1)
M(3)-M(4)	2.859(3)	2.8820(6)	2.882(1)	3.024(1)
M(4)-M(5)	2.879(2)	2.8347(5)	2.944(1)	2.899(1)

a) Mean of 2 molecules in asymmetric unit.

A number of similarities are evident. Firstly, the non-hydrido ligand bridges a basal bond and no example of a bridging group along an axial bond was found, indicating that such a conformation may be unfavourable in these types of structures. Secondly the bridging hydrido-atom in all the monohydride structures spans an axial edge on the far-side of the pyramid from the other bridging ligand. Even in the trisubstituted complex (34) all three hydrides are on axial bonds, strongly indicating that in these types of compounds hydrides bridge axial bonds in preference to basal bonds.

Table 2.3/10 shows the M-M bonds lengths for the reported structures and the parent cluster $\text{Ru}_5\text{C}(\text{CO})_{15}$. Since there is such a variation in bond length, only general conclusions can be drawn. In the parent carbide $\text{Ru}_5\text{C}(\text{CO})_{15}$ (1a) the average of the four axial bonds is slightly shorter, at $2.826(2) \text{ \AA}$, than the average of the basal bonds $2.855(2) \text{ \AA}$. [85] In all three reported ligand bridged structures (34), (45), and (46) the ligand bridged basal bond is markedly shortened with respect to the three unbridged basal bonds (Table 2.3/10). Similarly in both isomers of $\text{HRu}_5\text{C}(\text{CO})_{13}(\text{C}_5\text{H}_4\text{N})$ (XR4), the pyridyl bridge basal bond [Ru(3)-Ru(5) 2.736 \AA , mean value] is significantly shorter than the mean of the remaining three basal bonds (Table 2.3/2). In both the phosphido cluster (45) and thiol cluster (46), as the hydrido-bridged bond M(1)-M(4) is not the longest axial bond, evidence for the correct hydride sites was obtained from potential minimisation techniques and the distortions in the carbonyl sphere distribution. [88,90] This pattern is also evident for (XR4) (Table 2.3/2) with the same techniques being used to locate the hydride position (Chapter 6). In (46) the bond trans to the axially coordinated triphenylphosphine is the longest in the structure M(3)-M(4) $3.024(1) \text{ \AA}$, due to the trans influence of the terminal phosphorus ligand. [179]

2.4 Mechanistic Analysis.

One of the most challenging aspects of cluster chemistry is mechanistic analysis. Cluster reaction mechanisms are extremely difficult to study because of their complexity - intermediates are often hard to envisage and have rarely been isolated. The reaction of pyridine with the pentanuclear carbide $\text{Ru}_5\text{C}(\text{CO})_{15}$ (1a) has provided a opportunity to characterise an interrelated range of products.

In this section work by Johnson and Rodger will be discussed, [183,184] and used as a guide to develop a possible mechanism for the formation of the pyridyl derivatives reported in this chapter.

Johnson and Rodger classified the possible rearrangement mechanisms available to transition metal clusters according to a number of selection rules. These restrict the symmetry (and hence geometry) changes that are possible in each step of any reaction. Thus reaction pathways can be studied in two separate parts.

- a) The first stage, from geometrical and symmetry arguments, elicits all potentially feasible reaction mechanisms for systems of a given geometry.
- b) The second stage, a refinement, involves quantitative calculations on specific systems to determine which of these geometrically feasible reactions is the most likely pathway.

As cluster energy depends on the fine electronic structure, only the most qualitative general conclusions about mechanisms can be made. However this in itself can be advantageous, as it allows general trends to be formulated, which may then be supported by detailed quantum analysis on individual systems of interest. Clusters have certain features which separate them from mononuclear complexes, and these distinctions have a profound effect on reaction pathways. One important aspect is the

difference in mass between the metal atoms in the metal polyhedron and the atoms in the surrounding ligand system. This allows most normal modes of the system to be classified as largely metal, M_m , or largely ligand, L_n , based. Thus metal core rearrangement, to a first approximation, can be studied in isolation, followed by consideration of the effects of ligand motion. In general, the latter alter the relative energetics and so may be included in the quantum analysis stage of the study. The other important feature of clusters is the comparatively short range nature of metal-metal interactions. This can be used as a criterion for deciding which postulated mechanisms are most likely to be energetically feasible.

Keppert compared atom-atom interactions in the core of transition metal clusters with those found in closo boranes, and found that M-M interactions were shorter in range.[185] In an alternative interpretation, Wolley's 'cohesive energy' gives a useful empirical figure for metal-metal interaction energy in systems with high connectivity.[186] Thus, if the M-M interaction is short range, then it is energetically expensive to simultaneously break or significantly stretch many M-M links.

Johnson and Rodger proposed the following three hypotheses.

- a) In order to determine possible mechanisms, metal polyhedron rearrangements can be considered in isolation from ligand motion, the effect of ligand motion being on the relative energetics of postulated mechanisms.
- b) Rearrangement reactions of M_m (metal atoms in a polyhedron) proceed by successive breaking and formation of single M-M links.
- c) The point symmetry of a reacting system is the highest symmetry consistent with i) the atom-atom linkages present in the system, and ii) reactant and product geometry.

From the above Johnson and Rodger concluded that this type of approach would be less appropriate for systems with lower connectivity, where next-nearest neighbour distances would be small (i.e. it should only be used for clusters with nuclearity 5 or higher). In addition, an axiomatic feature of the theory is that M_m rearrangements will in general be multi-step.

2.5 A reaction pathway for pyridyl addition to pentanuclear clusters.

The structural characterisation of all products of the reaction of pyridine with the carbido-cluster $Ru_5C(CO)_{15}$ (1a) provides a opportunity to speculate on the possible reaction pathway. In Section 1.3 part of the network of metal core geometries available to pentanuclear clusters, via successive addition and loss of electron pairs, is illustrated. The structurally characterised compounds, (XR1) - (XR4), discussed in this chapter involve the interaction of pentanuclear carbido-clusters with pyridine. As a bifunctional ligand, pyridine can either bond terminally, or bridge two metals with transfer of hydrogen to the metal framework. In these molecules the central C-atom can be considered as an anchoring 'pivot' about which the metals rotate as the M-M bonds break and reform.

2.5.1 Proposed mechanism.

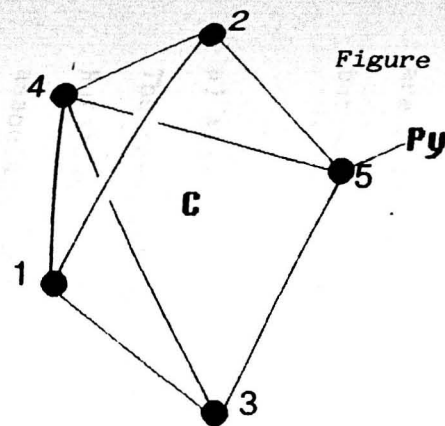
The metal atom environments in a square pyramidal geometry, such as $Ru_5C(CO)_{15}$, are either axial or basal.

Nucleophilic attack, through the lone pair of electrons on the pyridine nitrogen, can occur at either of these sites, but is more likely to occur at a basal ruthenium atom for the following reasons;

- a) $Ru_5C(CO)_{15}$ has a polyhedral electron count of 74 electrons, having seven skeletal electron pairs and as such is a nido-octahedron. It can therefore be considered as more 'electron deficient' at the basal metal atoms.

Figure 2.5/1 Initial products from reaction of

$\text{Ru}_5\text{C}(\text{CO})_{15}$ (1a) with pyridine.



Basal-axial cleavage

Basal-basal cleavage

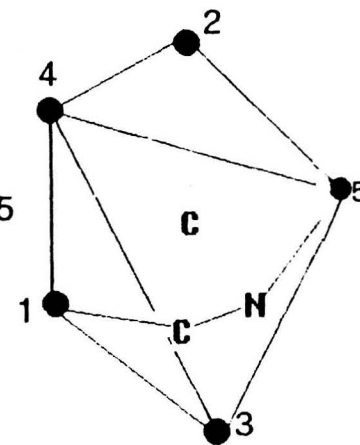
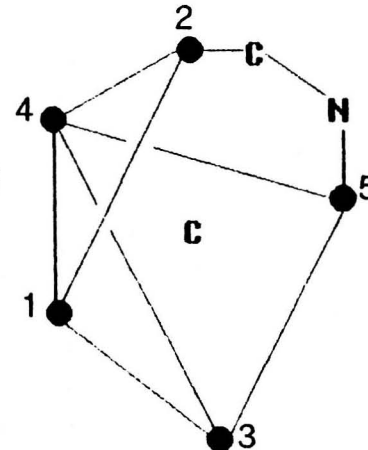
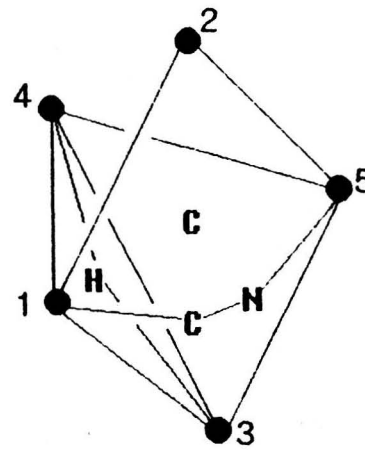
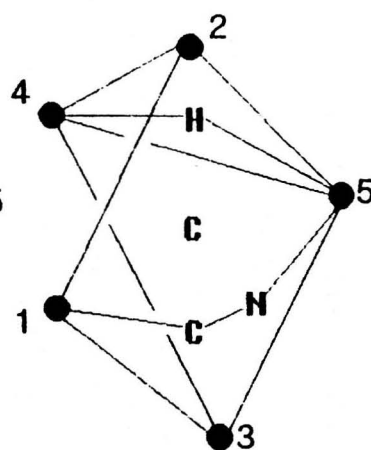
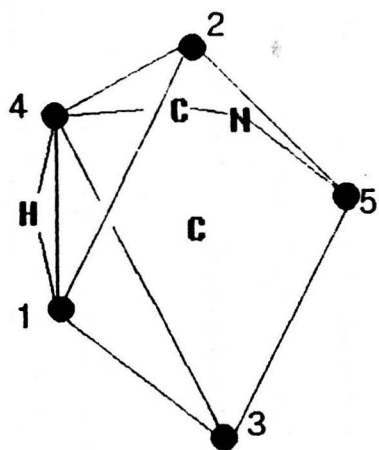
M(4)-M(5)

M(1)-M(4)

M(2)-M(4) or
M(3)-M(4)

M(2)-M(5) or
M(3)-M(5)

M(1)-M(2)
M(1)-M(3)



Wingtip bridge butterflies

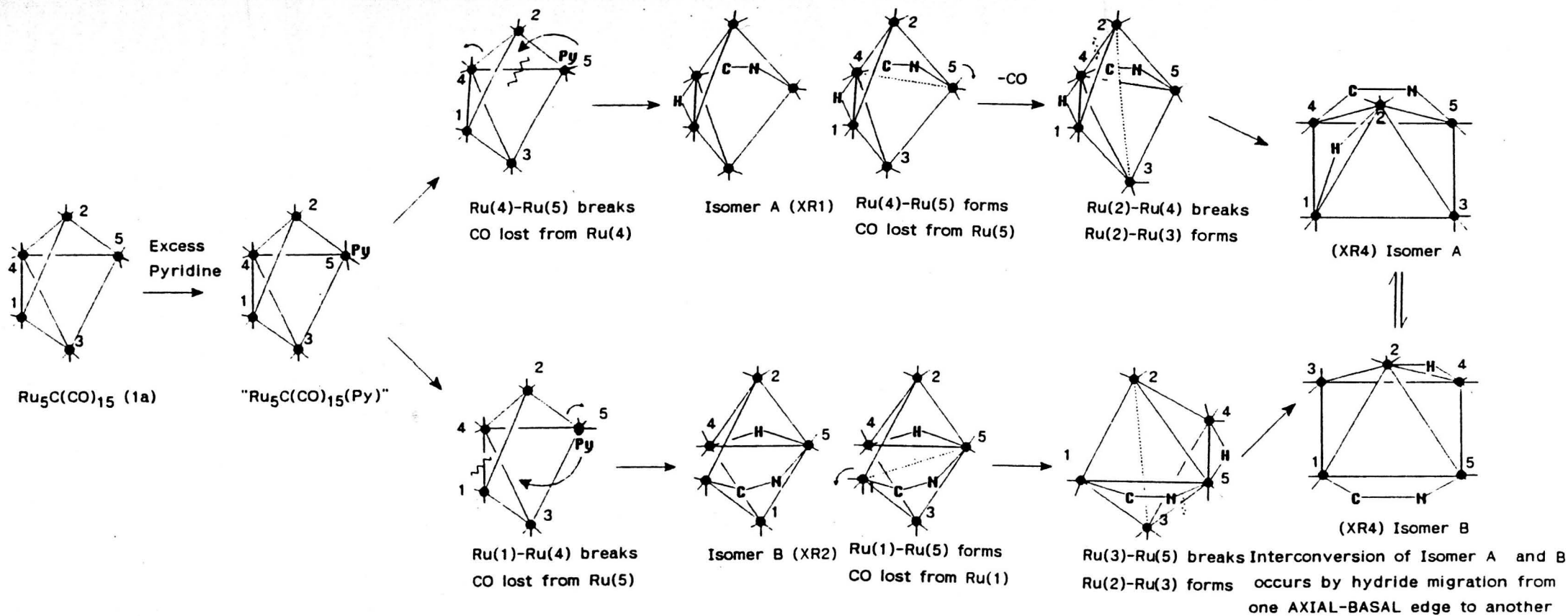
Hinge wingtip bridged butterflies

b) Perhaps more importantly, no complexes have been reported in which nucleophilic addition or substitution has occurred at an apical atom. Attack by the pyridine ligand at a basal ruthenium atom, leads to an unstable intermediate, $\text{Ru}_5\text{C}(\text{CO})_{15}(\text{C}_5\text{H}_5\text{N})$, a 76 electron species (Scheme 2.5/1). The next step, in which the pyridine swings over to occupy a bridging position with orthometallation, loss of a carbonyl ligand, and concomitant M-M bond fission, is crucial. A number of alternative structures are possible, but only two isomers are formed (Figure 2.5/1). In Section 1.3 the metal core geometries for a pentanuclear cluster were discussed. From a square pyramidal core only two alternative geometries are possible; a wingtip bridged butterfly and a hinge-wingtip bridged butterfly (Figure 1.3/5).

a) Axial-basal bond cleavage.

The terminal pyridine can swing over to bridge either Ru(4)-Ru(5) or Ru(1)-Ru(5). In both cases an axial-basal bond is cleaved and one carbonyl associated with the pyridyl bridged metal atom is lost. The isomers differ only in the attachment of the pyridyl ligand: in (XR1) the N-atom is bonded to a bridging ruthenium, whilst in (XR2) it is bonded to a hinge atom.

Cleavage of either of the other two axial-basal bonds, Ru(2)-Ru(4) or Ru(3)-Ru(4), would also give a wingtip-bridged butterfly metal core geometry, in which the pyridyl ligand spans across the outer wingtip atoms and the hydride lies along the hinge bond (Figure 2.5/1). A possible reason why this alternative isomer has not been detected is that the steric strain of such an arrangement would make it unfeasible. A review by Carty[91] considers the parameters associated with some tetranuclear butterflies and, although these will naturally be more flexible in nature



Scheme 2.5/1 Proposed mechanism for the formation of $\text{HRu}_5(\text{CO})_{14}(\text{C}_5\text{H}_4\text{N})$ Isomer A (XR1) and Isomer B (XR2) and $\text{HRu}_5(\text{CO})_{13}(\text{C}_5\text{H}_4\text{N})$ Isomer A and B (XR4).

than their pentanuclear bridged analogues, some interesting trends are evident. The dihedral angle between the two triangular faces in these butterflies varies considerably depending on the ligand sphere, ranging from extremely shallow in $\text{Ru}_4(\text{CO})_{13}(\text{PPh}_2)(\text{CCBut})$ (176.93°), with an associated long wingtip-wingtip distance (5.259 \AA), [91] to close contact of the two wingtip-wingtip metal atoms (2.802 \AA) in $\text{Ru}_4(\text{CO})_{13}\text{Cl}(\text{PPN})$ accompanied by an almost perpendicular dihedral angle of 91.0° . [187] In comparison, wingtip-wingtip distances of ca. 3.9 \AA with dihedral angles of ca. 107° (Table 2.3/1) are reported for the 3 bridged butterfly structures (XR1), (XR2) and (XR3) discussed in Section 2.3, in addition no examples of a ligand bridging a non-bonding contact of this type has been reported. The actual separation of non-bonded metal atoms bridged by a pyridyl ligand in the reported structures is ca. 3.6 \AA (Table 2.3/1), and restricting the outer wingtip atoms to such a short distance (which would be required in the unobserved isomers) would presumably impose a prohibitive degree of strain on the overall metal core geometry.

b) Basal-basal bond cleavage.

In addition to the four axial-basal bonds in $\text{Ru}_5\text{C}(\text{CO})_{15}$ (1a), there are four basal-basal bonds. Cleavage of these, in principle, leads to alternative hinge-wingtip bridged butterflies. One isomer, achieved by breaking either $\text{Ru}(2)\text{-Ru}(5)$ or $\text{Ru}(3)\text{-Ru}(5)$, has the pyridyl spanning a wingtip-bridging atom distance (Figure 2.5/1). Conversely, cleavage of $\text{Ru}(2)\text{-Ru}(4)$ or $\text{Ru}(3)\text{-Ru}(4)$ would lead to the pyridyl ligand bridging across a hinge-bridging distance (Figure 2.5/1). (The latter can also be described as a wingtip-wingtip distance, depending on which part of the metal core is taken as the butterfly. If such structures require definition, a sensible precedent would be to define the hinge bond as that bridged by a hydride or isolobal analogue, as all known examples have this arrangement.) A known structure with the hinge-wingtip bridged core is

$\text{Ru}_5(\text{CO})_{12}(\text{CCPh})(\text{PhC}=\text{CC}=\text{Ph})(\text{PPh}_2)$. [102] This has a wingtip-bridging atom distance of 3.628(7) Å with the alkyne, $\text{PhC}=\text{CC}=\text{CPh}$ spanning these two metal atoms and an alkenyl group bonding to all five metal atoms ($\mu_5\eta^2\delta_5$). In comparison, a bridged pyridyl structure may be too 'floppy' to exist as a stable isomer.

Thus, the parent square pyramid $\text{Ru}_5\text{C}(\text{CO})_{15}$ (1a) can be converted to isomeric wingtip-bridged butterflies by fission of 2 different apical-basal bonds (Scheme 2.5/1). Cleavage of either of the remaining two apical-basal bonds, or any of the four basal-basal bonds, would respectively, lead to alternative wingtip-bridged or hinge-wingtip bridged butterflies (see above). None of these structures have been observed in this reaction.

Decarbonylation of the isomers (XR1) and (XR2) yields the square pyramidal isomers of (XR4), with the pyridyl spanning a basal-basal edge. Formation of a metal-metal bond, Ru(4)-Ru(5) in Isomer A (XR1) or Ru(1)-Ru(5) in Isomer B (XR2), converts the bridged butterfly geometry of these isomers back into a square pyramid, with the pyridyl bridging an axial-basal bond (Scheme 2.5/1). An alternative square pyramid can be generated by simultaneous M-M bond cleavage and formation, resulting in the pyridyl bridging a basal-basal bond. Interconversion of these isomers is possible by simple hydride migration from one axial-basal bond to another. The overall proposed mechanism for this reaction is illustrated in Scheme 2.5/1.

2.6 Conclusion and summary.

In both isomers of $\text{HRu}_5\text{C}(\text{CO})_{14}(\text{C}_5\text{H}_4\text{N})$ (XR1) and (XR2) and in the disubstituted cluster (XR3), the hydride ligands bridges the hinge bond of the butterfly. A comparison with other bridged butterflies shows that this is the rule and no exceptions were found, with related clusters with isolobal gold-phosphine ligands adopting the same bonding mode.

The ligand spheres of all three bridged butterfly clusters (XR1), (XR2) and (XR3) are very similar and this feature is reflected in comparable M-M and M-C(carbide) bond lengths. Distinction of M-C and M-N bond lengths is observed in (XR1) and (XR3) but is not significant in (XR2) due to the relatively high e.s.d.'s in this structural determination. Comparison of these structures with clusters with related cores was considered in Section 2.3.3. This showed that variation in ligand spheres causes marked bond variation, the most significant of which is observed for structures with μ_2 -ligands across the M(hinge)-M(bridge) distance.

The latter part of this chapter dealt with a possible mechanism for the reaction pathway of all products from the reaction of $\text{Ru}_5\text{C}(\text{CO})_{15}$ (1a) with pyridine. From the structural results, the pathway is proposed to occur by a series of M-M cleavage and re-formation steps and this process provides a good illustration of how metal framework geometric flexibility distinguishes the reactions of clusters compounds from their mononuclear counterparts.

CHAPTER THREE

Derivatives of octahedral hexaruthenium clusters.

Chapter 3- Derivatives of octahedral hexaruthenium clusters.

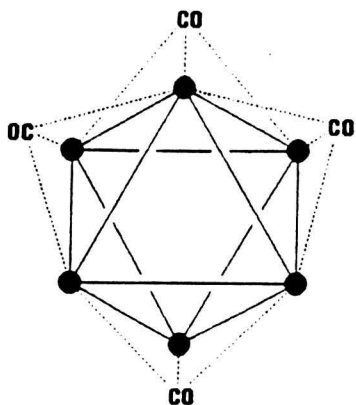
The range of hexanuclear clusters is immense, and an understanding of their reactivity, reaction pathways, and the bonding involved in such species is only now starting to emerge.[187-190] The combination of such compounds with small organic fragments is a particularly important area of current research and has uncovered novel cluster geometries and several unexpected modes of bonding for small organic fragments.[189]

The X-ray structures reported in this chapter are all based on the predominant octahedral geometry. Octahedral frameworks have only triangulated faces and so the type of organo-bonding observed for octahedral clusters will be comparable to that found for trinuclear clusters. Alternative metal core frameworks, which can give rise to unusual organo-fragments, and probably provide a closer analogy to metal surfaces, are discussed in the Chapter 4.

This chapter begins with a review of the range of hexanuclear cores observed with particular attention to organo-clusters. The introduction to Chapter 4 concentrates on the relationship clusters have to play with respect to metal surfaces and, importantly, to catalytic processes. These features are helping to develop our understanding of the mechanisms of reactions on heterogeneous surfaces and catalysis.

3.1 Historical Review.

The first octahedral cluster was structurally characterised as long ago as 1963.[191] It had been known since 1943 and formulated as $\text{Rh}_4(\text{CO})_{11}$. X-Ray structure analysis showed that there were six rhodium atoms occupying the corners of an octahedron and that the correct formulation was $\text{Rh}_6(\text{CO})_{16}$ (1) (Figure 3.1/1). Twelve of the sixteen carbonyl ligand are terminal with the remaining four adopt μ_3 -bridging modes above four tetrahedrally related faces of the octahedron.



$\text{Rh}_6(\text{CO})_{16}$ (1)

Figure 3.1/1 The octahedral metal core of $\text{Rh}_6(\text{CO})_{16}$ (1).

In succeeding years a range of clusters with octahedral geometries were reported; $\text{Co}_6(\text{CO})_{16}$, [192] its related anionic derivatives $[\text{Co}_6(\text{CO})_{15}]^{2-}$, [193] and $[\text{Co}_6(\text{CO})_{14}]^{4-}$. [192] And at about this time a ruthenium cluster, subsequently shown to be $\text{Ru}_6\text{C}(\text{CO})_{17}$ (2), [194] was wrongly assigned as $\text{Ru}_6(\text{CO})_{18}$. [195] Although the osmium analogue of this cluster was later synthesised, $\text{Ru}_6(\text{CO})_{18}$ has never been isolated.

The first reported examples of hexanuclear clusters containing interstitial carbides were discovered from the pyrolysis of $\text{Ru}_3(\text{CO})_{12}$ with arenes. [167, 196, 197] This reaction revealed a number of hexanuclear ruthenium clusters such as $\text{Ru}_6\text{C}(\text{CO})_{17}$ (2) and $\text{Ru}_6\text{C}(\text{CO})_{14}$ (arene) [arene = $\text{C}_6\text{H}_6\text{Me}_3$ (3), $m\text{-C}_6\text{H}_4\text{Me}_2$ or C_6H_5]. [167, 196, 197] These ruthenium compounds were all electronically related to the rhodium species (1) and the basic cores of (2) and (3) are illustrated in Figure 3.1/2. [167, 194, 196, 197] The X-ray structure analysis of the mesitylene derivative $\text{Ru}_6\text{C}(\text{CO})_{14}(\text{C}_6\text{H}_3\text{Me}_3)$ (3) established that the arene η^6 -bonds to one of the ruthenium atoms, donating 6e to the number of cluster valence electrons (CVE), with the interstitial carbido-atom acting as a 4e donor. [197] This gives a CVE of 86e characteristic of octahedral species. The octahedral carbido-dianion $[\text{Ru}_6\text{C}(\text{CO})_{16}]^{2-}$ was not reported for more than a decade and both the $[\text{Me}_4\text{N}]^+$ and the $[\text{Ph}_4\text{As}]^+$ salts have been structurally characterised. [198, 199] The $[\text{Me}_4\text{N}]^+$ salt is isostructural with its iron analogue and has three

μ_2 -bridging carbonyl ligands,[198] whereas the $[\text{Ph}_4\text{As}]^+$ salt has four μ_2 -bridging carbonyl groups.[199]

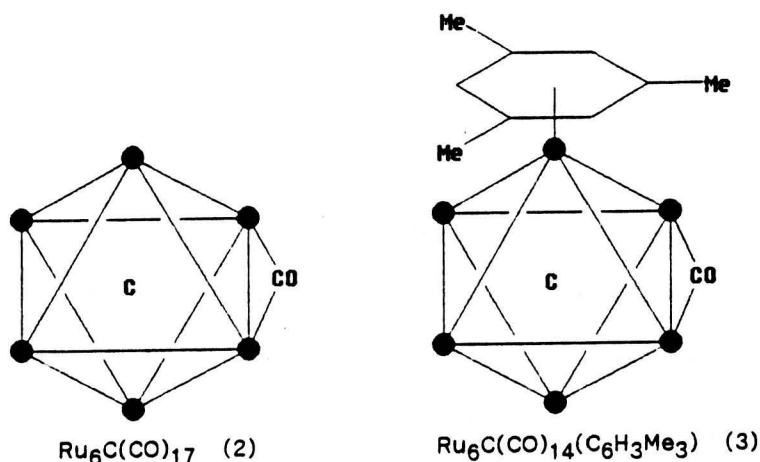


Figure 3.1/2 The metal cores of $\text{Ru}_6\text{C}(\text{CO})_{17}$ (2) and $\text{Ru}_6\text{C}(\text{CO})_{14}(\text{C}_6\text{H}_3\text{Me}_3)$ (3).

The origin of carbido-species has been the object of some discussion. Lewis identified the source of the carbido-atom in $\text{Ru}_6\text{C}(\text{CO})_{17}$ (2) as originating from a coordinated carbonyl group by heating $\text{Ru}_3(\text{CO})_{12}$ in a sealed tube such that no other source of carbon was present.[165] In contrast, Chini discovered that the carbido-atom in the trigonal prismatic cluster $[\text{Rh}_6\text{C}(\text{CO})_{15}]^{2-}$ originated from chloroform.[200]

Attention was turned to the remaining member of the iron triad, osmium. Surprisingly, pyrolysis of $\text{Os}_3(\text{CO})_{12}$ lead to a number of polynuclear clusters of nuclearities in the range 5 to 8: $\text{Os}_5(\text{CO})_{16}$, $\text{Os}_6(\text{CO})_{18}$, $\text{Os}_7(\text{CO})_{21}$, and $\text{Os}_8(\text{CO})_{23}$, with higher temperatures giving 2 new carbido-clusters, $\text{Os}_5\text{C}(\text{CO})_{15}$ and $\text{Os}_8\text{C}(\text{CO})_{21}$.[165] Again the reaction conditions indicated the source of the carbido-carbon as being from reduction of a coordinated carbonyl group.[165] Work on the present project has shed more light on the origin of interstitial carbides and this will be discussed in the next chapter. Surprisingly, no hexaosmium carbide has ever been structurally characterised, although some evidence for its existence has been proposed.[187,201]

The first hydrido-hexanuclear species, the dihydride $H_2Ru_6(CO)_{18}$ (4), was characterised by Churchill and Wormald.[34,35] The 6 rutheniums adopt an octahedral geometry and all eighteen carbonyl ligands are terminal (Figure 3.1/3). The hydrogen atoms could not be located directly, but evidence for their location came from two main structural features. Firstly, two opposite faces of the octahedron are significantly longer than the remaining six, with the Ru-Ru distances within these larger faces ranging from 2.950(3)-2.959(3) Å. This is in contrast to the remaining Ru-Ru distances which lie in the range 2.858(3)-2.874(3) Å. Secondly, the carbonyl ligands are bent away from the two enlarged 'open' faces. These features were attributed to the steric requirements of the two 1e-donor hydrido-ligands, which were assigned μ_3 -bonding modes on the enlarged faces.

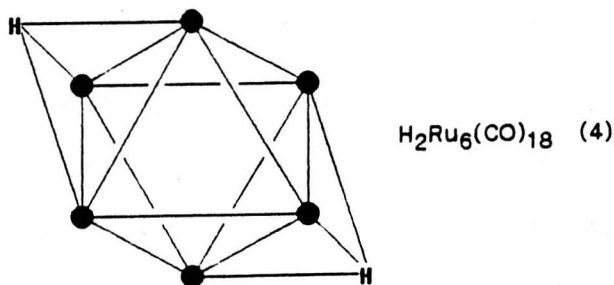


Figure 3.1/3 The first hydrido-hexanuclear cluster $H_2Ru_6(CO)_{18}$ (4).

The first interstitial hydride of the iron triad prepared was the monoanion $[HRu_6(CO)_{18}]^-$ (5).[202-204] The X-ray structure analysis of this revealed that, in contrast to the previously discussed dihydride (4), there was no enlargement of any of the M_3 faces and that the carbonyl ligand distribution was not distorted. In fact, the structure was almost indistinguishable from the nonhydrido-octahedral cluster $[Os_6(CO)_{18}]^{2-}$ (6) (discussed below). These structural features indicated that the hydrido-ligand could not occupy a surface position and must therefore reside interstitially in the octahedral hole (Figure 3.1/4). In the

initial work no proton signal was detected (in the range τ 0 to 40) for this cluster but after assignment of the hydrido-atom to an interstitial site a much broader spectral width (in the range τ -40 to 100) revealed a signal at $\tau = -6.43$. This is well outside the range expected for a transition metal hydride and so accounts for the failure to find it on initial investigation and confirms the evidence from X-ray structural work.

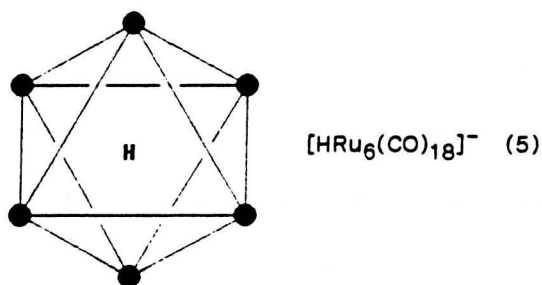


Figure 3.1/4 The interstitial hydride $[\text{HRu}_6(\text{CO})_{18}]^-$ (5).

Having established that hexanuclear clusters with 86e adopted an octahedral geometry the rule was unexpectedly broken by a series of hexanuclear osmium clusters which differed only in the charge and the number of hydride ligands present.[26] Two clusters of this series, $[\text{Os}_6(\text{CO})_{18}]^{2-}$ (6) and $[\text{HOs}_6(\text{CO})_{18}]^-$ (7), did adopt the predicted octahedral metal core but the third member of this group, $\text{H}_2\text{Os}_6(\text{CO})_{18}$ (8), was found to adopt an alternative monocapped square pyramidal arrangement (Figure 3.1/5).[25,26]

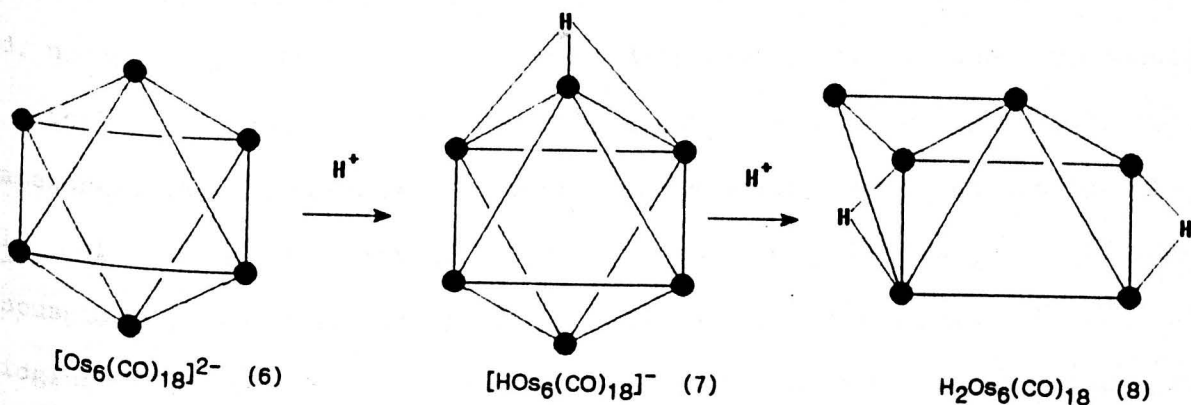


Figure 3.1/5 The M-core of $[\text{H}_{2-n}\text{Os}_6(\text{CO})_{18}]^{n-}$ [$n = 2$ (6), 1 (7), 0 (8)].

In the mono-hydrido anion $[\text{HOs}_6(\text{CO})_{18}]^-$ (7) one triangular face of the octahedron has significantly longer edges [mean Os-Os $2.973(3) \text{ \AA}$] than that found for the remaining M-M bonds [Os-Os $2.863(3) \text{ \AA}$]. [26] In addition, the carbonyl ligands belonging to the enlarged face appear to be pushed back. This is the same pattern as observed for the previously discussed dihydride $\text{H}_2\text{Ru}_6(\text{CO})_{18}$ (4). Thus, the hydride in $[\text{HOs}_6(\text{CO})_{18}]^-$ (7) was also envisaged as μ_3 -capping the enlarged face.

By analogy with the formally isoelectronic structure $\text{H}_2\text{Ru}_6(\text{CO})_{18}$ (4), [34, 35] $\text{H}_2\text{Os}_6(\text{CO})_{18}$ (8) was expected to be octahedral and indeed the i.r. spectrum of $\text{H}_2\text{Os}_6(\text{CO})_{18}$ (8) was similar to that of (4). However, the ^1H n.m.r. spectrum of (8) revealed a doublet of doublets [(CD_2Cl_2) 22.15/22.17, 31.69/31.71, 80 MHz, j 1.7 Hz] and so the hydrides were assigned as μ_2 - and μ_3 -bridging respectively. [25] X-Ray structure analysis showed that the metal core framework actually adopts a mono-capped square pyramidal metal core framework, with both hydrides adopting μ_2 -bonding modes; [26] this can be rationalised by PSEPT as an alternative geometry for an 86e CVE (Section 1.2).

The difference between the metal core geometries in the ruthenium and osmium dihydrides (4) and (8) cannot be simply explained in terms of the size of the atomic radii of ruthenium and osmium, as these are very similar. The energy differences between these frameworks are fairly small and, no doubt, sensitive to a number of different factors. One hypothesis is that the presence of hydrido-ligands favour capping metal core frameworks. [26] The variation in metal core geometry and in particular the role of bridging carbonyl ligands has been the subject of some discussion. [205-209] Johnson proposed that the number and distribution of bridging and terminal carbonyl groups in a polynuclear species reflect i) the polyhedral arrangement of the carbonyls and ii) the orientation of the metal unit within this polyhedron. [205-207] He suggested that the carbonyl

polyhedron could be proposed from simple packing arguments and that the orientation of the metal core could be deduced from the spaces and sites available within the carbonyl polyhedron and by the size of the metal atoms. Evans suggested that the occurrence of μ_2 -bridging carbonyl groups might be at least in part electronic in origin.[208] Bridging carbonyl groups have been structurally reviewed by Colton and McCormick.[209]

The above work on the series of complexes $H_2M_6(CO)_{18}$ [M=Os (8), Ru (4)], $[HM_6(CO)_{18}]^-$ [M=Ru (5), Os (7)], and $[M_6(CO)_{18}]^{2-}$ [M=Os (6)] was completed by the X-ray structure analysis of $[Ru_6(CO)_{18}]^{2-}$ (9),[210] which, although octahedral, differed from its osmium analogue in having four bridging carbonyl ligands (Figure 3.1/6). Thus, within this series no two clusters have the same structure. In those cases where the ruthenium and osmium analogues adopt the same metal core framework, the distribution of carbonyl ligands is different and thus the series is not isostructural, with the preferred structure depending on subtle quantitative factors.[203]

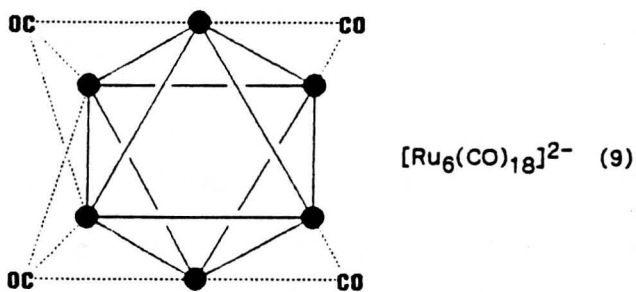


Figure 3.1/6 The dianion $[Ru_6(CO)_{18}]^{2-}$ (9).

Although one of the first hexanuclear clusters to be structurally characterised was the octahedral arene $Ru_6C(CO)_{14}(C_6H_3Me_3)$ (3), on the whole, the synthesis of organic-clusters developed late in the history of cluster chemistry and has been found to frequently lead to cluster rearrangement or breakdown rather than maintenance of the octahedral core.

Photolysis of the capped trigonal bipyramid $\text{Os}_6(\text{CO})_{18}$ (10) with phenylacetylene yielded $\text{Os}_6(\text{CO})_{16}(\text{CPh})_2$ (11) (Figure 3.1/7).[137] The six osmiums in (11) adopt a capped square pyramidal geometry, similar to that of the dihydrido-species $\text{H}_2\text{Os}_6(\text{CO})_{18}$ (8).[24,25] One of the benzyldiene groups caps the Os_4 square plane, while the other caps an adjacent Os_3 triangular face. Consequently, for both organo-ligands the CC backbone of the benzyldiene is approximately perpendicular to a cluster face. The benzyldiene ligands both act as 3e donors, and so the cluster maintains the 86 valence electron count expected for this geometry. The organo-ligands can be formally derived from the reactant, PhCCH , by fission of the acetylenic bond.

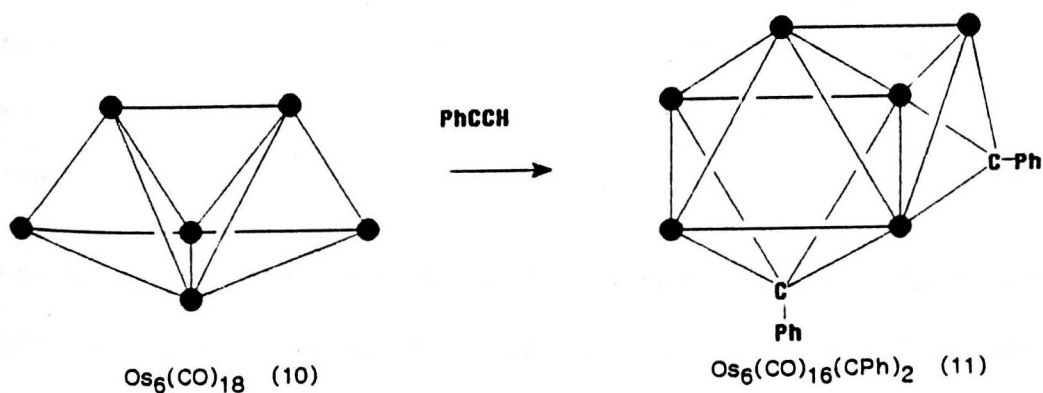
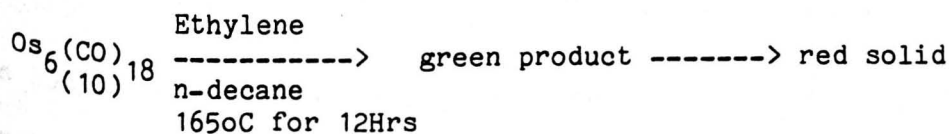


Figure 3.1/7 Core transformation from a trigonal bipyramidal core (10) to a capped square pyramidal core (11).

The reaction of $\text{Os}_6(\text{CO})_{18}$ (10) with ethylene yielded two distinctly different products.[136]



The first, $\text{Os}_6(\text{CO})_{16}(\text{CMe})_2$ (12), has a structure analogous to the benzyldiene complex (11) with the osmium atoms defining a capped square pyramidal geometry and the two methylidyne groups capping μ_3 - and μ_4 - respectively (Figure 3.1/8). Clearly, the 'bulkiness' of the organo-group,

perpendicularly bonded to the μ -C atom, does not alter the metal core framework. In contrast to the formation of $\text{Os}_6(\text{CO})_{16}(\text{CPh})_2$ (11), the organo-fragments in (12) are produced from the reactant ethylene by proton rearrangement to give the observed μ_3 - and μ_4 -bonding groups.

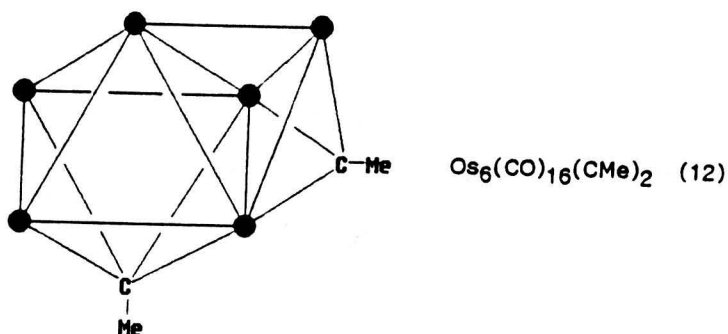


Figure 3.1/8 The capped square pyramid $\text{Os}_6(\text{CO})_{16}(\text{CMe}_2)$ (12).

The second reaction product, $\text{Os}_6\text{C}(\text{CO})_{16}(\text{MeC}:\text{CMe})$ (13), adopts an edge bridged square pyramidal metal core and was the first example of this type of geometry reported for a hexanuclear cluster (Figure 3.1/9).[136]

Interestingly, in this product the ethylene fragments have condensed together to form a but-2-yne fragment, with all four of the core carbon atoms of this new ligand co-planar. The but-2-yne ligand sits above an osmium triangular face, π -bonding to one osmium and σ -bonding to the remaining two osmium atoms. The cluster is an 88 electron system which, in terms of PSEPT (Section 1.3), is consistent with the cluster being derived from an 86e capped square-based pyramidal core by cleavage of a M-M bond, accompanied by addition of two electrons.

This compound is particularly interesting because a carbido-atom has been generated from a non-carbido-species and the but-2-yne results from condensation of 2 equivalents of ethylene. It will be shown in Chapter 4 that the generation of the carbido-atom in $\text{Ru}_6\text{C}(\text{CO})_{15}(\text{C}_6\text{H}_3\text{Me}_3)$ (3) can be expressed as a bimolecular process. It is interesting to speculate on the possibility of a similar mechanism occurring for the production of (13).

However, so far such a mechanism has not been established but must be of considerable interest, both with respect to the generation of a four carbon fragment and the formation of a carbido-species.

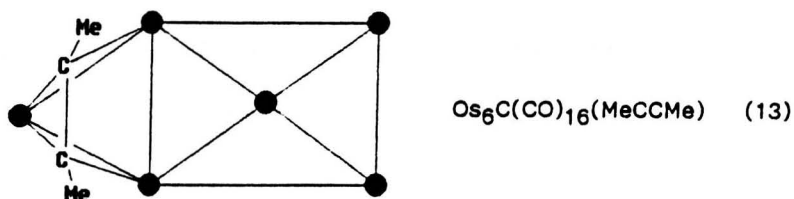


Figure 3.1/9 The edge-bridged square pyramid $\text{Os}_6\text{C}(\text{CO})_{16}(\text{MeCCMe})$ (13).

A further insight as to how ligand electron donating ability could be a key factor in determining cluster geometry, was obtained from the reaction of $\text{Os}_6(\text{CO})_{18}$ (10) with p-tolyl isocyanide.[211] This resulted in the addition of two molecules of isocyanide, to give $\text{Os}_6(\text{CO})_{18}(\text{CNC}_6\text{H}_4\text{CH}_3)_2$ (14) (Figure 3.1/10).

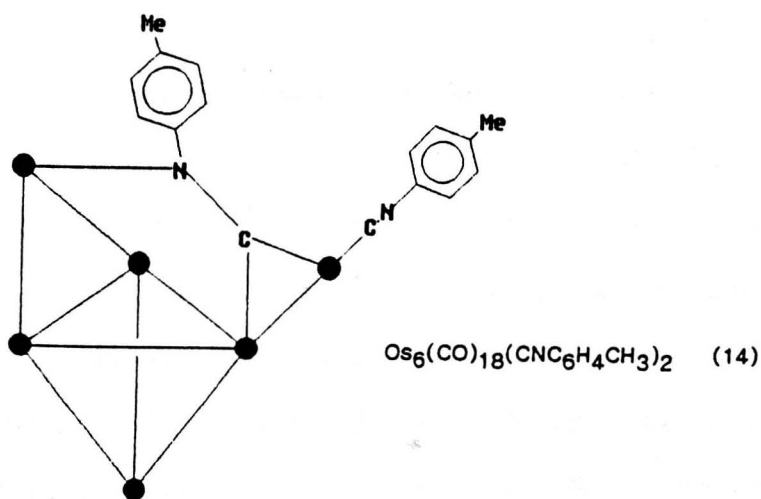


Figure 3.1/10 $\text{Os}_6(\text{CO})_{18}(\text{CNC}_6\text{H}_4\text{CH}_3)_2$ (14).

One of the isocyanides in (14) adopts a terminal bonding mode, donating 2e to the cluster framework, whereas the second isocyanide ligand donates a total of 4e by adopting an unusual μ_3 -bridging mode. The isocyanide ligands add directly to the cluster instead of replacing ligands. They, therefore, supply a total of six additional electrons and the change from 84 to 90 CVE is accompanied by a dramatic change in polyhedral geometry.

The observed framework, a spiked edge-bridged tetrahedron, results from scission of 3 M-M in the parent cluster $\text{Os}_6(\text{CO})_{18}$ (10).

Pyrolysis of $\text{Os}_3(\text{CO})_{11}(\text{CNCMe}_3)$ gives the related compound $\text{Os}_6(\text{CO})_{16}(\text{CNCMe}_3)_2$ (15), which maintains the metal framework and electron count of the parent carbonyl species with two carbonyls being replaced by isocyanide ligands (Figure 3.1/11).[211] The isocyanides both bond in equatorial sites to outer capping osmium atoms.

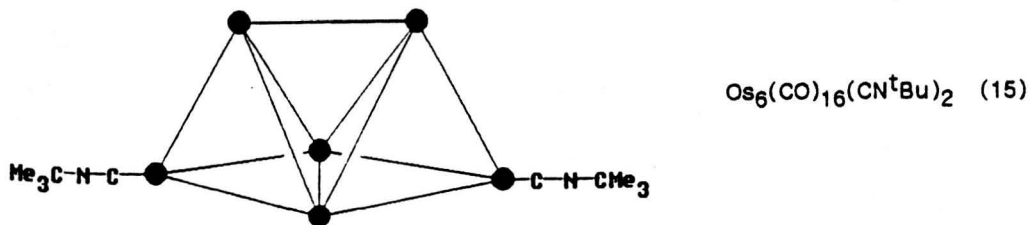


Figure 3.1/11 The capped trigonal bipyramidal M-core of (15).

An interstitial carbido-atom normally has a stabilising effect on cluster geometry with the octahedral metal core being maintained during most reactions. A rare example of cluster unravelling is seen for the reaction of $\text{Ru}_6\text{C}(\text{CO})_{17}$ (2) with EtSH, which gives two products; $\text{H}_2\text{Ru}_6\text{C}(\text{CO})_{15}(\text{EtS})_2$ and $\text{HRu}_6\text{C}(\text{CO})_{15}(\text{EtS})_3$ (16).[212] An X-ray structure analysis of $\text{HRu}_6\text{C}(\text{CO})_{15}(\text{EtS})_3$ (16) showed that the octahedral core has been destroyed, with five of the ruthenium atoms defining a wing-tip bridged butterfly arrangement and the remaining ruthenium atom bridging one of the wingtip-bridging bonds (Figure 3.1/12). The hydrido-ligand bridges the hinge bond and the SEt ligands act as 3e donors, giving a total CVE of 92e. This structure is of some relevance to the reverse process in which newly formed C-atoms become surrounded by six ruthenium metals (Chapter 4).

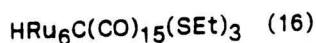
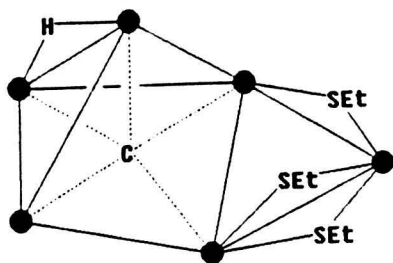


Figure 3.1/12 $\text{HRu}_6\text{C}(\text{CO})_{15}(\text{SEt})_3$ (16).

As $\text{Ru}_6(\text{CO})_{18}$ is unknown, reactions analogous to those discussed above for $\text{Os}_6(\text{CO})_{18}$ (10)) cannot be studied. The study of the reaction of ruthenium clusters with alkynes must therefore be produced from trinuclear precursors. The triruthenium cluster $\text{Ru}_3(\text{CO})_{12}$ reacts with ethylene to give both a tetranuclear alkyne $\text{Ru}_4(\text{CO})_{12}(\text{MeC}=\text{CMe})$ and a hexanuclear diene $\text{Ru}_6\text{C}(\text{CO})_{15}(\text{MeCH}=\text{CH}-\text{CH}=\text{CHMe})$ (17). [140] The latter was the first example of a six carbon atom linear chain bonded to a hexanuclear unit. The metal core in the diene (17) adopts an octahedral geometry (around the central carbide atom), with the trans,trans,hexa-2-4-diene ligand lying along one edge of the cluster (Figure 3.1/13). This organo-group donates a total of 4e (via two π -bonds) and it is evident that the 4e donating interstitial carbon must be important in allowing the accommodation of this bulky six-carbon fragment on the cluster surface. This is another example of organo-ligand condensation, with the six carbon chain in (17) being produced from the reactant ethylene. As in (13), where 2 equivalents of ethylene have condensed to give the product, here 3 equivalents of ethylene are condensed.

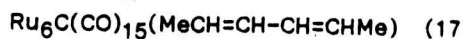
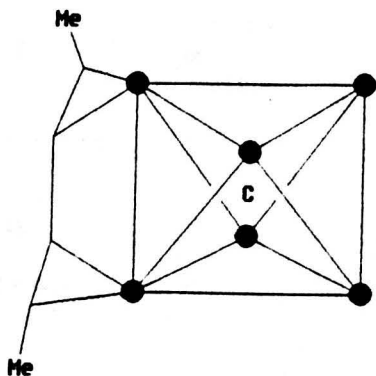


Figure 3.1/13 $\text{Ru}_6\text{C}(\text{CO})_{15}(\text{MeCH}=\text{CH}-\text{CH}=\text{CHMe})$ (17).

3- π interactions are evident in the hexanuclear carbide cluster $\text{Ru}_6\text{C}(\text{CO})_{14}(\text{bitropy})$ (18).[213] Six carbon atoms from one ring of the bitropy ligand bond to a triangular face of the cluster (π -bonding to three of the ruthenium atoms) and donating a total of 6e to the electron count of the cluster (Figure 3.1/14).

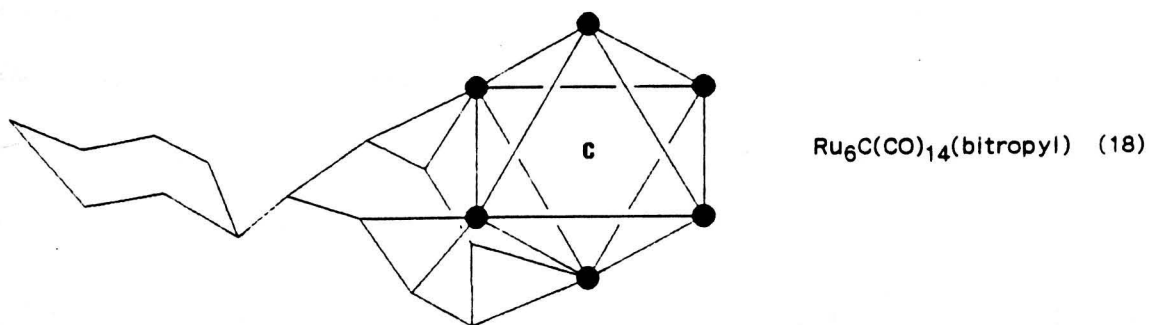


Figure 3.1/14 The carbido-octahedral M-core of the bitropy cluster (18). An extreme example of cluster-opening has been reported for the phosphite cluster $\text{Os}_6(\text{CO})_{17}\{\text{P}(\text{OMe})_3\}_4$ (19).[214] This cluster consists of a central triangle of osmium atoms, edge bridged on all sides by three more osmium atoms such that the 6 osmium atoms are approximately coplanar (Figure 3.1/15). This planar arrangement of atoms has also been observed in the basal plane of the pyramid metal skeleton of a number of decanuclear clusters, for example $[\text{HOs}_{10}\text{C}(\text{CO})_{24}]^-$, [104] these are discussed in more detail in Chapter 4. It has been noted that there is a close analogy between the arrangement of metal atoms in these clusters and the arrangement found for bulk metals.[104]

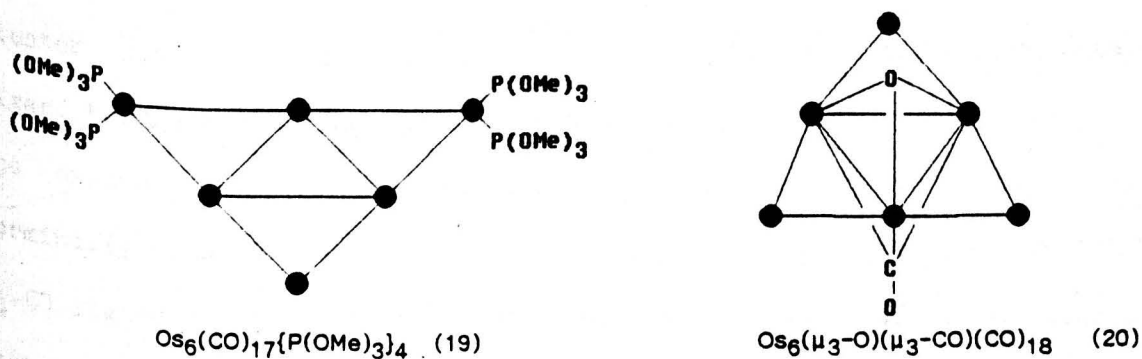


Figure 3.1/15 The giant equatorial triangular cores of (19) and (20).

A similar metal core geometry was reported for $\text{Os}_6(\mu_3\text{-O})(\mu_3\text{-CO})(\text{CO})_{18}$ (20) (although deviation from planarity was evident), [215] which contains both μ_3 -oxygen and μ_3 -carbonyl ligands (Figure 3.1/15). Both (19) and (20) are 90e clusters and can be envisaged as being derived from an 84e capped trigonal bipyramid [c.f. (10)] by the successive scission of three metal-metal bonds in the capped trigonal bipyramidal core of the parent cluster $\text{Os}_6(\text{CO})_{18}$ (10) (Figure 3.1/16).

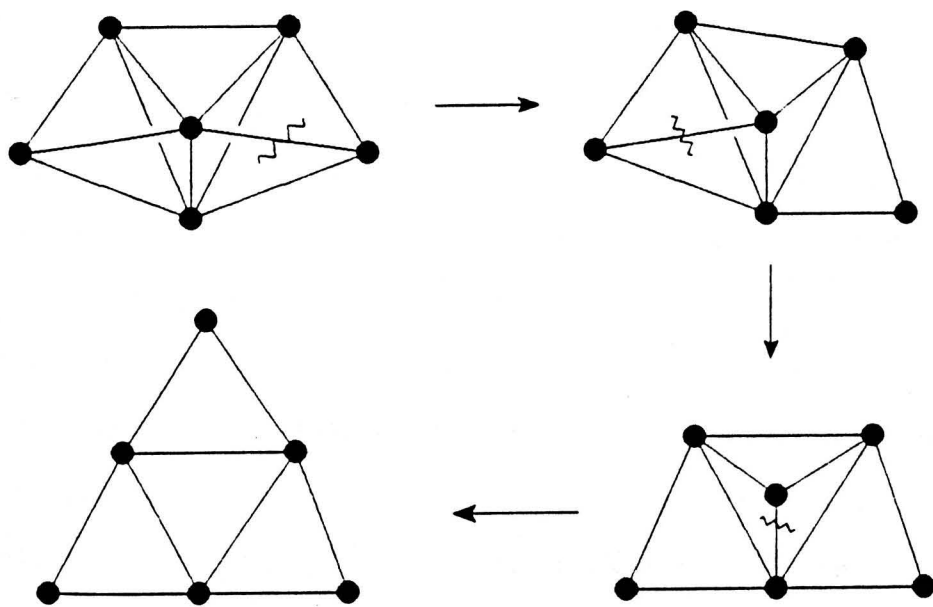


Figure 3.1/16 Successive M-M cleavage to produce a giant equatorial M-core. The reaction of $\text{Os}_6(\text{CO})_{18}$ (10) with pyridine produces two clusters of different nuclearity; the pentanuclear cluster $[\text{Os}_5(\text{CO})_{15}]^{2-}$ and the hexanuclear bis-pyridine $\text{Os}_6(\text{CO})_{17}(\text{Py})_2$ (21). [216] The bis-pyridine cluster (21) has a trigonal bipyramidal metal core with the sixth osmium bonded to an equatorial metal atom in a 'spiked' arrangement (Figure 3.1/17). The cluster contains the first example of a $\mu_4\eta^2\sigma_{4b}$ -carbonyl, which acts as a ligand bridge across the spike bond via σ -donation of two electrons from the oxygen atom to the terminal osmium atom. The two pyridine ligands terminally bond to the spiked osmium atom (and both donate 2e), whilst the μ_4 -CO ligand donates a total of 4e. This results in a CVE of 88e consistent with cleavage of 2 M-M bonds of the (84e) parent species $\text{Os}_6(\text{CO})_{18}$ (10).

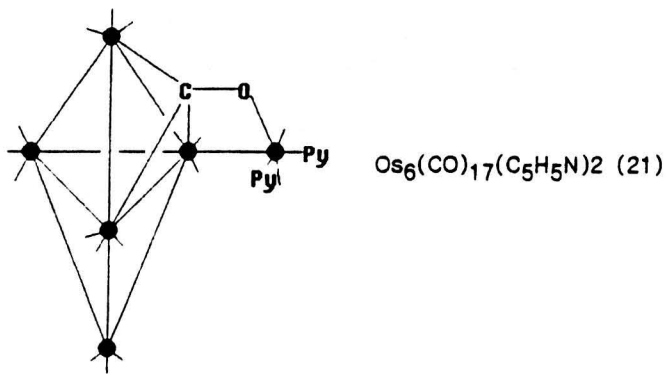


Figure 3.1/17 $\text{Os}_6(\text{CO})_{17}(\text{Py})_2$ (21).

The proposed mechanism for the formation of (21) is illustrated in Figure 3.1/18.[216] Initial attack, by the two pyridine ligands, results in rupture of two Os-Os bonds in one of the caps, this is then followed by an intramolecular attack on the 'spike' osmium atom by the carbonyl oxygen on an adjacent metal atom. This displaces a carbonyl group on the 'spiked' osmium to give the carbonyl bridged product (21).[216] The other product of this reaction, $[\text{Os}_5(\text{CO})_{15}]^{2-}$ can be produced if the intermediate $\text{Os}_6(\text{CO})_{18}(\text{C}_5\text{H}_5\text{N})_2$ (Figure 3.1/18) is further attacked by pyridine causing the sixth 'spiked' osmium atom to break off.

Prior to 1985, the few reports of arenes bonded to clusters involved either η^6 -coordination to one metal atom, as in $\text{Ru}_6\text{C}(\text{CO})_{14}(\eta^6\text{-C}_6\text{H}_3\text{Me}_3)$ (3), [197] or $\mu_3\eta^2\delta_4$ -bonding as observed for the benzyne ligand in the trinuclear cluster $\text{H}_2\text{Os}_3(\text{CO})_9(\mu_3\text{-}\eta^2\text{C}_6\text{H}_4)$. [217] Subsequent work revealed that in the bis-benzene cluster $\text{Ru}_6\text{C}(\text{CO})_{11}(\text{C}_6\text{H}_6)_2$ (22), [218] while one of the C_6H_6 rings adopts the conventional η^6 -terminal mode, the second ring adopts a $\mu_3\eta^6\delta_6$ -face capping mode (Figure 3.1/19). (The two carbonyl groups on each ruthenium atom of the triangular face, with the μ_3 -bonding benzyne ligand, are pushed back, such that they are almost co-planar with the metal triangle.)

The $\mu_3\eta^6$ -bonding mode adopted by one of the benzene ligands in the bis-benzene cluster $\text{Ru}_6\text{C}(\text{CO})_{11}(\text{C}_6\text{H}_6)_2$ (22) was the first example of this unusual bonding mode found for cluster compounds and significantly, it is exactly the mode of coordination found in a LEEDS study of benzene attached to a rhodium surface.[219]

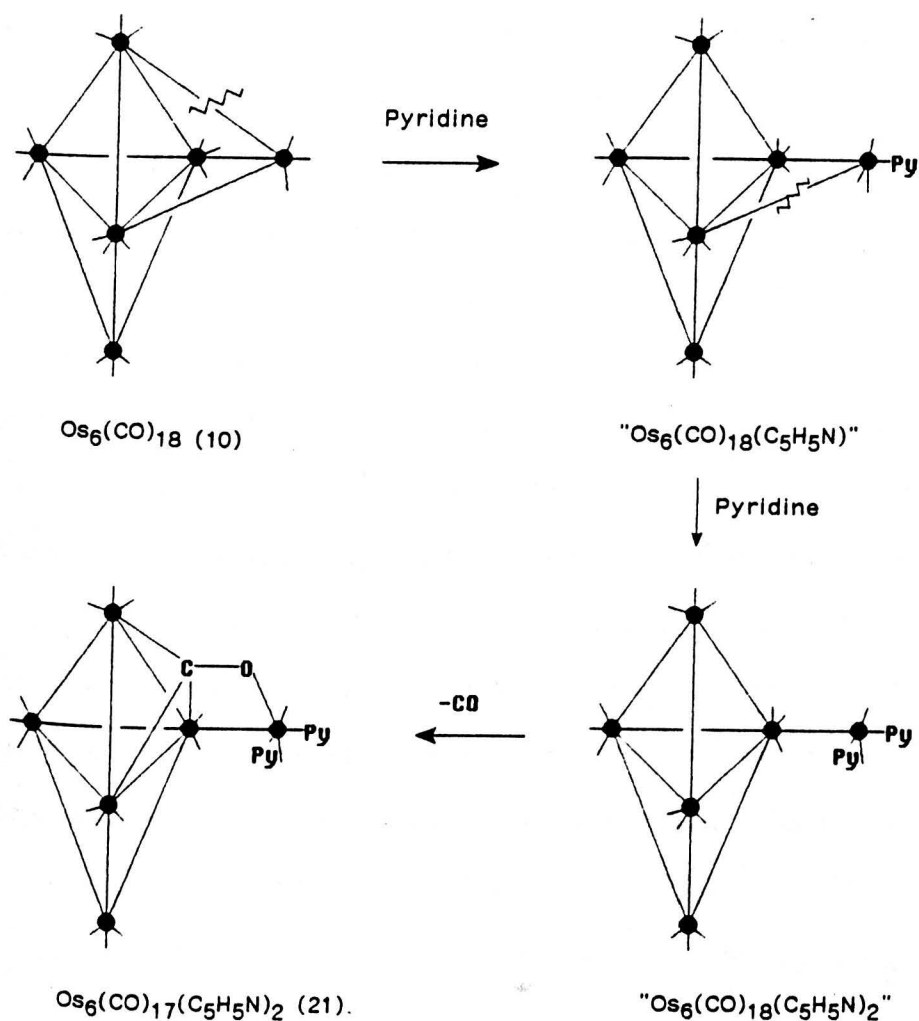


Figure 3.1/18 Proposed mechanism for the formation of (21).

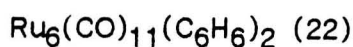
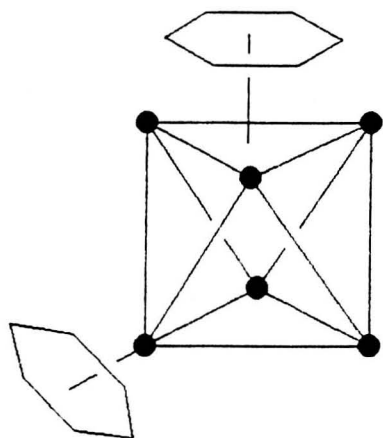


Figure 3.1/19 The bis-benzene cluster (22), with the two organo-groups adopting different bonds modes

The reaction of $\text{Os}_6(\text{CO})_{17}(\text{NCMe})$ with the mono-substituted alkyne $\text{HC}=\text{CET}$ yielded two main products.[152] The first, $\text{HOs}_6(\text{CO})_{17}(\mu_4\eta^2\delta_{5a}\text{-CCEt})$ (23), consists of a tetrahedron of osmiums, one edge of which is bridged by a fifth osmium, with the triangle thus formed being bridged by the sixth osmium atom (Figure 3.1/20). In this cluster, the alkyne hydrogen has migrated to the metal core and bridges one edge of the tetrahedron. The resulting alkynyl ligand caps the outermost triangle, σ -bonding to two metal atoms and π -bonding to the third osmium atom of the triangular face and, in addition, the α -carbon coordinates to one of the tetrahedral osmium atoms. The cluster has an 88 valence electron count, consistent with the presence of 10 Os-Os bonds, a 5e donating alkynyl fragment, CCEt, and a one electron donating μ_2 -hydride ligand.

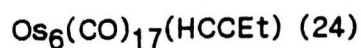
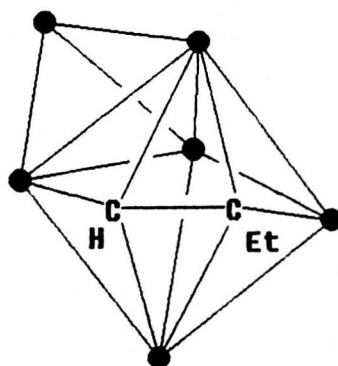
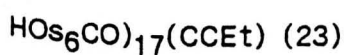
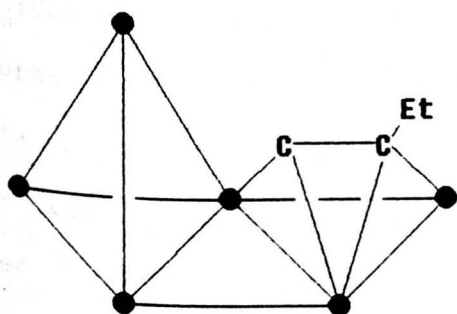


Figure 3.1/20 The alkenyl cluster (23) and the alkyne cluster (24).

The second product obtained from this reaction, $\text{Os}_6(\text{CO})_{17}(\text{HCCEt})$ (24), has a capped square pyramidal geometry (Figure 3.1/20). The alkyne ligand caps the base of the osmium square, coordinating to the cluster via 2σ - and 2π -bonds.[152] This results in the C-C vector lying approximately along the diagonal of the square base.

In contrast, the reaction of $\text{Os}_6(\text{CO})_{18}$ (10) with disubstituted alkynes gives $\text{Os}_6(\text{CO})_{16}(\text{RCCR}')$ (where R and R' are alkyl or aryl groups) as the major product. X-Ray structure analysis of the disubstituted cluster $\text{Os}_6(\text{CO})_{16}(\text{MeCCEt})$ (25) revealed that the capped trigonal bipyramidal core of the parent species is maintained with the alkyne group capping a triangular face in a $\mu_3\eta^2\delta_{4a}$ bonding mode (Figure 3.1/21).[84]

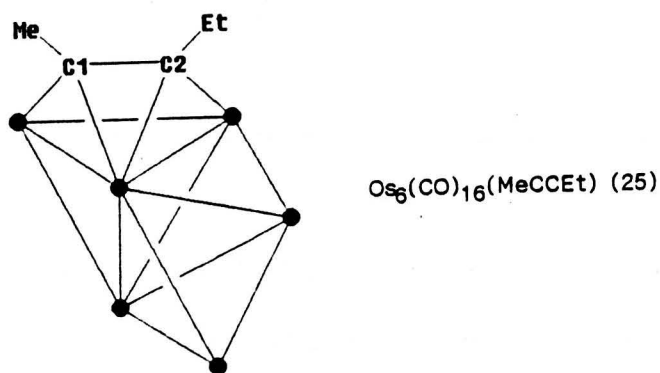


Figure 3.1/21 The capped trigonal bipyramidal M-core of (25).

The mid-eighties saw the development of a new synthetic strategy for preparing higher nuclearity clusters. An example of this was the reaction of $\text{H}_2\text{Os}(\text{CO})_4$ with $\text{Os}_5(\text{CO})_{15}(\text{MeCN})$, which gave the hexanuclear cluster $\text{H}_2\text{Os}_6(\text{CO})_{19}$ (26).[220] As with (21), the metal core of (26) is a 'spiked' trigonal bipyramid (Figure 3.1/22). In this complex, one of the hydrides adopts a terminal bonding mode to the 'spiked' osmium atom (this is the first example of a terminal hydrido-ligand for a cluster with nuclearity higher than four), and the other hydride bridges an equatorial-axial bond of the trigonal bipyramidal core. Similar synthetic strategy gives the spiked triangle $\text{H}_2\text{Os}_4(\text{CO})_{13}$, which has one terminal and one

μ_2 -hydride.[221] The 'spiked' metal configuration in these clusters appears to be the determining factor for one of the hydrides remaining terminal.[220,221]

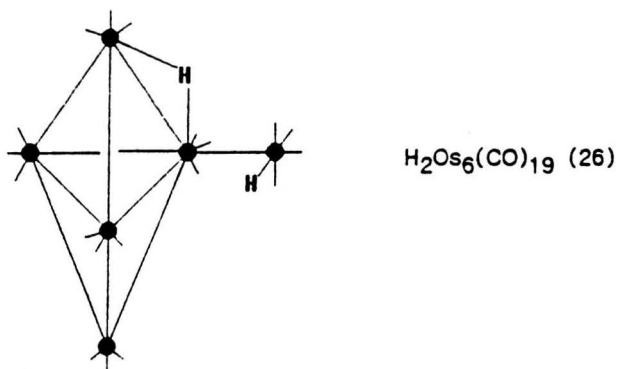


Figure 3.1/22 The spiked trigonal bipyramidal M-core of (26) with both terminal and μ_2 -bridging hydrides.

The first reported example of a ruthenium cluster, where the six metal atoms adopts the 'raft' configuration [seen for the osmium clusters (19) and (20)], was $\text{H}_2\text{Ru}_6(\text{CO})_{16}(\text{C}_6\text{H}_4\text{O})$ (27) (Figure 3.1/23).[222] This is a 90e-species, with the $\mu_5\eta^7\delta_9\text{-OC}_6\text{H}_4$ ligand acting as a 10 electron donor.

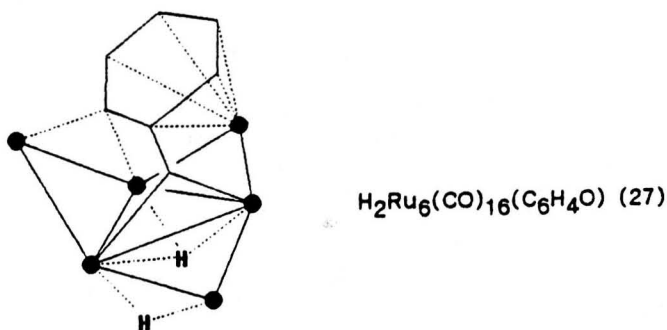
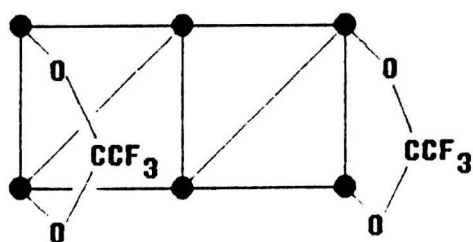


Figure 3.1/23 The giant equatorial triangular M-core of (27).

The reaction of $\text{Os}_6(\text{CO})_{18}$ (10) with $\text{Hg}(\text{O}_2\text{CCF}_3)_2$ produced a tetranuclear cluster $\text{Os}_4(\text{CO})_{12}(\text{O}_2\text{CCF}_3)_2$ and a hexanuclear cluster $\text{Os}_6(\text{CO})_{18}(\text{O}_2\text{CCF}_3)_2$ (28) (Figure 3.1/24).[223]



$\text{Os}_6(\text{CO})_{18}(\text{O}_2\text{CCF}_3)_2$ (28)

Figure 3.1/24 $\text{Os}_6(\text{CO})_{18}(\text{O}_2\text{CCF}_3)_2$ (28).

The metal core of (28) is an unusual Os_6 'ladder', in which the six metal atoms are not coplanar (Figure 3.1/24). This 90 electron system is an alternative geometry to the 'giant equatorial raft' framework seen in the osmium clusters (19), (20), and in the ruthenium cluster (27). The bidentate carboxylato ligands in (28) are approximately perpendicular to the Os_3 triangle and each trifluoroacetate ligand acts as a 3e donor. A similar mechanism to that proposed for the formation of (20) can be envisaged for the formation of (28) from (10). The pathway involves successive cleavage of 3 M-M bonds, but the alternative step involves the conversion of the 86 electron intermediate to an 88 electron species. The formation of (20) results from cleavage of an axial-equatorial bond of the 86e species, whereas in (28) an alternative axial-equatorial bond (adjacent to the bridging triangle) is broken (Figure 3.1/25).

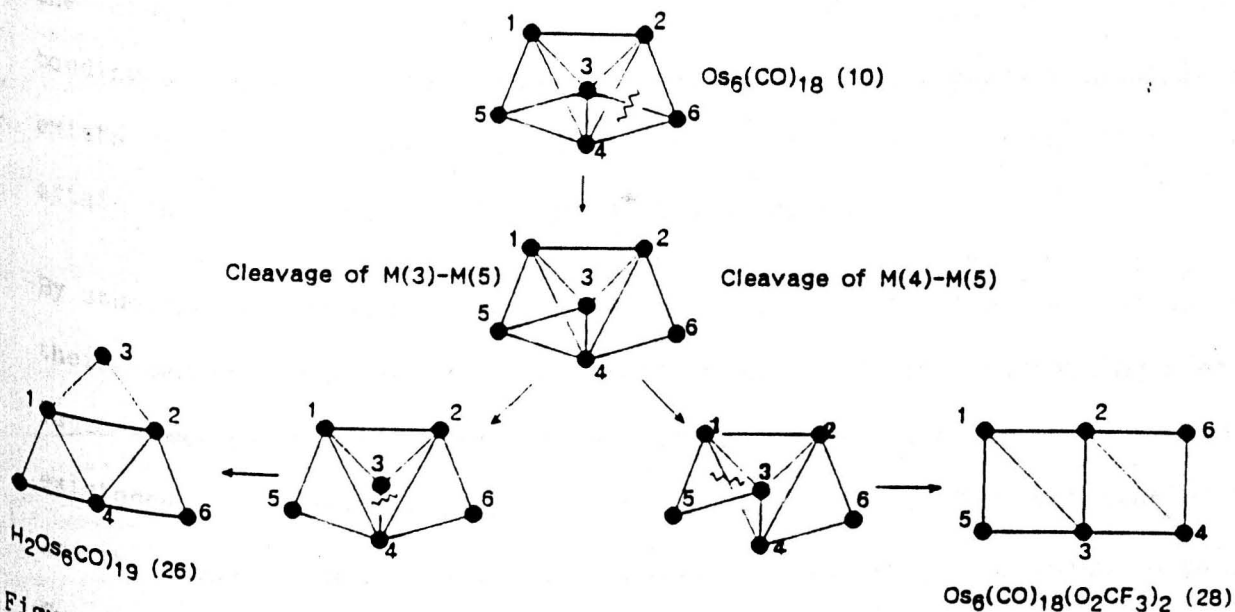


Figure 3.1/25 Mechanism for the formation of alternative 90e species.

This review of hexanuclear clusters has revealed both the predominance of the octahedral framework and the importance of carbido-species in maintaining this metal core geometry. It has shown that organo-fragments often have a profound effect on the metal framework and that the range of possible geometries is sensitive to a number of, often subtle, electronic differences. All X-ray structures reported in the remainder of this chapter are based on hexanuclear cores which contain interstitial carbido-atoms. One of the aims is to study the effect organo-fragments have on the metallic core and the type of bonding mode adopted, and to consider the role of the interstitial carbido-atom.

3.2 X-Ray structure analysis of $\text{Ru}_6\text{C}(\text{CO})_{15}(\text{C}_6\text{H}_8)$ (XR5) and a comparison with the linear analogue $\text{Ru}_6\text{C}(\text{CO})_{15}(\text{C}_6\text{H}_{10})$ (17).

3.2.1 Surface competition.

The study of organo-derivatives of polynuclear clusters, and specifically their surface topology, provides a useful analogy for understanding important processes such as catalysis at bulk metal surfaces. (This analogy is limited, as at present organo-derivatives of higher nuclearity clusters are rarely seen). One possible explanation for this is that as the cluster size increases the relative surface area available for ligand bonding decreases, and eventually becomes a limiting factor. Competition exists between surface availability and the need for the metal cluster to attain the correct number of polyhedral electrons.

By studying the structures of hexanuclear clusters of ruthenium, osmium and their organic derivatives, an understanding of the controlling steric factors may be gained. This can be extrapolated to predict the possible existence of higher nuclearity cluster hydrocarbons. One important class are the hexaruthenium carbonyl carbide derivatives, in which organic fragments have been found to replace some of the carbonyls of the parent cluster.

The two hexanuclear clusters discussed in this section differ only in the type of organo-fragment bonded to the cluster surface. This provides an opportunity to study the influence different organic fragments on the basic metal core unit, and the extent to which such ligands can distort the metal framework. Specifically, the two examples reported here, $\text{Ru}_6\text{C}(\text{CO})_{15}(\text{C}_6\text{H}_{10})$ (17) and $\text{Ru}_6\text{C}(\text{CO})_{15}(\text{C}_6\text{H}_8)$ (XR5), provide an opportunity to compare a linear and a cyclic hexadiene derivative of the same cluster core.

3.2.2 Structural description of the cyclohexadiene carbido-octahedral cluster $\text{Ru}_6\text{C}(\text{CO})_{15}(\text{C}_6\text{H}_8)$ (XR5).

An X-ray structure analysis of $\text{Ru}_6\text{C}(\text{CO})_{15}(\text{C}_6\text{H}_8)$ (XR5) established that the six ruthenium atoms adopt a carbido-centred octahedral geometry. There are fifteen carbonyl ligands, of which thirteen are terminal, one symmetrically bridges the Ru(4)-Ru(6) edge and one forms a very asymmetric bridge along Ru(3)-Ru(6). The cyclic organo-ligand bonds to one edge of the cluster via two π -bonds. The previously reported cluster $\text{Ru}_6\text{C}(\text{CO})_{15}(\text{C}_6\text{H}_{10})$ (17) adopts a very similar molecular configuration.

The X-ray structure solution of the linear hexadiene cluster $\text{Ru}_6\text{C}(\text{CO})_{15}(\text{C}_6\text{H}_{10})$ (17) was carried out by W.H. Nelson, [224] so only essential bond lengths and angles are quoted for comparison with the cyclohexadiene cluster $\text{Ru}_6\text{C}(\text{CO})_{15}(\text{C}_6\text{H}_8)$ (XR5). The structures $\text{Ru}_6\text{C}(\text{CO})_{15}(\text{C}_6\text{H}_{10})$ (17) and $\text{Ru}_6\text{C}(\text{CO})_{15}(\text{C}_6\text{H}_8)$ (XR5) are illustrated in Figure 3.2/1; essential crystallographic parameters for (XR5) are tabulated in Appendix A. Both clusters are numbered the same way for comparison.

3.2.3 Discussion.

The main difference between (XR5) and (17) lies in the mode of coordination of the cyclic and linear dienes. In the previously reported structure (17) the linear hexadiene lies on one side of the octahedron, forming two

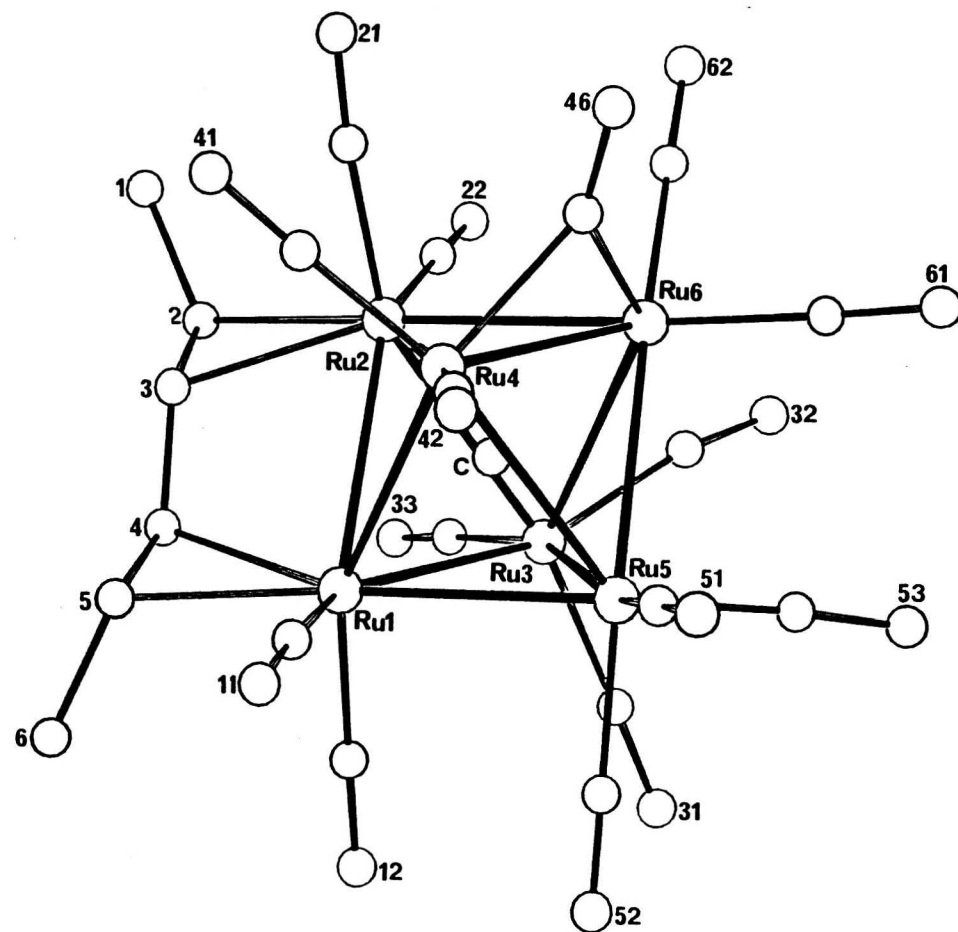
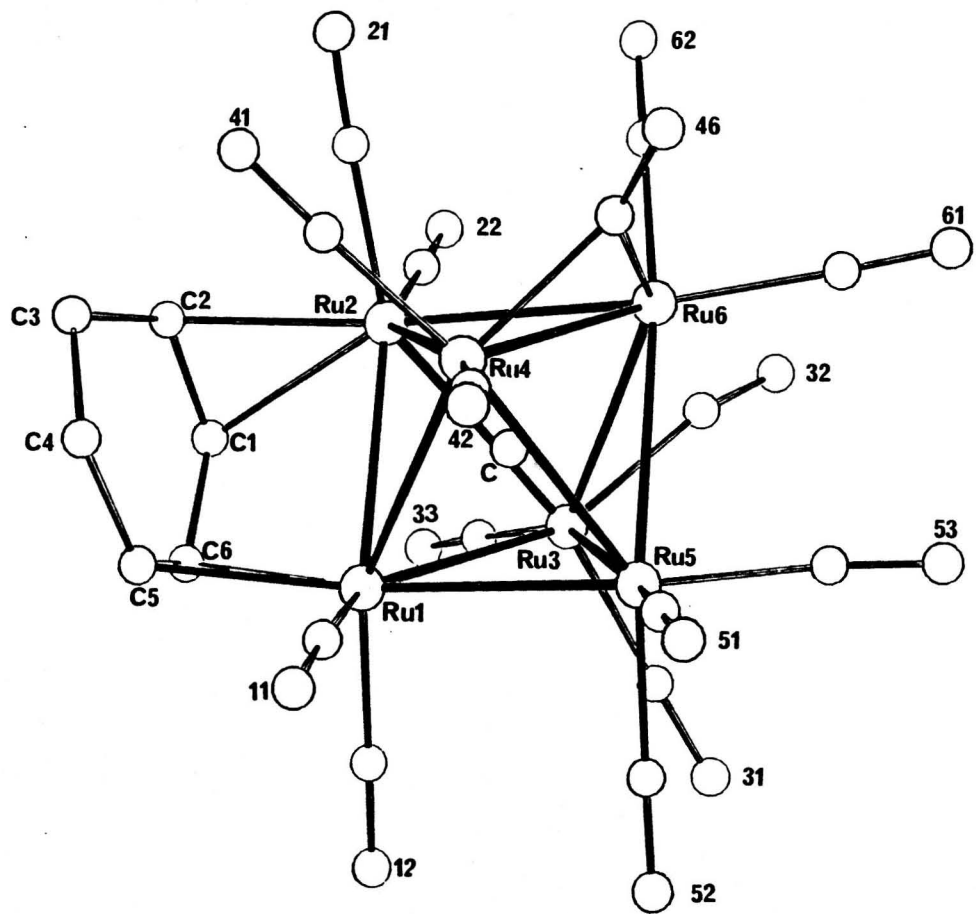


Figure 3.2/1 The molecular structure of $\text{Ru}_6\text{C}(\text{CO})_{15}(\text{C}_6\text{H}_8)$ (XR5) and

$\text{Ru}_6\text{C}(\text{CO})_{15}(\text{C}_6\text{H}_{10})$ (17). Only the O-atoms of the carbonyl ligands have been labelled for clarity.

π -bonds to two adjacent ruthenium atoms, Ru-C(organo) range 2.262(12)-2.311(19) Å (Table 3.2/1). The cyclohexadiene ligand in (XR5) adopts very similar bonding Ru-C(organo) range 2.254(7)-2.336(7) Å, lying along the Ru(1)-Ru(2) cluster edge, again π -bonding to the two adjacent metal atoms (Table 3.2/1).

Table 3.2/1 M-C(organo) bond lengths for (17) and (XR5) (Å).

	(17)	(XR5)
Ru(1)-C(4)	2.262(12)	Ru(1)-C(5) 2.265(6)
Ru(1)-C(5)	2.311(19)	Ru(1)-C(6) 2.254(7)
Ru(2)-C(2)	2.305(21)	Ru(2)-C(1) 2.336(7)
Ru(2)-C(3)	2.294(11)	Ru(2)-C(2) 2.278(6)

An interesting difference in the two structures is that in (XR5) the cyclic ligand is constrained to a cis-cis configuration, whereas the linear chain in (17) adopts a trans-trans configuration. Despite this difference a similarity in conjugation is evident. In both structures alternatively long and short bond lengths between the π -bonding unit are present. Significantly shorter bond lengths occur between the carbon atoms involved in π -bonding to the cluster: C(2)-C(3) 1.37(1) Å and C(4)-C(5) 1.34(2) Å for (17) and C(1)-C(2) 1.400(11) Å and C(5)-C(6) 1.385(9) Å for (XR5) than the remaining nominally single bonds [mean values - 1.50(2) Å (17) and 1.513(12) Å (XR5)] (Table 3.2/2). In both structures the C-C bonds between the two π -bond units, are shorter [C(3)-C(4) 1.42(1) Å (17) and C(5)-C(6) 1.385(9) Å (XR5)], consistent with some delocalisation of the electron density.

Table 3.2/2 Carbon-carbon bond lengths for the organofragments (Å).

	(17)	(XR5)	(18) ⁱ	(22) ⁱ
C(1)-C(2)	1.51(2)	1.400(11)	1.411(9)	1.42(2)
C(2)-C(3)	1.37(1)	1.496(8)	1.450(9)	1.46(2)
C(3)-C(4)	1.42(1)	1.543(12)	1.437(9)	1.39(2)
C(4)-C(5)	1.34(2)	1.510(11)	1.438(9)	1.50(2)
C(5)-C(6)	1.49(2)	1.385(9)	1.426(9)	1.37(2)
C(1)-C(6)	-	1.466(13)	1.522(9)	1.48(2)

i) The carbon atoms have been renumbered for comparison.

If the bonding at each metal atom is considered separately then a comparison with $\mu_1 \eta^1 \delta_2$ bonding ligands can be made. There are very few examples of hexanuclear ruthenium clusters with this mode of organo-bonding. One is the bitropyl cluster $\text{Ru}_6\text{C}(\text{CO})_{14}(\text{C}_{14}\text{H}_{14})$ (18), [213] which may be regarded as having three such bonds. This cluster has one less carbonyl ligand than either (XR5) or (17) in order to accommodate the third π -bond (Figure 3.1/14). The bond alternation seen in the cyclohexadiene ligand of (XR5) is less obvious for the bonds of the bitropyl ligand in (18) involved in bonding to the ruthenium atoms of one of the cluster faces, $\text{Ru-C}(\text{organo})$ 1.411(9)-1.522(9) Å (Table 3.2/2), but is evident in the related benzene cluster $\text{Ru}_6\text{C}(\text{CO})_{11}(\mu_3 \eta^6 \delta_6 - \text{C}_6\text{H}_6)(\eta^6 - \text{C}_6\text{H}_6)$ (22) (Figure 3.1/19), where one of the benzene ligands forms three $\mu_1 \eta^2 \delta_2$ bonding interactions to three ruthenium atoms of a cluster face. The mean of the three bonds in (22) involved in π -bonding to the cluster [C(1)-C(2), C(3)-C(4), and C(5)-C(6) mean 1.39(2) Å] is 0.09 Å ($>31\sigma$) shorter than the mean of the remaining three C-C benzene distances [C(2)-C(3), C(4)-C(5), and C(1)-C(6) mean 1.48(2) Å]. Distortion of bond lengths around aromatic rings has been noted previously when, for example, a metal atom is coordinated to just two of the carbon atoms in the ring. [226] In 'free' benzene, where complete delocalisation of π -electron density occurs, all the bonds are equivalent and of length ca. 1.397 Å (intermediate between a single (ca. 1.54 Å) and double (ca. 1.33 Å) bond. [225]

Despite the difference in the organo-ligands in (XR5) and (17) both the metal core and the remaining ligand distribution is very similar in both structures. Both structures (17) and (XR5) adopt slightly distorted octahedral frameworks of six ruthenium atoms, surrounding a carbide atom. The carbido-atom in the reported cluster (XR5) is not exactly in the centre

of the octahedron and the Ru-C distances lie in the range 2.015(6)-2.081(6) Å [Ru-C(carbide)_{mean} 2.052(6) Å]. A very similar range was noted in the earlier structure (17), with distances in the range 2.007(8)-2.099(8) Å [Ru-C(carbide)_{mean} 2.055(8) Å]. Both the bitropyl cluster (18) and the bis-benzene complex (22) have similar values, with the Ru-C range for (18) 2.022(5)-2.080(5) Å [Ru-C(carbide)_{mean} 2.055(5) Å] and the Ru-C(carbide)_{mean} for (22) 2.043 Å.

In the linear diene (17) the metal-metal bond lengths, for the two independent molecules, lie within the range 2.829(1)-2.982(1) Å, which is very similar to the range observed for the reported structure (XR5) [2.838(1)-2.961(1) Å]. There appears to be no obvious correlation between the variation in M-M bond lengths and the location of the bonding interaction with the organo-ligand. The bridged edge Ru(1)-Ru(2) is intermediate in length in (XR5) 2.889(1) Å, but is one of the longest bonds in (XR7) 2.963(1) Å (mean value). The parent carbido-cluster Ru₆C(CO)₁₇ (2)[194] has a larger Ru-Ru range, 2.827(5)-3.034(5) Å, and this is comparable to the range found for the phosphido-cluster Ru₆C(CO)₁₆(PPh₂Et) 2.850(1)-3.088(1) Å.[227] However, the organo-clusters Ru₆C(CO)₁₄(C₁₄H₁₄) (18) and Ru₆C(CO)₁₁(C₆H₆)₂ (22) have ranges closer to those observed for (XR5) and (17), Ru-Ru 2.778(1)-2.982(1) Å for (18) and 2.819(1)-3.006(1) Å for (22).

This suggests that organic ligands μ₃-bonded to a face of an octahedral cluster will slightly contract the core. Indeed, in both the bitropyl cluster (18) and the bis-benzene cluster (22) the triangular face involved in bonding to the μ₃-benzene is contracted [mean Ru-Ru 2.884(1) for (18) and 2.876(1) Å for (22)] compared with the remaining ruthenium bond lengths [Ru-Ru_{mean} 2.914(1) for (18) and 2.893(1) Å for (22)]. However this analogy cannot be directly compared in the clusters (XR5) and (17) where the hexacarbon fragments bond only to a cluster edge.

The range of Ru-C(carbonyl) distances and associated C-O distances were found to be very similar for both (XR5) and (17): Ru-C(carbonyl) range 1.871(8)-1.942(8) Å for (XR5) and 1.828(10)-1.901(12) Å for (17), and C-O(carbonyl) 1.117(9)-1.162(8) Å for (XR5) and 1.138(13)-1.192(14) Å for (17). These are typical and similar ranges are observed in other hexaruthenium clusters.[35,194,199,213,218,227,228] The similarity of carbonyl distribution in both structures, despite the difference in organo-ligands, is very striking - as can be seen in Figure 3.2/1 - and this will be discussed further in Section 3.2.3. Both clusters have thirteen terminal carbonyl ligands with very similar M-C-O bond angles, which lie in the range 172.5(8)-179.6(6)° for (17) and 172.0(8)-179.4(7)° for (XR5); the deviation from linearity is normal and has been discussed by Kettle.[178]

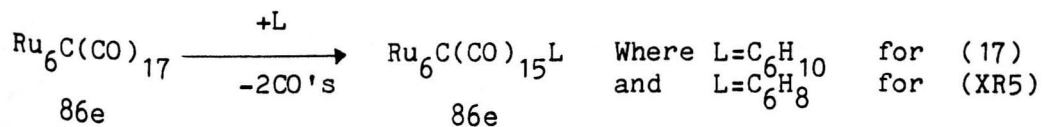
One of the remaining carbonyl ligands in both structures bonds in a slightly asymmetric mode with Ru(4)-C(46) 2.031(9) Å, Ru(6)-C(46) 2.120(9) Å for compound (17), and Ru(4)-C(46) 2.048(7) Å, Ru(6)-C(46) 2.133(6) Å for (XR5). Bridging carbonyl ligands have been observed in a number of other octahedral ruthenium clusters and all but one of the carbonyl ligands is terminal.[194,197,213,218,227,228] This is evident for Ru₆C(CO)₁₄(C₁₄H₁₄) (18) [Ru-C(bridging) 2.042(6) and 2.051(6) Å],[213] Ru₆C(CO)₁₆(PPh₂Et) [Ru-C(bridging) 2.079(14) and 2.038(14) Å],[227] and Ru₆C(CO)₁₅(Ph₂PCH₂PPh₂) [Ru-C(bridging) 2.05(1) and 2.06(1) Å].[228]

In both structures (XR5) and (17), the remaining carbonyl ligand may be regarded as very asymmetrically bridging, being strongly bonded to Ru(3), Ru(3)-C(32) 1.909(11) for (17), and Ru(3)-C(32) 1.942(8) Å for (XR5) and weakly bonded to Ru(6), Ru(6)-C(32) 2.594(11) for (17) and Ru(6)-C(32) 2.513(7) Å for (XR5). This is in marked contrast to osmium clusters where bridging carbonyl ligands are very rare indeed.

For the cluster solved by the author (XR5) there were no shorter intramolecular distances than that found between the cyclohexadiene hydrogen atom H(6) and the oxygen atom O(51) on an adjacent molecule [H(6)...O(51) 2.46 Å].

3.2.3 Comparison of the surface topology of (XR5) and (17).

Both molecules (17) and (XR5) may be formally considered as having been derived from $\text{Ru}_6\text{C}(\text{CO})_{17}$ (2) by replacement of two carbonyl ligands on adjacent metal atoms with an organic fragment.



The cyclic and linear dienes both bond to the cluster via two π -bonds to adjacent ruthenium atoms ($2\mu_1\eta^2\delta_2$ -bonding modes), and each contribute 4e (i.e. equivalent to two carbonyl ligands) to the overall polyhedral electron count. As mentioned in Section 3.2.2 the surface ligand distributions of the two clusters are similar. The surface topology of (17) and (XR5) can be illustrated by use of computed space filling models calculated from the X-ray coordinates (Figure 3.2/2). The interstitial carbon atom contributes 4e to the total electron count and therefore reduces the total number of carbonyl groups by two. Surprisingly, in spite of the difference in shape of the two hydrocarbon ligands, there is a close similarity in the distribution of the carbonyl groups. Both surfaces consist of a tightly packed array of carbonyl ligands and an organic fragment, which occupies a substantial percentage of the total surface of the sphere. This can be seen more clearly by removal of the organic fragments using computer simulation techniques. The space filling diagrams of these $\text{Ru}_6\text{C}(\text{CO})_{15}$ cores are illustrated in Figure 3.2/3. From these it is evident that there is enough space available for two more carbonyls, as is indeed the case in $\text{Ru}_6\text{C}(\text{CO})_{17}$ (2).

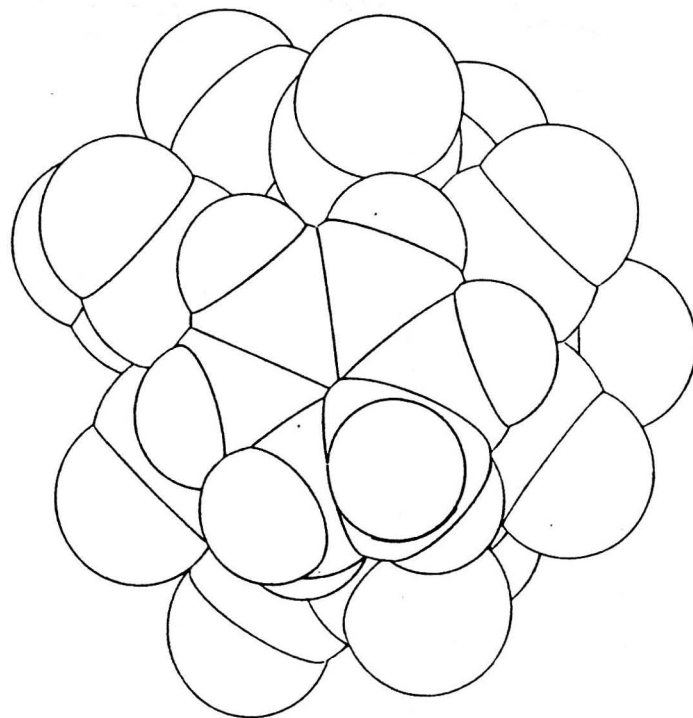
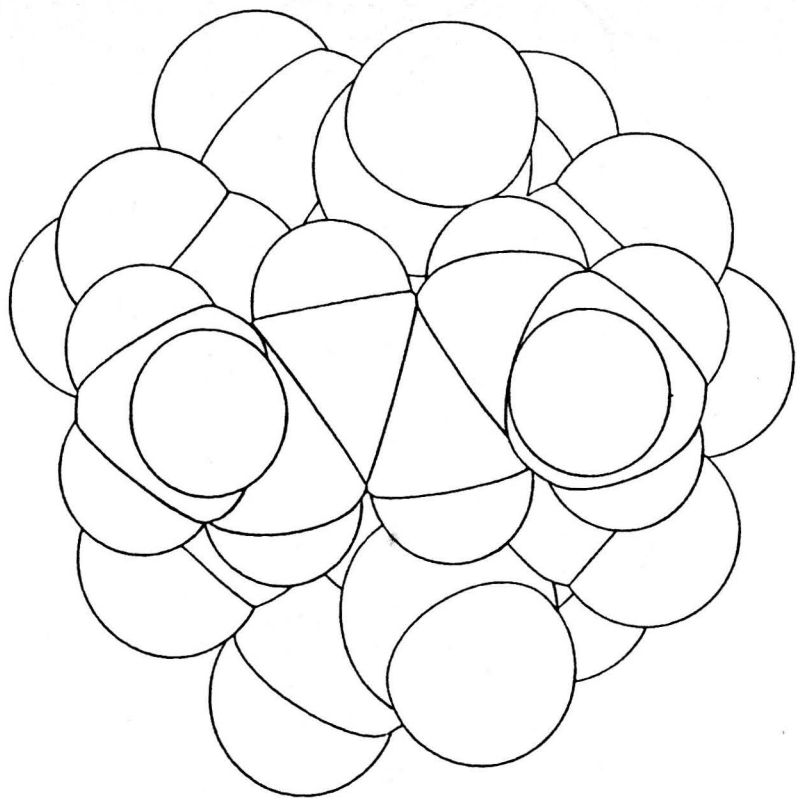


Figure 3.2/2 Computed 'space-filling' model of of $\text{Ru}_6\text{C}(\text{CO})_{15}(\text{C}_6\text{H}_8)$ (XR5) and $\text{Ru}_6\text{C}(\text{CO})_{15}(\text{C}_6\text{H}_{10})$ (17).

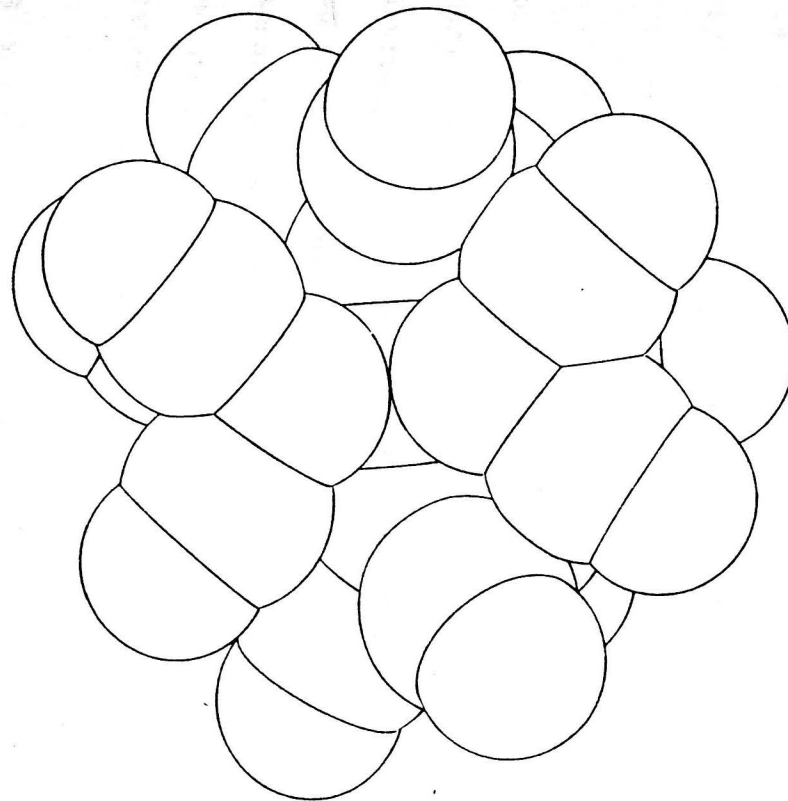
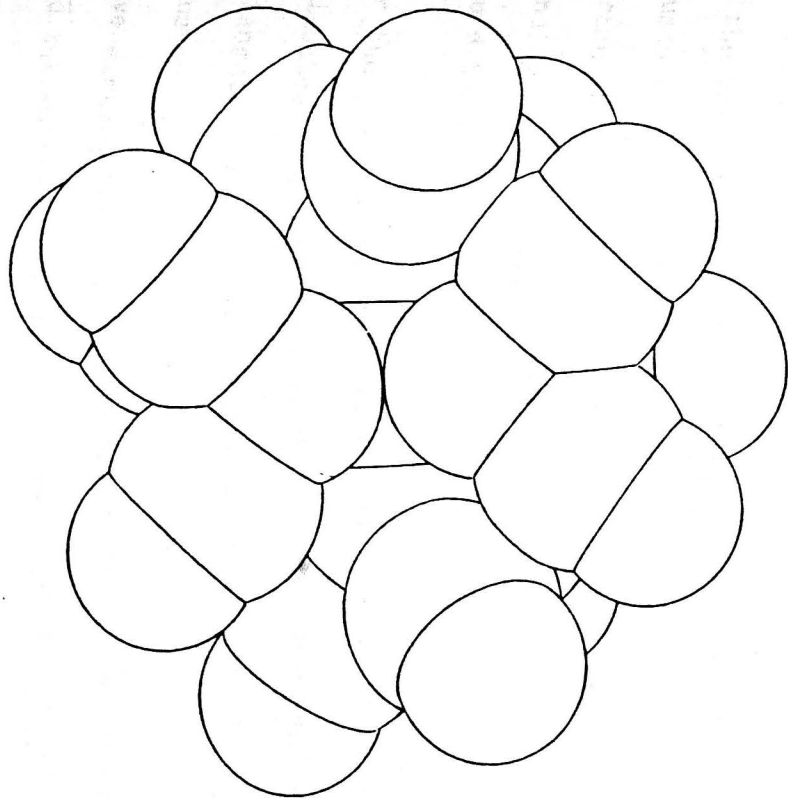


Figure 3.2/3 Computed 'space-filling' model of $\text{Ru}_6\text{C}(\text{CO})_{15}(\text{C}_6\text{H}_8)$ (XR5) and $\text{Ru}_6\text{C}(\text{CO})_{15}(\text{C}_6\text{H}_{10})$ (17),
with the organo-fragment removed.

3.2.4 Conclusion.

X-ray structure analysis of the carbido-cluster $\text{Ru}_6\text{C}(\text{CO})_{15}(\text{C}_6\text{H}_8)$ (XR5) established an octahedral metal core. The overall surface distribution of the cluster was remarkably similar to that found for the previously reported linear analogue $\text{Ru}_6\text{C}(\text{CO})_{15}(\text{C}_6\text{H}_{10})$ (17). In both cases, the central carbido-atom is considered essential in allowing coordination of relatively bulky organo-groups, such as C_6H_8 and C_6H_{10} . It is in keeping with this hypothesis that all other octahedral organo-clusters have an interstitial carbido-atom. No interstitial octahedral osmium clusters have been structurally characterised and in addition no organo-derivatives on octahedral osmium clusters are known.

3.3 X-Ray structure analysis of $\text{Ru}_6\text{C}(\text{CO})_{15}(\mu_3\text{n}^2\text{o}_{4a}-\text{PhCCH})$ (XR6) and $\text{Ru}_6\text{C}(\text{CO})_{15}(\mu_3\text{n}^2\text{o}_{4a}-\text{PhCCMe})$ (XR7).

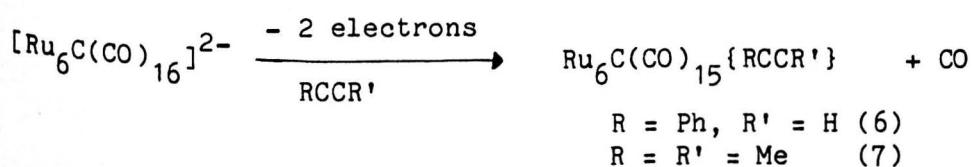
3.3.1 Introduction.

In the previous section a comparison was made between two octahedral clusters differing only in the organo-fragment; one contained a linear six carbon chain (17) and the other a cyclic hexacarbon ligand (XR5). The bonding modes adopted by the diene fragments in these two clusters was found to be very similar.

For the two structures discussed here, parallels can be drawn with trinuclear cluster chemistry. The bonding modes adopted onto the triangular faces of both clusters is similar to that found for simpler cluster species with three metal atoms (Section 1.4). Preliminary results have already been published.[229] Both the structures in this section and the related digold-derivative $\text{Ru}_6\text{C}(\text{CO})_{14}(\mu_3\text{n}^2\text{o}_{4a}-\text{PhCCH})(\text{AuPMe}_3)_2$ (XR8) discussed in Section 3.4 were synthesised by S.R. Drake at Cambridge University.

3.3.2 Synthesis.

The electrochemical two-electron oxidation of $[\text{Ru}_6\text{C}(\text{CO})_{16}]^{2-}$ under carbon monoxide atmosphere at a platinum electrode occurs at a potential of +0.5eV (vs Ag/AgCl) and on the same scale, the couples $\text{Fe}(\text{Cp})_2/[\text{Fe}(\text{Cp})_2]\text{BF}_4$ and $\text{Fe}(\text{Cp})_2/\text{FeCl}_3$ occur at similar values of 0.53 eV. This provides the basis for a recently discovered method of synthesis using either chemical or electrochemical oxidation of ruthenium cluster dianions in the presence of a ligand at room temperature.



The reaction of $[\text{Ru}_6\text{C}(\text{CO})_{16}]^{2-}$ with alkynes in the presence of 2 equivalents of either of the oxidants $[\text{Fe}(\text{Cp})_2]\text{BF}_4$ or FeCl_3 results in the formation of products of the general formula $\text{Ru}_6\text{C}(\text{CO})_{15}(\text{RCCR}')$. X-Ray structure analyses of two clusters were carried out, where $\text{R}=\text{Ph}$, $\text{R}'=\text{H}$ (XR6) and $\text{R}=\text{R}'=\text{Me}$ (XR7). The reaction permits an investigation of the differences in reactivity and the bonding mode adopted by mono- and disubstituted alkynes.

3.3.3 Structural description.

X-Ray structure analyses confirmed that the carbido-octahedral metal core was maintained in both $\text{Ru}_6\text{C}(\text{CO})_{15}(\text{PhCCH})$ (XR6) and $\text{Ru}_6\text{C}(\text{CO})_{15}(\text{MeCCMe})$ (XR7) (Figure 3.3/1). The only major difference between the two clusters is the organic ligand bonded to the cluster face. In (XR6) the mono-substituted alkyne, PhCCH , bonds to all three ruthenium atoms of one face of the cluster; forming σ -bonds to $\text{Ru}(1)$ and $\text{Ru}(2)$, and a π -bond to the remaining metal atom, $\text{Ru}(3)$. This results in the $\text{C}(1)$ - $\text{C}(2)$ backbone of the alkyne lying almost parallel to the $\text{Ru}(1)$ - $\text{Ru}(2)$ edge of the octahedron. The symmetrical disubstituted alkyne (but-2-yne) in (XR7) bonds to the octahedral core in an analogous fashion. All fifteen carbonyl ligands in

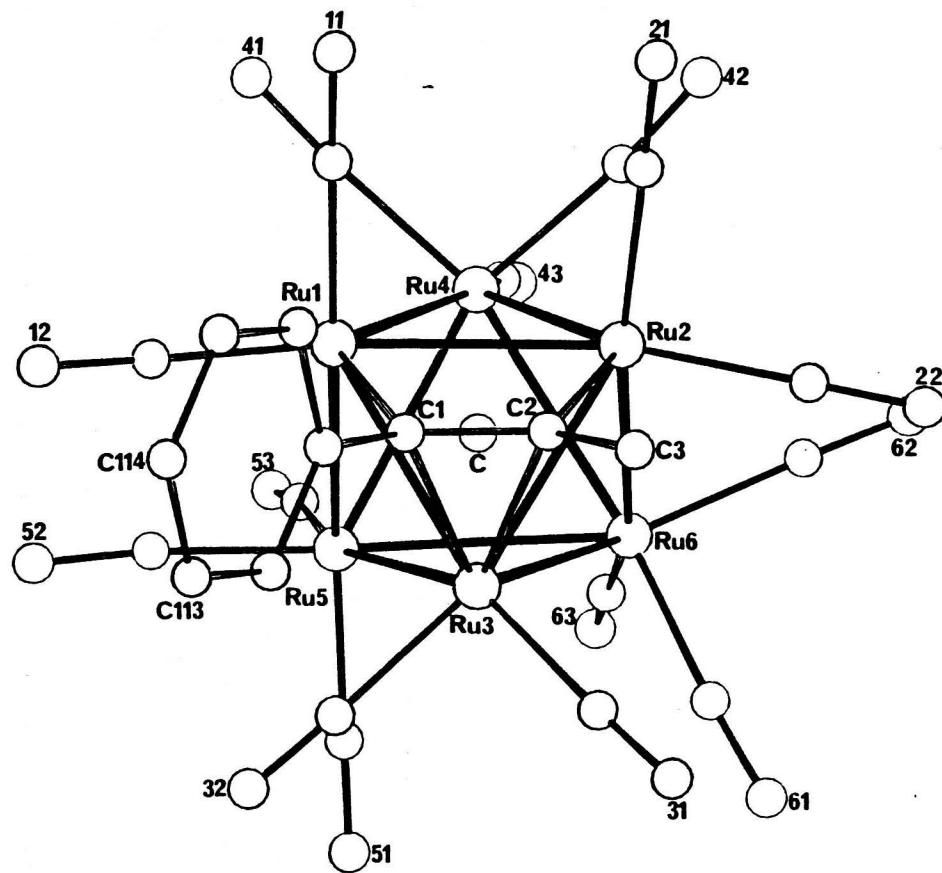
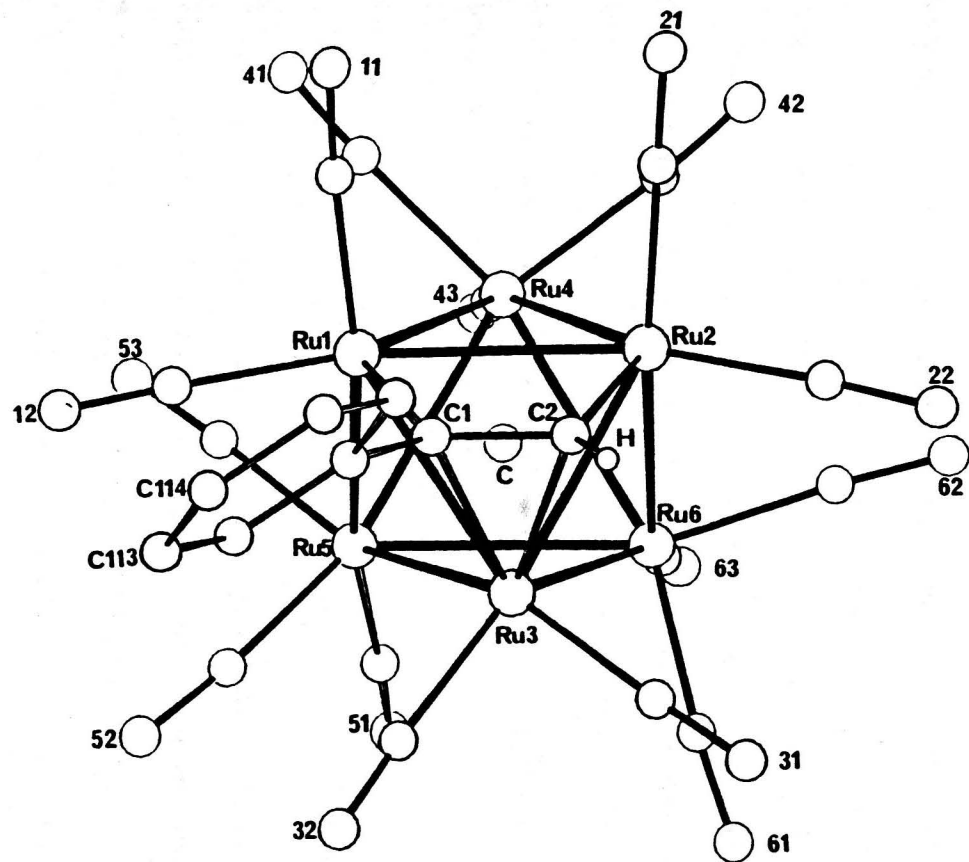


Figure 3.3/1 The molecular structure of $\text{Ru}_6\text{C}(\text{CO})_{15}(\text{PhCCH})$ (XR6) and

$\text{Ru}_6\text{C}(\text{CO})_{15}(\text{MeCCMe})$ (XR7). Only the O-atoms of the carbonyl ligands have been labelled for clarity.

each structure are terminally bonded, with the three ruthenium atoms involved in bonding to the alkyne groups having only two carbonyl ligands each. The remaining ruthenium atoms Ru(4), Ru(5), and Ru(6) all have three terminal carbonyl ligands.

3.3.4 Discussion.

The interstitial carbide atom lies almost at the centre of the octahedral framework in both structures, with the Ru-C(carbide) distances in the range 2.015(14)-2.073(15) Å for (XR6) [$\text{Ru-C(carbide)}_{\text{mean}} 2.046(18)$ Å] and 1.992(13)-2.098(11) Å for (XR7) [$\text{Ru-C(carbide)}_{\text{mean}} 2.045(14)$ Å]. These ranges are similar to those reported for the carbido-clusters $\text{Ru}_6\text{C(CO)}_{15}(\text{C}_6\text{H}_8)$ (XR5) and $\text{Ru}_6\text{C(CO)}_{15}(\text{C}_6\text{H}_{10})$ (17) discussed in the last section, and to other hexaruthenium clusters with interstitial C-atoms. [34, 194, 213, 218, 227, 228]

All 15 carbonyls are essentially linear for both structures, with Ru-C(carbonyl) distances in the range 1.862(21)-1.946(20) Å for (XR6) and 1.882(12)-1.929(12) Å for (XR7). The corresponding C-O distances lie in the range 1.098(20)-1.177(22) Å for (XR6) and 1.125(16)-1.157(17) Å for (XR7). The M-C-O bond angles lie within the range 172(1)-180(1)° for compound (XR6) and 168.8(8)-178.4(9)° for compound (XR7). These values are comparable to those observed for the terminal carbonyl ligands in (XR5) and the linear analogue (17) (Section 3.2), and to other carbido-octahedral structures. [35, 194, 199, 213, 218, 227, 228]

The metal-metal bond lengths are similar in both cases, lying within the range 2.764(2)-2.980(2) Å for (XR6) and 2.782(1)-2.991(1) Å for (XR7). For both structures (XR6) and (XR7) the bonds associated with the triangular face Ru(1), Ru(2), and Ru(3) are significantly shorter than the average of all the other metal-metal bond lengths, with the average bond length for a M-M bond in triangle 1,2,3 being 2.805(2) Å for compound (XR6) and

2.796(1) Å for compound (XR7). This compares with an average M-M bond length for the remaining nine metal bonds of 2.920(2) Å for (XR6) and 2.921(1) Å for (XR7). This constrained triangle is involved in bonding to the organo-fragment. The shorter bonds are significantly less than the shortest bond observed for (17), (XR5), the bitropyl cluster $\text{Ru}_6\text{C}(\text{CO})_{14}(\text{C}_{14}\text{H}_{14})$ (18), and the bis-benzene derivative $\text{Ru}_6\text{C}(\text{CO})_{11}(\text{C}_6\text{H}_6)_2$ (22) discussed previously (Section 3.2). This can be attributed to the presence of the organo-fragment μ_3 -bonding to a cluster face. As with the bitropyl cluster (18), the $\text{Ru-Ru}_{\text{mean}}$ of the Ru(1)-Ru(2)-Ru(3) face in both (XR6) and (XR7) is contracted with respect to the remaining Ru-Ru bond distances.

In structures (XR6) and (XR7) both carbon atoms of the alkyne group bond to Ru(3) [Ru(3)-C(1) 2.264(11) (XR6) and 2.181(11) (XR7), Ru(3)-(2) 2.174(11) (XR6) and 2.201(11) (XR7) Å]. In addition, each C-atom bonds to one other ruthenium atom of the triangular face [Ru(1)-C(1) 2.095(13) (XR6) and 2.069(8) (XR7); Ru(2)-C(2) 2.076(13) (XR6) and 2.078(9) Å (XR7)]. The alkyne C(1)-C(2) bond lies nearly parallel to the Ru(1)-Ru(2) edge of the two clusters (Figure 3.3/1), and in both cases a reduction in the formal C-C bond order upon coordination of the alkyne is indicated by the C(1)-C(2) bond lengths of 1.365(17) in (XR6) and 1.395(13) Å in (XR7). The interaction of the alkyne with metal atoms Ru(1) and Ru(2) in both structures may be formally described as σ -bonding in character, with that to Ru(3) being π -bonding (Figure 3.3/1). Similar bond lengths have been reported in other alkyne clusters which adopt this mode of bonding (Table 1.4/1). This 'parallel' $\mu_3\eta^2\delta_{4a}$ mode of bonding is more widely observed in clusters containing alkyne ligands than the alternative 'perpendicular' $\mu_3\eta^2\delta_{5a}$ mode. A variety of trinuclear clusters which have these 2 different forms are discussed in Section 1.4; typical M-C(organo) bond lengths are given.

3.3.5 Conclusion.

One point of interest is the similarity of the two structures, just as was found for the two previously discussed examples, (XR5) and (17). The mono- and disubstituted alkynes both adopt the same mode of bonding and, significantly, no H-migration to the metal core occurs for the mono-substituted alkyne. Organo-fragments often lead to cluster breakdown but this is not observed in either structures - evidence of the important role of the carbido-atom in stabilising the octahedral framework. As with (XR5) and (17), the metal core bond lengths and angles of both (XR6) and (XR7) are very similar. This differs from mono- and trinuclear clusters, where ligand fragmentation often occurs (Chapter 5). The fact that hydride migration does not occur with the terminal alkyne may be because this would result in cluster breakdown, caused by the inherent stability of octahedral clusters with interstitial carbido-ligands.

3.4 X-Ray structure analysis of $\text{Ru}_6\text{C}(\text{CO})_{14}(\text{PhCCH})(\text{AuPMe}_3)_2$ (XR8).

3.4.1 Synthesis.

The reaction of $[\text{PPN}]_2[\text{Ru}_6\text{C}(\text{CO})_{16}]$ with PhCCH in CH_2Cl_2 in the presence of FeCp_2BF_4 yields the alkyne complex $\text{Ru}_6\text{C}(\text{CO})_{15}(\text{PhCCH})$ (XR6) discussed in the last section. This cluster reacts rapidly with 2 equivalents of LiBu^n in THF at room temperature to give the dianionic intermediate $[\text{Ru}_6\text{C}(\text{CO})_{14}(\text{PhCCH})]^{2-}$. Subsequent addition of 2 equivalents of AuPMe_3Cl produces the novel alkyne-digold cluster species $\text{Ru}_6\text{C}(\text{CO})_{14}(\text{PhCCH})(\text{AuPMe}_3)_2$ (XR8) as the major product.

Two reasons for establishing the structure of this molecule were to see how the addition of AuPMe_3Cl would effect a) the metal core geometry, and b) the mode of bonding adopted by the alkyne fragment. The cation AuPMe_3^+ is isolobal to H^+ and so if this analogy is considered there are a number of possible reaction products. The AuPMe_3^+ might occupy a capping position

analogous to the μ_3 -hydrido ligands in $H_2Ru_6(CO)_{18}$ (4) (Section 3.1-Figure 3.1/3), [34,35] or it could replace the hydrogen atom in the terminal alkyne PhCCH. The second possibility could lead to a radical alteration of the mode of bonding adopted by the resultant organo-fragment, and at the same time cause the metal framework to open up. An X-ray structure analysis of this cluster was carried out to establish the molecular geometry of (XR8) and to consider the above points.

3.4.2 Structural description.

X-ray structure analysis established that the carbido-octahedral core of the precursor complex (XR6) is maintained. This is capped by one of the gold atoms and this is further capped by a second gold atom (Figure 3.4/1). The alkyne fragment bonds to a ruthenium face of the octahedron in an analogous fashion to that discussed above for the mono- and disubstituted alkyne clusters (XR6) and (XR7).

3.4.3 Discussion.

Clusters containing more than one $AuPR_3$ fragment (where R is usually an alkyl or aryl group) have been observed before. These gold-phosphine ligands can adopt two alternative forms of bonding. Firstly, each gold-phosphine fragment can act in isolation, this usually involves μ_2^- or μ_3 -bonding to the cluster face and so the isolobal analogy between an $AuPR_3$ unit and a hydrido-ligand remains applicable. Secondly, direct Au-Au bonds may arise and therefore the isolobal analogy no longer fully applies.

The isolobal analogy is evident for example in the di-gold cluster $Os_3(CO)_{10}(AuPEt_3)_2$ (29), [59] where the Au...Au separation is 4.304(2) Å and the gold atoms bridge the same Os-Os edge in a similar manner to the two hydride ligands in $H_2Os_3(CO)_{10}$ (30) (Figure 3.4/2). [60]

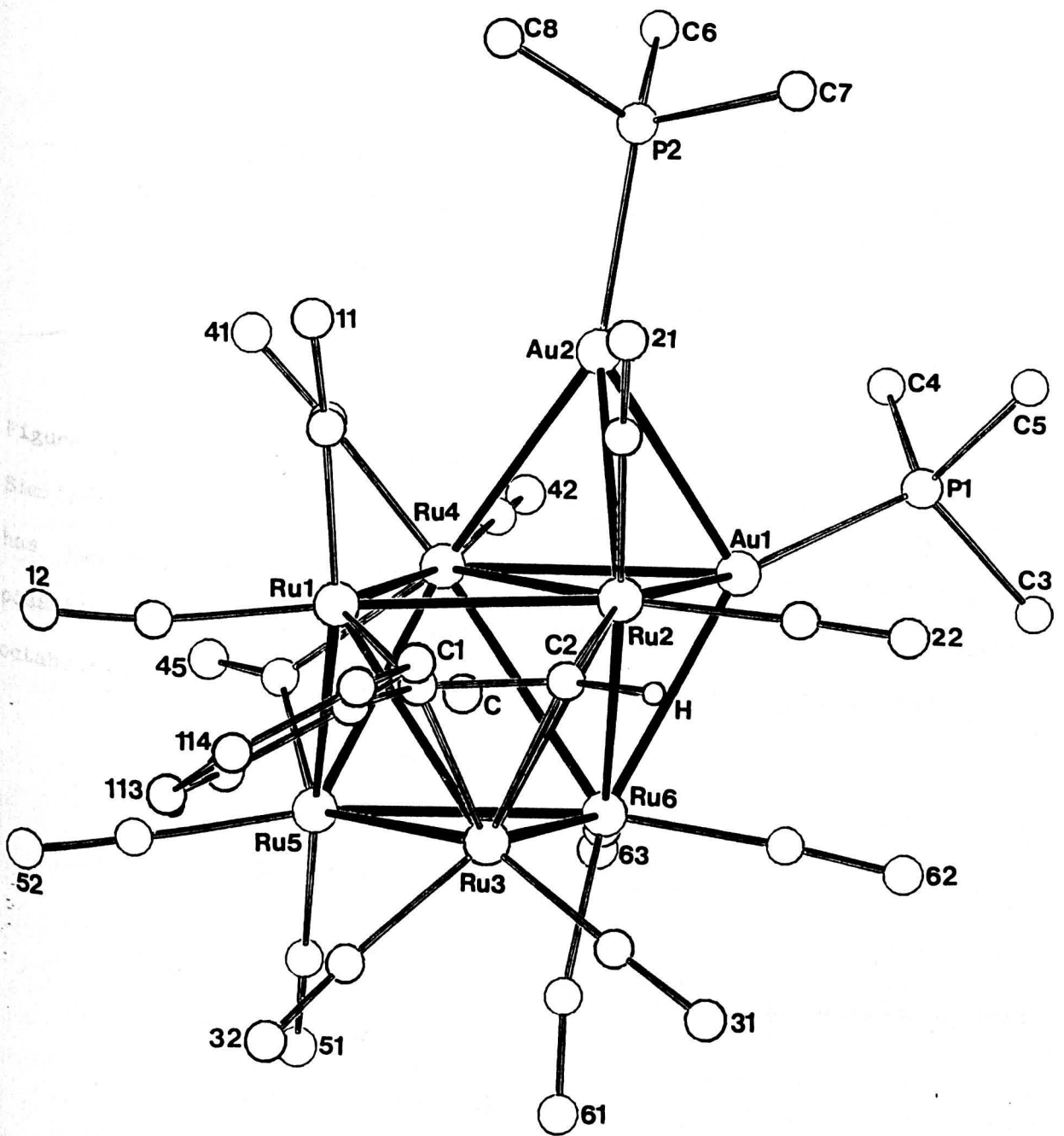
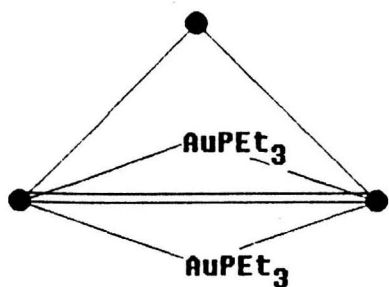
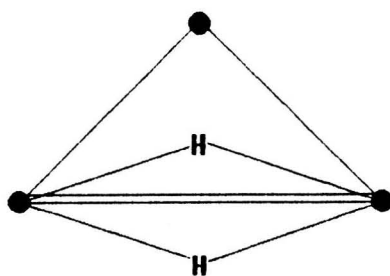


Figure 3.4/1 The molecular structure of $\text{Ru}_6\text{C}(\text{CO})_{14}(\text{PhCCH})(\text{AuPEt}_3)_2$ (XR8).

Only the O-atoms of the carbonyl ligands have been labelled for clarity.



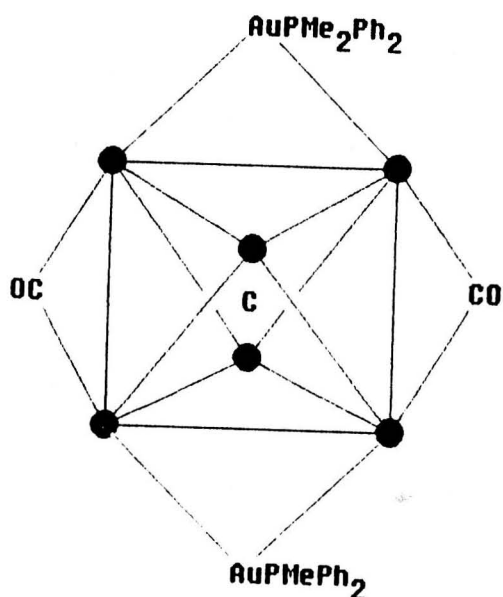
$\text{Os}_3(\text{CO})_{10}(\text{AuPET}_3)_2$ (29)



$\text{H}_2\text{Os}_3(\text{CO})_{10}$ (30)

Figure 3.4/2 Two isolobal clusters.

Similarly the octahedron of ruthenium atoms in $\text{Ru}_6\text{C}(\text{CO})_{16}(\text{AuPMePh}_2)_2$ (31) has two opposite edges bridged by gold fragments (Figure 3.4/3). [230] This possibly indicates that the hydride ligands in the related (unknown) octahedral cluster $\text{H}_2\text{Ru}_6\text{C}(\text{CO})_{16}$ would adopt an unusual μ_2 -bonding mode.



$\text{Ru}_6\text{C}(\text{CO})_{16}(\text{AuPMePh}_2)_2$ (31)

Figure 3.4/3 $\text{Ru}_6(\text{CO})_{16}(\text{AuPMePh}_2)_2$ (31).

Examples of the second type, where Au-Au bonds are formed, are found in a number of clusters. The heterometallic Ru_5W octahedron in $\text{Ru}_5\text{WC}(\text{CO})_{17}(\text{AuPET}_3)_2$ (32) is capped on a triangular Ru_3 face by an AuPET_3 unit. The tetrahedron so formed is then capped by the second AuPET_3 ligand and an Au-Au distance of $2.808(3) \text{ \AA}$ is observed (Figure 3.4/4). [230]

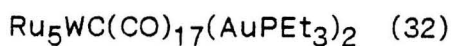
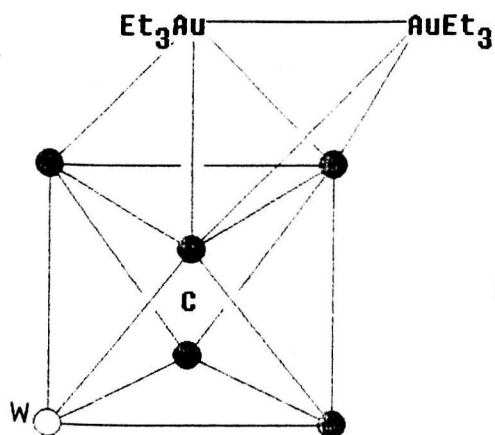


Figure 3.4/4 The heterometallic cluster $\text{Ru}_5\text{WC}(\text{CO})_{17}(\text{AuPEt}_3)_2$ (32), which contains two μ_3 - AuPEt_3 groups.

Several groups have synthesised a range of M_2Ru_3 and M_2Ru_4 [M=Au, Ag or Cu] cluster cores containing direct Au-Au bonding.[231-238] The metal core of the heterometallic cluster $\text{Au}_3\text{CoRu}_3(\text{CO})_{12}(\text{PPh}_3)_3$ (33) consists of a trigonal bipyramidal Ru_3CoAu core which is capped on adjacent faces by two more Au groups (Figure 3.4/5).[239] This is an example of the cis-bicapped trigonal bipyramidal core discussed in Section 1.3 (Figure 1.3/17), but no examples of this type of core are known for homonuclear clusters. The number of cluster valence electrons can be deduced in two alternative ways.

Despite the Au-Au bonds the gold triphenylphosphine groups can be considered as cluster ligands (isolobal with H) and therefore are assigned as one electron donors. This gives 60 CVE for the Ru_3Co core, the correct electron count for a tetrahedron. Secondly, the gold atoms can be considered as part of the metal framework, which gives a CVE of 96e, and subtracting 12e from each metal atom gives $S=6$, the correct number for a five vertex polyhedron, i.e., a trigonal bipyramid. Therefore the additional two metal atoms occupy capping positions.

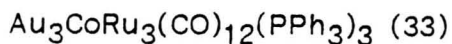
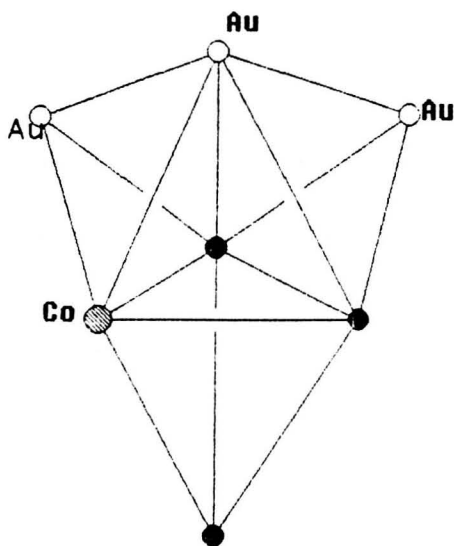
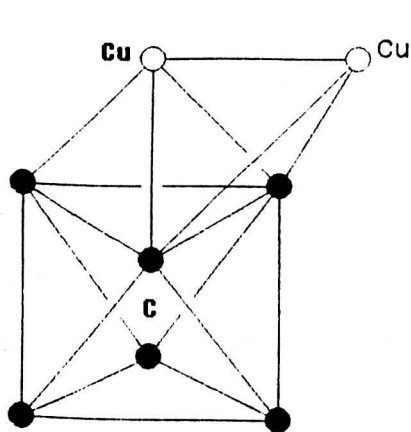


Figure 3.4/5 The M-core framework of $\text{Au}_3\text{CoRu}_3(\text{CO})_{12}(\text{PPh}_3)_3$ (33).

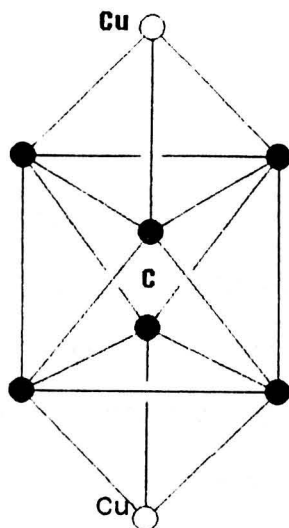
A similar core is observed in the hydrido-cluster $\text{HRu}_4(\text{CO})_{12}(\text{AuPPh}_3)_3$, [240] and in $\text{Ru}_3(\text{CO})_9(\text{COMe})(\text{AuPPh}_3)_3$ a related bicapped tetrahedral cluster core (a nido-trigonal bipyramid) occurs. [241] Nicholson noted that gold-gold bonding distances in these types of compounds vary between wide limits, and extremes of 2.784(1) to 3.010(1) Å have been reported. [241] An unusual tetragold unit $\text{Au}_4\{\text{P}(\text{C}_6\text{H}_{11})_3\}_3$ was observed in the high nuclearity cluster $\text{Au}_4\text{Os}_{10}\text{C}(\text{CO})_{24}(\text{P}(\text{C}_6\text{H}_{11})_3)_3$, which was bonded, via a naked μ_2 -Au atom, to the tetracapped octahedral Os_{10} unit. [242] The Au-Au bond lengths range from 2.665(2)-2.758(2) Å.

In the present work, X-ray structure analysis established that the six ruthenium atoms in $\text{Ru}_6\text{C}(\text{CO})_{14}(\text{PhCCH})(\text{AuPMe}_3)_2$ (XR18) adopt an octahedral geometry, with M-M bond lengths in the range 2.791(3)-3.111(3) Å (Figure 3.4/1). One gold atom asymmetrically caps the triangular face Ru(2)-Ru(4)-Ru(6) [Au(1)-Ru(2) 2.915(2), Au(1)-Ru(4) 2.920(2), and Au(1)-Ru(6) 2.799(2) Å], whilst the second gold atom caps a triangular face of this cap, namely, Ru(2)-Ru(4)-Au(1) [Au(2)-Ru(2) 2.996(2), Au(2)-Ru(4) 2.787(2), and Au(1)-Au(2) 2.795(2) Å], resulting in the formation of a direct gold-gold interaction.

This metal core has been observed before, in the cluster $\text{Cu}_2\text{Ru}_6\text{C}(\text{CO})_{16}(\text{CH}_3\text{CN})_2$ (34), [243] whereas a related Cu_2Ru_6 cluster $\text{Cu}_2\text{Ru}_6(\text{CO})_{18}(\text{C}_6\text{H}_5\text{CH}_3)_2$ (35) has the two Cu atoms capping the octahedron in a trans fashion (Figure 3.4/6). [244]



$\text{Cu}_2\text{Ru}_6\text{C}(\text{CO})_{16}(\text{CH}_3\text{CN})_2$ (34)



$\text{Cu}_2\text{Ru}_6\text{C}(\text{CO})_{18}(\text{C}_6\text{H}_5\text{CH}_3)_2$ (35)

Figure 3.4/6 Alternative bicapped octahedra.

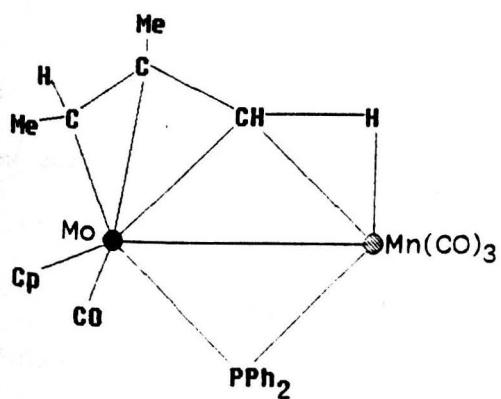
The alkyne group in $\text{Ru}_6\text{C}(\text{CO})_{14}(\text{PhCCH})(\text{AuPMe}_3)_2$ (XR8) bonds to the triangular face Ru(1)-Ru(2)-Ru(3) [Ru(1)-C(1) 2.083(21), Ru(2)-C(2) 2.051(23), Ru(3)-C(1) 2.228(22), and Ru(3)-C(2) 2.183(24) Å] in the same $\mu_3\eta^2\text{o}_{4a}$ (parallel) bonding mode observed in (XR6) and (XR7) (Section 3.3). One carbonyl ligand bridges the Ru(4)-Ru(5) edge of the cluster [Ru(4)-C(45) 2.09(3) and Ru(5)-C(45) 1.99(3) Å]; a feature not observed in either (XR6) or (XR7). However both the diene clusters (17) and (XR5) have one μ_2 -carbonyl ligand (Section 3.2 -Figure 3.2/1). All three ruthenium atoms in (XR8) involved in bonding to the phenylethyne ligand have in addition two linear carbonyl ligands, whereas Ru(6) is coordinated to three carbonyl ligands. In total thirteen carbonyl ligands are essentially linear, with the M-C-O angles in the range 165(3) to 177(2)°.

The carbido-atom in (XR8) lies almost at the centre of the octahedron of ruthenium atoms, with the metal-carbide bond lengths lying in the range 1.972(23) to 2.139(22) Å [mean M-C(carbide) 2.059(23) Å]. The gold-phosphorus bond lengths are identical, within experimental error, at Au(1)-P(1) 2.294(7) and Au(2)-P(2) 2.299(7) Å.

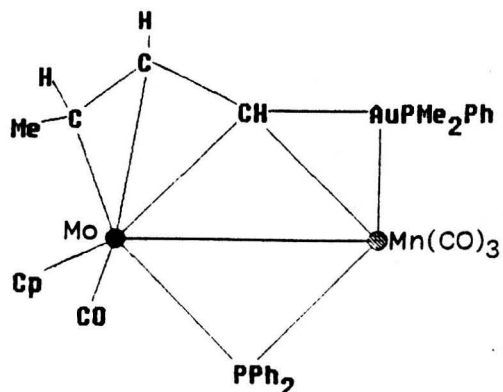
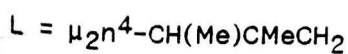
There are no shorter intramolecular distances than that between the oxygen atom O(42) and the methyl hydrogen atom H(61), and between O(61) and the alkyne hydrogen H, where the two oxygen atoms are on adjacent molecules [Os(42)...H(61) 2.43 and O(61)...H 2.43 Å].

Interestingly, ^{31}P n.m.r. evidence for a second isomer of (XR8) was obtained. It is thought that this isomer has no direct Au-Au bond and that interconversion between the two occurs by a low-energy process involving M-M bond cleavage/re-formation. This type of isomerism has been inferred before for $\text{Ru}_6\text{C}(\text{CO})_{16}(\text{AuPEt}_3)_2$. One isomer has a structure similar to the analogous methyl diphosphine cluster $\text{Ru}_6\text{C}(\text{CO})_{16}(\text{AuPMePh}_2)_2$ (31) (no Au-Au interaction), and the second isomer has a structure similar to $\text{Ru}_5\text{WC}(\text{CO})_{17}(\text{AuPEt}_3)_2$ (32) [Au-Au 2.803(3) Å] (Figures 3.4/3 and 3.4/4 respectively). The ^{31}P n.m.r. spectrum (in CH_2Cl_2 at room temperature) of $\text{Ru}_6\text{C}(\text{CO})_{16}(\text{AuPEt}_3)_2$ exhibits a single sharp resonance at δ -72.1 p.p.m. (relative to trimethylphosphite). On cooling, this resonance broadens and splits until, at -70°C , resonances of -69.8 and 76.2 p.p.m. (intensity 2:1) are observed. These were assigned to two different isomers of this complex which rapidly interconvert at room temperature. Lewis et. al. proposed that in one isomer the gold units adopt μ_2 -bridging bonding modes comparable to that found in the digold cluster $\text{Ru}_6(\text{CO})_{16}(\text{AuPMePh}_2)_2$ (31) (Figure 3.4/3), and in the other they are μ_3 -caps, as in the heteronuclear (Ru5W) octahedral cluster (32) (Figure 3.4/4).

The possible replacement of the alkynic hydrogen atom in $\text{Ru}_6\text{C}(\text{CO})_{15}(\text{PhCCH})$ (XR6) by a gold fragment was discussed at the beginning of this section. This type of isolobal replacement has only been observed before for a dinuclear compound. Both the hydride and isolobal analogue will be briefly discussed here.



MoMn(PPh₂)(L)(CO)₄(Cp) (36)



MoMn(PPh₂)(L)(CO)₄(Cp) (37)



Figure 3.4/7 Replacement of an allylic hydrogen atom by an Au(PR₃) unit.

The allylic compound MoMn(PPh₂)(Cp)(CO)₄(μ₂η⁴-CH(Me)CMeCH₂) (36) contains an allyl group which is η³-bonded to the Mo atom and, in addition, is bonded to the Mn atom via an agostic[245] C-H-Mn interaction (3-c,2-e) (Figure 3.4/7).[246] This can be deprotonated and the resultant anion reacted with AuClPMe₂Ph to give the isolobal gold derivative MoMn(PPh₂)(Cp)(CO)₄(μ₂η⁴-CH(Me)CHCHAu(PMe₂Ph) (37).[247] X-Ray analysis established that the structure of (37) is directly analogous to that of (36), with the agostic H-atom replaced by an isolobal Au(PMe₂Ph) group (Figure 3.4/7).[248] Mays suggested that this replacement is possible because an agostic interaction increases the acidity of the H-atom concerned, i.e. the H-atom is 'activated'. In the present work the failure of a gold atom to replace the alkyne hydrogen atom on the precursor cluster (XR6) may be because the H-atom of the mono-substituted alkyne does not interact with any metal atoms, and therefore has not been activated.

3.4.3 Conclusion.

The X-ray structure analysis of (XR8) established that the AuPMe₃⁺ group does not directly replace the hydrogen atom in the terminal alkyne PhCCH. Both the fundamental polyhedron of the precursor compound (XR6) and the mode of bonding adopted by the organo-fragment are retained. The first AuPMe₃⁺ group caps one of the triangular faces of the ruthenium octahedron

and could be considered analogous to that expected on reaction with H^+ . However, the isolobal analogy between H^+ and $AuPMe_3^+$ breaks down at this point, as a second $AuPMe_3^+$ group then further caps the cluster core with formation of an Au-Au bond. The cluster species (XR8) provides further evidence that the isolobal analogy cannot be carried too far. Not only does (XR8) contain a direct gold-gold bond, but replacement of the alkynic proton by a $AuPR_3$ unit (as might be expected) does not occur.

3.5 Overall Summary.

All five hexanuclear clusters discussed in this chapter consist of octahedral metal core frameworks with an interstitial carbido-atom. In addition, for (XR8) this fundamental polyhedron is bicapped by two $AuPMe_3^+$ groups, with the formation of a gold-gold bond. Two forms of organo-bonding have been found: for the dienes (XR5) and (17) two π -bonds are formed to one of the cluster edges, and in the remaining three clusters the alkynes lie parallel to a cluster edge bonding in a $\mu_3\eta^2\delta_{4a}$ fashion. There was no hydride migration to the metal core.

In Chapter 2, a mechanistic pathway for the reaction of pyridine with $Ru_5C(CO)_{15}$ was considered to proceed by successive M-M cleavage and formation, with the central carbido-atom acting as a 'pivot'. In the octahedral clusters discussed in this chapter, the carbido-atom adopts the role of stabilising the metal core polyhedron with major reactions occurring on the cluster surface by replacement of carbonyl ligands.

CHAPTER FOUR

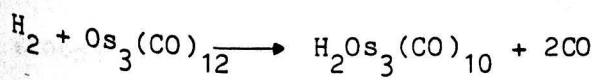
A key to carbide formation.

Chapter 4 - A key to carbide formation.

4.1 Cluster catalysis.

Three reasons have been cited as to why the study of metal clusters is relevant to that of catalytic processes.[248] Firstly, such clusters may serve as models of chemisorbed molecules or molecular fragments on the surfaces of metals. Secondly, clusters may enable the generation of reactive mononuclear fragments of high catalytic activity, by thermally or photochemically initiated scission of all M-M bonds in the cluster. Thirdly, clusters have additional flexibility in catalytic reactions when compared with their mononuclear counterparts.

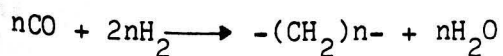
The third factor, flexibility, has been addressed in an article by Muettterties.[248] One of the most important catalytic processes is hydrogenation and oxidative addition. A specific illustration of how cluster chemistry provides an analogy for such a process is the addition of hydrogen to the triosmium cluster $\text{Os}_3(\text{CO})_{12}$:



In addition, the unsaturated dihydrido-product $\text{H}_2\text{Os}_3(\text{CO})_{10}$ can react with 2 equivalents of ethene to form the alkenyl cluster $\text{H}\text{Os}_3(\text{CO})_{10}(\text{CH}=\text{CH}_2)$. Subsequent loss of ethane and reaction with hydrogen regenerates the catalyst $\text{H}_2\text{Os}_3(\text{CO})_{10}$. [16,249] Analogous reactions occur with other terminal alkenes, and this series of reactions is discussed in more detail in Chapter 5. Another example is catalytic hydrogenation of ketones to alcohols, which is achieved by the tetranuclear cluster $\text{H}_4\text{Ru}_4(\text{CO})_{12}$. [250] Hydroformylation is catalysed by a variety of clusters, including $\text{H}_4\text{M}_4(\text{CO})_{12}$ [M = Ru or Os], [251] $\text{M}_3(\text{CO})_{12}$ [M = Ru or Os], and $\text{H}_2\text{Os}_3(\text{CO})_{10}$. [251,252]

4.1.1 Fischer-Tropsch Synthesis.

An important catalytic reduction process involving carbon monoxide is the Fischer-Tropsch reaction, which can be summarised by the following equation:



Depending on the conditions a range of different products can be obtained. These include straight chain alkanes, alkenes, alcohols, aldehydes, carboxylic acids, esters and arenes.

In 1982, Herrmann highlighted the following point when discussing possible mechanistic routes in this catalytic process:

"..Carbide cluster compounds....require further investigation into their capability for initiating Fischer-Tropsch-type reactions." [253] Herrmann cited tetranuclear examples to illustrate the role clusters could play in the analysis of the F-T synthesis. He noted that the addition of hydrogen to $[\text{Fe}_4\text{C}(\text{CO})_{12}]^{2-}$, giving $\text{HFe}_4(\eta^2\text{-CH})(\text{CO})_{12}$, demonstrates the reactivity of exposed low-coordinate carbido-atoms. [254-256] Furthermore, such carbido-atoms can be carbonylated to yield coordinated acyl groups. [253,257]

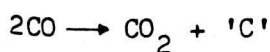
Five formal types of reaction are important in the Fischer-Tropsch synthesis. [258] These are: i) hydrogen atom transfer (from metal surface atoms or from surface intermediates) to carbon, leading to C-H bond formation; ii) hydrogen atom transfer to oxygen, resulting in O-H bond formation; iii) C-O bond scission; iv) C-C bond formation; v) C-O bond formation. In a Fischer-Tropsch synthesis reaction, there are probably a number of different surface intermediates, potentially leading to a mixture of products.

Although any of the five steps outlined above could be considered as the initial step, C-O cleavage is usually considered as the most likely. For

example, the hydrogenation of CO on surfaces composed of relatively electropositive metals, such as iron and ruthenium, appears to proceed largely by initial dissociative CO chemisorption to yield a reactive surface C species. The carbon monoxide bonds to one or more metal atoms, and then subsequently undergoes cleavage of the C-O bond. This type of process is of particular relevance to the formation of carbido-clusters discussed later in this chapter.

4.2 An early investigation of the process involved in carbido cluster formation.

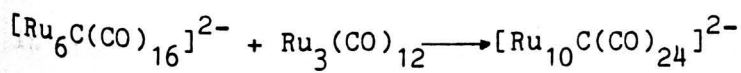
The thermolytic reactions of $M_3(CO)_x$ [$M=Ru$ or Os] clusters with a variety of small molecules yields a spectacular array of products with varying nuclearity and diverse ligand bonding modes (Sections 2.1 and 3.1). Mason and Robinson characterised the first example of a hexanuclear cluster containing an interstitial carbide atom from one of these reactions $Ru_6C(CO)_{14}(C_6H_3Me_3)$. [197] The origin of interstitial carbides has been the object of considerable discussion. For the trigonal prismatic carbido cluster $[Rh_6C(CO)_{15}]^{2-}$ ^{13}C labelling experiments established that it is derived from the solvent $CHCl_3$, [198] whereas, in contrast, similar experiments on ruthenium clusters showed that the interstitial C-atom forms by cleavage of coordinated carbon monoxide. Pyrolysis of $Ru_3(CO)_x$ in the absence of any other source of carbon gave the carbido-cluster $Ru_6C(CO)_{17}$. [165] The observation that CO_2 is evolved during the reaction is consistent with formation of the carbido-atom as a result of disproportion of two molecules of carbon monoxide.



This mechanism of carbonyl disproportionation is significant as the cleavage of the C-O bond of carbon monoxide is of fundamental importance, not only to the Fischer-Tropsch synthesis (Section 4.1), but also to many homogeneous and heterogeneous catalytic processes.

More recently, in the pyrolysis of $\text{Ru}_5(\text{CO})_{15}(\text{NCBu}^t)(\mu_5\text{-NCBu}^t)$ to give $\text{Ru}_6\text{C}(\text{CO})_{16}(\text{NCBu}^t)$, labelling of the NCBu^t ligands with ^{13}C established the carbido-atom originates from the cyano-carbon.[259]

In this chapter three hexanuclear carbido-species - all products of the same reaction - are characterised. It will be shown that these provide a key to understanding the mechanism of the formation of carbido-species. The decaruthenium cluster $[\text{Ru}_{10}\text{C}(\text{CO})_{24}]^{2-}$ with an interstitial carbido-atom was also obtained from this reaction and almost simultaneously by a different synthetic route.[260]



This method was exploited in the formation of the first decaruthenium interstitial nitrido-species $[\text{Ru}_{10}\text{N}(\text{CO})_{24}]^-$ (XR12) which has been structurally characterised as part of this work.

4.3 X-Ray structure analyses of $\text{Ru}_6\text{C}(\text{CO})_{14}(\eta^6\text{-C}_6\text{H}_3\text{Me}_3)$ (XR9), $\text{Ru}_6(\text{CO})_{15}(\eta^6\text{-C}_6\text{H}_3\text{Me}_3)$ (XR10) and $\text{HRu}_6(\text{CO})_{14}(\eta^7\text{-C}_6\text{H}_3\text{Me}_2\text{CH}_2)$ (XR11).

The structures of the clusters considered in this section offer an insight into the mechanism of formation of hexanuclear carbido-clusters. This is of importance in developing an understanding of the mechanisms involved in the F-T synthesis outlined above (Section 4.1), particularly with respect to the C-O scission step.

4.3.1 Synthesis.

All the synthetic work discussed in this chapter was carried out by P.J. Bailey at Cambridge University. $\text{Ru}_3(\text{CO})_{12}$ was reacted with a range of arenes (hexamethylbenzene, mesitylene, xylene, and toluene).[261,262] With mesitylene the products obtained were the known clusters $\text{Ru}_6\text{C}(\text{CO})_{17}$ (1) and $\text{Ru}_6\text{C}(\text{CO})_{14}(\eta^6\text{-C}_6\text{H}_3\text{Me}_3)$ (XR9). In addition, two complexes $\text{Ru}_6(\text{CO})_{13}(\mu_4\eta^6\delta_{5b}\text{-CO})_2(\eta^6\text{-C}_6\text{H}_3\text{Me}_3)$ (XR10) and

$\text{HRu}_6(\text{CO})_{13}(\mu_4\eta^2\delta_{5b}-\text{CO})(\eta^7-\text{C}_6\text{H}_3\text{Me}_2\text{CH}_2)$ (XR11) were produced. X-Ray structure analyses were carried out on the last three compounds. A further product of the reaction is the decaruthenium carbido-cluster dianion $[\text{Ru}_{10}\text{C}(\text{CO})_{24}]^{2-}$ (2), which has the tetracapped octahedral geometry. Almost simultaneously the synthesis of $[\text{Ru}_{10}\text{C}(\text{CO})_{24}]^{2-}$ (2) by an alternative route was reported.[260] This consisted of reaction of $\text{Ru}_3(\text{CO})_{12}$ with the dianion $[\text{Ru}_6\text{C}(\text{CO})_{16}]^{2-}$ to give $[\text{Ru}_{10}\text{C}(\text{CO})_{24}]^{2-}$ (2). A related reaction of the nitrido-cluster $[\text{Ru}_6\text{N}(\text{CO})_{16}]^-$ with $\text{Ru}_3(\text{CO})_{12}$ gave the decaruthenium monoanion $[\text{Ru}_{10}\text{N}(\text{CO})_{24}]^-$ (XR12), which has been structurally characterised in the present work and is discussed in Section 4.4.

The ^{13}C n.m.r. spectrum of $\text{Ru}_6\text{C}(\text{CO})_{14}(\text{C}_6\text{H}_3\text{Me}_3)$ (XR9) at 291 K indicated that there is total carbonyl fluxionality on the n.m.r. timescale since only one broad resonance is observed at 203.2 ppm in the terminal carbonyl region of the spectrum. Importantly, the carbido resonance appears at 442.8 ppm and its intensity shows that it is ^{13}C enriched, and must therefore have originated from a coordinated carbonyl ligand.

The solution infra-red spectrum of (XR11) shows two absorptions consistent with bridging carbonyl ligands and its electron impact (EI) mass spectrum showed a strong M^+ peak centred at $m/z = 1122$ with successive loss of 14 carbonyl ligands. The ^1H n.m.r. spectrum can be interpreted by assuming that the mesitylene ligand has lost a methyl hydrogen to the metal framework, and the resulting metal hydride ligand gives a singlet resonance at -19.5ppm (^1H). The methylene group so created is bonded to the cluster, giving rise to two doublets at 3.33 and 2.99 ppm ($J = 6\text{Hz}$). Other resonances are consistent with a $\mu_2\eta^7$ -coordination mode for the mesityl ligand. This anchors the ligand to the asymmetric cluster and prevents it from spinning, and so causes the inequivalence of the aryl hydrogens and the two sets of methyl hydrogens in the ligand. The EI mass spectrum of (XR10) showed an identical molecular ion to that given by (XR9) at $m/z=1136$

and successive loss of 14 carbonyl ligands. A peak at 44 daltons attributed to CO_2 was also observed to increase in intensity relative to that due to O_2 (32 daltons) during the experiment, showing that (XR10) is converting into (XR9) and CO_2 inside the spectrometer.

4.3.2 Structural descriptions.

a) The carbido-octahedral cluster $\text{Ru}_6\text{C}(\text{CO})_{14}(\eta^6\text{-C}_6\text{H}_3\text{Me}_3)$ (XR9).

The X-ray structure analysis of $\text{Ru}_6\text{C}(\text{CO})_{14}(\text{C}_6\text{H}_3\text{Me}_3)$ was first characterised by Mason and Robinson.[197] The X-ray structure analysis was repeated with much better data in the present work. $\text{Ru}_6\text{C}(\text{CO})_{14}(\text{C}_6\text{H}_3\text{Me}_3)$ (XR9) possesses an exact crystallographic mirror plane which passes through the centre of the octahedral Ru_6 unit. This contains two of the ruthenium atoms Ru(2), Ru(6), three carbon atoms of the mesitylene ring C(5), C(50), C(8), the central carbide and the two carbonyl ligands C(43), O(43), C(22), O(22) (Figure 4.3/1).

Of the 8 independent carbonyl ligands, 7 are essentially linear with the remaining carbonyl group bridging the Ru(4)-Ru(4') edge of the cluster. The mesitylene is involved in η^6 -coordination to Ru(6), with the six carbon atoms of the aryl ring essentially planar. The methyl groups of the η^6 -mesitylene ligand are staggered with respect to the η^2 -carbonyl ligands. The ^1H n.m.r. spectrum of (XR9) shows all methyl hydrogens to be equivalent at room temperature, indicating spinning of the mesitylene ring in solution.

b) $\text{Ru}_6(\text{CO})_{12}(\mu\text{-CO})(\mu_4\text{-}\eta^2\text{CO})_2(\eta^6\text{-C}_3\text{H}_3\text{Me}_3)$ (XR10).

X-Ray structure analysis established that the metal framework of $\text{Ru}_6(\text{CO})_{13}(\mu_4\eta^2\delta_{5b}\text{-CO})_2(\eta^6\text{-C}_3\text{H}_3\text{Me}_3)$ (XR10) consists of a tetranuclear Ru_4 core with two edge bridging ruthenium atoms (Figure 4.3/2), which is the first reported example of this type of geometry for a homonuclear cluster. The mesitylene ligand adopts the same bonding mode observed in (XR9), and

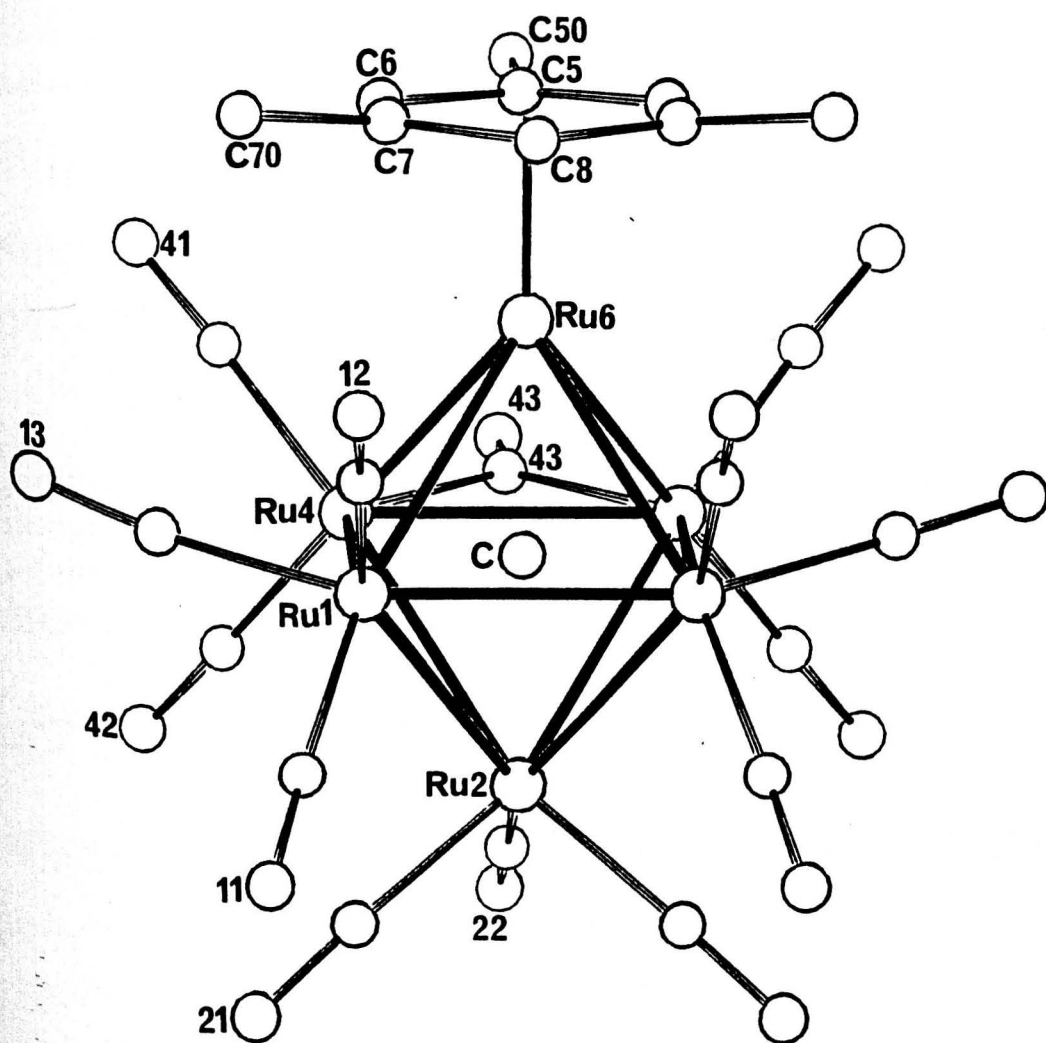


Figure 4.3/1 The molecular structure of $\text{Ru}_6\text{C}(\text{CO})_{15}(\text{C}_6\text{H}_3\text{Me}_3)$ (XR9).

Only the O-atoms of the carbonyl ligands have been labelled for clarity.

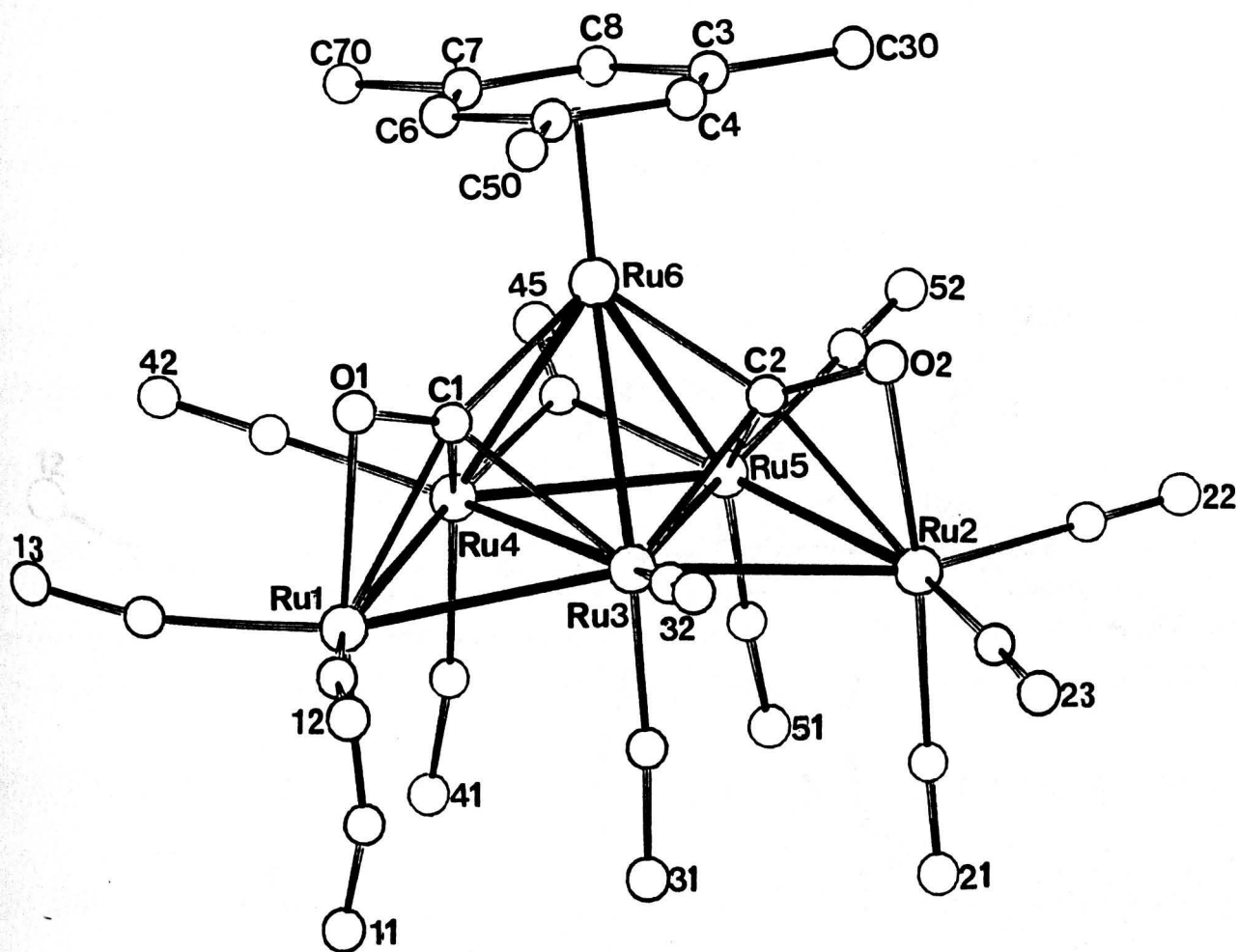


Figure 4.3/2 The molecular structure of $\text{Ru}_6(\text{CO})_{15}(\text{C}_6\text{H}_3\text{Me}_3)$ (XR10).

Only the O-atoms of the carbonyl ligands have been labelled for clarity.

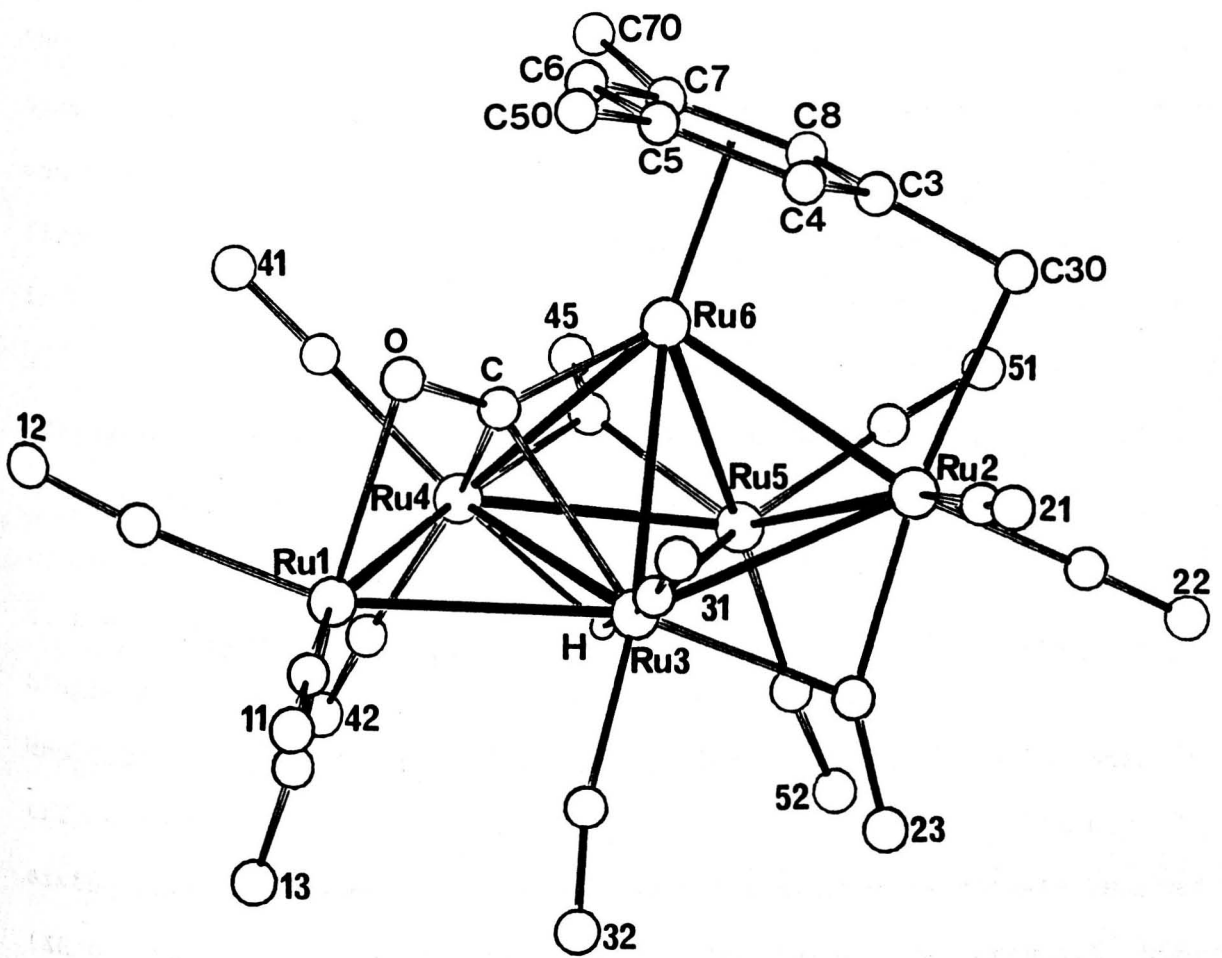


Figure 4.3/3 The molecular structure of $\text{HRu}_6(\text{CO})_{14}(\eta^7\text{-C}_6\text{H}_3\text{Me}_2\text{CH}_2)$ (XR11).
 Only the O-atoms of the carbonyl ligands have been labelled
 for clarity.

has all six carbon atoms of the aryl ring bonded to the apical atom Ru(6) of the central tetrahedron of ruthenium atoms. There are two 4e-donating ($\mu_4\eta^2\delta_{5b}$) carbonyl ligands situated in the two Ru_4 butterflies created by the two bridging ruthenium atoms [Ru(1) and Ru(2)], one carbonyl ligand symmetrically bridges the unique basal edge of the central Ru_4 tetrahedron, and the other twelve carbonyl ligands are essentially linear. This is the first example of a cluster containing two $\mu_4\eta^2\delta_{5b}$ -bridging carbonyl ligands in one molecule. The unusual bonding in each may be described as involving a four centre two electron (4c-2e) bond between the carbon atom and a triangular face of the tetrahedron, with the carbonyl unit involved in π -donation to a bridging ruthenium atom.

c) $HRu_6(CO)_{12}(\mu-CO)(\mu_4\eta^2\delta_{5b}-CO)(\mu_2\eta^7-C_6H_3Me_2CH_2)$ (XR11).

Single X-ray crystal structure analysis established that the metal core of $HRu_6(CO)_{13}(\mu_4\eta^2\delta_{5b}-CO)(\mu_2-\eta^7C_6H_3Me_2CH_2)$ (XR11) is a rare example of a trigonal bipyramid with one of the apical-equatorial edges bridged by a sixth ruthenium atom (Figure 4.3/3). The cluster is closely related to (XR10), having one less carbonyl ligand. Twelve of the carbonyl ligands are essentially linear; two carbonyl ligands symmetrically bridge M-M edges, Ru(2)-Ru(3) and Ru(4)-Ru(5). The remaining carbonyl ligand bridges the butterfly unit in a $\mu_4\eta^2\delta_{5b}$ -fashion, almost identical to the two carbonyl ligands in (XR10). The organo-ligand may be regarded as being derived from mesitylene by metallation at one of the methyl groups, with concomitant transfer of the hydrogen atom to the metal framework. The μ_3 -hydride, which bridges the basal plane defined by Ru(3), Ru(4), and Ru(5) of the central tetrahedron, was located by potential energy minimisation calculations.[263] A computed space filling diagram of (XR11), viewed onto the hydrido-capped face, is illustrated in Figure 4.3/4. It shows that the terminal carbonyl ligands associated with this face are 'pushed' back to accommodate the μ_3 -hydride ligand. A discussion of the

location of surface hydrido-ligands is given in Chapter 6. The hepta-hapto ligand has the six aryl carbon atoms bonded to Ru(6) (which may be formally regarded as an equatorial atom of the trigonal bipyramid) and is further bonded, via the methylene carbon atom C(30), to an edge bridging ruthenium atom Ru(2) [C(30)-Ru(2) 2.214(25) Å], resulting in an overall $\mu_2-\eta^7$ bonding mode.

4.3.3 Discussion.

The M-M bond lengths for the three hexanuclear structures (XR9), (XR10), and (XR11) are listed in Table 4.3/1.

Table 4.3/1 The Ru-Ru bond lengths (Å) for the three hexaruthenium clusters (XR9), (XR10), and (XR11).

Bond	(XR9)	(XR10)	(XR11)
Ru(1)-Ru(2)	2.906(1)		
Ru(1)-Ru(3)		2.839(1)	2.815(2)
Ru(1)-Ru(4)	2.966(1)	2.785(1)	2.744(2)
Ru(1)-Ru(5)			
Ru(1)-Ru(6)	2.872(1)		
Ru(2)-Ru(3)		2.842(1)	2.850(2)
Ru(2)-Ru(4)	2.851(1)		
Ru(2)-Ru(5)		2.776(1)	2.716(2)
Ru(2)-Ru(6)			2.788(2)
Ru(3)-Ru(4)		2.733(1)	2.858(2)
Ru(3)-Ru(5)		2.740(1)	2.934(2)
Ru(3)-Ru(6)		2.783(1)	2.754(2)
Ru(4)-Ru(5)		2.628(1)	2.679(2)
Ru(4)-Ru(6)	2.882(1)	2.843(1)	2.843(2)
Ru(5)-Ru(6)		2.820(1)	2.767(2)

The octahedral geometry observed in the carbido-cluster $\text{Ru}_6\text{C}(\text{CO})_{14}(\eta^6\text{-C}_6\text{H}_3\text{Me}_3)$ (XR9) is the most widely observed metal core framework for hexanuclear clusters. The Ru-Ru bond lengths in (XR9) lie in a range comparative to those observed for a number of related carbido-octahedral clusters (Table 4.3/2). Clusters of this type have been discussed in some detail in Chapter 3.

Table 4.3/2 The range of M-M bond lengths for (XR9) and related carbido-octahedral clusters. (Å).

Compound	Range	Ref.
$\text{Ru}_6\text{C}(\text{CO})_{14}(\text{C}_6\text{H}_3\text{Me}_3)$ (XR9)	2.851(1)-2.966(1)	[This work]
$\text{Ru}_6\text{C}(\text{CO})_{17}$ (1)	2.827(5)-3.034(5)	[194]
$\text{Ru}_6\text{C}(\text{CO})_{15}(\text{C}_6\text{H}_8)$ (XR5)	2.838(1)-2.961(1)	[Section 3.2]
$\text{Ru}_6\text{C}(\text{CO})_{15}(\text{C}_6\text{H}_{10})$	2.829(1)-2.982(1)	[140]
$\text{Ru}_6\text{C}(\text{CO})_{16}(\text{PPh}_2\text{Et})$	2.850(1)-3.088(1)	[227]
$\text{Ru}_6\text{C}(\text{CO})_{14}(\text{C}_{14}\text{H}_{14})$	2.778(1)-2.982(1)	[213]
$\text{Ru}_6\text{C}(\text{CO})_{11}(\text{C}_6\text{H}_6)_2$	2.819(1)-3.006(1)	[218]

The di-edge bridged metal core framework observed for $\text{Ru}_6(\text{CO})_{13}(\mu_4\eta^2\text{-CO})_2(\text{C}_6\text{H}_3\text{Me}_3)$ (XR10) is the first reported example for a homonuclear cluster. The Ru-Ru bond lengths are, on the whole, shorter than those found for the carbido-octahedral cluster (XR9) lying in the range 2.628(1)-2.843(1) Å, with that bridged by the $\mu_2\text{-CO}$ group being the shortest metal bond, Ru(4)-Ru(5) 2.628(1) Å. Similarly one of the carbonyl bridged M-M bonds in $\text{HRu}_6(\text{CO})_{14}(\eta^7\text{-C}_6\text{H}_3\text{Me}_2\text{CH}_2)$ (XR11) is also extremely short, Ru(4)-Ru(5) 2.679(2) Å, and in fact these are two of the shortest Ru-Ru bond lengths ever reported for a ruthenium cluster.

The carbido-atom in (XR9) lies almost at the centre of the octahedral core, Ru-C(carbide) range 1.923(11)-2.094(11) Å. Table 4.3/3 shows the M-C(carbide) range for (XR9) and a number of related carbido-octahedral clusters.

Table 4.3/3 M-C(carbido) bond lengths (Å).

Compound	Range	Mean
$\text{Ru}_6\text{C}(\text{CO})_{14}(\text{C}_6\text{H}_3\text{Me}_3)$ (XR9)	1.923(11)-2.094(11)	2.05(7)
$\text{Ru}_6\text{C}(\text{CO})_{15}(\text{C}_6\text{H}_8)$ (XR5)	2.015(6)-2.099(8)	2.052(6)
$\text{Ru}_6\text{C}(\text{CO})_{15}(\text{C}_6\text{H}_{10})$	2.007(8)-2.099(8)	2.055(8)
$\text{Ru}_6\text{C}(\text{CO})_{14}(\text{C}_{14}\text{H}_{14})$	2.022(5)-2.080(5)	2.055(5)
$\text{Ru}_6\text{C}(\text{CO})_{11}(\text{C}_6\text{H}_6)_2$		2.043(5)
$\text{Ru}_6\text{C}(\text{CO})_{16}(\text{PPh}_2\text{Et})$	2.010(7)-2.089(7)	2.058(7) ⁱ

i) The range given is for one of the molecules in the asymmetric unit.

Thirteen of the carbonyl ligands in (XR9) are essentially linear, lying in the range Ru-C(Carbonyl) 1.845(10)-1.931(12) Å, C-O(carbonyl) 1.160(12)-1.193(22) Å, and Ru-C-O 165(1)-180°C. The bridging carbonyl group lies in the mirror plane, with Ru(4)-C(43) 2.062(11) Å and Ru(4)-C(43)-O(43) 136.2(3)°. Table 4.3/4 lists comparative M-C(μ_2 -carbonyl) distances. The twelve terminal carbonyl ligands in (X10) lie in the range 1.861(9)-1.936(11) Å, C-O(carbonyl) 1.117(10)-1.167(10) Å, and Ru-C-O 175.0(7)-179.6(7)°. The eleven terminal carbonyl ligands in (XR11) lie in the range 1.82(3)-1.988(24) Å, C-O 1.05(3)-1.22(3) Å, and 171(2)-179(2)°.

Table 4.3/4 M-C(μ_2 -carbonyl) bond lengths (Å).

Compound	M1-C	M2-C
$\text{Ru}_6\text{C}(\text{CO})_{14}(\text{C}_6\text{H}_3\text{Me}_3)$ (XR9)	2.062(11)	
$\text{Ru}_6(\text{CO})_{15}(\text{C}_6\text{H}_3\text{Me}_3)$ (XR10)	2.091(11)	2.153(8)
$\text{HRu}_6(\text{CO})_{14}(\text{C}_6\text{H}_3\text{Me}_2\text{CH}_2)$ (XR11)	1.988(24)	2.183(22)
$\text{HRu}_6(\text{CO})_{14}(\text{C}_6\text{H}_3\text{Me}_2\text{CH}_2)$ (XR11)	1.99(3)	2.11(3)
$\text{Ru}_6\text{C}(\text{CO})_{15}(\text{C}_6\text{H}_8)$ (XR5)	2.048(7)	2.133(6)
$\text{Ru}_6\text{C}(\text{CO})_{15}(\text{C}_6\text{H}_{10})$	2.031(9)	2.120(9)
$\text{Ru}_6\text{C}(\text{CO})_{14}(\text{C}_{14}\text{H}_{14})$	2.042(6)	2.051(6)
$\text{Ru}_6\text{C}(\text{CO})_{16}(\text{PPh}_2\text{Et})$	2.079(14)	2.038(14)
$\text{Ru}_6\text{C}(\text{CO})_{15}(\text{Ph}_2\text{PCH}_2\text{PPh}_2)$	2.05(1)	2.06(1)

Table 4.3/5 shows that in $\text{Ru}_6\text{C}(\text{CO})_{14}(\eta^6\text{-C}_6\text{H}_3\text{Me}_3)$ (XR9) all six aryl carbon atoms of the mesitylene group bond to Ru(6), with the largest deviation from the mean [mean Ru(6)-C(aryl) 2.268(16) Å] being 0.056 Å for C(5). A similar mode of bonding is observed for the di-edge bridged tetrahedral cluster $\text{Ru}_6(\text{CO})_{15}(\text{C}_6\text{H}_3\text{Me}_3)$ (XR10), and here the largest deviation (0.024 Å) from the mean [mean Ru(6)-C(aryl) 2.280(9) Å] is observed for C(6). This type of η^6 -coordination has been observed in the bis-benzene cluster $\text{Ru}_6\text{C}(\text{CO})_{11}(\text{C}_6\text{H}_6)_2$, [218] and in the tetranuclear cluster $\text{Ru}_4(\text{CO})_9(\text{C}_6\text{H}_6)(\text{C}_6\text{H}_8)$ Ru-C(benzene) range 2.193(16)-2.274(16) Å. [264] The aryl carbon atoms of the mesitylene ligand in $\text{HRu}_6\text{C}(\text{CO})_{14}(\eta^7\text{-C}_6\text{H}_3\text{Me}_2\text{CH}_2)$ (XR11) are also all bonded in Ru(6) but, in addition, the methylene (CH_2) bonds to the bridging ruthenium atom Ru(2)-C(30) 2.214(25) Å. The largest deviation from the mean [mean Ru-C(aryl) 2.297(24) Å] in (XR11) is 0.017 Å.

Thirteen of the carbonyl ligands in (XR9) are essentially linear, lying in the range Ru-C(Carbonyl) 1.845(10)-1.931(12) Å, C-O(carbonyl) 1.160(12)-1.193(22) Å, and Ru-C-O 165(1)-180°C. The bridging carbonyl group lies in the mirror plane, with Ru(4)-C(43) 2.062(11) Å and Ru(4)-C(43)-O(43) 136.2(3)°. Table 4.3/4 lists comparative M-C(μ_2 -carbonyl) distances. The twelve terminal carbonyl ligands in (X10) lie in the range 1.861(9)-1.936(11) Å, C-O(carbonyl) 1.117(10)-1.167(10) Å, and Ru-C-O 175.0(7)-179.6(7)°. The eleven terminal carbonyl ligands in (XR11) lie in the range 1.82(3)-1.988(24) Å, C-O 1.05(3)-1.22(3) Å, and 171(2)-179(2)°.

Table 4.3/4 M-C(μ_2 -carbonyl) bond lengths (Å).

Compound	M1-C	M2-C
$\text{Ru}_6\text{C}(\text{CO})_{14}(\text{C}_6\text{H}_3\text{Me}_3)$ (XR9)	2.062(11)	
$\text{Ru}_6(\text{CO})_{15}(\text{C}_6\text{H}_3\text{Me}_3)$ (XR10)	2.091(11)	2.153(8)
$\text{HRu}_6(\text{CO})_{14}(\text{C}_6\text{H}_3\text{Me}_2\text{CH}_2)$ (XR11)	1.988(24)	2.183(22)
$\text{HRu}_6(\text{CO})_{14}(\text{C}_6\text{H}_3\text{Me}_2\text{CH}_2)$ (XR11)	1.99(3)	2.11(3)
$\text{Ru}_6\text{C}(\text{CO})_{15}(\text{C}_6\text{H}_8)$ (XR5)	2.048(7)	2.133(6)
$\text{Ru}_6\text{C}(\text{CO})_{15}(\text{C}_6\text{H}_{10})$	2.031(9)	2.120(9)
$\text{Ru}_6\text{C}(\text{CO})_{14}(\text{C}_{14}\text{H}_{14})$	2.042(6)	2.051(6)
$\text{Ru}_6\text{C}(\text{CO})_{16}(\text{PPh}_2\text{Et})$	2.079(14)	2.038(14)
$\text{Ru}_6\text{C}(\text{CO})_{15}(\text{Ph}_2\text{PCH}_2\text{PPh}_2)$	2.05(1)	2.06(1)

Table 4.3/5 shows that in $\text{Ru}_6\text{C}(\text{CO})_{14}(\eta^6\text{-C}_6\text{H}_3\text{Me}_3)$ (XR9) all six aryl carbon atoms of the mesitylene group bond to Ru(6), with the largest deviation from the mean [mean Ru(6)-C(aryl) 2.268(16) Å] being 0.056 Å for C(5). A similar mode of bonding is observed for the di-edge bridged tetrahedral cluster $\text{Ru}_6(\text{CO})_{15}(\text{C}_6\text{H}_3\text{Me}_3)$ (XR10), and here the largest deviation (0.024 Å) from the mean [mean Ru(6)-C(aryl) 2.280(9) Å] is observed for C(6). This type of η^6 -coordination has been observed in the bis-benzene cluster $\text{Ru}_6\text{C}(\text{CO})_{11}(\text{C}_6\text{H}_6)_2$, [218] and in the tetranuclear cluster $\text{Ru}_4(\text{CO})_9(\text{C}_6\text{H}_6)(\text{C}_6\text{H}_8)$ Ru-C(benzene) range 2.193(16)-2.274(16) Å. [264] The aryl carbon atoms of the mesitylene ligand in $\text{HRu}_6(\text{CO})_{14}(\eta^7\text{-C}_6\text{H}_3\text{Me}_2\text{CH}_2)$ (XR11) are also all bonded in Ru(6) but, in addition, the methylene (CH_2) bonds to the bridging ruthenium atom Ru(2)-C(30) 2.214(25) Å. The largest deviation from the mean [mean Ru-C(aryl) 2.297(24) Å] in (XR11) is 0.017 Å.

Table 4.3/5 M-C(aryl) bond lengths (Å).

Bond	(XR9)	(XR10)	(XR11)
Ru(6)-C(3)		2.302(9)	2.281(22)
Ru(6)-C(4)		2.271(7)	2.281(24)
Ru(6)-C(5)	2.237(16)	2.260(8)	2.314(21)
Ru(6)-C(6)	2.256(10)	2.256(8)	2.285(20)
Ru(6)-C(7)	2.324(9)	2.303(8)	2.311(23)
Ru(6)-C(8)	2.256(11)	2.285(10)	2.311(21)
Ru(2)-C(30)			2.214(25)

The organo-ligand in (XR11) is η^6 -bonded to the apical Ru(6) atom and is also bonded via the methylene carbon to Ru(2), C(30)-Ru(2) 2.25 Å, giving an overall $\mu_2\text{-}\eta^7$ -bonding mode as indicated by the ^1H n.m.r. spectrum.

This coordination is similar to that reported for the benzyl ligand in $\text{Ru}_8(\mu_8\text{-P})(\mu_2\text{-}\eta^7\text{-C}_6\text{H}_5\text{CH}_2)(\text{CO})_{19}$. [265] The bond angle C(3)-C(30)-Ru(2) in (XR11) is 92° and is reminiscent to that in the tetrabenzyl complex $\text{Ti}(\text{C}_6\text{H}_5\text{CH}_2)_4$, [266] which interestingly is a catalyst for the polymerisation of ethene and α -alkenes. [267] For each ligand in $\text{Ti}(\text{C}_6\text{H}_5\text{CH}_2)_4$, not only is the CH_2 group σ -bonded to the metal atom but there is also an interaction with the β -carbon atom and the Ti atom. A similar interaction may be present in (XR11), where there is a short intramolecular contact between Ru(2) and C(3) (2.75 Å).

Two of the carbonyl ligands in $\text{Ru}_6\text{C}(\text{CO})_{15}(\text{C}_6\text{H}_3\text{Me}_3)$ (XR10) bridge butterfly units of the metal core; in each of these the carbon atom σ -bonds to three of the ruthenium atoms with the C-O group forming a π -bond to the fourth metal atom, and in (XR11) one $\mu_4\eta^2\sigma_{5b}$ ligand is found. The C-O bond lengths of the η^2 -carbonyl ligands in (XR10) are equal within experimental error with a mean value of 1.255(10) Å, and are therefore considerably lengthened relative to the terminally coordinated ligands (mean 1.138(18) Å). This may be attributed to electron donation from the C-O π -bond, and increased electron density in the C-O π^* orbital due to the $d_\pi\text{-p}_\pi$ bonding from three metal atoms. These carbonyl ligands may therefore be regarded as 'activated'. In (XR11) there is one $\mu_4\eta^2\sigma_{5b}$ -carbonyl ligand coordinated in a similar position to those in

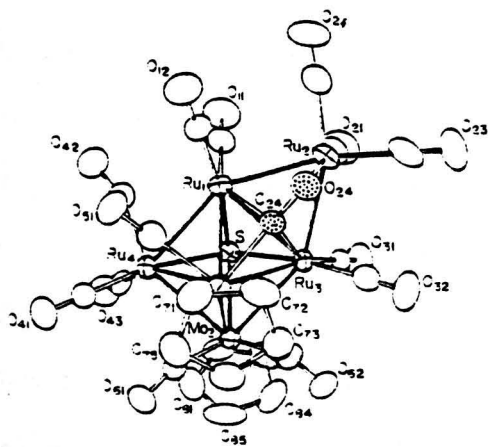
$[\text{Ru}_6(\mu_4\eta^2\delta_{5b}\text{-CO})_2(\text{CO})_{13}(\eta^6\text{-C}_6\text{H}_3\text{Me}_3)]$ (XR10) and this also shows lengthening of the C-O bond relative to the mean for the terminal carbonyls [1.21(2) and 1.13(2) Å respectively].

Clusters containing $\mu_4\eta^2\delta_{5b}$ bonded carbonyl ligands are extremely rare, and Table 4.3/6 lists the essential bond lengths for the $\mu_4\eta^2\delta_{5b}$ -carbonyl ligands in (XR10) and (XR11) and five other compounds with related bonding modes. The M(1)-C(μ_4 -carbonyl) bond lengths for the two μ_4 -carbonyl ligands in (XR10) [1.969(9) and 1.969(7) Å] and the one μ_4 -carbonyl ligand in (XR11) [1.913(23) Å] are significantly shorter than the mean of the remaining three M-C(μ_4 -carbonyl) bond lengths [mean Ru-C(μ_4 -carbonyl) 2.206(9) and 2.200(8) Å respectively for the two μ_4 -carbonyl groups in (XR10)] and [mean Ru-C(μ_4 -carbonyl) 2.278(22) Å for (XR11)]. The other two examples of $\mu_4\eta^2\delta_{5b}$ carbonyl groups occur in the monoanion $[\text{HFe}_4(\text{CO})_{13}]^-$ (6), [269] and the heterometallic cluster $\text{Co}_2\text{Mo}_2(\text{CO})_4(\text{C}_5\text{H}_5)(\text{C}_5\text{Me}_5)$ (7) (Figure 4.3/5). [270] Again, in both these compounds one M-C(μ_4 -carbonyl) bond length is significantly shorter than the mean of the remaining three.

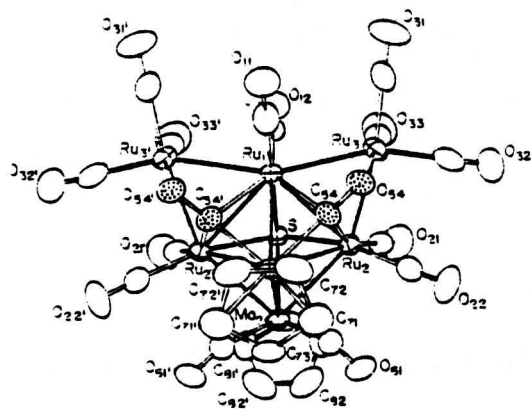
A related bonding mode in which the C-atom is bonded only to three metal atoms is observed in the heterometallic clusters $\text{Ru}_4\text{Mo}_2(\mu_4\text{-S})(\text{CO})_{12}(\text{C}_5\text{H}_5)_2$ (3) and $\text{Ru}_5\text{Mo}_2(\mu_4\text{-S})(\text{CO})_{14}(\text{C}_5\text{H}_5)_2$ (4), and in the spiked trigonal bipyramidal cluster $\text{Os}_6(\text{CO})_{17}(\text{Py})_2$ (5) (Figure 4.3/4). As with the $\mu_4\eta^2\delta_{5b}$ bonding mode, in all of these compounds the C-O bond is considerably activated, lying in the range 1.25(1)-1.283(3) Å (Table 4.3/7).

In (XR9) there are no shorter intramolecular contacts than that found between two adjacent carbonyl ligands C(41)...C(42) 2.58 Å. In (XR10) the shortest distance is between a mesitylene hydrogen atom and an oxygen atom of a near by carbonyl group H(6)...O(1) 2.47 Å. For the hydrido-cluster (XR11) the shortest intramolecular distance is between the μ_3 -hydrido-atom and the carbon atom of a carbonyl group H...C(42) 2.61 Å.

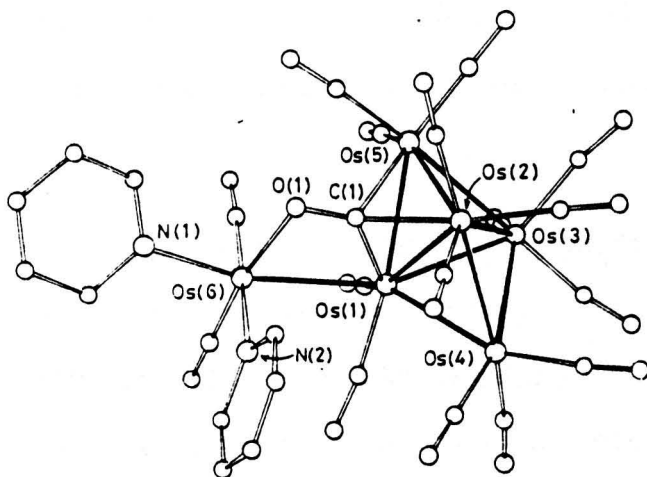
Figure 4.3/5 Clusters containing $\mu_4 n^2 \delta_{5b}$ and $\mu_3 n^2 \delta_{4b}$ -bonded carbonyl ligands.



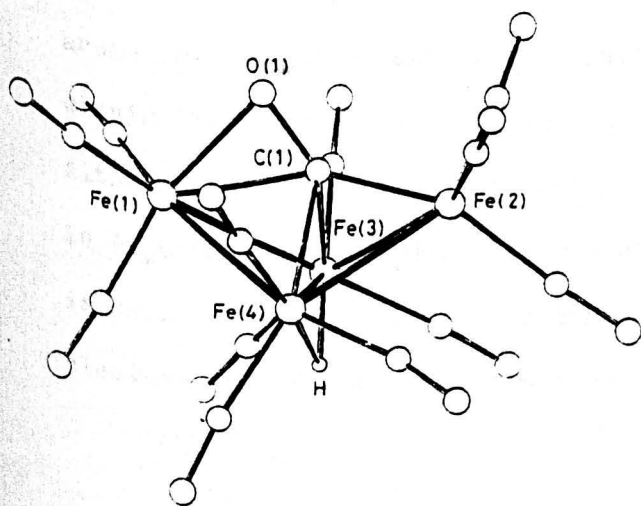
(3)



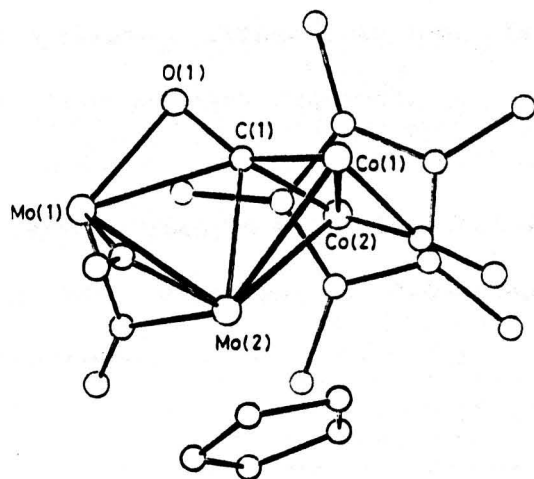
(4)



(5)



(6)



(7)

4.3.4 A structural pathway for the generation of interstitial C-atoms.

The isolation and full characterisation of this remarkable series of compounds has led to a detailed study of the reaction from which they were isolated. Initially the reaction of $\text{Ru}_3(\text{CO})_{12}$ with arenes (hexamethylbenzene, mesitylene, xylenes, toluene) had given a solid black deposit and deep red/brown solutions, from which $\text{Ru}_6\text{C}(\text{CO})_{17}$ (1) and clusters analogous to the structures $\text{Ru}_6\text{C}(\text{CO})_{15}(\text{C}_6\text{H}_3\text{Me}_3)$ (XR9), $\text{Ru}_6(\text{CO})_{15}(\text{C}_6\text{H}_3\text{Me}_3)$ (XR10), and $\text{HRu}_6\text{C}(\text{CO})_{14}(\eta^7\text{-C}_6\text{H}_3\text{Me}_2\text{CH}_2)$ (XR11) (containing the appropriate arene) had been isolated by thin layer chromatography (tlc).[261,262] Later investigations focussed on the mesitylene clusters, but there is some evidence that the chemistry applies equally well to the clusters derived from other methyl substituted arenes.

It was found that the yields of the four clusters $\text{Ru}_6\text{C}(\text{CO})_{17}$ (1), $\text{Ru}_6\text{C}(\text{CO})_{15}(\text{C}_6\text{H}_3\text{Me}_3)$ (XR9), $\text{Ru}_6(\text{CO})_{15}(\text{C}_6\text{H}_3\text{Me}_3)$ (XR10), and $\text{HRu}_6(\text{CO})_{14}(\text{C}_6\text{H}_3\text{Me}_2\text{CH}_2)$ (XR11) were dependent on the reaction time, with $\text{Ru}_6(\mu_4\eta^2\delta_{5b}\text{-CO})_2(\text{CO})_{13}(\eta^6\text{-C}_6\text{H}_3\text{Me}_3)$ (XR10) being the first product formed. The concentrations of (1), (XR9), and (XR11) increasing as the reaction proceeded, at the expense of (XR10) (Scheme 4.3/1). The reaction conditions can be optimized to give yields of approximately 15% for any one selected product. In general, the rate of the reaction is increased by methyl substitution of the arene, i.e., by higher electron density in the arene ring. For example, the reaction with hexamethylbenzene is complete within three days, but with toluene at least five days are required.

Although the ^{13}C n.m.r. and infrared evidence shows that the carbido-atom in $\text{Ru}_6\text{C}(\text{CO})_{14}(\eta^6\text{-C}_6\text{H}_3\text{Me}_3)$ (XR9) - and by inference that in $\text{Ru}_6\text{C}(\text{CO})_{17}$ (1) - is derived from a coordinated carbonyl group, the mechanism of C-O bond cleavage is not apparent from these arguments alone.

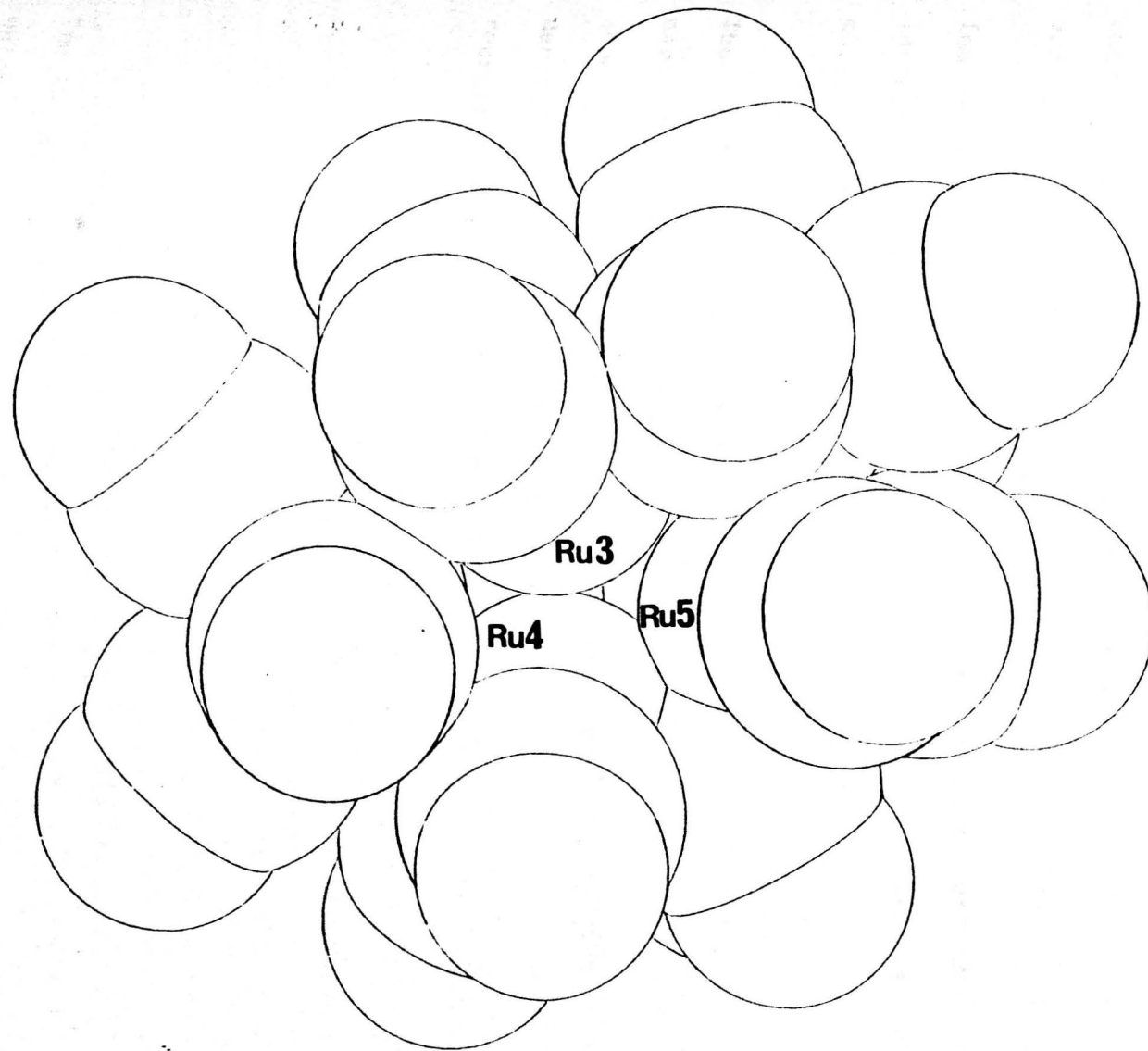
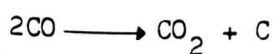


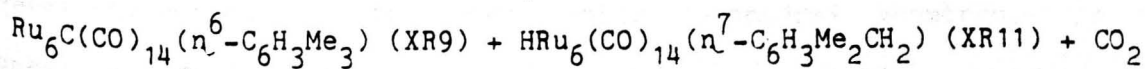
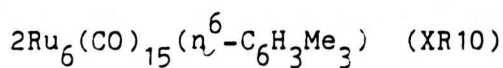
Figure 4.3/4 Computed 'space-filling' model of $\text{HRu}_6(\text{CO})_{14}(\eta^7\text{C}_6\text{H}_3\text{Me}_2\text{CH}_2)$ (XR11).

Further evidence was obtained by thermolysis of $\text{Ru}_6(\mu_4\eta^2\delta_{5b}\text{-CO})_2(\text{CO})_{13}(\text{C}_6\text{H}_3\text{Me}_3)$ (XR10) in an infrared gas cell, so that the gaseous products could be identified in situ by their infrared spectra. In the case of thermolysis of (XR10) in mesitylene, the infrared spectrum of the gaseous products (after the mesitylene solvent had been frozen out) showed strong absorptions at 2360 and 2344 cm^{-1} , characteristic of CO_2 . In addition the clusters (XR9) and (XR11) were formed in equal yield.

The observation of CO_2 in the reaction products confirms that the interstitial carbido atoms are the result of the disproportionation of two molecules of CO.



The two dihapto carbonyl groups in $\text{Ru}_6(\mu_4\eta^2\delta_{5b}\text{-CO})_2(\text{CO})_{13}(\text{C}_6\text{H}_3\text{Me}_3)$ (XR10) have very long C-O bond lengths and may be considered as activated, so it seems probable that the carbido-atom in $\text{Ru}_6\text{C}(\text{CO})_{14}(\text{C}_6\text{H}_3\text{Me}_3)$ (XR9) is derived from one of these groups. The thermolysis of (XR10) can be represented by the following equation:



The CO_2 generated from this reaction comes from the carbido-forming process which must involve two carbonyl ligands. However, an intramolecular process can be ruled out because the carbido-containing product $\text{Ru}_6\text{C}(\text{CO})_{15}(\eta^6\text{-C}_6\text{H}_3\text{Me}_3)$ (XR9) has an equal number of non-aryl carbon atoms to that of the reactant molecule $\text{Ru}_6(\text{CO})_{15}(\eta^6\text{-C}_6\text{H}_3\text{Me}_3)$ (XR10). In contrast, the other product of the thermolysis of (XR10), $\text{HRu}_6(\text{CO})_{14}(\eta^7\text{-C}_6\text{H}_3\text{Me}_2\text{CH}_2)$ (XR11), has one less carbonyl ligand than (XR10) and is produced in equal amounts to (XR9).

It is therefore proposed that the reaction involves a bimolecular first step, with two molecules of $\text{Ru}_6\text{C}(\text{CO})_{15}(\text{C}_6\text{H}_3\text{Me}_3)$ (XR10) reacting to eliminate CO_2 (Scheme 4.3/1). In one molecule of (XR10) [A] a μ_4 -carbonyl group unfolds and leans over to donate 2e to the second molecule of (XR10) [B] making this a 90e species. This results in bond cleavage, generating intermediate [D] (Scheme 4.3/1). The conversion of a μ_4 -carbonyl group in [A] to a terminally bonded linking carbonyl group causes bond formation and creation of the 86e edge-bridged trigonal bipyramid [C]. The formation of CO_2 may be envisaged as loss of the linking carbonyl group from [C] and an oxygen atom of the μ_4 -CO ligand on [D], leaving a naked C-atom. The loss of 2e as the CO_2 unit is generated leads to bond re-formation, generating an 88e edge-bridged square pyramidal core (intermediate [F] -Scheme 4.3/1). The loss of the carbonyl group from [C] gives an unstable 84e species [E].

The correct 86 CVE is achieved by formation of an M-C bond from one of the mesitylene methyl groups to an apical ruthenium of the trigonal bipyramid and transfer of hydrogen to the metal core. To compensate the apical ruthenium converts a terminal CO group to a μ_2 -CO group with the adjacent equatorial ruthenium atom. This results in the formation of the observed 86e-product $\text{HRu}_6(\mu_4\text{-}\eta^2\text{CO})(\text{CO})_{13}(\eta^7\text{-C}_6\text{H}_3\text{Me}_2\text{CH}_2)$ (XR11). The carbido-cluster $\text{Ru}_6\text{C}(\text{CO})_{14}(\eta^6\text{-C}_6\text{H}_3\text{Me}_3)$ (XR9) is generated from the 88e-species [F] by cluster rearrangement to the more stable octahedral geometry. In the process the $\mu_2\text{-}\eta^4\text{-CO}$ ligand is converted to a terminal CO group.

A similar mechanism can be envisaged for the formation of $\text{Ru}_6\text{C}(\text{CO})_{17}$ (1), with replacement of the η^6 -mesitylene by three terminal carbonyl ligands occurring at some stage during the reaction pathway. It is not possible at present to specify exactly when this happens.

4.4 The formation of a nitrido decaruthenium cluster.

In addition to the hexanuclear clusters discussed above, pyrolysis of $\text{Ru}_3(\text{CO})_{12}$ with mesitylene also gave the decanuclear dianion $[\text{Ru}_{10}\text{C}(\text{CO})_{24}]^{2-}$ (2). [262] On protonation this was converted to the monohydride $[\text{HRu}_{10}\text{C}(\text{CO})_{24}]^-$ (8). In this section a brief review of the reactivity of decanuclear clusters will be given. The X-ray structural analysis of the nitrido cluster $[\text{Ru}_{10}\text{N}(\text{CO})_{24}]^-$ (XR12) is reported and compared to $[\text{HRu}_{10}\text{C}(\text{CO})_{24}]^-$ (8).

A mechanism for the formation of the hexanuclear carbido clusters $\text{Ru}_6\text{C}(\text{CO})_{17}$ (1) and $\text{Ru}_6\text{C}(\text{CO})_{14}(\text{C}_6\text{H}_3\text{Me}_3)$ (XR9) is proposed in Section 4.3. Important intermediates in this process are believed to be the non-carbido clusters $\text{Ru}_6(\mu_4\eta^2\delta_{5b}\text{-CO})_2(\text{CO})_{13}(\text{C}_6\text{H}_3\text{Me}_3)$ (XR10) and $\text{HRu}_6(\mu_4\eta^2\delta_{5b}\text{-CO})(\text{CO})_{13}(\eta^7\text{-C}_6\text{H}_3\text{Me}_2\text{CH}_2)$ (XR11). Further reaction of $\text{Ru}_3(\text{CO})_{12}$ with mesitylene leads to the decanuclear ruthenium cluster, $[\text{Ru}_{10}\text{C}(\text{CO})_{24}]^{2-}$ (2). This ruthenium cluster was discovered at the same time via an alternative route by Yamazaki et al. [260]

It can be envisaged that in the mesitylene reaction the decaruthenium species is formed by some type of further reaction of the hexaruthenium cluster with $\text{Ru}(\text{CO})_3$ fragments generated from excess $\text{Ru}_3(\text{CO})_{12}$. A similar process must be involved with the nitride (which is generated by reaction of $\text{Ru}_3(\text{CO})_{12}$ with $[\text{Ru}_6\text{C}(\text{CO})_{16}]^{2-}$). The very stable decanuclear core seems to be an end product in this sequence of reactions.

4.4.1 The predominant decanuclear cluster core.

Before discussing the X-ray structure analysis of $[\text{Ru}_{10}\text{N}(\text{CO})_{24}]^-$ (XR12), a brief review of decanuclear clusters will be given. The first decanuclear cluster for the iron triad was prepared by pyrolysis of the pyridyl derivative $\text{Os}_3(\text{CO})_{11}(\text{Py})$, which gave the dianion $[\text{Os}_{10}\text{C}(\text{CO})_{24}]^{2-}$ (9). [271] This adopts a tetracapped octahedral metal core framework with the

carbido-atom located in the central octahedral cavity (Figure 4.4/1). There is a striking difference between the Os-Os bond lengths of the octahedron [ca. 2.88(1) Å] and those from the capping groups [ca. 2.79(1) Å]. This expansion of the octahedron can be attributed to the presence of the central carbon atom.

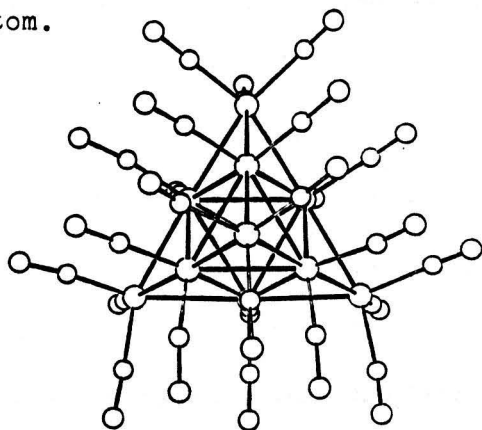


Figure 4.4/1 The tetra-capped metal core of the dianion (9).

The metal skeleton of (9) is a fragment of a cubic close packed (c.c.p.) array and corresponds to a face-centred cubic unit cell with four tetrahedrally related corners removed. Large rhodium[272] and niobium[273] clusters have been reported with hexagonal close packed (h.c.p.) arrangements, but, curiously, the reverse is observed for the metallic state; rhodium metal has a c.c.p lattice whilst osmium metal is h.c.p. One of the features that is considered important about the dianion $[\text{Os}_{10}\text{C}(\text{CO})_{24}]^{2-}$ (9) is its large planar surface of metal atoms, making it amenable to comparison of metal surfaces as a model for the chemisorption of carbon monoxide.

Electrophilic attack of I^+ on $[\text{Os}_{10}\text{C}(\text{CO})_{24}]^{2-}$ (9) leads to progressive cluster opening, with formation of the iodo-clusters $[\text{Os}_{10}\text{C}(\text{CO})_{24}\text{I}]^-$ (10) and $\text{Os}_{10}\text{C}(\text{CO})_{24}\text{I}_2$ (11) respectively (Figure 4.4/2).[274] Attack of I^+ occurs at the capping Os_4 groups, resulting in cleavage of two Os-Os bonds. The initial product, $[\text{Os}_{10}\text{C}(\text{CO})_{24}\text{I}]^-$ (10), is a tricapped octahedron with the remaining osmium atom edge bridging one side of the fundamental polyhedron. The iodine atom functions as a three electron bridge. The

second iodine in the neutral cluster $\text{Os}_{10}\text{C}(\text{CO})_{24}\text{I}_2$ (11) adopts the same bridging mode, such that the metal core is now a dicapped octahedron with two edge bridging osmium atoms and two μ_2 -iodines. This reduction is accompanied by a characteristic increase in electron count from 134e for (9), 136e for (10) and 138e for (11). The parent cluster has 134 valence electrons with seven skeletal electron pairs and therefore the fundamental polyhedron is an octahedron, as observed. The importance of this sequence of reactions is that it emphasises the ability of cluster systems to undergo reduction or electrophilic addition at capping Os tetrahedra.[274] All decanuclear species of the iron triad have interstitial atoms stabilising the core geometry and even on electrophilic attack with I^+ it is the tetrahedral caps which open out, with the basic core octahedral geometries remaining the same.

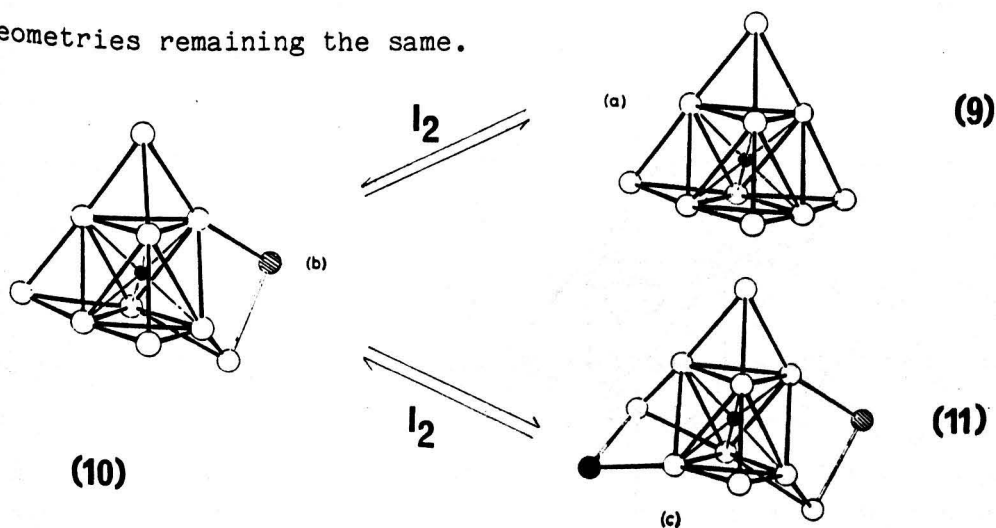


Figure 4.4/2 Electrophilic attack by I^+ on (9).

Protonation of $[\text{Os}_{10}\text{C}(\text{CO})_{24}]^{2-}$ (9) gave the monoanion $[\text{HOs}_{10}\text{C}(\text{CO})_{24}]^-$ (12) (Figure 4.4/3).[275] This, unlike the reaction of (9) with iodine discussed above, does not result in cluster opening or any significant displacement of the close packed carbonyl sphere (which would be expected if a surface hydride was present). Lewis et al concluded that the hydrido ligand in (12) was situated in one of the tetrahedral sites and, indeed, one of the cavities is enlarged (mean Os-Os 2.856 Å) in comparison with the remaining three tetrahedral caps (mean Os-Os 2.838 Å).

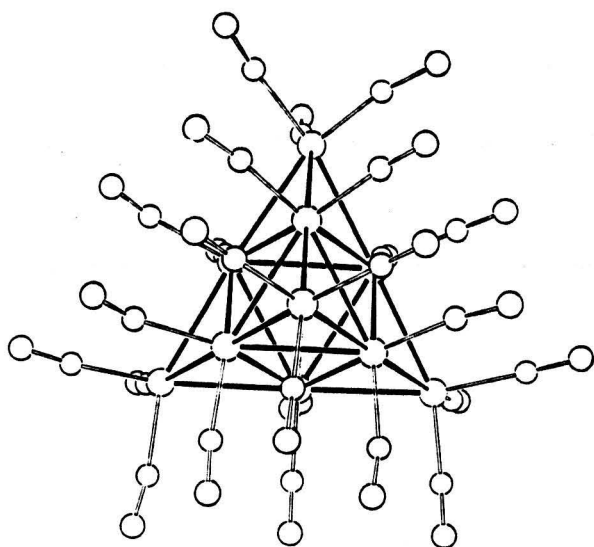


Figure 4.4/3 The monoanion $[\text{HOs}_{10}(\text{CCO})_{24}]^{2-}$ (12).

The first non-carbido decaosmium cluster was reported in 1983.[276] The tetrahydrido-cluster $[\text{H}_4\text{Os}_{10}(\text{CO})_{24}]^{2-}$ (13) has an interstitial hydrogen atom in the central Os_6 cavity, with the remaining hydrogen atoms in three of the osmium caps (Figure 4.4/4).

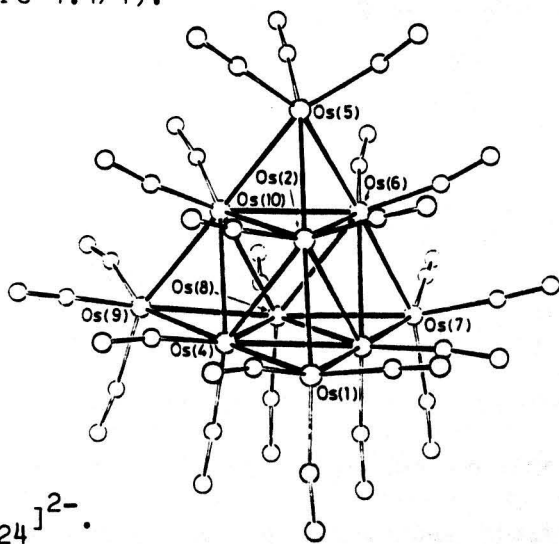


Figure 4.4/4 $[\text{H}_4\text{Os}_{10}(\text{CO})_{24}]^{2-}$.

Protonation of this dianion gave the penta-hydrido cluster $[\text{H}_5\text{Os}_{10}(\text{CO})_{24}]^{-}$ (14) (Figure 4.4/4). An X-ray structure analysis of the pentahydride (14), established that the tetracapped octahedral geometry of the parent cluster (14) has been maintained.[277] Again there is no distortion of the carbonyl sphere, and the overall spatial distribution is very similar to that observed for the non-hydrido carbide cluster $[\text{Os}_{10}\text{C}(\text{CO})_{10}]^{2-}$ (9). Four of the hydride ligands reside in tetrahedral caps and the fifth is located in the central octahedral cavity.

An alternative core has been reported for the disulphide cluster $\text{Os}_{10}(\text{S})_2(\text{CO})_{23}$ (15).[168] The metal core geometry of (15) consists of two square pyramidal units fused to two trigonal bipyramids, with the two sulphur atoms μ_4 -bridging the two pyramidal square bases (Figure 4.4/5).

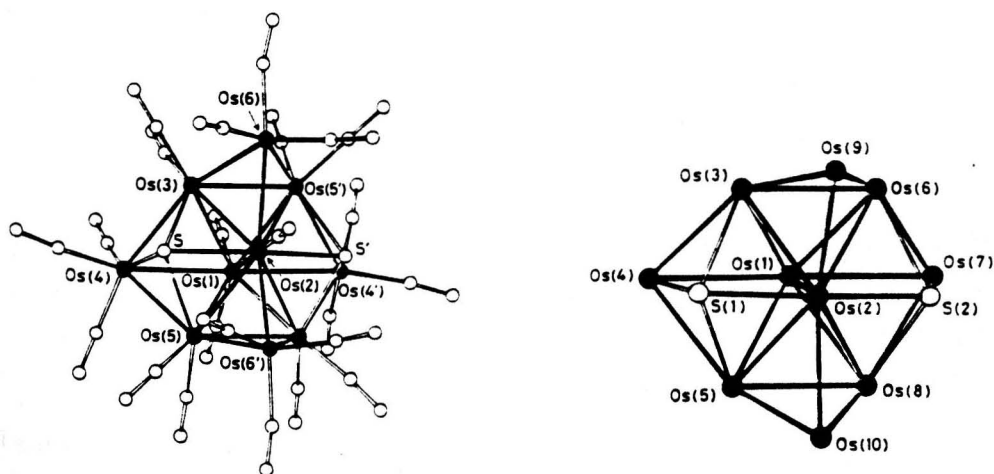


Figure 4.4/5 $\text{Os}_{10}(\text{S})_2(\text{CO})_{23}$ (15).

In comparison to the decaosmium clusters discussed above, surprisingly little is known of the decaruthenium clusters. As discussed in Section 4.3 the dianion $[\text{Ru}_{10}\text{C}(\text{CO})_{24}]^{2-}$ (2) was only reported recently.[260] Another example of a decaruthenium cluster is the edge-fused biocuboctahedral dicarbide $[\text{Ru}_{10}\text{C}_2(\text{CO})_{24}]^{2-}$ (16).[278] The framework is based on two octahedra fused along an edge, with the two carbido-atoms occupying interstitial sites (Figure 4.4/6). Previously bis-carbido-fragments had only been reported in cobalt and rhodium clusters. Examples of these are $[\text{Co}_{13}\text{C}_2(\text{CO})_{24}]^{4-}$ [279] and $[\text{Rh}_{15}\text{C}_2(\text{CO})_{23}]^-$,[280] where the two carbon atoms are well separated and occupy two distinct cavities (trigonal prismatic for Co, octahedral for Rh). In contrast a single C_2 unit is observed in $[\text{Co}_{11}(\text{C}_2)(\text{CO})_{22}]^{3-}$ [281] and $\text{Rh}_{12}(\text{C}_2)(\text{CO})_{25}$. [282]

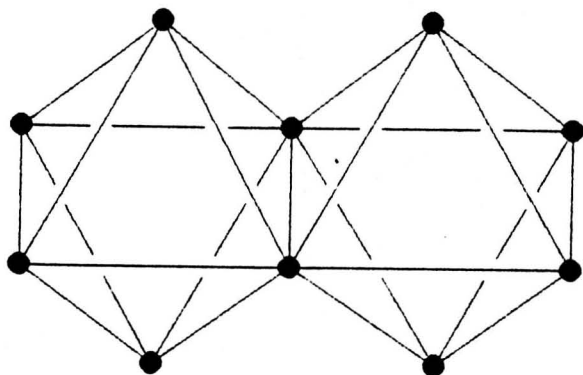


Figure 4.4/6 $[\text{Ru}_{10}\text{C}_2(\text{CO})_{24}]^{2-}$ (16).

Apart from $[\text{Ru}_{10}\text{N}(\text{CO})_{24}]^-$ (XR12) the only other decaruthenium cluster which does not contain an interstitial carbido-atom is the dihydrido-anion $[\text{H}_2\text{Ru}_{10}(\text{CO})_{25}]^{2-}$ (17) (Figure 4.4/7).[283] Interestingly this was synthesised in exactly the same way as (XR12), by redox condensation of the anion $[\text{HRu}_6(\text{CO})_{18}]^-$ with $\text{Ru}_3(\text{CO})_{12}$, or by thermolysis of $[\text{HRu}_6(\text{CO})_{18}]^-$ in ethanol. The metal core framework of (17) consists of a fused bicapped octahedron with a bicapped square pyramid through a planar array of five metal atoms. This is the first example of this type of metal framework and it is a fragment of the hcp system of metal atom packing. In Section 4.3 the thermolytic syntheses of ruthenium clusters were discussed; these reactions result in the formation of carbido-containing species (usually via the cleavage of a CO ligand). The reason for the non-formation of the carbido-atom in the case of $[\text{H}_2\text{Ru}_{10}(\text{CO})_{25}]^{2-}$ (17) is believed to be due to the relative acidity of the solvent (ethanol), which may liberate protons to fulfill the electronic role of the carbon atom in stabilising intermediate structures.[283]

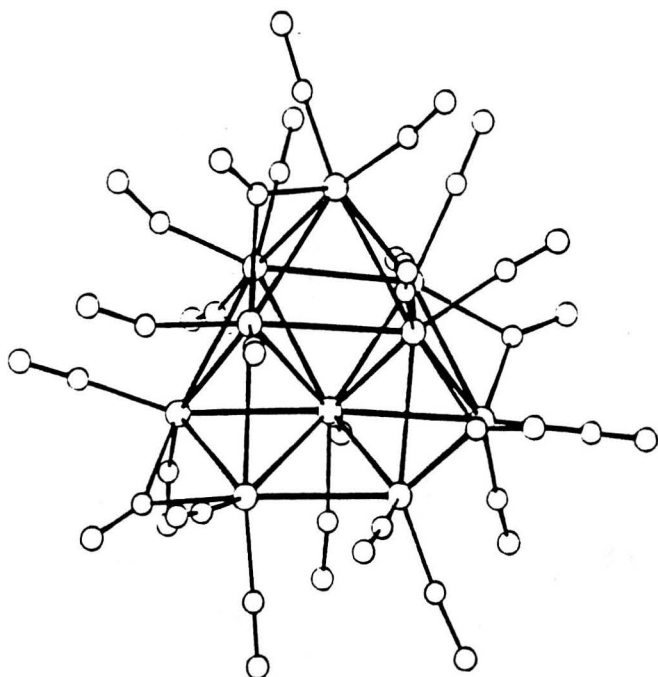


Figure 4.4/7 $[\text{H}_2\text{Ru}_{10}(\text{CO})_{25}]^{2-}$ (17).

This review has emphasised the predominance of the tetra-capped octahedral framework for decanuclear clusters and the fact that interstitial atoms such as C or H are vital for the maintenance of these cores. The nitrido decanuclear cluster $[\text{Ru}_{10}\text{N}(\text{CO})_{24}]^-$ (XR12) is the first reported example of a decaruthenium cluster with an interstitial nitrido-atom. It is compared to the isostructural cluster $[\text{HRu}_{10}(\text{CO})_{24}]^-$ (8).

4.4.2 X-Ray structure analysis of the nitrido-cluster $[\text{Ru}_{10}\text{N}(\text{CO})_{24}]^-$ (XR12).

a) Synthesis.

The decaruthenium nitrido-anion $[\text{Ru}_{10}\text{N}(\text{CO})_{24}]^-$ (XR12) was synthesised by redox condensation of the nitrido-monoanion $[\text{Ru}_6\text{N}(\text{CO})_{16}]^-$ with $\text{Ru}_3(\text{CO})_{12}$. Treatment of $[\text{PPN}][\text{Ru}_6\text{N}(\text{CO})_{16}]$ with $\text{Ru}_3(\text{CO})_{12}$ in diglyme under reflux (162°C) gave a green solution; the nitrido-cluster $[\text{Ru}_{10}\text{N}(\text{CO})_{24}]^-$ (XR12) was isolated by tlc. Crystals of $[\text{PPN}][\text{Ru}_{10}\text{N}(\text{CO})_{24}]^-$ (XR12) showed that the salt was isomorphous with $[\text{PPN}][\text{HRu}_{10}\text{C}(\text{CO})_{24}]^-$ (8).

b) Structural description.

X-ray structure analysis of the monoanion $[\text{Ru}_{10}\text{N}(\text{CO})_{24}]^-$ (XR12) established a tetra-capped octahedral metal core framework (Figure 4.4/8). The six ruthenium atoms, Ru(2), Ru(3), Ru(4), Ru(6), Ru(8), and Ru(10) define the

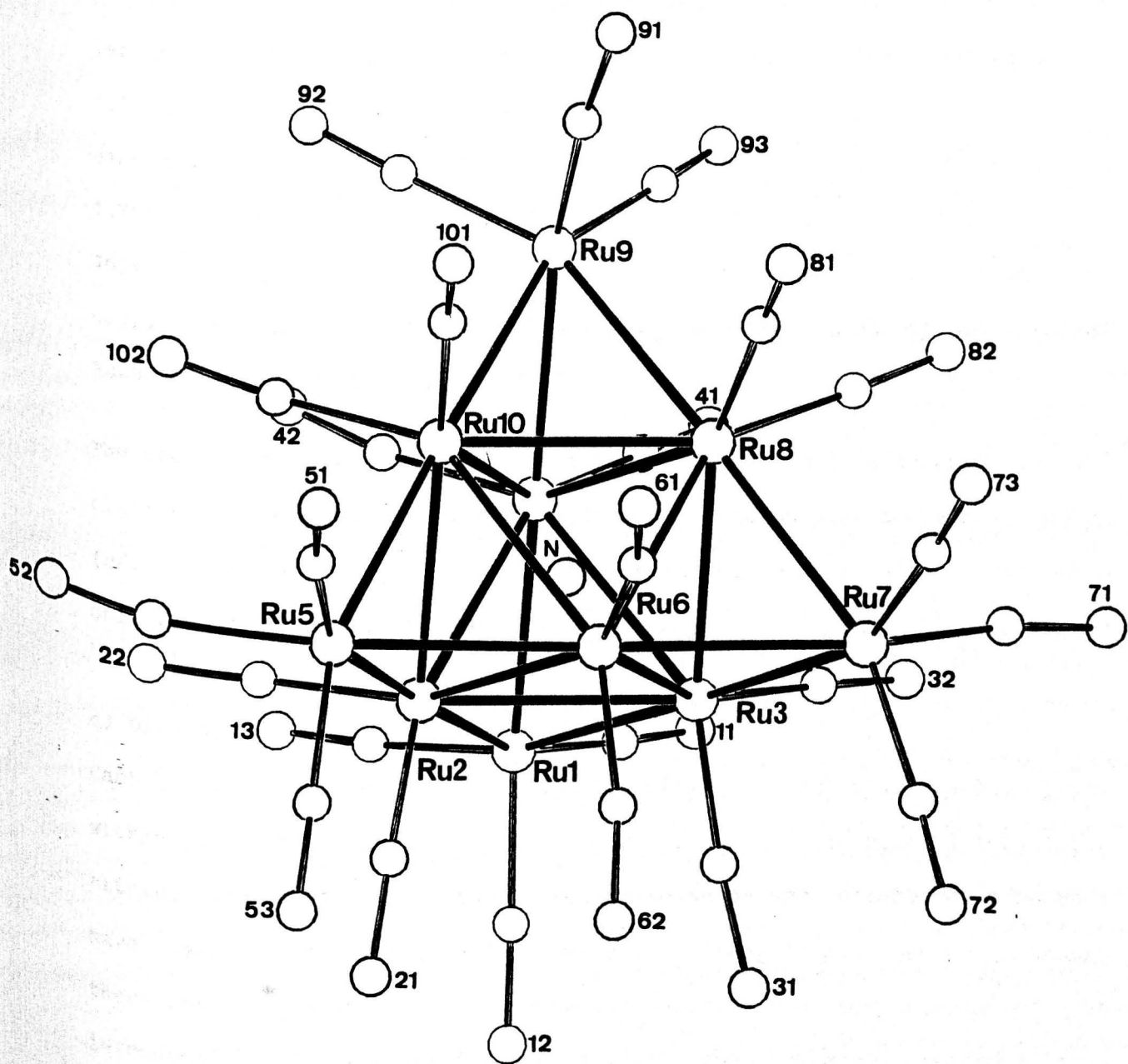


Figure 4.4/8 The molecular structure of $[\text{Ru}_{10}\text{N}(\text{CO})_{24}]^-$ (XR12).

Only the O-atoms of the carbonyl ligands have been labelled for clarity.

octahedron, with four triangular faces capped by the remaining four metal atoms. The triangular face defined by Ru(2), Ru(3), and Ru(4) is capped by Ru(1), the face defined by Ru(2), Ru(6), and Ru(10) by Ru(5), the face defined by Ru(3), Ru(6), and Ru(8) by Ru(7), and the face defined by Ru(4), Ru(8), and Ru(10) by Ru(9). All four capping ruthenium atoms have three terminal carbonyl ligands, whereas the six metal atoms defining the octahedron are bonded to two terminal carbonyl ligands each. All 24 carbonyl ligands are essentially linear and lie in the range; M-C(carbonyl) 1.70(5)-1.90(5) Å; C-O(carbonyl) 1.12(6)-1.28(5) Å; and M-C-O(carbonyl) 169(3) to 179(6)°. The nitrido atom is located in the central octahedral cavity and bonds to all six ruthenium atoms of the octahedral core (range Ru-N(nitrido) 1.966(25)-2.079(24) Å).

The nitrido atom in (XR12) contributes five valence electrons to the cluster valence electron count, resulting in this complex being a monoanion (cf. the dianion $[\text{Ru}_{10}\text{C}(\text{CO})_{24}]^{2-}$ (2), where the carbon atom contributes only four electrons).

c) Discussion.

Carbido-clusters, particularly those containing interstitial carbon atoms within an octahedral cavity, are now common. In contrast, interstitial nitrides are relatively unusual. Both disulphide and dicarbide compounds have been reported, [168,279,280] whereas dinitrogens are unknown (although there seems no reason for their non-existence). One consequence of the introduction of interstitial atoms with more valence electrons is an elevation of surface crowding. The series of ligands H, C, N, and S, contribute progressively more electrons, namely 1, 4, 5, and 6. Indeed this feature has been noted as an important feature of hydrido- and carbido-clusters.

Differentiation between carbon and nitrogen atoms is notoriously difficult as they differ by only one electron. In Chapter 2, the X-ray structure analyses of pentanuclear isomers which differed only in the orientation of a pyridine ligand were discussed, in this section decanuclear ruthenium clusters differing only in the type of interstitial atom are compared.

Table 4.4/1 Comparison of the Ru-Ru bond lengths in for the isostructural nitrido-species (XR12) and hydrido-species (8).

Bond length	$[\text{Ru}_{10}\text{N}(\text{CO})_{24}]^-$	$[\text{HRu}_{10}\text{C}(\text{CO})_{24}]^-$
Octahedron		
Ru(2)-Ru(3)	2.884(5)	2.875(4)
Ru(2)-Ru(4)	2.854(5)	2.845(4)
Ru(2)-Ru(6)	2.849(5)	2.850(4)
Ru(2)-Ru(10)	2.845(4)	2.847(4)
Ru(3)-Ru(4)	2.846(5)	2.850(4)
Ru(3)-Ru(6)	2.855(5)	2.859(4)
Ru(3)-Ru(8)	2.862(5)	2.873(4)
Ru(4)-Ru(8)	2.864(5)	2.874(4)
Ru(4)-Ru(10)	2.861(5)	2.859(4)
Ru(6)-Ru(8)	2.855(5)	2.860(4)
Ru(6)-Ru(10)	2.856(5)	2.855(4)
Ru(8)-Ru(10)	2.842(5)	2.852(4)
Ru-Ru(mean)	2.856(5)	2.858(4)
Capping atoms		
Ru(1)-Ru(2)	2.761(5)	2.778(4)
Ru(1)-Ru(3)	2.790(5)	2.795(4)
Ru(1)-Ru(4)	2.767(5)	2.780(4)
Ru-Ru(mean)	2.773(5)	2.784(4)
Ru(5)-Ru(2)	2.789(5)	2.785(4)
Ru(5)-Ru(6)	2.774(5)	2.774(4)
Ru(5)-Ru(10)	2.791(5)	2.799(4)
Ru-Ru(mean)	2.785(5)	2.786(4)
Ru(7)-Ru(3)	2.773(5)	2.783(4)
Ru(7)-Ru(6)	2.778(5)	2.793(4)
Ru(7)-Ru(8)	2.781(5)	2.782(4)
Ru-Ru(mean)	2.777(5)	2.786(4)
Ru(9)-Ru(4)	2.780(5)	2.794(4)
Ru(9)-Ru(8)	2.787(5)	2.789(4)
Ru(9)-Ru(10)	2.783(5)	2.804(4)
Ru-Ru(mean)	2.783(5)	2.796(4)

The metal-metal bond lengths for both structures are listed in Table 4.4/1, along with the mean values of the octahedral bond length and the capping unit bond lengths. From a comparison of the M-M bond lengths for (XR12) and (8) it can be seen that the two structures closely resemble each other, the difference between the means of the tetrahedral caps is not significant. The two structures are so similar it is not possible to say conclusively that (XR12) is the nitrido-cluster, although the X-ray

structure analysis was consistent with (XR12) being the nitrido-cluster (Chapter 6).

The I.R. spectra of (XR12) and (8) were very similar. However in the initial ^1H n.m.r. spectrum of (XR12) (which should have clearly indicated the difference between the two structures) a resonance was detected which was consistent with the presence of an interstitial hydride.[284] Thus a ^{14}N n.m.r. spectra was undertaken, this showed that (XR12) was indeed the new nitrido-cluster and it was concluded that characterisation problems were due to contamination with $[\text{HRu}_{10}\text{C}(\text{CO})_{24}]^-$. In Section 4.3 the products of the thermolysis of $\text{Ru}_3(\text{CO})_{12}$ with arenes were discussed and (significantly) one of the products was the dianion $[\text{Ru}_{10}\text{C}(\text{CO})_{24}]^{2-}$, which could be protonated to the hydrido-species $[\text{HRu}_{10}\text{C}(\text{CO})_{24}]^-$. The mechanism outlined in that section for the formation of carbido-octahedral clusters (and presumably decanuclear carbido-species) rests on the fact that the carbido-atom originates from a coordinated carbonyl ligand. Thus a similar reaction is probably occurring here and accounts for the trace amounts of $[\text{HRu}_{10}\text{C}(\text{CO})_{24}]^-$. The ^{14}N n.m.r. spectra of $[\text{PPN}][\text{Ru}_{10}\text{N}(\text{CO})_{24}]$ (XR12) consists of a singlet at 410 ppm. This was assigned to the nitride, with a second singlet at 310 ppm being assigned to the counterion. The low frequency shift of the interstitial nitride resonance relative to $[\text{Ru}_6\text{N}(\text{CO})_{16}]^{2-}$ (538 ppm) [282] follows the trend observed for $[\text{Ru}_{10}\text{C}(\text{CO})_{24}]^{2-}$ (5) (362 ppm) and $[\text{Ru}_6\text{C}(\text{CO})_{16}]^{2-}$ (461.2 ppm).[282]

4.5 Conclusion.

The hexanuclear clusters (XR10) and (XR11) are believed to offer a plausible mechanism for the formation of carbido-clusters such as (XR9). The interstitial carbido-atom in $\text{Ru}_6\text{C}(\text{CO})_{15}(\text{C}_6\text{H}_3\text{Me})$ (XR9) has long been believed to originate from a coordinated carbonyl ligand. The isolation of (XR10 and (XR11) from the reaction of $\text{Ru}_3(\text{CO})_{12}$ with mesitylene is believed

to shed light on this mechanism, and in Section 4.3 a plausible mechanism for the formation of (XR9) is presented. This mechanism is important as octahedral carbido-species dominate the chemistry of hexanuclear clusters of the iron triad, and because it offers a possible insight into the process of C-O cleavage - a vital, possibly primary, step in the Fischer-Tropsch synthesis.

The $\mu_4\eta^2\delta_{5b}$ -CO ligands have a number of important functions. Firstly, the high degree of coordination with even the O-atom involved in bonding to the cluster considerably reduces the C-O bond order, such that this ligand can be considered as activated and susceptible to cleavage. The cleavage and loss of the O-atom is the key step in the generation of a carbido-species. Secondly, the extra electrons donated in this mode of carbonyl bonding are vital in stabilising unusual metal core frameworks. In the formation of larger species the generation of an octahedral species encapsulating the created carbido-atom appears to be the first step in the generation of decanuclear species. Although there is no definite evidence of the intermediates, the formation of both $[\text{Ru}_{10}\text{C}(\text{CO})_{24}]^{2-}$ and $[\text{Ru}_{10}\text{N}(\text{CO})_{24}]^-$ by direct reaction of hexanuclear precursors (containing interstitial atoms) with $\text{Ru}_3(\text{CO})_{12}$ lend support to this view.

CHAPTER FIVE

Osmium clusters with alkyne fragments.

Chapter 5 - Osmium clusters with alkyne fragments.

In this chapter three X-ray structures are presented, which result from the interaction of alkynes with osmium clusters. The first two are trinuclear clusters with bridging gold atoms, and the third is a heptanuclear species with an unprecedented metal framework.

5.1 The reactivity of trinuclear clusters with alkenes and alkynes.

Trinuclear clusters have been studied in more depth than any other set of metal clusters.[171] They are important in their own right, and also as analogues to higher species that consist predominately of triangulated faces. The reactivity of trinuclear species with organo-derivatives has proved particularly interesting, leading to a wide range of organometallic bonding modes.

5.1.1 Trinuclear clusters with alkene ligands.

By the early seventies a number of reactions had been reported in which alkene carbon-hydrogen cleavage was observed to give coordinated organo-fragments and bridging hydrides.[285-292] For example, cyclo-octene (C_8H_{14}) reacts with $M_3(CO)_9$ ($M=Ru$ or Os) to give $H_2M_3(CO)_9(C_8H_{12})$ (1) [$M=Ru$ or Os],[291] and bicyclo[3.2.1]-2,6-octadiene (C_8H_{10}) reacts with $Ru_3(CO)_9$ to give $H_2Ru_3(CO)_9(C_8H_8)$ (2) (Figure 5.1/1).[293] A C=C double bond in both of these clusters has been dehydrogenated to give a coordinated alkyne, bridging three metal atoms (via two σ -bonds and one π -bond) in a $\mu_3\eta^2\delta_4$ bonding mode (section 1.4).

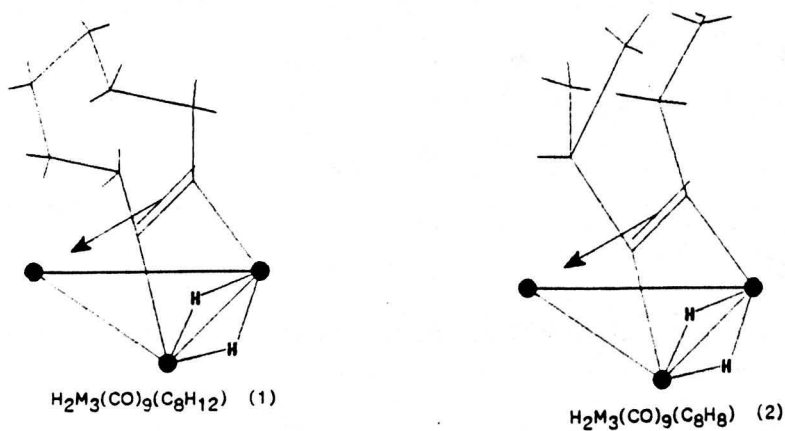


Figure 5.1/1 The $\mu_3\eta^2\delta_4$ organo-bonding mode in (1) and (2).

An alternative form of bonding is seen for hexadiene (C_6H_{10}) and cyclohexadiene (C_6H_8), which both react with $Ru_3(CO)_{12}$ to give the same product $HRu_3(CO)_9(C_6H_9)$ (3) (Figure 5.1/2).[287] In both of these complexes the unsaturated ligand bridges three metal atoms via one π -allyl and two σ -bonds, with hydrogen transfer to the metal core. For the cyclohexadiene C-C cleavage occurs in addition to hydrogen transfer to the metal framework. The reaction of $Ru_3(CO)_{12}$ with cyclododeca-1,5,9-triene gives $HRu_3(CO)_9(C_{12}H_{15})$ (4), in which the organo-ligand bonds to the cluster in an analogous fashion to the organo-fragment found in (3) (Figure 5.1/2.)[289] In all these reactions transfer of hydrogen to the metal framework has occurred.

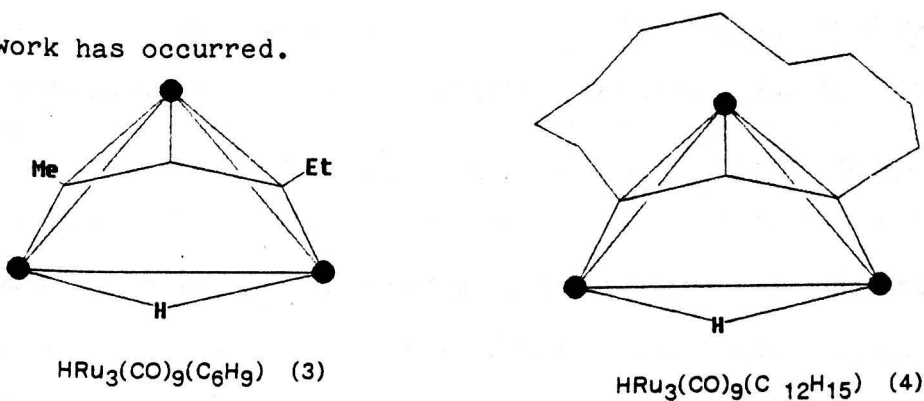


Figure 5.1/2 The $\mu_3\eta^2\delta_{4a}$ organo-bonding mode in (3) and (4).

In a study by Deeming, on the reactivity of $Os_3(CO)_{12}$ with simple alkenes, a number of significant features emerged. With ethene, the alkenylidene cluster $H_2Os_3(CO)_9(C=CH_2)$ (5) was produced, [285,288] whereas cyclopentene and benzene gave $H_2Os_3(CO)_9(C_5H_6)$ (6) and $H_2Os_3(CO)_9(C_6H_4)$ (7) respectively (Figure 5.1/3).[285]

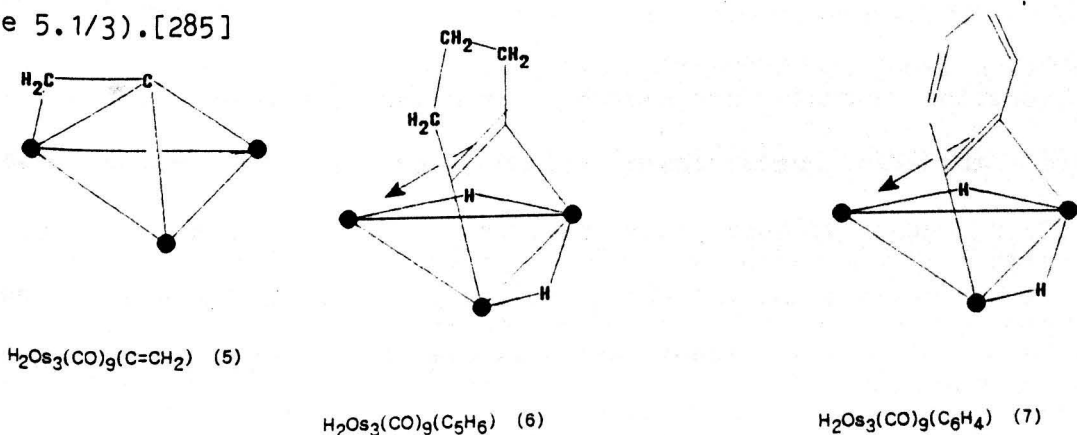


Figure 5.1/3 Alternative organo-bonding modes adopted by (5) ($\mu_3\eta^2\delta_{4b}$), (6) and (7) ($\mu_3\eta^2\delta_{4a}$).

The alkenylidene ligand in (5) donates four electrons to the cluster valence count (via σ -bonds to two of the metal atoms and a π -bond to the third metal atom). In contrast, the reaction of $\text{Os}_3(\text{CO})_{12}$ with cyclopentene produced $\text{H}_2\text{Os}_3(\text{CO})_9(\text{C}_5\text{H}_6)$ (6), [285] in which the alkyne lies parallel to one metal edge donating four electrons. Benzene produced a similar structural product, namely $\text{H}_2\text{Os}_3(\text{CO})_9(\text{C}_6\text{H}_4)$ (7). [285] Both structures (6) and (7) are analogous to the cyclooctene derivative $\text{H}_2\text{M}_3(\text{CO})_9(\text{C}_8\text{H}_{12})$ (1) [M=Ru or Os]. [291, 292]

Deeming proposed that these reactions occur as double oxidative additions of the respective alkene. For ethene, initial transfer of hydrogen to the metal core gives an alkenyl intermediate $\text{HOs}_3(\text{CO})_9(\text{HC}=\text{CH}_2)$. Similarly, the cyclic alkenes produce $\text{HOs}_3(\text{CO})_9(\text{C}_5\text{H}_7)$ and $\text{HOs}_3(\text{CO})(\text{C}_6\text{H}_5)$ respectively. For both the cyclic ligands the second C-H cleavage occurs from the β -carbon to give the observed products (6) and (7), and thus the overall process is 1,2-elimination. However the linear alkenylidene intermediate $\text{HOs}_3(\text{CO})_9(\text{CH}=\text{CH}_2)$ can eliminate the second hydrogen from either the α - or β -carbon atom. The observed product (5) shows that a second α -carbon hydrogen has been removed resulting in overall 1,1-elimination. Thus one hydrogen atom is removed from each unsaturated carbon atom in the cyclic alkenes, whereas with terminal alkenes both hydrogen atoms may be removed from the terminal carbon atom.

Much of our understanding of organic reactions on cluster surfaces has developed through use of the formally unsaturated triosmium cluster $\text{H}_2\text{Os}_3(\text{CO})_{10}$ (8), which forms derivatives more readily than $\text{Os}_3(\text{CO})_{12}$. Reaction of excess ethene with $\text{H}_2\text{Os}_3(\text{CO})_{10}$ (8) initially gives the alkenyl cluster $\text{HOs}_3(\text{CO})_{10}(\text{CHCH}_2)$ (9a) (Figure 5.1/4). [249]

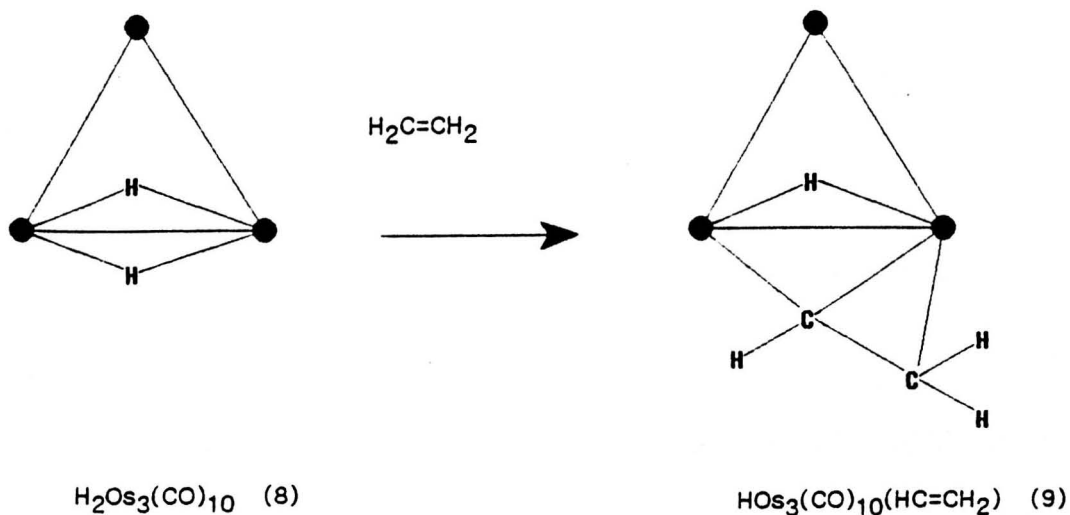
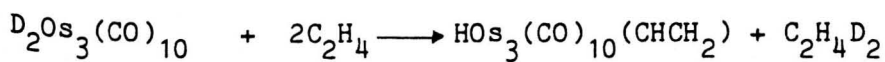
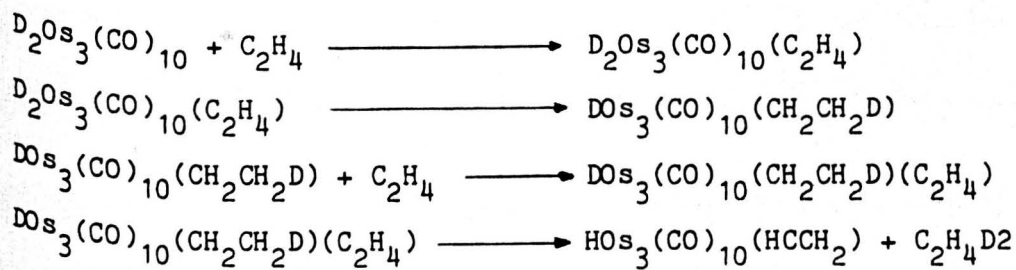


Figure 5.1/4 The reaction of $\text{H}_2\text{Os}_3(\text{CO})_{10}$ (8) to give an alkenyl cluster (9).

Shapley, in an elegant study of this reaction, showed that deuterated $\text{D}_2\text{Os}_3(\text{CO})_{10}$ gave the alkenyl product (9a). No deuterium had been incorporated into the alkenyl ligand, but deuterated ethane was evolved as a byproduct. [249]



Deeming developed this idea and proposed that one of the bridging hydrides in $\text{H}_2\text{Os}_3(\text{CO})_{10}$ (8) reduces a coordinated ethene to a σ -bonding ethyl ligand, and that this transfer is completed before a C-H of a second ethene molecule is cleaved to form an alkenyl ligand. [16] This can be represented by the following mechanism:



In this scheme, the alkene initially attaches to the cluster (via a π -bond), and hydrogen then reduces the coordinated ethene to an ethyl derivative (bonding via a σ -bond). The second ethene then coordinates and is converted to a bridging alkenyl ligand, with loss of the ethyl group as

an ethane molecule. During this sequence, the number of carbonyl ligands remain constant and the versatility is provided by variation of M-M bond order, hydrogen mobility, and by the coordination modes adopted by the organo-derivative.

Deeming extended this to a general mechanism for the reaction of alkenes with $\text{H}_2\text{Os}_3(\text{CO})_{10}$ (8), laying stress upon the variety of isomeric products possible via this pathway.[16] The major products isolated from this reaction are a hydrido cluster with a terminally attached alkane (resulting from reduction of the precursor alkene), and an alkenyl complex.

5.1.2 Reaction of $\text{H}_2\text{Os}(\text{CO})_{10}$ (8) with alkynes.

Transfer of hydrogen to the metal core occurs for all of the alkene ligands discussed above. In contrast, the reaction of trinuclear species with alkynes often produces 'intact' alkynes on the cluster surface.

An interesting feature of alkyne cluster chemistry is the effect the alkyne substituents have on ligand reactivity and the resultant product profile. Monosubstituted (terminal) alkynes are likely to be more reactive for a number of reasons. Firstly, they possess a dipole moment (not present in a symmetric disubstituted alkyne) and, as such, may be more susceptible to electrophilic and nucleophilic attack. Secondly, the α -hydrogen can migrate, either within the alkyne or to the metallic core, increasing the range of possible organo-products. Finally, a disubstituted alkyne will be sterically more hindered owing to the presence of two R groups instead of one.

The reaction of $\text{H}_2\text{Os}_3(\text{CO})_{10}$ (8)[60,294,295] with a variety of alkynes yielded a remarkable range of products (Figure 5.1/5).[143,149, 296-298] These range from relatively simple alkyne derivatives to clusters containing complex coupling fragments, including one which has an oxygen

atom of a carbonyl group incorporated into the organo-fragment. The two major products, formed with both mono- and disubstituted alkynes, are the hydrido σ -alkenyl cluster $\text{HOs}_3(\text{CO})_{10}(\text{RCCHR}') (9)$ and the $\mu_3\text{-}\eta^2$ alkyne derivative $\text{Os}_3(\text{CO})_{10}(\text{RCCR}') (10)$ (Figure 5.1/5).

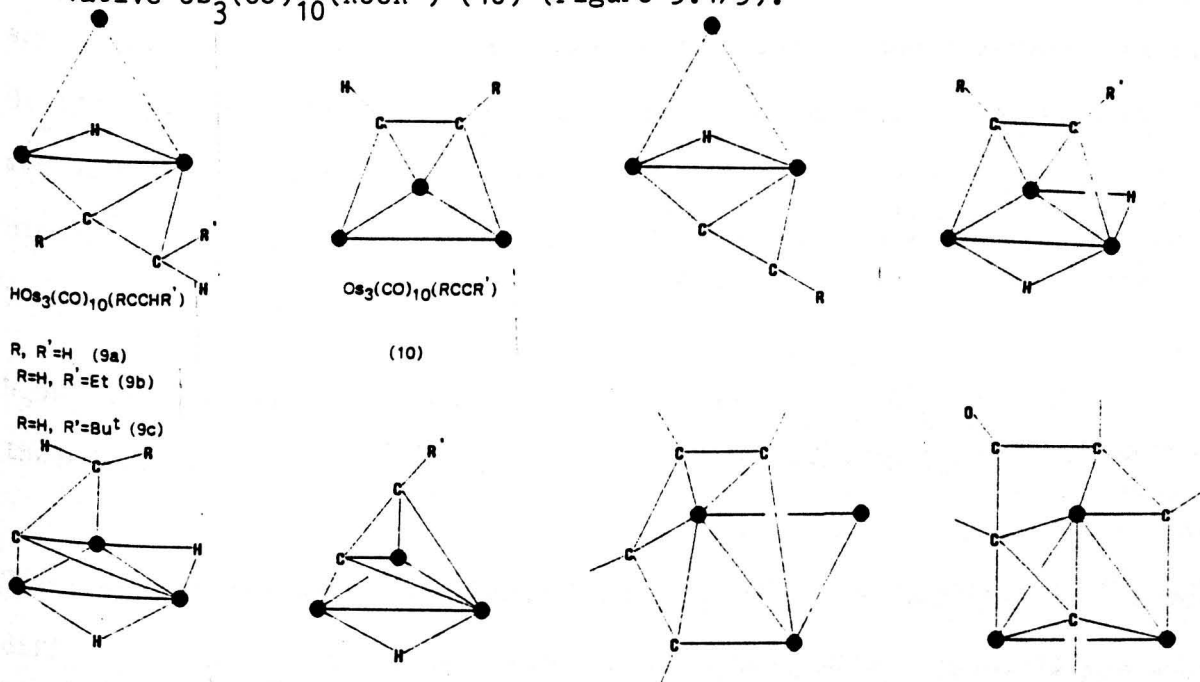
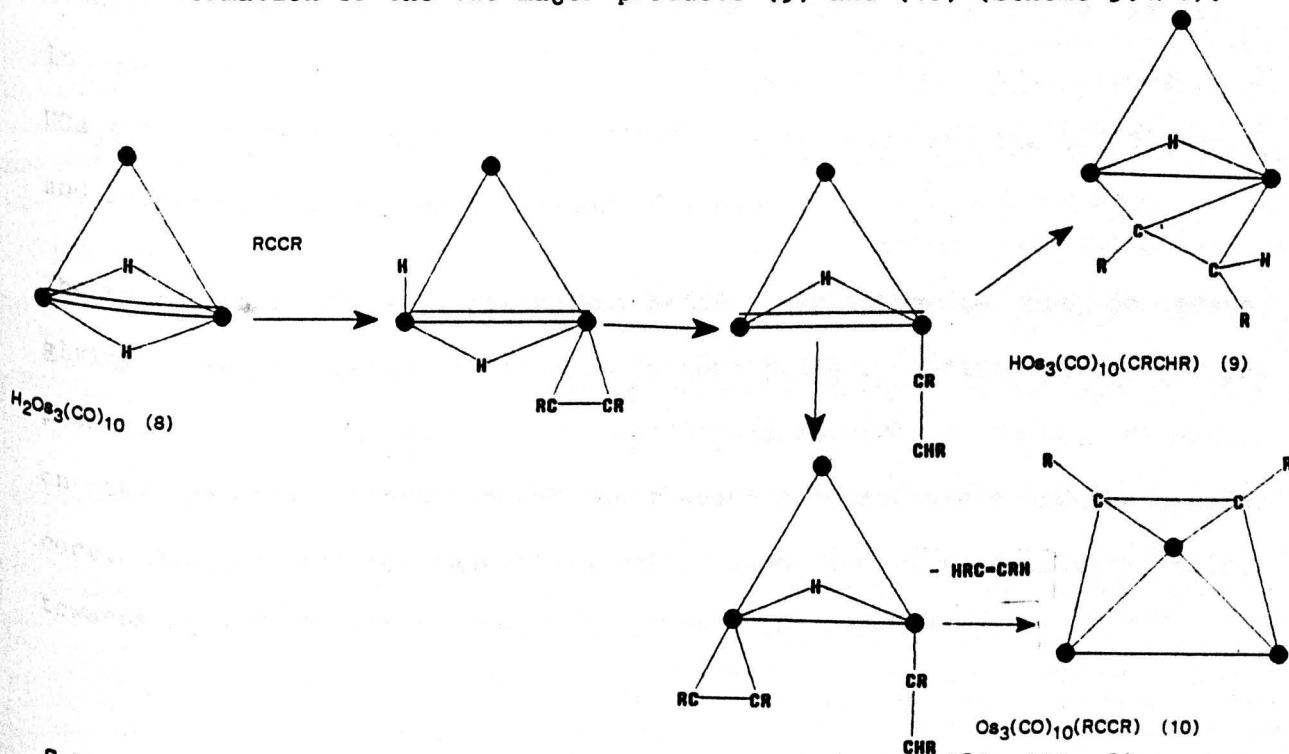


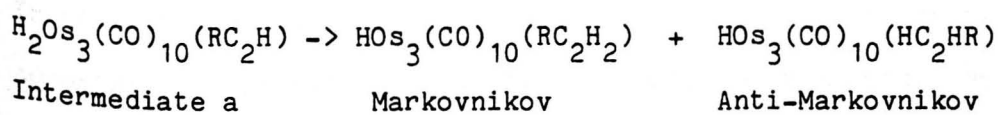
Figure 5.1/5 The organo-derivatives from reaction of (8) with alkynes.

Lunniss proposed a mechanism for the reaction of $\text{H}_2\text{Os}_3(\text{CO})_{10}$ (8) with alkynes based on that of (8) with alkenes, which satisfactorily accounts for the formation of the two major products (9) and (10) (Scheme 5.1/1).



Scheme 5.1/1 Mechanism for the reaction of $\text{H}_2\text{Os}_3(\text{CO})_{10}$ (8) with alkynes.

The initial step in the reaction of (8) with alkynes involves coordination of the alkyne as a two electron donor, followed by hydrogen migration from the metallic core to give a σ -bonded alkenyl.[299] This can then either rearrange to the σ - π -alkenyl cluster (9), or react with a second alkyne and reductively eliminate an alkene to give the alkyne cluster $\text{Os}_3(\text{CO})_{10}(\text{RCCR})$ (10). The second step in this mechanism involves hydride migration to the coordinated alkyne, and this is believed to proceed via a cis-addition step. In principle addition can lead to the following possible products:



These alkenyl triosmium compounds could exhibit a variety of isomers differing only in the orientation of the ligand with respect to the metal core triangle. Shapley defined two alternative configurations for σ - π -bonded clusters of this type, syn and anti.[143] For example, in the trans isomers of $\text{HOs}_3(\text{CO})_{10}(\text{RCCR}'\text{H})$ [R=H, R'=H (9a), Et (9b)] the α -hydrogen atom points towards the $\text{Os}(\text{CO})_4$ unit and is denoted as 'syn'. In contrast, the phenyl on the α -carbon in the cis isomer of $\text{HOs}_3(\text{CO})_{10}(\text{RCCR}'\text{H})$ [R=R'=Ph (9c)][143] points away from the $\text{Os}(\text{CO})_4$ unit, and is referred to as 'anti' (Figure 5.1/6).

The hydrogens in the anti-Markovnikov product may either be cis or trans, giving rise to geometric isomers (Figure 5.1/6). Additional isomers are possible for both the Markovnikov and anti-Markovnikov products, depending on the relative orientation of the α -carbon substituents and the cluster core. Syn and anti configurations arise when the α -substituent points towards or away from the core, respectively (Figure 5.1/6).

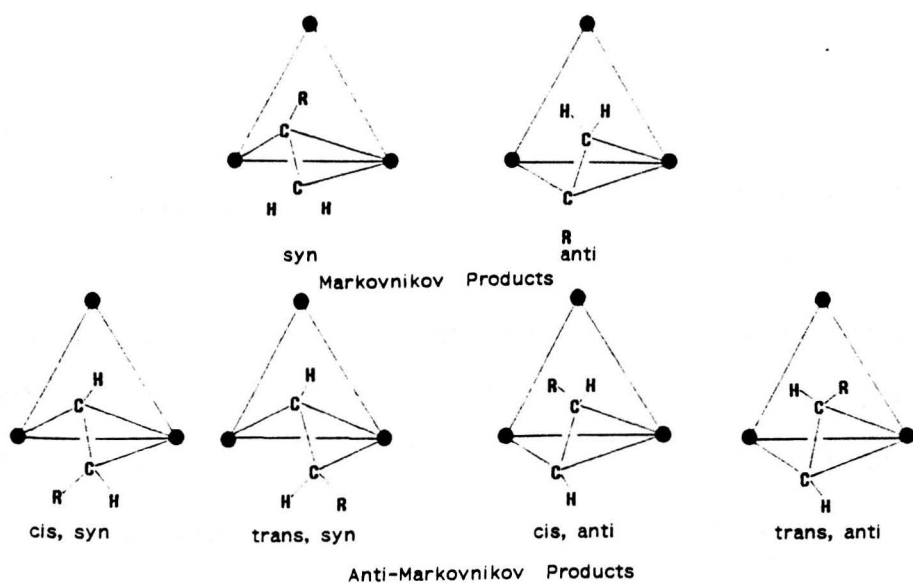


Figure 5.1/6 The 'syn' and 'anti' isomers possible for an alkenyl cluster (9).

In fact the reaction of $\text{H}_2\text{Os}_3(\text{CO})_{10}$ (8) with mono-substituted alkynes is surprisingly specific. The alkenyl products, $\text{HOs}_3(\text{CO})_{10}(\text{RC}_2\text{HR}')$ (9) ($\text{R}=\text{H}$, $\text{R}'=\text{H}$ (9a), [141, 142] Et (9b), [300] tBu (9c) [301], Ph (9d) [302]), all result from anti-Markovnikov insertion and only the trans-syn configurations are evident for mono-substituted alkynes.

Similarly, the reaction of $\text{H}_2\text{Os}_3(\text{CO})_{10}$ (8) with the gold alkyne derivative $\text{Au}(\text{C}_2\text{R})\text{PR}'_3$ [where R and R' are alkyl or aryl groups] gave analogous trans-syn products $\text{Os}_3(\text{CO})_{10}(\text{HC}_2\text{HR})\text{AuPR}'_3$ (11) [302], with the gold ligand bridging the same Os-Os bond as the σ - π -alkenyl (Figure 5.1/7). This is formally analogous to the mono-hydride alkenyl clusters (9).

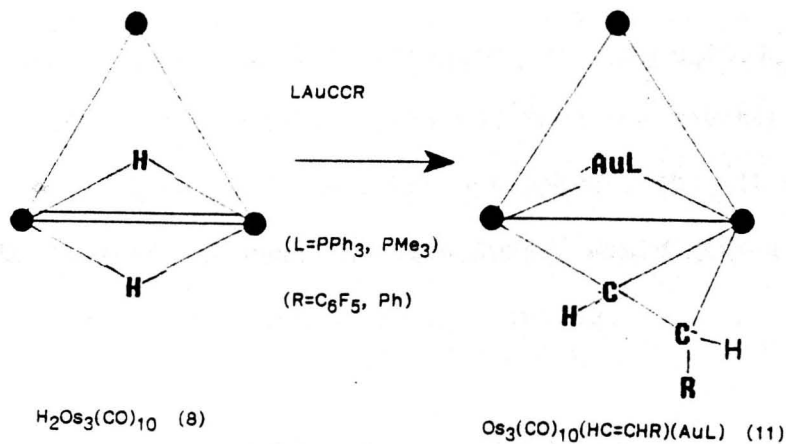


Figure 5.1/7 The gold-alkenyl cluster (11).

Recently, Lunniss has studied the related anion $[\text{HOs}_3(\text{CO})_{11}]^-$ (12) and it is the product of this reaction which has been studied as part of this thesis.

The anion $[\text{HOs}_3(\text{CO})_{11}]^-$ (12) was reacted with a variety of alkynes, and the resulting anions were then further reacted with H^+ or AuPR_3^+ . The products after electrophilic attack by H^+ were broadly similar to those observed from $\text{H}_2\text{Os}_3(\text{CO})_{10}$ (8), with the major products being the anti-Markovnikov alkenyl clusters $\text{HOs}_3(\text{CO})_{10}(\text{HC}_2\text{HR})$ (9) and the alkyne derivatives $\text{Os}_3(\text{CO})_{10}(\text{RC}_2\text{H})$ (10). The σ - π -alkenyl $\text{HOs}_3(\text{CO})_{10}(\text{HC}_2\text{HR})$ [$\text{R}=\text{H}$ (10a), Me (10b), Ph (10c)][297] again adopted the trans-syn bonding mode. Significantly, the reaction of $[\text{HOs}_3(\text{CO})_{11}]^-$ (12) with alkynes involves a decarbonylation and, furthermore, the products are very similar to those for $\text{H}_2\text{Os}_3(\text{CO})_{10}$ (8). It therefore seems likely that they share a common mechanism.

The proposed mechanism is analogous to that discussed for the reaction with $\text{H}_2\text{Os}_3(\text{CO})_{10}$ (8), and is illustrated in Scheme 5.1/2. The initial step involves loss of CO to give an ionic intermediate $[\text{HOs}_3(\text{CO})_{10}]^-$ analogous to $\text{H}_2\text{Os}_3(\text{CO})_{10}$ (8). The alkyne then π -bonds to one of the osmium atoms, followed by a 1,2-hydrogen migration to give a σ -coordinated alkenyl ligand. This can then either π -bond across to an adjacent osmium atom giving the μ_2 -alkenyl cluster (9), or a second alkyne can coordinate to the cluster core, followed by protonation and alkene elimination to give (10).

As H^+ and AuPR_3^+ gave similar products for $\text{H}_2\text{Os}_3(\text{CO})_{10}$ (8), and the protonation of the intermediate obtained from the reaction of alkynes with $[\text{Os}_3(\text{CO})_{11}]^-$ (12) gave the same trans-syn product (9), it was considered of interest to see if the reaction with AuPR_3^+ would give a cluster with the same metal framework and form of organo-bonding.

5.2 X-Ray analysis of $\text{Os}_3(\text{CO})_{10}(\text{PhCCH}_2)(\text{AuPET}_3)$ (XR13).

5.2.1 Synthesis

Addition of the electrophile AuPET_3Cl to the mixture obtained from reaction of $[\text{HOs}_3(\text{CO})_{11}]^-$ (12) with HCCR gave fewer products than the analogous

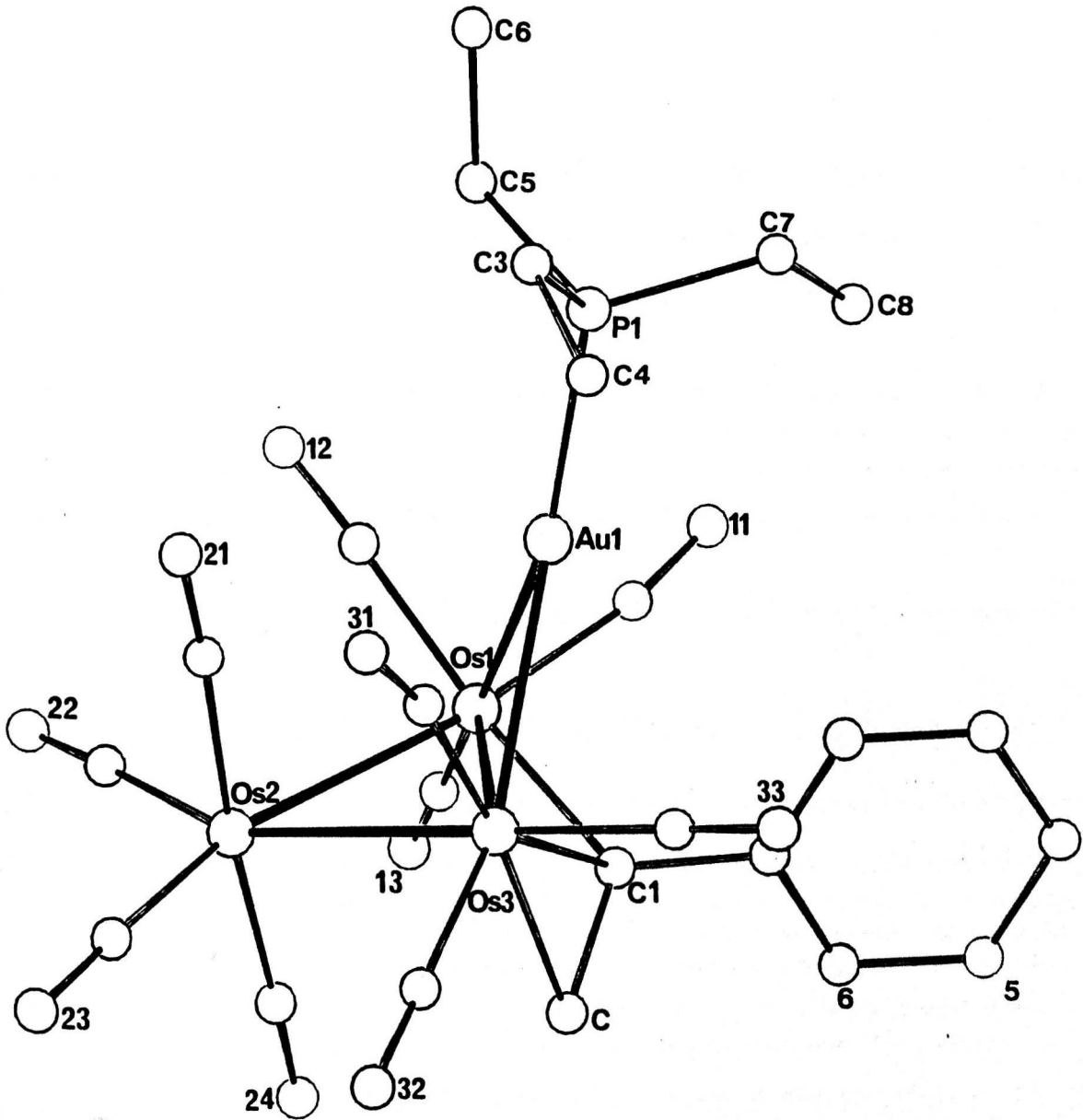


Figure 5.2/1 The molecular structure of $\text{Os}_3(\text{CO})_{10}(\text{PhC}=\text{CH}_2)(\text{AuPEt}_3)$ (XR13).

Only the O-atoms of the carbonyl ligands have been labelled for clarity.

protonation reaction.[297] With phenylethyne the major product is $\text{Os}_3(\text{CO})_{10}(\text{PhC}_2\text{H}_2)\text{AuPEt}_3$ (XR13).

The spectroscopic data obtained for (13) was consistent with this formula. No signals characteristic of metal bound H-atoms were found in the ^1H n.m.r. spectrum, indicating that the compound did not contain any hydride ligands, and two singlets at ca. 5.5 ppm and 4.6 ppm were assigned to the alkenyl geminal protons. An X-ray structure analysis was carried out to confirm the presence of the alkenyl group, PhC_2H_2 , and to determine its bonding mode and the isomer present.

5.2.2 Structural Description.

X-Ray structure analysis confirmed that the metal core of the cluster $\text{Os}_3(\text{CO})_{10}(\text{PhCCH}_2)(\text{AuPEt}_3)$ (XR13) consists of a triangle of osmium atoms, with one edge bridged by both the $\text{Au}(\text{PEt}_3)$ group and the organo-ligand (Figure 5.2/1). Hydride addition to the mono-substituted alkyne fragment has resulted in a coordinated alkenyl ligand, which bonds in a σ, π -fashion. The non-bridged osmium Os(2) has four terminally bonded carbonyl ligands attached to it, two of which are equatorial and two of which are axial. The bridged osmium atoms Os(1) and Os(2) both have three terminally bonded carbonyl ligands.

Two of the carbonyl ligands on Os(1) lie axially with respect to the triangle defined by the three osmium atoms, and the remaining carbonyl ligand C(13)-O(13) lies axially with respect to the Os(1)-Au(1) bond. The three terminal carbonyl groups on Os(2) are slightly twisted due to the presence of the alkenylidene ligand, which spans the Os(1)-Os(2) edge. The α -carbon C(1) bonds to both Os(1) and Os(2), whilst the β -carbon bonds solely to Os(2). This structure represents the first example of a Markovnikov addition of a metallic hydride to an alkyne. The β -carbon atom carries two geminal hydrogens and the phenyl substituent on the α -carbon

atom adopts the anti configuration (rather than the more common syn configuration discussed in the previous section) (Figure 5.1/6). The σ, π -alkenyl ligand donates three electrons to the cluster valence count and the bridging gold triphenylphosphine donates one electron; this results in the expected total valence electron count of 48e.

5.2.3 Discussion.

For the metal core the bridged bond Os(1)-Os(3) is the shortest, at 2.874(1) Å. The longest bond is Os(2)-Os(3) 2.917(1) Å, which is adjacent to the metal atom involved in π -bonding to the organo-fragment. The third bond [Os(1)-Os(2) 2.881(1) Å] is closer in length to the bridged bond. This is similar to the bonding trends observed in the related complexes $\text{HOs}_3(\text{CO})_{10}(\text{CHCHR})$ (R=H (9a), [141,142] or Et (9b)[300]), where for each structure the osmium-osmium bond lengths exceed 2.9 Å for the bond between the $\text{Os}(\text{CO})_4$ unit and the atom involved in π -bonding to the organo-fragment (Section 1.4).

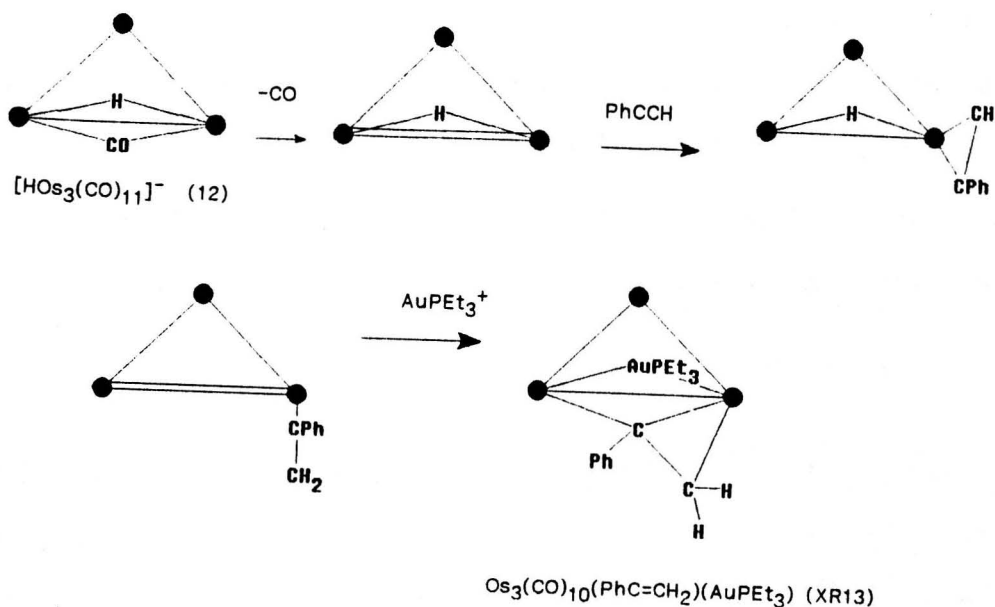
The gold triethylphosphine asymmetrically bridges the Os(1)-Os(3) bond [Au(1)-Os(1) 2.771(1) and Au(1)-Os(3) 2.812(1) Å] and is also bridged by the alkenyl ligand. The σ - π -bonding of the ligand to the cluster is reflected in the variation of osmium-carbon bond lengths, with the σ -bond significantly shorter at Os(1)-C(1) 2.076(1) Å, compared to values of Os(3)-C(1) 2.300(1) and Os(3)-C(2) 2.296(1) Å for the π -bonding lengths. All carbonyl ligands are essentially linear, lying in the range M-C(carbonyl) 1.814(1)-1.940(1) Å, C-O(carbonyl) 1.110(1)-1.238(1) Å, and M-C-O 164.0(1)-177.1(1)°. There are no shorter intramolecular contacts than that found between an aryl hydrogen atom and the bridging gold atom, H(111).. Au(1) 2.62 Å.

An alternative description of the framework is as a mixed-metal butterfly with the alkenyl bridging the Os-Os hinge bond. The angle between the planes defined by the atoms Os(1), Os(2), Os(3) and Os(1), Os(3), Au(1) is 118.69°.

As previously noted, the hydrogen ligand has been transferred from the metal framework via Markovnikov addition to the β -carbon atom of the mono-substituted alkyne. Although these geminal hydrogen atoms were deduced from the X-ray structure analysis, they could not be directly located. The two singlet peaks at ca. 5.5 ppm and 4.6 ppm in the ^1H n.m.r. spectroscopy (see above) were assigned to these two geminal hydrogens. The C(1)-C(2) bond length [1.434(18) Å] is longer than that expected for a formal double bond and this can be attributed to back donation of the metal d-orbital to the π^* -antibonding orbital of the ligand. Alkenyl bonding of this type has been observed before, both in trinuclear and higher nuclearity systems (Section 1.4).

5.2/4 Mechanism for the formation of $\text{Os}_3(\text{CO})_{10}(\text{PhCCH}_2)(\text{AuPET}_3)$ (XR13).

The proposed mechanism for the formation of $\text{Os}_3(\text{CO})_{10}(\text{PhCCH}_2)(\text{AuPET}_3)$ (XR13) is illustrated in Scheme 5.2/1. Initial loss of CO from the saturated anion $[\text{HOs}_3(\text{CO})_{11}]^-$ (12) gives the reactive unsaturated intermediate $[\text{HOs}_3(\text{CO})_{10}]^-$, which can be considered as directly analogous to the dihydrido-cluster $\text{H}_2\text{Os}_3(\text{CO})_{12}$ (8) discussed in the previous section. The phenylethyne then coordinates to one osmium atom via a π -bond and the μ_2 -hydride is then transferred to the alkyne ligand in such a way that the overall addition is Markovnikov rather than the anti-Markovnikov addition discussed above. The σ -alkenyl ligand produced then π -bonds across to an adjacent osmium atom, and reaction with AuPET_3^+ give the observed product (XR13).



Scheme 5.2/1 Mechanism for formation of $\text{Os}_3(\text{CO})_{10}(\text{CPhCH}_2)(\text{AuPEt}_3)$ (XR13).

5.2.5 Conclusion.

Three features were of interest in this work.

- A comparison of the reactivity and product types from $\text{H}_2\text{Os}_3(\text{CO})_{10}$ (8) and $[\text{HOs}_3(\text{CO})_{11}]^-$ (12).
- The effect of electrophilic attack by the isolobally related H^+ and AuPR_3^+ on the nature of the products formed.
- The effect of different alkyne substituents.

The dihydrido-cluster $\text{H}_2\text{Os}_3(\text{CO})_{10}$ (8) undergo a wide range of reactions with alkyne molecules. The addition of alkyne molecules to (8) to give σ - π complexes $\text{HOs}_3(\text{CO})_{10}(\text{CR}=\text{CR}_2)$ (9) is surprisingly specific, resulting in trans,syn products. However, the equivalent reaction with $[\text{HOs}_3(\text{CO})_{11}]^-$, followed by auration, gives an alternative cluster $\text{Os}_3(\text{CO})_{10}(\text{CPh}=\text{H}_2)\text{AuPEt}_3$ (XR13) which contains has two geminal hydrogen atoms on the β -carbon atom.

From the reaction schemes (Scheme 5.1/1 and Scheme 5.2/1) it is evident that the only difference in these reactions is the final step. This involves addition of H^+ in the reaction of $H_2Os_3(CO)_{10}$ (8) (Scheme 5.1/1), whereas the isolobal $AuPEt_3^+$ group is added in the reaction with $[HOs_3(CO)_{11}]^-$ (12). That this gives rise to different products indicates that the electrophilic groups may in fact be involved at an earlier stage in the mechanism, with the H^+ favouring anti-Markovnikov addition and the $AuPEt_3^+$ group favouring Markovnikov addition.

5.3 X-Ray structure analysis of $HOs_3(CO)_9(MeCCMe)(AuPPh_3)$ (XR14).

5.3.1 Synthesis.

The alkenyl cluster $Os_3(CO)_{10}(PhCCH_2)(AuPEt_3)$ (XR13) discussed above is obtained by the reaction of $[HOs_3(CO)_{11}]^-$ (12) with the mono-substituted alkyne $PhCCH$ followed by coordination of $AuPEt_3$. The second trinuclear structure solved by X-ray structure analysis involves a similar reaction but the alkyne used is the disubstituted molecule $MeCCMe$.

At $60^\circ C$ the reaction of $[HOs_3(CO)_{11}]^-$ (12) with $MeCCMe$, followed by reaction with $AuPR_3Cl$ gives as the major product the alkenyl derivative $Os_3(CO)_{10}(MeC_2HMe)(AuPR_3)$, which appears to be an analogue of the hydrido alkenyl species $HOs_3(CO)_{10}(MeC_2HMe)$ (9e), from spectroscopic evidence. In addition, an alkyne-derivative $HOs_3(CO)_9(MeC_2Me)(AuPPh_3)$ (XR14) was isolated. An X-ray structure analysis of this product has been carried out to establish the molecular geometry.

5.3.2 Structural description.

As in (XR13), the metal core consists of a triangle of osmium atoms (Figure 5.3/1). One edge is bridged by a gold triphenylphosphine ligand and a second edge is bridged by both the organo-fragment and a hydride ligand. The alkyne σ -bonds to the two osmium atoms and π -bonds to the third in the

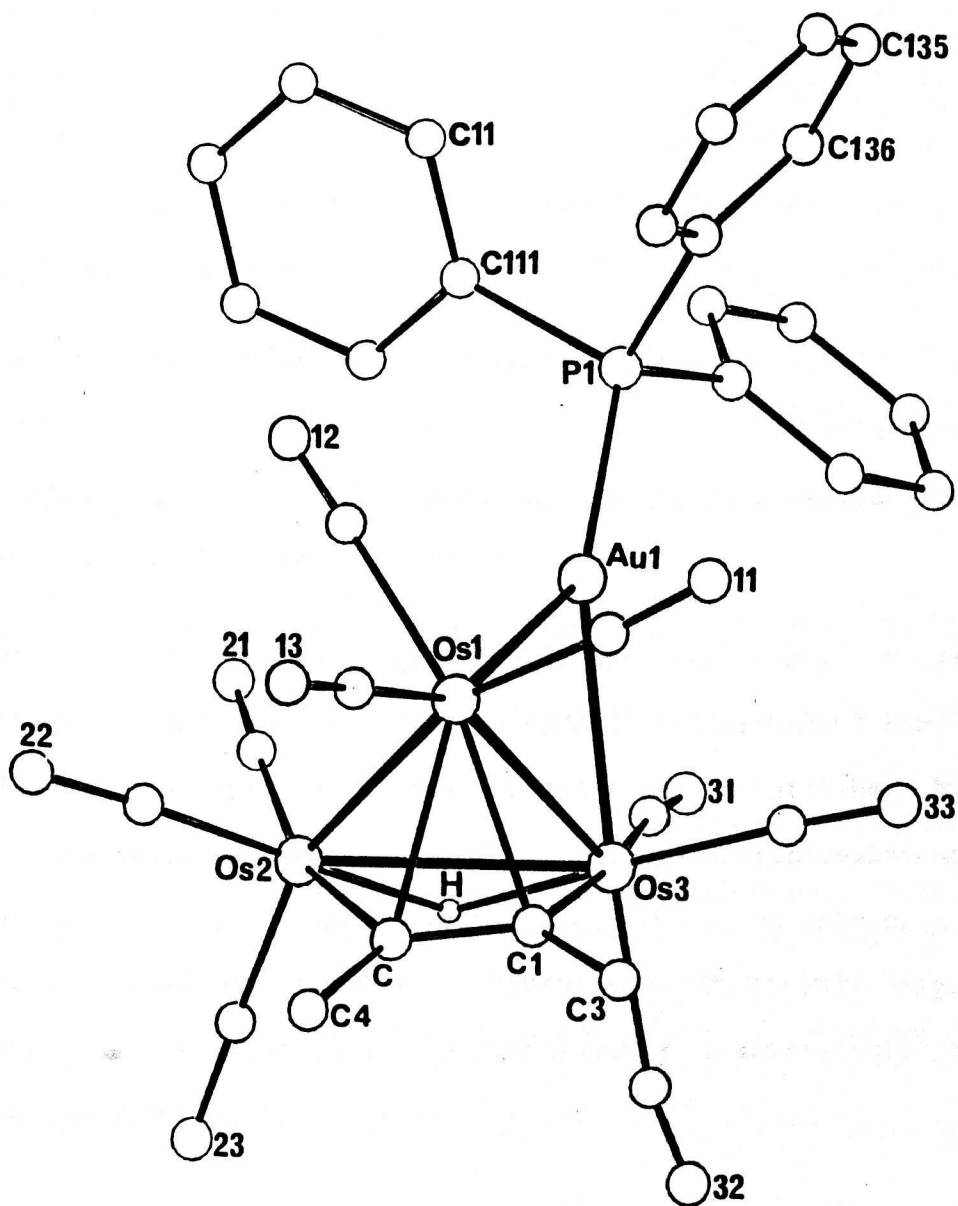


Figure 5.3/1 The molecular structure of $\text{HOs}_3(\text{CO})_9(\text{MeCCMe})(\text{AuPPh}_3)$ (XR14).
 Only the O-atoms of the carbonyl ligands have been labelled
 for clarity.

commonly seen 'parallel' ($\mu_3\eta^2\delta_{4a}$) mode (Section 1.4). However, the carbon backbone is distorted from parallel to the Os-Os bond.

5.3.3 Discussion.

If the metal core is considered as a mixed-metal butterfly, the alkyne bridges a wingtip-hinge Os-Os bond, in contrast to (XR13) where the alkenyl bridges the hinge bond. The angle between the two triangles of the butterfly is 103.82° in comparison to 118.69° for (XR13), a factor which can be attributed to the bulky substituents on the gold atom and steric repulsion by the alkyne.

In both (XR13) and (XR14), the organo-fragments bond on the outside of the butterfly, since bonding to the inside is sterically unfavourable. It is interesting that the hydride ligand and the gold triphenylphosphine ligand bridge non-equivalent metallic edges.

The metallic bond lengths in (XR14) vary more than those of (XR13), with the longest bond evident for the hydride bridged metal bond Os(2)-Os(3) $3.001(1) \text{ \AA}$. The position of the hydride was established by potential energy minimisation techniques, [264] The gold triphenylphosphine ligand bridges Os(1)-Os(3), of length $2.898(3) \text{ \AA}$. The third unbridged bond is the shortest, with Os(1)-Os(2) $2.769(3) \text{ \AA}$. The gold ligand bridges asymmetrically with Au(1)-Os(1) $2.796(3)$ being significantly longer than Au(1)-Os(3) $2.731(3) \text{ \AA}$.

The organo-fragment is a parallel bonded alkyne, σ -bonding to two metal atoms, Os(2)-C(2) $2.13(4)$ and Os(3)-C(1) $2.12(4) \text{ \AA}$ and π - to the third metal atom Os(1)-(C(1) $2.24(5)$ and Os(1)-C(2) $2.32(6) \text{ \AA}$, and as for (XR13), the σ -bonds are significantly shorter than the M-ligand π -bonds.

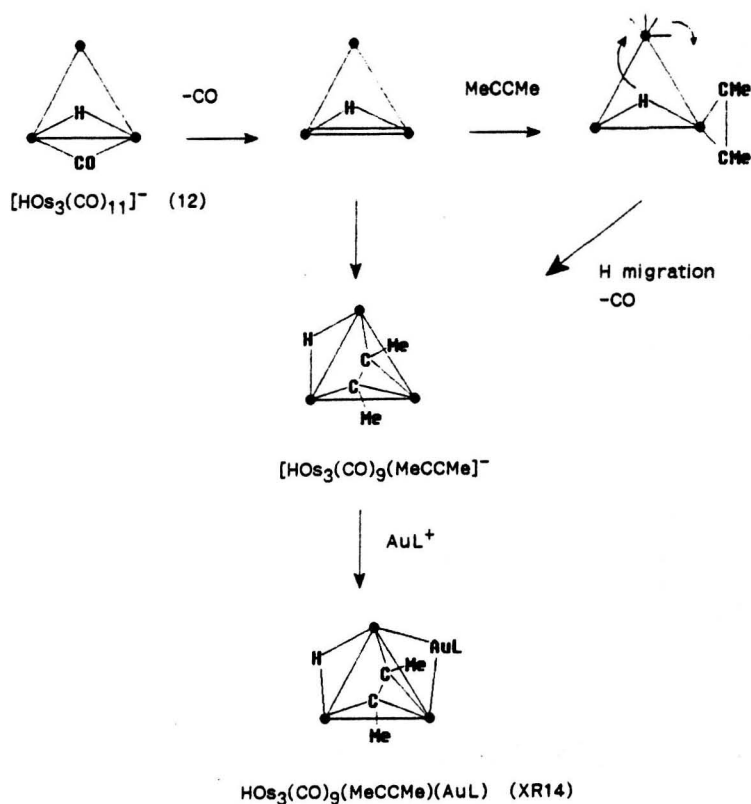
All nine carbonyl ligands are essentially linear and lie within the range M-C(carbonyl) 1.78(5)-1.95(5) Å, C-O(carbonyl) 0.98(7)-1.21(6) Å, and M-C-O 169(4) to 179(4)°. There are no shorter intramolecular contacts than that found between the μ_2 -hydride and a nearby carbonyl ligand H...C(23) 2.33 Å. The alkenyl ligand in (XR13) donates only three electrons, whilst the alkyne in (XR14) donates four electrons. The alkyne formally donates four electrons to the cluster valence count, whilst the bridging gold triphenylphosphine and the hydride each donate one electron. This gives the expected cluster count of 48 electrons for a triangular species.

Only one methyl singlet was observed in the ^1H n.m.r. spectrum of (XR14) in the temperature range 20-80°C. This is not consistent with the solid state structure, which implies that a low energy fluxional process is responsible for equilibration of the two methyl groups.

5.3.4 Mechanism.

The proposed mechanism for the formation of the hydrido-cluster $\text{HOs}_3(\text{CO})_9(\text{MeCCMe})(\text{AuPPh}_3)$ (XR14) is illustrated in Scheme 5.3/1. The initial steps are similar to those proposed for the formation of (XR13), with loss of CO being followed by alkyne addition to one of the osmium atoms. The next step is completely different: it involves hydride migration and decarbonylation, and the alkyne ligand then bridges across the triangular face to form two σ -bonds to the other two osmium atoms. This anion is then reacted with AuPPh_3 , which occupies a bridging position adjacent to the hydride bridged edge in the product (XR14). The hydride ligand does not leave the metal framework but migrates with decarbonylation, and the alkyne swings across the triangular face to form two σ -bonds to the two osmium atoms bridged by the hydrogen atom. This gives a symmetrical intermediate (Scheme 5.3/1). On structural grounds, it can be envisaged that the fluxionality in solution of (XR14) occurs via a

tetrahedral heterometallic intermediate. Both μ_2 - and μ_3 - bonding modes, are known for gold ligands.



Scheme 5.3/1 Mechanism for the formation of the alkyne cluster $\text{HOs}_3(\text{CO})_9(\text{MeCCMe})(\text{AuPPh}_3)$ (XR14).

5.3.5 Conclusion.

The two triosmium clusters which have been structurally characterised in this section and Section 5.3 are gold/triosmium clusters with coordinated organo-fragments derived from alkyne precursors. These form part of a series of related clusters derived from mono- and di-substituted alkynes. Part of their interest stems from a comparison of the reactivity of $\text{H}_2\text{Os}_3(\text{CO})_{10}$ (8) and the anion $[\text{HOs}_3(\text{CO})_{11}]^-$ (12). Both structures (XR13) and (XR14) result from reaction of $[\text{HOs}_3(\text{CO})_{11}]^-$ (12) with alkynes, followed by electrophilic attack of AuPR_3^+ . [297] In the case of (XR13) the organo-reagent is a monosubstituted alkyne (PhCCH), whilst (XR14) is derived from a disubstituted alkyne (MeCCMe).

The reaction of trinuclear clusters with alkynes produces a wide array of products but predominantly the alkenyl cluster $\text{HOs}_3(\text{CO})_9(\text{CH}=\text{CH}_2)$ and the alkyne cluster $\text{Os}_3(\text{CO})_{10}(\text{RCCR})$.

5.4 Interaction of heptanuclear clusters with mono- and disubstituted alkynes.

A study of the reaction of mono- and disubstituted alkynes with heptanuclear clusters was carried out by J.A. Lunniss at Cambridge University. This gave a variety of products. The most complicated of these is $\text{Os}_7(\text{CO})_{16}(\text{MeCCMe})$ (XR15), the X-ray structure analysis of which is reported here. Core geometries available for heptanuclear clusters are discussed first and then a number of important features of Lunniss' work will be highlighted.

5.4.1 Heptanuclear metal core geometries.

In comparison with pentanuclear and hexanuclear clusters there are still relatively few reports of heptanuclear clusters. Whereas hexanuclear clusters are, on the whole, based on an octahedral metal core (Chapter 3), an additional metal atom in the fundamental polyhedron results in a plethora of unusual geometries with no equivalent predominant metal framework. The valence count for these clusters varies between 98 and 102 electrons.

Heptanuclear clusters with 98e have $S=7$ and can therefore be considered as being derived from the 86e octahedron by addition of one metal atom and 12 electrons (see Section 1.2). The expected mono-capped octahedron has been reported for the rhodium cluster $[\text{Rh}_7(\text{CO})_{16}]^{3-}$ (13), [303,304] the rhenium cluster $[\text{Re}_7\text{C}(\text{CO})_{21}]^{3-}$ (14), [305] and the osmium cluster $\text{Os}_7(\text{CO})_{21}$ (15) (Figure 5.4/1). [306] Interestingly, the rhenium cluster (14) contains an interstitial carbide, essential if this d_7 metal is to achieve this geometry without surface ligand overcrowding.

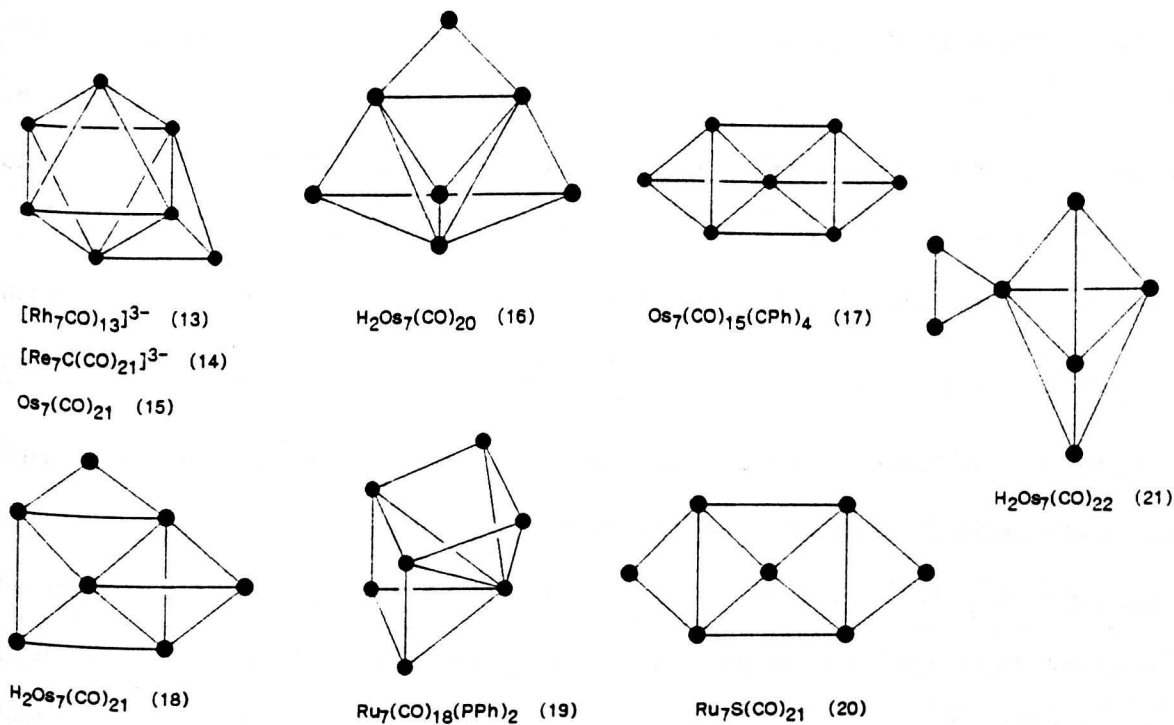


Figure 5.4/1 Observed metal frameworks for heptanuclear clusters.

The hydrido osmium cluster H₂Os₇(CO)₂₀ (16) (Figure 5.4/1), also a 98e species, adopts the capped trigonal bipyramid metal core with the seventh metal atom edge bridging; [221,307] this may be rationalised for S=7 as being a tricapped butterfly (arachno-octahedron). The third possible 98 electron core is the bicapped square pyramid, which is observed in the benzylidyne cluster Os₇(CO)₁₅(μ₃-CPh)₄ (17) (Figure 5.4/1). [138]

The 100e cluster H₂Os₇(CO)₂₁ (18) (Figure 5.4/1), with an edge bridged capped square pyramidal core, can be formally derived from the edge bridged capped trigonal bipyramidal core seen in (16) by cleavage of one M-M bond. An alternative metal framework for 100 electron species is the highly unusual fused square pyramidal geometry. This has been reported for Ru₇(CO)₁₈(μ₄-PPh)₂ (19) (Figure 5.4/1), [308] and is an example of one of a growing group of metal cores made by the fusion of common units such as square pyramids and octahedra.

The di-edge bridged square pyramid seen in the sulphide cluster $\text{Ru}_7\text{S}(\text{CO})_{21}$ (20) (Figure 5.4/1) is related to the bicapped square pyramidal core seen in (17) by rupture an M-M bond of each of the metal caps, and has a valence count of 102e.[309] One of the most unusual frameworks for this family of clusters is that observed in the 102e species $\text{H}_2\text{Os}_7(\text{CO})_{22}$ (21). The metal core in (21) can be described as a trigonal bipyramid sharing a vertex with a triangle, or as a bicapped bow-tie.[307]

Thus, heptanuclear clusters display a wider range of metal cores than any of the lower cluster species. By extension, additional metal atoms would be expected to continue this trend and proportionally increase the range of possible cores. Tantalisingly, this does not appear to be the case. Some nuclearities seem to particularly favour one geometry. For example, in the iron triad, the symmetrical quadruply capped octahedral metal core framework is predominant for decanuclear species (Section 4.4). A better understanding of the energetics of these species and the energy barriers involved will be required to interpret these observations, but it seems that highly symmetric species such as the octahedron and the M10 tetrahedron are often preferred.

The series of clusters $\text{H}_2\text{Os}_7(\text{CO})_{22-n}$ [$n=0$ (21), 1 (18), or 2 (16)] provide an insight into the reactivity of heptanuclear species. Decarbonylation of $\text{H}_2\text{Os}_7(\text{CO})_{22}$ (21) first produces $\text{H}_2\text{Os}_7(\text{CO})_{21}$ (18) and then $\text{H}_2\text{Os}_7(\text{CO})_{20}$ (16), with sequential closure of the metal core polyhedron due to successive loss of two pairs of electrons (Figure 5.4/2).[306,307] There are thought to be two isomers of $\text{H}_2\text{Os}_7(\text{CO})_{22}$ (21) but only one form has been characterised by X-ray structure analysis.[307] The ease with which decarbonylation occurs in this sequence of reactions indicates that the energy barrier between these metal frameworks is low.

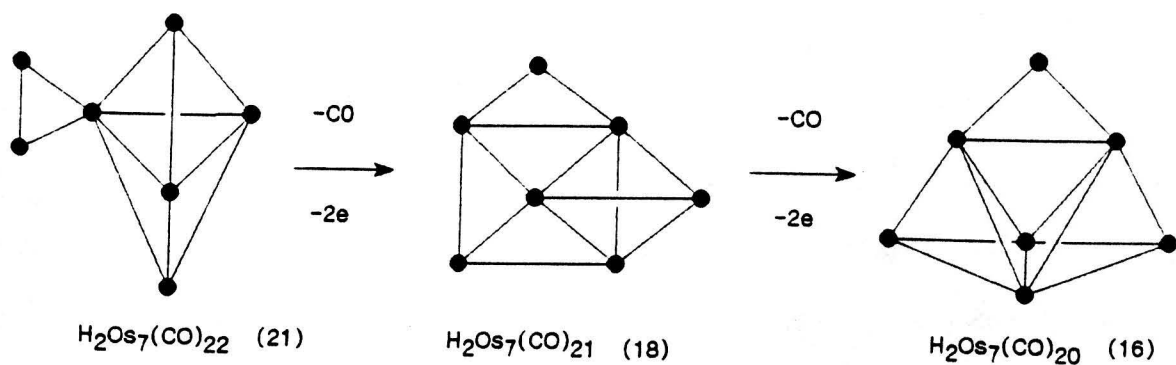
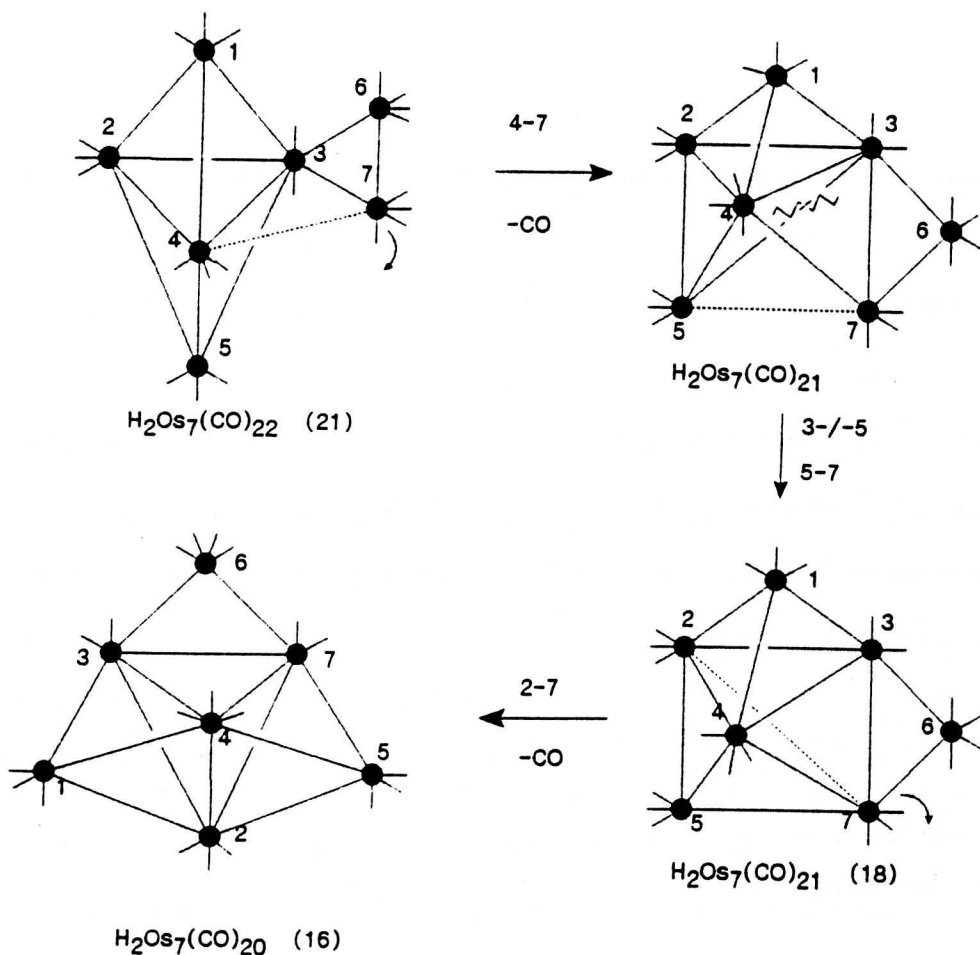


Figure 5.4/2 $\text{H}_2\text{Os}_7(\text{CO})_{2-n}$ [$n=0$ (21), 1 (18), 2 (16)].

This mechanism has been studied by Lunniss, using a phosphite label throughout the decarbonylation sequence.[297] The position of the phosphite ligand at each stage appears to agree with the above proposed pathway. This reaction provides a good example of the lability of heptanuclear metal frameworks even with very simple reactions. The initial step from (21) involves bond formation [Os(4)-Os(7)] together with the loss of a 2e carbonyl ligand from Os(7) [between the triangle and the trigonal bipyramid] to give an intermediate trigonal bipyramid with a bridging M-atom, which is further bridged by the seventh metal atom. This species rearranges to $\text{H}_2\text{Os}_7(\text{CO})_{21}$ by simultaneous rupture of an axial-equatorial bond [Os(3)-Os(5)] and formation of a bond to an axial atom [Os(5)-Os(7)]. Further decarbonylation is accompanied by bond formation across the diagonal of the square pyramid in $\text{H}_2\text{Os}_7(\text{CO})_{21}$ (18) and subsequent loss of a second carbonyl group from Os(7) to give $\text{H}_2\text{Os}_7(\text{CO})_{20}$ (16).



Scheme 5.4/1 Mechanism for the interconversion of three heptanuclear clusters.

5.4.2 The reactions of heptanuclear clusters with mono-substituted alkynes.

The reaction of $\text{H}_2\text{Os}_7(\text{CO})_{20}$ (16) with both mono- and disubstituted alkynes has been studied.[299] The reaction of (16) with PhCCH gave $\text{Os}_7(\text{CO})_{20}(\text{CCHPh})$ (22). Both hydrides of the parent cluster (16) have been lost and the alkyne has undergone a 1,2-hydrogen shift to produce a coordinated alkenylidene ligand (Figure 5.4/3).

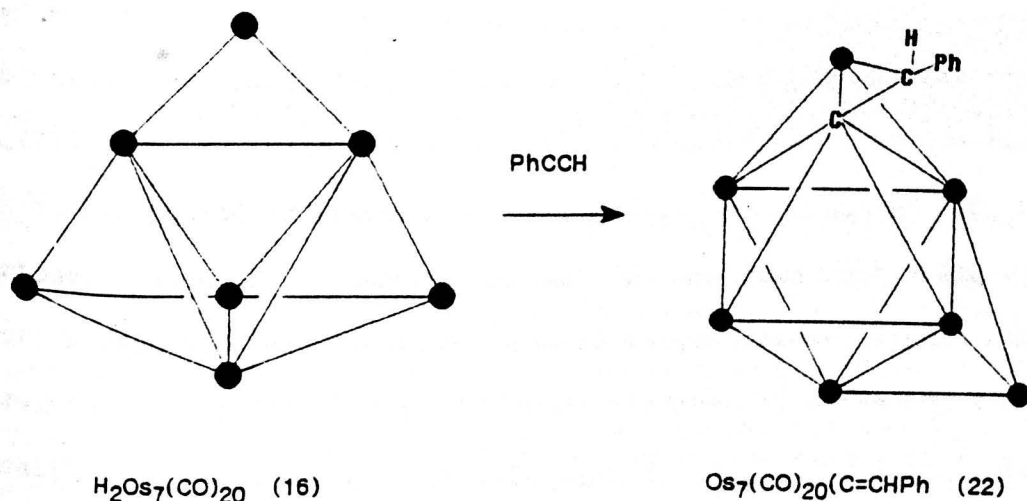


Figure 5.4/3 The alkenylidene cluster (22).

Addition of two electrons to the cluster count has resulted in metal framework rearrangement, the capped trigonal bipyramidal unit in (16) changing to form the mono-capped square pyramidal unit in (22). The α -carbon atom of the ($\mu_3\eta^{2,6}_5$) alkenylidene ligand caps the square base of the pyramid [mean Os-C(1) 2.25(3) Å]. Furthermore, both carbon atoms of the alkenylidene ligand are involved in a highly asymmetric π -bond to the seventh osmium atom [C(1)-Os(7) 2.63(3) and C(2)-Os(7) 2.13(3) Å]. Asymmetrical π -bonds have been observed in a number of organic-clusters, including the alkenyl ligands found on a number of trinuclear and tetranuclear clusters.[123,124,142] However, the difference in the two bond lengths in these clusters does not exceed 0.2 Å (Section 1.4). The extreme asymmetry observed for the alkenylidene ligand in $\text{Os}_7(\text{CO})_{20}(\text{CCHPh})$ (22) may arise from the steric constraints of two carbon atoms spanning five metal atoms.

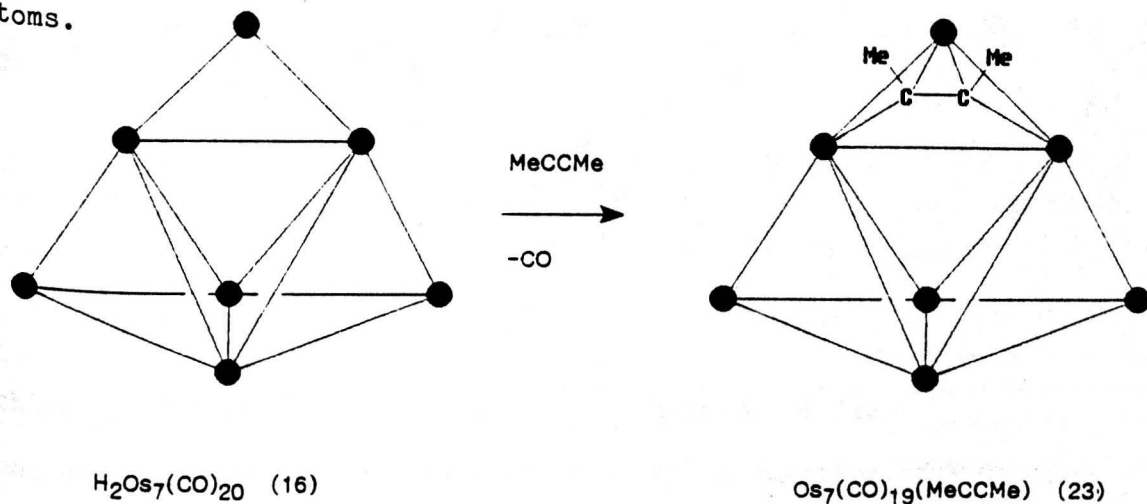
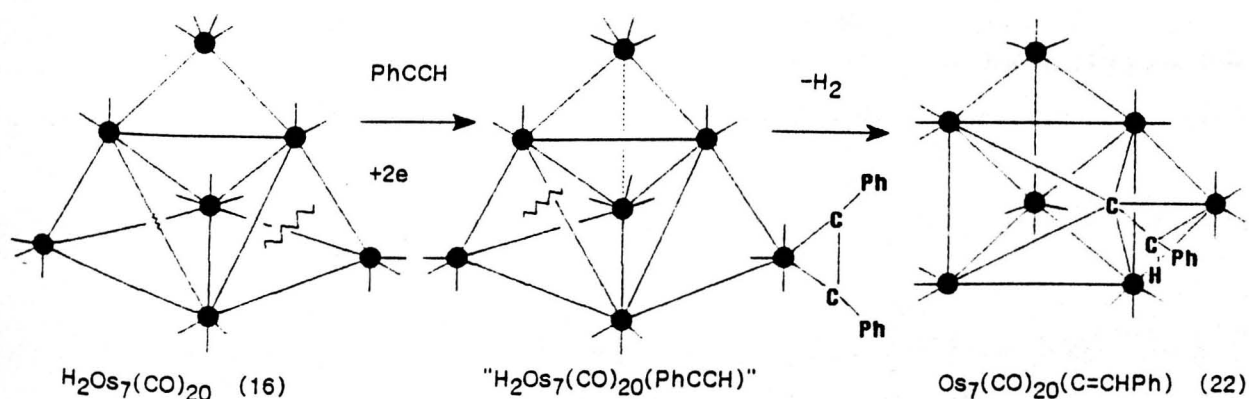


Figure 5.4/4

Thermolysis of $\text{H}_2\text{Os}_7(\text{CO})_{20}$ (16) with the disubstituted alkyne MeCCMe gave $\text{Os}_7(\text{CO})_{19}(\text{MeCCMe})$ (23) (Figure 5.4/4). This differs from the reaction with the mono-substituted alkyne discussed above in a number of ways. One carbonyl ligand of the parent species (16) has been lost along with the two hydride groups. The incoming disubstituted alkyne ligand donates 4e, resulting in a CVE of 98e. Although a number of different frameworks are possible for a cluster with 98e (Section 5.4.1), in (23) the core of (16) is retained in preference to the alternative cores. Finally the

observation that the organo-ligand does not undergo any rearrangement may be related to the fact that, unlike the mono-substituted alkyne, it has no hydrogen atom to transfer to the metal core. The bonding mode adopted by the alkyne ligand in (23) is the familiar $2-\sigma, \pi$ -parallel mode ($\mu_3 \eta^2 \delta_{4a}$) and, as this occurs on the bridging triangle of the metal core, it closely resembles triangular cluster species. Interestingly in the thermolysis of (16), in spite of the wide variety of geometries available to clusters with 98e, the reaction with disubstituted alkynes appears only to involve the triangular edge-bridging unit; the cluster framework remains unchanged.

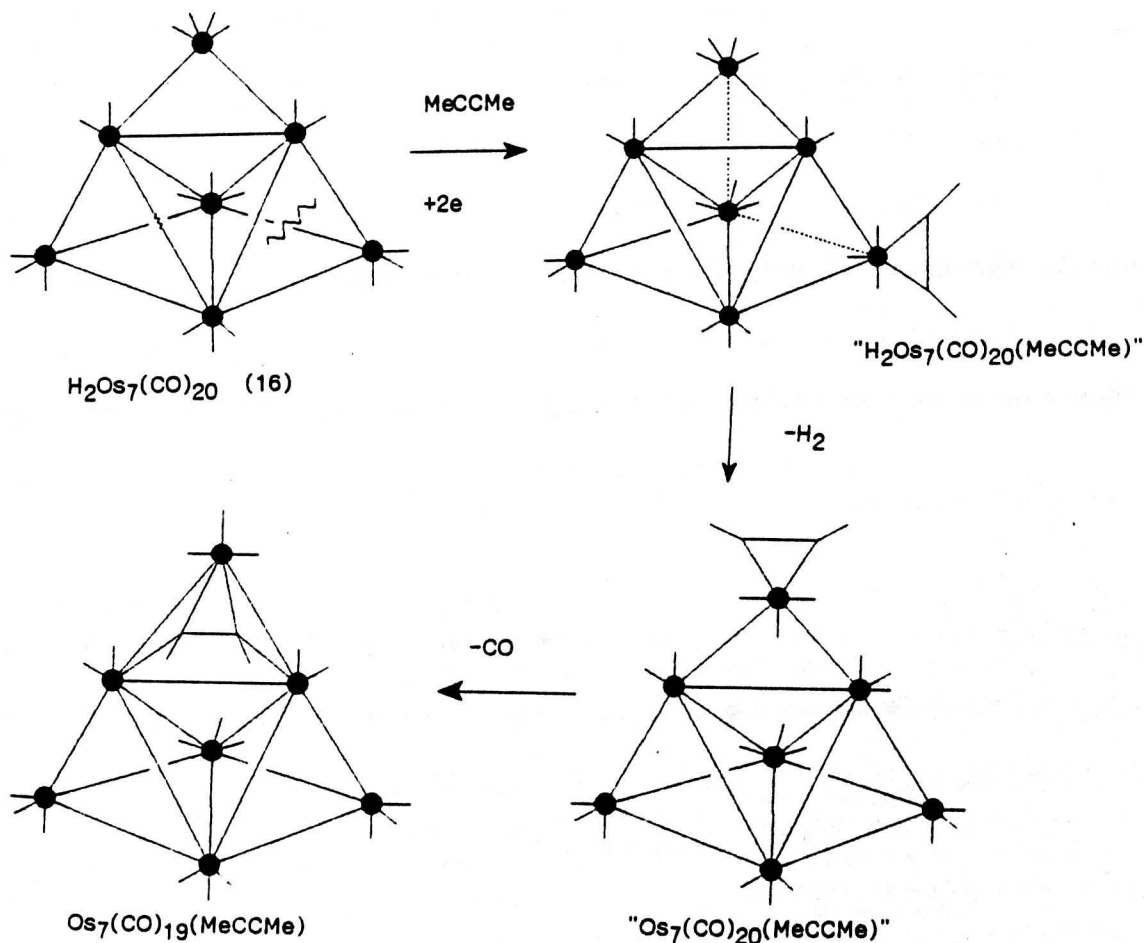


Scheme 5.4/2 Proposed mechanism for the formation of (22).

Lunniss suggested that the initial step in the reaction of $\text{H}_2\text{Os}_7(\text{CO})_{20}$ (16) with the mono-substituted alkyne PhCCH is nucleophilic addition of the alkyne, which coordinates as a two electron donor (Scheme 5.4/2). [297] This is accompanied by cleavage of a metal bond to give an transition state intermediate, " $\text{H}_2\text{Os}_7(\text{CO})_{20}(\text{PhCCH})$ ", with a doubly bridged trigonal bipyramidal metal core. Simultaneous bond cleavage/formation, hydride loss, and alkyne rearrangement to the alkenylidene ligand, gives the observed product, $\text{Os}_7(\text{CO})_{20}(\text{C}_2\text{HPh})$ (22) (Scheme 5.4/2).

By analogy with this mechanism, Lunniss suggested that the first step in the reaction of $\text{H}_2\text{Os}_7(\text{CO})_{20}$ (16) with the disubstituted alkyne MeCCMe to

give $\text{Os}_7(\text{CO})_{19}(\text{MeCCMe})$ (23), would be alkyne coordination, π -bonding to a capping osmium atom (Scheme 5.4/3). This is accompanied by Os-Os cleavage to give a di-edge bridged trigonal bipyramid. Subsequent elimination of the μ_2 -hydrides results in the creation of a new M-M bond regenerating the metal core of the parent cluster (16), with the alkyne now π -bonding to the bridging osmium atom. Rearrangement from a 2e to a 4e donor proceeds with the loss of a coordinated CO ligand rather than by cleavage of a M-M bond.



Scheme 5.4/3 Proposed mechanism for the formation of (23).

The reaction of $\text{H}_2\text{Os}_7(\text{CO})_{20}$ (16) with the disubstituted alkyne PhCCPh gave three products and X-Ray structure analysis has been carried out on two of these. One of the products $\text{Os}_7(\text{CO})_{18}(\mu_3\text{-CPh})_2$ (24) contains two benzyldiene ligands, which can be envisaged as being derived from the precursor alkyne by C-C bond rupture (Figure 5.4/5). Although no change in cluster valence electron count is observed the metal core has rearranged to the mono-capped octahedron geometry. One benzyldiene asymmetrically caps a triangular face associated with the μ_3 -capping osmium atom, whilst the second caps one of the faces of the octahedron on the other side of the cluster.

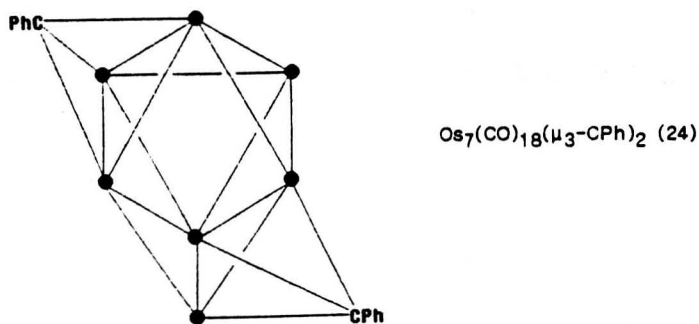
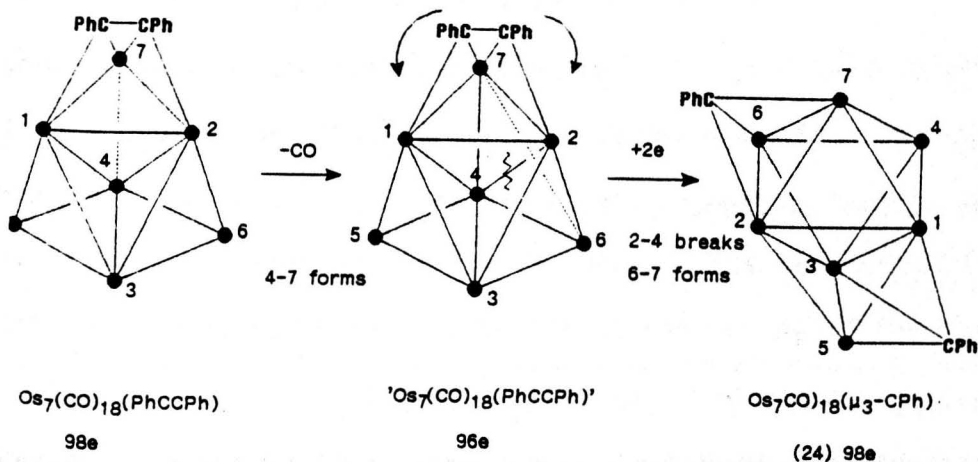


Figure 5.4/5 The mono-capped octahedral core of (24).

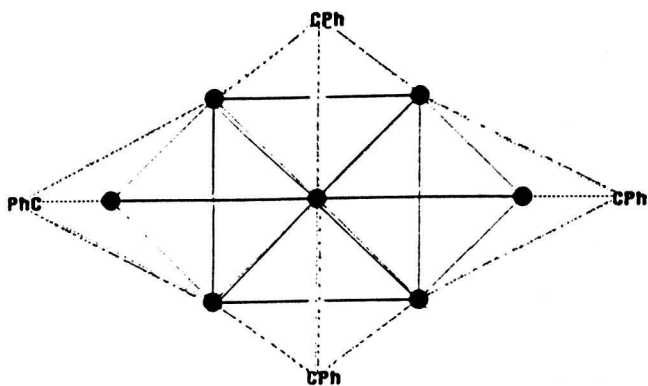
This can be derived from the PhC_2Ph analogue of the edge-bridged capped trigonal bipyramid $\text{Os}_7(\text{CO})_{19}(\text{MeCCMe})$ (23) (Scheme 5.4/3). Decarbonylation and bond formation $[\text{Os}(4)\text{-Os}(7)]$ converts the metal core of $\text{Os}_7(\text{CO})_{19}(\text{PhCCPh})$ into a 96e bi-capped trigonal bipyramid. Cleavage of the C-C to produce two benzylidyne fragments and simultaneous bond cleavage/formation $[\text{Os}(2)\text{-Os}(4), \text{Os}(6)\text{-Os}(7)]$ give the 98e mono-capped octahedral product $\text{Os}_7(\text{CO})_{18}(\mu_3\text{-CPh})_2$ (24) (Scheme 5.4/3).



Scheme 5.4/3 Proposed mechanism for the formation of (24).

The reaction of $\text{H}_2\text{Os}_7(\text{CO})_{20}$ (16) with PhCCPh requires more severe reaction conditions than the reaction of (16) with MeCCMe . In the product (24) the alkyne PhCCPh has been cleaved and this difference in reactivity can presumably be attributed to the difference in nature of the substituent R groups. The bulkier nature of a phenyl group as compared to a methyl group

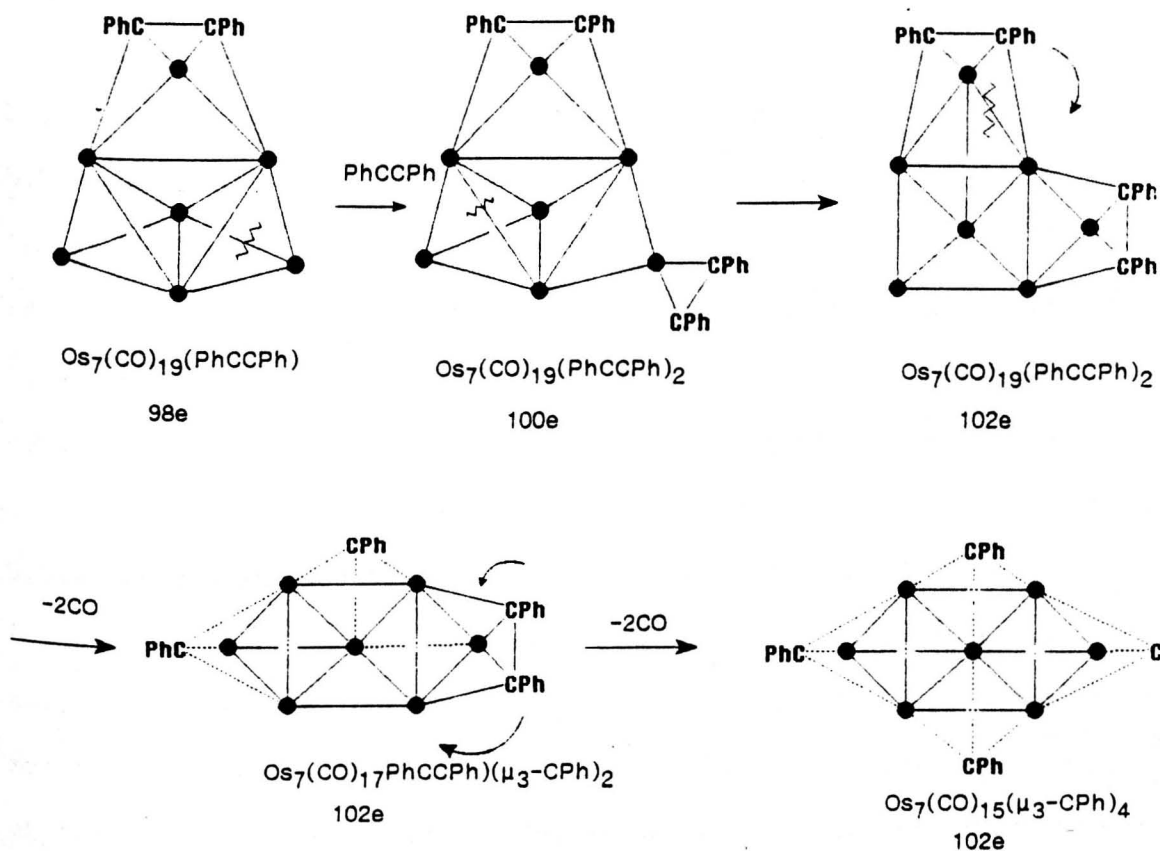
is almost certainly an important factor. It would be interesting to see what effect strongly electron donating or withdrawing groups would have on this sequence of reactions.



$\text{Os}_7\text{CO}_{15}(\mu_3\text{-CPh})_4$ (17)

Figure 5.4/6 The dicapped square pyramidal core of (17).

A second product of the reaction of $\text{H}_2\text{Os}_7(\text{CO})_{20}$ (16) with PhCCPh was the alkylidyne cluster $\text{Os}_7(\text{CO})_{15}(\text{CPh})_4$ (17) (Figure 5.4/6). The metal core has rearranged to the highly unusual bi-capped square pyramid, which has a cluster valence electron count of 98e. From the diphenyl analogue of $\text{Os}_7(\text{CO})_{19}(\text{MeCCMe})$, addition of a second PhCCPh on one of the osmium caps, with cleavage of Os(4)-Os(6), gives an 100e dedge bridged trigonal bipyramidal species $\text{Os}_7(\text{CO})_{19}(\text{PhCCPh})_2$. Decarbonylation and bond cleavage [Os(1)-Os(3)] gives the 102e dedge bridged square pyramidal cluster $\text{Os}_7(\text{CO})_{18}(\text{PhCCPh})_2$. Further decarbonylation and cleavage of one of the PhCCPh fragments causes the core to rearrange to an edge-bridged capped square pyramidal 100e species $\text{Os}_7(\text{CO})_{17}(\text{PhCCPh})(\mu_3\text{-CPh})_2$. Loss of two more CO-groups, bond formation [Os(4)-Os(6)] and fission of the second alkyne fragment gives the observed 98e bicapped square pyramidal cluster $\text{Os}_7(\text{CO})_{15}(\mu_3\text{-CPh})_4$ (17).



Scheme 5.4/4 Proposed mechanism for the formation of (17).

The edge capped trigonal bipyramid $\text{Os}_7(\text{CO})_{19}(\text{MeCCMe})$ (23) can also be produced from the activated cluster $\text{H}_2\text{Os}_7(\text{CO})_{19}(\text{NCMe})$ and this is expected to proceed by a similar mechanism. Another product from the reaction of (16) with MeCCMe is $\text{H}_2\text{Os}_7(\text{CO})_{19}(\text{MeC}_2\text{Me})$ (25). In this cluster the hydrides [present in the precursor (16)] are retained - an unusual occurrence in this sequence of reactions. The metal core of (25) is a mono-capped square pyramid with an edge bridging osmium along one of the basal edges (Figure 5.4/7).

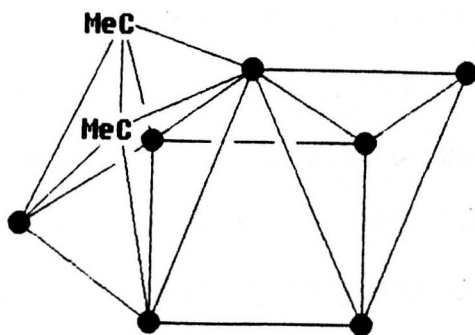


Figure 5.4/7 The metal core framework of (25).

5.5 X-Ray structure analysis of $\text{Os}_7(\text{CO})_{16}(\text{MeCCMe})_3$ (XR15).

5.5.1 Synthesis.

Prolonged thermolysis of $\text{H}_2\text{Os}_7(\text{CO})_{20}$ (16) or $\text{Os}_7(\text{CO})_{19}(\text{MeCCMe})$ (23) gave a product with the empirical formula $\text{Os}_7(\text{CO})_{16}(\text{MeCCMe})_3$ (XR15). [297] In order to establish the molecular geometry of the most complicated product obtained from this reaction a X-ray structure analysis was carried out.

5.5.2 Structural description.

Despite the very high e.s.d.'s observed in this structure, X-ray structure analysis established that $\text{Os}_7(\text{CO})_{16}(\text{MeCCMe})_3$ (XR15) adopts an unprecedented metal core geometry, which is illustrated in Figure 5.5/1. The metal core of (XR15) can be described as consisting of a highly distorted square based pyramid [defined by Os(1), Os(2), Os(3), Os(4), and Os(5)], which shares a triangular face [Os(1), Os(2), and Os(5)] with a butterfly unit [defined by the osmium atoms Os(1), Os(2), Os(5) and Os(6)]. The butterfly unit is edge-bridged by a seventh osmium atom, Os(7) (Figure 5.5/1). The unusual framework of (XR15) appears to be twisted to accommodate the three organo-fragments bonded to the metal surface. One of the alkyne ligands bonds to the triangular face defined by Os(1), Os(2), and Os(6) in the commonly observed parallel ($\mu_3\eta^2\delta_{4a}$) mode of bonding adopted by a variety of triangulated clusters (Section 1.4). The second alkyne fragments links the Os(1)...Os(7) non-bonding distance of the edge-bridged butterfly unit, with the C-C backbone of the alkyne lying perpendicular to the M-M bond vector. Both carbon atoms σ -bond to wingtip osmium atoms [Os(2) and Os(6)] and, in addition, form π -bonds to Os(1) and Os(7). A similar mode of bonding is adopted by the third alkyne group, which bridges to all four osmium atoms of the square base of the distorted square pyramidal unit, in an analogous $\mu_4\eta^2\delta_{6a}$ bonding mode (Section 1.4).

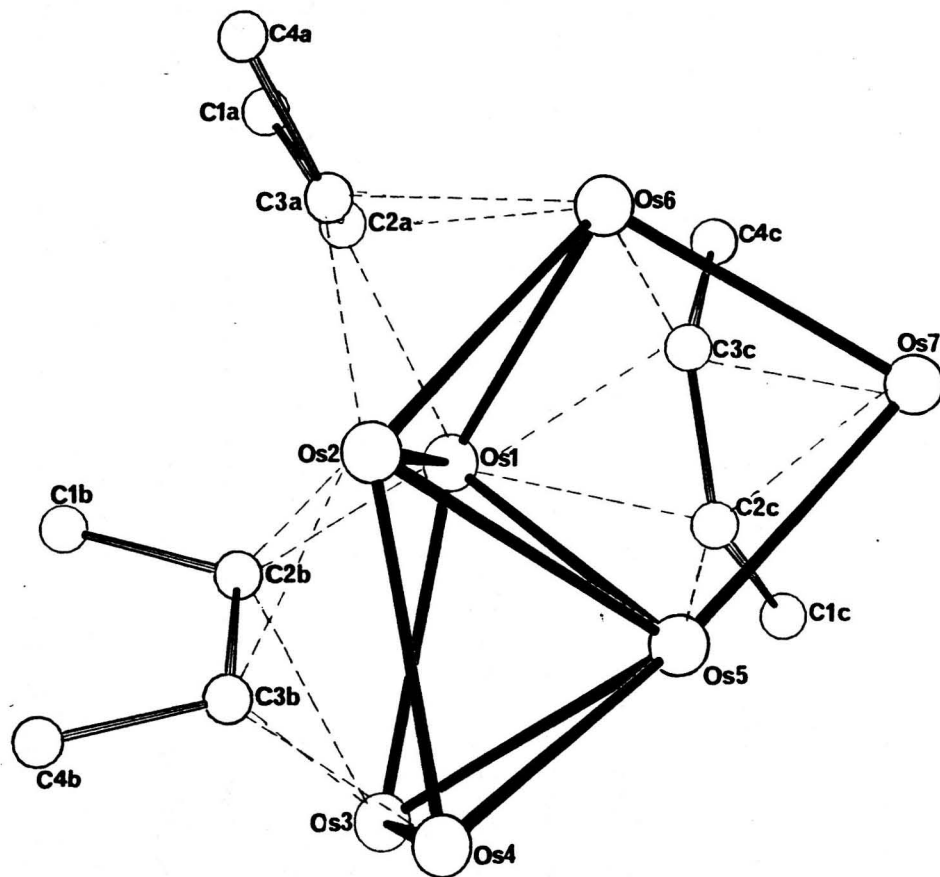
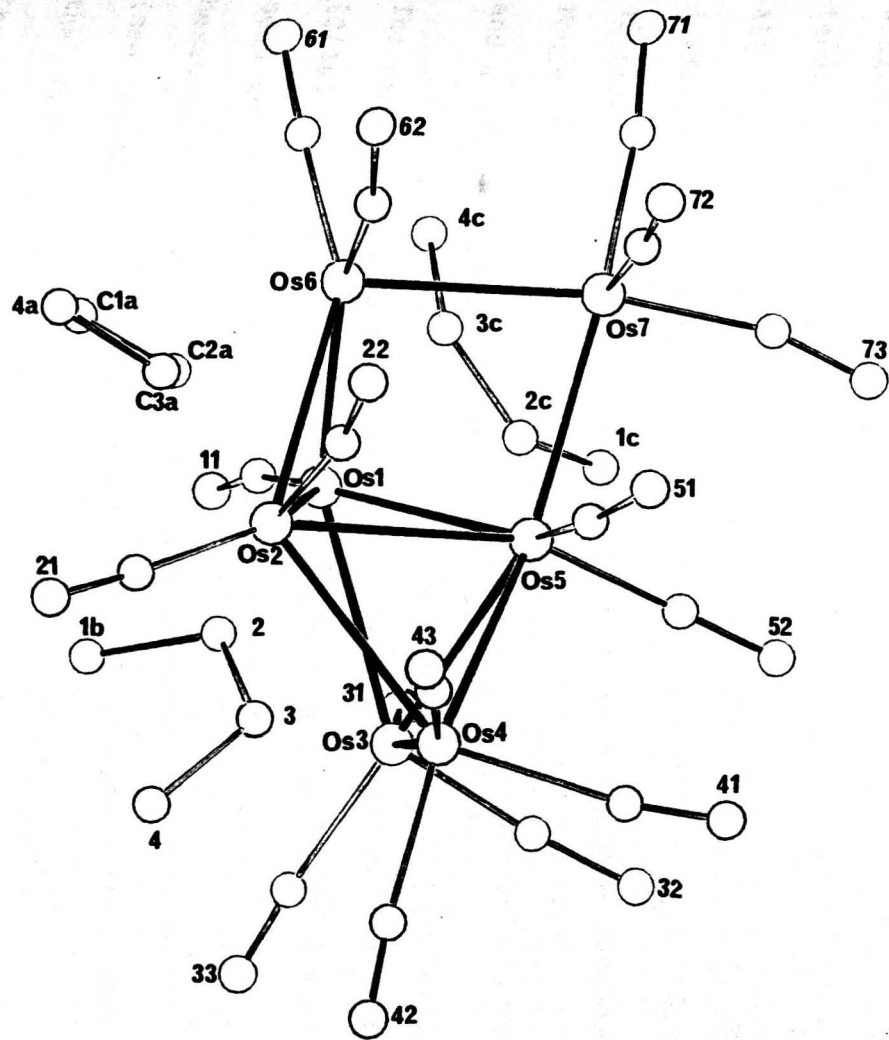


Figure 5.5/1 The molecular structure of $\text{Os}_7(\text{CO})_{16}(\text{MeCCMe})$ (XR15).

Only the O-atoms of the carbonyl ligands have been labelled for clarity.

5.5.3 Discussion.

The metal-metal bond distances in (XR15) lie within the unusually wide range 2.604(2) - 3.034(2) Å. The two M(wingtip)-M(hinge) bonds, on the same side of the cluster as the alkyne fragment that bridges the bridged-butterfly unit, are markedly shorter [Os(1)-Os(5) 2.694(2) and Os(1)-Os(6) 2.604(2) Å] than the remaining two M(wingtip)-M(hinge) bonds [Os(2)-Os(5) 3.034(2) and Os(2)-Os(6) 3.008(2) Å], with each set being respectively among the shortest and longest Os-Os bonds ever reported. This type of asymmetry in bridged butterfly units, which have organo-groups spanning a M(hinge)-M(bridge) distance, has been observed for a number of pentanuclear clusters. This was also observed in the pyridyl derivatives $\text{HRu}(\text{CO})_{13}\text{L}(\text{C}_5\text{H}_4\text{N})$ [L=CO (XR1) Isomer A and (XR2) Isomer B, and L=C₅H₅N (XR3)] studied by X-ray structure analysis in the present work; although the difference of ca. 0.1 Å was considerably less (Chapter 2). The edge bridging atom, Os(7), and two of the basal atoms of the distorted square pyramid, Os(3) and Os(4), have a total of three carbonyls each, both wing-tip atoms Os(5) and Os(6), and one of the hinge atoms, Os(2), have two terminal carbonyl ligands, whilst the last hinge atom, Os(1), has only one. All sixteen carbonyl ligands are essentially linear, M-C(carbonyl) 1.78-2.03(5) Å, C-O(carbonyl) 1.08(7)-1.29(5) Å, and M-C-O(carbonyl) 161(5)-179(3)°. There were no shorter intramolecular distances than that found between one of the methyl hydrogen atoms on one of the alkyne ligands and a nearby carbonyl ligand H(43b)...C(21) 2.28 Å.

The remaining surface is taken up by the three organo-fragments. The first [C(1a) to C(4a)], bonds in the $\mu_4\eta^2\delta_{6a}$ parallel mode of bonding commonly seen in trinuclear clusters, [171,303] and described in this report for the hexanuclear clusters (XR6) and (XR7), and the heterometallic clusters (XR8) (see Chapter 3) and (XR14) (Section 5.3). In (XR15) the alkynic bond in the first ligand [defined by C(2a) and C(3a)] lies virtually parallel to the Os(1)-Os(2) bond vector, forming a π -bond to Os(6) [Os(6)-C(2a)

2.19(3), Os(6)-C(3a) 2.21(3) Å] and two σ -bonds, one to Os(1) and one to Os(2) [Os(1)-C(2a) 2.08(3), Os(2)-C(3a) 2.07(3) Å]. With the formation of two σ -bonds the alkyne ligand might be expected to exhibit a bond order of 2, the length observed [C(2a)-C(3a) 1.521 Å] is rather long, but due to the relatively high e.s.d.'s, no conclusions can be drawn from this. The second alkyne fragment caps the highly distorted base of the square pyramid, two σ -bonds hook the fragment to Os(1) and Os(4) [Os(1)-C(2b) 2.08(3), Os(4)-C(3b) 2.12(4) Å] and two π -bonds link to Os(2) [Os(2)-C(2b) 2.37(4), Os(2)-C(3b) 2.28(4) Å] and Os(3) [Os(3)-C(2b) 2.26(3) and Os(3)-C(3b) 2.29(3) Å]. The third alkyne fragment spans the wingtip bridged butterfly, linking the bridging osmium, Os(7), with the hinge atom, Os(1). This bonding can be considered as two σ -bonds 'hooking' the wing-tip atoms Os(5) and Os(6) [Os(5)-C(2c) 2.09(3), Os(6)-C(3c) 2.19(4) Å] with two π -bonds, one to the bridging Os(7) [Os(7)-C(2c) 2.31(4), Os(7)-C(3c) 2.30(4) Å], and one to the hinge atom Os(1) [Os(1)-C(2c) 2.21(3) and Os(1)-C(3c) 2.15(4) Å].

This is somewhat reminiscent of the pyridyl clusters described in Chapter 2, but there is a marked difference in that the C-C backbone of the organo-fragment in (XR15) lies perpendicular to the Os(1)...Os(7) vector. The $\mu_4 \eta^2 \delta_{6a}$ bonding mode adopted by the last two alkyne groups has been observed in a number of tetranuclear butterfly clusters, but in these the C-C vector lies parallel to the hinge bond of the M-butterfly unit. The 'perpendicular' orientation observed for the two $\mu_4 \eta^2 \delta_{6a}$ alkyne ligands in (XR15) is more akin to the $\mu_4 \eta^2 \delta_{6a}$ bonding mode adopted by the alkyne ligand in the capped square pyramidal cluster Os₆(CO)₁₇(HCCEt) (Figure 1.4/17), where the C-C vector is diagonally orientated with respect to the square face to which it bonds.[152]

The condensed polyhedral principle (see Section 1.2), [45,46] is possibly the best approach for discussing the electron count for the very unusual metal framework in (XR15). Consider first the 'top' half of the molecule, as defined by atoms Os(1), Os(2), Os(5), Os(6) and Os(7). This wingtip bridged butterfly has 8 skeletal electron pairs (76e) and as such can be described as an arachno-pentagonal bipyramid with two of the vertices missing. This shares a triangular face (48e) with the highly distorted square pyramidal unit (74e) and, using the condensation principle, gives a total electron count of $76 + 74 - 48 = 102e$. However, the formulation established by the X-ray structure analysis corresponds to a CVE of only 100e. The presence of two hydrido-ligands supplying the missing pair of electrons can be ruled out on the basis of ^1H n.m.r., which showed no signals in the hydrido-region of the spectrum.

The only alternative is to consider the rather long osmium-osmium distance Os(5)-Os(6) $3.387(1) \text{ \AA}$ as a valid bonding distance. Then the structure is a capped square pyramid with the cap to apex bond bridged by the seventh metal atom. Electron counting now gives the observed count of 100e [square pyramid(74) + tetrahedron(60) + triangle(48) - triangle(48) - edge(34) = 100e].

As the observed electron count is 100e it is useful to compare this cluster to the dihydrido-cluster $\text{H}_2\text{Os}_7(\text{CO})_{19}(\text{MeCCMe})$ (25), [580, 581] which has a predicted and observed CVE of 100e. This has a capped square based pyramidal structure with one edge of the base bridged by a seventh osmium atom (Figure 5.3/7).

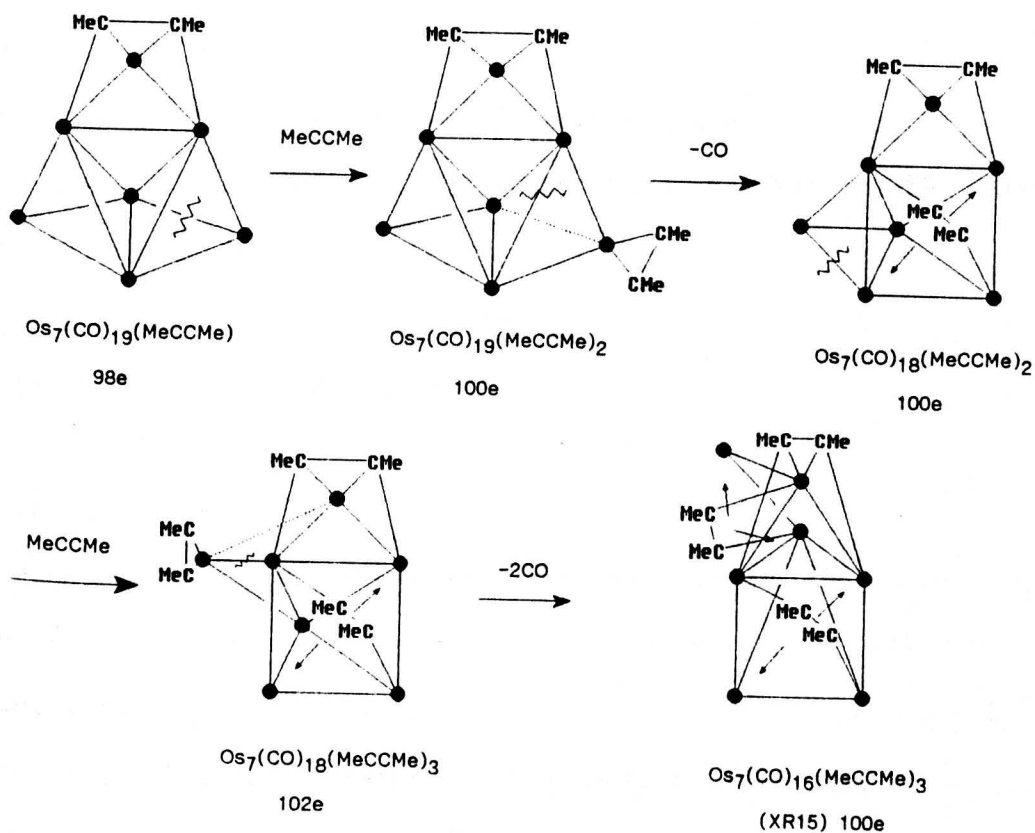
One of the interesting features of the metal frameworks adopted by heptanuclear clusters is the propensity of edge bridging metal atoms. Another way of viewing these structures is by relating them to the unbridged hexanuclear analogues. Thus, the monocapped octahedron in

$\text{Os}_7(\text{CO})_{21}$ (18)[97] is related to the octahedron common for so many hexanuclear structures. $\text{H}_2\text{Os}_7(\text{CO})_{20}$ (16) has the same geometry as $\text{Os}_6(\text{CO})_{18}$, [24] with one metal edge bridged. The di-edge bridged square pyramid reported for $\text{Ru}_7\text{S}(\text{CO})_{21}$ (20)[102] is related to the geometry in $\text{Os}_6(\text{CO})_{16}(\text{MeCCMe})_2$. [191] The mono-capped square pyramidal core of $\text{H}_2\text{Os}_6(\text{CO})_{18}$ (27)[63,62] can be formally viewed as a 'precursor' to $\text{H}_2\text{Os}_7(\text{CO})_{21}$ (18)[100] and the structure $\text{H}_2\text{Os}_7(\text{CO})_{22}$ (21)[100] is formally created by bridging of the spike of the unusual core in $\text{Os}_6(\text{CO})_{17}(\text{Py})_2$. [216] A related methodology can be applied to the metal core of $\text{Os}_7(\text{CO})_{16}(\text{MeCCMe})_3$. Bridging between the apex of the square pyramidal unit and the μ_2 -M atom of the wingtip bridged butterfly unit gives the observed geometry. This core is observed in $\text{Os}_6(\text{CO})_{16}(\text{MeCCMe})$ [124] and $\text{Os}_6\text{C}(\text{CO})_{16}(\text{MeCCMe})$ [136] and indeed both of these clusters have alkynes coordinating in a similar fashion to that observed in $\text{Os}_7(\text{CO})_{16}(\text{MeCCMe})_3$.

5.5.4 Proposed mechanism for the formation of (XR15).

The proposed mechanism for the formation of $\text{Os}_7(\text{CO})_{16}(\text{MeCCMe})_3$ (XR15) is illustrated in Scheme 5.5/5. The reaction of $\text{H}_2\text{Os}_7(\text{CO})_{20}$ (16) with MeCCMe gives $\text{Os}_7(\text{CO})_{20}(\text{MeCCMe})$; a mechanism for the reaction pathway is proposed in Section 5.4. Further reaction of (16) with MeCCMe gives the trialkyne cluster $\text{Os}_7(\text{CO})_{16}(\text{MeCCMe})_3$ (XR15). Thus the first stage in the formation of (XR15) may be considered analogous to that proposed for the formation of $\text{Os}_7(\text{CO})_{19}(\text{MeCCMe})$. From this 98e species addition of a second π -donating alkyne cause bond rupture to give the di-edge bridged trigonal bipyramidal cluster $\text{Os}_7(\text{CO})_{19}(\text{MeCCMe})_2$ (100e). Decarbonylation and concomitant bond cleavage and formation converts this to a edge-bridged capped square pyramid $\text{Os}_7(\text{CO})_{18}(\text{MeCCMe})_2$. The second alkyne ligand now bonds to all four osmium atoms of the base as a 4e donor and therefore the cluster is still an 100e species. Addition of the third alkyne cause M-M cleavage to give a di-edge bridged square pyramidal cluster $\text{Os}_7(\text{CO})_{18}(\text{MeCCMe})_3$ (102e).

Further decarbonylation, bond cleavage/formation rearrangement of the third alkyne group gives the observed 100e cluster $\text{Os}_7(\text{CO})_{16}(\text{MeCCMe})_3$ (XR15).



Scheme 5.5.5 Proposed mechanism for the formation of (XR15).

5.5.5 Conclusion.

Although this cluster contains three intact alkyne ligands in close proximity, ligand fragmentation, coupling or rearrangement has not occurred. This structure is exciting not only because of the novel twisted metal core geometry, but because of the paradoxical of the nature of the bonding modes of the organic fragments. It gives some insight into the enormous variety of possible frameworks and bonding modes available these types of clusters.

CHAPTER SIX

Background crystallography and experimental details.

The following reference text books were used:

X-Ray structure determination - A practical guide.

G.H. Stout and L.H. Jensen, J. Wiley and Sons, New York, 1989, (2nd Ed.).

Crystal structure analysis.

M.J. Buerger, Wiley, New York, 1960.

The determination of crystal structures.

H. Lipson and W. Cochran, Bell, London, 1957.

Chemical crystallography.

C.W. Bunn, 2nd ed., Oxford University Press, London, 1961.

Modern X-ray analysis on single crystals. by P. Luger, Walter de Gruyter, Berlin, 1980.

International Tables for X-ray crystallography, Vol. 1.

N.F.M. Henry and K. Lonsdale, Eds., Kynoch Press, Birmingham, England, 1952.

All the main computing operations were performed using the SHELX suite of programmes - G.M. Sheldrick, SHELX76 programme for crystal structure determination, 1976, University of Cambridge.

Diagrams were plotted using OR TEP-II - C.K. Johnson, 1976,

Oak Ridge National Laboratory and the space filling diagrams were plotted using SCHAKAL - E. Keller, 1982, University of Fribourg.

Chapter 6 - Background crystallography and experimental details.

This chapter outlines background crystallography, along with the experimental details of the 15 structures solved by X-ray structural methods (Section 6.5). The detailed discussion of these clusters can be found in the preceding chapters. Appendix A includes selected bond lengths and angles and the Patterson solutions are listed in Appendix B. As the most important application of X-ray diffraction is the investigation of the solid state, crystal symmetry is discussed in the early part of this chapter.

Crystals are composed of a regularly repeating array of atoms, ions or molecules in three-dimensions. A crystal lattice is an array of points (each of identical environment) separated by unit cell translations. The unit cell is the defined repeat unit of a crystal and is a parallelepiped characterised by six parameters (the edge lengths a , b , c , and the angles α , β , and γ between pairs of sides). Fractional coordinates x , y , and z are used to define any point or atom in the unit cell, where $x = X/a$, $y = Y/b$, and $z = Z/c$. The coordinates are defined parallel to the corresponding unit cell axis and X , Y , and Z are in \AA .

6.1 Conditions for X-ray diffraction and fundamental symmetry concepts.

6.1.1 Geometry of X-ray diffraction by crystals.

X-Rays were discovered at the end of the last century by Roentgen but it was Laue in 1912 who demonstrated their wave like behaviour and showed that their wavelengths are of a suitable order of magnitude to produce diffraction effects in crystals. Laue described the diffraction of X-rays by crystals in terms of diffraction from a three-dimensional atomic array and defined the conditions for diffraction of X-rays of crystals in three-dimensional terms (Figure 6.1/1).

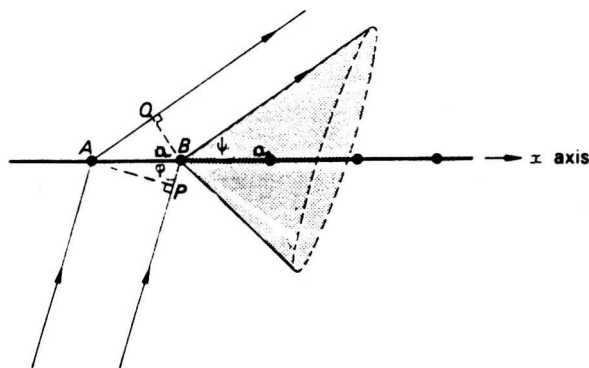


Figure 6.1/1. Diagram showing conditions for Laue diffraction.

With reference to Figure 6.1/1, for a row of scattering centres of regular spacing a , X-rays are incident at an angle ϕ and scattered at an angle ψ . The path difference between rays scattered by neighbouring centres is given by:

$$\text{Path difference} = AQ - BP \text{ or}$$

$$\text{Path difference} = a(\sin \psi - \sin \phi)$$

For reinforcement of the scattering rays, the path difference must be an integral number of wavelengths. Generalising to three-dimensions gives the three Laue equations:

$$h\lambda = a(\sin \psi_1 - \sin \phi_1)$$

$$k\lambda = b(\sin \psi_2 - \sin \phi_2)$$

$$l\lambda = c(\sin \psi_3 - \sin \phi_3)$$

where λ is the wavelength of the X-ray radiation. For constructive interference to occur all 3 of these simultaneous equations must be satisfied.

In a simpler approach W.L. Bragg noted the similarity of the result of diffraction to ordinary reflection, and deduced an equation treating diffraction as a type of reflection from mathematically defined planes in the lattice (Figure 6.1/2).

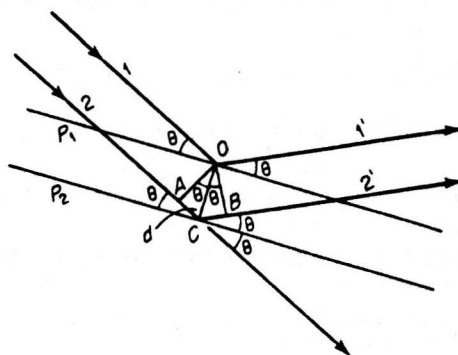


Figure 6.1/2 Conditions for Bragg reflection.

Each set of planes is denoted by the indices h, k, l , and has characteristic spacing d_{hkl} . The planes cut the unit cell axes with intercepts a/h , b/k , and c/l . Diffraction only occurs if the X-ray beam strikes a set of planes (hkl) at an angle θ_{hkl} such that:

$$\lambda = 2d_{hkl} \sin\theta_{hkl}$$

where λ is the wavelength of the X-radiation, θ is the Bragg angle and d_{hkl} is the perpendicular spacing between successive planes and the diffracted beam emerges as if reflected (i.e. at an angle θ_{hkl})

This gives the direction of the diffracted beam and conversely from the measurement of the angles of the diffracted beam d_{hkl} the unit cell dimensions may be deduced. (The nature and positions of the atoms within the unit cell determine the intensities of the diffracted beams.)

6.1.2 The reciprocal lattice.

Bragg's equation shows there is an inverse relationship between $\sin\theta_{hkl}$ and d_{hkl} (the interplanar spacing for a set of planes, hkl). To facilitate interpretation of X-ray diffraction patterns a reciprocal lattice is defined, for which any point within the crystal may be taken as the origin.

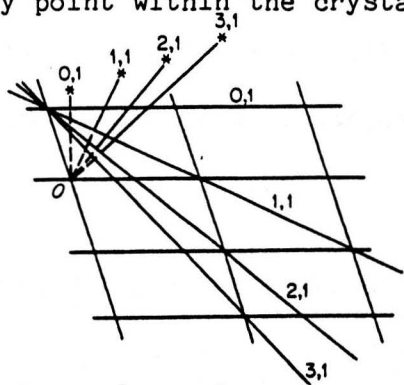


Figure 6.1/3. Points in reciprocal space are related to planes in direct space.

Normals from the origin to all sets of direct-lattice hkl planes are drawn and each terminates in a point at distance $1/d_{hkl}$ from the origin. A two-dimensional representation of this process is illustrated in Figure 6.1/3. This gives a regular array of points constituting the reciprocal lattice, with rows of parallel and regularly spaced points related to

planes in direct space. To envisage the condition for diffraction a sphere of reflection can be constructed such that any reciprocal lattice point passing through the sphere as the crystal rotates will meet the requirements for diffraction as stipulated in Bragg's equation.

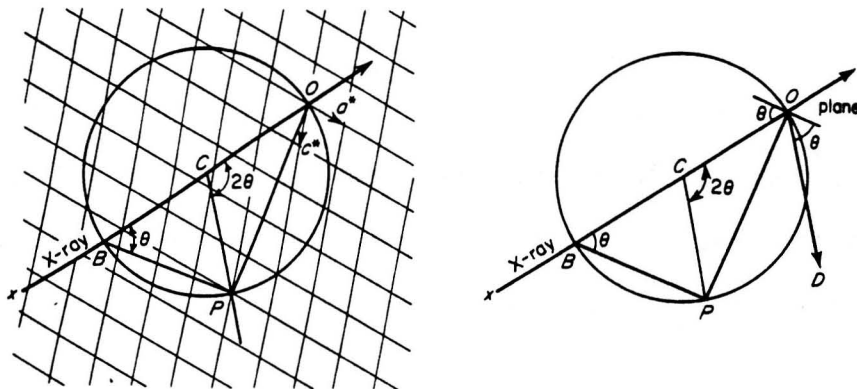


Figure 6.1/4. The relationship between the reciprocal lattice and diffraction.

The sphere of reflection may be constructed as illustrated in two-dimensions in Figure 6.1/4, where it is assumed that the crystal is orientated with the X-ray beam parallel to the a^*c^* plane of the reciprocal lattice. The line XO is drawn in the direction of the beam passing through the reciprocal lattice origin, O. A circle of radius $1/\lambda$ is constructed with centre C on XO and located such that O falls on the circumference. From this circle the properties of a reciprocal lattice point, P, lying on the sphere of reflection are as follows.

The angle OPB is inscribed in the semi-circle and is therefore 90° . From trigonometry

$$\sin \theta = \frac{OP}{OB} = \frac{OP}{(2/\lambda)}$$

$$\sin \theta = (OP/2)\lambda$$

As P is a reciprocal lattice point the length OP by definition is $1/d_{hkl}$, giving:

$$\sin \theta = [(1/d_{hkl})/2]\lambda$$

$$= \lambda/2d_{hkl}$$

$$\lambda = 2d_{hkl} \sin \theta.$$

Therefore, when P lies on this circle the Bragg equation is satisfied and reflection will occur. The reflecting plane is perpendicular to OP and

therefore parallel to BP, making an angle of θ with BO. The direction of the diffracted beam OD is parallel to CP making (as required) an angle of 2θ with the incident beam. The whole sphere of reflection in three-dimensions, of radius $1/\lambda$, is generated by rotating the circle about OB. The maximum number of reflections which can be detected for a crystal where radiation of wavelength λ is used and rotating the lattice about the origin O generates a limiting sphere of radius $2/\lambda$. Changing the wavelength corresponds to a change in size of the sphere of reflection and therefore in the number of reflections which can be observed.

6.1.3 Symmetry Elements.

The last section outlined the conditions necessary for diffraction, this section will consider the symmetry of a crystal. Almost all crystals have some symmetry and since this depends on the way in which atoms are arranged in the crystal a knowledge of the symmetry of atomic arrangement is very useful in structure determination.

The symmetry within a crystal gives rise to seven crystal systems which impose special restrictions on the unit cell dimensions. These range from none for triclinic crystals to $a=b=c$ and $\alpha = \beta = \gamma = 90$ for cubic crystals. Remarkably, for crystals of metal cluster compounds examples of crystal systems other than triclinic and monoclinic are rare and none were encountered in the present project. In monoclinic systems one axis is unique (conventionally this is the b axis) and is perpendicular to the remaining two axes. The notation used for the symmetry elements in crystallography are those of Hermann-Mauguin in contrast to the Schoenflies notation used in spectroscopy.

Two types of symmetry are possible in crystals: a) point group symmetry and b) translational symmetry.

a) Point group symmetry.

There are two types of point group symmetry elements, rotational axes (n) and inversion axes (\bar{n}). Rotation of $360/n^\circ$ occurring about an axis constitutes a rotational axis. This is described as an n -fold axis. In contrast to the symmetry of isolated molecules, the values of n possible for crystals are restricted to $n = 1, 2, 3, 4$ or 6 because of the necessity to generate regular repetitions. A rotation inversion axis is created by the combination of one these axes with a centre of symmetry. Thus this point is the centre of symmetry or inversion centre. and there are two special cases. Firstly, there is the $\bar{1}$ inversion axis, the operation of which consists of rotation of 360° followed by inversion, which is equivalent to the inversion centre C_i of the Schoenflies notation. The second case is the 2-fold inversion axis, the operation of which is rotation of 180° followed by inversion. This is equivalent to reflection in a plane and is therefore given the symbol m , equivalent to C_s .

b) Translational symmetry.

In an extended array of atoms, types of symmetry other than rotation and inversion axes are possible. Symmetry operations whose continued operation bring a point not into self coincidence but into coincidence with a point in a neighbouring unit cell are known as translational symmetry operations. Thus translational symmetry arises from the combination of point group symmetry with the translations possible in three-dimensions. These do not occur in the triclinic crystal system and in monoclinic only the 2_1 screw axis and the c -glide plane are standard. The combination of a rotation axis and a translation parallel to the axis produces a screw axis. Screw axes are designated by an integer n and a subscript m , where $n = 1, 2, 3, 4$

or 6 is the order of the axis and m is an integer factor of n . Thus the operation of a 2_1 screw axis consists of a rotation of 180° followed by translation of a fraction $1/2 (m/n)$ of the unit cell length parallel to an axis. The combination of a reflection and a translation parallel to the axis is the operation of a glide plane. The translation in such a plane is parallel to an edge or diagonal of the unit cell. Thus the operation of a c-glide in a monoclinic crystal is reflection in a plane perpendicular to b followed by $1/2$ a unit cell translation parallel to the c axis.

6.1.4 Crystal systems.

There are seven crystal systems and each one has associated lattice symmetry. Lattices are always centrosymmetric and this is the only symmetry possessed by triclinic lattices. All monoclinic crystals have a lattice symmetry of $2/m$ whilst the remaining five crystal systems possess progressively higher symmetry. When the unit cell is selected so that lattice points occur only at its corners the lattice is primitive. Additional lattice points, within the unit cell, give rise to non-primitive lattices A, B, C, I or F-faced. A C-face centred lattice has a pair of lattice points per unit cell in the centre of each C-face (the face defined by the a and b axes) in addition to the lattice points at all 8 corners of the unit cell. These non-primitive lattices are essential to describe the maximum symmetry of some crystals. Thus there are seven primitive and seven non-primitive lattices arising from the seven crystal systems and these are known as the 14 Bravais lattices. The symmetry results in unit cell restrictions, of which there are none for triclinic and for monoclinic $\alpha = \gamma = 90^\circ$. For each crystal system the lattice symmetry is the highest point group symmetry possible but the actual point group symmetry may be lower. For example, the monoclinic crystal system has a lattice symmetry of $2/m$ but point groups 2 , m , and $2/m$. In total, there are 32 unique point groups for the seven crystal systems. The combination of lattice types with crystal symmetry give 230 unique space groups.

Centred lattices give rise to general systematic absences in the diffraction data. For example a C-face centred lattice causes all data with $h + k = (2n+1)$ to be unobserved. The presence of a 2_1 screw axis is denoted by systematic absences in the diffraction data of the type $0k0$; $k = 2n+1$, whilst a c-glide is recognised by lack of data of the type $h0l$; $l = 2n+1$.

The symmetry of the X-ray diffraction pattern corresponds to one of 11 Laue groups. All X-ray diffraction patterns have $I_{hkl} = I_{\bar{h}\bar{k}\bar{l}}$ (Friedels Law) and higher crystal systems have correspondingly more complicated intensity relationships, e.g., in monoclinic systems the relationships are $I_{hkl} = I_{\bar{h}k\bar{l}} = I_{h\bar{k}l}$. The Laue groups for the triclinic and monoclinic space groups are $\bar{1}$ and $2/m$ respectively.

6.2 Intensity of X-ray diffraction.

6.2.1 The atomic scattering factor.

Since X-rays are diffracted by the electrons of an atom, the degree of diffraction depends on the number of electrons, and therefore on the atomic number of the element. The expression for the scattering power of an atom is known as the atomic scattering factor (f). The atomic scattering factor (f) is a function of $\sin\theta/\lambda$ and decreases with increasing angle of diffraction.

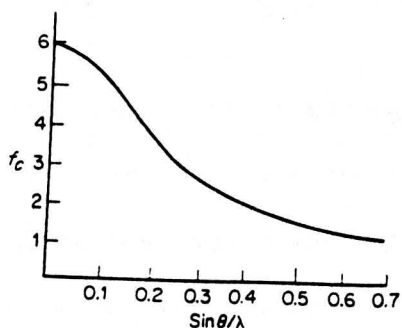


Figure 6.2/1 The atomic scattering factor curve for carbon.

Figure 6.2/1 shows the relationship between the scattering factor (f) and $\sin\theta/\lambda$ for the element carbon. For other atoms the shape of the curve is

similar, with the vertical intercept equal to the atomic number Z of the element concerned.

6.2.2 The Structure Factor.

The structure factor, F_{hkl} , is a measure of the total diffraction by all atoms in the unit cell by a particular set of planes hkl . It is the resultant of N waves scattered in the direction of the reflection hkl by the N atoms in the unit cell and may be expressed:

$$F_{hkl} = \sum_n^{n=N} f_n \exp[2\pi i(hx_n + ky_n + lz_n)]$$

This can be represented as: $F_{hkl} = A + iB$, where

$$A = \sum_{n=1}^N f_n \cos 2\pi(hx_n + ky_n + lz_n) \text{ and } B = \sum_{n=1}^N f_n \sin 2\pi(hx_n + ky_n + lz_n)$$

The scattering factor of the n^{th} atom is f_n , where x_n , y_n , and z_n are the fractional coordinates of the n^{th} atom. Figure 6.2/2 shows the corresponding Argand diagram where A and B are expressed in terms of the structure factor modulus, F_{hkl} and the phase angle, α_{hkl} . The experimentally measured intensity, I_{hkl} , is proportional to the square of the structure factor, $(F_{hkl})^2$.

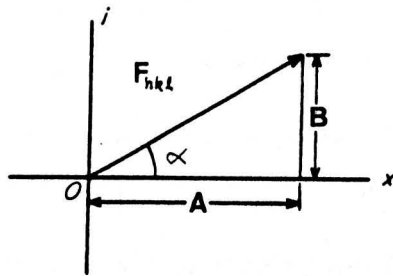


Figure 6.2/2 The structure factor on an Argand diagram.

All structures discussed in this work had a centre of symmetry and so the expression for the structure factor is real and simplifies to:

$$F_{hkl} = 2 \sum [f_o \cos 2\pi(hx_n + ky_n + lz_n)]$$

6.3 The use of the diffractometer.

6.3.1 Selection and mounting of a crystal.

Certain features are of importance in choosing a crystal. Firstly it

should be a real single crystal, since double crystals can cause numerous problems during data collection and subsequent structure analysis. Where possible well formed crystals of regular shape are selected and examination under a polarising microscope can be useful in assessing the crystal quality. In practice for cluster compounds the crystallisation process often proves difficult and irregular dark crystals are often obtained. The quality of such crystals is normally assessed by scanning the diffraction profile of individual reflections on the diffractometer. Photographic methods are often used at this stage but were not employed in this project. In principle a large crystal is desirable because the scattering power is proportional to the crystal volume, but the optimum size of the crystal is limited practically by the dimensions of the X-ray beam. As such, the crystal must be smaller than the uniform cross section of X-ray beam (ca. 0.5 mm). Both the incident and diffracted beam will be absorbed by the crystal, and absorption increases exponentially with the linear dimensions of the crystal. For this reason the smallest osmium crystals compatible with a reasonable diffracting ability were selected for data collection.

6.3.2 Mounting and centring the crystal.

The crystals were held on the end of a thin quartz fibre by epoxy resin adhesive and the fibre was then secured in a brass pin. The pin was placed in the goniometer head of the diffractometer and, using translational adjustment only, it was aligned precisely in the centre of rotation of the diffractometer head.

The Philips PW1100 diffractometer has four circles, which allow the mounted crystal to be brought into various orientations. Two circles, ϕ and χ , are used to adjust the crystal orientation relative to the diffractometer coordinate system (Figure 6.3/1).

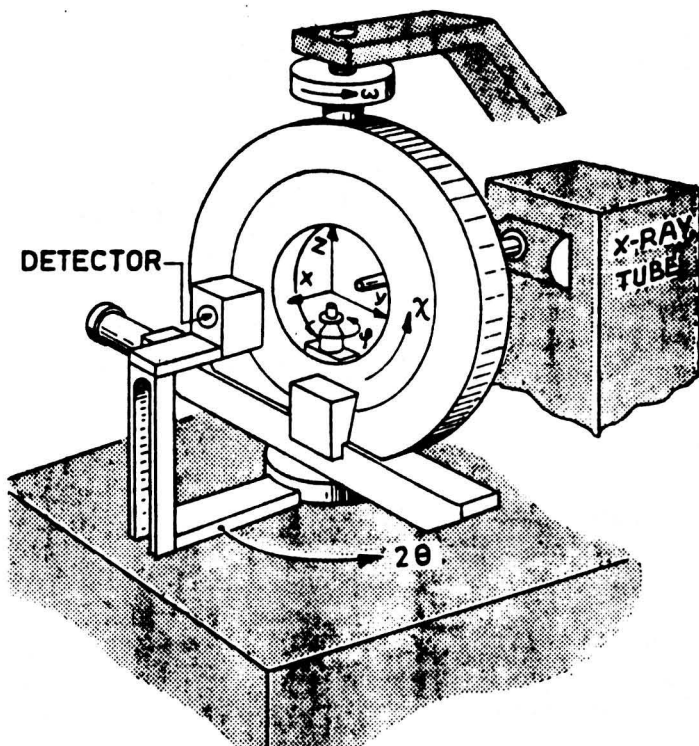
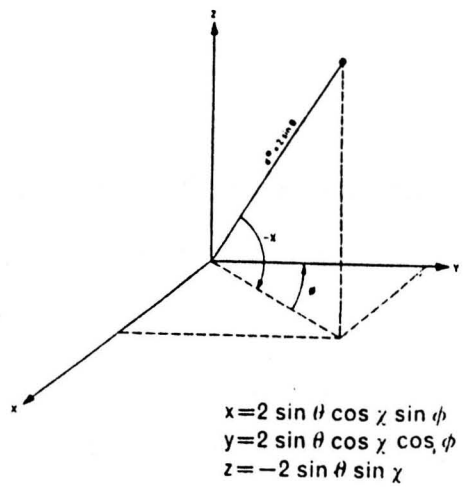
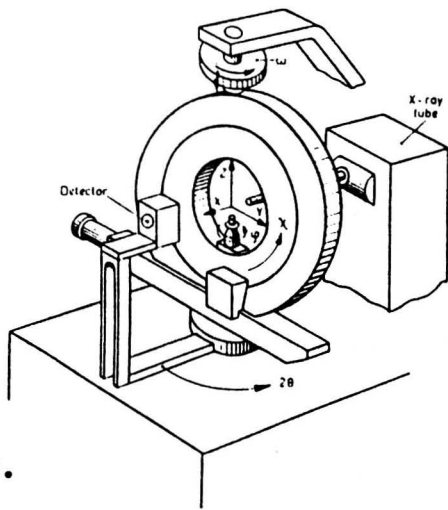


Figure 6.3/1. The 4-circle diffractometer.

The ω circle permits orientation of the crystal relative to the direction of the primary beam and the detector can be moved to an angle 2θ to the primary beam. During data collection ω scans through the values θ_{hkl} of each reflection hkl and its movement and the 2θ setting are synchronised. Thus the crystal orientation is defined by the three angular settings ϕ , χ , ω , with the detector position being defined by the fourth angle, 2θ . The geometry of the 4-circle diffractometer is shown in Figure 6.3/1.

6.3.3 Peak hunting.

An automatic peak hunting routine was used to find the unit cell parameters and the orientation of each crystal. A volume of reciprocal space was systematically scanned until a radiation intensity (above a preset minimum) was sensed. The four circles were then adjusted to optimise diffraction and the four setting angle values stored. This procedure was continued until 25 maxima had been measured and their setting angles were converted to reciprocal space lattice points, with coordinates x, y, z relative to the diffractometer axes X, Y, Z . A set of lattice planes is represented by a vector d^* , and the x, y, z components of the vector d^* can be defined from the setting angles ϕ, χ , and ω . This is illustrated in Figure 6.3/2.



$$\begin{aligned} x &= 2 \sin \theta \cos \chi \sin \phi \\ y &= 2 \sin \theta \cos \chi \cos \phi \\ z &= -2 \sin \theta \sin \chi \end{aligned}$$

Figure 6.3/2.

Next, the three shortest non-coplanar reciprocal lattice vectors were identified by calculating the distance between all pairs of reciprocal lattice points found in the peak hunt. The first shortest vector was assigned as a^* , the second as b^* , and the third as c^* . This information is stored in a matrix known as the UB matrix, which is defined as:

$$\begin{matrix} a_X^* & b_X^* & c_X^* \\ a_Y^* & b_Y^* & c_Y^* \\ a_Z^* & b_Z^* & c_Z^* \end{matrix}$$

where the columns signify the components of a^* , b^* and c^* along the axes X, Y, and Z. If the crystal is in a random orientation the coordinates of the reciprocal lattice point can be represented in matrix form as:

$$\begin{pmatrix} x \\ y \\ z \end{pmatrix} = \begin{pmatrix} a^* & b^* & c^* \\ a^* x & b^* x & c^* x \\ a^* y & b^* y & c^* y \\ a^* z & b^* z & c^* z \end{pmatrix} \begin{pmatrix} h \\ k \\ l \end{pmatrix} \quad \text{or} \quad \begin{pmatrix} x \\ y \\ z \end{pmatrix} = UB \begin{pmatrix} h \\ k \\ l \end{pmatrix}$$

Implicit in this matrix, and of central importance in data collection, are the six parameters of the unit cell and the three parameters connected with the orientation of the crystal. Abstraction of the six unit cell parameters as the three vectors a^* , b^* , and c^* is possible by use of:

$$M = \begin{pmatrix} a^* \cdot a^* & a^* \cdot b^* & a^* \cdot c^* \\ b^* \cdot a^* & b^* \cdot b^* & b^* \cdot c^* \\ c^* \cdot a^* & c^* \cdot b^* & c^* \cdot c^* \end{pmatrix}$$

where a , b , and c are the unit cell sides. The M matrix is derived from the UB matrix so that $M=UB \cdot UB$, where UB is the transpose of the UB matrix. The scalar elements of M are equal to the scalar products of the reciprocal

axes vectors, i.e. $M_{11} = a^* \cdot a^*$, $M_{12} = a^* \cdot b^*$, etc, and therefore the scalar results are $M_{11} = (a^*)^2$, $M_{12} = a^* b^* \cos \gamma^*$, etc. This means that M is symmetrical and independent of the orientation of the crystal, depending only on the dimensions of the repeat unit. The M matrix can also be used to give a preliminary indication of the crystal system. Thus if two reciprocal axes have the same length (as would occur for a tetragonal or hexagonal crystal), the corresponding diagonal elements of the M matrix will be equal. If two of the axes are perpendicular to each other (as would occur for any crystal system other than triclinic) the corresponding off diagonals will be zero. In practice most crystals are not so straightforward at this stage, because the initial a^* , b^* , and c^* , selected by the diffractometer do not necessarily reflect the full crystal symmetry.

The reflections found in the above peak hunt can be assigned hkl values by use of the relationship:

$$\begin{pmatrix} h \\ k \\ l \end{pmatrix} = UB^{-1} \begin{pmatrix} x \\ y \\ z \end{pmatrix}$$

After the 25 peaks have been indexed, they are used to refine the UB matrix by a least-squares refinement. The transformation of the initially found primitive unit cell to the corresponding Bravais lattice usually only requires axes to be interchanged or changed in direction. In the case of centered lattices the procedure is more complicated but all crystals discussed in this thesis had primitive unit cells.

At this stage the crystal system is confirmed by checking that the Laue symmetry holds for a reasonable number of reflections. More accurate unit cell parameters and orientation matrix are obtained by replacing the 25 initially found reflections by 25 reflections with θ ca. 10° , evenly distributed throughout reciprocal space.

6.3.4 Automatic data collection.

The intensities of the diffracted beams are measured by a scintillation counter. In using a counter the precision of measurements is proportional to the square root of the total number of counts, so it would be necessary to increase the counting time by a factor of four to double the precision. Several strong reflections are initially scanned to examine their peak profile and to decide on the optimum scan width. All structures reported in this study had data collected at a constant scan speed of 0.05 s^{-1} . In order not to waste time scanning insignificant reflections, the diffractometer applies a criterion - reflections which gave $I_t - 2(I_t)^{1/2} < I_b$ on the first scan are not re-examined. (I_t is the count rate at the top of reflection profile and I_b is the average count rate of two background measurements on either side of peak profile). The Laue symmetry of the crystal system determines what portion of the data is unique and for triclinic systems only half the data need be collected ($I_{hkl} = I_{\bar{h}\bar{k}\bar{l}}$), whereas for monoclinic systems only a quarter of the data need be collected ($I_{hkl} = I_{\bar{h}k\bar{l}} = I_{h\bar{k}l} = I_{\bar{h}\bar{k}l}$).

During data collection weak reflections were scanned a second time to improve their precision. Finally, three strong reference reflections were chosen, with θ in the range 3 to 4.5, as close to each of the three reciprocal axes as possible. These were then remeasured every five hours during data collection to check that neither decomposition nor crystal movement had occurred.

6.3.5 Data reduction.

The conversion of measured intensities I_{hkl} to structure factor amplitudes, $|F_{hkl}|_{\text{obs}}$ or $|F_o|$, is known as data reduction. This involves the application of a number of correction factors to the values of F_o and to their estimated standard deviations (e.s.d.'s) $\sigma(F_o)$.

Data reduction was achieved by use of a program written for the PW1100 diffractometer. This also corrects for Lorenz and polarisation errors. The Lorentz correction is geometric and for the Philips four circle diffractometer involves multiplying each reflection by $\sin 2\theta$. In addition, the X-ray beam is partially polarised during reflection, giving rise to the need for a polarisation correction: $P = (1 + \cos 2\theta) / 2$.

Absorption of the X-ray beam by the crystal is another source of error and can be corrected at this stage providing the crystal has well defined faces that may be measured and indexed. However, for all the compounds discussed in this study an empirical correction was made after structure solution and partial refinement. This is discussed in Section 6.4.5

6.4 Structure determination.

6.4.1 The phase problem.

The object of X-ray structure determination is to establish the position of the atoms in the crystal and hence the complete geometry of the molecules present. In theory the fractional coordinates x_n, y_n, z_n for each of the N atoms in the unit cell may be obtained by calculating the electron density, ρ_{xyz} , at a grid of points x, y, z using a Fourier series:

$$\rho_{xyz} = \frac{1}{V} \sum_{hkl} F_{hkl} e^{-2\pi i(hx+ky+lz)} \quad (4),$$

where V is the volume of the unit cell.

Although the magnitude of the structure factor, F_{hkl} , may be directly obtained from the corrected intensity values, I_{hkl} , the phase angle is not known. The unknown phase angles must be estimated before an electron density map can be calculated and this is known as the phase problem. Solving this is the key step in X-ray structure determination.

6.4.2 Solving the phase problem.

Nearly all methods for solving the phase problem rely on initially deducing the coordinates for one or more atoms of relatively high scattering power. These atomic coordinates can be used to calculate approximate values of the structure factor, F_c , for each reflection. If the atoms of the 'partial structure' contribute significantly to the diffraction many of the calculated phases will be reasonably close to the correct value. The strategy then employed is to assign these calculated phases to the corresponding observed structure factor amplitude F_o and use them in the Fourier series for the calculation of electron density. From this the positions of more atoms should be evident and these may then be used to improve the 'partial structure'. This iterative process is repeated until all the non-hydrogen atoms have been found, and even hydrogen atoms may be located using techniques described below.

For crystals with centrosymmetric space groups, which includes all those studied in this project, the expression for the calculation of structure factor simplifies to:

$$F_{hkl} = 2 \sum f_n \cos(hx_n + hy_n + z_n)$$

The phase problem is therefore reduced to a 'sign problem' and it is the sign of F_{hkl} (Sc, + or -) which has to be determined in structure solution.

The expression for the electron density during structure solution also simplifies to:

$$\rho_{xyz} = 1/V \sum S_c F_o \cos 2\pi (hx+ky+lz).$$

In the later stages of structure determination, when only a few atoms and any hydrogen atoms remain to be located, it is usual to use a difference-Fourier synthesis. This has the advantage of minimising termination of series errors:

$$\rho = 1/V \sum S_c (|F_o| - |F_c|) \cos 2\pi (hx+ky+lz)$$

The resulting electron density synthesis show only the atoms omitted from

the calculation of F_{hkl} , together with residual peaks due to errors in the positions of those atoms already included. A fully determined structure should show residual electron density of not more than $1e \text{ \AA}^{-3}$, except in the region of very large metal atoms.

Hydride ligand location using X-ray crystallography techniques is particularly difficult for metal cluster compounds, since as it is the electrons that scatter X-rays, the presence of metal atoms, such as ruthenium and osmium, will swamp out the electron density of a nearby hydride ligand. The best solution to this problem is to use neutron diffraction. However, there are two distinct deterrents to using nuclear diffraction. Firstly, access to a neutron source is necessary and secondly, the crystal used must be about 1000 times the volume of crystals used in X-ray analysis. Unsurprisingly, only the most important of hydrido-clusters are structurally characterised in this way. In this project it was usually difficult to get crystals suitable for X-ray structure analysis and none of neutron quality were isolated, so a number of direct and indirect techniques were employed. The X-ray scattering ability of hydrogen is relatively higher at low angle compared to other atoms, and therefore the hydrogen peaks may be resolved more easily from a difference-Fourier synthesis based on data with the high angle reflections excluded. In this work it was found that data with $\sin\theta < 0.35$ was the most effective in giving suitable maxima for H-atoms in ruthenium clusters but (not surprisingly) no success by this method was achieved for osmium. Some of the qualitative techniques which proved invaluable included identifying the lengthening effect bridging hydrides often have on metal-metal bond lengths and examining surface ligand distribution, evidence of the presence of an H-atom being signalled by a 'pushing back' of the carbonyl ligands surrounding it. Computed space-filling models, calculated from the observed coordinates of the non-hydrogen atoms, were

often useful at this stage to show gaps in the surface ligands. The hydride positions could often be deduced from a more quantitative technique using potential energy minimisation calculations.[263] This is usually successful for symmetrical μ_2 - or μ_3 -hydride ligand location, but often fails for asymmetric hydrogen bonding modes.

6.4.3 The Patterson synthesis

For metal coordination compounds the Patterson synthesis provides a method of deducing the position of the metal atom and this, having a relatively high number of electrons, provides a suitable starting 'partial structure'. The interpretation of Patterson syntheses becomes rapidly more difficult as the number of independent metal atoms in a molecule increases. However, it proved a reliable method of deducing the positions of the metal atoms in nearly all the metal cluster compounds studied here and the strategy adopted in the solution of these multi-metal problems will be explained here in some detail (see also Appendix B).

Patterson showed that a Fourier-synthesis employing values of $(F_{hkl})^2$ (all positive and directly obtained from I_{hkl}) could be used to give information about interatomic vectors in crystals and that this could be unravelled to give fractional coordinates of atoms in favourable cases. This expression calculated is:

$$P_{uvw} = 1/V \sum (F_{hkl})^2 e^{-2\pi i(hv+kw+lw)}$$

In the Patterson there is a maximum in P_{uvw} at fractional coordinate u, v, w , corresponding to the vector between every pair of atoms in the unit cell of fractional coordinates x_1, y_1, z_1 , and x_2, y_2, z_2 in the following way:

$$u = x_1 - x_2$$

$$v = y_1 - y_2$$

$$w = z_1 - z_2$$

The Patterson summation will always involve a large peak at the origin (and all corners of the unit cell) due to the superposition of all vectors which arise from every atom to the identical atom in the adjacent unit cells. In general, if an atom i contains Z_i electrons and an atom j contains Z_j electrons then the peak in the Patterson summation, which represents the vector between atoms i and j , will have a height proportional to $Z_i Z_j$. Thus heavier atoms will give rise to higher peaks in the map and are readily distinguished, which accounts for the use of Patterson synthesis as a method for determining the positions of metal atoms.

In addition to determining the fractional coordinates of the metal atoms in a structure, the Patterson synthesis can be used as a means of identifying any point group symmetry elements (which cannot be recognised at an earlier stage because they do not give rise to systematic absences in the reflection data).

6.4.4 Refinement.

Once all the atoms in the crystal have been located the model is systematically adjusted to obtain the best fit between the observed data and the calculated structure factors. The latter depend on a large number of parameters made up of the fractional coordinates of the atoms and their thermal parameters. The atomic thermal parameters are applied in structure factor calculation as an addition factor $e^{-B(\sin^2\theta)/\lambda^2}$, where B is related to the mean-square amplitude (μ^2) of atomic vibration and is given by $B = 8\pi^2\mu^2$. This addition factor may be considered to allow for the thermal motion of the atoms in the solid state, as well as slight variations in the exact siting of each atom of the given type in the thousands of unit cells that make up the crystal. Additionally an overall scale factor, K , is applied to all the observed structure factors to bring them onto the same scale as the calculated values. The method of least-squares refinement

involves systematically altering the parameters to minimise the function $\sum w_{hkl} (F_o - 1/K F_c)^2$. The weighting factor w_{hkl} is assigned to each reflection to take into account the different precision of the observed structure amplitudes, $(F_o)_{hkl}$, and throughout this work the standard weight $1/\sigma^2(F_o)_{hkl}$ was used.

6.4.5 Absorption corrections.

Absorption effects pose one of the most serious errors in measuring the data for cluster compounds. For all complexes discussed in this study absorption corrections were made using the empirical method of Stuart and Walker.[310]

In addition to being scattered, the incident and diffracted X-ray beams are also absorbed by a crystal. The intensity I of a beam after passing through a thickness t of crystal is given by the equation

$$I = I_o e^{-\mu t}$$

where I_o is the intensity of the incident beam and μ the linear absorption coefficient. The value of the linear absorption coefficient is dependent on the wavelength of the X-rays used, the type of atoms present, and the density of the crystal. Using molybdenum K_{α} radiation it is relatively low for ruthenium, but very high for osmium clusters.

The method of Stuart and Walker proved valuable in this work because the crystals obtained were often very irregular in shape which would have made direct quantitative corrections almost impossible to assess. It involves use of a Fourier series to model the discrepancy between the calculated and observed structure factor amplitudes. The correction is evaluated using observed structure factors of the full data set without averaging symmetry-equivalent or Friedel-pair reflections. The calculated structure factors are based on the best model obtained with isotropic thermal parameters for all atoms.

Reduction of the thermal co-efficients of all atoms to more reasonable values was used as one criterion for assessing the success of the correction.

6.5 Experimental

This section outlines the experimental X-ray structural solution for all fifteen compounds discussed in this thesis. Table 6.5/1 lists the structures solved and indicates in which chapter each is discussed. Essential bond lengths and angles for all 15 structures are presented in Appendix A.

6.5.1 X-Ray Structure Analyses of $\text{HRu}_5\text{C}(\text{CO})_{14}(\text{C}_5\text{H}_4\text{N})$ Isomer A (XR1), Isomer B (XR2), $\text{HRu}_5\text{C}(\text{CO})_{13}(\text{C}_5\text{H}_4\text{N})(\text{C}_5\text{H}_5\text{N})$ (XR3) and $\text{HRu}_5\text{C}(\text{CO})_{13}(\text{C}_5\text{H}_4\text{N})$ (XR4).

These four structures are discussed in more detail in Chapter 2, where labelled diagrams may be found. Principal bond lengths and angles are presented in Appendix A and the Patterson solution for (XR1) and (XR3) is listed in Appendix B.

a) Crystal Data and Data Collection.

The crystal data and method of data collection for all four structures are presented in Table 6.5/2.

b) Structural Solution and Refinement.

All four structures were found to have primitive lattices and both (XR1) and (XR3) were found to be monoclinic from the intensity relationships. In addition both (XR1) and (XR3) had systematic absences of the type $0k0$, $k=2n+1$ and this indicated the presence of a 2_1 -screw axis in both crystals. In addition, (XR1) had systematic absences of the type $h0l$, $l=2n+1$, and

Table 6.5/1 Structures solved.

Structure	No.	Chapter
$\text{HRu}_5\text{C}(\text{CO})_{14}(\text{C}_5\text{H}_4\text{N})$	(XR1)	2
$\text{HRu}_5\text{C}(\text{CO})_{14}(\text{C}_5\text{H}_4\text{N})$	(XR2)	2
$\text{HRu}_5\text{C}(\text{CO})_{13}(\text{C}_5\text{H}_4\text{N})(\text{C}_5\text{H}_5\text{N})$	(XR3)	2
$\text{HRu}_5\text{C}(\text{CO})_{13}(\text{C}_5\text{H}_4\text{N})$	(XR4)	2
$\text{Ru}_6\text{C}(\text{CO})_{15}(\text{C}_6\text{H}_8)$	(XR5)	3
$\text{Ru}_6\text{C}(\text{CO})_{15}(\text{PhCCH})$	(XR6)	3
$\text{Ru}_6\text{C}(\text{CO})_{15}(\text{PhCCMe})$	(XR7)	3
$\text{Ru}_6\text{C}(\text{CO})_{14}(\text{PhCCH})\text{AuPMe}_3$	(XR8)	3
$\text{Ru}_6\text{C}(\text{CO})_{15}(\text{C}_6\text{H}_3\text{Me}_3)$	(XR9)	4
$\text{Ru}_6(\text{CO})_2(\text{CO})_{13}(\text{C}_6\text{H}_3\text{Me}_3)$	(XR10)	4
$\text{HRu}_6(\text{CO})(\text{CO})_{13}(\text{C}_6\text{H}_3\text{Me}_2\text{CH}_2)$	(XR11)	4
$[\text{Ru}_{10}\text{N}(\text{CO})_{24}]^-$	(XR12)	4
$\text{Os}_3(\text{CO})_{10}(\text{PhCCH}_2)\text{AuPEt}_3$	(XR13)	5
$\text{HOs}_3(\text{CO})_9(\text{PhCCH})\text{AuPPh}_3$	(XR14)	5
$\text{Os}_7(\text{CO})_{14}(\text{MeCCMe})_3$	(XR15)	5

Table 6.5/2.

	(XR1)	(XR2)	(XR3)	(XR4)
CRYSTAL DATA				
Molecular Formula	: $C_{20}H_5N_{10}Ru_5$: $C_{20}H_5N_{10}Ru_5$: $C_{24}H_{10}N_2O_{13}Ru_5$: $C_{19}H_5N_{10}Ru_5$
Molecular Weight	: 988.25	: 988.25	: 1039.34	: 960.60
Crystal System	: monoclinic	: triclinic	: monoclinic	: triclinic
Space Group	: $P2_1/c$: $P1(\text{No. } 2)$: $P2_1/n$: $\bar{P}1(\text{No. } 2)$
Unit Cell Dimensions				
a (Å)	: 8.864(2)	: 19.095(4)	: 17.325(3)	: 16.468(3)
b (Å)	: 17.962(3)	: 17.870(3)	: 16.405(3)	: 13.686(2)
c (Å)	: 17.200(3)	: 9.4790(2)	: 10.726(2)	: 11.570(2)
alpha°	: -	: 97.86(3)	: -	: 89.63(3)
beta°	: 95.84(3)	: 106.52(3)	: 95.95(3)	: 96.83(3)
gamma°	: -	: 93.02(3)	: -	: 90.34(3)
Volume (Å ³)	: 2724.29	: 2763.39	: 3032.08	: 2589.07
Z	: 4	: 4	: 4	: 4
Density (g m ⁻³)	: 2.41	: 2.38	: 2.28	: 2.46
F(000)	: 1856	: 1856	: 1968	: 1800

Table 6.5/2 (Continued).

DATA COLLECTION

crystal colour	: light red	light red	red	light red
crystal size(mm)	: 0.16x0.42x0.13	0.27x0.40x0.47	0.21x0.30x0.35	0.32x0.25x0.16
$\mu(\text{Mo } -K_{\alpha})$: 25.21	25.1	22.65	26.8
scan speed(s^{-1})	: 0.05	0.05	0.05	0.05
scan width($^{\circ}$)	: 0.80	0.90	0.80	0.90
	2 -5 -2	2 -1 -1	-3 2 0	0 0 2
standard reflections:	1 4 1	0 -2 -1	2 3 4	1 3 1
	-1 -1 2	1 -1 -2	1 4 3	2 -2 0
θ range($^{\circ}$)	: 3 - 25	3 - 25	3 - 25	3 -25
Systematic	0k0; k=2n+1		0k0; k=2n+1	
Absences	: h0l; l=2n+1		h0l; h+1=2n+1	

(XR3) had $h0l$; $h+l=2n+1$, therefore these structures were assigned the space groups $P2_1/c$ and $P2_1/n$ respectively. For (XR2) and (XR4), the diffraction data showed only triclinic Laue symmetry ($Ihkl=I\bar{h}\bar{k}\bar{l}$ only) and it was concluded that the space group, for both structures, would probably be the centrosymmetric $P\bar{1}$ (No.2). Density calculations (see Table 6.6/2) indicated four molecules per unit cell for all four structures, thus unexpectedly for both (XR2) and (XR4) there were two molecules per equivalent position. Application of Delauney reduction did not produce an alternative lattice of higher symmetry for either of these triclinic crystals and the assignment of the space group as $P\bar{1}$ was confirmed by the eventual satisfactory structure solution and refinement.

Structures (XR1) and (XR3) were solved by interpretation of Patterson synthesis, from which the coordinates of the five ruthenium atoms, forming the cluster core, were found for each structure. The assignment of the Patterson vectors is given in Appendix B. For the triclinic structures, (XR2) and (XR4), with two molecules per equivalent position, the coordinates of the metal atoms in the two non-equivalent clusters could not be deduced from Patterson syntheses. These structures were solved by direct methods, using the sigma-two (σ_2) sign equation (EES) available in the SHELX suite of programs. For both structures an initial minimum E-value of 1.2 was used, which was subsequently raised to a value of 1.4, and reflections with $E > 3.0$ were omitted. The tangent map calculated showed high peaks corresponding to all metal atoms of the two independent molecules in the asymmetric unit for both structures.

Once the coordinates of all the metal atoms in the four structures were known the overall scale factor K was initially refined alone and then again in two further cycles, along with the metal atom coordinates and isotropic thermal parameters. For all four structures this gave both reasonable reliability factors and isotropic thermal parameters (Table 6.5/3-[a]). A

Table 6.5/3 : Reliability factors during structure solution and refinement.

	(XR1)		(XR2)		(XR3)		(XR4)	
	R	R _w						
[a]	0.1855	0.2014	0.2143	0.2303	0.1890	0.2008	0.1909	0.2037
[b]	0.0564	0.0642	0.0962	0.1035	0.0639	0.0664	0.0729	0.0764
[c]	0.0524	0.0609	0.0595	0.0668	0.0564	0.0592	0.0603	0.0653
[d]	0.0281	0.0297	0.0435	0.0477	0.0423	0.0441	0.0505	0.0544

[a] - refinement on metal atom coordinates

[b] - two cycles of least-square full-matrix refinement on each independent molecule, with all atoms assigned isotropic thermal parameters

[c] - two further cycles as in [b], after absorption corrections have been applied

[d] - Final R-values.

Fourier synthesis was calculated at this stage and from this and from subsequent difference-Fourier syntheses (calculated after later refinement with anisotropic thermal parameters assigned to the metal atoms) all remaining atomic coordinates were located. At each stage in the determinations, 'newly' found atomic coordinates were included in refinement with isotropic thermal parameters, and weights of $w = 1/\sigma F_o$ were assigned to the individual reflections.

One of the most important aspects of these four crystal structures is the mode of attachment of the bridging pyridyl ligand to the metal framework: interchange of the relative positions of the metal-bonded C- and N-atoms potentially gives rise to different isomeric forms. Both $\text{HRu}_5\text{C}(\text{CO})_{14}(\text{C}_5\text{H}_4\text{N})$ [in crystals (XR1) and (XR2)] and $\text{HRu}_5\text{C}(\text{CO})_{13}(\text{C}_5\text{H}_4\text{N})$ [in crystal (XR4)] were found to be present in the two isomeric forms. For $\text{HRu}_5\text{C}(\text{CO})_{14}(\text{C}_5\text{H}_4\text{N})$ the two isomers (A) and (B) proved to be present in the one crystal of (XR4), not as the two independent molecules, but disordered at the site of one of them. As the difference in the (A) and (B) type of isomer lies only in the orientation of the pyridine ligand, and as C- and N-atoms are so similar in terms of electron density, extremely careful work was necessary to establish the correct atomic assignment. Confirmation of the N-atom sites in the two sets of isomers [in crystals (XR1), (XR2), and in (XR4)] and in the single isomer for $\text{HRu}_5\text{C}(\text{CO})_{13}(\text{C}_5\text{H}_4\text{N})(\text{C}_5\text{H}_5\text{N})$ found in (XR3) was obtained by reversal of the assignment of the coordinates of the N-atom and C-atom of the bridging pyridyl ligand in all 5 unique molecules, the model which gave unreasonable thermal parameters for these two atoms on refinement being rejected (Table 6.5/4).

From Table 6.5/4 it is clear that reversal of the nitrogen and carbon atoms leads to unambiguous distinction between the two atoms in all cases, except that of the second independent molecule (b) in (XR4). For molecule (b) of (XR4) the thermal parameter of the atom assigned as N was higher both times

Table 6.5/4 : Refined thermal parameters on reversal of assignment of the coordinates of the N and C(1) atoms of the bridging pyridine ligand.

	(XR1)	(XR2)		(XR3)	(XR4)	
		a	b		a	b
Correct assignment						
N	0.035(3)	0.042(2)	0.041(2)	0.037(3)	0.031(3)	0.037(3)
C(1)	0.036(3)	0.041(3)	0.038(3)	0.039(3)	0.027(3)	0.023(2)
Incorrect assignment, N and C reversed						
N	0.054(3)	0.064(3)	0.061(3)	0.061(2)	0.044(3)	0.040(3)
C(1)	0.022(2)	0.024(3)	0.021(3)	0.020(1)	0.015(2)	0.021(2)

a and b refer to the two independent molecules in the asymmetric unit cell of (XR2) and (XR4).

(0.037 and 0.040 Å²) than the atom assigned as C (0.023 and 0.021 Å²). An explanation of this was achieved by considering both atomic positions as 0.5N/0.5C, equivalent to a statistical disorder of the two isomer types (A) and (B) at this site. The atomic coordinates of each site were tied to the same free variables, with fixed isotropic thermal parameters of 0.03 Å², and the site occupation factors were allowed to refine and gave values of 0.5 for the partial C- and N- atoms assigned to each of the two sites. In final refinement the site occupation factors were fixed as 0.5C and 0.5N and the thermal parameters of the two components at each site were tied to the same free variable and were allowed to refine. These gave reasonable and similar values of 0.031(2) and 0.033(2) Å² for the two atomic position.

For (XR1) the hydrogen atoms of the bridging pyridyl ligand were located in a difference-Fourier synthesis calculated using data with $\sin \theta < 0.35$. In the case of the other three crystals not all the H-atoms on these ligands could be located and for consistency they were included at calculated positions and constrained to 'ride' on the relevant C-atom (C-H 1.08 Å) with fixed isotropic thermal parameters of 0.08 Å². From subsequent difference-Fouriers, using data with $\sin \theta < 0.35$, reasonable maxima which could be assigned as metal-bridging H-atoms were found.

All the methods discussed in Section 6.4.2 for the location of surface hydride atoms were employed in the determination of the hydride positions in these compounds. Using low angle data ($\sin \theta < 0.35$) a reasonable peak, which could be assigned as a bridging hydride for Isomer A of $\text{HRu}_5\text{C}(\text{CO})_{14}(\text{C}_5\text{H}_4\text{N})$ (XR1), was found to be bridging the hinge bond, Ru(1)-Ru(4). A labelled diagram of this structure is illustrated in Figure 2.3/1. This was verified by use of Orpen's potential energy minimisation programme[263] which again showed the hydride as clearly μ_2 -bridging the Ru(1)-Ru(4) hinge bond. A space filling diagram of (XR1) viewed directly on to the Ru(1)-Ru(4) bond is illustrated in Figure 6.5/1 and shows that

the carbonyl ligands are clearly pushed back to accommodate the H-atom. Bond lengths of Ru(1)-H 1.85 and Ru(4)-H 1.85 Å were also reasonable and only one intramolecular contact of less than 2.50 Å was noted [H...C(11) 2.4712 Å].

For both molecules in the asymmetric unit of $\text{HRu}_5\text{C}(\text{CO})_{14}(\text{C}_5\text{H}_4\text{N})$ (XR4) (Figure 2.3/3) use of low angle data did not reveal the position of the μ_2 -hydride but both Orpens's potential energy minimisation programme[263] and space filling diagrams (Figure 6.5/2 clearly located the H-atom as bridging the Ru(1)-Ru(4) hinge bond, as was found for (XR1).

For the remaining two structures (XR3) and (XR4) no area of electron density could be assigned with certainty to the metal-bonded hydrogen atoms. In these cases the hydride was found by use of Orpen's potential energy minimisation technique.[263] One final check on the validity of these positions was by use of space filling models of the clusters, showing the carbonyl displacement along the hydride bridge edge. Figures 6.5/1 - 6.5/4 show the view onto the μ_2 -hydride bridged edge of the cluster, clearly showing that the surrounding carbonyl ligands are pushed back to accommodate the surface hydride ligand.

For all four crystals the bridging hydride ligands were included in the structure factor calculations with thermal factors of $U = 0.08 \text{ \AA}^2$ but their parameters were not refined.

Absorption corrections were not applied to the four sets of data until after location of all the atoms. Isotropic thermal parameters were reassigned to the metal atoms and the parameters of all the atoms in each of the four structures were given two cycles of full-matrix least-squares refinement (Table 6.5/3), with the H-atoms treated as mentioned above in the individual cases. Application of absorption corrections[310] and

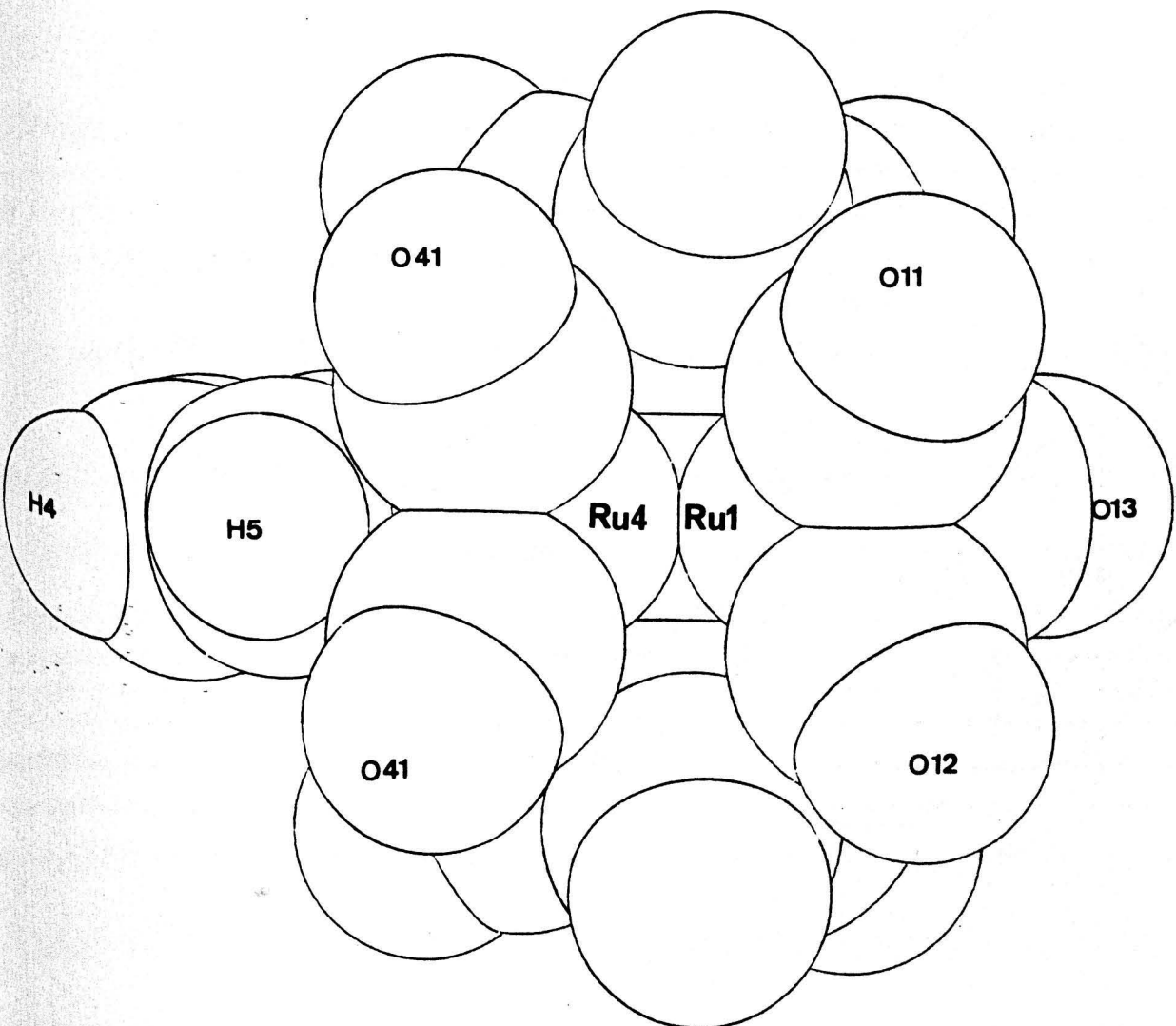


Figure 6.5/1 Computed 'space-filling' model of $\text{HRu}_5\text{C}(\text{CO})_{14}(\text{C}_5\text{H}_4\text{N})$

Isomer A (XR1).

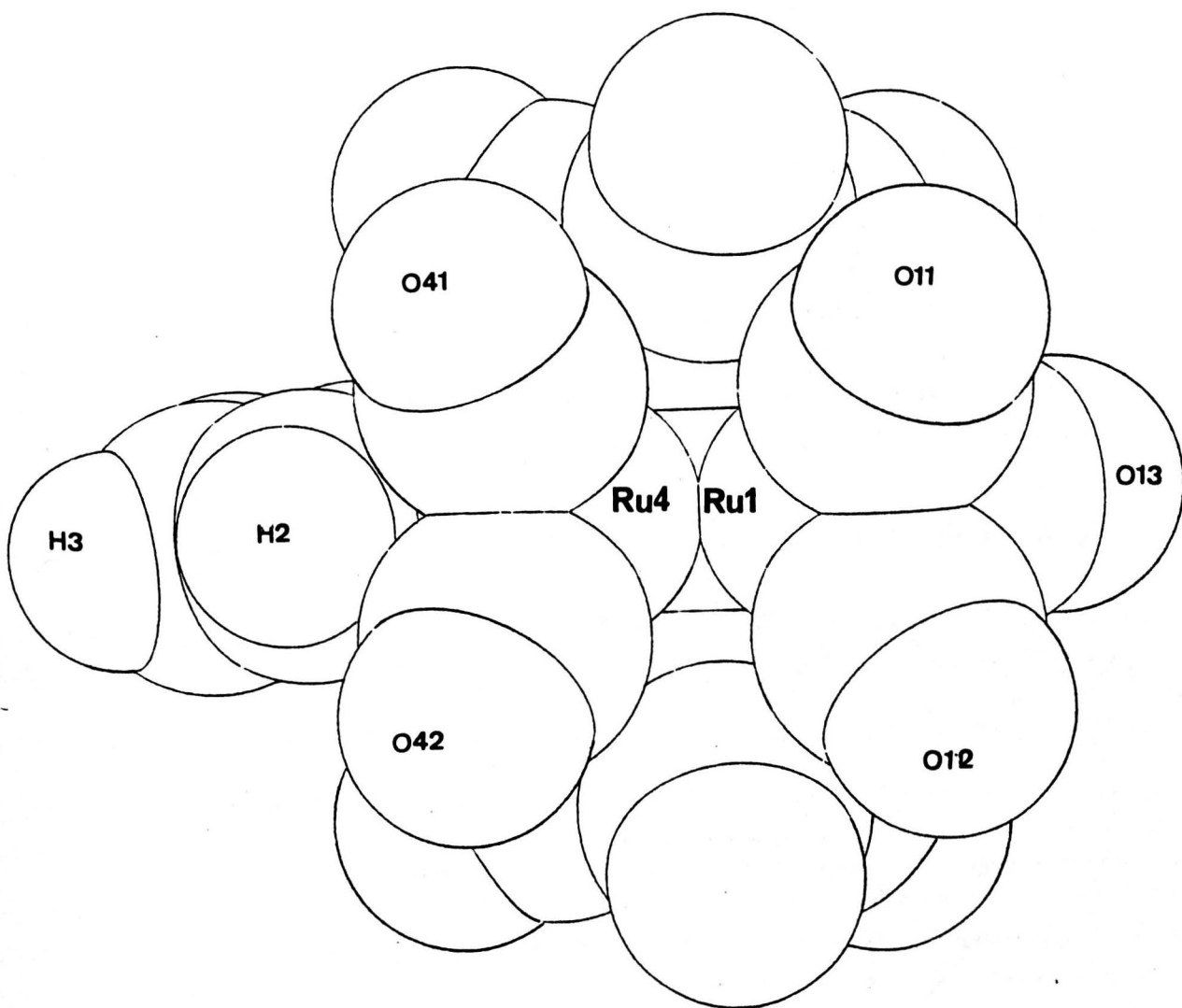


Figure 6.5/2 Computed 'space-filling' model of HRu₅C(CO)₁₄(C₅H₄N)

Isomer B (XR2).

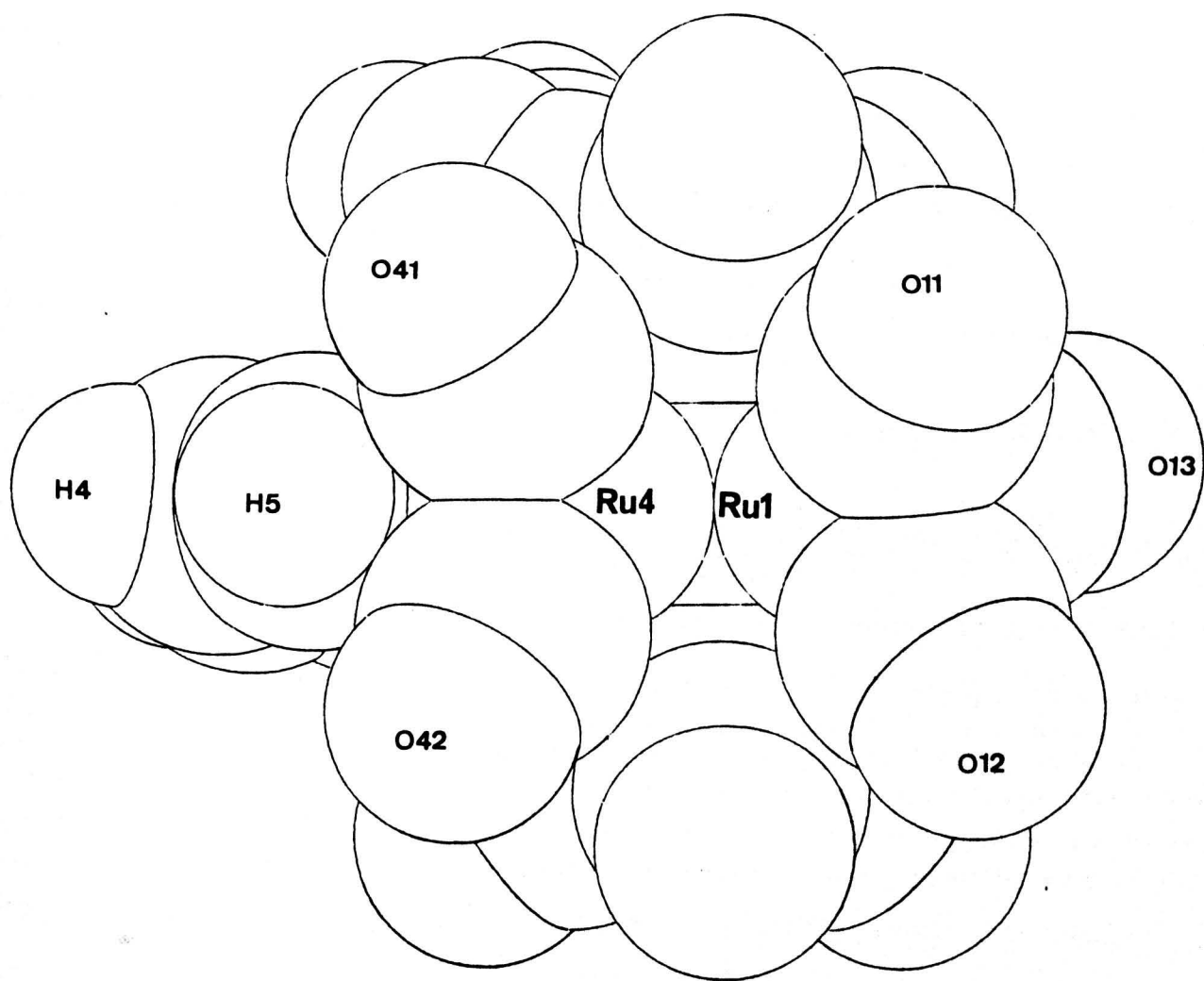


Figure 6.5/3 Computed 'space-filling' model of $\text{HRu}_5\text{C}(\text{CO})_{13}(\text{C}_5\text{H}_4\text{N})(\text{C}_5\text{H}_5\text{N})$
(XR3).

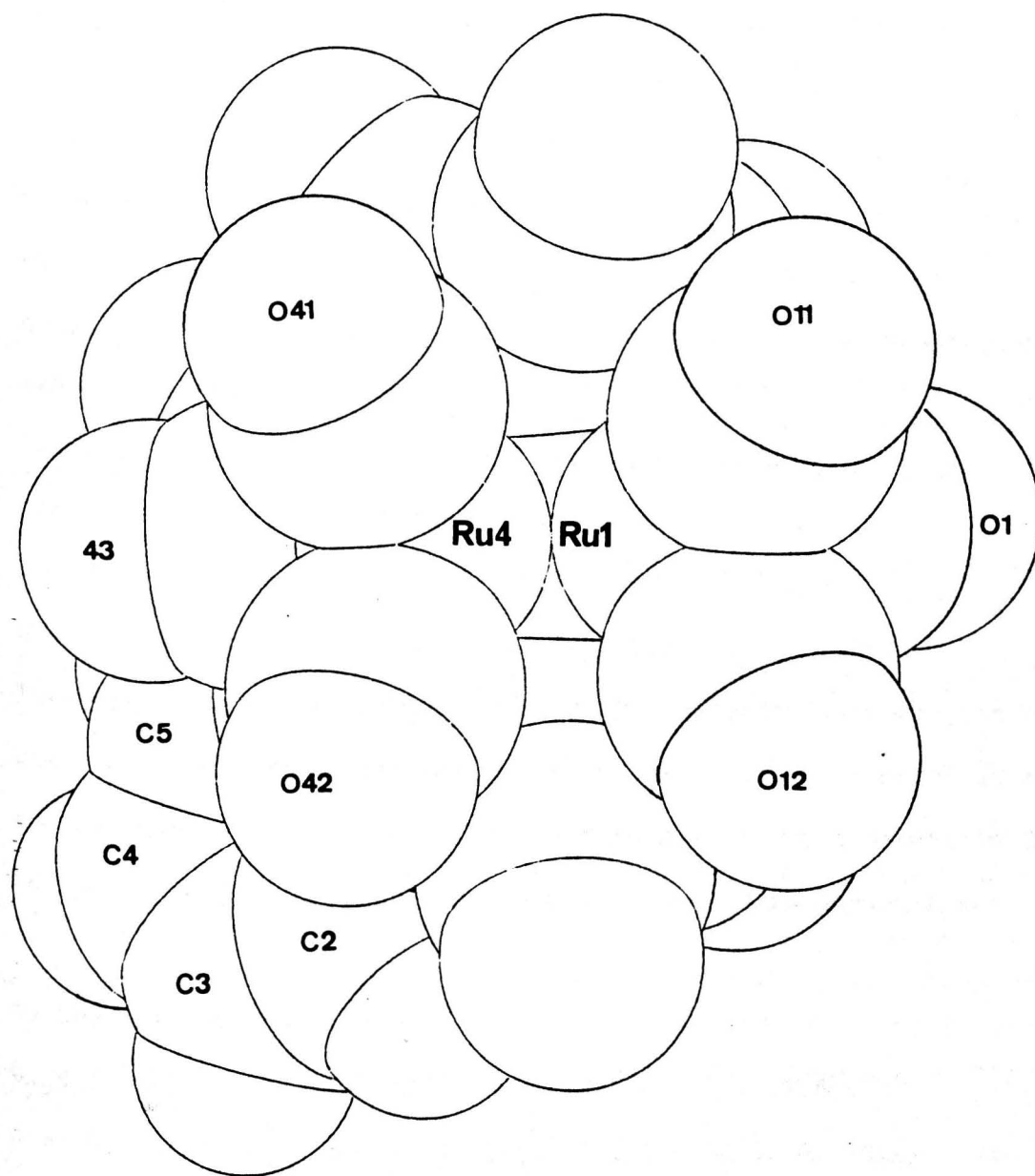


Figure 6.5/4 Computed 'space-filling' model of $\text{HRu}_5\text{C}(\text{CO})_{13}(\text{C}_5\text{H}_4\text{N})$

Isomer A and Isomer B (XR4).

further refinement of atomic parameters gave improved R values in all cases. Two further cycles of refinement were applied after absorption corrections and the results are summarised in Table 6.5/3.

In the final stages of refinement for (XR1) all the non-hydrogen atoms were assigned anisotropic thermal parameters, whilst for the remaining three structures only the metal atoms (and in the case of (XR3) and (XR4) the nitrogen and carbon atoms of the pyridine ligands) were assigned anisotropic thermal parameters. All cycles of refinement were full-matrix, except for (XR2) and (XR4), where the atoms of the two independent molecules in the asymmetric unit were refined in separate blocks. For (XR1) to (XR3) no residual electron density of greater than one electron remained. However for (XR4) residual electron density of ca. $2 \text{ e } \text{Å}^{-3}$ was present in the region of the metal atoms of molecule (b).

6.5.2 X-Ray structure analysis of $\text{Ru}_6\text{C}(\text{CO})_{15}\{\text{C}_6\text{H}_8\}$ (XR5).

This structure was originally solved by a undergraduate project student but was not completed. The structure was resolved in a corrected space group and refined in this project. It is discussed in more detail in Chapter 3; essential bond lengths and angles are presented in Appendix A.

a) Crystal data for (XR5).

$\text{C}_{22}\text{H}_{18}\text{O}_{15}\text{Ru}_6$, $M = 1118.72$, Monoclinic, $a = 17.809(3)$, $b = 9.523(2)$,
 $c = 18.340(3) \text{ Å}^3$, $\beta = 115.379(2)^\circ$, $U = 2810.20$, Space group $P2_1/c$,
 $Z = 4$, $D_c = 2.644 \text{ g cm}^{-3}$, $F(000) = 2096$, $\mu(\text{Mo-K}\alpha) = 29.5 \text{ cm}^{-1}$.

b) Data collection.

A clear crystal of size $0.28 \times 0.25 \times 0.19 \text{ mm}$ was used for collection, in the θ -range, $3 - 25^\circ$, with a scan width of 0.90° . Equivalent reflections were merged to give 3792 data with $I/\sigma(I) > 3.0$.

c) Structural solution and refinement.

The structure was originally solved in the space group $P2_1$. However the two apparently independent molecules in the asymmetric unit were shown to have massive correlations in refinement between parameters of equivalent atoms. It was demonstrated that the two molecules were related by a c-glide, and the structure refined in the space group $P2_1/c$ with one molecule per equivalent position. The problem had arisen because the systematic absences for the c-glide ($h0l, l=2n+1$) were violated by a number of reflections. Furthermore the Patterson synthesis contained a number of high vectors with coordinates nearly zero, making solution difficult. Eventually the coordinates for the two sets of six metal atoms found from the initial solution in $P2_1$ (which had arbitrary y coordinates) were adjusted to put the c glide, which was midway between the two clusters, at $y=0.25$. Six metal atoms of one cluster were deleted from the list of atoms. The remaining atoms were then shown to account for the major Patterson peaks and a table of vector assignments from the Patterson synthesis is presented in Appendix B.

The coordinates of the six ruthenium atoms were used as the basis to calculate a Fourier synthesis. The overall scale factor was initially refined alone and then two further refinement cycles with the parameters of the metal atoms were carried out. This gave reasonable isotropic thermal parameters for all six metal atoms. From this and subsequent difference-Fourier synthesis all remaining non-hydrogen atoms were found. At each stage 'newly' found atomic coordinates were included in refinement with isotropic thermal parameters. Weights of $w = 1/\sigma^2$ were assigned to the individual reflections.

IMAGING SERVICES NORTH

Boston Spa, Wetherby

West Yorkshire, LS23 7BQ

www.bl.uk

**PAGE MISSING IN
ORIGINAL**

The ligand hydrogen atoms were located in a difference-Fourier synthesis by use of low angle data, with $\sin \theta < 0.35$, and these were included in structure factor calculation with fixed thermal parameters of 0.08 \AA^2 but were not refined. In the final stages of least-square refinement all atoms were assigned anisotropic thermal parameters. Refinement converged at $R = 0.0301$ and $R_w = 0.0319$. No residual electron density of more than 1 e \AA^{-3} remained, and no reason for the slight break in the systematic absences due to the glide plane was deduced from the structure.

6.5.3 X-Ray structure analysis of $\text{Ru}_6\text{C}(\text{CO})_{15}(\text{PhCCH})$ (XR6) and $\text{Ru}_6\text{C}(\text{CO})_{15}(\text{PhCCMe})$ (XR7).

These structures are discussed in more detail in Chapter 3, where fully numbered diagrams may be found. Principal bond lengths and angles are presented in Appendix A.

a) Crystal data for (XR6).

$\text{C}_{24}\text{H}_6\text{O}_{15}\text{Ru}_6$, $M = 1140.72$, monoclinic, space group $P2_1/c$, $a = 9.853(2)$, $b = 16.911(3)$, $c = 19.312(4) \text{ \AA}$, $\beta = 111.79(2)^\circ$, $U = 2987.93 \text{ \AA}^3$, $Z = 4$, $D_c = 2.536 \text{ g cm}^{-3}$, $F(000) = 2136$, $\mu(\text{Mo-K}\alpha) = 27.8 \text{ cm}^{-1}$.

Crystal data for (XR7). $\text{C}_{25}\text{H}_8\text{O}_{15}\text{Ru}_6 \cdot 0.5\text{CH}_2\text{Cl}_2$, $M = 1197.22$, triclinic, space group $P1$ (No 2), $a = 17.809(3)$, $b = 10.567(2)$, $c = 9.310(2) \text{ \AA}$, $\alpha = 106.99(2)$, $\beta = 98.135(2)$, $\gamma = 98.824(2)^\circ$, $U = 1623.23 \text{ \AA}^3$, $Z = 2$, $D_c = 2.449 \text{ g cm}^{-3}$, $F(000) = 1126$, $\mu(\text{Mo-K}\alpha) = 26.4 \text{ cm}^{-1}$.

b) Data collection.

Dark red crystals of size $0.38 \times 0.26 \times 0.18 \text{ mm}$ for (XR6) and of size $0.25 \times 0.20 \times 0.18 \text{ mm}$ for (XR7) were used for collection, in the θ -range, $3 - 25^\circ$, with scan widths of 0.90° for (XR6) and 0.80° for (XR7). Equivalent reflections for both structures were merged to give 3033 and 4037 data respectively, with $I/\sigma(I) > 3.0$.

c) Structure solution and refinement for $\text{Ru}_6\text{C}(\text{CO})_{15}\{\text{PhCCH}\}$ (XR6) and $\text{Ru}_6\text{C}(\text{CO})_{15}\{\text{PhCCMe}\}$ (XR7).

The coordinates of the six ruthenium atoms in each structure were deduced from a Patterson synthesis (Appendix B). The solution of (XR6) is discussed in some detail here and the pattern of solution for (XR7) was very similar, so only the points of difference will be mentioned. A Fourier synthesis for (XR6) based on the phases from refinement of the six metal atoms alone gave the positions of all six atoms of the phenyl ring, along with the two backbone carbons of the organo-fragment, the central carbide, and the carbon and oxygen atoms of all fifteen carbonyls. All these atoms were included in structure factor calculation but only the overall scale factor and the metal atom parameters were refined, giving a reliability factor of $R = 0.119$ and $R_w = 0.123$. The thermal parameters for all six metal atoms were reasonable, with none over 0.035 \AA^2 . Further refinement with isotropic thermal parameters for all atoms and the carbon atoms of the phenyl ring constrained to regular hexagonal geometry (C-C 1.395 \AA) gave $R = 0.0987$ and $R_w = 0.1017$. A difference-Fourier calculated at this stage using data with $\sin\theta < 0.35$ showed maxima corresponding to the alkyne H-atom in (XR6), which was included in the structure factor calculation with a fixed thermal parameter of 0.08 \AA^2 but not in refinement. For both structures some H-atoms of the phenyl ring were located, but for consistency all the hydrogens of the phenyl rings of both structures and the methyl group of (XR7) were included at calculated positions (C-H 1.08 \AA) with fixed isotropic thermal parameters of 0.08 \AA^2 . Absorption corrections were then carried out using the method of Stewart and Walker; [310] the final refinement before absorption gave $R = 0.0889$, $R_w = 0.0890$ for (XR6). Further refinement after absorption correction, with all thermal parameters still isotropic, gave $R = 0.0628$ and $R_w = 0.0632$ for (XR6) and there were no regions of significant electron density in a difference-Fourier synthesis calculated at this stage.

Complications arose at the stage before absorption correction for the second structure (XR7), as residual peaks of ca. $6 \text{ e } \text{\AA}^{-3}$ were found. These were at a suitable distance from each other to be assigned to the two chlorine atoms of a dichloromethane solvent of crystallisation and so were included in refinement as chlorine atoms at half occupancy along with the C-atom of the solvent molecule. Refinement of (XR7) with all atoms assigned isotropic thermal parameters gave $R = 0.1119$ and $R_w = 0.1153$, and after absorption corrections these reduced to $R = 0.0844$ and $R_w = 0.0896$. A difference-Fourier calculated at this stage showed a suitable peak for the carbon atom of the dichloromethane and it was included in the refinement with a population parameter of 0.5.

For both structures the metal atoms, the atoms of the carbonyl ligands, and for (XR7) the two half chlorine atoms were assigned anisotropic thermal parameters in the final cycles of full-matrix refinement. Weights of $w = 1/\sigma^2 F_o$ were assigned to the individual reflections. Refinement converged at $R = 0.0487$ and $R_w = 0.0483$ for (XR6) and $R = 0.0460$ and $R_w = 0.0469$ for (XR7). The maximum residual electron density located in a final difference-Fourier was ca. $2 \text{ e } \text{\AA}^{-3}$ and $1.5 \text{ e } \text{\AA}^{-3}$ for (XR6) and (XR7) respectively, in the vicinity of the metal atoms.

6.5.4 X-Ray Structural analysis of $\text{Ru}_6\text{C}(\text{CO})_{14}(\text{PhCCH})(\text{AuPEt}_3)_2$ (XR8).

a) Crystal data for (XR8).

$\text{C}_{29}\text{H}_{24}\text{Au}_2\text{O}_{14}\text{P}_2\text{Ru}_6$, $M = 1658.8$, monoclinic, space group $P2_1/c$, $a = 16.172(4)$, $b = 13.590(3)$, $c = 18.698(4) \text{ \AA}$, $\beta = 93.50(1)^\circ$, $U = 4101.75 \text{ \AA}^3$, $Z = 4$, $D_c = 2.69 \text{ g cm}^{-3}$, $F(000) = 3048$. A dark red crystal of size $0.26 \times 0.21 \times 0.18 \text{ mm}$, $\mu(\text{Mo-K}\alpha) = 89.42 \text{ cm}^{-1}$, was used in the data collection.

b) Data collection.

Data were collected in the θ -range 3-25°, with a scan width of 0.70°. Equivalent reflections were merged to give 2841 unique data with $I/\sigma(I) > 3.0$.

c) Structure solution and refinement.

The coordinates of the six ruthenium metal atoms and the two gold atoms were deduced with some difficulty from a Patterson synthesis (Appendix B), and the remaining non-hydrogen atoms were located from subsequent difference-Fourier syntheses. No hydrogen atoms could be located from limited difference-Fourier syntheses carried out after preliminary refinement with anisotropic thermal parameters assigned to the metal atoms. Three cycles of refinement of all the atoms with isotropic thermal parameters were then carried out and absorption corrections were applied using the method of Stuart and Walker.

Two cycles of full-matrix refinement with isotropic thermal parameters for all atoms were followed by two with isotropic thermal parameters assigned to the two gold and six ruthenium atoms. The alkyne hydrogen atom and half the remaining H-atoms were located in a difference-Fourier synthesis calculated at this stage using data with $\sin \theta < 0.35$. The alkyne H-atom was included in the structure factor calculations with a thermal factor of 0.08 \AA^2 but its parameters were not refined. For consistency all the remaining hydrogen atoms were included in geometrically idealised positions and were constrained to 'ride' on the relevant carbon atoms with a fixed isotropic thermal parameter of 0.08 \AA^2 . All eight metal atoms, the two phosphorus atoms, two alkyne carbon atoms, and six ethyl carbon atoms were assigned anisotropic thermal parameters in the final cycles of full-matrix refinement, which converged at R 0.0489 and R_w 0.0470 with weights of $w = 1/\sigma^2 F_o$ assigned to the individual reflections. There was no residual electron density of greater than 1 e \AA^{-3} .

6.5.5 X-Ray structure analysis of $\text{Ru}_6\text{C}(\text{CO})_{15}\{\text{C}_6\text{H}_3\text{Me}_3\}$ (XR9).

The X-ray crystal structure of (XR9) was first reported in 1968.[197] This earlier structural analysis suffered from a lack of data due to poor diffraction by the crystal. As this cluster plays such a major role in the context of the structures discussed in Chapter 4, when better crystals were obtained a re-determination was undertaken.

a) Crystal data for (XR9).

$\text{C}_{24}\text{H}_{12}\text{O}_{14}\text{Ru}_6$, $M = 1130.77$, monoclinic, space group $P2_1/m$, $a = 10.573(2)$,
 $b = 15.885(3)$, $c = 9.481(2) \text{ \AA}$, $\beta = 110.37(3)^\circ$, $U = 1492.77 \text{ \AA}^3$, $Z = 2$,
 $D_c = 2.52 \text{ g cm}^{-3}$, $F(000) = 1064$, $\mu(\text{Mo-K}\alpha) = 27.50 \text{ cm}^{-1}$,

b) Data collection. Data were collected in the θ -range $3\text{--}25^\circ$, with a scan width of 0.80° , using a red crystal of dimensions $0.32 \times 0.31 \times 0.26 \text{ mm}$. Equivalent reflections were merged to give 2316 data with $I/\sigma(I) > 3.0$.

c) Structure solution and refinement.

Satisfactory solution and refinement were achieved in the space group $P2/m$, which is very rarely observed for metal compounds. The cluster has exact C_s symmetry and the mirror plane passing through the molecule has a total of 10 atoms lying in it, namely the opposite vertex metal atoms Ru(2) and Ru(6), the central carbide atom C, two of the arene carbon atoms C(5) and C(8), the methyl carbon, C(5) and the atoms of one terminal and one bridging carbonyl ligand, CO(22) and CO(43) respectively. This structure is illustrated in Chapter 4, where a numbered diagram is given. The coordinates of the four independent metal atoms were deduced from a Patterson synthesis (Appendix A) (the coordinates of the earlier determination were not available) and the remaining non-hydrogen atoms were located from subsequent difference-Fourier syntheses. Absorption corrections were applied to the data after initial refinement with isotropic thermal parameters for all atoms. Refinement before gave $R = 0.0819$, $R_w = 0.0834$ and, after application of absorption corrections,

further isotropic refinement gave $R = 0.0759$ and $R_w = 0.0876$. The four independent ruthenium metal atoms were assigned anisotropic thermal parameters in the final cycles of full-matrix refinement of the overall scale factor and the atomic parameters which converged at $R = 0.0507$ and $R_w = 0.0621$ with weights of $w = 1/\sigma^2 F_o$ assigned to the individual reflections.

No residual electron density of greater than ca. $1 \text{ e } \text{Å}^{-3}$ was observed in the difference-Fourier synthesis calculated at this stage. Subsequent use of data with $\sin\theta < 0.35$ and 0.30 failed to give satisfactory maxima for any of the ligand hydrogen atoms.

6.5.6 X-Ray structure analysis of $\text{Ru}_6\text{C}(\mu_2\text{-CO})_2(\text{CO})_{13}(\text{C}_6\text{H}_3\text{Me}_3)$ (XR10).

This is the second in a series of three related hexanuclear clusters discussed in Chapter 4, where fully numbered diagrams of the molecular species may be found. Principal bond lengths and angles are presented in Appendix A.

a) Crystal data for (XR10).

$\text{C}_{24}\text{H}_{12}\text{O}_{15}\text{Ru}_6$, $M = 1146.57$, triclinic, space group $P1$ (No.2), $a = 14.123(4)$, $b = 11.573(3)$, $c = 9.624(3) \text{ Å}$, $\alpha = 101.19(3)$, $\beta = 96.19(3)$, $\gamma = 87.15(2)^\circ$, $U = 1533.42 \text{ Å}^3$, $Z = 2$, $D_c = 2.48 \text{ g cm}^{-3}$, $\mu(\text{Mo-K}\alpha) = 27.1 \text{ cm}^{-1}$, $F(000) = 1080$.

b) Data collection.

A red crystal of size $0.34 \times 0.40 \times 0.11 \text{ mm}$, $\mu(\text{Mo-K}\alpha) = 27.1 \text{ cm}^{-1}$, was used in the data collection. Data were collected in the θ -range $3\text{-}25^\circ$, with a scan width of 0.80° . Equivalent reflections were merged to give 3434 unique data with $I/\sigma(I) > 3.0$.

c) Structure solution and refinement.

Density calculations assuming two molecules per unit cell gave a reasonable value of 2.48 g cm^{-3} , which is comparable to previously reported values for related hexanuclear ruthenium clusters. The space group was assumed to be $P\bar{1}$ (No.2). This was confirmed both by the use of the Delaunay reduction programme Tracer (which did not find an alternative lattice of higher symmetry) and by the satisfactory solution and refinement of the structure.

The coordinates of four of the six metal atoms, forming a tetrahedron, were deduced from a Patterson synthesis. One cycle of refinement was given to the overall scale factor in this stage and a Fourier synthesis showed high peaks due to the two 'missing' ruthenium atoms. These were included in the structure factor calculation and the overall scale factor was refined alone in one cycle of refinement and the six sets of metal atom positional and isotropic thermal parameters were also refined in the two subsequent cycles. This gave reasonable isotropic parameters for all six atoms and a reliability index of $R = 0.2145$, $R_w = 0.2238$. From a Fourier calculated at this stage the carbon and oxygen atoms of ten carbonyl ligands were located, along with all 9 carbon atoms of the mesitylene ring. Blocked full-matrix refinement with the overall scale refined in the first cycle, the metal atom parameters refining in cycles 2 and 4 and the remaining parameters in cycles 3 and 5 ($R = 0.1624$ and $R_w = 0.1824$) were carried out. A difference-Fourier map showed suitable maxima for five new carbonyl ligands. This made the total number of carbonyl groups present 15, although the original formulation of the molecule had predicted only 14 carbonyls. Full-matrix refinement of all the atoms with isotropic thermal parameters ($R = 0.0778$) was followed by absorption correction on the data using the method of Stuart and Walker. Two cycles of refinement, with all the atoms isotropic, then gave $R = 0.0647$.

After two cycles of full-matrix refinement, with anisotropic thermal parameters assigned to the metal atoms, a difference-Fourier synthesis was calculated. Only two phenyl type hydrogen atoms of the mesitylene ligand could be located, so the remaining phenyl ring hydrogen and all nine methyl hydrogen atoms of the mesitylene ligand were included in geometrically idealised positions [$d(\text{C-H}) 1.08 \text{ \AA}$] and were constrained to 'ride' on the relevant carbon atoms with fixed isotropic thermal parameters of 0.08 \AA^2 . The six metal atoms, and all carbon and oxygen atoms of the fourteen carbonyl ligands were assigned anisotropic thermal parameters in the final cycles of blocked full-matrix refinement (metal atoms refining in cycles 1 and 3 and the remaining atoms in cycles 2 and 4), which converged at $R 0.0334$ and $R_w 0.0365$ with weights of $w = 1/\sigma^2 F_o$ assigned to the individual reflections. Only residual electron density of less than 1 e \AA^{-3} remained in the final difference-Fourier synthesis.

6.5.7 X-Ray structure analysis of $\text{HRu}_6(\text{CO})_{12}(\mu\text{-CO})(\mu_4\text{-}\eta^2\text{-CO})(\eta^7\text{-C}_6\text{H}_3\text{Me}_2\text{CH}_2)$ (XR11).

This is the third structure of the three related hexanuclear species which are discussed in Chapter 4, where full labelled diagrams are given. Principal bond lengths and angles are in Appendix A. The initial steps in this structure analysis were carried out by Dr. H.R. Powell, but the final stages were done as part of this project when the nature of the cluster was discovered.

a) Crystal data for (XR11). $(\text{C}_6\text{H}_{14})$:

$\text{C}_{29}\text{H}_{26}\text{O}_{14}\text{Ru}_6$, $M = 1204.51$, monoclinic, space group $P2_1/c$, $a = 9.876(3)$,

$b = 16.050(5)$, $c = 22.563(6) \text{ \AA}$, $\beta = 91.55(2)^\circ$, $U = 3575.15 \text{ \AA}^3$, $Z = 4$,

$D_c = 2.24 \text{ g cm}^{-3}$, $\mu(\text{Mo-K}\alpha) = 23.00 \text{ cm}^{-1}$, $F(000) = 2304$.

b) Data collection.

A green crystal of size 0.05 x 0.35 x 0.24 mm was used in the data collection. Data were collected in the θ -range 3-25°, with a scan width of 0.80°. Equivalent reflections were merged to give 3582 unique data with $I/\sigma(I) > 3.0$.

c) Structure solution and refinement.

The coordinates of the metal atoms were deduced from a Patterson synthesis, and the remaining non-hydrogen atoms were located from subsequent difference-Fourier syntheses. The position of the hydride ligand was deduced by potential energy minimisation techniques, [263] but the hydrogen atoms of the organic ligand were not located. The completion of the structure from this stage formed a part of the work of this project. Six regions of very extended electron density in difference-Fourier syntheses calculated at this point have been assigned as due to a disordered hexane solvent molecule of crystallisation. Although considerable effort was used in studying very fine grid difference-Fourier syntheses in the region of the peaks it was not possible to resolve them into more than 6 peaks or to obtain a set of good geometry for a linear hexane. Carbon atoms with full occupancy factors were assigned to these peaks, and they were assigned isotropic thermal parameters. All non-hydrogen atoms in the cluster molecule were assigned anisotropic thermal parameters in the final cycles of full-matrix refinement, which converged at R 0.0650 and R_w 0.0679, with weights of $w = 1/\sigma^2 F_o$ assigned to the individual reflections.

6.5.8 X-Ray Structure Analysis of $[N(PPh_3)_2][Ru_{10}N(CO)_{24}]$ (XR12).

This structure is discussed in detail in Chapter 4, where fully labelled diagrams are given. The principal bond lengths and angles are in Appendix A.

a) Crystal data for (XR12).

$C_{61}H_{32}Cl_2N_2O_{24}P_2Ru_{10}$, $M = 2319.87$, monoclinic, space group $P2_1/c$,
 $a = 11.763(2)$, $b = 17.817(4)$, $c = 35.330(5)$ Å, $\beta = 94.33(1)^\circ$, $U = 7383.38$
 Å^3 , $D_c = 2.09 \text{ g cm}^{-3}$, $Z = 4$, $\mu(\text{Mo-K}\alpha) = 19.72 \text{ cm}^{-1}$, $F(000) = 4432$.

b) Data collection.

A dark orange crystal of size 0.20 x 0.25 x 0.19 mm, was used in the data collection, in the θ -range 3-25°, with a scan width of 0.90°. Equivalent reflections were merged to give 2300 unique data with $I/\sigma(I) > 3.0$.

c) Structure solution and refinement.

The coordinates of the ten metal atoms from the related decanuclear cluster $[\text{HRu}_{10}\text{C}(\text{CO})_{24}]^-$ were used as a 'partial structure', and the remaining non-hydrogen atoms were located from subsequent difference-Fourier syntheses. One cycle of refinement was given to the overall scale factor, followed by two cycles in which the atomic parameters of the metal atoms were included. A difference-Fourier calculated at this stage showed suitable peaks for all non-hydrogen atoms. The carbon atoms of the phenyl rings were constrained to idealised hexagonal geometry (C-C 1.395 Å) with the attached H-atoms in calculated sites (C-H 1.08 Å) with fixed isotropic thermal parameters of 0.08 Å^2 . The interstitial nitrido atom (the first to have been located in a decanuclear cluster) refined satisfactorily giving a final isotropic thermal parameter of 0.0283 Å^2 . In view of the very close similarity of the unit cell dimensions and the atomic parameters to those of the corresponding salt of the monohydrido carbido cluster dianion $[\text{HRu}_{10}(\text{C})(\text{CO})_{24}]^{2-}$, the possibility that this species had been isolated in the synthesis was carefully considered. Repetition of the refinement of the structure with the central atom assigned as a C-atom instead of nitrogen resulted in a very low thermal parameter of 0.0001 Å^2 . Conclusive proof of the presence of an interstitial N-atom was later obtained from ^{15}N n.m.r. and this is discussed in Chapter 4. Refinement of the

structure was very difficult (as it had been on the case of the isomorphous $[N(PPh_3)_2][HRu_{10}(C)(CO)_{24}]$ structure) as four of the metal atoms lie close to $Y = 0$ and the remaining metals occur in pairs lying almost equally either side of this plane. Effectively the cluster near mirror symmetry about the plane $y = 0.0$ and this causes correlations between 'pseudo-symmetry' related atomic parameters on either side of this plane. The correlations were prevented by refining these atoms in alternate cycles of blocked full-matrix refinement. The ten ruthenium atoms and the phosphorus and nitrogen atoms of the counter ion were assigned anisotropic thermal parameters in the final cycles of blocked full-matrix refinement, which converged at R 0.0613 and R_w 0.0582, with weights of $w = 1/\sigma^2 F_o$ assigned to the individual reflections.

6.5.9 X-Ray structure analysis of $Os_3(CO)_{10}AuPET_3(PhCCH_2)$ (XR13).

This structure is one of two trinuclear cluster which have certain features in common with the heptanuclear cluster $Os_7(CO)_{16}(MeCCMe)_3$ (XR15). All three structures are discussed in Chapter 5.

a) Crystal data for (XR13).

$C_{24}H_{22}Au_{10}Os_3P$, $M = 1268.97$, monoclinic, space group $P2_1/c$
 $a = 14.005(3)$, $b = 12.242(2)$, $c = 17.599(4)$ Å, $\beta = 86.41(3)^\circ$,
 $U = 3011.41$ Å³, $Z = 4$, $D_c = 2.80$ g cm⁻³, $\mu(Mo-K\alpha) = 169.2$ cm⁻¹,
 $F(000) = 2272$.

b) Data collection.

A black crystal of size 0.16 x 0.42 x 0.13 mm, was used in the data collection. Data were collected in the θ -range 3-25°, with a scan width of 0.80°. Equivalent reflections were merged to give 3766 data with $I/\sigma(I) > 3.0$.

c) Structure solution and refinement.

Systematic absences in the data of the type $0k0$, $k = 2n + 1$ and $h0l$, $l = 2n + 1$, indicated that the space group was $P2_1/c$. From the Patterson synthesis the positions of all three osmium atoms and the gold atom were deduced (Appendix B). These were included in structure factor calculation and the overall structure factor was refined in two cycles of least-squares refinement and the parameters of the metal atoms were also included in the second cycle. A difference-Fourier synthesis calculated at this stage gave suitable positions for all the non-hydrogen atoms. Refinement of the parameters of all the atoms in two cycles gave very high thermal parameters for some of the carbonyl ligand atoms. Some improvement was possible by refinding these peaks from a subsequent difference-Fourier synthesis. Use of low angle data with $\sin\theta < 0.35$ in a difference-Fourier synthesis gave some hydrogen positions but most of these were associated with rather bad angles at the carbon atoms. For consistency, the phenyl and methyl hydrogen positions were included in refinement at calculated positions riding on the relevant carbon atoms with fixed isotropic thermal parameters of 0.08 \AA^2 . The geminal hydrogen atoms of the organo ligand were not located and were not included.

Absorption corrections were applied to the data after refinement with all atoms having isotropic thermal parameters. This led to a lowering in the R factor from 0.0745 to 0.0458, and overall lower thermal parameters. In the final cycles of refinement anisotropic thermal parameters were assigned to the four metal and the phosphorus atoms, and this converged at $R = 0.0345$, $R_w = 0.0367$. The residual electron density in the final difference-Fourier synthesis was less than 1 e \AA^{-3} .

6.5.10 X-Ray structure analysis of $\text{HOs}_3(\text{CO})_9(\text{MeCCMe})(\text{AuPPh}_3)$ (XR14).

This is the second of the two trinuclear clusters discussed together with the related heptanuclear cluster (XR15) in Chapter 5.

a) Crystal data for (XR14).

$C_{31}H_{22}Au_{10}Os_3P$, $M = 1337.05$, monoclinic, space group $P2_1/c$,
 $a = 15.691(4)$, $b = 9.614(2)$, $c = 25.022(5)$ Å, $\beta = 115.82(3)^\circ$,
 $U = 3397.81$ Å³, $Z = 4$, $D_c = 2.61$ g cm⁻³, $\mu(\text{Mo-K}\alpha) = 150.0$ cm⁻¹, $F(000) =$
2408.

b) Data collection.

A black crystal of size 0.16 x 0.16 x 0.11 mm, was used in the data collection which covered the range θ -range 3-25°, with a scan width of 0.70°. Equivalent reflections were merged to give 2015 independent data with $I/\sigma(I) > 3.0$.

c) Structure solution and refinement.

From a Patterson synthesis the positions of three osmium atoms and the gold atom were deduced. These were included in structure factor calculation and three cycles of refinement of the overall scale factor and two of the atomic parameters were carried out. From a difference-Fourier synthesis at this point the positions of the phosphorus atom and the carbon and oxygen atoms of one carbonyl were located and included in refinement. The metal atom parameters were refined in a separate block from those of the other atoms. This reduced the reliability factor slightly, to $R = 0.2005$, $R_w = 0.1969$. A difference-Fourier then gave all carbon atoms of one phenyl ring, a total of six carbon atoms for the remaining two phenyl groups and two more carbonyl ligands ($R = 0.1029$, $R_w = 0.1032$). The difference-Fourier then calculated revealed positions for all four carbon atoms of the butyne group (C_2Me_2) and one carbonyl ligand. Refinement of all atoms with isotropic thermal parameters in two cycles gave $R = 0.0798$, $R_w = 0.0764$.

Use of low angle data ($\sin\theta < 0.35$) in a difference-Fourier synthesis did not reveal the hydrogen ligand position, which was found by use of the Orpen potential energy minimisation technique [bridging the Os(1)-Os(2) bond (Figure 5.4/1).[263] This was included in structure factor calculations with an isotropic thermal parameter of 0.08 \AA^2 but was not refined. The phenyl rings were given idealised geometry (C-H 1.395 \AA) and their hydrogen atoms and those of the methyl groups were included in calculated positions (C-H 1.08 \AA) with fixed thermal parameters of 0.08 \AA^2 . Absorption corrections were applied using the method of Stewart and Walker after refinement of all atoms with isotropic thermal parameters ($R = 0.0728$). Two further cycles of refinement with isotropic thermal parameters gave $R = 0.0664$.

In the final cycles of full-matrix refinement anisotropic thermal parameters were assigned to all four metal atoms and the phosphorus atom. Refinement converged at $R = 0.0589$, $R_w = 0.0560$. Residual electron density of ca. 1 e \AA^{-3} remained after all atomic positions had been assigned and fully refined.

6.5.11 X-Ray structure analysis of $\text{Os}_7(\text{CO})_{16}(\text{MeCCMe})_3$ (XR15).

This structure is discussed together with the two preceding trinuclear osmium species (XR13) and (XR14) in Chapter 5, where the fully labelled diagrams are given. The principal bond lengths and angles are given in Appendix A.

a) Crystal data for $\text{Os}_7(\text{CO})_{16}(\text{MeCCMe})_3$ (XR15).

$\text{C}_{28}\text{H}_{18}\text{O}_{16}\text{Os}_7 \cdot (0.5\text{C}_6\text{H}_{12}) \cdot 0.5(\text{C}_2\text{H}_6\text{O})$, $M = 2006.96$, monoclinic, space group $P2_1/c$, $a = 33.655(7)$, $b = 12.225(2)$, $c = 10.356(2) \text{ \AA}$, $\beta = 105.38(3)^\circ$, $U = 4108.11 \text{ \AA}^3$, $Z = 4$, $D_c = 3.25 \text{ g cm}^{-3}$, $\mu(\text{Mo-K}\alpha) = 208.1 \text{ cm}^{-1}$, $F(000) = 3532$.

b) Data collection.

Data were collected in the θ -range 3-25°, with a scan width of 0.80°, using a black crystal of dimensions 0.29 x 0.13 x 0.07 mm, and equivalent reflections were merged to give 3253 unique data with $I/\sigma(I) > 3.0$.

c) Structure solution and refinement.

Systematic absences in the data of the type:

$$0\ k\ 0, \quad k = 2n + 1 \quad \text{and} \quad h\ 0\ 1, \quad (h + 1) = 2n + 1$$

indicated that there was a 2_1 screw axis parallel to the b axis and an n-glide perpendicular to it. This indicates the crystal setting corresponded to the non-standard space group $P2_1/n$, an alternative setting of space group $P2_1/c$.

The Patterson map was used to deduce the fractional coordinates of five of the seven metal atoms. These were included in structure factor calculation and refinement of the overall scale factor alone gave $R = 0.4750$, $R_w = 0.4758$. In a Fourier synthesis calculated at this stage suitable peaks corresponding to the two remaining metal atoms were readily identified.

The parameters of all seven atoms were included in structure factor calculation and three cycles of refinement were carried out. The overall scale factor refined in all three cycles and the metal atom parameters in cycles 2 and 3. All refined isotropic thermal parameters were under 0.05 \AA^2 with $R = 0.1211$, $R_w = 0.1249$. A difference-Fourier synthesis calculated at this stage revealed the 13 carbonyl groups and the four carbon atoms of the organo-fragments. The parameters of these 'new' atoms were included in refinement and gave a lowered reliability factor of $R = 0.1102$, $R_w = 0.1158$. Subsequent difference-Fourier maps revealed all remaining non-hydrogen atoms.

A difference-Fourier, calculated after all the cluster atoms had been included in structure factor calculation and refinement, showed residual electron density, indicating the presence of solvent of crystallisation. As crystallisation had been carried out in a mixture of solvents, identification of the atoms present proved very difficult. Ultimately a compromise was adopted and the most significant peaks were included as one oxygen and eight carbon atoms all at half occupancy. On refinement they gave reasonable thermal parameters in all cases. It proved possible to attribute these atoms to a 50/50 disorder of hexane and ethanol, corresponding to random distribution of hexane and ethanol molecules in equal proportions throughout the crystal. All methyl hydrogen atoms were included at calculated positions 'riding' on the C-atoms and were assigned fixed thermal parameters of 0.08 \AA^2 . Absorption corrections were applied using the method of Stewart and Walker, after refinement of all atoms with isotropic thermal parameters ($R = 0.742$). Two further cycles of refinement with isotropic thermal parameters gave $R = 0.0583$. In the final stages of full-matrix refinement the seven osmium atoms were assigned anisotropic thermal parameters and convergence occurred at $R = 0.0576$ and $R_w = 0.0548$. In the final difference-Fourier residual electron density of ca. 2 e \AA^{-3} was evident in the neighbourhood of the osmium atoms.

References.

References.

1. A.F. Dyke, S.A.R. Knox, M.J. Morris and P.J. Naish, *J. Chem. Soc., Dalton Trans.*, 1983, 1417.
2. G.S. Lewandos, N.M. Doherty, S.A.R. Knox, K.A. Macpherson and A.G. Orpen, *Polyhedron*, 1988, 7, 837.
3. D.M. Skinner, E. Rosenberg, J. Bracker-Navak, S. Aime, D. Osella, R. Gobetto and L. Milone *Organometallics*, 1988, 7, 856.
4. A.A. Cherkas, L.H. Randall, S.A. MacLaughlin, G.N. Mott, N.J. Taylor and A.J. Carty, *Organometallics*, 1988, 7, 969.
5. G. Conole, K. Hendrick, A.H. Horton, M. McPartlin and M.J. Mays, *Nouv. J. Chim.*, 1988, 12, 559.
6. G. Conole, K.A. Hill, M. McPartlin, M.J. Mays and M.J. Morris, *J. Chem. Soc., Chem. Commun.*, 1989, 688.
7. G. Conole, M. McPartlin, M.J. Mays and M.J. Morris, *J. Chem. Soc., Dalton Trans.*, 1990, 2359.
8. G. Conole, K. Hendrick, A.D. Horton, M. McPartlin, M.J. Mays and E. Sappa, *J. Chem. Soc., Dalton Trans.*, 1990, 2367.
9. G.E. Kimbell, *J. Chem. Phys.*, 1940, 8, 188.
10. R.B. Woodward and R. Hoffmann, *Angew. Chem. Int. Ed.*, 1969, 8, 781.
11. D.M.P. Mingos and R.L. Johnston, *Structure Bonding*, 1987, 68, 31.

12. S.M. Owen, *Polyhedron*, 1988, 7, 253.
13. C.A. Tolman, *Chem. Soc. Rev.*, 1972, 1, 337.
14. P.R. Mitchell and R.V. Parish, *J. Chem. Ed.*, 1969, 46, 811.
15. T.A. Albright, *Tetrahedron*, 1982, 38, 1339.
16. A.J. Deeming and S. Hasso, *J. Organometal. Chem.*, 1976, 114, 313.
17. M. McPartlin and W.J.H. Nelson, *J. Chem. Soc., Dalton Trans.*, 1986, 1557.
18. B.F.G. Johnson, J. Lewis, B.E. Reichert, K.T. Schorpp, G.M. Sheldrick, *J. Chem. Soc., Dalton Trans.*, 1977,
19. P.F. Heveldt, B.F.G. Johnson, J. Lewis, P.R. Raithby and G.M. Sheldrick, *J. Chem. Soc., Chem. Commun.*, 1978, 340.
20. G.R. John, B.F.G. Johnson, J. Lewis, W.J. Nelson and M. McPartlin, *J. Organometal. Chem.*, 1979, 171, C14.
21. C.R. Eady, B.F.G. Johnson, J. Lewis and T. Matheson, *J. Organometal. Chem.*, 1973, 57, C82.
22. P.F. Jackson, B.F.G. Johnson, J. Lewis, J.N. Nicholls, M. McPartlin and W.J.H. Nelson, *J. Chem. Soc., Chem. Commun.*, 1980, 564.
23. B.F.G. Johnson, J. Lewis, W.J.H. Nelson, J.N. Nicholls, J. Puga, P.R. Raithby, M.J. Rosales, M. Schroder and M.D. Vargas, *J. Chem. Soc., Dalton. Trans.*, 1983, 2447.

24. R. Mason, K.M. Thomas, D.M.P. Mingos, J. Am. Chem. Soc., 1973, 95, 3802.
25. C.R. Eady, B.F.G. Johnson and J. Lewis, J. Chem. Soc., Chem. Commun., 1976, 302.
26. M. McPartlin, C.R. Eady, B.F.G. Johnson and J. Lewis, J. Chem. Soc., Chem. Commun., 1976, 883.
27. G.R. John, B.F.G. Johnson, J. Lewis and A.L. Mann, J. Organometal. Chem., 1979, 171, C9.
28. R.E. Williams, Inorg. Chem., 1971, 10, 210.
29. K. Wade, Chem. Commun., 1971, 792;
30. K. Wade, Inorg. Nucl. Chem. Letters, 1972, 8, 559;
31. K. Wade, Inorg. Nucl. Chem. Letters, 1972, 8, 563;
32. K. Wade, Inorg. Nucl. Chem. Letters, 1972, 8, 823;
33. K. Wade, Adv. Inorg. Chem. Radiochem., 1976, 18, 1.
34. M.R. Churchill, J. Wormald, J. Knight and M.J. Mays and Chem. Commun., 1970, 458.
35. M.R. Churchill and J. Wormald, J. Am. Chem. Soc., 1971, 93, 5670.
36. D.M.P. Mingos, J. Chem. Soc., Dalton Trans., 1974, 133.
37. J.W. Lauher, J. Am. Chem. Soc., 1978, 100, 5305.

38. D.M.P. Mingos and M.I. Forsyth, *J. Chem. Soc., Dalton Trans.*, 1977, 610.
39. J. Evans, *J. Chem. Soc., Dalton Trans.*, 1978, 18.
40. J. Evans, *J. Chem. Soc., Dalton Trans.*, 1978, 25.
41. D.M.P. Mingos, *Nat. Phys. Sci.*, 1972, 236, 99.
42. D.M.P. Mingos, *Acc. Chem. Res.*, 1984, 17, 311.
43. M. McPartlin, *Polyhedron*, 1984, 3, 1279.
44. M. McPartlin and D.M.P. Mingos, *Polyhedron*, 1984, 3, 1321.
45. D.M.P. Mingos and D.G. Evans, *J. Organometal. Chem.*, 1983, 251, C13.
46. D.M.P. Mingos, *J. Chem. Soc., Chem. Commun.*, 1983, 706.
47. M. Elian, M.M.L. Chen, D.M.P. Mingos and R. Hoffmann, *Inorg. Chem.*, 1976, 15, 1148.
48. R. Hoffmann, *Angew. Chem. Int. Ed. Engl.*, 1982, 21, 711.
49. K. Fukui, *Angew. Chem. Int. Ed. Engl.*, 1982, 21, 801.
50. R. Hoffmann, *Science*, 1981, 211, 995.
51. M. Elian and R. Hoffmann, *Inorg. Chem.*, 1975, 14, 1058.
52. D.G. Evans and D.M.P. Mingos, *J. Organometal. Chem.*, 1982, 232, 171.
53. D.M.P. Mingos, *Polyhedron*, 1984, 3, 1289.

54. K.P. Hall and D.M.P. Mingos, *Prog. Inorg. Chem.*, 1984, 32, 237.
55. F.G.A. Stone, *Angew. Chem. Int. Ed. Engl.*, 1984, 23, 89.
56. J.W. Lauher and K. Wald, *J. Am. Chem. Soc.*, 1981, 103, 7648.
57. L.W. Bateman, M. Green, J.A.K. Howard, K.A. Mead, R.M. Mills, I.D. Salter, F.G.A. Stone and P. Woodward, *J. Chem. Soc., Chem. Commun.*, 1982, 773.
58. B.F.G. Johnson, D.A. Kaner, J. Lewis and P.R. Raithby, *J. Organometal. Chem.*, 1981, 215, C33.
59. K. Burgess, B.F.G. Johnson, D.A. Kaner, J. Lewis, P.R. Raithby, A.N. Azman and B. Syed-Mustaffa, *J. Chem. Soc., Chem. Commun.*, 1983, 455.
60. M.R. Churchill, F.J. Hollander and J.P. Hutchinson, *Inorg. Chem.*, 1977, 16, 2697.
61. B.T. Huie, C.B. Knobler and H.D. Kaesz, *J. Am. Chem. Soc.*, 1978, 100, 3059.
62. J.A.K. Howard, I.D. Salter and F.G.A. Stone, *Polyhedron*, 1984, 3, 567.
63. B.K. Teo, *Inorg. Chem.*, 1984, 23, 1251.
64. B.K. Teo, G. Longoni and F.R.K. Chung, *Inorg. Chem.*, 1984, 23, 1257.
65. D.M.P. Mingos, *Inorg. Chem.*, 1985, 24, 114.

66. B.K. Teo, *Inorg. Chem.*, 1985, 24, 115.
67. B.K. Teo, *Inorg. Chem.*, 1985, 24, 1627.
68. B.K. Teo, *Inorg. Chem.*, 1985, 24, 4209.
69. C.R. Boyer and U.C. Merzbach, *A History of Mathematics* (2 Ed.), 1989, J. Wiley and sons.
70. R.B. King and D.H. Rouvray, *J. Am. Chem. Soc.*, 1977, 99, 7834.
71. A.J. Stone, *Inorg. Chem.*, 1981, 20, 563.
72. M.J. Alderton and A.J. Stone, *Inorg. Chem.*, 1982, 21, 2297.
73. A.J. Stone, *Polyhedron*, 1984, 3, 1299.
74. C.R. Eady, B.F.G. Johnson, J. Lewis, B.E. Reichert and G.M. Sheldrick., *J. Chem. Soc., Chem. Commun.*, 1976, 271.
75. B.E. Reichert and G.M. Sheldrick, *Acta Cryst.*, 1977, B33, 173.
76. C.R. Eady, J.J. Guy, B.F.G. Johnson, J. Lewis, M.C. Malatesta, and G.M. Sheldrick, *J. Chem. Soc., Chem. Commun.*, 1976, 807.
77. J.J. Guy and G.M. Sheldrick, *Acta. Cryst.*, 1978, B34, 1722.
78. B.F.G. Johnson, J. Lewis, P.R. Raithby, and M.J. Rosales, *J. Organometal. Chem.*, 1983, 259, C9.
79. A.V. Rivera, G.M. Sheldrick and M.B. Hursthouse, *Acta. Cryst.*, 1978, B34, 3376.
80. B.F.G. Johnson, J. Lewis, W.J.H. Nelson, M.A. Pearsall, P.R. Raithby, M.J. Rosales, M. McPartlin and A. Sironi, *J. Chem. Soc., Dalton. Trans.*, 1987, 327.

31. J.J. Guy and G.M. Sheldrick, *Acta Cryst.*, 1978, B34, 1725.
32. Z. Dawoodi, M.J. Mays and P.R. Raithby, *J. Chem. Soc., Chem. Commun.*, 1981, 801.
33. J.G. Jeffrey, B.F.G. Johnson, J. Lewis, P.R. Raithby, and D.A. Welch, *J. Chem. Soc., Chem. Commun.*, 1986, 318.
34. D.H. Farrar, P.F. Jackson, B.F.G. Johnson, J. Lewis, J.N. Nicholls and M. McPartlin, *J. Chem. Soc., Chem. Commun.*, 1981, 415.
35. B.F.G. Johnson, J. Lewis, J.N. Nicholls, J. Puga, P.R. Raithby, M.J. Rosales, M. McPartlin and W. Clegg, *J. Chem. Soc., Dalton. Trans.*, 1983, 277.
36. J. Evans, B.P. Gracey, L.R. Gray, M. Webster, *J. Organometal. Chem.*, 1982, 240, C61.
37. K. Henrick, B.F.G. Johnson, J. Lewis, J. Mace, M. McPartlin and J. Morris, *J. Chem. Soc., Chem. Commun.*, 1985, 1617.
38. S.L. Cook, J. Evans, L.R. Gray and M. Webster, *J. Chem. Soc., Dalton. Trans.*, 1986, 2149.
39. M.I. Bruce, B.W. Skelton, A.H. White and M.L. Williams, *J. Chem. Soc., Chem. Commun.*, 1985, 744.
90. A.G. Cowie, B.F.G. Johnson, J. Lewis, J.N. Nicholls, P.R. Raithby and M.J. Rosales, *J. Chem. Soc., Dalton. Trans.*, 1983, 2311.
91. A.J. Carty, *Pure and Appl. Chem.*, 1982, 54, 113.

92. A.J. Carty, S.A. MacLaughlin and N.J. Taylor, J. Am. Chem. Soc., 1981, 103, 2456.
93. J. Daran, E. Cabrera, M.I. Bruce, and M.L. Williams, J. Organometal. Chem., 1987, 319, 239.
94. M.L. Blohm, D.E. Fjare and W.L. Gladfelter, Inorg. Chem., 1983, 22, 1004.
95. M.L. Blohm, W.L. Gladfelter, Organometallics, 1985, 4, 45.
96. K. Natarajan, L. Zsolnai and G. Huttner, J. Organometal. Chem., 1981, 209, 85.
97. A.G. Orpen and G.M. Sheldrick, Acta Cryst., 1978, B34, 1992.
98. J.M. Fernandez, B.F.G. Johnson, J. Lewis, and P.R. Raithby, Acta Cryst., 1979, B35, 1711.
99. K. Kwek, N.J. Taylor and A.J. Carty, J. Am. Chem. Soc., 1984, 106, 4636.
100. M.I. Bruce, J.G. Matison, J.R. Rodgers and R.C. Wallis, J. Chem. Soc., Chem. Commun., 1081, 1070.
101. D.H. Farrar, G.R. John, B.F.G. Johnson, J. Lewis, P.R. Raithby, and M.J. Rosales, J. Chem. Soc., Chem. Commun., 1981, 886
102. S.A. MacLaughlin, N.J. Taylor and A.J. Carty, Organometallics, 1984, 3, 392.
103. M.I. Bruce, M.L. Williams, J.M. Patrick and A.H. White, J. Chem. Soc., Dalton Trans., 1985, 1229.

104. P.F. Jackson, B.F.G. Johnson, J. Lewis, W.J.H. Nelson and M. McPartlin, *J. Chem. Soc., Dalton. Trans.*, 1982, 2099.
105. B.F.G. Johnson, J. Lewis, W.J.H. Nelson, J.N. Nicholls, D. Braga, K. Henrick and M. McPartlin, *J. Chem. Soc., Dalton Trans.*, 1984, 1809.
106. D. Braga, B.F.G. Johnson, J. Lewis, M. McPartlin, W.J.H. Nelson, J.N. Nicholls and M.D. Vargas, *J. Chem. Soc., Chem. Commun.*, 1982, 966.
107. B.F.G. Johnson, J. Lewis, P.R. Raithby, M.J. Rosales and D.A. Welch, *J. Chem. Soc., Dalton. Trans.*, 1986, 453.
108. J.M. Fernandez, B.F.G. Johnson, J. Lewis, and P.R. Raithby, *J. Chem. Soc., Dalton Trans.*, 1981, 2250.
109. B.F.G. Johnson, J. Lewis, J.N. Nicholls, J. Puga and K.H. Whitmire, *J. Chem. Soc., Dalton Trans.*, 1983, 787.
110. A.G. Cowie, B.F.G. Johnson, J. Lewis, J.N. Nicholls, P.R. Raithby and A.G. Swanson, *J. Chem. Soc., Chem. Commun.*, 1984, 637.
111. J.M. Fernandez, B.F.G. Johnson, J. Lewis, P.R. Raithby, and G.M. Sheldrick, *Acta Cryst.*, 1978, B34, 1994.
112. Z. Dawoodi, M.J. Mays, and P.R. Raithby, *J. Chem. Soc., Chem. Commun.*, 1980, 712.
113. S.A.R. Knox, B.R. Lloyd, A.G. Orpen, J.M. Vinas, and M. Weber, *J. Chem. Soc., Chem. Commun.*, 1987, 1498.

114. R.D. Adams, J.E. Babin, M. Tasi and T.A. Wolfe, *Organometallics*, 1987, 6, 2228.
115. D. Nucciarone, N.J. Taylor, A.J. Carty, *Organometallics*, 1986, 2565.
116. D.H. Farrar, B.F.G. Johnson, J. Lewis, J.N. Nicholls, P.R. Raithby, and M.J. Rosales, *J. Chem. Soc., Chem. Commun.*, 1981, 273.
117. D.H. Farrar, B.F.G. Johnson, J. Lewis, P.R. Raithby and M.J. Rosales, *J. Chem. Soc., Dalton Trans.*, 1982, 2051.
118. B.F.G. Johnson, J. Lewis, P.R. Raithby and M.J. Rosales, *J. Chem. Soc., Dalton Trans.*, 1983, 2645.
119. K. Kwek, N.J. Taylor, and A.J. Carty, *J. Chem. Soc., Chem. Commun.*, 1986, 230.
120. J. Evans, A.C. Street and M. Webster, *J. Chem. Soc., Chem. Commun.*, 1987, 637.
121. D.L. Davies, J.A.K. Howard, S.A.R. Knox, K.A. Mead, M.J. Morris and M.C. Rendle, *J. Organometal. Chem.*, 1985, 279, C37.
122. S. Han, G.L. Geoffroy and A.L. Rheingold, *Organometallics*, 1986, 5, 2561.
123. E. Sappa, A. Tiripicchio and P. Braunstein, *Chem. Revs.*, 1983, 83, 203.
124. P.R. Raithby and M.J. Rosales, *Adv. Inorg. Chem. Radiochem.*, 1985, 29, 169.

125. M. Ciriano, J.A.K. Howard, J.L. Spencer, F.G.A. Stone and H. Wadepohl, *J. Chem. Soc., Dalton Trans.*, 1979, 1749.
126. K. Henrick, M. McPartlin, A.J. Deeming, S. Hasso, and P. Manning, *J. Chem. Soc., Dalton Trans.*, 1982, 899.
127. A.J. Carty, N.J. Taylor and W.F. Smith, *J. Chem. Soc., Chem. Commun.*, 1979, 750.
128. A.J. Deeming, M.S.B. Felix, P.A. Bates and M.B. Hursthouse, *J. Chem. Soc., Chem. Commun.*, 1987, 461.
129. M. Green, A.G. Orpen and C.J. Schaverien, *J. Chem. Soc., Chem. Commun.*, 1984, 37.
130. B.F.G. Johnson, J.W. Kelland, J. Lewis, A.L. Mann and P.R. Raithby, *J. Chem. Soc., Chem. Commun.*, 1980, 547.
131. J.R. Shapley, M. Tachikawa, M.R. Churchill and R.A. Lashewycz, *J. Organometal. Chem.*, 1978, 162, C39.
132. M.R. Churchill and R.A. Lashewycz, *Inorg. Chem.*, 1978, 18, 848.
133. G.M. Sheldrick and J.P. Yesinowski, *J. Chem. Soc., Dalton Trans.*, 1975, 873.
134. M. Castiglioni, G. Gervasio and E. Sappa, *Inorg. Chim. Acta.*, 1981, 49, 217.
135. W. Yeh, J.R. Shapley, J.W. Ziller and M.R. Churchill, *Organometallics*, 1986, 1757.
136. C.R. Eady, J.M. Fernandez, B.F.G. Johnson, J. Lewis, P.R. Raithby and G.M. Sheldrick, *J. Chem. Soc., Chem. Commun.*, 1978, 421.

137. J.M. Fernandez, B.F.G. Johnson, J. Lewis and P.R. Raithby, *Acta Cryst.*, 1978, B34, 3086.
138. B.F.G. Johnson, J. Lewis, J.A. Lunniss, D. Braga and F. Grepioni, *J. Chem. Soc., Chem. Commun.*, 1988, 972.
139. B.F.G. Johnson, J. Lewis, D. Pippard and P.R. Raithby, *J. Chem. Soc., Chem. Commun.*, 1978, 551.
140. P.F. Jackson, B.F.G. Johnson, J. Lewis, P.R. Raithby, G.J. Will, M. McPartlin and W.J.H. Nelson, *J. Chem. Soc., Chem. Commun.*, 1980, 1190.
141. A.G. Orpen, A.V. Rivera, E.G. Bryan, D. Pippard, G.M. Sheldrick and K.D. Rouse, *J. Chem. Soc., Chem. Commun.*, 1978, 723.
142. A.G. Orpen, D. Pippard, G.M. Sheldrick and K.D. Rouse, *Acta Cryst.*, 1978, B34, 2466.
143. A.D. Clauss, M. Tachikawa, J.R. Shapley and C.G. Pierpont, *Inorg. Chem.*, 1981, 20, 1528.
144. R.D. Adams and S. Wang, *Organometallics*, 1986, 5, 1274.
145. B.F.G. Johnson, J. Lewis, P.R. Raithby, I.C.D. Rouse, *J. Chem. Soc., Dalton Trans.*, 1981, 788.
146. Z. Dawoodi, M.J. Mays and P.R. Raithby, *J. Chem. Soc., Chem. Commun.*, 1979, 721.
147. N.M. Boag, M. Green, J.A.K. Howard, J.L. Spencer, R.F.D. Stansfield, F.G.A. Stone, M.D.O. Thomas, J. Vicente and P. Woodward, *J. Chem. Soc., Chem. Commun.*, 1977, 930.

148. Z. Nomikou, J. Halet, R. Hoffmann, J.T. Tanner and R.D. Adams, and 1990, 9, 588.
149. M. Laing, P. Sommerville, Z. Dawoodi, M.J. Mays, and P.J. Wheatley, J. Chem. Soc., Chem. Commun., 1978, 1035.
150. E. Boyar, A.J. Deeming, M.S.B. Felix, S.E. Kabir, T. Adatia, R. Bhusate, M. McPartlin, and H.Powell, J. Chem. Soc., Dalton Trans., 1989, 5.
151. D. Braga, F. Grepioni, B.F.G. Johnson, J. Lewis, M. Martinelli and M.A. Gallop, J. Chem. Soc., Chem. Commun., 1990, 53.
152. M.P. Gomez-Sal, B.F.G. Johnson, R.A. Kamarudin, J. Lewis and P.R. Raithby, J. Chem. Soc., Chem. Commun., 1985, 1622.
153. E. Sappa, A.M.M. Lanfredi, G. Predieri, A. Tiripicchio, Inorg. Chim. Acta., 1982, 61, 217.
154. C.G. Pierpont, Inorg. Chem., 1977, 16, 636.
155. C. Barner-Thorsen, K.I. Hardcastle, E. Rosenberg, J. Siegel, A.M.M. Landfredi, A. Tiripicchio and M.T. Camellini, Inorg. Chem., 1981, 20, 4306.
156. M. Catti, G. Gervasio and S.A. Mason, J. Chem. Soc., Dalton Trans., 1977, 2260.
157. A.J. Carty, S.A. MacLaughlin, N.J. Taylor and E. Sappa, Inorg. Chem., 1981, 20, 4437.
158. A.J. Carty, S.A. MacLaughlin and N.J. Taylor, J. Chem. Soc., Chem. Commun., 1981, 476.

159. R. Jackson, B.F.G. Johnson, J. Lewis, P.R. Raithby and S.W. Sankey, *J. Organomet. Chem.*, 1980, 193, C1.
160. A.G. Albano, P. Chini, S. Martinengo, M. Sansini and D. Strumolo, *J. Chem. Soc., Dalton Trans.*, 1978, 459.
161. B.F.G. Johnson, J. Lewis, W.J.H. Nelson, J.N. Nicholls and M. Vargas, *J. Organometal. Chem.*, 1983, 249, 255.
162. M.D. Vargas and J. Nicholls, *Adv. Inorg. Chem and Radiochem.*, 1986, 30, 123.
163. R.D. Adams and I.T. Horvath, *Prog. Inorg. Chem.*, 1985, 33, 127.
164. M. McPartlin, *Fourth International Conference on The Chemistry Of The Platinum Group Metals*, 1990, 0.4.
165. C.R. Eady, B.F.G. Johnson and J. Lewis, *J. Chem. Soc., Dalton Trans.*, 1975, 2606.
166. C.R. Eady, B.F.G. Johnson, and J. Lewis, *J. Chem. Soc., Dalton Trans.*, 1977, 838.
167. B.F.G. Johnson, R.D. Johnston and J. Lewis, *J. Chem. Soc. (A)*, 1968, 2865.
168. J.P. Attard, B.F.G. Johnson, J. Lewis, J.M. Mace, M. McPartlin, and A. Sironi, *J. Chem. Soc., Chem. Commun.*, 1984, 595.
169. R.D. Adams, J.E. Babin, R. Mahtab, Suning Wang, *Inorg. Chem.*, 1986, 25, 1623.
170. S.A. MacLaughlin, N.J. Taylor and A.J. Carty, *Inorg. Chem.*, 1983, 22, 1409.

171. A.J. Deeming, *Advances in Organometallic Chem.*, 1986, 26, 1.
172. E. Sappa, A. Tiripicchio, A.J. Carty and G.E. Toogood, *Prog. Inorg. Chem.*, 1987, 35, 438.
173. E.L. Muetterties, *Pure Appl. Chem.*, 1982, 54, 83.
174. M.I. Bruce, M.L. Williams, *J. Organometal. Chem.*, 1985, 282, C11.
175. M. Green, D.R. Hankey, M. Murray, A.G. Orpen and F.G.A. Stone, *J. Chem. Soc., Chem., Commun.*, 1981, 689.
176. M.A. Pearsall, Ph. D thesis, Cambridge.
177. G. Conole, M. McPartlin, H.R. Powell, T. Dutton, B.F.G. Johnson and J. Lewis, *J. Organometal. Chem.*, 1989, 370, C1.
178. S.F.A. Kettle, *Inorg. Chem.*, 1965, 4, 1661.
179. T.G. Appleton, H.C. Clark and L.E. Manzer, *Coord. Chem. Revs.*, 1973, 10, 335.
180. K. Hendrick, M. McPartlin and J. Morris, *Angew. Chem. Int.*, 1986, 25, 853.
181. R.G. Teller and R. Bau, *Structure and Bonding*, 1981, 44, 1.
182. D.S. Moore, D. Robison, *Prog. Inorg. Chem.*, 1979, 25, 145.
183. A. Rodger and B.F.G. Johnson, *Polyhedron*, 1988, 7, 1107.
184. B.F.G. Johnson, *J. Chem. Soc., Chem. Commun.*, 1986, 27.

185. D.J. Fuller and D.L. Keppert, *Inorg. Chem.*, 1984, 23, 3273.
186. R.G. Wolley, *Transition metal clusters* (edited by B.F.G. Johnson) John Wiley, London (1980).
187. J. Lewis and B.F.G. Johnson, *Pure and Appl. Chem.*, 1982, 54, 97.
188. M. Tachikawa and E.L. Muetterties, *Prog. Inorg. Chem.*, 1981, 28, 203.
189. J. Lewis and B.F.G. Johnson, *Pure and Appl. Chem.*, 1975, 44, 43.
190. J.F. Halet, D.G. Evans, D.M.P. Mingos, *J. Am. Chem. Soc.*, 1988, 110, 87.
191. E.R. Corey, L.F. Dahl and W. Beck, *J. Am. Chem. Soc.*, 1963, 85, 1202.
192. P. Chini, *Chem. Commun.*, 1967, 440.
193. P. Chini, *Chem. Commun.*, 1967, 29.
194. M. Bianchi, E. Benedetti and A. Sirigu, *Chemical Communications*, 1969, 596.
195. F. Piacenti, M. Bianchi and E. Benedetti, *Chem. Commun.*, 1967, 775.
196. B.F.G. Johnson, R.D. Johnston and J. Lewis, *Chemical Communications*, 1967, 1057.

197. R. Mason and W.R. Robinson, Chem. Commun., 1968, 468.
198. J.S. Bradley, G.B. Ansell and E.W. Hill, J. Organometal. Chem., 1980, 184, C33.
199. B.F.G. Johnson, J. Lewis, S.W. Sankey, K. Wong, M. McPartlin and W.J.H. Nelson, J. Organometal. Chem., 1980, 191, C3.
200. V.G. Albano, M. Sansoni, P. Chini and S. Martinengo, J. Chem. Soc., Dalton. Trans., 1973, 651.
201. C.T. Hayward and J.R. Shapley, Inorg. Chem., 1982, 21, 3816.
202. C.R. Eady, B.F.G. Johnson, J. Lewis, M. McPartlin, P. Machin and M.C. Malatesta, J. Chem. Soc., Chem. Commun., 1976, 945.
203. J. Allibon, P.F. Jackson, B.F.G. Johnson, J. Lewis, M. McPartlin, W.J.H. Nelson, P.R. Raithby and K.D. Rouse, J. Chem. Soc., Chem. Commun., 1980, 295.
204. C.R. Eady, P.F. Jackson, B.F.G. Johnson, J. Lewis, M. McPartlin, M.C. Malatesta and W.J.H. Nelson, J. Chem. Soc., Dalton Trans., 1980, 383.
205. B.F.G. Johnson, J. Chem. Soc., Chem. Commun., 1976, 211.
206. B.F.G. Johnson and R.E. Benfield, J. Chem. Soc., Dalton Trans., 1978, 1554.
207. R.E. Benfield and B.F.G. Johnson, J. Chem. Soc., Dalton Trans., 1980, 1743.
208. D.G. Evans, J. Chem. Soc., Chem. Commun., 1983, 675.

209. R. Colton and M.J. McCormick, *Coord. Chem. Revs.*, 1980, 31, 1.
210. P.F. Jackson, B.F.G. Johnson, J. Lewis, M. McPartlin and W.J.H. Nelson, *J. Chem. Soc., Chem. Commun.*, 1979, 735.
211. C.R. Eady, P.D. Gavens, B.F.G. Johnson, J. Lewis, M.C. Malatesta, M.J. Mays, A.G. Orpen, A.V. Rivera, G.M. Sheldrick and M.B. Hursthouse, *J. Organometal. Chem.*, 1978, 149, C43.
212. B.F.G. Johnson, J. Lewis, M. McPartlin and K. Wong, *J. Organometal. Chem.*, 1980, 185, C17.
213. G.B. Ansell and J.S. Bradley, *Acta. Cryst.*, 1980, B36, 1930.
214. R.J. Goudsmit, B.F.G. Johnson, J. Lewis, P.R. Raithby and K.H. Whitmire, *J. Chem. Soc., Chem. Commun.*, 1982, 640.
215. R.J. Goudsmit, B.F.G. Johnson, J. Lewis, P.R. Raithby and K.H. Whitmire, *J. Chem. Soc., Chem. Commun.*, 1983, 246.
216. B.F.G. Johnson, J. Lewis, M. McPartlin, M.A. Pearsall, A. Sironi, *J. Chem. Soc., Chem. Commun.*, 1984, 1089.
217. R.J. Goudsmit, B.F.G. Johnson, J. Lewis, P.R. Raithby and M.J. Rosales, *J. Chem. Soc., Dalton Trans.*, 1983, 2257.
218. M.P. Gomez-Sal, B.F.G. Johnson, J. Lewis, P.R. Raithby and A.H. Wright, *J. Chem. Soc., Chem. Commun.*, 1985, 1682.
219. M.A. Van Hove, R. Lin and G.A. Somorjai, *Phys. Rev. Letts.*, 1983, 51, 778.
220. B.F.G. Johnson, R. Khattar, J. Lewis, M. McPartlin, J. Morris and G.L. Powell, *J. Chem. Soc., Chem. Commun.*, 1986, 507.

221. E.J. Ditzel, H.D. Holden, B.F.G. Johnson, J. Lewis, A. Saunders and M.J. Taylor, J. Chem. Soc., Chem. Commun., 1982, 1373.
222. S. Bhaduri, K. Sharma and P.G. Jones, J. Chem. Soc., Chem. Commun., 1987, 1769.
223. M.P. Dielbold, S.R. Drake, B.F.G. Johnson, J. Lewis, M. McPartlin and H. Powell, J. Chem. Soc., Chem. Commun., 1988, 1358.
224. W. H. Nelson, Ph. D thesis (C.N.A.A.), 1980.
225. Tables of Interatomic distances and configurations in molecules and ions, 1958, Ed. L.E. Sutton, Chem. Soc., London.
226. J. Browning, M. Green, B.R. Penfold, J.L. Spencer and F.G.A. Stone, J. Chem. Soc., Chem. Commun., 1973, 31.
227. S.C. Brown, J. Evans and M. Webster, J. Chem. Soc., Dalton Trans., 1981, 2263.
228. B.P. Gracey, J. Evans, A.G. Jones and M. Webster, Acta. Cryst., 1987, C43, 2286.
229. G. Conole, M. McPartlin, S.R. Drake, B.F.G. Johnson and J. Lewis, J. Chem. Soc., Dalton Trans., 1990, 995.
230. S.R. Bunkhall, H.D. Holden, B.F.G. Johnson, J. Lewis, G.N. Pain, P.R. Raithby and M.J. Taylor, J. Chem. Soc., Chem. Commun., 1984, 25.
231. L.J. Farrugia, M.J. Freeman, M. Green, A.G. Orpen, F.G.A. Stone and I.D. Salter, J. Organometal. Chem., 1983, 249, 273.

232. P.A. Bates, S.S.D. Brown, A.J. Dent, M.B. Hursthouse, G.F.M. Kitchen, A.G. Orpen, I.D. Salter and V. Sik, J. Chem. Soc., Chem. Commun., 1986, 600.
233. M.J. Freeman, A.G. Orpen and I.D. Salter, J. Chem. Soc., Chem. Commun., 1987, 379.
234. S.S.D. Brown, S. Hudson, I.D. Salter and M. McPartlin, J. Chem. Soc., Chem. Commun., 1987, 1967.
235. S.S.D. Brown, I.D. Salter, T. Adatia and M. McPartlin, J. Organometal. Chem., 1987, 332, C6.
236. M.J. Freeman, A.G. Orpen and I.D. Salter, J. Chem. Soc., Dalton Trans., 1987, 1001.
237. S.S.D. Brown, I.D. Salter, P.A. Bates and M.B. Hursthouse, J. Chem. Soc., Dalton Trans., 1988, 1795.
238. S.S.D. Brown, I.D. Salter and L. Toupet, J. Chem. Soc., Dalton Trans., 1988, 757.
239. M.I. Bruce and B.K. Nicholson, J. Chem. Soc., Chem. Commun., 1982, 1141.
240. M.I. Bruce and B.K. Nicholson, J. Organometal. Chem., 1983, 252, 243.
241. L.W. Bateman, M. Green, K.A. Mead, R.M. Mills, I.D. Salter, F.G.A. Stone and P. Woodward, J. Chem. Soc., Dalton Trans., 1983, 2599.

242. V. Dearing, S.R. Drake, B.F.G. Johnson, J Lewis, M. McPartlin and H.R. Powell, J. Chem. Soc., Chem. Commun., 1988, 1331.
243. G.B. Ansell, M.A. Modrick and J. Bradley, Acta. Cryst., 1984, C40, 365.
244. A.D. Horten, M.J. Mays and P.R. Raithby, J. Chem. Soc., Chem. Commun., 1985, 247.
245. M. Brookhart and M.L.H. Green, J. Organometal. Chem., 1983, 250, 395.
246. A.D. Horton, M.J. Mays and P.R. Raithby, J. Chem. Soc., Chem. Commun., 1985, 247.
247. A.D. Horten, M.J. Mays and M. McPartlin, J. Chem. Soc., Chem. Commun., 1987, 424.
248. E.L. Muettertides and M.J. Krause, Angew. Chem. Int. Ed. Engl., 1983, 22, 135.
249. J.B. Keister and J.R. Shapley, J. Organometal. Chem., 1975, 85, C29.
250. P. Frediani, U. Matteoli, M. Bianchi, F. Piacenti and G. Menchi, J. Organometal. Chem., 1978, 150, 273.
251. H. Kang, C.H. Mauldin, T. Cole, W. Slegeir, K. Cann and R. Pettit, J. Am. Chem. Soc., 1977, 99, 8323.
252. R.M. Laine, J. Am. Chem. Soc., 1978, 100, 645.
253. W.A. Hermann, Angew. Chem., Int. Ed. Engl., 1982, 117

254. M. Tachikawa and E.L. Muetterties, J. Am. Chem. Soc., 1980, 102, 4541;
255. M.A. Beno, J.M. Williams, M. Tachikawa and E.L. Muetterties, J. Am. Chem. Soc., 1981, 102, 4542.
256. M.A. Beno, J.M. Williams, M. Tachikawa and E.L. Muetterties, J. Am. Chem. Soc., 1981, 103, 1485
257. J.S. Bradley, G.B. Ansell, E.W. Hill, J. Am. Chem. Soc., 1979, 7417.
258. E.L. Muetterties and J. Stein, Chem. Revs., 1979, 79, 479.
259. E.C. Constable, B.F.G. Johnson, J. Lewis, G.N. Pain and M.J. Taylor, J. Chem. Soc., Chem. Commun., 1982, 754.
260. T. Chihara, R. Komoto, K. Kobayashi, H. Yamazaki and Y. Matsuura, Inorg. Chem., 1989, 28, 964.
261. C.E. Anson, P.J. Bailey, G. Conole, B.F.G. Johnson, J. Lewis, M. McPartlin and H. Powell, J. Chem. Soc., Chem. Commun., 1989, 442.
262. P.J. Bailey, M.J. Duer, B.F.G. Johnson, J. Lewis, G. Conole, M. McPartlin, H.R. Powell and C.E. Anson, J. Organometal. Chem., 1990, 383, 441.
263. A.G. Orpen, J. Chem. Soc., Dalton Trans., 1980, 2509.
264. S. Aime, L. Milone, D. Osella, G.A. Vaglio, M. Valle, A. Tiripicchio and M.T. Camellini, Inorg. Chem. Acta., 1979, 34, 49.

265. L.M. Bullock, J.S. Field, R.J. Haines, E. Minsel, D.N. Smit, G.M. Sheldrick, *J. Organometal. Chem.*, 1986, 310, C47.
266. G.R. Davies, J.A.J. Jarvis, B.T. Kilbourne, A. Pioli, *J. Chem. Soc., Chem. Commun.*, 1971, 667 and *J. Chem. Soc., Chem. Commun.*, 1971, 1511, *J. Am. Chem. Soc.*, 1971, 93, 3787.
267. U. Gianni, U. Zucchini, E. Albizzati, *J. Polym. Sci., Part B*, 1970, 8, 405.
268. R.D. Adams, J.E. Balsin, M. Tasi, *Angew. Chem. Int., Engl. Ed.*, 1987, 26, 685.
269. M. Manassero, M. Sansoni and G. Longoni, *J. Chem. Soc., Chem. Commun.*, 1976, 919.
270. P. Brun, G.M. Dawkins, M. Green, A.D. Miles, A.G. Orpen and F.G.A. Stone, *J. Chem. Soc., Chem. Commun.*, 1982, 926.
271. P.F. Jackson, B.F.G. Johnson, J. Lewis, M. McPartlin and W.J.H. Nelson, *J. Chem. Soc., Chem. Commun.*, 1980, 224.
272. S. Martinengo, G. Chiani, A. Sironi and P. Chini, *J. Am. Chem. Soc.*, 1978, 100, 7096.
273. R.W. Broach, L.F. Dahl, G. Longoni, P. Chini, A.J. Schultz and J.M. Williams, *Adv. Chem. Series*, 1978, 167, 93.
274. D.H. Farrar, P.G. Jackson, B.F.G. Johnson, J. Lewis, W.J.H. Nelson and M.D. Vargas, *J. Chem. Soc., Chem. Commun.*, 1981, 1009.

275. P.F. Jackson, B.F.G. Johnson, J. Lewis, M. McPartlin and W.J.H. Nelson, J. Chem. Soc., Chem. Commun., 1982, 49.
276. D. Braga, B.F.G. Johnson, J. Lewis, M. McPartlin, W.J.H. Nelson and M.D. Vargas, J. Chem. Soc., Chem. Commun., 1983, 241.
277. T. Adatia, Ph.D thesis (C.N.A.A.), 1988.
278. C. Bueno, M.R. Churchill, C.J. Hayward, A.L. Rheingold and J.R. Shapley, J. Am. Chem. Soc., 1982, 7347.
279. V.G. Albano, D. Braga, P. Chini, G. Ciani, S.J. Martinengo, J. Chem. Soc., Dalton Trans., 1982, 645.
280. V.G. Albano, M. Sansoni, P. Chini, S. Martinengo, D. Strumolo, J. Chem. Soc., Dalton Trans., 1976, 970.
281. V.G. Albano, D. Braga, G. Ciani, S. Martinengo, J. Organometal. Chem., 1981, 213, 293.
282. V.G. Albano, P. Chini, S. Martinengo, M. Sansoni, D. Strumolo, J. Chem. Soc., Dalton Trans., 1978, 459.
283. P.J. Bailey, E. Charalambous, J. Hoyle, B.F.G. Johnson, J. Lewis and M. McPartlin, J. Chem. Soc., Chem. Commun., 1990, in press.
284. P.J. Bailey, G. Conole, B.F.J. Johnson, J. Lewis, M. McPartlin, A. Moule, D. Wilkinson, J. Chem. Soc., Chem. Commun., 1990, to be submitted.
285. A.J. Deeming and M. Underhill, J. Chem. Soc., Dalton Trans., 1974, 1415.

286. A.J. Deeming and M. Underhill, J. Chem. Soc., Chem. Commun., 1973, 277
287. T.H. Whitesides and R.A. Budnik, J. Chem. Soc., Chem. Commun., 1973, 87.
288. A.J. Deeming and M. Underhill, J. Organometal. Chem., 1972, 42, C60.
289. M.I. Bruce, M.A. Cairns, A. Cox, M. Green, M.D.H. Smith and P. Woodward, Chem. Commun. 1970, 735.
290. M. Evans, M. Hursthouse, L. Miloni, E.W. Randell, E. Rosenberg and M. Valle, J. Chem. Soc., Chem. Commun., 1972, 545.
291. A.J. Canty, A.J.P. Domingos, B.F.G. Johnson and J. Lewis, J. Chem. Soc., Dalton Trans., 1973, 2056.
292. A.J. Canty, B.F.G. Johnson and J. Lewis, J. Organometal. Chem., 1972, 43, C35.
293. A.J.P. Domingos, B.F.G. Johnson and J. Lewis, J. Organometal. Chem., 1972, 36, C43.
294. M.R. Churchill and B.G. Deboer, Inorg. Chem., 1977, 16, 878.
295. R.W. Broach and J.M. Williams, Inorg. Chem., 1979, 18, 314.
296. A.J. Deeming, S. Hasso and M. Underhill, J. Chem. Soc., Dalton. Trans., 1975, 1614.
297. W.G. Jackson, B.F.G. Johnson, J.W. Kelland, J. Lewis and K.T. Schorpp, J. Organometal. Chem., 1975, 87, C27.

298. W.G. Jackson, B.F.G. Johnson, J.W. Kelland, J. Lewis and K.T. Schorpp, *J. Organometal. Chem.*, 1975, 88, C17.
299. J.A. Lunniss, Ph. D. Thesis, University of Cambridge, 1988.
300. J.J. Guy, E. Reichert and G.M. Sheldrick, *Acta. Cryst.*, 1976, B32, 3319.
301. E. Sappa, A. Tiripicchio and A.M. Mannetti, *J. Organometal. Chem.*, 1983, 249, 391.
302. M.I. Bruce, E. Horn, J.G. Matison and M.R. Snow, *J. Organometal. Chem.*, 1985, 286, 271.
303. V.G. Albano, P.L. Bellon and G.F. Ciani, *Chemical Communications*, 1969, 1024.
304. V.G. Albano, P.L. Bellon and G.F. Ciani, *J. Chem. Soc., Dalton Trans.*, 1988, 1103.
305. G.F. Ciani, G. D'Alfonso, M. Freni, P. Romiti and A. Sironi, *J. Chem. Soc., Chem. Commun.*, 1982, 339.
306. C.R. Eady, B.F.G. Jackson, J. Lewis, *J. Chem. Soc., Chem. Commun.*, 1977, 385.
307. B.F.G. Johnson, J. Lewis, M. McPartlin, J. Morris, G.L. Powell, P.R. Raithby and M.D. Vargas, *J. Chem. Soc., Chem. Commun.*, 1986, 429.
308. F. Van Gastel, N.J. Taylor and A.J. Carty, *J. Chem. Soc., Chem. Commun.*, 1987, 1049.

309. R.D. Adams, J.E. Babin and M. Tasi, *Organometallics*, 1988, 7, 503.

310. D. Stuart and N. Walker, *Acta Cryst.*, 1983, A39, 158.

Appendix A

Fractional coordinates and thermal parameters,
bond lengths (Å) and selected angles(°).

Table A1.1 Fractional atomic coordinates and thermal

parameters (\AA^2) for $\text{HRu}_5\text{C}(\text{CO})_{14}(\text{C}_5\text{H}_4\text{N})$ (XR1)

Atom	x	y	z	U_{iso} or U_{eq}
Ru(1)	0.00088(5)	0.21734(2)	0.17801(2)	0.0324(2)
Ru(2)	0.17168(5)	0.08988(2)	0.13602(2)	0.0327(2)
Ru(3)	0.21534(5)	0.22788(2)	0.31524(2)	0.0298(2)
Ru(4)	0.05755(5)	0.09292(2)	0.28397(2)	0.0308(2)
Ru(5)	0.42835(5)	0.14188(2)	0.23717(2)	0.0307(2)
C	0.1940(5)	0.1590(3)	0.2258(3)	0.028(2)
C(11)	-0.1509(7)	0.1983(4)	0.0927(4)	0.055(4)
O(11)	-0.2452(6)	0.1905(3)	0.0426(3)	0.086(4)
C(12)	-0.1243(7)	0.2894(3)	0.2222(4)	0.048(3)
O(12)	-0.2041(6)	0.3317(3)	0.2446(3)	0.076(3)
C(13)	0.1024(7)	0.2898(4)	0.1218(4)	0.051(3)
O(13)	0.1590(6)	0.3364(3)	0.0896(3)	0.094(4)
C(21)	0.2603(7)	-0.0083(3)	0.1401(3)	0.046(3)
O(21)	0.3089(6)	-0.0658(3)	0.1387(3)	0.079(3)
C(22)	-0.0132(7)	0.0512(4)	0.0849(4)	0.059(4)
O(22)	-0.1205(5)	0.0251(3)	0.0553(3)	0.091(3)
C(23)	0.2571(7)	0.1193(4)	0.0419(3)	0.049(3)
O(23)	0.3097(7)	0.1365(3)	-0.0122(3)	0.083(4)
C(31)	0.3284(7)	0.1960(3)	0.4107(3)	0.045(3)
O(31)	0.3923(6)	0.1738(3)	0.4653(2)	0.070(3)
C(32)	0.3237(6)	0.3201(3)	0.3024(3)	0.044(3)
O(32)	0.3939(5)	0.3713(3)	0.2932(3)	0.078(3)
C(33)	0.0630(7)	0.2718(4)	0.3731(3)	0.051(3)
O(33)	-0.0216(5)	0.2984(3)	0.4090(3)	0.085(3)
C(41)	-0.0418(7)	0.0019(3)	0.2561(4)	0.054(4)
O(41)	-0.0946(6)	-0.0542(3)	0.2419(4)	0.089(4)
C(42)	-0.0217(7)	0.1020(3)	0.3821(4)	0.049(3)
O(42)	-0.0675(6)	0.1048(3)	0.4413(3)	0.084(4)
C(51)	0.4587(6)	0.2222(3)	0.1689(3)	0.040(3)
O(51)	0.4803(5)	0.2694(2)	0.1280(3)	0.066(3)
C(52)	0.5856(6)	0.1801(3)	0.3133(3)	0.044(3)
O(52)	0.6755(5)	0.2040(3)	0.3580(3)	0.073(3)
C(53)	0.5526(6)	0.0770(3)	0.1804(3)	0.044(3)
O(53)	0.6230(5)	0.0402(3)	0.1453(3)	0.076(3)
N	0.3850(5)	0.0513(2)	0.3152(2)	0.035(2)
C(1)	0.2445(6)	0.0341(3)	0.3346(3)	0.036(3)
C(2)	0.2314(7)	-0.0226(3)	0.3887(3)	0.047(3)
C(3)	0.3552(8)	-0.0611(3)	0.4225(4)	0.057(4)
C(4)	0.4984(7)	-0.0438(3)	0.4002(4)	0.052(4)
C(5)	0.5087(7)	0.0119(3)	0.3477(3)	0.044(3)

For this and all subsequent Tables, values in parenthesis refer to estimated standard deviations (e.s.d.'s).

Table A1.2 Fractional atomic coordinates for the
hydrogen atoms for $\text{HRu}_5\text{C}(\text{CO})_{14}(\text{C}_5\text{H}_4\text{N})$ (XR1)

Atom	x	y	z
H	-0.0751	0.1447	0.2303
H(2)	0.1250	-0.0345	0.4027
H(3)	0.3542	-0.1015	0.4640
H(4)	0.5930	-0.0697	0.4193
H(5)	0.6080	0.0294	0.3303

Table A1.3 Anisotropic thermal parameters (\AA^2) for $\text{HRu}_5\text{C}(\text{CO})_{14}(\text{C}_5\text{H}_4\text{N})$ (XR1)

Atom	U_{11}	U_{22}	U_{33}	U_{23}	U_{13}	U_{12}
Ru(1)	0.0304(2)	0.0355(2)	0.0313(2)	0.0025(2)	0.0016(2)	0.0044(2)
Ru(2)	0.0348(2)	0.0346(2)	0.0287(2)	-0.0059(2)	0.0030(2)	0.0011(2)
Ru(3)	0.0329(2)	0.0277(2)	0.0288(2)	-0.0030(2)	0.0012(2)	0.0011(2)
Ru(4)	0.0297(2)	0.0294(2)	0.0335(2)	0.0011(2)	0.0058(2)	-0.0016(2)
Ru(5)	0.0266(2)	0.0319(2)	0.0335(2)	0.0032(2)	0.0042(2)	0.0013(2)
C	0.030(2)	0.029(2)	0.026(2)	-0.001(S)	0.003(2)	-0.002(2)
C(11)	0.044(3)	0.073(4)	0.048(3)	0.003(3)	0.005(3)	0.010(3)
O(11)	0.063(3)	0.137(5)	0.058(3)	-0.016(3)	-0.023(3)	0.003(3)
C(12)	0.047(3)	0.045(3)	0.051(3)	0.000(3)	0.002(3)	0.007(3)
O(12)	0.078(3)	0.071(3)	0.080(3)	-0.007(3)	0.014(3)	0.028(3)
C(13)	0.044(3)	0.054(4)	0.054(3)	0.018(3)	0.005(3)	0.009(3)
O(13)	0.079(4)	0.098(4)	0.104(4)	0.052(4)	0.024(3)	0.001(3)
C(21)	0.049(3)	0.042(3)	0.046(3)	-0.002(3)	0.009(3)	-0.004(3)
O(21)	0.084(4)	0.041(3)	0.111(4)	0.005(3)	0.012(3)	0.010(2)
C(22)	0.050(4)	0.071(4)	0.055(3)	-0.034(3)	0.016(3)	-0.002(3)
O(22)	0.045(3)	0.139(4)	0.090(3)	-0.075(3)	0.006(2)	-0.017(3)
C(23)	0.059(4)	0.052(4)	0.037(3)	0.000(3)	0.001(3)	0.007(3)
O(23)	0.110(4)	0.091(4)	0.048(3)	0.016(3)	0.027(3)	0.001(3)
C(31)	0.048(3)	0.046(3)	0.039(3)	-0.001(3)	0.004(3)	0.006(3)
O(31)	0.086(3)	0.087(4)	0.037(2)	0.006(2)	-0.014(2)	0.020(3)
C(32)	0.042(3)	0.039(3)	0.052(3)	-0.003(3)	-0.002(3)	0.008(3)
O(32)	0.068(3)	0.039(2)	0.127(4)	-0.001(3)	0.007(3)	-0.019(2)

Table A1.3 continued

C(33)	0.043(3)	0.063(4)	0.048(3)	-0.017(3)	0.004(3)	0.008(3)
O(33)	0.056(3)	0.118(4)	0.082(3)	-0.045(3)	0.016(3)	0.015(3)
C(41)	0.045(3)	0.044(3)	0.072(4)	0.002(3)	0.003(3)	-0.009(3)
O(41)	0.083(3)	0.045(3)	0.139(5)	0.001(3)	-0.019(3)	-0.033(2)
C(42)	0.045(3)	0.055(4)	0.048(3)	0.008(3)	0.007(3)	0.009(3)
O(42)	0.090(4)	0.109(4)	0.052(3)	0.016(3)	0.034(3)	0.014(3)
C(51)	0.034(3)	0.045(3)	0.039(3)	0.004(3)	0.002(2)	-0.003(2)
O(51)	0.072(3)	0.061(3)	0.066(3)	0.024(2)	0.018(2)	-0.009(2)
C(52)	0.035(3)	0.052(3)	0.046(3)	0.003(3)	0.001(3)	0.001(3)
O(52)	0.049(3)	0.094(4)	0.075(3)	-0.014(3)	-0.011(2)	-0.010(3)
C(53)	0.041(3)	0.039(3)	0.051(3)	0.003(3)	0.007(3)	0.001(2)
O(53)	0.066(3)	0.066(3)	0.096(3)	-0.012(3)	0.039(3)	0.016(2)
N	0.042(3)	0.030(2)	0.034(2)	0.004(2)	0.003(2)	0.005(2)
C(1)	0.044(3)	0.028(3)	0.036(3)	-0.001(2)	0.001(2)	0.000(2)
C(2)	0.049(3)	0.041(3)	0.050(3)	0.009(3)	0.009(3)	0.001(3)
C(3)	0.077(5)	0.043(3)	0.051(3)	0.015(3)	0.003(3)	0.007(3)
C(4)	0.054(4)	0.050(4)	0.053(3)	0.009(3)	-0.001(3)	0.015(3)
C(5)	0.044(3)	0.040(3)	0.048(3)	0.002(3)	0.000(3)	0.012(3)

Table A1.4 Bond lengths (\AA) for $\text{HRu}_5\text{C}(\text{CO})_{14}(\text{C}_5\text{H}_4\text{N})$ (XR1)

Ru(1) -Ru(2)	2.877(1)	Ru(1) -Ru(3)	2.882(1)
Ru(1) -Ru(4)	2.895(1)	Ru(1) -C	2.102(5)
Ru(1) -C(11)	1.918(6)	Ru(1) -C(12)	1.912(6)
Ru(1) -C(13)	1.901(6)	Ru(2) -Ru(4)	2.833(1)
Ru(2) -Ru(5)	2.876(1)	Ru(2) -C	1.975(5)
Ru(2) -C(21)	1.929(6)	Ru(2) -C(22)	1.910(6)
Ru(2) -C(23)	1.930(6)	Ru(3) -Ru(4)	2.823(1)
Ru(3) -Ru(5)	2.876(1)	Ru(3) -C	1.969(5)
Ru(3) -C(31)	1.922(5)	Ru(3) -C(32)	1.939(6)
Ru(3) -C(33)	1.926(6)	Ru(4) -C	2.030(5)
Ru(4) -C(41)	1.896(6)	Ru(4) -C(42)	1.900(6)
Ru(4) -C(1)	2.080(5)	Ru(5) -C	2.089(5)
Ru(5) -C(51)	1.897(6)	Ru(5) -C(52)	1.938(6)
Ru(5) -C(53)	1.935(6)	Ru(5) -N	2.169(4)
C(11) -O(11)	1.146(8)	C(12) -O(12)	1.131(8)
C(13) -O(13)	1.148(9)	C(21) -O(21)	1.121(8)
C(22) -O(22)	1.134(8)	C(23) -O(23)	1.124(8)
C(31) -O(31)	1.119(7)	C(32) -O(32)	1.131(8)
C(33) -O(33)	1.125(8)	C(41) -O(41)	1.127(8)
C(42) -O(42)	1.135(8)	C(51) -O(51)	1.130(7)
C(52) -O(52)	1.134(7)	C(53) -O(53)	1.126(8)
N -C(1)	1.357(7)	N -C(5)	1.375(7)
C(1) -C(2)	1.393(8)	C(2) -C(3)	1.375(9)
C(3) -C(4)	1.398(10)	C(4) -C(5)	1.357(9)

Table A1.5 Bond angles ($^{\circ}$) for $\text{HRu}_5\text{C}(\text{CO})_{14}(\text{C}_5\text{H}_4\text{N})$ (XR1)

C(1)	-Ru(4)	-Ru(3)	89.9(1)	N	-Ru(5)	-Ru(2)	87.2(1)
N	-Ru(5)	-Ru(3)	87.0(1)	O(11)	-C(11)	-Ru(1)	176.4(6)
O(12)	-C(12)	-Ru(1)	176.0(5)	O(13)	-C(13)	-Ru(1)	176.2(6)
O(21)	-C(21)	-Ru(2)	176.6(5)	O(22)	-C(22)	-Ru(2)	176.9(6)
O(23)	-C(23)	-Ru(2)	178.6(6)	O(31)	-C(31)	-Ru(3)	176.5(5)
O(32)	-C(32)	-Ru(3)	175.7(5)	O(33)	-C(33)	-Ru(3)	177.3(5)
O(41)	-C(41)	-Ru(4)	176.2(6)	O(42)	-C(42)	-Ru(4)	177.5(6)
O(51)	-C(51)	-Ru(5)	178.2(5)	O(52)	-C(52)	-Ru(5)	178.3(5)
O(53)	-C(53)	-Ru(5)	177.9(5)	C(1)	-N	-Ru(5)	123.1(3)
C(5)	-N	-Ru(5)	117.0(4)	C(5)	-N	-C(1)	119.8(4)
N	-C(1)	-Ru(4)	119.6(4)	C(2)	-C(1)	-Ru(4)	122.3(4)
C(2)	-C(1)	-N	118.1(5)	C(3)	-C(2)	-C(1)	122.3(6)
C(4)	-C(3)	-C(2)	118.6(6)	C(5)	-C(4)	-C(3)	118.1(6)
C(4)	-C(5)	-N	123.1(6)				

Table A2.1 Fractional atomic coordinates and thermal

parameters (\AA^2) for $\text{HRu}_5\text{C}(\text{CO})_{14}(\text{C}_5\text{H}_4\text{N})$ (XR2)

Atom	x	y	z	U_{iso} or U_{eq}
Ru(1a)	0.33372(5)	0.14717(5)	0.06921(15)	0.0409(8)
Ru(2a)	0.37698(5)	0.23655(6)	-0.09170(16)	0.0464(8)
Ru(3a)	0.17602(5)	0.21375(5)	-0.13102(15)	0.0410(8)
Ru(4a)	0.24054(5)	0.32237(5)	0.02702(15)	0.0379(8)
Ru(5a)	0.24509(5)	0.24317(6)	-0.34136(16)	0.0444(9)
Ca	0.2764(6)	0.2246(6)	-0.1139(17)	0.037(3)
C(11a)	0.4291(8)	0.1263(8)	0.2240(20)	0.070(4)
O(11a)	0.4854(6)	0.1132(6)	0.3219(14)	0.091(3)
C(12a)	0.2920(8)	0.1044(9)	0.1818(21)	0.074(4)
O(12a)	0.2704(7)	0.0734(7)	0.2424(16)	0.111(4)
C(13a)	0.3828(7)	0.0457(8)	-0.0281(20)	0.066(4)
O(13a)	0.4112(6)	-0.0169(6)	-0.0856(14)	0.091(3)
C(21a)	0.3725(8)	0.3300(8)	-0.1703(20)	0.063(4)
O(21a)	0.3688(6)	0.3901(7)	-0.2118(14)	0.098(3)
C(22a)	0.4558(8)	0.2414(8)	0.0763(20)	0.063(4)
O(22a)	0.5053(6)	0.2462(6)	0.1785(15)	0.100(4)
C(23a)	0.4534(8)	0.1513(9)	-0.1888(20)	0.072(4)
O(23a)	0.4948(6)	0.0946(6)	-0.2428(14)	0.089(3)
C(31a)	0.0781(7)	0.3028(7)	-0.2278(18)	0.052(3)
O(31a)	0.0195(5)	0.3588(5)	-0.2801(12)	0.068(3)
C(32a)	0.1634(8)	0.1238(8)	-0.2443(20)	0.064(4)
O(32a)	0.1553(6)	0.0699(7)	-0.3192(15)	0.096(3)
C(33a)	0.1289(9)	0.2035(9)	0.0167(23)	0.073(5)
O(33a)	0.0998(7)	0.2003(7)	0.1028(17)	0.115(4)
C(41a)	0.2949(7)	0.3830(8)	0.1389(19)	0.065(4)
O(41a)	0.3308(5)	0.4191(6)	0.2093(13)	0.081(3)
C(42a)	0.1558(9)	0.3687(9)	0.1177(22)	0.078(4)
O(42a)	0.1034(8)	0.3968(8)	0.1782(16)	0.121(4)
C(51a)	0.3026(8)	0.1222(9)	-0.3824(20)	0.075(4)
O(51a)	0.3338(6)	0.0532(7)	-0.4057(15)	0.101(4)
C(52a)	0.1527(8)	0.2543(8)	-0.4926(20)	0.062(4)
O(52a)	0.0930(6)	0.2624(6)	-0.5776(14)	0.085(3)
C(53a)	0.2941(9)	0.2686(9)	-0.4628(23)	0.087(5)
O(53a)	0.3225(7)	0.2896(7)	-0.5284(16)	0.110(4)
Na	0.1803(5)	0.4035(5)	-0.1614(15)	0.042(2)
C(1a)	0.1813(6)	0.3747(7)	-0.3007(19)	0.041(3)
C(2a)	0.1400(8)	0.4306(8)	-0.4131(19)	0.064(4)
C(3a)	0.0946(8)	0.5156(8)	-0.3913(22)	0.067(4)
C(4a)	0.0904(7)	0.5430(8)	-0.2469(22)	0.062(4)
C(5a)	0.1346(7)	0.4869(7)	-0.1355(18)	0.055(3)

Table A2.1 continued

Ru(1b)	0.67840(6)	0.35507(6)	0.88030(16)	0.0532(9)
Ru(2b)	0.82274(6)	0.19941(6)	0.92050(17)	0.0538(9)
Ru(3b)	0.65154(5)	0.31932(5)	0.57212(16)	0.0425(8)
Ru(4b)	0.79938(5)	0.32180(5)	0.73163(15)	0.0405(8)
Ru(5b)	0.75542(5)	0.14295(5)	0.63602(16)	0.0498(8)
Cb	0.7362(6)	0.2575(6)	0.7444(16)	0.044(3)
C(11b)	0.7098(9)	0.3891(9)	1.0809(24)	0.083(5)
O(11b)	0.7292(8)	0.4092(8)	1.1984(19)	0.132(5)
C(12b)	0.5887(8)	0.4612(9)	0.8368(20)	0.074(4)
O(12b)	0.5327(7)	0.5270(7)	0.8131(16)	0.110(4)
C(13b)	0.6155(9)	0.3113(9)	0.9222(21)	0.086(5)
O(13b)	0.5734(7)	0.2848(7)	0.9412(16)	0.106(4)
C(21b)	0.9261(9)	0.1211(9)	0.9012(21)	0.077(4)
O(21b)	0.9886(7)	0.0755(7)	0.8801(15)	0.104(4)
C(22b)	0.8691(9)	0.2456(10)	1.0853(23)	0.088(5)
O(22b)	0.9018(7)	0.2725(7)	1.1869(17)	0.121(4)
C(23b)	0.8050(10)	0.1303(11)	1.0219(25)	0.114(6)
O(23b)	0.7913(7)	0.0858(8)	1.0795(17)	0.122(4)
C(31b)	0.6703(8)	0.2907(9)	0.3788(30)	0.070(5)
O(31b)	0.6856(7)	0.2751(7)	0.2699(18)	0.100(4)
C(32b)	0.5521(7)	0.3095(7)	0.5293(19)	0.061(4)
O(32b)	0.4935(5)	0.2991(6)	0.5099(13)	0.082(3)
C(33b)	0.6052(7)	0.4347(7)	0.5288(18)	0.056(3)
O(33b)	0.5811(5)	0.5044(5)	0.4976(13)	0.071(3)
C(41b)	0.8913(6)	0.3278(7)	0.8617(17)	0.051(3)
O(41b)	0.9455(5)	0.3361(5)	0.9416(13)	0.072(3)
C(42b)	0.7798(7)	0.4087(7)	0.6093(18)	0.056(3)
O(42b)	0.7679(5)	0.4633(6)	0.5426(13)	0.082(3)
C(51b)	0.6763(8)	0.1333(8)	0.7141(21)	0.074(4)
O(51b)	0.6295(7)	0.1276(7)	0.7564(16)	0.119(4)
C(52b)	0.7112(7)	0.1161(8)	0.4445(21)	0.063(4)
O(52b)	0.6820(6)	0.1032(6)	0.3230(15)	0.085(3)
C(53b)	0.8314(7)	0.0306(8)	0.6895(19)	0.058(3)
O(53b)	0.8792(5)	-0.0374(6)	0.7182(13)	0.081(3)
Nb	0.8612(5)	0.2232(5)	0.5972(13)	0.041(2)
C(1b)	0.8419(6)	0.1575(6)	0.5573(16)	0.038(3)
C(2b)	0.8845(6)	0.0960(7)	0.4640(17)	0.050(3)
C(3b)	0.9448(7)	0.0992(7)	0.4160(19)	0.061(4)
C(4b)	0.9628(6)	0.1662(7)	0.4618(18)	0.051(3)
C(5b)	0.9198(6)	0.2265(7)	0.5451(17)	0.048(3)

Table A2.2 Fractional atomic coordinates for the
hydrogen atoms for $\text{HRu}_5\text{C}(\text{CO})_{14}(\text{C}_5\text{H}_4\text{N})$ (XR2)

Atom	x	y	z
Ha	0.2916	0.2446	0.1770
H(2a)	0.1423	0.4096	-0.5286
H(3a)	0.0596	0.5610	-0.4803
H(4a)	0.0529	0.6089	-0.2258
H(5a)	0.1331	0.5101	-0.0268
Hb	0.7363	0.3935	0.8335
H(2b)	0.8692	0.0448	0.4274
H(3b)	0.9767	0.0507	0.3472
H(4b)	1.0104	0.1705	0.4257
H(5b)	0.9304	0.2832	0.5749

Table A2.3 Anisotropic thermal parameters (\AA^2) for $\text{HRu}_5\text{C}(\text{CO})_{14}(\text{C}_5\text{H}_4\text{N})$ (XR2)

Atom	U_{11}	U_{22}	U_{33}	U_{23}	U_{13}	U_{12}
Ru(1a)	0.043(1)	0.040(1)	0.040(1)	0.003(1)	0.005(1)	-0.011(1)
Ru(2a)	0.037(1)	0.053(1)	0.050(1)	-0.002(1)	0.009(1)	-0.019(1)
Ru(3a)	0.037(1)	0.041(1)	0.045(1)	0.004(1)	0.007(1)	-0.016(1)
Ru(4a)	0.043(1)	0.038(1)	0.032(1)	-0.002(1)	0.009(1)	-0.014(1)
Ru(5a)	0.046(1)	0.054(1)	0.034(1)	-0.004(1)	0.012(1)	-0.021(1)
Ru(1b)	0.056(1)	0.052(1)	0.051(2)	-0.005(1)	0.022(1)	-0.025(1)
Ru(2b)	0.057(1)	0.050(1)	0.054(1)	0.014(1)	0.008(1)	-0.023(1)
Ru(3b)	0.038(1)	0.041(1)	0.048(2)	0.001(1)	0.009(1)	-0.016(1)
Ru(4b)	0.041(1)	0.037(1)	0.043(1)	-0.001(1)	0.011(1)	-0.020(1)
Ru(5b)	0.045(1)	0.037(1)	0.068(1)	-0.001(1)	0.017(1)	-0.022(1)

Table A2.4 Bond lengths (Å) for $\text{HRu}_5\text{C}(\text{CO})_{14}(\text{C}_5\text{H}_4\text{N})$ (XR2)

Ru(1a)-Ru(2a)	2.853(2)	Ru(1a)-Ru(3a)	2.864(1)
Ru(1a)-Ru(4a)	2.830(1)	Ru(1a)-Ca	2.080(14)
Ru(1a)-C(11a)	1.903(14)	Ru(1a)-C(12a)	1.902(22)
Ru(1a)-C(13a)	1.873(14)	Ru(2a)-Ru(4a)	2.824(2)
Ru(2a)-Ru(5a)	2.894(2)	Ru(2a)-Ca	1.977(12)
Ru(2a)-C(21a)	1.877(18)	Ru(2a)-C(22a)	1.877(15)
Ru(2a)-C(23a)	1.914(15)	Ru(3a)-Ru(4a)	2.803(1)
Ru(3a)-Ru(5a)	2.899(2)	Ru(3a)-Ca	1.972(13)
Ru(3a)-C(31a)	1.896(10)	Ru(3a)-C(32a)	1.879(16)
Ru(3a)-C(33a)	1.934(24)	Ru(4a)-Ru(5a)	3.593(2)
Ru(4a)-Ca	2.025(12)	Ru(4a)-C(41a)	1.859(15)
Ru(4a)-C(42a)	1.849(19)	Ru(4a)-Na	2.154(12)
Ru(5a)-Ca	2.098(16)	Ru(5a)-C(51a)	1.972(14)
Ru(5a)-C(52a)	1.879(14)	Ru(5a)-C(53a)	1.884(23)
Ru(5a)-C(1a)	2.140(11)	C(11a)-O(11a)	1.155(18)
C(12a)-O(12a)	1.11(3)	C(13a)-O(13a)	1.137(17)
C(21a)-O(21a)	1.160(22)	C(22a)-O(22a)	1.170(19)
C(23a)-O(23a)	1.129(18)	C(31a)-O(31a)	1.141(12)
C(32a)-O(32a)	1.156(20)	C(33a)-O(33a)	1.13(3)
C(41a)-O(41a)	1.164(19)	C(42a)-O(42a)	1.173(25)
C(51a)-O(51a)	1.121(17)	C(52a)-O(52a)	1.153(17)
C(53a)-O(53a)	1.12(3)	Na -C(1a)	1.352(22)
Na -C(5a)	1.373(13)	C(1a) -C(2a)	1.362(22)
C(2a) -C(3a)	1.387(17)	C(3a) -C(4a)	1.40(3)
C(4a) -C(5a)	1.360(22)		
Ru(1b)-Ru(2b)	2.866(1)	Ru(1b)-Ru(3b)	2.853(2)
Ru(1b)-Ru(4b)	2.838(2)	Ru(1b)-Cb	2.089(12)
Ru(1b)-C(11b)	1.926(21)	Ru(1b)-C(12b)	1.889(12)
Ru(1b)-C(13b)	1.849(21)	Ru(2b)-Ru(4b)	2.814(2)
Ru(2b)-Ru(5b)	2.899(2)	Ru(2b)-Cb	1.986(12)
Ru(2b)-C(21b)	1.876(14)	Ru(2b)-C(22b)	1.851(19)
Ru(2b)-C(23b)	1.86(3)	Ru(3b)-Ru(4b)	2.815(1)
Ru(3b)-Ru(5b)	2.898(1)	Ru(3b)-Cb	1.968(12)
Ru(3b)-C(31b)	1.92(3)	Ru(3b)-C(32b)	1.910(15)
Ru(3b)-C(33b)	1.889(13)	Ru(4b)-Ru(5b)	3.599(1)
Ru(4b)-Cb	2.043(14)	Ru(4b)-C(41b)	1.876(12)
Ru(4b)-C(42b)	1.901(17)	Ru(4b)-Nb	2.115(10)
Ru(5b)-Cb	2.083(11)	Ru(5b)-C(51b)	1.941(21)
Ru(5b)-C(52b)	1.869(17)	Ru(5b)-C(53b)	1.901(11)
Ru(5b)-C(1b)	2.121(15)	C(11b)-O(11b)	1.13(3)
C(12b)-O(12b)	1.171(15)	C(13b)-O(13b)	1.16(3)
C(21b)-O(21b)	1.155(19)	C(22b)-O(22b)	1.163(23)
C(23b)-O(23b)	1.18(3)	C(31b)-O(31b)	1.12(3)
C(32b)-O(32b)	1.175(20)	C(33b)-O(33b)	1.164(16)
C(41b)-O(41b)	1.153(16)	C(42b)-O(42b)	1.135(20)
C(51b)-O(51b)	1.13(3)	C(52b)-O(52b)	1.171(21)
C(53b)-O(53b)	1.151(14)	Nb -C(1b)	1.359(16)
Nb -C(5b)	1.371(20)	C(1b) -C(2b)	1.409(18)
C(2b) -C(3b)	1.378(24)	C(3b) -C(4b)	1.373(20)
C(4b) -C(5b)	1.340(19)		

Table A2.5 Bond angles ($^{\circ}$) for $\text{HRu}_5\text{C}(\text{CO})_{14}(\text{C}_5\text{H}_4\text{N})$ (XR2)

Na	-Ru(4a)-Ru(1a)	134.9(3)	Na	-Ru(4a)-Ru(2a)	89.0(3)	
Na	-Ru(4a)-Ru(3a)	88.2(3)	Na	-Ru(4a)-Ru(5a)	57.8(3)	
C(1a)	-Ru(5a)-Ru(2a)	89.0(4)	C(1a)	-Ru(5a)-Ru(3a)	87.7(5)	
C(1a)	-Ru(5a)-Ru(4a)	59.3(5)	O(11a)	-C(11a)-Ru(1a)	177(2)	
O(12a)	-C(12a)-Ru(1a)	174(1)	O(13a)	-C(13a)-Ru(1a)	178(2)	
O(21a)	-C(21a)-Ru(2a)	176(1)	O(22a)	-C(22a)-Ru(2a)	178(2)	
O(23a)	-C(23a)-Ru(2a)	171(2)	O(31a)	-C(31a)-Ru(3a)	177(1)	
O(32a)	-C(32a)-Ru(3a)	177(2)	O(33a)	-C(33a)-Ru(3a)	178(1)	
O(41a)	-C(41a)-Ru(4a)	178.2(9)	O(42a)	-C(42a)-Ru(4a)	178(1)	
O(51a)	-C(51a)-Ru(5a)	178(2)	O(52a)	-C(52a)-Ru(5a)	175(2)	
O(53a)	-C(53a)-Ru(5a)	174(1)	C(1a)	-Na	-Ru(4a)	123.0(7)
C(5a)	-Na	-Ru(4a)	C(5a)	-Na	-C(1a)	120(1)
Na	-C(1a)	-Ru(5a)	C(2a)	-C(1a)	-Ru(5a)	121(1)
C(2a)	-C(1a)	-Na	C(3a)	-C(2a)	-C(1a)	123(2)
C(4a)	-C(3a)	-C(2a)	C(5a)	-C(4a)	-C(3a)	119(1)
C(4a)	-C(5a)	-Na	Nb	-Ru(4b)-Ru(1b)	135.4(3)	
Nb	-Ru(4b)-Ru(2b)	88.3(3)	Nb	-Ru(4b)-Ru(3b)	89.8(2)	
Nb	-Ru(4b)-Ru(5b)	58.5(3)	C(1b)	-Ru(5b)-Ru(3b)	86.9(2)	
C(1b)	-Ru(5b)-Ru(4b)	57.7(3)	O(11b)	-C(11b)-Ru(1b)	179(2)	
O(12b)	-C(12b)-Ru(1b)	178(2)	O(13b)	-C(13b)-Ru(1b)	176(1)	
O(21b)	-C(21b)-Ru(2b)	175(2)	O(22b)	-C(22b)-Ru(2b)	177(2)	
O(23b)	-C(23b)-Ru(2b)	177(2)	O(31b)	-C(31b)-Ru(3b)	175(2)	
O(32b)	-C(32b)-Ru(3b)	175(1)	O(33b)	-C(33b)-Ru(3b)	175(1)	
O(41b)	-C(41b)-Ru(4b)	176.3(9)	O(42b)	-C(42b)-Ru(4b)	176(1)	
O(51b)	-C(51b)-Ru(5b)	178(1)	O(52b)	-C(52b)-Ru(5b)	177(1)	
O(53b)	-C(53b)-Ru(5b)	177(2)	C(1b)	-Nb	-Ru(4b)	121(1)
C(5b)	-Nb	-Ru(4b)	C(5b)	-Nb	-C(1b)	119(1)
Nb	-C(1b)	-Ru(5b)	C(2b)	-C(1b)	-Ru(5b)	120(1)
C(2b)	-C(1b)	-Nb	C(3b)	-C(2b)	-C(1b)	123(1)
C(4b)	-C(3b)	-C(2b)	C(5b)	-C(4b)	-C(3b)	119(1)
C(4b)	-C(5b)	-Nb				

Table A3.1 Fractional atomic coordinates and thermal

parameters (\AA^2) for $\text{HRu}_5\text{C}(\text{CO})_{13}(\text{C}_5\text{H}_4\text{N})(\text{C}_5\text{H}_5\text{N})$ (XR3)

Atom	x	y	z	U_{iso} or U_{eq}
Ru(1)	0.06877(4)	0.09445(4)	0.26521(7)	0.0380(4)
Ru(2)	0.04512(4)	0.22468(4)	0.43588(7)	0.0376(4)
Ru(3)	0.14722(4)	0.21044(4)	0.12165(7)	0.0370(4)
Ru(4)	-0.00412(4)	0.24553(4)	0.18019(6)	0.0350(4)
Ru(5)	0.17637(4)	0.30743(4)	0.34480(6)	0.0324(4)
N(1)	0.0946(4)	0.3924(4)	0.2492(6)	0.037(4)
C(1)	0.0227(5)	0.3691(5)	0.1948(8)	0.039(5)
C(2)	-0.0277(5)	0.4300(6)	0.1453(9)	0.049(6)
C(3)	-0.0083(6)	0.5115(6)	0.1514(10)	0.057(6)
C(4)	0.0654(7)	0.5327(6)	0.1979(10)	0.066(7)
C(5)	0.1150(6)	0.4722(5)	0.2474(9)	0.051(6)
N(2)	0.2026(4)	0.3910(4)	0.5054(7)	0.040(4)
C(6)	0.1566(6)	0.4516(7)	0.5358(10)	0.062(7)
C(7)	0.1750(7)	0.5019(7)	0.6366(11)	0.069(7)
C(8)	0.2406(7)	0.4922(8)	0.7100(12)	0.086(9)
C(9)	0.2888(7)	0.4325(9)	0.6784(13)	0.099(10)
C(10)	0.2690(6)	0.3855(7)	0.5773(11)	0.072(8)
C	0.0980(4)	0.2193(5)	0.2813(7)	0.034(2)
C(11)	-0.0041(6)	0.0287(6)	0.3348(9)	0.053(2)
O(11)	-0.0520(4)	-0.0123(4)	0.3715(7)	0.071(2)
C(12)	0.0798(6)	0.0167(6)	0.1372(9)	0.055(3)
O(12)	0.0870(4)	-0.0333(5)	0.0658(8)	0.079(2)
C(13)	0.1529(5)	0.0526(6)	0.3746(9)	0.051(2)
O(13)	0.2027(4)	0.0260(5)	0.4422(7)	0.075(2)
C(21)	0.0079(6)	0.3258(6)	0.4834(9)	0.053(2)
O(21)	-0.0186(5)	0.3875(5)	0.5095(8)	0.086(2)
C(22)	-0.0462(7)	0.1721(7)	0.4805(11)	0.068(3)
O(22)	-0.1039(5)	0.1439(5)	0.4998(8)	0.097(3)
C(23)	0.1083(6)	0.2024(7)	0.5859(11)	0.063(3)
O(23)	0.1505(6)	0.1905(6)	0.6756(9)	0.106(3)
C(31)	0.1605(6)	0.3042(6)	0.0240(10)	0.059(3)
O(31)	0.1684(4)	0.3614(5)	-0.0353(7)	0.079(2)
C(32)	0.2491(6)	0.1692(7)	0.1190(10)	0.062(3)
O(32)	0.3134(5)	0.1475(6)	0.1174(9)	0.100(3)
C(33)	0.1074(6)	0.1522(6)	-0.0235(10)	0.062(3)
O(33)	0.0799(5)	0.1183(5)	-0.1106(8)	0.083(2)
C(41)	-0.1027(6)	0.2642(6)	0.2349(9)	0.052(2)
O(41)	-0.1611(5)	0.2812(5)	0.2679(8)	0.084(2)
C(42)	-0.0356(5)	0.2535(6)	0.0090(9)	0.052(2)
O(42)	-0.0548(4)	0.2592(5)	-0.0987(8)	0.075(2)
C(51)	0.2426(5)	0.2284(5)	0.4196(8)	0.045(2)
O(51)	0.2852(4)	0.1797(4)	0.4637(7)	0.063(2)
C(52)	0.2596(5)	0.3501(6)	0.2649(9)	0.047(2)
O(52)	0.3137(4)	0.3703(5)	0.2200(7)	0.077(2)

Table A3.2 Fractional atomic coordinates for the

hydrogen atoms for $\text{HRu}_5\text{C}(\text{CO})_{13}(\text{C}_5\text{H}_4\text{N})(\text{C}_5\text{H}_5\text{N})$ (XR3)

Atom	x	y	z
H	-0.0152	0.1337	0.1613
H(2)	-0.0841	0.4130	0.1013
H(3)	-0.0497	0.5579	0.1195
H(4)	0.0846	0.5952	0.1965
H(5)	0.1728	0.4888	0.2861
H(6)	0.1026	0.4619	0.4780
H(7)	0.1358	0.5501	0.6563
H(8)	0.2547	0.5302	0.7914
H(9)	0.3432	0.4222	0.7344
H(10)	0.3098	0.3406	0.5503

Table A3.3 Anisotropic thermal parameters (\AA^2) for

$\text{HRu}_5\text{C}(\text{CO})_{13}(\text{C}_5\text{H}_4\text{N})(\text{C}_5\text{H}_5\text{N}) (\text{XR3})$

Atom	U_{11}	U_{22}	U_{33}	U_{23}	U_{13}	U_{12}
Ru(1)	0.0440(4)	0.0306(4)	0.0394(4)	0.0030(3)	-0.0005(3)	-0.0029(3)
Ru(2)	0.0380(4)	0.0414(4)	0.0334(4)	0.0031(3)	0.0073(3)	-0.0039(3)
Ru(3)	0.0405(4)	0.0363(4)	0.0342(4)	0.0015(3)	0.0077(3)	0.0038(3)
Ru(4)	0.0316(4)	0.0377(4)	0.0356(4)	0.0021(3)	0.0000(3)	0.0007(3)
Ru(5)	0.0304(3)	0.0312(4)	0.0357(4)	0.0022(3)	0.0027(3)	-0.0005(3)
N(1)	0.041(4)	0.027(4)	0.042(4)	0.007(3)	0.004(3)	0.000(3)
C(1)	0.043(5)	0.036(5)	0.037(5)	0.009(4)	0.011(4)	0.011(4)
C(2)	0.052(6)	0.050(6)	0.046(5)	0.000(5)	-0.001(5)	0.015(5)
C(3)	0.059(7)	0.049(6)	0.062(7)	0.010(5)	-0.001(5)	0.016(5)
C(4)	0.116(10)	0.025(5)	0.058(7)	0.004(5)	-0.005(7)	0.004(6)
C(5)	0.062(6)	0.036(5)	0.054(6)	0.001(5)	0.005(5)	-0.004(4)
N(2)	0.034(4)	0.038(4)	0.047(4)	-0.002(3)	0.000(3)	0.005(3)
C(6)	0.054(6)	0.073(7)	0.060(7)	-0.001(6)	0.001(5)	-0.002(6)
C(7)	0.069(7)	0.071(8)	0.068(7)	-0.021(6)	-0.003(6)	0.009(6)
C(8)	0.082(9)	0.095(10)	0.081(9)	-0.043(8)	-0.002(8)	0.002(8)
C(9)	0.084(9)	0.119(12)	0.093(10)	-0.047(9)	-0.044(8)	0.015(8)
C(10)	0.066(7)	0.066(7)	0.084(8)	-0.025(6)	-0.025(7)	0.020(6)

Table A3.4 Bond lengths (Å) for HRu₅C(CO)₁₃(C₅H₄N)(C₅H₅N) (XR3)

Ru(1) -Ru(2)	2.870(1)	Ru(1) -Ru(3)	2.876(1)
Ru(1) -Ru(4)	2.886(1)	Ru(1) -C	2.113(8)
Ru(1) -C(11)	1.873(10)	Ru(1) -C(12)	1.899(10)
Ru(1) -C(13)	1.902(9)	Ru(2) -Ru(4)	2.807(1)
Ru(2) -Ru(5)	2.903(1)	Ru(2) -C	1.978(8)
Ru(2) -C(21)	1.869(10)	Ru(2) -C(22)	1.906(12)
Ru(2) -C(23)	1.886(11)	Ru(3) -Ru(4)	2.818(1)
Ru(3) -Ru(5)	2.875(1)	Ru(3) -C	1.995(8)
Ru(3) -C(31)	1.888(11)	Ru(3) -C(32)	1.894(11)
Ru(3) -C(33)	1.895(11)	Ru(4) -C	2.023(7)
Ru(4) -C(41)	1.887(10)	Ru(4) -C(42)	1.865(10)
Ru(4) -C(1)	2.083(8)	Ru(5) -C	2.050(8)
Ru(5) -C(51)	1.857(9)	Ru(5) -C(52)	1.887(10)
Ru(5) -N(1)	2.168(6)	Ru(5) -N(2)	2.212(7)
C(11) -O(11)	1.168(13)	C(12) -O(12)	1.137(13)
C(13) -O(13)	1.153(12)	C(21) -O(21)	1.159(13)
C(22) -O(22)	1.140(15)	C(23) -O(23)	1.163(14)
C(31) -O(31)	1.150(13)	C(32) -O(32)	1.172(14)
C(33) -O(33)	1.148(13)	C(41) -O(41)	1.142(13)
C(42) -O(42)	1.172(13)	C(51) -O(51)	1.155(11)
C(52) -O(52)	1.145(13)	N(1) -C(1)	1.374(10)
N(1) -C(5)	1.358(11)	C(1) -C(2)	1.395(12)
C(2) -C(3)	1.378(14)	C(3) -C(4)	1.367(16)
C(4) -C(5)	1.383(14)	N(2) -C(6)	1.336(13)
N(2) -C(10)	1.320(13)	C(6) -C(7)	1.371(16)
C(7) -C(8)	1.323(17)	C(8) -C(9)	1.352(20)
C(9) -C(10)	1.346(18)		

Table A3.5 Bond angles ($^{\circ}$) for $\text{HRu}_5\text{C}(\text{CO})_{13}(\text{C}_5\text{H}_4\text{N})(\text{C}_5\text{H}_5\text{N})$ (XR3)

C(1) -Ru(4) -Ru(1)	136.5(2)	C(1) -Ru(4) -Ru(2)	90.1(2)
C(1) -Ru(4) -Ru(3)	90.6(2)	N(1) -Ru(5) -Ru(2)	87.9(2)
N(1) -Ru(5) -Ru(3)	85.0(2)	N(2) -Ru(5) -Ru(2)	97.6(2)
N(2) -Ru(5) -Ru(3)	174.7(2)	N(2) -Ru(5) -N(1)	92.4(2)
O(11) -C(11) -Ru(1)	176.1(8)	O(12) -C(12) -Ru(1)	176.0(9)
O(13) -C(13) -Ru(1)	178.5(9)	O(21) -C(21) -Ru(2)	176.7(8)
O(22) -C(22) -Ru(2)	175(1)	O(23) -C(23) -Ru(2)	176(1)
O(31) -C(31) -Ru(3)	179.7(5)	O(32) -C(32) -Ru(3)	177(1)
O(33) -C(33) -Ru(3)	177(1)	O(41) -C(41) -Ru(4)	175.2(9)
O(42) -C(42) -Ru(4)	179.2(9)	O(51) -C(51) -Ru(5)	178.1(8)
O(52) -C(52) -Ru(5)	174.2(8)	C(1) -N(1) -Ru(5)	122.8(5)
C(5) -N(1) -Ru(5)	117.9(6)	C(5) -N(1) -C(1)	119.2(7)
N(1) -C(1) -Ru(4)	119.2(6)	C(2) -C(1) -Ru(4)	122.9(6)
C(2) -C(1) -N(1)	117.9(7)	C(3) -C(2) -C(1)	122.5(8)
C(4) -C(3) -C(2)	118.5(9)	C(5) -C(4) -C(3)	118.6(9)
C(4) -C(5) -N(1)	123.0(9)	C(6) -N(2) -Ru(5)	124.9(6)
C(10) -N(2) -Ru(5)	120.6(7)	C(10) -N(2) -C(6)	114.5(8)
C(7) -C(6) -N(2)	122.9(9)	C(8) -C(7) -C(6)	121(1)
C(9) -C(8) -C(7)	117(1)	C(10) -C(9) -C(8)	120(1)
C(9) -C(10) -N(2)	124(1)		

Table A4.1 Fractional atomic coordinates and thermal

parameters (\AA^2) for $\text{HRu}_5\text{C}(\text{CO})_{13}(\text{C}_5\text{H}_4\text{N})$ (XR4)

Atom	x	y	z	U_{iso} or U_{eq}
Ru(1a)	0.27772(6)	0.24650(6)	0.30698(8)	0.0326(5)
Ru(2a)	0.39578(5)	0.21124(6)	0.50504(8)	0.0328(5)
Ru(3a)	0.17155(5)	0.32818(6)	0.46447(8)	0.0298(5)
Ru(4a)	0.23670(5)	0.13594(6)	0.50600(8)	0.0288(5)
Ru(5a)	0.29027(5)	0.30185(6)	0.64969(8)	0.0295(5)
Na	0.1778(5)	0.3344(6)	0.7121(8)	0.035(5)
C(1a)	0.1203(6)	0.3494(7)	0.6201(9)	0.030(6)
C(2a)	0.0439(7)	0.3799(8)	0.6392(11)	0.043(7)
C(3a)	0.0260(8)	0.3937(9)	0.7499(13)	0.052(8)
C(4a)	0.0839(8)	0.3766(10)	0.8422(12)	0.054(8)
C(5a)	0.1616(8)	0.3475(9)	0.8232(10)	0.045(7)
Ca	0.2862(6)	0.2767(7)	0.4794(9)	0.030(2)
C(11a)	0.3343(8)	0.1740(9)	0.2035(12)	0.047(3)
O(11a)	0.3684(6)	0.1297(8)	0.1371(10)	0.079(3)
C(12a)	0.1815(7)	0.2594(9)	0.1981(11)	0.043(3)
O(12a)	0.1268(6)	0.2647(7)	0.1282(9)	0.070(3)
C(13a)	0.3221(7)	0.3677(9)	0.2668(11)	0.046(3)
O(13a)	0.3516(6)	0.4436(8)	0.2481(9)	0.072(3)
C(21a)	0.4524(7)	0.1712(9)	0.6479(11)	0.043(3)
O(21a)	0.4900(6)	0.1450(7)	0.7350(10)	0.073(3)
C(22a)	0.4520(7)	0.1196(9)	0.4198(11)	0.044(3)
O(22a)	0.4866(6)	0.0628(7)	0.3699(9)	0.071(3)
C(23a)	0.4671(8)	0.3166(10)	0.4843(12)	0.051(3)
O(23a)	0.5046(6)	0.3857(8)	0.4702(10)	0.074(3)
C(32a)	0.1731(7)	0.4617(9)	0.4392(11)	0.046(3)
O(32a)	0.1755(6)	0.5434(8)	0.4245(10)	0.079(3)
C(33a)	0.0655(7)	0.3126(9)	0.3819(11)	0.043(3)
O(33a)	0.0012(7)	0.3030(8)	0.3327(10)	0.080(3)
C(41a)	0.2907(8)	0.0117(10)	0.5057(12)	0.051(3)
O(41a)	0.3203(6)	-0.0625(8)	0.5134(10)	0.079(3)
C(42a)	0.1233(8)	0.1060(9)	0.4680(11)	0.044(3)
O(42a)	0.0559(6)	0.0822(7)	0.4452(8)	0.061(2)
C(43a)	0.2278(8)	0.1191(9)	0.6674(12)	0.046(3)
O(43a)	0.2140(6)	0.0954(7)	0.7591(9)	0.069(3)
C(51a)	0.3339(7)	0.4272(9)	0.6668(10)	0.039(3)
O(51a)	0.3611(6)	0.5012(7)	0.6747(9)	0.067(3)
C(53a)	0.3429(7)	0.2630(8)	0.7988(11)	0.040(3)
O(53a)	0.3751(6)	0.2440(7)	0.8881(9)	0.068(3)

Table A4.1 continued

Ru(1b)	0.36371(5)	0.67261(6)	-0.00849(8)	0.0309(5)
Ru(2b)	0.25021(5)	0.75230(6)	-0.19421(8)	0.0303(5)
Ru(3b)	0.24137(5)	0.70173(6)	0.14497(8)	0.0279(5)
Ru(4b)	0.29320(5)	0.86273(6)	0.01013(8)	0.0290(5)
Ru(5b)	0.13291(5)	0.77223(6)	-0.03166(7)	0.0260(4)
C(2b)	0.0233(7)	0.8544(9)	0.1532(12)	0.047(8)
C(3b)	0.0126(8)	0.8729(9)	0.2650(13)	0.055(9)
C(4b)	0.0683(9)	0.8423(11)	0.3540(12)	0.059(9)
C(5b)	0.1356(8)	0.7894(9)	0.3301(11)	0.048(8)
Cb	0.2466(6)	0.7216(7)	-0.0247(9)	0.027(2)
C(11b)	0.4537(9)	0.6787(11)	-0.0984(13)	0.062(4)
O(11b)	0.5106(8)	0.6838(9)	-0.1493(12)	0.105(4)
C(12b)	0.4300(8)	0.6465(9)	0.1330(12)	0.049(3)
O(12b)	0.4725(6)	0.6262(7)	0.2183(9)	0.068(3)
C(13b)	0.3438(8)	0.5391(9)	-0.0344(11)	0.046(3)
O(13b)	0.3285(7)	0.4582(9)	-0.0502(11)	0.086(3)
C(21b)	0.1803(7)	0.8386(8)	-0.2872(11)	0.040(3)
O(21b)	0.1410(6)	0.8910(7)	-0.3478(9)	0.069(3)
C(22b)	0.3365(8)	0.7599(9)	-0.2895(12)	0.050(3)
C(22b)	0.3888(7)	0.7640(8)	-0.3476(10)	0.084(3)
C(23b)	0.2047(7)	0.6386(9)	-0.2653(11)	0.046(3)
O(23b)	0.1734(6)	0.5695(8)	-0.3035(9)	0.072(3)
C(32b)	0.1964(7)	0.5782(9)	0.1581(10)	0.040(3)
O(32b)	0.1661(6)	0.5024(7)	0.1540(9)	0.064(3)
C(33b)	0.3047(9)	0.6936(10)	0.2934(14)	0.059(4)
O(33b)	0.3420(7)	0.6895(9)	0.3837(12)	0.096(4)
C(41b)	0.3496(11)	0.9429(13)	-0.0823(17)	0.114(5)
O(41b)	0.3897(8)	0.9924(10)	-0.1440(12)	0.141(4)
C(42b)	0.3198(9)	0.8926(10)	0.1691(13)	0.059(4)
O(42b)	0.3347(7)	0.9259(8)	0.2625(11)	0.086(3)
C(43b)	0.2089(8)	0.9563(10)	-0.0011(12)	0.053(3)
O(43b)	0.1652(6)	1.0231(8)	0.0028(10)	0.076(3)
C(51b)	0.0653(6)	0.6648(7)	-0.0589(9)	0.029(2)
O(51b)	0.0286(5)	0.5941(6)	-0.0762(8)	0.055(2)
C(53b)	0.0548(7)	0.8515(9)	-0.1189(11)	0.043(3)
O(53b)	0.0061(6)	0.9003(8)	-0.1725(10)	0.074(3)
Nb(1)	0.1460(6)	0.7705(7)	0.2148(8)	0.031(2)
C(1b1)	0.1460(6)	0.7705(7)	0.2148(8)	0.031(2)
Nb(2)	0.0926(6)	0.8040(7)	0.1295(9)	0.033(2)
C(1B ₂)	0.0926(6)	0.8040(7)	0.1295(9)	0.033(2)

Table A4.2 Fractional atomic coordinates for the

hydrogen atoms for $\text{HRu}_5\text{C}(\text{CO})_{13}(\text{C}_5\text{H}_4\text{N})$ (XR4)

Atom	x	y	z
Ha	0.2375	0.1259	0.3465
H(2a)	-0.0019	0.3941	0.5667
H(3a)	-0.0340	0.4176	0.7651
H(4a)	0.0693	0.3851	0.9300
H(5a)	0.2088	0.3361	0.8952
Hb	0.3923	0.8039	-0.0060
H(2b)	-0.0210	0.8781	0.0834
H(3b)	-0.0406	0.9126	0.2837
H(4b)	0.0601	0.8589	0.4430
H(5b)	0.1796	0.7632	0.4000

Table A4.3 Anisotropic thermal parameters (\AA^2) for $\text{HRu}_5\text{C}(\text{CO})_{13}(\text{C}_5\text{H}_4\text{N})$ (XR4)

Atom	U_{11}	U_{22}	U_{33}	U_{23}	U_{13}	U_{12}
Ru(1a)	0.0378(5)	0.0327(5)	0.0271(5)	0.0014(4)	0.0072(4)	0.0029(4)
Ru(2a)	0.0258(5)	0.0325(5)	0.0401(5)	-0.0009(4)	0.0045(4)	0.0040(4)
Ru(3a)	0.0278(5)	0.0313(5)	0.0303(5)	0.0009(4)	0.0026(4)	0.0034(4)
Ru(4a)	0.0311(5)	0.0263(4)	0.0291(5)	0.0006(4)	0.0042(4)	-0.0022(3)
Ru(5a)	0.0288(5)	0.0314(5)	0.0284(5)	-0.0029(4)	0.0024(4)	-0.0007(4)
Na	0.037(5)	0.034(5)	0.034(6)	-0.003(4)	0.009(4)	0.006(4)
C(1a)	0.026(5)	0.032(6)	0.032(6)	-0.007(5)	0.010(5)	0.000(4)
C(2a)	0.040(7)	0.035(6)	0.055(8)	-0.006(6)	0.018(6)	0.001(5)
C(3a)	0.042(7)	0.055(8)	0.058(9)	-0.005(7)	0.022(7)	0.004(6)
C(4a)	0.059(9)	0.052(8)	0.051(8)	-0.007(7)	0.034(7)	-0.012(7)
C(5a)	0.060(8)	0.045(7)	0.029(7)	-0.005(5)	0.012(6)	-0.007(6)
Ru(1b)	0.0247(4)	0.0319(5)	0.0362(5)	-0.0039(4)	0.0038(4)	0.0007(4)
Ru(2b)	0.0362(5)	0.0298(5)	0.0249(5)	-0.0003(4)	0.0059(4)	-0.0047(4)
Ru(3b)	0.0278(4)	0.0315(5)	0.0244(5)	0.0032(4)	0.0016(4)	0.0014(4)
Ru(4b)	0.0303(5)	0.0249(4)	0.0316(5)	-0.0022(4)	0.0030(4)	-0.0055(3)
Ru(5b)	0.0251(4)	0.0258(4)	0.0272(5)	0.0018(4)	0.0016(3)	0.0008(3)
C(2b)	0.037(7)	0.044(7)	0.060(9)	-0.002(6)	0.011(6)	0.005(5)
C(3b)	0.059(9)	0.043(7)	0.063(10)	-0.003(7)	0.029(8)	0.014(6)
C(4b)	0.065(9)	0.068(9)	0.045(8)	-0.020(7)	0.022(7)	0.007(7)
C(5b)	0.060(8)	0.044(7)	0.040(7)	-0.005(6)	0.010(6)	-0.007(6)

Table A4.4 Bond lengths (Å) for $\text{HRu}_5\text{C}(\text{CO})_{13}(\text{C}_5\text{H}_4\text{N})$ (XR4)

Ru(1a)-Ru(2a)	2.864(1)	Ru(1a)-Ru(3a)	2.904(1)
Ru(1a)-Ru(4a)	2.892(1)	Ru(1a)-Ca	2.028(11)
Ru(1a)-C(11a)	1.891(14)	Ru(1a)-C(12a)	1.912(12)
Ru(1a)-C(13a)	1.886(13)	Ru(2a)-Ru(4a)	2.811(1)
Ru(2a)-Ru(5a)	2.846(1)	Ru(2a)-Ca	2.010(10)
Ru(2a)-C(21a)	1.879(12)	Ru(2a)-C(22a)	1.911(13)
Ru(2a)-C(23a)	1.886(13)	Ru(3a)-Ru(4a)	2.863(1)
Ru(3a)-Ru(5a)	2.747(1)	Ru(3a)-Ca	2.006(10)
Ru(3a)-C(32a)	1.849(13)	Ru(3a)-C(33a)	1.901(12)
Ru(3a)-C(1a)	2.100(11)	Ru(4a)-Ru(5a)	2.894(1)
Ru(4a)-Ca	2.123(10)	Ru(4a)-C(41a)	1.924(13)
Ru(4a)-C(42a)	1.909(12)	Ru(4a)-C(43a)	1.903(14)
Ru(5a)-Ca	1.996(11)	Ru(5a)-C(43a)	2.714(12)
Ru(5a)-C(51a)	1.859(12)	Ru(5a)-C(53a)	1.911(12)
Ru(5a)-Na	2.117(9)	C(11a)-O(11a)	1.178(18)
C(12a)-O(12a)	1.139(15)	C(13a)-O(13a)	1.174(16)
C(21a)-O(21a)	1.173(16)	C(22a)-O(22a)	1.163(17)
C(23a)-O(23a)	1.147(17)	C(32a)-O(32a)	1.131(17)
C(33a)-O(33a)	1.147(16)	C(41a)-O(41a)	1.127(17)
C(42a)-O(42a)	1.156(15)	C(43a)-O(43a)	1.154(18)
C(51a)-O(51a)	1.104(15)	C(53a)-O(53a)	1.133(16)
Na -C(1a)	1.354(13)	Na -C(5a)	1.357(16)
C(1a)-C(2a)	1.372(16)	C(2a)-C(3a)	1.362(20)
C(3a)-C(4a)	1.363(18)	C(4a)-C(5a)	1.385(19)
Ru(1b)-Ru(2b)	2.888(1)	Ru(1b)-Ru(3b)	2.871(1)
Ru(1b)-Ru(4b)	2.875(1)	Ru(1b)-Cb	2.033(10)
Ru(1b)-C(11b)	1.911(16)	Ru(1b)-C(12b)	1.890(13)
Ru(1b)-C(13b)	1.874(13)	Ru(2b)-Ru(4b)	2.830(1)
Ru(2b)-Ru(5b)	2.867(1)	Ru(2b)-Cb	2.011(10)
Ru(2b)-C(21b)	1.893(11)	Ru(2b)-C(22b)	1.901(14)
Ru(2b)-C(23b)	1.875(12)	Ru(3b)-Ru(4b)	2.875(1)
Ru(3b)-Ru(5b)	2.725(1)	Ru(3b)-Cb	1.992(10)
Ru(3b)-C(32b)	1.854(12)	Ru(3b)-C(33b)	1.903(15)
Ru(3b)-Nb(1)	2.083(10)	Ru(3b)-C(1b1)	2.083(10)
Ru(3b)-C(1B ₂)	2.815(10)	Ru(4b)-Ru(5b)	2.898(1)
Ru(4b)-Cb	2.098(10)	Ru(4b)-C(41b)	1.850(20)
Ru(4b)-C(42b)	1.887(15)	Ru(4b)-C(43b)	1.887(13)
Ru(5b)-Cb	1.992(10)	Ru(5b)-C(43b)	2.812(13)
Ru(5b)-C(51b)	1.845(10)	Ru(5b)-C(53b)	1.882(12)
Ru(5b)-C(1b1)	2.834(10)	Ru(5b)-Nb(2)	2.102(10)
Ru(5b)-C(1B ₂)	2.102(10)	C(11b)-O(11b)	1.165(21)
C(12b)-O(12b)	1.172(16)	C(13b)-O(13b)	1.144(17)
C(21b)-O(21b)	1.147(15)	C(22b)-C(22b)	1.154(19)
C(23b)-O(23b)	1.140(16)	C(32b)-O(32b)	1.147(15)
C(33b)-O(33b)	1.149(20)	C(41b)-O(41b)	1.227(24)
C(42b)-O(42b)	1.173(19)	C(43b)-O(43b)	1.171(17)
C(51b)-O(51b)	1.144(13)	C(53b)-O(53b)	1.165(16)
Nb(1)-Nb(2)	1.322(13)	Nb(1)-C(1B ₂)	1.322(13)
Nb(1)-C(5b)	1.390(16)	C(1b1)-Nb(2)	1.322(13)
C(1b1)-C(1B ₂)	1.322(13)	C(1b1)-C(5b)	1.390(16)
Nb(2)-C(2b)	1.392(16)	C(1B ₂)-C(2b)	1.392(16)
C(2b)-C(3b)	1.352(21)	C(3b)-C(4b)	1.361(19)
C(4b)-C(5b)	1.383(20)		

Table A4.5 Bond angles ($^{\circ}$) for $\text{HRu}_5\text{C}(\text{CO})_{13}(\text{C}_5\text{H}_4\text{N})$ (XR4)

C(1a) -Ru(3a)-Ru(1a)	158.2(3)	C(1a) -Ru(3a)-Ru(4a)	99.9(3)
C(1a) -Ru(3a)-Ru(5a)	70.8(3)	Na -Ru(5a)-Ru(2a)	156.5(2)
Na -Ru(5a)-Ru(3a)	70.6(2)	Na -Ru(5a)-Ru(4a)	98.5(2)
O(11a)-C(11a)-Ru(1a)	179(1)	O(12a)-C(12a)-Ru(1a)	176(1)
O(13a)-C(13a)-Ru(1a)	176(1)	O(21a)-C(21a)-Ru(2a)	178(1)
O(22a)-C(22a)-Ru(2a)	179(1)	O(23a)-C(23a)-Ru(2a)	174(1)
O(32a)-C(32a)-Ru(3a)	179(1)	O(33a)-C(33a)-Ru(3a)	179(1)
O(41a)-C(41a)-Ru(4a)	175(1)	O(42a)-C(42a)-Ru(4a)	176(1)
O(51a)-C(51a)-Ru(5a)	178(1)	O(53a)-C(53a)-Ru(5a)	177(1)
C(1a) -Na -Ru(5a)	108.9(7)	C(5a) -Na -Ru(5a)	129.3(8)
C(5a) -Na -C(1a)	122(1)	Na -C(1a) -Ru(3a)	109.7(7)
C(2a) -C(1a) -Ru(3a)	130.9(8)	C(2a) -C(1a) -Na	119(1)
C(3a) -C(2a) -C(1a)	120(1)	C(4a) -C(3a) -C(2a)	120(1)
C(5a) -C(4a) -C(3a)	120(1)	C(4a) -C(5a) -Na	119(1)
Nb(1) -Ru(3b)-Ru(1b)	157.6(3)	Nb(1) -Ru(3b)-Ru(4b)	98.5(3)
Nb(1) -Ru(3b)-Ru(5b)	70.8(3)	C(1b1)-Ru(3b)-Ru(1b)	157.6(3)
C(1b1)-Ru(3b)-Ru(4b)	98.5(3)	C(1b1)-Ru(3b)-Ru(5b)	70.8(3)
C(1B ₁)-Ru(3b)-Ru(1b)	134.7(2)	C(1B ₂)-Ru(3b)-Ru(4b)	84.0(2)
C(1B ₂)-Ru(3b)-Ru(5b)	44.5(2)	C(1b1)-Ru(5b)-Ru(2b)	133.1(2)
C(1b1)-Ru(5b)-Ru(3b)	43.9(2)	C(1b1)-Ru(5b)-Ru(4b)	82.8(2)
Nb(2) -Ru(5b)-Ru(2b)	155.9(3)	Nb(2) -Ru(5b)-Ru(3b)	70.0(3)
Nb(2) -Ru(5b)-Ru(4b)	98.0(3)		

TABLE A5.1 Fractional atomic coordinates and thermal

parameters (\AA^2) for $\text{Ru}_6\text{C}(\text{CO})_{15}(\text{C}_6\text{H}_8)$ (XR5)

Atom	x	y	z	U_{iso} or U_{eq}
Ru(1)	0.76025(3)	0.58673(5)	0.83861(3)	0.0343(3)
Ru(2)	0.82201(3)	0.63595(5)	0.71864(3)	0.0315(3)
Ru(3)	0.64495(3)	0.62236(5)	0.66820(3)	0.0332(3)
Ru(4)	0.83997(3)	0.35478(5)	0.79279(3)	0.0281(2)
Ru(5)	0.66007(3)	0.35919(5)	0.74547(3)	0.0339(3)
Ru(6)	0.73145(3)	0.39756(5)	0.62768(3)	0.0342(3)
C	0.7442(3)	0.4947(5)	0.7340(3)	0.027(3)
C(1)	0.8372(4)	0.8349(6)	0.7983(4)	0.044(4)
C(2)	0.9149(4)	0.7924(6)	0.8041(4)	0.044(4)
C(3)	0.9825(4)	0.7424(7)	0.8819(4)	0.047(4)
C(4)	0.9514(4)	0.6719(8)	0.9396(4)	0.046(4)
C(5)	0.8658(4)	0.7174(7)	0.9281(4)	0.047(4)
C(6)	0.8157(4)	0.8039(7)	0.8654(4)	0.050(4)
C(11)	0.8010(5)	0.4617(7)	0.9264(4)	0.054(4)
O(11)	0.8203(4)	0.3941(6)	0.9834(3)	0.082(4)
C(12)	0.6754(5)	0.6679(8)	0.8595(5)	0.065(5)
O(12)	0.6237(4)	0.7181(8)	0.8728(5)	0.122(6)
C(21)	0.9161(4)	0.5894(6)	0.7029(4)	0.041(4)
O(21)	0.9730(3)	0.5639(5)	0.6903(3)	0.069(3)
C(22)	0.7888(4)	0.7556(7)	0.6279(4)	0.045(4)
O(22)	0.7704(3)	0.8243(6)	0.5712(3)	0.068(4)
C(31)	0.5350(5)	0.6230(7)	0.6576(5)	0.055(5)
O(31)	0.4674(3)	0.6241(6)	0.6506(4)	0.080(4)
C(32)	0.6151(4)	0.5685(8)	0.5571(4)	0.051(4)
O(32)	0.5786(3)	0.5754(7)	0.4886(3)	0.068(4)
C(33)	0.6407(5)	0.8189(8)	0.6546(5)	0.063(5)
O(33)	0.6389(4)	0.9373(6)	0.6500(5)	0.103(5)
C(41)	0.9537(4)	0.3805(6)	0.8317(4)	0.037(3)
O(41)	1.0252(3)	0.3922(5)	0.8554(3)	0.052(3)
C(42)	0.8691(4)	0.1961(7)	0.8608(4)	0.041(4)
O(42)	0.8916(3)	0.1037(5)	0.9048(3)	0.056(3)
C(46)	0.8265(4)	0.2483(7)	0.6909(4)	0.042(4)
O(46)	0.8532(3)	0.1504(6)	0.6732(3)	0.072(4)
C(51)	0.6898(4)	0.1928(8)	0.8082(5)	0.055(4)
O(51)	0.6996(3)	0.0904(6)	0.8443(4)	0.087(4)
C(52)	0.5783(5)	0.4063(7)	0.7824(5)	0.058(5)
O(52)	0.5292(4)	0.4315(6)	0.8047(4)	0.104(5)
C(53)	0.5819(4)	0.2571(7)	0.6558(5)	0.047(4)
O(53)	0.5320(3)	0.1959(6)	0.6050(3)	0.066(4)
C(61)	0.6709(5)	0.2542(8)	0.5519(4)	0.053(4)
O(61)	0.6371(4)	0.1706(6)	0.5071(4)	0.086(4)
C(62)	0.7782(5)	0.4486(7)	0.5575(4)	0.054(4)
O(62)	0.8080(4)	0.4811(7)	0.5161(3)	0.101(5)

TABLE A5.2 Fractional atomic coordinates for the
hydrogen atoms for $\text{Ru}_6\text{C}(\text{CO})_{15}(\text{C}_6\text{H}_8)$ (XR5)

Atom	x	y	z
H(1)	0.7926	0.8876	0.7474
H(2)	0.9249	0.8459	0.7564
H(3)	1.0152	0.6874	0.8660
H(3')	1.0116	0.7997	0.9067
H(4)	0.9628	0.5645	0.9435
H(4')	0.9832	0.6863	1.0000
H(5)	0.8668	0.7166	0.9777
H(6)	0.7646	0.8568	0.8673

TABLE A5.3 Anisotropic thermal parameters (\AA^2) for $\text{Ru}_6\text{C}(\text{CO})_{15}(\text{C}_6\text{H}_8)$ (XR5)

Atom	U_{11}	U_{22}	U_{33}	U_{23}	U_{13}	U_{12}
Ru(1)	0.0362(3)	0.0318(3)	0.0349(3)	-0.0033(2)	0.0232(2)	0.0008(2)
Ru(2)	0.0347(3)	0.0265(2)	0.0334(3)	0.0017(2)	0.0202(2)	-0.0025(2)
Ru(3)	0.0322(3)	0.0267(3)	0.0408(3)	0.0050(2)	0.0146(2)	0.0057(2)
Ru(4)	0.0280(2)	0.0259(2)	0.0305(3)	0.0015(2)	0.0149(2)	0.0033(2)
Ru(5)	0.0292(3)	0.0266(3)	0.0459(3)	0.0051(2)	0.0200(2)	0.0003(2)
Ru(6)	0.0404(3)	0.0349(3)	0.0273(3)	-0.0045(2)	0.0157(2)	-0.0044(2)
C	0.027(3)	0.020(3)	0.034(3)	-0.002(2)	0.017(2)	-0.003(2)
C(1)	0.056(4)	0.026(3)	0.048(4)	-0.003(3)	0.019(3)	-0.002(3)
C(2)	0.053(4)	0.038(3)	0.040(4)	-0.009(3)	0.025(3)	-0.016(3)
C(3)	0.042(4)	0.053(4)	0.048(4)	-0.008(3)	0.017(3)	-0.014(3)
C(4)	0.039(4)	0.065(4)	0.034(4)	0.004(3)	0.005(3)	-0.008(3)
C(5)	0.054(4)	0.042(4)	0.044(4)	-0.012(3)	0.029(3)	-0.007(3)
C(6)	0.056(4)	0.034(4)	0.059(4)	-0.015(3)	0.031(4)	-0.008(3)
C(11)	0.064(5)	0.042(4)	0.055(5)	0.005(4)	0.025(4)	-0.004(4)
O(11)	0.129(6)	0.066(4)	0.050(3)	0.018(3)	0.040(4)	0.012(4)
C(12)	0.063(5)	0.055(4)	0.076(6)	-0.025(4)	0.047(4)	-0.004(4)
O(12)	0.080(5)	0.118(6)	0.167(7)	-0.054(5)	0.084(5)	0.008(4)
C(21)	0.043(4)	0.030(3)	0.050(4)	-0.005(3)	0.025(3)	-0.008(3)
O(21)	0.062(3)	0.054(3)	0.092(4)	0.003(3)	0.055(3)	0.006(3)
C(22)	0.049(4)	0.043(4)	0.044(4)	0.003(3)	0.021(3)	-0.001(3)
O(22)	0.080(4)	0.076(4)	0.049(3)	0.033(3)	0.027(3)	0.008(3)
C(31)	0.049(4)	0.043(4)	0.073(5)	0.000(4)	0.028(4)	0.010(3)
O(31)	0.050(3)	0.075(4)	0.114(5)	-0.011(3)	0.046(3)	0.007(3)
C(32)	0.046(4)	0.058(5)	0.050(4)	-0.001(4)	0.014(4)	-0.007(4)
O(32)	0.072(4)	0.093(4)	0.040(3)	0.001(3)	-0.002(3)	0.022(3)

Table A5.3 continued

C(33)	0.059(5)	0.036(4)	0.095(6)	0.005(4)	0.037(5)	0.006(4)	
O(33)	0.101(5)	0.044(4)	0.162(7)	0.019(4)		0.064(5)	0.018(3)
C(41)	0.036(4)	0.034(3)	0.041(4)	0.006(3)		0.022(3)	0.006(3)
O(41)	0.034(3)	0.065(3)	0.058(3)	0.002(2)		0.019(2)	0.000(2)
C(42)	0.040(4)	0.036(4)	0.046(4)	-0.004(3)		0.020(3)	-0.002(3)
						0.024(3)	0.005(2)

TABLE A5.4 Bond lengths (Å) for Ru₆C(CO)₁₅(C₆H₈) (XR5)

Ru(1) -Ru(2)	2.889(1)	Ru(1) -Ru(3)	2.932(1)
Ru(1) -Ru(4)	2.937(1)	Ru(1) -Ru(5)	2.861(1)
Ru(1) -C	2.015(6)	Ru(1) -C(5)	2.265(6)
Ru(1) -C(6)	2.254(7)	Ru(1) -C(11)	1.880(7)
Ru(1) -C(12)	1.877(10)	Ru(2) -Ru(3)	2.884(1)
Ru(2) -Ru(4)	2.958(1)	Ru(2) -Ru(6)	2.869(1)
Ru(2) -C	2.036(6)	Ru(2) -C(1)	2.336(7)
Ru(2) -C(2)	2.278(6)	Ru(2) -C(21)	1.871(8)
Ru(2) -C(22)	1.890(7)	Ru(3) -Ru(5)	2.835(1)
Ru(3) -Ru(6)	2.914(1)	Ru(3) -C	2.056(5)
Ru(3) -C(31)	1.884(9)	Ru(3) -C(32)	1.942(8)
Ru(3) -C(33)	1.886(7)	Ru(4) -Ru(5)	2.939(1)
Ru(4) -Ru(6)	2.838(1)	Ru(4) -C	2.067(5)
Ru(4) -C(41)	1.852(6)	Ru(4) -C(42)	1.885(6)
Ru(4) -C(46)	2.048(7)	Ru(5) -Ru(6)	2.961(1)
Ru(5) -C	2.055(6)	Ru(5) -C(51)	1.895(8)
Ru(5) -C(52)	1.905(10)	Ru(5) -C(53)	1.903(6)
Ru(6) -C	2.081(6)	Ru(6) -C(32)	2.513(7)
Ru(6) -C(46)	2.133(6)	Ru(6) -C(61)	1.917(7)
Ru(6) -C(62)	1.872(9)	C(1) -C(2)	1.400(11)
C(1) -C(6)	1.466(13)	C(2) -C(3)	1.496(8)
C(3) -C(4)	1.543(12)	C(4) -C(5)	1.510(11)
C(5) -C(6)	1.385(9)	C(11) -O(11)	1.148(9)
C(12) -O(12)	1.154(13)	C(21) -O(21)	1.158(10)
C(22) -O(22)	1.151(9)	C(31) -O(31)	1.154(11)
C(32) -O(32)	1.143(9)	C(33) -O(33)	1.129(9)
C(41) -O(41)	1.162(8)	C(42) -O(42)	1.144(8)
C(46) -O(46)	1.153(10)	C(51) -O(51)	1.150(10)
C(52) -O(52)	1.139(13)	C(53) -O(53)	1.135(8)
C(61) -O(61)	1.117(9)	C(62) -O(62)	1.140(12)

TABLE A5.5 Bond angles ($^{\circ}$) for $\text{Ru}_6\text{C}(\text{CO})_{15}(\text{C}_6\text{H}_8)$ (XR5)

C(5) -Ru(1) -Ru(2)	89.7(2)	C(5) -Ru(1) -Ru(3)	133.9(2)
C(5) -Ru(1) -Ru(4)	105.5(2)	C(5) -Ru(1) -Ru(5)	163.8(2)
C(6) -Ru(1) -Ru(2)	75.1(2)	C(6) -Ru(1) -Ru(3)	99.6(2)
C(6) -Ru(1) -Ru(4)	122.1(2)	C(6) -Ru(1) -Ru(5)	158.1(2)
C(6) -Ru(1) -C(5)	35.7(2)	C(1) -Ru(2) -Ru(1)	68.6(2)
C(1) -Ru(2) -Ru(3)	93.2(2)	C(1) -Ru(2) -Ru(4)	119.1(2)
C(1) -Ru(2) -Ru(6)	153.0(2)	C(2) -Ru(2) -Ru(1)	89.0(2)
C(2) -Ru(2) -Ru(3)	128.4(2)	C(2) -Ru(2) -Ru(4)	111.8(2)
C(2) -Ru(2) -Ru(6)	168.2(2)	C(2) -Ru(2) -C(1)	35.3(3)
C(2) -C(1) -Ru(2)	70.1(4)	C(6) -C(1) -Ru(2)	111.0(4)
C(6) -C(1) -C(2)	118.8(6)	C(1) -C(2) -Ru(2)	74.6(4)
C(3) -C(2) -Ru(2)	119.9(4)	C(3) -C(2) -C(1)	122.0(7)
C(4) -C(3) -C(2)	114.4(6)	C(5) -C(4) -C(3)	114.6(6)
C(4) -C(5) -Ru(1)	114.7(5)	C(6) -C(5) -Ru(1)	71.7(4)
C(6) -C(5) -C(4)	122.6(8)	C(1) -C(6) -Ru(1)	104.5(4)
C(5) -C(6) -Ru(1)	72.6(4)	C(5) -C(6) -C(1)	120.7(7)
O(11) -C(11) -Ru(1)	172.0(8)	O(12) -C(12) -Ru(1)	179.6(5)
O(21) -C(21) -Ru(2)	177.2(6)	O(22) -C(22) -Ru(2)	176.9(7)
O(31) -C(31) -Ru(3)	179.4(7)	Ru(6) -C(32) -Ru(3)	80.6(2)
O(32) -C(32) -Ru(3)	155.4(7)	O(32) -C(32) -Ru(6)	124.0(7)
O(33) -C(33) -Ru(3)	176.9(9)	O(41) -C(41) -Ru(4)	177.8(5)
O(42) -C(42) -Ru(4)	175.6(5)	Ru(6) -C(46) -Ru(4)	85.5(3)
O(46) -C(46) -Ru(4)	139.1(5)	O(46) -C(46) -Ru(6)	135.4(5)
O(51) -C(51) -Ru(5)	173.2(7)	O(52) -C(52) -Ru(5)	178.6(6)
O(53) -C(53) -Ru(5)	175.5(8)	O(61) -C(61) -Ru(6)	178.2(9)
O(62) -C(62) -Ru(6)	178.6(6)		

Table A6.1 Fractional atomic coordinates and

thermal parameters (\AA^2) for $\text{Ru}_6\text{C}(\text{CO})_{15}(\text{PhCCH})$ (XR6)

Atom	x	y	z	U_{iso} or U_{eq}
Ru(1)	-0.34780(12)	0.31726(6)	0.04907(6)	0.0324(6)
Ru(2)	-0.31918(12)	0.16252(6)	-0.00065(6)	0.0351(6)
Ru(3)	-0.11141(12)	0.27584(6)	0.00783(6)	0.0302(6)
Ru(4)	-0.27323(12)	0.18485(7)	0.15868(6)	0.0386(7)
Ru(5)	-0.06582(12)	0.30721(6)	0.16620(6)	0.0344(6)
Ru(6)	-0.02955(12)	0.14802(6)	0.11814(6)	0.0374(7)
C(11)	-0.5548(16)	0.3176(10)	0.0106(9)	0.059(11)
O(11)	-0.6784(12)	0.3155(7)	-0.0127(8)	0.086(9)
C(12)	-0.3486(17)	0.4271(9)	0.0681(8)	0.045(9)
O(12)	-0.3455(13)	0.4920(6)	0.0791(6)	0.067(8)
C(21)	-0.5224(17)	0.1418(9)	-0.0378(9)	0.058(11)
O(21)	-0.6435(12)	0.1304(8)	-0.0561(7)	0.092(9)
C(22)	-0.2938(17)	0.0828(9)	-0.0619(8)	0.049(10)
O(22)	-0.2715(13)	0.0343(7)	-0.1001(7)	0.076(9)
C(31)	-0.0217(16)	0.2276(8)	-0.0509(7)	0.037(8)
O(31)	0.0287(13)	0.1960(6)	-0.0881(6)	0.074(8)
C(32)	-0.0085(15)	0.3685(8)	-0.0023(7)	0.036(8)
O(32)	0.0528(12)	0.4202(6)	-0.0121(6)	0.062(7)
C(41)	-0.4311(20)	0.2430(8)	0.1731(9)	0.059(11)
O(41)	-0.5165(13)	0.2721(7)	0.1886(7)	0.079(9)
C(42)	-0.3675(18)	0.0834(9)	0.1332(10)	0.064(11)
O(42)	-0.4256(15)	0.0266(7)	0.1224(7)	0.108(10)
C(43)	-0.1811(18)	0.1579(8)	0.2629(9)	0.053(10)
O(43)	-0.1246(13)	0.1456(7)	0.3233(6)	0.069(8)
C(51)	0.1180(17)	0.2835(9)	0.2421(9)	0.059(10)
O(51)	0.2246(14)	0.2715(9)	0.2887(8)	0.114(10)
C(52)	0.0059(19)	0.4078(11)	0.1506(9)	0.066(12)
O(52)	0.0446(16)	0.4706(7)	0.1456(7)	0.105(10)
C(53)	-0.1486(17)	0.3505(10)	0.2312(8)	0.050(10)
O(53)	-0.1953(14)	0.3785(8)	0.2719(7)	0.082(9)
C(61)	0.1429(18)	0.1581(9)	0.0955(9)	0.055(11)
O(61)	0.2495(12)	0.1567(7)	0.0850(7)	0.080(9)
C(62)	-0.0710(17)	0.0434(9)	0.0816(9)	0.055(10)
O(62)	-0.0843(15)	-0.0220(6)	0.0640(8)	0.098(10)
C(63)	0.0658(24)	0.1106(12)	0.2148(12)	0.056(15)
O(63)	0.1265(19)	0.0820(10)	0.2712(10)	0.100(14)
C	-0.1944(16)	0.2321(8)	0.0842(8)	0.028(3)
C(1)	-0.3385(13)	0.3225(7)	-0.0575(6)	0.030(3)
C(2)	-0.3210(14)	0.2474(7)	-0.0787(7)	0.037(3)
C(111)	-0.3793(9)	0.3916(4)	-0.1076(4)	0.029(3)
C(112)	-0.3186(9)	0.4666(4)	-0.0872(4)	0.034(3)
C(113)	-0.3643(9)	0.5292(4)	-0.1376(4)	0.053(4)
C(114)	-0.4707(9)	0.5169(4)	-0.2083(4)	0.055(4)
C(115)	-0.5314(9)	0.4419(4)	-0.2287(4)	0.049(4)
C(116)	-0.4857(9)	0.3792(4)	-0.1784(4)	0.040(3)

Table A6.2 Fractional atomic coordinates for the
hydrogen atoms for $\text{Ru}_6\text{C}(\text{CO})_{15}(\text{PhCCH})$ (XR6)

Atom	x	y	z
H(112)	-0.2367	0.4760	-0.0323
H(113)	-0.3175	0.5875	-0.1213
H(114)	-0.5054	0.5659	-0.2472
H(115)	-0.6124	0.4328	-0.2840
H(116)	-0.5315	0.3213	-0.1950
H(2)	-0.3395	0.2502	-0.1397

Table A6.3 Anisotropic thermal parameters (\AA^2) $\text{Ru}_6\text{C}(\text{CO})_{15}(\text{PhCCH})$ (XR6)

Atom	U_{11}	U_{22}	U_{33}	U_{23}	U_{13}	U_{12}
Ru(1)	0.031(1)	0.034(1)	0.032(1)	-0.002(1)	0.013(1)	0.001(1)
Ru(2)	0.035(1)	0.031(1)	0.039(1)	-0.005(1)	0.013(1)	-0.006(1)
Ru(3)	0.030(1)	0.031(1)	0.030(1)	0.000(1)	0.012(1)	-0.001(1)
Ru(4)	0.041(1)	0.039(1)	0.036(1)	0.002(1)	0.019(1)	-0.003(1)
Ru(5)	0.034(1)	0.036(1)	0.033(1)	-0.004(1)	0.009(1)	-0.002(1)
Ru(6)	0.036(1)	0.033(1)	0.043(1)	0.004(1)	0.015(1)	0.003(1)
C(11)	0.032(8)	0.071(12)	0.073(12)	-0.005(9)	0.021(8)	-0.002(8)
O(11)	0.040(7)	0.075(9)	0.144(12)	-0.018(8)	0.028(7)	-0.007(6)
C(12)	0.057(10)	0.039(9)	0.040(9)	-0.001(7)	0.024(8)	-0.002(8)
O(12)	0.084(9)	0.046(7)	0.073(8)	-0.011(6)	0.034(7)	-0.005(7)
C(21)	0.043(9)	0.049(10)	0.083(13)	-0.023(9)	0.014(9)	-0.010(8)
O(21)	0.040(7)	0.113(11)	0.122(10)	-0.059(8)	0.012(7)	-0.029(7)
C(22)	0.046(10)	0.055(10)	0.047(10)	-0.006(8)	0.022(8)	-0.008(8)
O(22)	0.075(9)	0.076(8)	0.077(9)	-0.033(7)	0.029(7)	-0.014(7)
C(31)	0.045(9)	0.041(8)	0.026(7)	0.000(6)	0.005(7)	0.017(7)
O(31)	0.082(9)	0.061(7)	0.079(8)	-0.019(6)	0.045(7)	0.008(7)
C(32)	0.028(8)	0.044(9)	0.034(8)	0.004(7)	0.010(6)	0.005(7)
O(32)	0.063(8)	0.049(7)	0.074(8)	-0.002(6)	0.041(7)	-0.015(6)
C(41)	0.079(13)	0.033(8)	0.064(11)	-0.009(8)	0.033(10)	-0.014(8)
O(41)	0.067(8)	0.075(8)	0.096(10)	0.001(7)	0.050(8)	0.017(7)
C(42)	0.062(11)	0.048(9)	0.082(13)	-0.001(9)	0.046(10)	-0.012(8)
O(42)	0.136(12)	0.076(8)	0.113(10)	-0.034(8)	0.084(10)	-0.059(9)
C(43)	0.068(11)	0.034(8)	0.056(11)	0.007(7)	0.042(9)	0.016(8)
O(43)	0.085(9)	0.083(8)	0.041(7)	0.019(6)	0.028(7)	0.019(7)
C(51)	0.058(10)	0.056(10)	0.063(11)	-0.021(8)	-0.003(9)	0.000(8)
O(51)	0.079(8)	0.146(13)	0.117(10)	-0.049(9)	-0.070(8)	0.047(9)
C(52)	0.067(12)	0.072(12)	0.060(11)	-0.027(9)	0.033(10)	-0.021(10)
O(52)	0.133(12)	0.068(8)	0.115(11)	-0.038(8)	0.076(10)	-0.053(8)
C(53)	0.043(10)	0.071(11)	0.035(9)	-0.001(8)	0.006(8)	0.002(8)

Table A6.3 continued

O(53)	0.073(9)	0.103(10)	0.070(9)	-0.020(8)	0.037(7)	0.003(8)
C(61)	0.052(10)	0.061(11)	0.053(11)	-0.001(8)	0.025(9)	-0.010(8)
O(61)	0.050(7)	0.100(10)	0.089(9)	0.019(7)	0.040(7)	0.000(7)
C(62)	0.041(10)	0.047(10)	0.076(12)	0.001(9)	0.002(9)	0.014(8)
O(62)	0.087(10)	0.034(7)	0.171(14)	-0.020(8)	0.012(10)	0.007(7)
C(63)	0.042(15)	0.068(14)	0.059(15)	0.032(12)	0.020(12)	0.021(12)
O(63)	0.089(15)	0.149(13)	0.062(14)	0.051(11)	0.031(12)	0.046(11)

Table A6.4 Bond lengths (Å) for Ru₆C(CO)₁₅(PhCCH) (XR6)

Ru(1) -Ru(2)	2.837(2)	Ru(1) -Ru(3)	2.815(2)
Ru(1) -Ru(4)	2.980(2)	Ru(1) -Ru(5)	2.863(1)
Ru(1) -C	2.015(14)	Ru(1) -C(11)	1.894(15)
Ru(1) -C(12)	1.895(15)	Ru(1) -C(1)	2.095(13)
Ru(2) -Ru(3)	2.764(2)	Ru(2) -Ru(4)	2.963(2)
Ru(2) -Ru(6)	2.934(1)	Ru(2) -C	2.021(13)
Ru(2) -C(21)	1.892(16)	Ru(2) -C(22)	1.871(17)
Ru(2) -C(2)	2.076(13)	Ru(3) -Ru(5)	2.969(2)
Ru(3) -Ru(6)	2.930(2)	Ru(3) -C	2.070(18)
Ru(3) -C(31)	1.864(17)	Ru(3) -C(32)	1.915(15)
Ru(3) -C(1)	2.264(11)	Ru(3) -C(2)	2.174(11)
Ru(4) -Ru(5)	2.874(2)	Ru(4) -Ru(6)	2.857(2)
Ru(4) -C	2.035(18)	Ru(4) -C(41)	1.946(20)
Ru(4) -C(42)	1.925(16)	Ru(4) -C(43)	1.930(16)
Ru(5) -Ru(6)	2.912(2)	Ru(5) -C	2.059(13)
Ru(5) -C(51)	1.902(14)	Ru(5) -C(52)	1.908(19)
Ru(5) -C(53)	1.880(18)	Ru(6) -C	2.073(15)
Ru(6) -C(61)	1.913(19)	Ru(6) -C(62)	1.893(16)
Ru(6) -C(63)	1.862(21)	C(11) -O(11)	1.131(18)
C(12) -O(12)	1.116(19)	C(21) -O(21)	1.128(20)
C(22) -O(22)	1.177(22)	C(31) -O(31)	1.146(22)
C(32) -O(32)	1.119(19)	C(41) -O(41)	1.107(25)
C(42) -O(42)	1.098(20)	C(43) -O(43)	1.111(19)
C(51) -O(51)	1.120(18)	C(52) -O(52)	1.144(23)
C(53) -O(53)	1.150(24)	C(61) -O(61)	1.140(24)
C(62) -O(62)	1.149(20)	C(63) -O(63)	1.14(3)
C(1) -C(2)	1.365(17)	C(1) -C(111)	1.475(13)
C(111) -C(112)	1.395	C(111) -C(116)	1.395
C(112) -C(113)	1.395	C(113) -C(114)	1.395
C(114) -C(115)	1.395	C(115) -C(116)	1.395

Table A6.5 Bond angles ($^{\circ}$) for $\text{Ru}_6\text{C}(\text{CO})_{15}(\text{PhCCH})$ (XR6)

C(1) -Ru(1) -Ru(2)	70.1(3)	C(1) -Ru(1) -Ru(3)	52.4(3)
C(1) -Ru(1) -Ru(4)	129.8(3)	C(1) -Ru(1) -Ru(5)	113.3(3)
C(2) -Ru(2) -Ru(1)	68.5(4)	C(2) -Ru(2) -Ru(3)	51.0(3)
C(2) -Ru(2) -Ru(4)	128.5(4)	C(2) -Ru(2) -Ru(6)	111.7(3)
C(1) -Ru(3) -Ru(1)	47.2(4)	C(1) -Ru(3) -Ru(2)	69.6(3)
C(1) -Ru(3) -Ru(5)	104.6(3)	C(1) -Ru(3) -Ru(6)	127.6(3)
C(2) -Ru(3) -Ru(1)	67.8(4)	C(2) -Ru(3) -Ru(2)	47.9(4)
C(2) -Ru(3) -Ru(5)	124.6(4)	C(2) -Ru(3) -Ru(6)	108.8(3)
O(11) -C(11) -Ru(1)	178(1)	O(12) -C(12) -Ru(1)	178(2)
O(21) -C(21) -Ru(2)	176(2)	O(22) -C(22) -Ru(2)	177(1)
O(31) -C(31) -Ru(3)	177(1)	O(32) -C(32) -Ru(3)	175(1)
O(41) -C(41) -Ru(4)	172(1)	O(42) -C(42) -Ru(4)	175(2)
O(43) -C(43) -Ru(4)	177(1)	O(51) -C(51) -Ru(5)	177(2)
O(52) -C(52) -Ru(5)	174(2)	O(53) -C(53) -Ru(5)	178(1)
O(61) -C(61) -Ru(6)	173(1)	O(62) -C(62) -Ru(6)	174(1)
O(63) -C(63) -Ru(6)	174(2)	Ru(3) -C(1) -Ru(1)	80.4(4)
C(2) -C(1) -Ru(1)	108.2(9)	C(2) -C(1) -Ru(3)	68.5(7)
C(111)-C(1) -Ru(1)	125.3(8)	C(111)-C(1) -Ru(3)	127.9(8)
C(111)-C(1) -C(2)	125(1)	Ru(3) -C(2) -Ru(2)	81.1(4)
C(1) -C(2) -Ru(2)	113(1)	C(1) -C(2) -Ru(3)	75.7(7)
C(112)-C(111)-C(1)	123.4(7)	C(116)-C(111)-C(1)	116.6(7)
C(116)-C(111)-C(112)	120.0	C(113)-C(112)-C(111)	120.0
C(114)-C(113)-C(112)	120.0	C(115)-C(114)-C(113)	120.0
C(116)-C(115)-C(114)	120.0	C(115)-C(116)-C(111)	120.0

TABLE A7.1 Fractional atomic coordinates and thermal

parameters (\AA^2) for $\text{Ru}_6\text{C}(\text{CO})_{15}(\text{PhCCMe})$ (XR7)

Atom	x	y	z	U_{iso} or U_{eq}
Ru(1)	-0.34026(4)	-0.16929(8)	0.06342(8)	0.0301(4)
Ru(2)	-0.18220(4)	-0.07217(8)	0.07753(8)	0.0307(4)
Ru(3)	-0.23152(4)	-0.12032(8)	0.33074(8)	0.0297(4)
Ru(4)	-0.25276(5)	-0.35748(8)	-0.11674(8)	0.0314(4)
Ru(5)	-0.29979(5)	-0.39829(8)	0.15663(8)	0.0338(4)
Ru(6)	-0.14053(4)	-0.30112(8)	0.15424(8)	0.0335(4)
C(11)	-0.3685(6)	-0.0860(11)	-0.0836(11)	0.048(6)
O(11)	-0.3857(5)	-0.0331(9)	-0.1700(9)	0.071(6)
C(12)	-0.4426(6)	-0.1882(11)	0.0965(12)	0.047(6)
O(12)	-0.5049(5)	-0.1954(11)	0.1157(12)	0.090(7)
C(21)	-0.1975(6)	0.0316(11)	-0.0563(12)	0.047(6)
O(21)	-0.2085(5)	0.0945(9)	-0.1373(10)	0.084(6)
C(22)	-0.0766(6)	0.0143(10)	0.1400(11)	0.041(6)
O(22)	-0.0129(4)	0.0695(9)	0.1808(10)	0.064(5)
C(31)	-0.1554(6)	-0.0112(11)	0.5063(11)	0.046(6)
O(31)	-0.1092(5)	0.0555(9)	0.6066(9)	0.070(6)
C(32)	-0.2949(6)	-0.1612(10)	0.4660(11)	0.047(6)
O(32)	-0.3341(5)	-0.1867(9)	0.5428(10)	0.082(6)
C(41)	-0.3501(6)	-0.3898(10)	-0.2528(12)	0.042(6)
O(41)	-0.4058(5)	-0.4169(8)	-0.3425(10)	0.061(5)
C(42)	-0.1922(6)	-0.2664(11)	-0.2221(11)	0.044(6)
O(42)	-0.1596(5)	-0.2308(9)	-0.3049(8)	0.062(5)
C(43)	-0.2288(9)	-0.5255(17)	-0.2231(18)	0.058(10)
O(43)	-0.2136(7)	-0.6283(14)	-0.2794(15)	0.102(10)
C(51)	-0.2683(7)	-0.4521(11)	0.3308(12)	0.050(7)
O(51)	-0.2491(6)	-0.4871(8)	0.4309(9)	0.079(6)
C(52)	-0.4045(9)	-0.4227(16)	0.1728(17)	0.060(10)
O(52)	-0.4676(8)	-0.4476(13)	0.1884(15)	0.097(9)
C(53)	-0.3153(6)	-0.5748(12)	0.0135(12)	0.049(7)
O(53)	-0.3259(6)	-0.6863(8)	-0.0566(10)	0.073(6)
C(61)	-0.0787(7)	-0.2336(12)	0.3588(14)	0.058(7)
O(61)	-0.0375(5)	-0.2026(10)	0.4734(9)	0.078(6)
C(62)	-0.0532(6)	-0.2681(13)	0.0662(14)	0.059(7)
O(62)	-0.0005(5)	-0.2551(11)	0.0138(13)	0.108(8)
C(63)	-0.1350(6)	-0.4836(13)	0.1189(14)	0.057(7)
O(63)	-0.1298(6)	-0.5946(9)	0.0977(12)	0.085(7)
C1(1)	-0.0546(5)	-0.5528(10)	-0.3032(13)	0.116(7)
C1(2)	0.0231(8)	-0.5093(13)	-0.5408(16)	0.139(11)
C	-0.2422(7)	-0.2377(12)	0.1013(13)	0.029(2)
C(1)	-0.2995(5)	0.0073(9)	0.2461(10)	0.035(2)
C(2)	-0.2216(5)	0.0575(9)	0.2517(10)	0.036(2)
C(3)	-0.1794(6)	0.2021(11)	0.3388(12)	0.047(3)
C(111)	-0.3505(4)	0.0965(7)	0.3215(8)	0.040(2)
C(112)	-0.3665(4)	0.1013(7)	0.4653(8)	0.081(4)
C(113)	-0.4160(4)	0.1825(7)	0.5286(8)	0.095(5)
C(114)	-0.4496(4)	0.2590(7)	0.4481(8)	0.065(3)
C(115)	-0.4336(4)	0.2542(7)	0.3044(8)	0.073(4)
C(116)	-0.3841(4)	0.1729(7)	0.2411(8)	0.069(3)
C(s)	-0.0201(31)	-0.4293(52)	-0.3593(59)	0.121(20)

TABLE A7.2 Fractional atomic coordinates for the
hydrogen atoms for $\text{Ru}_6\text{C}(\text{CO})_{15}(\text{PhCCMe})$ (XR7)

Atom	x	y	z
H(3a)	-0.1197	0.2142	0.3255
H(3b)	-0.1815	0.2248	0.4589
H(3c)	-0.2070	0.2702	0.2934
H(112)	-0.3400	0.0433	0.5285
H(113)	-0.4284	0.1869	0.6395
H(114)	-0.4891	0.3198	0.4944
H(115)	-0.4614	0.3091	0.2385
H(116)	-0.3730	0.1655	0.1276

TABLE A7.3 Anisotropic thermal parameters (\AA^2) for

Atom	$\text{Ru}_6\text{C}(\text{CO})_{15}(\text{PhCCMe})$ (XR7)					
	U_{11}	U_{22}	U_{33}	U_{23}	U_{13}	U_{12}
Ru(1)	0.0302(4)	0.0320(4)	0.0281(3)	0.0074(3)	0.0032(3)	0.0072(3)
Ru(2)	0.0343(4)	0.0307(4)	0.0271(3)	0.0115(3)	0.0084(3)	0.0045(3)
Ru(3)	0.0338(4)	0.0325(4)	0.0229(3)	0.0093(3)	0.0060(3)	0.0056(3)
Ru(4)	0.0355(5)	0.0329(4)	0.0258(3)	0.0060(3)	0.0058(3)	0.0063(3)
Ru(5)	0.0351(5)	0.0313(4)	0.0350(4)	0.0136(3)	0.0070(3)	0.0020(3)
Ru(6)	0.0302(4)	0.0366(5)	0.0336(4)	0.0149(3)	0.0054(3)	0.0095(3)
C(11)	0.055(7)	0.054(7)	0.035(5)	0.016(5)	0.003(5)	0.018(6)
O(11)	0.078(6)	0.073(6)	0.061(5)	0.036(5)	0.007(5)	0.025(5)
C(12)	0.044(6)	0.048(7)	0.049(6)	0.018(5)	0.010(5)	0.013(5)
O(12)	0.040(5)	0.122(8)	0.107(8)	0.044(7)	0.024(5)	0.023(5)
C(21)	0.050(6)	0.042(6)	0.048(6)	0.019(5)	0.016(5)	0.006(5)
O(21)	0.097(7)	0.081(6)	0.073(6)	0.056(5)	0.020(5)	0.024(5)
C(22)	0.047(7)	0.046(6)	0.031(5)	0.009(5)	0.004(5)	-0.005(5)
O(22)	0.044(5)	0.082(6)	0.066(5)	0.023(5)	0.001(4)	-0.015(4)
C(31)	0.054(7)	0.053(7)	0.032(5)	0.012(5)	0.009(5)	0.011(6)
O(31)	0.072(6)	0.087(7)	0.050(4)	0.006(5)	-0.010(4)	-0.018(5)
C(32)	0.063(7)	0.037(6)	0.042(5)	0.013(5)	0.017(5)	0.012(5)
O(32)	0.088(6)	0.086(7)	0.072(5)	0.034(5)	0.051(5)	0.007(5)
C(41)	0.045(6)	0.037(6)	0.043(6)	0.008(5)	0.010(5)	0.000(5)
O(41)	0.053(5)	0.060(5)	0.069(5)	0.015(5)	-0.011(5)	0.005(4)
C(42)	0.041(6)	0.057(7)	0.033(5)	0.011(5)	0.003(5)	0.006(5)
O(42)	0.062(5)	0.080(6)	0.043(4)	0.023(4)	0.015(4)	-0.005(4)
C(43)	0.089(10)	0.054(10)	0.032(9)	0.012(8)	0.021(8)	0.029(8)
O(43)	0.184(10)	0.060(10)	0.061(10)	0.010(8)	0.048(8)	0.073(8)
C(51)	0.063(8)	0.043(7)	0.044(6)	0.021(5)	0.006(5)	0.008(6)

Table A7.3 continued

O(51)	0.122(8)	0.061(6)	0.052(5)	0.029(4)	0.004(5)	0.022(5)
C(52)	0.047(10)	0.056(10)	0.078(9)	0.038(8)	0.009(8)	0.002(8)
O(52)	0.045(10)	0.098(9)	0.149(9)	0.059(8)	0.038(8)	0.014(8)
C(53)	0.049(7)	0.056(8)	0.042(6)	0.010(6)	0.005(5)	-0.003(6)
O(53)	0.101(7)	0.046(5)	0.072(6)	-0.007(5)	0.029(5)	-0.014(5)
C(61)	0.053(7)	0.063(8)	0.058(7)	0.021(6)	0.009(6)	0.021(6)
O(61)	0.075(6)	0.117(8)	0.041(4)	0.010(5)	-0.010(4)	0.036(6)
C(62)	0.042(6)	0.069(8)	0.065(7)	0.032(6)	0.011(6)	0.024(6)
O(62)	0.063(6)	0.128(9)	0.132(9)	0.075(8)	0.059(6)	0.042(6)
C(63)	0.039(6)	0.062(8)	0.071(8)	0.025(7)	0.010(6)	0.014(6)
O(63)	0.089(7)	0.049(5)	0.117(8)	0.028(5)	0.019(6)	0.031(5)
C1(1)	0.076(6)	0.125(8)	0.149(9)	0.014(7)	0.025(6)	0.020(5)
C1(2)	0.164(13)	0.103(8)	0.151(13)	0.041(9)	0.047(8)	0.027(8)

TABLE A7.4 Bond lengths (\AA) for $\text{Ru}_6\text{C}(\text{CO})_{15}(\text{PhCCMe})$ (XR7)

Ru(1) -Ru(2)	2.815(1)	Ru(1) -Ru(3)	2.791(1)
Ru(1) -Ru(4)	2.989(1)	Ru(1) -Ru(5)	2.952(1)
Ru(1) -C	2.015(14)	Ru(1) -C(11)	1.883(13)
Ru(1) -C(12)	1.882(12)	Ru(1) -C(1)	2.069(8)
Ru(2) -Ru(3)	2.782(1)	Ru(2) -Ru(4)	2.991(1)
Ru(2) -Ru(6)	2.885(1)	Ru(2) -C	1.992(13)
Ru(2) -C(21)	1.904(13)	Ru(2) -C(22)	1.888(10)
Ru(2) -C(2)	2.078(9)	Ru(3) -Ru(5)	2.880(1)
Ru(3) -Ru(6)	2.974(1)	Ru(3) -C	2.098(11)
Ru(3) -C(31)	1.906(9)	Ru(3) -C(32)	1.902(12)
Ru(3) -C(1)	2.181(11)	Ru(3) -C(2)	2.201(11)
Ru(4) -Ru(5)	2.915(1)	Ru(4) -Ru(6)	2.836(1)
Ru(4) -C	2.019(11)	Ru(4) -C(41)	1.916(11)
Ru(4) -C(42)	1.894(12)	Ru(4) -C(43)	1.908(17)
Ru(5) -Ru(6)	2.870(1)	Ru(5) -C	2.079(14)
Ru(5) -C(51)	1.910(13)	Ru(5) -C(52)	1.876(17)
Ru(5) -C(53)	1.902(11)	Ru(6) -C	2.069(14)
Ru(6) -C(61)	1.929(12)	Ru(6) -C(62)	1.890(13)
Ru(6) -C(63)	1.880(14)	C(11) -O(11)	1.140(16)
C(12) -O(12)	1.143(15)	C(21) -O(21)	1.157(17)
C(22) -O(22)	1.147(13)	C(31) -O(31)	1.125(11)
C(32) -O(32)	1.125(16)	C(41) -O(41)	1.140(13)
C(42) -O(42)	1.141(15)	C(43) -O(43)	1.151(22)
C(51) -O(51)	1.128(16)	C(52) -O(52)	1.153(22)
C(53) -O(53)	1.139(14)	C(61) -O(61)	1.134(14)
C(62) -O(62)	1.127(17)	C(63) -O(63)	1.152(17)
C(1) -C(2)	1.395(13)	C(1) -C(111)	1.504(12)
C(2) -C(3)	1.519(13)	C(111) -C(112)	1.395
C(111) -C(116)	1.395	C(112) -C(113)	1.395
C(113) -C(114)	1.395	C(114) -C(115)	1.395
C(115) -C(116)	1.395	Cl(1) -C((s))	1.61(6)
Cl(2) -C((s))	1.97(6)	Cl(2) -Cl(2)	1.20(3)

TABLE A7.5 Bond angles ($^{\circ}$) for $\text{Ru}_6\text{C}(\text{CO})_{15}(\text{PhCCMe})$ (XR7)

C(1) -Ru(1) -Ru(2)	70.0(3)	C(1) -Ru(1) -Ru(3)	50.7(3)
C(1) -Ru(1) -Ru(4)	129.8(3)	C(1) -Ru(1) -Ru(5)	109.0(3)
C(2) -Ru(2) -Ru(1)	69.9(2)	C(2) -Ru(2) -Ru(3)	51.4(3)
C(2) -Ru(2) -Ru(4)	129.8(3)	C(2) -Ru(2) -Ru(6)	112.9(3)
C(1) -Ru(3) -Ru(1)	47.2(2)	C(1) -Ru(3) -Ru(2)	69.4(3)
C(1) -Ru(3) -Ru(5)	108.1(2)	C(1) -Ru(3) -Ru(6)	126.1(3)
C(2) -Ru(3) -Ru(1)	69.0(2)	C(2) -Ru(3) -Ru(2)	47.6(2)
C(2) -Ru(3) -Ru(5)	128.4(2)	C(2) -Ru(3) -Ru(6)	106.0(3)
C(2) -Ru(3) -C(1)	37.1(4)	O(11) -C(11) -Ru(1)	178.4(9)
O(12) -C(12) -Ru(1)	177(1)	O(21) -C(21) -Ru(2)	178(1)
O(22) -C(22) -Ru(2)	178.2(9)	O(31) -C(31) -Ru(3)	177(1)
O(32) -C(32) -Ru(3)	178.2(9)	O(41) -C(41) -Ru(4)	174(1)
O(42) -C(42) -Ru(4)	168.8(8)	O(43) -C(43) -Ru(4)	176(2)
O(51) -C(51) -Ru(5)	178(1)	O(52) -C(52) -Ru(5)	173(2)
O(53) -C(53) -Ru(5)	171(1)	O(61) -C(61) -Ru(6)	173(1)
O(62) -C(62) -Ru(6)	176(1)	O(63) -C(63) -Ru(6)	178(1)
Ru(3) -C(1) -Ru(1)	82.0(4)	C(2) -C(1) -Ru(1)	110.2(6)
C(2) -C(1) -Ru(3)	72.2(6)	C(111)-C(1) -Ru(1)	124.1(6)
C(111)-C(1) -Ru(3)	130.7(7)	C(111)-C(1) -C(2)	121.8(7)
Ru(3) -C(2) -Ru(2)	81.0(3)	C(1) -C(2) -Ru(2)	109.8(6)
C(1) -C(2) -Ru(3)	70.7(6)	C(3) -C(2) -Ru(2)	123.6(7)
C(3) -C(2) -Ru(3)	128.7(7)	C(3) -C(2) -C(1)	124.4(9)
C(112)-C(111)-C(1)	122.1(8)	C(116)-C(111)-C(1)	117.9(8)
C(116)-C(111)-C(112)	120.0	C(113)-C(112)-C(111)	120.0
C(114)-C(113)-C(112)	120.0	C(115)-C(114)-C(113)	120.0
C(116)-C(115)-C(114)	120.0	C(115)-C(116)-C(111)	120.0
Cl(2) -C(s)-Cl(1)	106(3)		

Table A8.1 Fractional atomic coordinates and thermal

parameters (\AA^2) for $\text{Ru}_6\text{C}(\text{CO})_{14}(\text{PhCCH})\{\text{Au}(\text{PMe}_3)\}_2$ (XR8)

Atom	x	y	z	U_{iso} or U_{eq}
Au(1)	0.25942(7)	0.00095(9)	0.03719(6)	0.0433(7)
Au(2)	0.16742(7)	0.14129(8)	0.10737(7)	0.0460(7)
Ru(1)	0.21764(11)	-0.00569(14)	0.29595(10)	0.0320(11)
Ru(2)	0.31642(12)	0.04977(15)	0.18383(11)	0.0374(12)
Ru(3)	0.36395(12)	-0.10831(15)	0.27229(11)	0.0375(13)
Ru(4)	0.14777(12)	-0.05444(14)	0.14743(11)	0.0353(12)
Ru(5)	0.20245(13)	-0.20792(15)	0.23902(11)	0.0395(13)
Ru(6)	0.30962(13)	-0.15289(16)	0.12946(11)	0.0425(13)
C(1)	0.3368(13)	0.0212(16)	0.3401(13)	0.039(15)
C(2)	0.3859(13)	0.0500(18)	0.2794(13)	0.042(16)
P(1)	0.2627(5)	0.0558(5)	-0.0786(4)	0.053(5)
P(2)	0.1143(4)	0.2955(5)	0.0832(4)	0.053(5)
C(3)	0.3202(19)	-0.0238(18)	-0.1381(15)	0.080(21)
C(4)	0.1649(16)	0.0628(19)	-0.1288(15)	0.066(19)
C(5)	0.3089(18)	0.1792(19)	-0.0835(16)	0.076(22)
C(6)	0.0393(17)	0.3063(22)	0.0103(17)	0.081(23)
C(7)	0.2001(16)	0.3842(17)	0.0617(17)	0.069(20)
C(8)	0.0700(17)	0.3516(21)	0.1624(16)	0.079(22)
C(11)	0.1742(16)	0.1191(20)	0.3058(14)	0.051(8)
O(11)	0.1456(13)	0.1962(17)	0.3158(12)	0.096(7)
C(12)	0.1643(15)	-0.0442(18)	0.3756(14)	0.045(7)
O(12)	0.1291(11)	-0.0616(13)	0.4280(11)	0.067(6)
C(21)	0.2942(15)	0.1799(20)	0.2031(14)	0.051(7)
O(21)	0.2871(11)	0.2633(14)	0.2190(11)	0.072(6)
C(22)	0.4026(21)	0.0860(25)	0.1321(18)	0.089(11)
O(22)	0.4623(15)	0.1108(17)	0.1078(13)	0.106(8)
C(31)	0.4714(18)	-0.1230(20)	0.2611(15)	0.060(8)
O(31)	0.5442(16)	-0.1320(18)	0.2504(13)	0.117(8)
C(32)	0.3647(15)	-0.1978(19)	0.3502(14)	0.049(7)
O(32)	0.3714(12)	-0.2496(15)	0.3984(12)	0.080(6)
C(41)	0.0600(16)	0.0152(20)	0.1819(14)	0.056(8)
O(41)	0.0044(13)	0.0556(15)	0.2049(11)	0.084(7)
C(42)	0.0905(14)	-0.0722(17)	0.0560(13)	0.039(6)
O(42)	0.0566(11)	-0.0887(14)	0.0029(11)	0.070(6)
C(45)	0.0947(17)	-0.1834(20)	0.1853(15)	0.061(8)
O(45)	0.0278(13)	-0.2205(15)	0.1729(11)	0.084(7)
C(51)	0.2071(21)	-0.3391(28)	0.2113(19)	0.096(11)
O(51)	0.2059(14)	-0.4195(19)	0.1922(13)	0.112(8)
C(52)	0.1576(15)	-0.2503(18)	0.3230(14)	0.046(7)
O(52)	0.1296(12)	-0.2828(15)	0.3737(12)	0.079(6)
C(61)	0.3702(20)	-0.2572(25)	0.1771(19)	0.089(11)
O(61)	0.4087(12)	-0.3278(15)	0.1909(11)	0.078(6)
C(62)	0.3953(19)	-0.1271(23)	0.0736(18)	0.082(10)
O(62)	0.4553(14)	-0.1147(16)	0.0391(12)	0.097(7)
C(63)	0.2497(16)	-0.2230(20)	0.0620(15)	0.056(8)
O(63)	0.2156(14)	-0.2751(17)	0.0225(13)	0.099(8)
C	0.2521(14)	-0.0751(17)	0.2101(12)	0.037(6)
C(111)	0.3628(10)	0.0385(12)	0.4158(7)	0.044(7)
C(112)	0.3399(10)	-0.0256(12)	0.4694(7)	0.052(8)
C(113)	0.3690(10)	-0.0103(12)	0.5403(7)	0.065(8)
C(114)	0.4210(10)	0.0692(12)	0.5576(7)	0.078(10)
C(115)	0.4439(10)	0.1333(12)	0.5040(7)	0.061(8)
C(116)	0.4148(10)	0.1180(12)	0.4331(7)	0.050(7)

Table A8.2 Fractional atomic coordinates for the

hydrogen atoms for $\text{Ru}_6\text{C}(\text{CO})_{14}(\text{PhCCH})\{\text{Au}(\text{PMe}_3)\}_2$ (XR8)

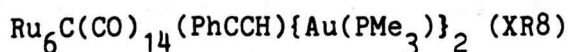
Atom	x	y	z
H(112)	0.2999	-0.0870	0.4574
H(113)	0.3520	-0.0586	0.5829
H(114)	0.4443	0.0828	0.6126
H(115)	0.4845	0.1957	0.5168
H(116)	0.4324	0.1673	0.3913
H(31)	0.3822	-0.0360	-0.1151
H(32)	0.3231	0.0114	-0.1897
H(33)	0.2885	-0.0935	-0.1447
H(41)	0.1228	0.1081	-0.1005
H(42)	0.1392	-0.0102	-0.1356
H(43)	0.1738	0.0947	-0.1807
H(51)	0.3683	0.1797	-0.0538
H(52)	0.2685	0.2323	-0.0606
H(53)	0.3171	0.1979	-0.1387
H(61)	-0.0117	0.2573	0.0188
H(62)	0.0669	0.2869	-0.0389
H(63)	0.0170	0.3811	0.0069
H(71)	0.2488	0.3819	0.1039
H(72)	0.1752	0.4579	0.0574
H(73)	0.2250	0.3636	0.0115
H(81)	0.1142	0.3466	0.2080
H(82)	0.0140	0.3129	0.1740
H(83)	0.0557	0.4279	0.1514
H	0.4573	0.0942	0.2856

Table A8.3 Anisotropic thermal parameters (\AA^2) for

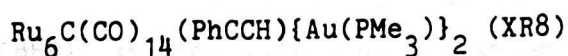
$\text{Ru}_6\text{C}(\text{CO})_{14}(\text{PhCCH})\{\text{Au}(\text{PMe}_3)\}_2$ (XR8)

Atom	U_{11}	U_{22}	U_{33}	U_{23}	U_{13}	U_{12}
Au(1)	0.043(1)	0.056(1)	0.030(1)	0.009(1)	0.004(1)	0.001(1)
Au(2)	0.061(1)	0.027(1)	0.050(1)	0.007(1)	0.003(1)	0.002(1)
Ru(1)	0.027(1)	0.033(1)	0.036(1)	-0.005(1)	0.001(1)	0.002(1)
Ru(2)	0.030(1)	0.045(1)	0.037(1)	0.004(1)	0.002(1)	-0.005(1)
Ru(3)	0.029(1)	0.046(1)	0.038(1)	-0.005(1)	-0.001(1)	0.010(1)
Ru(4)	0.032(1)	0.033(1)	0.041(1)	0.002(1)	-0.003(1)	-0.004(1)
Ru(5)	0.049(1)	0.031(1)	0.039(1)	-0.001(1)	-0.001(1)	-0.003(1)
Ru(6)	0.043(1)	0.050(1)	0.035(1)	-0.006(1)	0.001(1)	0.009(1)
C(1)	0.036(14)	0.025(14)	0.056(16)	-0.027(13)	-0.026(13)	0.009(11)
C(2)	0.032(14)	0.054(17)	0.041(16)	-0.008(14)	0.012(13)	-0.009(13)
P(1)	0.066(5)	0.047(5)	0.046(5)	0.011(4)	0.002(4)	-0.013(4)
P(2)	0.046(4)	0.039(4)	0.074(6)	0.006(4)	-0.006(4)	0.004(4)
C(3)	0.134(25)	0.039(19)	0.068(20)	-0.006(15)	0.055(19)	-0.004(17)
C(4)	0.061(19)	0.057(18)	0.079(21)	0.027(17)	-0.027(17)	-0.002(15)
C(5)	0.092(23)	0.055(19)	0.082(24)	0.002(17)	0.025(19)	-0.029(17)
C(6)	0.080(21)	0.076(23)	0.088(26)	0.001(20)	-0.024(19)	0.011(18)
C(7)	0.058(18)	0.038(15)	0.110(25)	0.028(16)	0.011(18)	-0.007(14)
C(8)	0.086(22)	0.071(20)	0.081(22)	-0.033(18)	0.026(19)	0.029(17)

Table A8.4 Bond lengths (Å) for

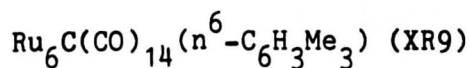


Au(1) -Au(2)	2.795(2)	Au(1) -Ru(2)	2.915(2)
Au(1) -Ru(4)	2.920(2)	Au(1) -Ru(6)	2.799(2)
Au(1) -P(1)	2.294(7)	Au(2) -Ru(2)	2.996(2)
Au(2) -Ru(4)	2.787(2)	Au(2) -C(21)	2.690(24)
Au(2) -P(2)	2.299(7)	Ru(1) -Ru(2)	2.815(3)
Ru(1) -Ru(3)	2.805(3)	Ru(1) -Ru(4)	3.008(3)
Ru(1) -Ru(5)	2.952(3)	Ru(1) -C(11)	1.85(3)
Ru(1) -C(12)	1.84(3)	Ru(1) -C	1.972(23)
Ru(1) -C(1)	2.083(21)	Ru(2) -Ru(3)	2.791(3)
Ru(2) -Ru(4)	3.111(3)	Ru(2) -Ru(6)	2.935(3)
Ru(2) -C(21)	1.85(3)	Ru(2) -C(22)	1.81(4)
Ru(2) -C	2.066(23)	Ru(2) -C(2)	2.051(23)
Ru(3) -Ru(5)	2.974(3)	Ru(3) -Ru(6)	2.826(3)
Ru(3) -C(31)	1.77(3)	Ru(3) -C(32)	1.90(3)
Ru(3) -C(61)	2.70(3)	Ru(3) -C	2.139(22)
Ru(3) -C(1)	2.228(22)	Ru(3) -C(2)	2.183(24)
Ru(4) -Ru(5)	2.807(3)	Ru(4) -Ru(6)	2.977(3)
Ru(4) -C(41)	1.85(3)	Ru(4) -C(42)	1.909(24)
Ru(4) -C(45)	2.09(3)	Ru(4) -C	2.013(22)
Ru(5) -Ru(6)	2.862(3)	Ru(5) -C(45)	1.99(3)
Ru(5) -C(51)	1.86(4)	Ru(5) -C(52)	1.86(3)
Ru(5) -C	2.061(23)	Ru(6) -C(61)	1.91(3)
Ru(6) -C(62)	1.82(3)	Ru(6) -C(63)	1.81(3)
Ru(6) -C	2.104(23)	C(11) -O(11)	1.16(3)
C(12) -O(12)	1.19(3)	C(21) -O(21)	1.18(3)
C(22) -O(22)	1.14(4)	C(31) -O(31)	1.21(4)
C(32) -O(32)	1.14(3)	C(41) -O(41)	1.16(3)
C(42) -O(42)	1.13(3)	C(45) -O(45)	1.20(3)
C(51) -O(51)	1.15(5)	C(52) -O(52)	1.16(3)
C(61) -O(61)	1.16(4)	C(62) -O(62)	1.21(4)
C(63) -O(63)	1.14(3)	C(1) -C(2)	1.48(3)
C(1) -C(111)	1.47(3)	C(111) -C(112)	1.395
C(111) -C(116)	1.395	C(112) -C(113)	1.395
C(113) -C(114)	1.395	C(114) -C(115)	1.395
C(115) -C(116)	1.395	P(1) -C(3)	1.84(3)
P(1) -C(4)	1.79(3)	P(1) -C(5)	1.84(3)
P(2) -C(6)	1.77(3)	P(2) -C(7)	1.90(3)
P(2) -C(8)	1.85(3)		

Table A8.5 Bond angles ($^{\circ}$) for

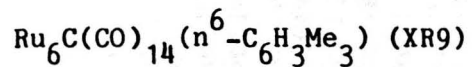
C(1) -Ru(1) -Ru(2)	72.2(7)	C(1) -Ru(1) -Ru(3)	51.7(6)
C(1) -Ru(1) -Ru(4)	133.7(7)	C(1) -Ru(1) -Ru(5)	111.2(6)
C(2) -Ru(2) -Au(1)	160.8(7)	C(2) -Ru(2) -Au(2)	142.8(7)
C(2) -Ru(2) -Ru(1)	69.9(7)	C(2) -Ru(2) -Ru(3)	50.8(7)
C(2) -Ru(2) -Ru(4)	128.1(7)	C(2) -Ru(2) -Ru(6)	108.0(7)
C(1) -Ru(3) -Ru(2)	70.9(6)	C(1) -Ru(3) -Ru(5)	106.1(6)
C(1) -Ru(3) -Ru(6)	130.3(6)	C(2) -Ru(3) -Ru(1)	68.6(6)
C(2) -Ru(3) -Ru(2)	46.8(6)	C(2) -Ru(3) -Ru(5)	126.8(6)
C(2) -Ru(3) -Ru(6)	108.0(6)	C(2) -Ru(3) -C(1)	39.1(9)
O(11) -C(11) -Ru(1)	176(2)	O(12) -C(12) -Ru(1)	175(2)
Ru(2) -C(21) -Au(2)	80.4(9)	O(21) -C(21) -Au(2)	106(2)
O(21) -C(21) -Ru(2)	174(2)	O(22) -C(22) -Ru(2)	171(3)
O(31) -C(31) -Ru(3)	177(2)	O(32) -C(32) -Ru(3)	175(2)
O(41) -C(41) -Ru(4)	177(2)	O(42) -C(42) -Ru(4)	176(2)
Ru(5) -C(45) -Ru(4)	87(1)	O(45) -C(45) -Ru(4)	132(2)
O(45) -C(45) -Ru(5)	141(2)	O(51) -C(51) -Ru(5)	176(3)
O(52) -C(52) -Ru(5)	176(2)	Ru(6) -C(61) -Ru(3)	73(1)
O(61) -C(61) -Ru(3)	121(2)	O(61) -C(61) -Ru(6)	165(3)
O(62) -C(62) -Ru(6)	176(3)	O(63) -C(63) -Ru(6)	173(2)
Ru(3) -C(1) -Ru(1)	81.1(8)	C(2) -C(1) -Ru(1)	106(1)
C(2) -C(1) -Ru(3)	69(1)	C(111) -C(1) -Ru(1)	128(1)
C(111) -C(1) -Ru(3)	128(1)	C(111) -C(1) -C(2)	124(2)
Ru(3) -C(2) -Ru(2)	82.4(8)	C(1) -C(2) -Ru(2)	112(1)
C(1) -C(2) -Ru(3)	72(1)	C(112) -C(111) -C(1)	121(1)
C(116) -C(111) -C(1)	119(1)	C(116) -C(111) -C(112)	120
C(113) -C(112) -C(111)	120	C(114) -C(113) -C(112)	120
C(115) -C(114) -C(113)	120	C(116) -C(115) -C(114)	120
C(115) -C(116) -C(111)	120	C(3) -P(1) -Au(1)	114.9(9)
C(4) -P(1) -Au(1)	116(1)	C(4) -P(1) -C(3)	100(1)
C(5) -P(1) -Au(1)	112(1)	C(5) -P(1) -C(3)	106(1)
C(5) -P(1) -C(4)	106(1)	C(6) -P(2) -Au(2)	117(1)
C(7) -P(2) -Au(2)	110.6(8)	C(7) -P(2) -C(6)	105(1)
C(8) -P(2) -Au(2)	112(1)	C(8) -P(2) -C(6)	107(1)
C(8) -P(2) -C(7)	103(1)		

TABLE A9.1 Fractional atomic coordinates and

thermal parameters (\AA^2) for

Atom	x	y	z	U_{iso} or U_{eq}
Ru(1)	-0.26166(8)	0.34028(5)	-0.20245(8)	0.0338(5)
Ru(2)	-0.47405(10)	0.25000	-0.43241(13)	0.0363(6)
Ru(4)	-0.28128(7)	0.33989(4)	-0.52223(8)	0.0291(4)
Ru(6)	-0.06929(9)	0.25000	-0.29649(11)	0.0234(5)
C	-0.2629(11)	0.2500	-0.3596(12)	0.025(2)
C(11)	-0.3817(13)	0.3751(9)	-0.1109(15)	0.074(4)
O(11)	-0.4529(11)	0.3940(8)	-0.0421(14)	0.114(4)
C(12)	-0.1244(11)	0.3470(7)	-0.0167(13)	0.049(3)
O(12)	-0.0408(9)	0.3514(5)	0.1011(10)	0.070(2)
C(13)	-0.2355(10)	0.4492(7)	-0.2785(13)	0.051(3)
O(13)	-0.2068(9)	0.5189(6)	-0.2903(11)	0.075(3)
C(21)	-0.5769(12)	0.3382(8)	-0.3973(14)	0.060(3)
O(21)	-0.6486(10)	0.3918(7)	-0.3888(11)	0.089(3)
C(22)	-0.5773(20)	0.2500	-0.6353(24)	0.079(5)
O(22)	-0.6434(18)	0.2500	-0.7640(21)	0.119(6)
C(41)	-0.1641(10)	0.4072(6)	-0.5795(11)	0.042(2)
O(41)	-0.0956(8)	0.4515(5)	-0.6201(10)	0.070(2)
C(42)	-0.4225(11)	0.4031(7)	-0.6468(13)	0.052(3)
O(42)	-0.5111(9)	0.4439(6)	-0.7309(11)	0.084(3)
C(43)	-0.2904(13)	0.2500	-0.6824(16)	0.037(3)
O(43)	-0.2965(11)	0.2500	-0.8085(13)	0.060(3)
C(5)	0.0825(13)	0.2500	-0.4122(15)	0.036(3)
C(6)	0.0953(9)	0.1725(6)	-0.3332(10)	0.034(2)
C(7)	0.1223(10)	0.1709(6)	-0.1730(11)	0.040(2)
C(8)	0.1264(12)	0.2500	-0.0991(14)	0.034(3)
C(50)	0.0658(14)	0.2500	-0.5792(16)	0.041(3)
C(70)	0.1477(11)	0.0894(7)	-0.0924(12)	0.053(3)

TABLE A9.3 Anisotropic thermal parameters (\AA^2) for



Atom	U_{11}	U_{22}	U_{33}	U_{23}	U_{13}	U_{12}
Ru(1)	0.0392(5)	0.0331(5)	0.0292(5)	-0.0034(3)	0.0144(4)	0.0054(3)
Ru(2)	0.0236(5)	0.0427(7)	0.0424(7)	0.0000(1)	0.0117(5)	0.0000(1)
Ru(4)	0.0310(4)	0.0267(4)	0.0297(4)	0.0055(3)	0.0089(3)	0.0052(3)
Ru(6)	0.0228(5)	0.0244(5)	0.0230(5)	0.0000(1)	0.0054(4)	0.0000(1)

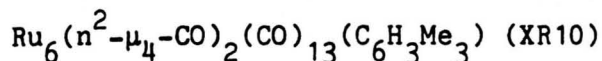
TABLE A9.4 Bond lengths (Å) for Ru₆C(CO)₁₄(n⁶-C₆H₃Me₃) (XR9)

Ru(1) - Ru(2)	2.906(1)	Ru(1) - Ru(4)	2.966(1)
Ru(1) - Ru(6)	2.872(1)	Ru(1) - C	2.065(9)
Ru(1) - C(11)	1.854(16)	Ru(1) - C(12)	1.855(10)
Ru(1) - C(13)	1.931(12)	Ru(1) - Ru(1)	2.868(2)
Ru(2) - Ru(4)	2.851(1)	Ru(2) - C	2.094(11)
Ru(2) - C(21)	1.873(13)	Ru(2) - C(22)	1.852(20)
Ru(4) - Ru(6)	2.882(1)	Ru(4) - C	2.060(8)
Ru(4) - C(41)	1.855(11)	Ru(4) - C(42)	1.845(10)
Ru(4) - C(43)	2.062(11)	Ru(4) - Ru(4)	2.856(1)
Ru(6) - C	1.923(11)	Ru(6) - C(5)	2.237(16)
Ru(6) - C(6)	2.256(10)	Ru(6) - C(7)	2.324(9)
Ru(6) - C(8)	2.256(11)	C(11) - O(11)	1.193(22)
C(12) - O(12)	1.160(12)	C(13) - O(13)	1.164(15)
C(21) - O(21)	1.161(17)	C(22) - O(22)	1.18(3)
C(41) - O(41)	1.167(15)	C(42) - O(42)	1.189(13)
C(43) - O(43)	1.175(20)	C(5) - C(6)	1.423(12)
C(5) - C(50)	1.530(21)	C(6) - C(7)	1.445(14)
C(7) - C(8)	1.432(12)	C(7) - C(70)	1.480(15)

TABLE A9.5 Bond angles ($^{\circ}$) for $\text{Ru}_6\text{C}(\text{CO})_{14}(\eta^6\text{-C}_6\text{H}_3\text{Me}_3)$ (XR9)

C(5) -Ru(6) -Ru(1)	149.2(1)	C(5) -Ru(6) -Ru(4)	98.1(3)
C(6) -Ru(6) -Ru(1)	171.2(2)	C(6) -Ru(6) -Ru(4)	126.8(2)
C(6) -Ru(6) -C(5)	36.9(3)	C(7) -Ru(6) -Ru(1)	134.5(3)
C(7) -Ru(6) -Ru(4)	163.4(3)	C(7) -Ru(6) -C(5)	66.4(4)
C(7) -Ru(6) -C(6)	36.7(4)	C(8) -Ru(6) -Ru(1)	106.6(3)
C(8) -Ru(6) -Ru(4)	150.2(1)	C(8) -Ru(6) -C(5)	78.4(5)
C(8) -Ru(6) -C(6)	66.0(4)	C(8) -Ru(6) -C(7)	36.4(3)
O(11) -C(11) -Ru(1)	175(1)	O(12) -C(12) -Ru(1)	178(1)
O(13) -C(13) -Ru(1)	165(1)	O(21) -C(21) -Ru(2)	174(1)
C(21) -Ru(2) -C(21)	96.8(8)	O(22) -C(22) -Ru(2)	180(1)
O(41) -C(41) -Ru(4)	176.8(8)	O(42) -C(42) -Ru(4)	177(1)
O(43) -C(43) -Ru(4)	136.2(3)	C(6) -C(5) -Ru(6)	72.2(8)
C(50) -C(5) -Ru(6)	131.5(9)	C(50) -C(5) -C(6)	120.0(6)
C(5) -C(6) -Ru(6)	70.8(7)	C(7) -C(6) -Ru(6)	74.2(6)
C(7) -C(6) -C(5)	121.1(9)	C(6) -Ru(6) -C(6)	66.2(5)
C(6) -C(5) -C(6)	120(1)	C(6) -C(7) -Ru(6)	69.0(5)
C(8) -C(7) -Ru(6)	69.2(6)	C(8) -C(7) -C(6)	117.4(9)
C(70) -C(7) -Ru(6)	134.7(8)	C(70) -C(7) -C(6)	119.5(9)
C(70) -C(7) -C(8)	123(1)	C(7) -Ru(6) -C(7)	65.5(5)
C(7) -C(8) -C(7)	123(2)	C(7) -C(8) -Ru(6)	74.4(5)

Table A10.1 Fractional atomic coordinates and

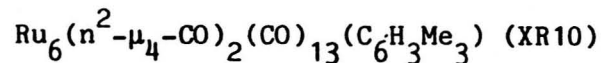
thermal parameters (\AA^2) for

Atom	x	y	z	U_{iso} or U_{eq}
Ru(1)	-0.41090(4)	0.15218(5)	-0.10814(8)	0.0391(4)
Ru(2)	-0.03405(4)	0.18553(5)	-0.23105(8)	0.0351(4)
Ru(3)	-0.22050(4)	0.20018(5)	-0.14240(8)	0.0291(4)
Ru(4)	-0.36588(4)	0.24587(5)	-0.33761(8)	0.0279(4)
Ru(5)	-0.18965(4)	0.26457(5)	-0.39280(7)	0.0270(4)
Ru(6)	-0.25764(4)	0.43343(5)	-0.17041(7)	0.0266(4)
C(11)	-0.3832(8)	0.1196(8)	0.0783(15)	0.057(8)
O(11)	-0.3652(6)	0.1053(7)	0.1919(11)	0.080(7)
C(12)	-0.5486(7)	0.1588(6)	-0.1269(12)	0.058(6)
O(12)	-0.6287(4)	0.1644(6)	-0.1342(10)	0.081(5)
C(13)	-0.4121(6)	-0.0064(7)	-0.1970(11)	0.048(6)
O(13)	-0.4159(5)	-0.1040(5)	-0.2457(9)	0.076(5)
C(21)	0.0422(7)	0.1382(8)	-0.0748(14)	0.065(8)
O(21)	0.0863(6)	0.1036(7)	0.0125(10)	0.112(7)
C(22)	0.0689(6)	0.2189(7)	-0.3336(12)	0.056(6)
O(22)	0.1293(5)	0.2423(7)	-0.3911(10)	0.095(6)
C(23)	-0.0373(6)	0.0285(8)	-0.3230(12)	0.050(6)
O(23)	-0.0329(4)	-0.0695(5)	-0.3747(7)	0.055(4)
C(31)	-0.1696(7)	0.1939(8)	0.0459(13)	0.052(7)
O(31)	-0.1395(6)	0.1901(7)	0.1595(10)	0.091(7)
C(32)	-0.2165(5)	0.0365(7)	-0.2117(11)	0.043(6)
O(32)	-0.2160(4)	-0.0630(5)	-0.2605(8)	0.056(4)
C(41)	-0.4960(6)	0.2973(7)	-0.3692(11)	0.046(6)
O(41)	-0.5716(4)	0.3267(7)	-0.3916(9)	0.080(5)
C(42)	-0.3874(5)	0.0963(7)	-0.4533(11)	0.042(6)
O(42)	-0.3985(4)	0.0053(5)	-0.5294(8)	0.062(5)
C(45)	-0.3203(5)	0.3285(7)	-0.4925(11)	0.038(6)
O(45)	-0.3439(4)	0.3819(6)	-0.5801(8)	0.066(5)
C(51)	-0.1173(6)	0.3476(8)	-0.4945(11)	0.049(6)
O(51)	-0.0789(5)	0.3997(6)	-0.5604(9)	0.083(6)
C(52)	-0.1802(5)	0.1216(7)	-0.5257(11)	0.038(5)
O(52)	-0.1779(4)	0.0366(5)	-0.6072(8)	0.058(5)
C(1)	-0.3421(5)	0.3240(6)	-0.1140(10)	0.035(5)
O(1)	-0.4009(4)	0.3365(4)	-0.0244(6)	0.039(4)
C(2)	-0.1364(5)	0.3417(6)	-0.1777(10)	0.035(5)
O(2)	-0.0510(3)	0.3663(4)	-0.1322(7)	0.037(3)
C(30)	-0.0976(7)	0.6216(9)	-0.2474(12)	0.063(3)
C(50)	-0.2550(7)	0.5519(9)	0.1762(12)	0.067(3)
C(70)	-0.4535(6)	0.6022(8)	-0.2703(12)	0.057(3)
C(3)	-0.1844(6)	0.6056(7)	-0.1760(11)	0.044(2)
C(4)	-0.1790(5)	0.5901(7)	-0.0370(10)	0.037(2)
C(5)	-0.2598(5)	0.5737(6)	0.0287(10)	0.036(2)
C(6)	-0.3479(5)	0.5788(6)	-0.0529(10)	0.035(2)
C(7)	-0.3566(5)	0.5948(7)	-0.1911(11)	0.039(2)
C(8)	-0.2738(6)	0.6039(7)	-0.2585(11)	0.044(2)

Table A10.2 Fractional atomic coordinates for the

hydrogen atoms for $\text{Ru}_6(\eta^2\text{-}\mu_4\text{-CO})_2(\text{CO})_{13}(\text{C}_6\text{H}_3\text{Me}_3)$ (XR10)

Atom	x	y	z
H(30a)	-0.0357	0.6183	-0.1717
H(30b)	-0.1027	0.7063	-0.2795
H(30c)	-0.0911	0.5527	-0.3396
H(50a)	-0.1813	0.5511	0.2199
H(50b)	-0.2853	0.4680	0.1758
H(50c)	-0.2941	0.6211	0.2404
H(70a)	-0.4455	0.6146	-0.3767
H(70b)	-0.4947	0.6753	-0.2166
H(70c)	-0.4897	0.5212	-0.2758
H(8)	-0.2812	0.6527	-0.3442
H(4)	-0.1139	0.5747	0.0200
H(6)	-0.4136	0.5521	-0.0102

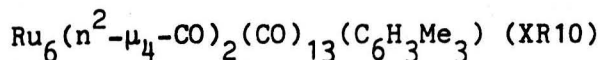
Table A10.3 Anisotropic thermal parameters (\AA^2) for

Atom	U_{11}	U_{22}	U_{33}	U_{23}	U_{13}	U_{12}
Ru(1)	0.0453(4)	0.0308(3)	0.0412(6)	0.0081(3)	0.0152(3)	-0.0081(3)
Ru(2)	0.0288(3)	0.0372(3)	0.0393(6)	-0.0002(3)	-0.0043(3)	0.0055(2)
Ru(3)	0.0344(3)	0.0269(3)	0.0260(6)	0.0067(3)	0.0006(3)	-0.0006(2)
Ru(4)	0.0242(3)	0.0305(3)	0.0289(5)	0.0057(3)	0.0026(3)	-0.0024(2)
Ru(5)	0.0251(3)	0.0329(3)	0.0230(5)	0.0047(3)	0.0035(3)	-0.0008(2)
Ru(6)	0.0274(3)	0.0238(3)	0.0287(5)	0.0046(3)	0.0051(3)	-0.0018(2)
C(11)	0.072(7)	0.048(5)	0.051(12)	0.017(6)	0.023(7)	-0.013(5)
O(11)	0.106(6)	0.074(5)	0.059(9)	0.028(5)	0.025(5)	-0.008(4)
C(12)	0.076(6)	0.022(4)	0.075(9)	0.004(4)	0.033(6)	-0.011(4)
O(12)	0.040(4)	0.066(4)	0.137(8)	0.003(5)	0.020(4)	-0.005(3)
C(13)	0.045(5)	0.048(5)	0.051(9)	0.015(5)	0.014(5)	-0.009(4)
O(13)	0.068(4)	0.034(3)	0.126(7)	0.000(4)	0.030(4)	-0.013(3)
C(21)	0.073(7)	0.044(5)	0.079(11)	0.000(6)	-0.033(7)	0.012(5)
O(21)	0.154(7)	0.094(6)	0.089(8)	0.012(5)	-0.072(6)	0.018(5)
C(22)	0.048(5)	0.041(4)	0.079(10)	-0.012(5)	0.000(5)	-0.004(4)
O(22)	0.068(4)	0.100(6)	0.117(8)	-0.027(5)	0.039(5)	-0.038(4)
C(23)	0.033(4)	0.050(5)	0.067(9)	0.005(5)	0.003(5)	0.007(4)
O(23)	0.063(4)	0.046(4)	0.055(6)	-0.009(3)	0.005(4)	0.004(3)
C(31)	0.066(6)	0.062(6)	0.027(10)	0.015(5)	-0.011(5)	-0.017(5)
O(31)	0.106(7)	0.116(7)	0.052(8)	0.034(5)	-0.020(5)	-0.020(5)
C(32)	0.037(4)	0.045(5)	0.048(8)	0.014(5)	0.004(4)	0.004(4)
O(32)	0.047(3)	0.033(3)	0.087(6)	-0.003(3)	0.005(3)	0.002(2)
C(41)	0.040(5)	0.042(4)	0.056(8)	0.012(4)	0.014(5)	0.005(4)
O(41)	0.041(4)	0.098(5)	0.101(7)	0.031(5)	0.010(4)	0.012(4)
C(42)	0.034(4)	0.043(5)	0.048(8)	0.004(5)	0.010(4)	0.003(3)

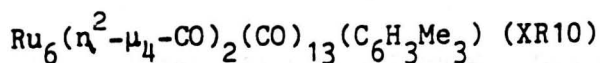
Table A10.3 continued

O(42)	0.069(4)	0.051(4)	0.065(6)	-0.017(4)	0.013(4)	-0.023(3)
C(45)	0.029(4)	0.055(5)	0.030(8)	0.012(5)	-0.005(4)	-0.002(3)
O(45)	0.053(4)	0.098(5)	0.045(6)	0.052(4)	-0.007(3)	0.001(3)
C(51)	0.053(5)	0.059(5)	0.036(8)	-0.006(5)	0.015(5)	-0.016(4)
O(51)	0.086(5)	0.091(5)	0.071(7)	0.021(5)	0.035(5)	-0.036(4)
C(52)	0.032(4)	0.040(5)	0.042(8)	0.010(5)	-0.003(4)	-0.002(3)
O(52)	0.065(4)	0.053(4)	0.057(6)	-0.012(4)	0.006(4)	0.015(3)
C(1)	0.043(4)	0.022(3)	0.041(8)	0.006(4)	0.009(4)	-0.006(3)
O(1)	0.047(3)	0.037(3)	0.033(5)	0.002(3)	0.022(3)	-0.009(2)
C(2)	0.037(4)	0.036(4)	0.031(7)	0.000(4)	0.008(4)	0.000(3)
O(2)	0.031(3)	0.039(3)	0.041(5)	-0.005(3)	-0.003(3)	-0.001(2)

Table A10.4 Bond lengths (Å) for



Ru(1) - Ru(3)	2.839(1)	Ru(1) - Ru(4)	2.785(1)
Ru(1) - C(11)	1.900(14)	Ru(1) - C(12)	1.933(10)
Ru(1) - C(13)	1.868(8)	Ru(1) - C(1)	2.269(8)
Ru(1) - O(1)	2.135(5)	Ru(2) - Ru(3)	2.842(1)
Ru(2) - Ru(5)	2.776(1)	Ru(2) - C(21)	1.906(12)
Ru(2) - C(22)	1.936(11)	Ru(2) - C(23)	1.861(9)
Ru(2) - C(2)	2.272(7)	Ru(2) - O(2)	2.137(5)
Ru(3) - Ru(4)	2.733(1)	Ru(3) - Ru(5)	2.740(1)
Ru(3) - Ru(6)	2.783(1)	Ru(3) - C(31)	1.890(13)
Ru(3) - C(32)	1.883(8)	Ru(3) - C(1)	2.187(7)
Ru(3) - C(2)	2.168(8)	Ru(4) - Ru(5)	2.628(1)
Ru(4) - Ru(6)	2.843(1)	Ru(4) - C(41)	1.914(8)
Ru(4) - C(42)	1.887(8)	Ru(4) - C(45)	2.091(11)
Ru(4) - C(1)	2.163(9)	Ru(5) - Ru(6)	2.820(1)
Ru(5) - C(45)	2.153(8)	Ru(5) - C(51)	1.899(11)
Ru(5) - C(52)	1.893(8)	Ru(5) - C(2)	2.159(8)
Ru(6) - C(3)	2.302(9)	Ru(6) - C(4)	2.271(7)
Ru(6) - C(5)	2.260(8)	Ru(6) - C(6)	2.256(8)
Ru(6) - C(7)	2.303(8)	Ru(6) - C(8)	2.285(10)
Ru(6) - C(1)	1.969(9)	Ru(6) - C(2)	1.969(7)
C(11) - O(11)	1.137(18)	C(12) - O(12)	1.125(11)
C(13) - O(13)	1.137(10)	C(21) - O(21)	1.117(15)
C(22) - O(22)	1.137(14)	C(23) - O(23)	1.149(10)
C(31) - O(31)	1.138(16)	C(32) - O(32)	1.156(10)
C(41) - O(41)	1.117(10)	C(42) - O(42)	1.167(10)
C(45) - O(45)	1.151(13)	C(51) - O(51)	1.146(14)
C(52) - O(52)	1.134(10)	C(30) - C(3)	1.505(15)
C(50) - C(5)	1.483(16)	C(70) - C(7)	1.500(12)
C(3) - C(4)	1.377(15)	C(3) - C(8)	1.416(12)
C(4) - C(5)	1.401(12)	C(5) - C(6)	1.403(11)
C(6) - C(7)	1.370(14)	C(7) - C(8)	1.415(13)
C(1) - O(1)	1.245(11)	C(2) - O(2)	1.265(9)

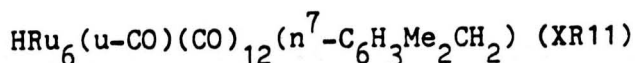
Table A10.5 Bond angles ($^{\circ}$) for

C(1) -Ru(1) -Ru(3)	49.2(2)	C(1) -Ru(1) -Ru(4)	49.4(2)
C(1) -Ru(1) -C(13)	141.3(4)	O(1) -Ru(1) -Ru(3)	76.6(1)
O(1) -Ru(1) -Ru(4)	76.2(2)	O(1) -Ru(1) -C(1)	32.6(3)
C(2) -Ru(2) -Ru(3)	48.6(2)	C(2) -Ru(2) -Ru(5)	49.4(2)
O(2) -Ru(2) -Ru(3)	76.3(1)	O(2) -Ru(2) -Ru(5)	76.7(1)
O(2) -Ru(2) -C(2)	33.2(2)	C(1) -Ru(3) -Ru(1)	51.7(2)
C(1) -Ru(3) -Ru(2)	140.4(2)	C(1) -Ru(3) -Ru(4)	50.7(2)
C(1) -Ru(3) -Ru(5)	91.9(3)	C(1) -Ru(3) -Ru(6)	44.7(2)
C(2) -Ru(3) -Ru(1)	140.5(2)	C(2) -Ru(3) -Ru(2)	51.8(2)
C(2) -Ru(3) -Ru(4)	92.6(2)	C(2) -Ru(3) -Ru(5)	50.6(2)
C(2) -Ru(3) -Ru(6)	44.8(2)	C(2) -Ru(3) -C(1)	89.2(3)
C(1) -Ru(4) -Ru(1)	52.8(2)	C(1) -Ru(4) -Ru(3)	51.5(2)
C(1) -Ru(4) -Ru(5)	95.6(2)	C(1) -Ru(4) -Ru(6)	43.8(2)
C(2) -Ru(5) -Ru(2)	53.0(2)	C(2) -Ru(5) -Ru(3)	50.9(2)
C(2) -Ru(5) -Ru(4)	95.8(2)	C(2) -Ru(5) -Ru(6)	44.2(2)
C(3) -Ru(6) -Ru(3)	142.7(2)	C(3) -Ru(6) -Ru(4)	144.3(3)
C(3) -Ru(6) -Ru(5)	105.5(2)	C(4) -Ru(6) -Ru(3)	124.7(2)
C(4) -Ru(6) -Ru(4)	176.6(2)	C(4) -Ru(6) -Ru(5)	127.3(2)
C(4) -Ru(6) -C(3)	35.0(4)	C(5) -Ru(6) -Ru(3)	118.7(2)
C(5) -Ru(6) -Ru(4)	141.9(2)	C(5) -Ru(6) -Ru(5)	161.0(2)
C(5) -Ru(6) -C(3)	64.5(3)	C(5) -Ru(6) -C(4)	36.0(3)
C(6) -Ru(6) -Ru(3)	132.1(2)	C(6) -Ru(6) -Ru(4)	113.4(2)
C(6) -Ru(6) -Ru(5)	160.8(2)	C(6) -Ru(6) -C(3)	74.6(3)
C(6) -Ru(6) -C(4)	63.5(3)	C(6) -Ru(6) -C(5)	36.2(3)
C(7) -Ru(6) -Ru(3)	153.6(2)	C(7) -Ru(6) -Ru(4)	102.0(2)
C(7) -Ru(6) -Ru(5)	127.4(2)	C(7) -Ru(6) -C(3)	63.6(3)
C(7) -Ru(6) -C(4)	74.7(3)	C(7) -Ru(6) -C(5)	64.6(3)
C(7) -Ru(6) -C(6)	34.9(4)	C(8) -Ru(6) -Ru(3)	163.0(2)
C(8) -Ru(6) -Ru(4)	113.7(2)	C(8) -Ru(6) -Ru(5)	104.5(2)
C(8) -Ru(6) -C(3)	35.9(3)	C(8) -Ru(6) -C(4)	64.2(3)
C(8) -Ru(6) -C(5)	77.2(3)	C(8) -Ru(6) -C(6)	64.0(3)
C(8) -Ru(6) -C(7)	35.9(3)	C(1) -Ru(6) -Ru(3)	51.4(2)
C(1) -Ru(6) -Ru(4)	49.4(3)	C(1) -Ru(6) -Ru(5)	94.4(2)
C(1) -Ru(6) -C(3)	160.0(3)	C(1) -Ru(6) -C(4)	130.0(4)
C(1) -Ru(6) -C(5)	96.8(3)	C(1) -Ru(6) -C(6)	86.1(3)
C(1) -Ru(6) -C(7)	103.0(3)	C(1) -Ru(6) -C(8)	137.2(3)
C(2) -Ru(6) -Ru(3)	50.8(2)	C(2) -Ru(6) -Ru(4)	93.9(2)
C(2) -Ru(6) -Ru(5)	49.8(2)	C(2) -Ru(6) -C(3)	92.5(3)
C(2) -Ru(6) -C(4)	89.5(3)	C(2) -Ru(6) -C(5)	112.6(3)
C(2) -Ru(6) -C(6)	148.7(3)	C(2) -Ru(6) -C(7)	155.2(3)
C(2) -Ru(6) -C(8)	119.8(3)	C(2) -Ru(6) -C(1)	101.8(3)
O(11) -C(11) -Ru(1)	176.9(9)	O(12) -C(12) -Ru(1)	178.1(9)
O(13) -C(13) -Ru(1)	176(1)	O(21) -C(21) -Ru(2)	175.8(9)
O(22) -C(22) -Ru(2)	177.7(8)	O(23) -C(23) -Ru(2)	175.0(7)
O(31) -C(31) -Ru(3)	179.6(7)	O(32) -C(32) -Ru(3)	176.7(9)
O(41) -C(41) -Ru(4)	178(1)	O(42) -C(42) -Ru(4)	177.0(9)
Ru(5) -C(45) -Ru(4)	76.5(3)	O(45) -C(45) -Ru(4)	145.3(6)
O(45) -C(45) -Ru(5)	138.2(7)	O(51) -C(51) -Ru(5)	175.7(8)
O(52) -C(52) -Ru(5)	177.5(7)	C(30) -C(3) -Ru(6)	128.5(6)
C(4) -C(3) -Ru(6)	71.2(5)	C(4) -C(3) -C(30)	122.5(8)
C(8) -C(3) -Ru(6)	71.4(5)	C(8) -C(3) -C(30)	117.4(9)
C(8) -C(3) -C(4)	120.1(9)	C(3) -C(4) -Ru(6)	73.7(5)
C(5) -C(4) -Ru(6)	71.6(4)	C(5) -C(4) -C(3)	122.4(7)

Table A10.5 continued

C(50)	-C(5)	-Ru(6)	125.6(6)	C(4)	-C(5)	-Ru(6)	72.4(5)
C(4)	-C(5)	-C(50)	123.1(8)	C(6)	-C(5)	-Ru(6)	71.8(5)
C(6)	-C(5)	-C(50)	120.5(8)	C(6)	-C(5)	-C(4)	116.3(9)
C(5)	-C(6)	-Ru(6)	72.1(4)	C(7)	-C(6)	-Ru(6)	74.4(5)
C(7)	-C(6)	-C(5)	123.2(8)	C(70)	-C(7)	-Ru(6)	130.1(5)
C(6)	-C(7)	-Ru(6)	70.7(5)	C(6)	-C(7)	-C(70)	120.0(8)
C(8)	-C(7)	-Ru(6)	71.4(5)	C(8)	-C(7)	-C(70)	120.4(9)
C(8)	-C(7)	-C(6)	119.6(7)	C(3)	-C(8)	-Ru(6)	72.7(5)
C(7)	-C(8)	-Ru(6)	72.7(5)	C(7)	-C(8)	-C(3)	118.2(9)
Ru(3)	-C(1)	-Ru(1)	79.1(2)	Ru(4)	-C(1)	-Ru(1)	77.8(2)
Ru(4)	-C(1)	-Ru(3)	77.9(3)	Ru(6)	-C(1)	-Ru(1)	159.1(4)
Ru(6)	-C(1)	-Ru(3)	83.9(3)	Ru(6)	-C(1)	-Ru(4)	86.8(4)
O(1)	-C(1)	-Ru(1)	67.7(4)	O(1)	-C(1)	-Ru(3)	129.6(6)
O(1)	-C(1)	-Ru(4)	127.0(5)	O(1)	-C(1)	-Ru(6)	133.1(5)
C(1)	-O(1)	-Ru(1)	79.6(4)	Ru(3)	-C(2)	-Ru(2)	79.5(3)
Ru(5)	-C(2)	-Ru(2)	77.5(3)	Ru(5)	-C(2)	-Ru(3)	78.6(2)
Ru(6)	-C(2)	-Ru(2)	158.9(4)	Ru(6)	-C(2)	-Ru(3)	84.4(3)
Ru(6)	-C(2)	-Ru(5)	86.1(3)	O(2)	-C(2)	-Ru(2)	67.5(4)
O(2)	-C(2)	-Ru(3)	129.2(6)	O(2)	-C(2)	-Ru(5)	126.8(6)
O(2)	-C(2)	-Ru(6)	133.5(5)	C(2)	-O(2)	-Ru(2)	79.3(4)

TABLE A11.1 Fractional atomic coordinates and

thermal parameters (\AA^2) for

Atom	x	y	z	U_{iso} or U_{eq}
Ru(1)	0.19075(18)	0.25253(11)	0.32779(8)	0.0442(10)
Ru(2)	0.25254(18)	0.03726(10)	0.13945(8)	0.0450(11)
Ru(3)	0.17692(16)	0.12201(10)	0.24451(7)	0.0361(9)
Ru(4)	0.15644(17)	0.29306(10)	0.21019(8)	0.0377(10)
Ru(5)	0.11041(16)	0.18084(11)	0.12410(7)	0.0380(10)
Ru(6)	0.37037(16)	0.18863(10)	0.17269(8)	0.0358(9)
C(11)	0.2180(27)	0.1916(15)	0.4024(11)	0.064(17)
O(11)	0.2282(21)	0.1552(17)	0.4419(9)	0.121(18)
C(12)	0.2356(22)	0.3588(16)	0.3598(11)	0.056(15)
O(12)	0.2652(19)	0.4203(12)	0.3792(9)	0.084(14)
C(13)	0.0068(26)	0.2684(15)	0.3382(10)	0.056(15)
O(13)	-0.1067(18)	0.2788(12)	0.3454(8)	0.080(13)
C(21)	0.3406(22)	-0.0554(14)	0.1783(11)	0.053(15)
O(21)	0.3913(18)	-0.1071(11)	0.2021(9)	0.085(14)
C(22)	0.1684(28)	-0.0286(16)	0.0841(11)	0.066(18)
O(22)	0.1033(24)	-0.0684(15)	0.0501(11)	0.124(19)
C(23)	0.0842(24)	0.0292(14)	0.1855(10)	0.051(15)
O(23)	-0.0211(17)	-0.0084(10)	0.1889(7)	0.066(11)
C(31)	0.2947(27)	0.0527(14)	0.2917(10)	0.062(16)
O(31)	0.3704(18)	0.0135(11)	0.3167(9)	0.085(14)
C(32)	0.0319(25)	0.0942(15)	0.2984(10)	0.056(15)
O(32)	-0.0534(18)	0.0690(11)	0.3249(9)	0.087(14)
C(41)	0.2575(24)	0.3935(15)	0.2217(11)	0.058(16)
O(41)	0.3114(18)	0.4549(11)	0.2239(10)	0.095(15)
C(42)	-0.0087(22)	0.3456(13)	0.2182(10)	0.047(13)
O(42)	-0.1150(16)	0.3754(11)	0.2185(8)	0.073(12)
C(45)	0.1378(40)	0.3035(17)	0.1172(13)	0.120(26)
O(45)	0.1368(22)	0.3585(12)	0.0802(8)	0.094(15)
C(51)	0.1547(23)	0.1557(13)	0.0477(12)	0.055(15)
O(51)	0.1737(20)	0.1469(11)	-0.0050(8)	0.080(13)
C(52)	-0.0769(24)	0.1596(14)	0.1011(9)	0.048(14)
O(52)	-0.1771(16)	0.1426(13)	0.0896(8)	0.079(13)
C(30)	0.4200(23)	0.0352(15)	0.0761(12)	0.070(17)
C(50)	0.6794(24)	0.1767(17)	0.2493(11)	0.070(17)
C(70)	0.4815(26)	0.3521(19)	0.0822(11)	0.083(19)
C(3)	0.4830(19)	0.1151(15)	0.1029(10)	0.050(14)
C(4)	0.5557(22)	0.1074(16)	0.1575(12)	0.069(18)
C(5)	0.6023(21)	0.1825(16)	0.1897(11)	0.059(16)
C(6)	0.5677(19)	0.2623(15)	0.1672(11)	0.052(14)
C(7)	0.4976(23)	0.2682(14)	0.1095(11)	0.059(15)
C(8)	0.4579(19)	0.1939(12)	0.0788(9)	0.042(12)
C(1)	0.3349(20)	0.2250(12)	0.2515(10)	0.044(13)
O(1)	0.3962(13)	0.2448(9)	0.2970(6)	0.044(9)
C(81)	0.6681(35)	0.0694(22)	0.4308(16)	0.152(11)
C(82)	0.5925(31)	0.1553(20)	0.4121(14)	0.114(10)
C(83)	0.6496(32)	0.2274(20)	0.4419(15)	0.133(10)
C(84)	0.7742(30)	0.2034(19)	0.4808(14)	0.101(9)
C(85)	0.7877(35)	0.1168(23)	0.4807(16)	0.159(11)
C(86)	0.8535(38)	0.0611(24)	0.4979(18)	0.204(13)

Table A11.2 Fractional atomic coordinates for the
hydrogen atoms for $\text{HRu}_6(\text{u-CO})(\text{CO})_{12}(\text{n}^7\text{-C}_6\text{H}_3\text{Me}_2\text{CH}_2)$ (XR11)

H	0.07470	0.19360	0.20150	0.0800
---	---------	---------	---------	--------

TABLE A11.3 Anisotropic thermal parameters (\AA^2) for

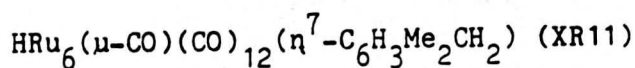
$\text{HRu}_6(\text{u-CO})(\text{CO})_{12}(\text{n}^7\text{-C}_6\text{H}_3\text{Me}_2\text{CH}_2)$ (XR11)

Atom	U_{11}	U_{22}	U_{33}	U_{23}	U_{13}	U_{12}
Ru(1)	0.048(1)	0.049(1)	0.035(1)	-0.003(1)	0.003(1)	-0.001(1)
Ru(2)	0.046(1)	0.036(1)	0.052(1)	-0.007(1)	0.001(1)	0.001(1)
Ru(3)	0.035(1)	0.037(1)	0.036(1)	0.004(1)	0.000(1)	-0.001(1)
Ru(4)	0.040(1)	0.034(1)	0.039(1)	0.002(1)	0.002(1)	0.003(1)
Ru(5)	0.038(1)	0.042(1)	0.034(1)	0.001(1)	-0.002(1)	0.003(1)
Ru(6)	0.033(1)	0.037(1)	0.038(1)	-0.001(1)	0.004(1)	0.000(1)
C(11)	0.098(21)	0.055(16)	0.040(15)	0.013(13)	-0.003(14)	0.022(14)
O(11)	0.121(18)	0.196(25)	0.047(13)	0.047(15)	-0.007(12)	-0.001(16)
C(12)	0.048(14)	0.061(16)	0.059(16)	-0.005(13)	-0.038(12)	-0.006(12)
O(12)	0.100(15)	0.065(12)	0.086(15)	-0.017(11)	-0.011(12)	-0.003(11)
C(13)	0.064(16)	0.064(16)	0.041(14)	-0.010(12)	0.015(12)	0.014(13)
O(13)	0.062(12)	0.091(14)	0.086(15)	-0.003(11)	0.014(11)	0.000(10)
C(21)	0.038(13)	0.048(14)	0.073(18)	-0.001(13)	0.015(12)	0.000(11)
O(21)	0.072(12)	0.066(13)	0.116(17)	0.015(12)	-0.024(11)	0.027(10)
C(22)	0.083(20)	0.071(18)	0.045(15)	-0.009(14)	-0.007(14)	-0.006(15)
O(22)	0.131(19)	0.122(19)	0.120(20)	-0.011(16)	-0.036(16)	-0.049(15)
C(23)	0.066(16)	0.045(14)	0.041(14)	-0.007(11)	0.009(12)	-0.006(12)
O(23)	0.075(12)	0.065(11)	0.058(11)	-0.007(9)	0.000(9)	-0.017(9)
C(31)	0.097(20)	0.051(15)	0.039(14)	0.012(12)	-0.015(13)	-0.023(14)
O(31)	0.086(13)	0.067(12)	0.102(16)	0.023(11)	-0.038(12)	0.028(10)
C(32)	0.066(17)	0.058(15)	0.043(14)	-0.008(12)	-0.019(13)	0.019(13)
O(32)	0.067(12)	0.079(13)	0.114(16)	0.026(12)	0.045(11)	-0.021(10)
C(41)	0.059(16)	0.049(15)	0.066(17)	-0.001(13)	-0.005(13)	0.009(12)
O(41)	0.082(13)	0.063(12)	0.139(20)	-0.016(12)	0.018(13)	-0.044(10)
C(42)	0.049(14)	0.034(12)	0.058(15)	-0.004(11)	0.008(12)	0.000(10)

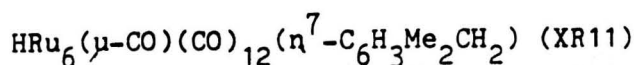
Table A11.3 continued

O(42)	0.055(10)	0.074(12)	0.090(13)	0.011(10)	-0.005(10)	0.014(9)
C(45)	0.233(38)	0.051(18)	0.077(21)	-0.029(16)	0.082(23)	-0.022(21)
O(45)	0.155(19)	0.088(14)	0.039(11)	0.018(11)	0.000(11)	-0.018(14)
C(51)	0.054(14)	0.032(12)	0.080(20)	0.003(13)	-0.005(13)	0.004(10)
O(51)	0.121(16)	0.074(12)	0.044(11)	-0.013(10)	0.018(11)	0.017(11)
C(52)	0.052(14)	0.058(15)	0.034(13)	0.004(11)	-0.016(11)	0.008(12)
O(52)	0.035(9)	0.126(16)	0.075(13)	0.006(12)	-0.019(9)	-0.019(10)
C(30)	0.059(15)	0.060(16)	0.090(20)	-0.026(15)	0.042(14)	0.004(12)
C(50)	0.065(16)	0.101(21)	0.045(15)	0.028(15)	-0.016(13)	0.023(15)
C(70)	0.073(17)	0.125(24)	0.049(16)	0.032(16)	0.032(13)	-0.010(17)
C(3)	0.026(11)	0.072(17)	0.052(15)	-0.014(13)	-0.004(10)	0.007(11)
C(4)	0.046(14)	0.083(19)	0.077(19)	-0.024(16)	0.033(14)	0.021(13)
C(5)	0.035(12)	0.073(17)	0.069(17)	-0.007(15)	0.016(12)	0.000(12)
C(6)	0.025(11)	0.068(16)	0.063(16)	0.030(13)	-0.011(11)	0.012(11)
C(7)	0.065(15)	0.048(14)	0.064(16)	0.003(13)	0.044(13)	-0.002(12)
C(8)	0.039(12)	0.037(12)	0.051(14)	-0.011(11)	0.032(10)	-0.006(9)
C(1)	0.042(12)	0.039(12)	0.052(15)	0.017(11)	0.006(11)	0.007(10)
O(1)	0.044(8)	0.048(9)	0.041(9)	0.003(7)	-0.002(7)	-0.007(7)

TABLE A11.4 Bond lengths (Å) for



Ru(1) - Ru(3)	2.815(2)	Ru(1) - Ru(4)	2.744(2)
Ru(1) - C(11)	1.961(25)	Ru(1) - C(12)	1.900(25)
Ru(1) - C(13)	1.86(3)	Ru(1) - C(1)	2.306(22)
Ru(1) - O(1)	2.166(13)	Ru(2) - Ru(3)	2.850(2)
Ru(2) - Ru(5)	2.716(2)	Ru(2) - Ru(6)	2.788(2)
Ru(2) - C(21)	1.922(23)	Ru(2) - C(22)	1.82(3)
Ru(2) - C(23)	1.988(24)	Ru(2) - C(30)	2.214(25)
Ru(2) - C(3)	2.742(20)	Ru(3) - Ru(4)	2.858(2)
Ru(3) - Ru(5)	2.934(2)	Ru(3) - Ru(6)	2.754(2)
Ru(3) - C(23)	2.183(22)	Ru(3) - C(31)	1.912(24)
Ru(3) - C(32)	1.955(25)	Ru(3) - C(1)	2.275(20)
Ru(3) - H	1.797(2)	Ru(4) - Ru(5)	2.679(2)
Ru(4) - Ru(6)	2.843(2)	Ru(4) - C(41)	1.910(24)
Ru(4) - C(42)	1.849(22)	Ru(4) - C(45)	2.11(3)
Ru(4) - C(1)	2.254(20)	Ru(4) - H	1.797(2)
Ru(5) - Ru(6)	2.767(2)	Ru(5) - C(45)	1.99(3)
Ru(5) - C(51)	1.84(3)	Ru(5) - C(52)	1.938(23)
Ru(5) - H	1.803(2)	Ru(6) - C(3)	2.281(22)
Ru(6) - C(4)	2.281(24)	Ru(6) - C(5)	2.314(21)
Ru(6) - C(6)	2.285(20)	Ru(6) - C(7)	2.311(23)
Ru(6) - C(8)	2.311(21)	Ru(6) - C(1)	1.913(23)
C(11) - O(11)	1.07(3)	C(12) - O(12)	1.12(3)
C(13) - O(13)	1.15(3)	C(21) - O(21)	1.10(3)
C(22) - O(22)	1.18(3)	C(23) - O(23)	1.21(3)
C(31) - O(31)	1.12(3)	C(32) - O(32)	1.12(3)
C(41) - O(41)	1.12(3)	C(42) - O(42)	1.15(3)
C(45) - O(45)	1.22(3)	C(51) - O(51)	1.22(3)
C(52) - O(52)	1.05(3)	C(30) - C(3)	1.54(3)
C(50) - C(5)	1.53(3)	C(70) - C(7)	1.49(4)
C(3) - C(4)	1.41(3)	C(3) - C(8)	1.40(3)
C(4) - C(5)	1.48(4)	C(5) - C(6)	1.41(3)
C(6) - C(7)	1.46(3)	C(7) - C(8)	1.43(3)
C(1) - O(1)	1.22(3)	C(81) - C(82)	1.62(5)
C(81) - C(85)	1.78(5)	C(82) - C(83)	1.44(5)
C(83) - C(84)	1.54(4)	C(84) - C(85)	1.40(5)
C(85) - C(86)	1.16(5)		

TABLE A11.5 Bond angles ($^{\circ}$) for

C(1) -Ru(1) -Ru(3)	51.6(5)	C(1) -Ru(1) -Ru(4)	52.1(5)
O(1) -Ru(1) -Ru(3)	76.8(4)	O(1) -Ru(1) -Ru(4)	78.2(4)
O(1) -Ru(1) -C(1)	31.5(6)	C(30) -Ru(2) -Ru(3)	139.5(6)
C(30) -Ru(2) -Ru(5)	108.8(6)	C(30) -Ru(2) -Ru(6)	82.7(6)
C(3) -Ru(2) -Ru(3)	105.7(5)	C(3) -Ru(2) -Ru(5)	90.3(5)
C(3) -Ru(2) -Ru(6)	48.7(5)	C(3) -Ru(2) -C(30)	34.2(8)
C(1) -Ru(3) -Ru(1)	52.6(6)	C(1) -Ru(3) -Ru(2)	102.1(6)
C(1) -Ru(3) -Ru(4)	50.5(5)	C(1) -Ru(3) -Ru(5)	88.1(6)
C(1) -Ru(3) -Ru(6)	43.4(6)	H -Ru(3) -Ru(1)	84.3(1)
H -Ru(3) -Ru(2)	90.7(1)	H -Ru(3) -Ru(4)	37.3(1)
H -Ru(3) -Ru(5)	35.5(1)	H -Ru(3) -Ru(6)	79.8(1)
H -Ru(3) -C(1)	87.0(5)	C(1) -Ru(4) -Ru(1)	53.9(6)
C(1) -Ru(4) -Ru(3)	51.2(5)	C(1) -Ru(4) -Ru(5)	95.1(5)
C(1) -Ru(4) -Ru(6)	42.1(6)	H -Ru(4) -Ru(1)	86.5(1)
H -Ru(4) -Ru(3)	37.3(1)	H -Ru(4) -Ru(5)	42.0(1)
H -Ru(4) -Ru(6)	77.2(1)	H -Ru(4) -C(1)	87.6(5)
H -Ru(5) -Ru(2)	95.0(1)	H -Ru(5) -Ru(3)	35.3(1)
H -Ru(5) -Ru(4)	41.8(1)	H -Ru(5) -Ru(6)	79.3(1)
C(3) -Ru(6) -Ru(2)	64.6(5)	C(3) -Ru(6) -Ru(3)	124.3(6)
C(3) -Ru(6) -Ru(4)	152.9(5)	C(3) -Ru(6) -Ru(5)	99.7(5)
C(4) -Ru(6) -Ru(2)	78.0(6)	C(4) -Ru(6) -Ru(3)	116.0(7)
C(4) -Ru(6) -Ru(4)	170.9(7)	C(4) -Ru(6) -Ru(5)	130.9(6)
C(4) -Ru(6) -C(3)	36.1(8)	C(5) -Ru(6) -Ru(2)	114.3(6)
C(5) -Ru(6) -Ru(3)	125.8(6)	C(5) -Ru(6) -Ru(4)	135.7(6)
C(5) -Ru(6) -Ru(5)	165.3(6)	C(5) -Ru(6) -C(3)	66.0(8)
C(5) -Ru(6) -C(4)	37.4(9)	C(6) -Ru(6) -Ru(2)	141.9(6)
C(6) -Ru(6) -Ru(3)	147.0(6)	C(6) -Ru(6) -Ru(4)	110.7(6)
C(6) -Ru(6) -Ru(5)	141.8(6)	C(6) -Ru(6) -C(3)	78.3(8)
C(6) -Ru(6) -C(4)	66.3(8)	C(6) -Ru(6) -C(5)	35.8(8)
C(7) -Ru(6) -Ru(2)	123.1(6)	C(7) -Ru(6) -Ru(3)	167.2(6)
C(7) -Ru(6) -Ru(4)	106.2(6)	C(7) -Ru(6) -Ru(5)	107.1(6)
C(7) -Ru(6) -C(3)	65.0(8)	C(7) -Ru(6) -C(4)	76.8(9)
C(7) -Ru(6) -C(5)	64.8(8)	C(7) -Ru(6) -C(6)	37.1(8)
C(8) -Ru(6) -Ru(2)	87.1(5)	C(8) -Ru(6) -Ru(3)	146.7(5)
C(8) -Ru(6) -Ru(4)	123.4(5)	C(8) -Ru(6) -Ru(5)	90.3(5)
C(8) -Ru(6) -C(3)	35.4(8)	C(8) -Ru(6) -C(4)	64.0(8)
C(8) -Ru(6) -C(5)	76.1(8)	C(8) -Ru(6) -C(6)	65.8(8)
C(8) -Ru(6) -C(7)	36.0(8)	C(1) -Ru(6) -Ru(2)	115.5(6)
C(1) -Ru(6) -Ru(3)	54.8(6)	C(1) -Ru(6) -Ru(4)	52.2(6)
C(1) -Ru(6) -Ru(5)	101.0(6)	C(1) -Ru(6) -C(3)	154.7(8)
C(1) -Ru(6) -C(4)	118.8(9)	C(1) -Ru(6) -C(5)	93.7(9)
C(1) -Ru(6) -C(6)	94.0(8)	C(1) -Ru(6) -C(7)	121.4(8)
C(1) -Ru(6) -C(8)	157.4(8)	O(11) -C(11) -Ru(1)	176(2)
O(12) -C(12) -Ru(1)	178(2)	O(13) -C(13) -Ru(1)	179(2)
O(21) -C(21) -Ru(2)	178(2)	O(22) -C(22) -Ru(2)	174(2)
Ru(3) -C(23) -Ru(2)	86.1(9)	O(23) -C(23) -Ru(2)	143(2)
O(23) -C(23) -Ru(3)	130(2)	O(31) -C(31) -Ru(3)	175(2)
O(32) -C(32) -Ru(3)	171(2)	O(41) -C(41) -Ru(4)	174(2)
O(42) -C(42) -Ru(4)	174(2)	Ru(5) -C(45) -Ru(4)	81(1)
O(45) -C(45) -Ru(4)	138(2)	O(45) -C(45) -Ru(5)	141(2)
O(51) -C(51) -Ru(5)	172(2)	O(52) -C(52) -Ru(5)	175(2)
C(3) -C(30) -Ru(2)	92(1)	Ru(6) -C(3) -Ru(2)	66.7(5)
C(30) -C(3) -Ru(2)	54(1)	C(30) -C(3) -Ru(6)	120(1)

Table A11.5 continued

C(4)	-C(3)	-Ru(2)	96(1)	C(4)	-C(3)	-Ru(6)	72(1)
C(4)	-C(3)	-C(30)	117(2)	C(8)	-C(3)	-Ru(2)	113(1)
C(8)	-C(3)	-Ru(6)	73(1)	C(8)	-C(3)	-C(30)	122(2)
C(8)	-C(3)	-C(4)	120(2)	C(3)	-C(4)	-Ru(6)	72(1)
C(5)	-C(4)	-Ru(6)	72(1)	C(5)	-C(4)	-C(3)	120(2)
C(50)	-C(5)	-Ru(6)	128(2)	C(4)	-C(5)	-Ru(6)	70(1)
C(4)	-C(5)	-C(50)	122(2)	C(6)	-C(5)	-Ru(6)	71(1)
C(6)	-C(5)	-C(50)	119(2)	C(6)	-C(5)	-C(4)	120(2)
C(5)	-C(6)	-Ru(6)	73(1)	C(7)	-C(6)	-Ru(6)	72(1)
C(7)	-C(6)	-C(5)	119(2)	C(70)	-C(7)	-Ru(6)	135(2)
C(6)	-C(7)	-Ru(6)	70(1)	C(6)	-C(7)	-C(70)	118(2)
C(8)	-C(7)	-Ru(6)	72(1)	C(8)	-C(7)	-C(70)	122(2)
C(8)	-C(7)	-C(6)	120(2)	C(3)	-C(8)	-Ru(6)	71(1)
C(7)	-C(8)	-Ru(6)	72(1)	C(7)	-C(8)	-C(3)	122(2)
Ru(3)	-C(1)	-Ru(1)	75.8(6)	Ru(4)	-C(1)	-Ru(1)	74.0(6)
Ru(4)	-C(1)	-Ru(3)	78.2(6)	Ru(6)	-C(1)	-Ru(1)	152(1)
Ru(6)	-C(1)	-Ru(3)	81.8(8)	Ru(6)	-C(1)	-Ru(4)	85.7(8)
O(1)	-C(1)	-Ru(1)	68(1)	O(1)	-C(1)	-Ru(3)	125(2)
O(1)	-C(1)	-Ru(4)	126(1)	O(1)	-C(1)	-Ru(6)	140(2)
C(1)	-O(1)	-Ru(1)	81(1)	C(85)	-C(81)	-C(82)	95(2)
C(83)	-C(82)	-C(81)	113(3)	C(84)	-C(83)	-C(82)	111(3)
C(85)	-C(84)	-C(83)	109(3)	C(84)	-C(85)	-C(81)	111(3)
C(86)	-C(85)	-C(81)	104(3)	C(86)	-C(85)	-C(84)	145(4)
Ru(4)	-H	-Ru(3)	105.4(1)	Ru(5)	-H	-Ru(3)	109.2(1)
Ru(5)	-H	-Ru(4)	96.2(1)				

Table A12.1 Fractional atomic coordinates and

thermal parameters (\AA^2) for $[\text{Ru}_{10}\text{N}(\text{CO})_{24}]^-$ (XR12)

Atom	x	y	z	U_{iso} or U_{eq}
Ru(1)	0.3167(3)	0.0133(2)	0.1349(1)	0.050(3)
Ru(2)	0.1103(3)	0.0077(2)	0.1672(1)	0.039(2)
Ru(3)	0.3025(3)	-0.0786(2)	0.1983(1)	0.038(3)
Ru(4)	0.3027(3)	0.0806(2)	0.2050(1)	0.036(2)
Ru(5)	-0.0940(3)	-0.0003(2)	0.2022(1)	0.041(2)
Ru(6)	0.0895(3)	-0.0850(2)	0.2319(1)	0.035(3)
Ru(7)	0.2769(3)	-0.1658(2)	0.2622(1)	0.040(3)
Ru(8)	0.2792(3)	-0.0106(2)	0.2707(1)	0.033(2)
Ru(9)	0.2797(3)	0.1455(2)	0.2756(1)	0.038(2)
Ru(10)	0.0905(3)	0.0746(2)	0.2395(1)	0.033(2)
P(1)	0.3535(12)	-0.2664(6)	0.4729(3)	0.045(9)
P(2)	0.1646(11)	-0.1571(6)	0.4902(3)	0.047(9)
N(1)	0.2542(31)	-0.2231(16)	0.4868(7)	0.046(25)
N(2)	0.1950(23)	-0.0037(18)	0.2169(7)	0.028(7)
C(11)	0.4688(39)	0.0110(27)	0.1326(11)	0.052(14)
O(11)	0.5728(28)	0.0115(19)	0.1322(8)	0.088(10)
C(12)	0.2900(56)	-0.0522(32)	0.0983(16)	0.090(22)
O(12)	0.2697(39)	-0.0980(24)	0.0734(12)	0.134(17)
C(13)	0.2989(48)	0.0906(29)	0.1041(14)	0.078(17)
O(13)	0.2847(35)	0.1442(22)	0.0840(10)	0.119(14)
C(21)	0.0453(53)	-0.0531(30)	0.1353(15)	0.076(19)
O(21)	-0.0014(32)	-0.0985(20)	0.1114(9)	0.098(12)
C(22)	0.0620(40)	0.0878(23)	0.1397(11)	0.053(13)
O(22)	0.0250(30)	0.1407(18)	0.1211(8)	0.075(11)
C(31)	0.2767(48)	-0.1596(30)	0.1707(14)	0.079(18)
O(31)	0.2662(32)	-0.2173(19)	0.1506(9)	0.095(12)
C(32)	0.4513(43)	-0.0863(23)	0.2009(11)	0.041(13)
O(32)	0.5580(30)	-0.0954(16)	0.2034(8)	0.070(9)
C(41)	0.4592(47)	0.0928(26)	0.2092(12)	0.046(15)
O(41)	0.5608(37)	0.1021(20)	0.2125(10)	0.082(13)
C(42)	0.2778(41)	0.1743(25)	0.1810(12)	0.047(14)
O(42)	0.2580(26)	0.2352(16)	0.1713(8)	0.060(9)
C(51)	-0.2002(38)	-0.0013(28)	0.2403(12)	0.056(14)
O(51)	-0.2507(28)	-0.0047(20)	0.2659(9)	0.094(11)
C(52)	-0.1761(40)	0.0773(24)	0.1778(11)	0.067(14)
O(52)	-0.2265(28)	0.1284(17)	0.1653(8)	0.075(10)
C(53)	-0.1689(45)	-0.0704(26)	0.1746(13)	0.040(15)
O(53)	-0.2237(33)	-0.1176(19)	0.1558(9)	0.077(12)
C(61)	0.0234(39)	-0.1034(23)	0.2754(11)	0.078(13)
O(61)	-0.0375(27)	-0.1072(16)	0.3039(8)	0.062(9)
C(62)	0.0335(46)	-0.1690(28)	0.2074(13)	0.045(17)
O(62)	-0.0062(27)	-0.2213(17)	0.1903(8)	0.082(10)
C(71)	0.4232(42)	-0.1863(23)	0.2717(11)	0.055(13)
O(71)	0.5230(29)	-0.2042(16)	0.2766(8)	0.062(10)
C(72)	0.2411(38)	-0.2599(22)	0.2435(11)	0.046(12)
O(72)	0.2166(27)	-0.3202(16)	0.2326(8)	0.051(10)
C(73)	0.2326(37)	-0.1871(22)	0.3115(11)	0.051(13)
O(73)	0.2078(29)	-0.1978(17)	0.3437(9)	0.076(11)
C(81)	0.2363(38)	-0.0133(26)	0.3203(13)	0.065(15)

Table A12.1 continued

O(81)	0.2054(25)	-0.0198(16)	0.3493(8)	0.064(10)
C(82)	0.4318(39)	-0.0164(23)	0.2870(11)	0.041(13)
O(82)	0.5300(29)	-0.0194(17)	0.2997(8)	0.081(11)
C(91)	0.2422(47)	0.1581(27)	0.3231(15)	0.098(17)
O(91)	0.2298(36)	0.1650(21)	0.3555(11)	0.104(14)
C(92)	0.2376(44)	0.2444(26)	0.2621(13)	0.040(15)
O(92)	0.2222(29)	0.3054(17)	0.2539(8)	0.073(10)
C(93)	0.4258(49)	0.1610(25)	0.2882(13)	0.083(16)
O(93)	0.5219(36)	0.1769(19)	0.2913(9)	0.107(12)
C(101)	0.0137(40)	0.0832(23)	0.2877(12)	0.063(13)
O(101)	-0.0331(31)	0.0815(18)	0.3133(9)	0.059(11)
C(102)	0.0305(39)	0.1646(23)	0.2186(11)	0.061(13)
O(102)	-0.0092(27)	0.2210(16)	0.2093(8)	0.049(10)
C(112)	0.3957(27)	-0.4180(24)	0.4802(8)	0.143(24)
C(113)	0.3755(27)	-0.4925(24)	0.4696(8)	0.193(30)
C(114)	0.2841(27)	-0.5103(24)	0.4437(8)	0.121(19)
C(115)	0.2129(27)	-0.4535(24)	0.4284(8)	0.127(21)
C(116)	0.2330(27)	-0.3790(24)	0.4390(8)	0.128(20)
C(111)	0.3244(27)	-0.3613(24)	0.4650(8)	0.086(17)
C(122)	0.4336(24)	-0.1523(15)	0.4297(6)	0.085(17)
C(123)	0.4862(24)	-0.1219(15)	0.3992(6)	0.050(12)
C(124)	0.5133(24)	-0.1679(15)	0.3692(6)	0.056(13)
C(125)	0.4878(24)	-0.2443(15)	0.3698(6)	0.064(14)
C(126)	0.4352(24)	-0.2748(15)	0.4004(6)	0.072(16)
C(121)	0.4081(24)	-0.2288(15)	0.4304(6)	0.045(12)
C(132)	0.4447(22)	-0.2649(15)	0.5448(9)	0.078(18)
C(133)	0.5308(22)	-0.2687(15)	0.5741(9)	0.071(14)
C(134)	0.6445(22)	-0.2747(15)	0.5657(9)	0.079(16)
C(135)	0.6720(22)	-0.2770(15)	0.5280(9)	0.084(17)
C(136)	0.5859(22)	-0.2732(15)	0.4987(9)	0.034(11)
C(131)	0.4723(22)	-0.2672(15)	0.5071(9)	0.044(13)
C(212)	0.2084(24)	-0.0227(16)	0.4516(7)	0.069(14)
C(213)	0.2678(24)	0.0441(16)	0.4473(7)	0.078(17)
C(214)	0.3476(24)	0.0684(16)	0.4759(7)	0.074(16)
C(215)	0.3680(24)	0.0257(16)	0.5088(7)	0.075(16)
C(216)	0.3087(24)	-0.0411(16)	0.5131(7)	0.070(15)
C(211)	0.2289(24)	-0.0654(16)	0.4845(7)	0.054(13)
C(222)	-0.0601(28)	-0.1485(13)	0.4672(6)	0.064(14)
C(223)	-0.1539(28)	-0.1515(13)	0.4406(6)	0.094(19)
C(224)	-0.1384(28)	-0.1685(13)	0.4027(6)	0.067(15)
C(225)	-0.0292(28)	-0.1825(13)	0.3915(6)	0.059(12)
C(226)	0.0646(28)	-0.1794(13)	0.4181(6)	0.082(16)
C(221)	0.0491(28)	-0.1624(13)	0.4559(6)	0.027(10)
C(232)	0.1047(26)	-0.2246(13)	0.5541(9)	0.079(17)
C(233)	0.0582(26)	-0.2265(13)	0.5893(9)	0.091(18)
C(234)	0.0201(26)	-0.1603(13)	0.6053(9)	0.090(16)
C(235)	0.0286(26)	-0.0923(13)	0.5861(9)	0.066(14)
C(236)	0.0751(26)	-0.0905(13)	0.5509(9)	0.065(14)
C(231)	0.1132(26)	-0.1566(13)	0.5350(9)	0.050(13)
C1(1)	0.2562(13)	0.0073(9)	0.6303(4)	0.119(5)
C1(2)	0.4275(17)	-0.0998(10)	0.6176(5)	0.148(7)
C(1)	0.3031(45)	-0.0855(27)	0.6413(13)	0.095(17)

Table A12.2 Fractional atomic coordinates for the
hydrogen atoms for $[\text{Ru}_{10}\text{N}(\text{CO})_{24}]^-$ (XR12)

Atom	x	y	z
H(112)	0.4664	-0.4042	0.5003
H(113)	0.4306	-0.5364	0.4814
H(114)	0.2685	-0.5679	0.4354
H(115)	0.1421	-0.4673	0.4083
H(116)	0.1779	-0.3351	0.4272
H(122)	0.4127	-0.1167	0.4530
H(123)	0.5060	-0.0627	0.3987
H(124)	0.5540	-0.1443	0.3455
H(125)	0.5087	-0.2799	0.3466
H(126)	0.4154	-0.3339	0.4008
H(132)	0.3568	-0.2602	0.5512
H(133)	0.5095	-0.2669	0.6033
H(134)	0.7112	-0.2777	0.5884
H(135)	0.7600	-0.2817	0.5215
H(136)	0.6072	-0.2750	0.4695
H(212)	0.1467	-0.0415	0.4294
H(213)	0.2520	0.0771	0.4218
H(214)	0.3935	0.1201	0.4725
H(215)	0.4298	0.0445	0.5310
H(216)	0.3245	-0.0741	0.5386
H(222)	-0.0721	-0.1353	0.4964
H(223)	-0.2384	-0.1407	0.4492
H(224)	-0.2110	-0.1709	0.3822
H(225)	-0.0172	-0.1956	0.3623
H(226)	0.1491	-0.1902	0.4095
H(232)	0.1342	-0.2758	0.5418
H(233)	0.0516	-0.2791	0.6041
H(234)	-0.0160	-0.1618	0.6325
H(235)	-0.0009	-0.0411	0.5985
H(236)	0.0817	-0.0379	0.5361

Table A12.3 Anisotropic thermal parameters (\AA^2) $[\text{Ru}_{10}\text{N}(\text{CO})_{24}]^-$ (XR12)

Atom	U_{11}	U_{22}	U_{33}	U_{23}	U_{13}	U_{12}
Ru(1)	0.056(3)	0.052(3)	0.042(2)	0.004(2)	0.013(2)	-0.001(2)
Ru(2)	0.050(3)	0.031(2)	0.037(2)	0.002(2)	-0.005(2)	0.000(2)
Ru(3)	0.038(3)	0.033(2)	0.043(2)	-0.001(2)	0.006(2)	0.009(2)
Ru(4)	0.030(3)	0.032(2)	0.044(2)	0.005(2)	0.005(2)	-0.001(2)
Ru(5)	0.035(2)	0.031(2)	0.058(2)	-0.001(2)	-0.001(2)	0.001(2)
Ru(6)	0.040(3)	0.027(2)	0.038(2)	0.002(2)	0.003(2)	0.000(2)
Ru(7)	0.048(3)	0.026(2)	0.046(3)	0.006(2)	-0.003(2)	0.006(2)
Ru(8)	0.035(2)	0.027(2)	0.037(2)	0.001(2)	-0.001(2)	-0.002(2)
Ru(9)	0.038(3)	0.030(2)	0.045(2)	0.000(2)	0.001(2)	-0.003(2)
Ru(10)	0.031(3)	0.027(2)	0.040(2)	-0.003(2)	0.004(2)	0.002(2)
P(1)	0.059(11)	0.034(7)	0.042(8)	-0.002(6)	-0.005(7)	0.008(7)
P(2)	0.057(11)	0.033(7)	0.052(8)	0.002(6)	0.007(7)	0.002(7)
N(1)	0.056(32)	0.054(23)	0.029(20)	-0.002(17)	0.009(19)	0.008(23)

Table A12.4 Bond lengths (Å) for $[\text{Ru}_{10}\text{N}(\text{CO})_{24}]^-$ (XR12)

Ru(1) -Ru(2)	2.761(5)	Ru(1) -Ru(3)	2.790(5)
Ru(1) -Ru(4)	2.767(5)	Ru(1) -C(11)	1.80(5)
Ru(1) -C(12)	1.75(6)	Ru(1) -C(13)	1.76(5)
Ru(2) -Ru(3)	2.884(5)	Ru(2) -Ru(4)	2.854(5)
Ru(2) -Ru(5)	2.789(5)	Ru(2) -Ru(6)	2.849(5)
Ru(2) -Ru(10)	2.845(4)	Ru(2) -N(1)	1.966(25)
Ru(2) -C(21)	1.70(5)	Ru(2) -C(22)	1.79(4)
Ru(3) -Ru(4)	2.846(5)	Ru(3) -Ru(6)	2.855(5)
Ru(3) -Ru(7)	2.773(5)	Ru(3) -Ru(8)	2.862(5)
Ru(3) -N(1)	1.98(3)	Ru(3) -C(31)	1.76(5)
Ru(3) -C(32)	1.75(5)	Ru(4) -Ru(8)	2.864(5)
Ru(4) -Ru(9)	2.780(5)	Ru(4) -Ru(10)	2.861(5)
Ru(4) -N(1)	2.03(3)	Ru(4) -C(41)	1.85(5)
Ru(4) -C(42)	1.89(4)	Ru(5) -Ru(6)	2.774(5)
Ru(5) -Ru(10)	2.791(5)	Ru(5) -C(51)	1.90(5)
Ru(5) -C(52)	1.86(4)	Ru(5) -C(53)	1.78(5)
Ru(6) -Ru(7)	2.778(5)	Ru(6) -Ru(8)	2.855(5)
Ru(6) -Ru(10)	2.856(5)	Ru(6) -N(1)	2.00(3)
Ru(6) -C(61)	1.80(4)	Ru(6) -C(62)	1.83(5)
Ru(7) -Ru(8)	2.781(5)	Ru(7) -C(71)	1.77(5)
Ru(7) -C(72)	1.84(4)	Ru(7) -C(73)	1.90(4)
Ru(8) -Ru(9)	2.787(5)	Ru(8) -Ru(10)	2.842(5)
Ru(8) -N(1)	2.079(24)	Ru(8) -C(81)	1.86(5)
Ru(8) -C(82)	1.85(4)	Ru(9) -Ru(10)	2.783(5)
Ru(9) -C(91)	1.78(5)	Ru(9) -C(92)	1.88(5)
Ru(9) -C(93)	1.76(6)	Ru(10) -N(1)	2.06(3)
Ru(10) -C(101)	1.99(4)	Ru(10) -C(102)	1.88(4)
C(11) -O(11)	1.22(6)	C(12) -O(12)	1.21(7)
C(13) -O(13)	1.19(6)	C(21) -O(21)	1.26(6)
C(22) -O(22)	1.21(5)	C(31) -O(31)	1.25(6)
C(32) -O(32)	1.26(6)	C(41) -O(41)	1.20(7)
C(42) -O(42)	1.16(5)	C(51) -O(51)	1.12(6)
C(52) -O(52)	1.15(5)	C(53) -O(53)	1.22(6)
C(61) -O(61)	1.28(5)	C(62) -O(62)	1.19(6)
C(71) -O(71)	1.22(6)	C(72) -O(72)	1.17(5)
C(73) -O(73)	1.21(5)	C(81) -O(81)	1.12(5)
C(82) -O(82)	1.21(5)	C(91) -O(91)	1.17(7)
C(92) -O(92)	1.14(6)	C(93) -O(93)	1.16(7)
C(101) -O(101)	1.10(6)	C(102) -O(102)	1.15(5)
P(1) -N(2)	1.51(4)	P(1) -C(111)	1.74(4)
P(1) -C(121)	1.81(3)	P(1) -C(131)	1.78(3)
P(2) -N(2)	1.59(3)	P(2) -C(211)	1.82(3)
P(2) -C(221)	1.75(3)	P(2) -C(231)	1.73(3)
C(112) -C(113)	1.39	C(112) -C(111)	1.39
C(113) -C(114)	1.39	C(114) -C(115)	1.39
C(115) -C(116)	1.39	C(116) -C(111)	1.39
C(122) -C(123)	1.39	C(122) -C(121)	1.39
C(123) -C(124)	1.39	C(124) -C(125)	1.39
C(125) -C(126)	1.39	C(126) -C(121)	1.39
C(132) -C(133)	1.39	C(132) -C(131)	1.39
C(133) -C(134)	1.39	C(134) -C(135)	1.39
C(135) -C(136)	1.39	C(136) -C(131)	1.39
C(212) -C(213)	1.39	C(212) -C(211)	1.39

Table A12.4 continued

C(213)-C(214)	1.39	C(214)-C(215)	1.39
C(215)-C(216)	1.39	C(216)-C(211)	1.39
C(222)-C(223)	1.39	C(222)-C(221)	1.39
C(223)-C(224)	1.39	C(224)-C(225)	1.39
C(225)-C(226)	1.39	C(226)-C(221)	1.39
C(232)-C(233)	1.39	C(232)-C(231)	1.39
C(233)-C(234)	1.39	C(234)-C(235)	1.39
C(235)-C(236)	1.39	C(236)-C(231)	1.39
C1(1) -C(1)	1.78(5)	C1(2) -C(1)	1.76(6)

Table A12.5 Bond angles ($^{\circ}$) for $[\text{Ru}_{10}\text{N}(\text{CO})_{24}]^{-}$ (XR12)

N(1) -Ru(2) -Ru(1)	88.3(8)	N(1) -Ru(2) -Ru(3)	43.3(9)
N(1) -Ru(2) -Ru(4)	45.3(9)	N(1) -Ru(2) -Ru(5)	89.6(8)
N(1) -Ru(2) -Ru(6)	44.7(9)	N(1) -Ru(2) -Ru(10)	46.4(9)
N(1) -Ru(3) -Ru(1)	87.1(8)	N(1) -Ru(3) -Ru(2)	42.9(7)
N(1) -Ru(3) -Ru(4)	45.5(9)	N(1) -Ru(3) -Ru(6)	44.6(9)
N(1) -Ru(3) -Ru(7)	89.8(8)	N(1) -Ru(3) -Ru(8)	46.6(7)
N(1) -Ru(4) -Ru(1)	86.9(8)	N(1) -Ru(4) -Ru(2)	43.5(7)
N(1) -Ru(4) -Ru(3)	44.2(8)	N(1) -Ru(4) -Ru(8)	46.5(7)
N(1) -Ru(4) -Ru(9)	91.0(8)	N(1) -Ru(4) -Ru(10)	46.0(8)
N(1) -Ru(6) -Ru(2)	43.6(7)	N(1) -Ru(6) -Ru(3)	44.0(9)
N(1) -Ru(6) -Ru(5)	89.2(8)	N(1) -Ru(6) -Ru(7)	89.2(8)
N(1) -Ru(6) -Ru(8)	46.7(7)	N(1) -Ru(6) -Ru(10)	46.2(9)
N(1) -Ru(8) -Ru(3)	43.9(8)	N(1) -Ru(8) -Ru(4)	45.1(8)
N(1) -Ru(8) -Ru(6)	44.6(8)	N(1) -Ru(8) -Ru(7)	87.7(9)
N(1) -Ru(8) -Ru(9)	89.8(9)	N(1) -Ru(8) -Ru(10)	46.3(8)
N(1) -Ru(10)-Ru(2)	43.7(7)	N(1) -Ru(10)-Ru(4)	45.2(8)
N(1) -Ru(10)-Ru(5)	87.7(8)	N(1) -Ru(10)-Ru(6)	44.6(8)
N(1) -Ru(10)-Ru(8)	46.9(7)	N(1) -Ru(10)-Ru(9)	90.3(8)
Ru(3) -N(1) -Ru(2)	94(1)	Ru(4) -N(1) -Ru(2)	91(1)
Ru(4) -N(1) -Ru(3)	90(1)	Ru(6) -N(1) -Ru(2)	92(1)
Ru(6) -N(1) -Ru(3)	91(1)	Ru(6) -N(1) -Ru(4)	177(1)
Ru(8) -N(1) -Ru(2)	177(2)	Ru(8) -N(1) -Ru(3)	89(1)
Ru(8) -N(1) -Ru(4)	88(1)	Ru(8) -N(1) -Ru(6)	89(1)
Ru(10)-N(1) -Ru(2)	90(1)	Ru(10)-N(1) -Ru(3)	176(1)
Ru(10)-N(1) -Ru(4)	89(1)	Ru(10)-N(1) -Ru(6)	89(1)
Ru(10)-N(1) -Ru(8)	87(1)	O(11) -C(11) -Ru(1)	177(4)
O(12) -C(12) -Ru(1)	179(6)	O(13) -C(13) -Ru(1)	178(5)
O(21) -C(21) -Ru(2)	179(5)	O(22) -C(22) -Ru(2)	177(4)
O(31) -C(31) -Ru(3)	176(5)	O(32) -C(32) -Ru(3)	177(3)
O(41) -C(41) -Ru(4)	178(4)	O(42) -C(42) -Ru(4)	170(4)
O(51) -C(51) -Ru(5)	171(4)	O(52) -C(52) -Ru(5)	174(4)
O(53) -C(53) -Ru(5)	178(4)	O(61) -C(61) -Ru(6)	169(3)
O(62) -C(62) -Ru(6)	177(4)	O(71) -C(71) -Ru(7)	176(3)
O(72) -C(72) -Ru(7)	178(4)	O(73) -C(73) -Ru(7)	177(3)
O(81) -C(81) -Ru(8)	174(4)	O(82) -C(82) -Ru(8)	176(3)
O(91) -C(91) -Ru(9)	173(5)	O(92) -C(92) -Ru(9)	174(5)
O(93) -C(93) -Ru(9)	170(4)	O(101)-C(101)-Ru(10)	173(4)
O(102)-C(102)-Ru(10)	173(4)	C(111)-P(1) -N(2)	114(2)
C(121)-P(1) -N(2)	114(1)	C(121)-P(1) -C(111)	108(1)
C(131)-P(1) -N(2)	112(2)	C(131)-P(1) -C(111)	104(1)
C(131)-P(1) -C(121)	105(1)	C(211)-P(2) -N(2)	112(2)
C(221)-P(2) -N(2)	113(1)	C(221)-P(2) -C(211)	106(1)
C(231)-P(2) -N(2)	111(1)	C(231)-P(2) -C(211)	106(1)
C(231)-P(2) -C(221)	109(1)	P(2) -N(2) -P(1)	159(2)
C(112)-C(111)-P(1)	122(2)	C(116)-C(111)-P(1)	117(3)
C(122)-C(121)-P(1)	118(2)	C(126)-C(121)-P(1)	122(2)
C(132)-C(131)-P(1)	115(2)	C(136)-C(131)-P(1)	125(2)
C(212)-C(211)-P(2)	122(2)	C(216)-C(211)-P(2)	117(2)
C(222)-C(221)-P(2)	118(2)	C(226)-C(221)-P(2)	122(2)
C(232)-C(231)-P(2)	119(2)	C(236)-C(231)-P(2)	121(2)
C(236)-C(231)-C(232)	120(3)	Cl(2) -C(1) -Cl(1)	107(3)

Table A13.1 Fractional atomic coordinates and thermal

parameters (\AA^2) for $\text{Os}_3(\text{CO})_{10}\{\text{PhCCH}_2\}(\text{AUPet}_3)$ (XR13)

Atom	x	y	z	U_{iso} or U_{eq}
Os(1)	0.24301(4)	0.21695(4)	-0.21092(3)	0.0367(3)
Os(2)	0.04305(4)	0.18270(4)	-0.16941(3)	0.0425(3)
Os(3)	0.17915(4)	0.21489(4)	-0.05253(3)	0.0367(3)
Au(1)	0.26553(4)	0.40030(4)	-0.12152(3)	0.0457(3)
P(1)	0.3118(3)	0.5796(3)	-0.1238(3)	0.065(3)
C(3)	0.2411(15)	0.6723(17)	-0.0520(13)	0.104(7)
C(4)	0.2384(16)	0.6222(19)	0.0278(13)	0.116(7)
C(5)	0.2842(16)	0.6414(18)	-0.2222(13)	0.111(7)
C(6)	0.2949(15)	0.7635(18)	-0.2309(13)	0.109(7)
C(7)	0.4395(16)	0.6044(17)	-0.1041(13)	0.108(7)
C(8)	0.5030(21)	0.5319(23)	-0.1467(17)	0.143(10)
C(1)	0.2902(9)	0.1149(11)	-0.1238(7)	0.047(3)
C(2)	0.2327(9)	0.0395(10)	-0.0785(7)	0.044(3)
C(112)	0.4489(6)	0.2033(6)	-0.0936(5)	0.052(3)
C(113)	0.5463(6)	0.1942(6)	-0.0826(5)	0.066(4)
C(114)	0.5907(6)	0.0922(6)	-0.0870(5)	0.082(5)
C(115)	0.5376(6)	-0.0007(6)	-0.1025(5)	0.074(5)
C(116)	0.4401(6)	0.0084(6)	-0.1135(5)	0.056(4)
C(111)	0.3958(6)	0.1104(6)	-0.1091(5)	0.049(3)
C(11)	0.3697(10)	0.2602(11)	-0.2407(8)	0.049(3)
O(11)	0.4423(8)	0.2874(9)	-0.2670(7)	0.077(3)
C(12)	0.1960(10)	0.3309(12)	-0.2727(8)	0.054(3)
O(12)	0.1680(8)	0.3981(9)	-0.3123(7)	0.081(3)
C(13)	0.2373(10)	0.1095(12)	-0.2842(8)	0.057(4)
O(13)	0.2327(9)	0.0402(10)	-0.3299(7)	0.086(4)
C(21)	0.0302(11)	0.3365(13)	-0.1621(9)	0.064(4)
O(21)	0.0181(8)	0.4303(9)	-0.1573(6)	0.076(3)
C(22)	0.0023(12)	0.1887(13)	-0.2687(9)	0.063(4)
O(22)	-0.0202(9)	0.1938(10)	-0.3313(7)	0.086(4)
C(23)	-0.0725(12)	0.1523(13)	-0.1127(9)	0.068(4)
O(23)	-0.1445(9)	0.1301(10)	-0.0757(8)	0.097(4)
C(24)	0.0714(9)	0.0295(10)	-0.1836(7)	0.042(3)
O(24)	0.0861(7)	-0.0595(8)	-0.1961(6)	0.061(3)
C(31)	0.1201(11)	0.3447(13)	-0.0203(9)	0.062(4)
O(31)	0.0754(9)	0.4198(10)	0.0062(7)	0.084(3)
C(32)	0.0918(11)	0.1356(13)	0.0077(9)	0.064(4)
O(32)	0.0327(8)	0.0919(9)	0.0475(7)	0.078(3)
C(33)	0.2728(10)	0.2338(11)	0.0210(8)	0.049(3)
O(33)	0.3222(8)	0.2480(9)	0.0698(7)	0.076(3)

Table A13.2 Fractional atomic coordinates for the

hydrogen atoms for $\text{Os}_3(\text{CO})_{10}\{\text{PhCCH}_2\}(\text{AUPet}_3)$ (XR13)

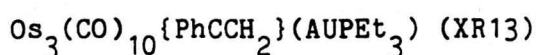
Atom	x	y	z
H(112)	0.4153	0.2828	-0.0914
H(113)	0.5870	0.2648	-0.0681
H(114)	0.6640	0.0827	-0.0731
H(115)	0.5693	-0.0813	-0.1016
H(116)	0.3975	-0.0633	-0.1249

Table A13.3 Anisotropic thermal parameters (\AA^2) for

$\text{Os}_3(\text{CO})_{10}\{\text{PhCCH}_2\}(\text{AUPEt}_3)$ (XR13)

Atom	U_{11}	U_{22}	U_{33}	U_{23}	U_{13}	U_{12}
Os(1)	0.0396(3)	0.0388(3)	0.0317(3)	-0.0002(2)	-0.0014(2)	0.0008(2)
Os(2)	0.0371(3)	0.0434(3)	0.0472(3)	-0.0003(2)	-0.0064(2)	0.0009(2)
Os(3)	0.0386(3)	0.0382(3)	0.0332(3)	-0.0001(2)	-0.0009(2)	0.0000(2)
Au(1)	0.0470(3)	0.0382(3)	0.0518(3)	-0.0029(2)	-0.0022(2)	-0.0025(2)
P(1)	0.080(3)	0.043(2)	0.071(3)	-0.004(2)	0.009(2)	-0.009(2)

Table A13.4 Bond lengths (Å) for



Os(1) -Os(2)	2.880(1)	Os(1) -Os(3)	2.874(1)
Os(1) -Au(1)	2.770(1)	Os(1) -C(1)	2.115(13)
Os(1) -C(11)	1.895(13)	Os(1) -C(12)	1.911(14)
Os(1) -C(13)	1.847(15)	Os(2) -Os(3)	2.917(1)
Os(2) -C(21)	1.894(16)	Os(2) -C(22)	1.874(17)
Os(2) -C(23)	1.885(16)	Os(2) -C(24)	1.930(12)
Os(3) -Au(1)	2.812(1)	Os(3) -C(1)	2.290(13)
Os(3) -C(2)	2.311(12)	Os(3) -C(31)	1.864(16)
Os(3) -C(32)	1.843(15)	Os(3) -C(33)	1.913(14)
Au(1) -P(1)	2.288(4)	Au(1) -C(31)	2.707(15)
P(1) -C(3)	1.927(22)	P(1) -C(5)	1.950(23)
P(1) -C(7)	1.868(23)	C(3) -C(4)	1.53(3)
C(5) -C(6)	1.51(3)	C(7) -C(8)	1.43(4)
C(1) -C(2)	1.434(18)	C(1) -C(111)	1.519(16)
C(112)-C(113)	1.395	C(112)-C(111)	1.395
C(113)-C(114)	1.395	C(114)-C(115)	1.395
C(115)-C(116)	1.395	C(116)-C(111)	1.395
C(11) -O(11)	1.140(17)	C(12) -O(12)	1.162(19)
C(13) -O(13)	1.175(19)	C(21) -O(21)	1.164(19)
C(22) -O(22)	1.166(21)	C(23) -O(23)	1.196(20)
C(24) -O(24)	1.129(16)	C(31) -O(31)	1.191(20)
C(32) -O(32)	1.179(19)	C(33) -O(33)	1.151(18)

Table A13.5 Bond angles ($^{\circ}$) for $\text{Os}_3(\text{CO})_{10}\{\text{PhCCH}_2\}(\text{AUPet}_3)$ (XR13)

Os(3) -Os(1) -Os(2)	60.9(1)	Au(1) -Os(1) -Os(2)	96.7(1)
Au(1) -Os(1) -Os(3)	59.7(1)	C(1) -Os(1) -Os(2)	94.2(3)
C(1) -Os(1) -Os(3)	52.0(3)	C(1) -Os(1) -Au(1)	90.9(4)
C(11) -Os(1) -Os(2)	171.9(4)	C(11) -Os(1) -Os(3)	120.0(4)
C(11) -Os(1) -Au(1)	78.1(4)	C(11) -Os(1) -C(1)	92.1(5)
Os(3) -Os(2) -Os(1)	59.4(1)	Os(2) -Os(3) -Os(1)	59.6(1)
Au(1) -Os(3) -Os(1)	58.3(1)	Au(1) -Os(3) -Os(2)	95.0(1)
C(1) -Os(3) -Os(1)	46.7(3)	C(1) -Os(3) -Os(2)	89.6(3)
C(1) -Os(3) -Au(1)	86.3(3)	C(2) -Os(3) -Os(1)	74.9(3)
C(2) -Os(3) -Os(2)	87.3(3)	C(2) -Os(3) -Au(1)	122.6(3)
C(2) -Os(3) -C(1)	36.3(4)	Os(3) -Au(1) -Os(1)	62.0(1)
P(1) -Au(1) -Os(1)	144.0(1)	P(1) -Au(1) -Os(3)	153.6(1)
C(3) -P(1) -Au(1)	114.9(7)	C(5) -P(1) -Au(1)	108.4(9)
C(5) -P(1) -C(3)	103.4(9)	C(7) -P(1) -Au(1)	115.2(7)
C(7) -P(1) -C(3)	104(1)	C(7) -P(1) -C(5)	110(1)
C(4) -C(3) -P(1)	110(1)	C(6) -C(5) -P(1)	117(2)
C(8) -C(7) -P(1)	112(1)	Os(3) -C(1) -Os(1)	81.3(4)
C(2) -C(1) -Os(1)	126.4(9)	C(2) -C(1) -Os(3)	72.6(7)
C(111) -C(1) -Os(1)	119.8(8)	C(111) -C(1) -Os(3)	124.1(8)
C(111) -C(1) -C(2)	114(1)	C(1) -C(2) -Os(3)	71.1(7)
C(111) -C(112) -C(113)	120.0	C(114) -C(113) -C(112)	120.0
C(115) -C(114) -C(113)	120.0	C(116) -C(115) -C(114)	120.0
C(111) -C(116) -C(115)	120.0	C(112) -C(111) -C(1)	122.7(8)
C(116) -C(111) -C(1)	117.2(8)	C(116) -C(111) -C(112)	120.0(8)
O(11) -C(11) -Os(1)	172(1)	O(12) -C(12) -Os(1)	178(1)
O(13) -C(13) -Os(1)	179(1)	O(21) -C(21) -Os(2)	177(1)
O(22) -C(22) -Os(2)	178(1)	O(23) -C(23) -Os(2)	178(1)
O(24) -C(24) -Os(2)	176(1)	Au(1) -C(31) -Os(3)	73.3(5)
O(31) -C(31) -Os(3)	172(1)	O(31) -C(31) -Au(1)	115(1)
O(32) -C(32) -Os(3)	175(1)	O(33) -C(33) -Os(3)	174(1)

TABLE A14.1 Fractional atomic coordinates and thermal

parameters (\AA^2) for $\text{HOs}_3(\text{CO})_9(\text{MeCCMe})(\text{AuPPh}_3)$ (XR14)

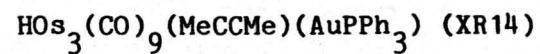
Atom	x	y	z	U_{iso} or U_{eq}
Os(1)	0.21054(12)	0.34750(19)	0.01481(9)	0.0566(13)
Os(2)	0.39015(12)	0.26262(20)	0.03384(9)	0.0562(12)
Os(3)	0.23165(11)	0.05508(18)	-0.00488(9)	0.0518(12)
Au(1)	0.21871(12)	0.14053(19)	0.09543(9)	0.0591(13)
P(1)	0.2109(8)	0.1054(13)	0.1830(5)	0.064(8)
C(111)	0.3092(20)	0.1890(29)	0.2488(12)	0.067(13)
C(112)	0.2929(20)	0.2806(29)	0.2866(12)	0.066(13)
C(113)	0.3687(20)	0.3491(29)	0.3315(12)	0.097(17)
C(114)	0.4608(20)	0.3261(29)	0.3385(12)	0.131(23)
C(115)	0.4771(20)	0.2345(29)	0.3007(12)	0.120(19)
C(116)	0.4013(20)	0.1660(29)	0.2558(12)	0.107(19)
C(121)	0.2162(21)	-0.0781(24)	0.2052(15)	0.058(12)
C(122)	0.1650(21)	-0.1712(24)	0.1596(15)	0.073(14)
C(123)	0.1644(21)	-0.3125(24)	0.1720(15)	0.092(17)
C(124)	0.2149(21)	-0.3609(24)	0.2300(15)	0.103(19)
C(125)	0.2661(21)	-0.2678(24)	0.2755(15)	0.089(16)
C(126)	0.2668(21)	-0.1265(24)	0.2631(15)	0.094(17)
C(131)	0.1078(15)	0.1720(28)	0.1861(13)	0.050(11)
C(132)	0.0747(15)	0.3005(28)	0.1591(13)	0.077(14)
C(133)	-0.0062(15)	0.3590(28)	0.1597(13)	0.097(17)
C(134)	-0.0541(15)	0.2891(28)	0.1873(13)	0.069(13)
C(135)	-0.0211(15)	0.1605(28)	0.2143(13)	0.089(16)
C(136)	0.0598(15)	0.1020(28)	0.2137(13)	0.085(16)
C(11)	0.0828(37)	0.3381(54)	-0.0094(24)	0.095(17)
O(11)	0.0041(22)	0.3251(32)	-0.0181(14)	0.084(10)
C(12)	0.2742(30)	0.4152(46)	0.1030(22)	0.065(14)
O(12)	0.3021(22)	0.4606(36)	0.1431(16)	0.091(11)
C(13)	0.1980(29)	0.5286(47)	-0.0109(20)	0.069(13)
O(13)	0.1910(23)	0.6463(39)	-0.0275(15)	0.122(11)
C(21)	0.4604(28)	0.2099(42)	0.1144(21)	0.058(13)
O(21)	0.5015(25)	0.1773(39)	0.1644(18)	0.150(13)
C(22)	0.4331(33)	0.4368(56)	0.0502(23)	0.104(16)
O(22)	0.4656(23)	0.5537(39)	0.0593(16)	0.127(12)
C(23)	0.4771(32)	0.1972(47)	0.0129(21)	0.081(14)
O(23)	0.5329(21)	0.1604(33)	-0.0070(14)	0.094(10)
C(31)	0.2808(31)	-0.0897(48)	0.0557(22)	0.081(14)
O(31)	0.3026(21)	-0.1838(34)	0.0868(15)	0.089(11)
C(32)	0.2558(27)	-0.0617(48)	-0.0694(21)	0.056(13)
O(32)	0.2543(25)	-0.1229(40)	-0.1012(17)	0.140(13)
C(33)	0.1047(38)	0.0100(55)	-0.0337(24)	0.099(18)
O(33)	0.0276(24)	-0.0303(36)	-0.0516(16)	0.101(11)
C(3)	0.1235(26)	0.2291(42)	-0.1186(18)	0.063(12)
C(1)	0.2030(30)	0.2266(46)	-0.0637(21)	0.069(14)
C(2)	0.2783(29)	0.3125(45)	-0.0502(20)	0.067(13)
C(4)	0.2860(27)	0.4238(40)	-0.0912(19)	0.056(12)

TABLE A14.2 Fractional atomic coordinates for the

hydrogen atoms for $\text{HOs}_3(\text{CO})_9(\text{MeCCMe})(\text{AuPPh}_3)$ (XR14)

Atom	x	y	z
H(112)	0.2216	0.2984	0.2812
H(113)	0.3561	0.4200	0.3607
H(114)	0.5195	0.3792	0.3732
H(115)	0.5483	0.2167	0.3061
H(116)	0.4138	0.0951	0.2266
H(122)	0.1259	-0.1338	0.1147
H(123)	0.1248	-0.3846	0.1368
H(124)	0.2144	-0.4703	0.2396
H(125)	0.3052	-0.3052	0.3204
H(126)	0.3064	-0.0545	0.2984
H(132)	0.1118	0.3546	0.1378
H(133)	-0.0318	0.4585	0.1388
H(134)	-0.1168	0.3344	0.1878
H(135)	-0.0582	0.1064	0.2357
H(136)	0.0854	0.0025	0.2346
H(3a)	0.0734	0.1509	-0.1197
H(3b)	0.1443	0.2095	-0.1538
H(3c)	0.0911	0.3307	-0.1247
H(4a)	0.3524	0.4787	-0.0692
H(4b)	0.2281	0.4967	-0.1038
H(4c)	0.2832	0.3729	-0.1304
H	0.3615	0.0748	0.0280

TABLE A14.3 Anisotropic thermal parameters (\AA^2) for



Atom	U_{11}	U_{22}	U_{33}	U_{23}	U_{13}	U_{12}
Os(1)	0.056(1)	0.047(1)	0.066(2)	0.023(1)	0.029(1)	0.005(1)
Os(2)	0.048(1)	0.060(1)	0.061(1)	0.007(1)	0.026(1)	-0.008(1)
Os(3)	0.042(1)	0.047(1)	0.066(2)	0.020(1)	0.014(1)	0.001(1)
Au(1)	0.052(1)	0.062(1)	0.063(2)	0.030(1)	0.020(1)	0.001(1)
P(1)	0.062(7)	0.080(9)	0.050(9)	0.041(7)	0.031(7)	0.003(6)

TABLE A14.4 Bond lengths (Å) for $\text{HOs}_3(\text{CO})_9(\text{MeCCMe})(\text{AuPPh}_3)$ (XR14)

Os(1) -Os(2)	2.769(3)	Os(1) -Os(3)	2.898(3)
Os(1) -Au(1)	2.796(3)	Os(1) -C(11)	1.83(6)
Os(1) -O(11)	2.98(3)	Os(1) -C(12)	2.09(5)
Os(1) -C(13)	1.84(4)	Os(1) -O(13)	3.03(4)
Os(1) -C(1)	2.24(5)	Os(1) -C(2)	2.32(6)
Os(2) -Os(3)	3.001(2)	Os(2) -Au(1)	3.821(3)
Os(2) -C(21)	1.90(4)	Os(2) -C(22)	1.78(5)
Os(2) -O(22)	3.00(4)	Os(2) -C(23)	1.78(6)
Os(2) -O(23)	3.00(4)	Os(2) -C(1)	2.91(4)
Os(2) -C(2)	2.13(4)	Os(3) -Au(1)	2.731(3)
Os(3) -C(31)	1.95(5)	Os(3) -C(32)	2.13(5)
Os(3) -C(33)	1.85(6)	Os(3) -O(33)	3.01(4)
Os(3) -C(3)	3.09(4)	Os(3) -C(1)	2.12(5)
Os(3) -C(2)	2.94(5)	Au(1) -P(1)	2.272(15)
Au(1) -C(12)	2.76(4)	Au(1) -C(31)	2.77(5)
P(1) -C(111)	1.88(3)	P(1) -C(121)	1.84(3)
P(1) -C(131)	1.77(3)	C(111)-C(112)	1.39
C(111)-C(116)	1.39	C(112)-C(113)	1.39
C(113)-C(114)	1.39	C(114)-C(115)	1.39
C(115)-C(116)	1.39	C(121)-C(122)	1.39
C(121)-C(126)	1.39	C(122)-C(123)	1.39
C(123)-C(124)	1.39	C(124)-C(125)	1.39
C(125)-C(126)	1.39	C(131)-C(132)	1.39
C(131)-C(136)	1.39	C(132)-C(133)	1.39
C(133)-C(134)	1.39	C(134)-C(135)	1.39
C(135)-C(136)	1.39	C(11) -O(11)	1.16(7)
C(12) -O(12)	1.00(6)	C(13) -O(13)	1.19(6)
C(21) -O(21)	1.17(6)	C(22) -O(22)	1.21(6)
C(23) -O(23)	1.23(7)	C(31) -O(31)	1.14(6)
C(32) -O(32)	0.98(7)	C(33) -O(33)	1.16(7)
C(3) -C(1)	1.40(5)	C(1) -C(2)	1.36(6)
C(2) -C(4)	1.52(7)		

TABLE A14.5 Bond angles ($^{\circ}$) for $\text{HOs}_3(\text{CO})_9(\text{MeCCMe})(\text{AuPPh}_3)$ (XR14)

Os(3) -Os(1) -Os(2)	63.9(1)	Au(1) -Os(1) -Os(2)	86.7(1)
Au(1) -Os(1) -Os(3)	57.3(1)	C(1) -Os(1) -Os(2)	70(1)
C(1) -Os(1) -Os(3)	47(1)	C(1) -Os(1) -Au(1)	103(1)
C(2) -Os(1) -Os(2)	48.4(9)	C(2) -Os(1) -Os(3)	68(1)
C(2) -Os(1) -Au(1)	121(1)	C(2) -Os(1) -C(1)	35(2)
Os(3) -Os(2) -Os(1)	60.1(1)	Au(1) -Os(2) -Os(1)	46.9(1)
Au(1) -Os(2) -Os(3)	45.2(1)	C(1) -Os(2) -Os(1)	46(1)
C(1) -Os(2) -Os(3)	42(1)	C(1) -Os(2) -Au(1)	71(1)
C(2) -Os(2) -Os(1)	55(1)	C(2) -Os(2) -Os(3)	68(1)
C(2) -Os(2) -Au(1)	93(1)	C(2) -Os(2) -C(1)	26(2)
Os(2) -Os(3) -Os(1)	56.0(1)	Au(1) -Os(3) -Os(1)	59.5(1)
Au(1) -Os(3) -Os(2)	83.5(1)	C(3) -Os(3) -Os(1)	64.8(8)
C(3) -Os(3) -Os(2)	89.0(7)	C(3) -Os(3) -Au(1)	116.9(9)
C(1) -Os(3) -Os(1)	50(1)	C(1) -Os(3) -Os(2)	67(1)
C(1) -Os(3) -Au(1)	109(1)	C(1) -Os(3) -C(3)	23(1)
C(2) -Os(3) -Os(1)	47(1)	C(2) -Os(3) -Os(2)	41.9(7)
C(2) -Os(3) -Au(1)	103(1)	C(2) -Os(3) -C(3)	47(1)
C(2) -Os(3) -C(1)	25(1)	Os(2) -Au(1) -Os(1)	46.3(1)
Os(3) -Au(1) -Os(1)	63.2(1)	Os(3) -Au(1) -Os(2)	51.3(1)
P(1) -Au(1) -Os(1)	142.8(3)	P(1) -Au(1) -Os(2)	141.0(3)
P(1) -Au(1) -Os(3)	153.9(3)	C(111)-P(1) -Au(1)	114(1)
C(121)-P(1) -Au(1)	115(1)	C(121)-P(1) -C(111)	103(1)
C(131)-P(1) -Au(1)	115(1)	C(131)-P(1) -C(111)	103(1)
C(131)-P(1) -C(121)	105(2)	C(112)-C(111)-P(1)	123(2)
C(116)-C(111)-P(1)	117(2)	C(116)-C(111)-C(112)	120(2)
C(113)-C(112)-C(111)	120	C(114)-C(113)-C(112)	120
C(115)-C(114)-C(113)	120	C(116)-C(115)-C(114)	120
C(115)-C(116)-C(111)	120	C(122)-C(121)-P(1)	116(2)
C(126)-C(121)-P(1)	124(2)	C(126)-C(121)-C(122)	120
C(123)-C(122)-C(121)	120	C(124)-C(123)-C(122)	120
C(125)-C(124)-C(123)	120	C(126)-C(125)-C(124)	120
C(125)-C(126)-C(121)	120	C(132)-C(131)-P(1)	117(2)
C(136)-C(131)-P(1)	123(2)	C(136)-C(131)-C(132)	120
C(133)-C(132)-C(131)	120	C(134)-C(133)-C(132)	120
C(135)-C(134)-C(133)	120	C(136)-C(135)-C(134)	120
C(135)-C(136)-C(131)	120	O(11) -C(11) -Os(1)	172(5)
C(11) -O(11) -Os(1)	5(3)	Au(1) -C(12) -Os(1)	69(1)
O(12) -C(12) -Os(1)	172(4)	O(12) -C(12) -Au(1)	118(4)
O(13) -C(13) -Os(1)	179(4)	C(13) -O(13) -Os(1)	1(3)
O(21) -C(21) -Os(2)	178(5)	O(22) -C(22) -Os(2)	176(6)
C(22) -O(22) -Os(2)	2(3)	O(23) -C(23) -Os(2)	173(4)
C(23) -O(23) -Os(2)	4(2)	Au(1) -C(31) -Os(3)	68(1)
O(31) -C(31) -Os(3)	173(4)	O(31) -C(31) -Au(1)	116(4)
O(32) -C(32) -Os(3)	169(4)	O(33) -C(33) -Os(3)	174(5)
C(33) -O(33) -Os(3)	4(3)	C(1) -C(3) -Os(3)	36(2)
Os(2) -C(1) -Os(1)	63(1)	Os(3) -C(1) -Os(1)	83(2)
Os(3) -C(1) -Os(2)	71(1)	C(3) -C(1) -Os(1)	122(4)
C(3) -C(1) -Os(2)	165(4)	C(3) -C(1) -Os(3)	122(3)
C(2) -C(1) -Os(1)	76(3)	C(2) -C(1) -Os(2)	43(2)
C(2) -C(1) -Os(3)	114(3)	C(2) -C(1) -C(3)	123(5)
Os(2) -C(2) -Os(1)	77(2)	Os(3) -C(2) -Os(1)	65(1)
Os(3) -C(2) -Os(2)	70(1)	C(1) -C(2) -Os(1)	69(3)
C(1) -C(2) -Os(2)	111(3)	C(1) -C(2) -Os(3)	41(2)
C(4) -C(2) -Os(1)	124(3)	C(4) -C(2) -Os(2)	123(3)
C(4) -C(2) -Os(3)	163(3)	C(3) -C(2) -C(1)	125(3)

TABLE A15.1 Fractional atomic coordinates and thermal

parameters (\AA^2) for $\text{Os}_7(\text{CO})_{16}(\text{MeCCMe})_3$ (XR15)

Atom	x	y	z	U_{iso} or U_{eq}
Os(1)	0.11216(4)	-0.06068(12)	-0.05471(14)	0.0374(8)
Os(2)	0.10699(5)	0.05491(13)	-0.29099(14)	0.0384(9)
Os(3)	0.10161(5)	0.14982(13)	0.04780(15)	0.0454(10)
Os(4)	0.12988(5)	0.26173(13)	-0.14807(16)	0.0470(10)
Os(5)	0.17551(4)	0.07878(13)	-0.03455(14)	0.0382(9)
Os(6)	0.15135(5)	-0.15775(13)	-0.20799(15)	0.0461(10)
Os(7)	0.22581(5)	-0.09982(14)	-0.03130(16)	0.0516(10)
C(1a)	0.0614(12)	-0.2541(32)	-0.2166(40)	0.067(12)
C(2a)	0.0854(10)	-0.1586(28)	-0.2189(32)	0.037(8)
C(3a)	0.0900(10)	-0.1067(27)	-0.3326(32)	0.039(9)
C(4a)	0.0705(13)	-0.1483(37)	-0.4731(39)	0.077(13)
C(1b)	0.0218(9)	0.0146(29)	-0.1570(32)	0.044(9)
C(2b)	0.0668(10)	0.0549(28)	-0.1347(32)	0.044(9)
C(3b)	0.0748(11)	0.1705(30)	-0.1787(34)	0.047(10)
C(4b)	0.0367(11)	0.2238(30)	-0.2535(36)	0.053(10)
C(1c)	0.1880(12)	-0.0736(34)	0.2315(38)	0.074(12)
C(2c)	0.1757(10)	-0.0636(29)	0.0776(32)	0.042(9)
C(3c)	0.1661(12)	-0.1616(34)	0.0116(38)	0.059(11)
C(4c)	0.1685(12)	-0.2815(31)	0.0762(38)	0.059(11)
C(11)	0.0855(13)	-0.1459(36)	0.0471(40)	0.066(12)
O(11)	0.0650(9)	-0.1887(25)	0.1102(30)	0.084(9)
C(21)	0.0677(12)	0.0950(31)	-0.4416(38)	0.053(11)
O(21)	0.0420(10)	0.1211(28)	-0.5408(35)	0.102(11)
C(22)	0.1445(15)	0.0678(40)	0.6021(48)	0.082(14)
O(22)	0.1675(11)	0.0662(32)	0.5340(38)	0.120(13)
C(31)	0.1018(14)	0.0633(39)	0.1911(46)	0.080(14)
O(31)	0.0974(10)	0.0157(29)	0.2879(36)	0.109(12)
C(32)	0.1379(15)	0.2536(42)	0.1559(50)	0.090(16)
O(32)	0.1561(11)	0.3143(31)	0.2411(37)	0.117(12)
C(33)	0.0534(14)	0.2074(38)	0.0597(44)	0.077(14)
O(33)	0.0243(12)	0.2562(33)	0.0764(38)	0.130(14)
C(41)	0.1769(12)	0.3533(32)	0.9507(38)	0.055(11)
O(41)	0.2067(11)	0.3924(28)	0.0062(34)	0.106(11)
C(42)	0.0974(14)	0.3914(38)	0.8383(44)	0.076(14)
O(42)	0.0786(10)	0.4676(30)	0.8463(34)	0.110(12)
C(43)	0.1417(15)	0.2972(43)	-0.3233(52)	0.092(16)
O(43)	0.1503(11)	0.3142(30)	-0.4143(36)	0.103(12)
C(51)	0.2056(11)	0.1394(32)	-0.1424(37)	0.056(11)
O(51)	0.2323(9)	0.1702(24)	-0.2039(27)	0.078(9)
C(52)	0.2098(12)	0.1498(34)	0.1134(39)	0.059(11)
O(52)	0.2315(8)	0.1954(22)	0.2008(26)	0.066(8)
C(61)	0.1768(13)	-0.1505(38)	-0.3413(43)	0.072(13)
O(61)	0.1924(10)	-0.1656(29)	-0.4360(36)	0.112(12)
C(62)	0.1525(12)	-0.3024(36)	-0.2232(40)	0.065(12)
O(62)	0.1526(9)	-0.4038(27)	-0.2358(31)	0.091(10)
C(71)	0.2531(13)	-0.2492(41)	0.0022(45)	0.079(14)
O(71)	0.2608(10)	-0.3368(31)	-0.0069(33)	0.100(11)
C(72)	0.2538(17)	-0.0763(47)	-0.1633(56)	0.109(19)
O(72)	0.2697(11)	-0.0441(31)	-0.2409(38)	0.114(12)

Table A15.1 continued

C(73)	0.2733(15)	-0.0385(43)	0.1070(51)	0.096(16)
O(73)	0.2913(11)	0.0074(31)	0.1950(39)	0.126(13)
O(1s)	0.0650(20)	0.5291(53)	0.1918(66)	0.131(21)
C(2s)	0.0242(25)	0.5143(74)	0.4013(82)	0.086(25)
C(3s)	0.0794(30)	0.5665(81)	0.3328(82)	0.103(29)
C(4s)	0.1294(31)	0.5651(81)	0.4002(85)	0.144(31)
C(5s)	0.0737(30)	0.4913(78)	0.4542(87)	0.093(27)
C(6s)	0.0361(28)	0.4864(78)	0.2815(95)	0.097(29)
C(7s)	0.0997(30)	0.5515(81)	0.4377(96)	0.104(28)
C(8s)	0.0444(31)	0.4386(86)	0.3925(84)	0.130(32)
C(9s)	0.1051(32)	0.5616(82)	0.2658(99)	0.119(31)

TABLE A15.2 Fractional atomic coordinates for the
hydrogen atoms for $\text{Os}_7(\text{CO})_{16}(\text{MeCCMe})_3$ (XR15)

Atom	x	y	z
H(11a)	0.0631	-0.2781	-0.1149
H(12a)	0.0723	-0.3203	-0.2671
H(12a)	0.0298	-0.2354	-0.2686
H(41a)	0.0787	-0.0939	-0.5441
H(42a)	0.0374	-0.1508	-0.4917
H(43a)	0.0819	-0.2295	-0.4841
H(11b)	0.0219	-0.0680	-0.1201
H(12b)	0.0061	0.0166	-0.2625
H(13b)	0.0061	0.0676	-0.1032
H(41b)	0.0436	0.3048	-0.2830
H(42b)	0.0158	0.2298	-0.1906
H(43b)	0.0225	0.1764	-0.3417
H(11c)	0.1951	0.0059	0.2770
H(12c)	0.2149	-0.1255	0.2612
H(13c)	0.1630	-0.1099	0.2638
H(41c)	0.1588	-0.3424	-0.0013
H(42c)	0.1491	-0.2858	0.1440
H(43c)	0.2001	-0.2966	0.1308

TABLE A15.3 Anisotropic thermal parameters (\AA^2) for $\text{Os}_7(\text{CO})_{16}(\text{MeCCMe})_3$ (XR15)

Atom	U_{11}	U_{22}	U_{33}	U_{23}	U_{13}	U_{12}
Os(1)	0.037(1)	0.037(1)	0.039(1)	0.006(1)	0.013(1)	0.002(1)
Os(2)	0.040(1)	0.041(1)	0.034(1)	0.004(1)	0.006(1)	-0.005(1)
Os(3)	0.047(1)	0.042(1)	0.047(1)	-0.005(1)	0.016(1)	-0.002(1)
Os(4)	0.053(1)	0.034(1)	0.054(1)	0.004(1)	0.012(1)	-0.007(1)
Os(5)	0.032(1)	0.046(1)	0.037(1)	0.002(1)	0.005(1)	-0.003(1)
Os(6)	0.048(1)	0.046(1)	0.045(1)	0.005(1)	0.018(1)	0.009(1)
Os(7)	0.040(1)	0.064(1)	0.050(1)	0.010(1)	0.012(1)	0.012(1)

TABLE A15.4 Bond lengths (Å) for Os₇(CO)₁₆(MeCCMe)₃ (XR15)

Os(1) -Os(2)	2.791(2)	Os(1) -Os(3)	2.842(2)
Os(1) -Os(5)	2.694(2)	Os(1) -Os(6)	2.604(2)
Os(1) -C(2a)	2.08(3)	Os(1) -C(2b)	2.08(3)
Os(1) -C(2c)	2.21(3)	Os(1) -C(3c)	2.15(4)
Os(1) -C(11)	1.87(5)	Os(2) -Os(4)	2.928(2)
Os(2) -Os(5)	3.034(2)	Os(2) -Os(6)	3.008(2)
Os(2) -C(3a)	2.07(3)	Os(2) -C(2b)	2.37(4)
Os(2) -C(3b)	2.28(4)	Os(2) -C(21)	1.82(3)
Os(2) -C(22)	1.89(6)	Os(3) -Os(4)	2.814(2)
Os(3) -Os(5)	2.965(2)	Os(3) -C(2b)	2.26(3)
Os(3) -C(3b)	2.29(3)	Os(3) -C(31)	1.82(5)
Os(3) -C(32)	1.90(5)	Os(3) -C(33)	1.80(5)
Os(4) -Os(5)	2.790(2)	Os(4) -C(3b)	2.12(4)
Os(4) -C(41)	1.99(4)	Os(4) -C(42)	1.91(5)
Os(4) -C(43)	2.01(6)	Os(5) -Os(6)	3.387(2)
Os(5) -Os(7)	2.757(2)	Os(5) -C(2c)	2.09(3)
Os(5) -C(51)	1.85(4)	Os(5) -C(52)	1.87(4)
Os(6) -Os(7)	2.774(2)	Os(6) -C(2a)	2.19(3)
Os(6) -C(3a)	2.21(3)	Os(6) -C(3c)	2.19(4)
Os(6) -C(61)	1.81(5)	Os(6) -C(62)	1.78(4)
Os(7) -C(2c)	2.31(4)	Os(7) -C(3c)	2.30(4)
Os(7) -C(71)	2.03(5)	Os(7) -C(72)	1.88(6)
Os(7) -C(73)	1.99(5)	C(1a) -C(2a)	1.42(5)
C(2a) -C(3a)	1.38(5)	C(3a) -C(4a)	1.52(5)
C(1b) -C(2b)	1.55(5)	C(2b) -C(3b)	1.53(5)
C(3b) -C(4b)	1.47(5)	C(1c) -C(2c)	1.54(5)
C(2c) -C(3c)	1.37(5)	C(3c) -C(4c)	1.61(6)
C(11) -O(11)	1.19(6)	C(21) -O(21)	1.20(5)
C(22) -O(22)	1.18(7)	C(31) -O(31)	1.20(6)
C(32) -O(32)	1.19(6)	C(33) -O(33)	1.20(7)
C(41) -O(41)	1.12(5)	C(42) -O(42)	1.14(6)
C(43) -O(43)	1.08(7)	C(51) -O(51)	1.29(5)
C(52) -O(52)	1.14(4)	C(61) -O(61)	1.24(6)
C(62) -O(62)	1.25(5)	C(71) -O(71)	1.11(6)
C(72) -O(72)	1.15(8)	C(73) -O(73)	1.10(6)
O(1s) -C(3s)	1.48(9)	O(1s) -C(6s)	1.60(9)
O(1s) -C(9s)	1.42(9)	C(2s) -C(5s)	1.64(9)
C(2s) -C(6s)	1.44(9)	C(2s) -C(8s)	1.17(9)
C(3s) -C(4s)	1.64(9)	C(3s) -C(5s)	1.61(9)
C(3s) -C(6s)	1.72(9)	C(3s) -C(7s)	1.13(9)
C(3s) -C(9s)	1.24(9)	C(4s) -C(7s)	1.17(9)
C(4s) -C(9s)	1.42(9)	C(5s) -C(6s)	1.90(9)
C(5s) -C(7s)	1.19(9)	C(5s) -C(8s)	1.21(9)
C(6s) -C(8s)	1.25(9)	C(7s) -C(9s)	1.84(9)

TABLE A15.5 Bond angles ($^{\circ}$) for $\text{Os}_7(\text{CO})_{16}(\text{MeCCMe})_3$ (XR15)

C(2a) -Os(1) -Os(2)	70(1)	C(2a) -Os(1) -Os(3)	139.2(9)
C(2a) -Os(1) -Os(5)	126(1)	C(2a) -Os(1) -Os(6)	54(1)
C(2b) -Os(1) -Os(2)	56(1)	C(2b) -Os(1) -Os(3)	51.9(9)
C(2b) -Os(1) -Os(5)	95(1)	C(2b) -Os(1) -Os(6)	120(1)
C(2b) -Os(1) -C(2a)	87(1)	C(2c) -Os(1) -Os(2)	112(1)
C(2c) -Os(1) -Os(3)	88.8(9)	C(2c) -Os(1) -Os(5)	49.3(9)
C(2c) -Os(1) -Os(6)	79(1)	C(2c) -Os(1) -C(2a)	129(1)
C(2c) -Os(1) -C(2b)	138(1)	C(3c) -Os(1) -Os(2)	115(1)
C(3c) -Os(1) -Os(3)	125(1)	C(3c) -Os(1) -Os(5)	76(1)
C(3c) -Os(1) -Os(6)	54(1)	C(3c) -Os(1) -C(2a)	94(1)
C(3c) -Os(1) -C(2b)	169(1)	C(3c) -Os(1) -C(2c)	37(1)
C(3a) -Os(2) -Os(1)	69.4(9)	C(3a) -Os(2) -Os(4)	162(1)
C(3a) -Os(2) -Os(5)	112.2(8)	C(3a) -Os(2) -Os(6)	47.4(8)
C(2b) -Os(2) -Os(1)	46.7(8)	C(2b) -Os(2) -Os(4)	77.1(8)
C(2b) -Os(2) -Os(5)	80.8(7)	C(2b) -Os(2) -Os(6)	97.7(8)
C(2b) -Os(2) -C(3a)	88(1)	C(3b) -Os(2) -Os(1)	78.1(9)
C(3b) -Os(2) -Os(4)	45.9(9)	C(3b) -Os(2) -Os(5)	81.2(8)
C(3b) -Os(2) -Os(6)	131.1(9)	C(3b) -Os(2) -C(3a)	124(1)
C(3b) -Os(2) -C(2b)	38(1)	C(2b) -Os(3) -Os(1)	46.5(8)
C(2b) -Os(3) -Os(4)	81.2(9)	C(2b) -Os(3) -Os(5)	84.1(9)
C(3b) -Os(3) -Os(1)	76.8(9)	C(3b) -Os(3) -Os(4)	47.6(9)
C(3b) -Os(3) -Os(5)	83(1)	C(3b) -Os(3) -C(2b)	39(1)
C(3b) -Os(4) -Os(2)	51(1)	C(3b) -Os(4) -Os(3)	53.2(9)
C(3b) -Os(4) -Os(5)	90(1)	C(2c) -Os(5) -Os(1)	53.3(8)
C(2c) -Os(5) -Os(2)	107.2(8)	C(2c) -Os(5) -Os(3)	88(1)
C(2c) -Os(5) -Os(4)	145(1)	C(2c) -Os(5) -Os(6)	63.2(9)
C(2c) -Os(5) -Os(7)	55(1)	C(2a) -Os(6) -Os(1)	50.5(9)
C(2a) -Os(6) -Os(2)	64.6(9)	C(2a) -Os(6) -Os(5)	97.4(9)
C(2a) -Os(6) -Os(7)	139.5(9)	C(3a) -Os(6) -Os(1)	71.5(9)
C(3a) -Os(6) -Os(2)	43.5(9)	C(3a) -Os(6) -Os(5)	97.1(9)
C(3a) -Os(6) -Os(7)	148.4(9)	C(3a) -Os(6) -C(2a)	37(1)
C(3c) -Os(6) -Os(1)	52(1)	C(3c) -Os(6) -Os(2)	106(1)
C(3c) -Os(6) -Os(5)	61(1)	C(3c) -Os(6) -Os(7)	53(1)
C(3c) -Os(6) -C(2a)	90(1)	C(3c) -Os(6) -C(3a)	122(1)
C(2c) -Os(7) -Os(5)	47.8(9)	C(2c) -Os(7) -Os(6)	73.8(7)
C(3c) -Os(7) -Os(5)	72(1)	C(3c) -Os(7) -Os(6)	50.2(9)
C(3c) -Os(7) -C(2c)	35(1)	Os(6) -C(2a) -Os(1)	75(1)
C(1a) -C(2a) -Os(1)	126(3)	C(1a) -C(2a) -Os(6)	125(3)
C(3a) -C(2a) -Os(1)	108(2)	C(3a) -C(2a) -Os(6)	73(2)
C(3a) -C(2a) -C(1a)	126(3)	Os(6) -C(3a) -Os(2)	89(1)
C(2a) -C(3a) -Os(2)	110(2)	C(2a) -C(3a) -Os(6)	71(2)
C(4a) -C(3a) -Os(2)	123(2)	C(4a) -C(3a) -Os(6)	124(3)
C(4a) -C(3a) -C(2a)	123(3)	Os(2) -C(2b) -Os(1)	77(1)
Os(3) -C(2b) -Os(1)	82(1)	Os(3) -C(2b) -Os(2)	108(1)
C(1b) -C(2b) -Os(1)	115(2)	C(1b) -C(2b) -Os(2)	128(2)
C(1b) -C(2b) -Os(3)	124(2)	C(3b) -C(2b) -Os(1)	125(2)
C(3b) -C(2b) -Os(2)	68(2)	C(3b) -C(2b) -Os(3)	71(2)
C(3b) -C(2b) -C(1b)	119(3)	Os(3) -C(3b) -Os(2)	110(1)
Os(4) -C(3b) -Os(2)	83(1)	Os(4) -C(3b) -Os(3)	79(1)
C(2b) -C(3b) -Os(2)	74(2)	C(2b) -C(3b) -Os(3)	69(2)
C(2b) -C(3b) -Os(4)	131(2)	C(4b) -C(3b) -Os(2)	118(2)
C(4b) -C(3b) -Os(3)	130(3)	C(4b) -C(3b) -Os(4)	117(3)
C(4b) -C(3b) -C(2b)	112(3)	Os(5) -C(2c) -Os(1)	77(1)

Table A15.5 continued

Os(7) -C(2c) -Os(1)	114(1)	Os(7) -C(2c) -Os(5)	77(1)
C(1c) -C(2c) -Os(1)	126(3)	C(1c) -C(2c) -Os(5)	127(2)
C(1c) -C(2c) -Os(7)	117(2)	C(3c) -C(2c) -Os(1)	69(2)
C(3c) -C(2c) -Os(5)	119(3)	C(3c) -C(2c) -Os(7)	72(2)
C(3c) -C(2c) -C(1c)	114(3)	Os(6) -C(3c) -Os(1)	74(1)
Os(7) -C(3c) -Os(1)	117(2)	Os(7) -C(3c) -Os(6)	76(1)
C(2c) -C(3c) -Os(1)	74(2)	C(2c) -C(3c) -Os(6)	117(3)
C(2c) -C(3c) -Os(7)	73(2)	C(4c) -C(3c) -Os(1)	127(3)
C(4c) -C(3c) -Os(6)	115(2)	C(4c) -C(3c) -Os(7)	116(2)
C(4c) -C(3c) -C(2c)	127(3)	O(11) -C(11) -Os(1)	171(4)
O(21) -C(21) -Os(2)	180(2)	O(22) -C(22) -Os(2)	174(4)
O(31) -C(31) -Os(3)	171(4)	O(32) -C(32) -Os(3)	167(5)
O(33) -C(33) -Os(3)	172(4)	O(41) -C(41) -Os(4)	170(4)
O(42) -C(42) -Os(4)	172(4)	O(43) -C(43) -Os(4)	176(4)
O(51) -C(51) -Os(5)	169(3)	O(52) -C(52) -Os(5)	177(4)
O(61) -C(61) -Os(6)	168(4)	O(62) -C(62) -Os(6)	179(3)
O(71) -C(71) -Os(7)	163(3)	O(72) -C(72) -Os(7)	169(5)
O(73) -C(73) -Os(7)	161(5)	C(6s) -O(1s) -C(3s)	68(6)
C(9s) -O(1s) -C(3s)	51(6)	C(9s) -O(1s) -C(6s)	114(7)
C(6s) -C(2s) -C(5s)	76(6)	C(8s) -C(2s) -C(5s)	48(6)
C(8s) -C(2s) -C(6s)	56(8)	C(4s) -C(3s) -O(1s)	117(9)
C(5s) -C(3s) -O(1s)	121(8)	C(5s) -C(3s) -C(4s)	89(7)
C(6s) -C(3s) -O(1s)	59(5)	C(6s) -C(3s) -C(4s)	145(8)
C(6s) -C(3s) -C(5s)	69(6)	C(7s) -C(3s) -O(1s)	148.2(5)
C(7s) -C(3s) -C(4s)	46(8)	C(7s) -C(3s) -C(5s)	48(7)
C(7s) -C(3s) -C(6s)	117(9)	C(9s) -C(3s) -O(1s)	62(7)
C(9s) -C(3s) -C(4s)	57(7)	C(9s) -C(3s) -C(5s)	131(9)
C(9s) -C(3s) -C(6s)	117(9)	C(9s) -C(3s) -C(7s)	101.3(1)
C(7s) -C(4s) -C(3s)	44(7)	C(9s) -C(4s) -C(3s)	47(7)
C(9s) -C(4s) -C(7s)	90(9)	C(3s) -C(5s) -C(2s)	88(6)
C(6s) -C(5s) -C(2s)	47(5)	C(6s) -C(5s) -C(3s)	58(5)
C(7s) -C(5s) -C(2s)	125(9)	C(7s) -C(5s) -C(3s)	45(6)
C(7s) -C(5s) -C(6s)	102(8)	C(8s) -C(5s) -C(2s)	45(7)
C(8s) -C(5s) -C(3s)	98(8)	C(8s) -C(5s) -C(6s)	40(6)
C(8s) -C(5s) -C(7s)	11.4(8)	C(2s) -C(6s) -O(1s)	141(8)
C(3s) -C(6s) -O(1s)	53(5)	C(3s) -C(6s) -C(2s)	90(7)
C(5s) -C(6s) -O(1s)	100(6)	C(5s) -C(6s) -C(2s)	57(5)
C(5s) -C(6s) -C(3s)	53(5)	C(8s) -C(6s) -O(1s)	131(8)
C(8s) -C(6s) -C(2s)	51(7)	C(8s) -C(6s) -C(3s)	91(7)
C(8s) -C(6s) -C(5s)	39(6)	C(4s) -C(7s) -C(3s)	90.6(5)
C(5s) -C(7s) -C(3s)	88(9)	C(5s) -C(7s) -C(4s)	149(2)
C(9s) -C(7s) -C(3s)	41(7)	C(9s) -C(7s) -C(4s)	50(7)
C(9s) -C(7s) -C(5s)	116(8)	C(5s) -C(8s) -C(2s)	87(9)
C(6s) -C(8s) -C(2s)	73(8)	C(6s) -C(8s) -C(5s)	100.9(1)
C(3s) -C(9s) -O(1s)	67(7)	C(4s) -C(9s) -O(1s)	139.3(3)
C(4s) -C(9s) -C(3s)	76(8)	C(7s) -C(9s) -O(1s)	100(8)
C(7s) -C(9s) -C(3s)	37(6)	C(7s) -C(9s) -C(4s)	40(6)

Appendix B

Patterson solution and vector assignment

Appendix B Patterson solutions.

Included in this appendix are the vector assignments made to the Patterson syntheses, only heavy metal atom co-ordinates were obtained for each structure.

B.1 Location of the six ruthenium atoms in $\text{Ru}_6\text{C}(\text{CO})_{15}\text{PhCCH}$ (XR6) by use of Patterson synthesis.

The number of molecules in the unit cell was assumed to be four, since this gave a calculated density of 2.534 gcm^{-3} , a value typical of similar heanuclear species. Systematic absences in the data of the type: $0k0$; $k = 2n + 1$ and $h0l$; $h = 2n + 1$, indicated that the space group was $P2_1/a$. Interchange of the a and c axes converts this into the standard space group $P2_1/c$.

The equivalent positions for the space group $P2_1/c$ are obtainable from International Tables (Vol 1) and are as follows:

$$x, \quad y, \quad z,$$

$$x, \quad y, \quad z,$$

$$x, \quad 1/2-y, \quad 1/2+z,$$

$$x, \quad 1/2+y, \quad 1/2-z.$$

The series of unique vectors between two atoms (i) and (j) are given by:

$$x_i - x_j, \quad y_i - y_j, \quad z_i - z_j$$

$$x_i + x_j, \quad y_i + y_j, \quad z_i + z_j$$

$$x_i - x_j, \quad 1/2 + (y_i + y_j), \quad 1/2 + (z_i - z_j)$$

$$x_i + x_j, \quad 1/2 + (y_i - y_j), \quad 1/2 + (z_i + z_j)$$

The first of these vectors for any pair of metal atoms is usually assigned to the shortest distance (i.e., two atoms within one molecule). Previous structures reported have Ru-Ru bond distances ca. 2.8 \AA . For an octahedral cluster there will be six metal atoms and twelve vectors of

about this length would be expected but this reduces to six as the edges of an octahedron occur in parallel pairs. From the Patterson map six 'short' vectors of this type were found and these are listed below together with their relative height (R.H.).

R.H.	u	v	w	$\overset{\circ}{\text{A}}$
258	0.288	0.000	0.117	2.898
150	0.244	0.039	-0.042	2.885
142	0.046	0.019	0.159	2.950
138	0.038	0.159	-0.046	2.899
130	0.204	0.120	0.005	2.833
123	0.069	0.132	0.104	2.910

Five of these vectors have a similar height, of about 135, as expected, since peak heights in a Patterson synthesis are proportional to the product of the atom number of the two atoms. The sixth vector is approximately double the peak height, at 258, due to the value of 0 in v, which causes vectors of the type uvw and uvw (equivalent in monoclinic Patterson maps) to superimpose.

From these six metal-metal vectors a cluster geometry can be generated, by forming triangles between triplets of these 'short' vectors, and then linking these to build up a metal framework. Note that the following vector pairs (or pairs of atoms) are parallel in the octahedron: -

$$\begin{array}{lll}
 2-6 = 1-5 & 2-3 = 4-5 & 3-1 = 6-4 \\
 2-1 = 6-5 & 2-4 = 3-5 & 3-6 = 1-4
 \end{array}$$

Considering the triangle of metal atoms [Ru(1), Ru(2) and Ru(3)], the positions of the ruthenium atoms Ru(1), Ru(2), and Ru(3) can be obtained as follows (applying appropriate Patterson symmetry as necessary).

$$\begin{array}{r}
 (3-1) \quad 0.244 \quad -0.039 \quad -0.042 \\
 - (2-1) \quad 0.038 \quad -0.159 \quad -0.046 \\
 \hline
 (3-2) \quad 0.206 \quad 0.120 \quad 0.004
 \end{array}$$

The calculated value for the vector (3-2) is very similar to the observed 'short' vector at height 130 and can be used to solve for the positions of Ru(2) and Ru(3) as shown later. Continuing this approach the following short vectors were assigned:

M-M	u	v	w
2-1	0.038	-0.159	-0.046
2-3	-0.204	-0.120	-0.005
2-4	-0.046	-0.019	-0.159
2-6	-0.290	0.000	-0.117
3-1	0.244	-0.041	-0.042
3-6	-0.069	0.132	-0.104

In the next stage, each short vector can be used to solve for the real cell x,y,z, values of the related metal atoms. For example, consider the vector between Ru(2) and Ru(3):

$$\begin{array}{r}
 (x_3-x_2) \quad (y_3-y_2) \quad (z_3-z_2) \quad i) \\
 0.206 \quad 0.120 \quad 0.004
 \end{array}$$

A vector of the following type can be searched for:

$$\begin{array}{r}
 (x_3-x_2) \quad 1/2+(y_3+y_2) \quad 1/2+(z_3-z_2) \quad ii) \\
 0.206 \quad ? \quad 0.504
 \end{array}$$

The suitable peak is found at height 62:-

$$\begin{array}{r}
 0.205 \quad 0.946 \quad 0.504
 \end{array}$$

Therefore, $(y_3+y_2) = 0.446$, this can be use to look for:-

$$\begin{array}{r}
 (x_3+x_2) \quad (y_3+y_2) \quad (z_3+z_2) \quad iii) \\
 ? \quad 0.446 \quad ?
 \end{array}$$

A possible maximum was found at peak height 65:-

-0.432	0.439	0.003
--------	-------	-------

To check the values of (x_3+x_2) and (z_3+z_2) indicated here and using the (y_3-y_2) value, the following vector must be searched for:

(x_3+x_2)	$1/2+(y_3-y_2)$	$1/2+(z_3+z_2)$ iv)
-0.432	0.620	0.503

This was found at height 61:-

-0.431	0.613	0.503
--------	-------	-------

If vectors i) and iii) are used as simultaneous equations the positions of the two metal atoms can be obtained.

Ru(3)+Ru(2)	-0.432	0.439	0.003
Ru(3)-Ru(2)	0.206	0.120	0.004

2Ru(3)	-0.226	0.559	0.007
2Ru(2)	-0.638	0.319	-0.001

These $2x, 2y, 2z$ vectors were found on the map at heights 40 and 43 respectively. It is also important to check for the other vectors between symmetry related atoms.

The two vectors of the type :-

0	$1/2+2y$	$1/2$	should occur at
0	1.059	$1/2$	
0	0.819	$1/2$	

but were both attributed to the peak of height 205, at $0 \ 1.0 \ 1/2$, as the values of $2y$ are not resolved into separate peaks. This is not uncommon with c-glides as the Patterson density along the line $0 \ v \ 1/2$ may be almost continuous, all atoms contributing to it. Finally vectors of the type:

$2x$	$1/2$	$1/2+2z$
------	-------	----------

were searched for and found at peak heights 82 and 68 respectively.

-0.226	$1/2$	0.507
-0.638	$1/2$	0.499

The above method is followed for all six vector pairs, each individual atom position is therefore calculated twice, and it is essential that exactly the same value is obtained both times. This does not usually happen with the first attempt at solution and adjustment of signs on some of the starting triangles may be necessary before a completely consistent set is obtained. The procedure adopted above is used throughout, and ultimately gave the following six metal atom positions:

Ru(1)	-0.348	0.317	0.049
Ru(2)	-0.319	0.162	-0.001
Ru(3)	-0.111	0.276	0.008
Ru(4)	-0.273	0.185	0.159
Ru(5)	-0.066	0.307	0.166
Ru(6)	-0.023	0.148	0.118

B.2 The transformed vectors of the Patterson synthesis used to solve

$\text{HRu}_5\text{C}(\text{CO})_{14}(\text{C}_5\text{H}_4\text{N})$ Isomer A (XR1).

R.H.	u	v	w	Vector assignment		
170	0.000	0.682	0.500	(x1+x4)	(y1+y4)	(z1+z4)
169	0.119	0.000	-0.149	(x2-x4)	(y2-y4)	(z2-z4)
169	0.228	0.500	0.919	(x2+x4)	0.5+(y2-y4)	0.5+(z2+z4)
163	0.000	0.945	0.500	0	0.5+2y1	0.5
				0	0.5+2y3	0.5
157	-0.215	0.000	-0.139	(x1-x3)	(y1-y3)	(z1-z3)
149	0.212	0.500	0.995	(x1+x3)	0.5+(y1-y3)	0.5+(z1+z3)
102	-0.046	-0.138	-0.179	(x2-x3)	(y2-y3)	(z2-z3)
100	-0.218	0.943	0.361	(x1-x3)	0.5+(y1+y3)	0.5+(z1-z3)
99	0.500	0.234	0.500	(x4+x5)	(y4+y5)	(z4+z5)
98	-0.215	0.088	0.080	(x3-x5)	(y3-y5)	(z3-z5)
96	-0.428	0.078	-0.060	(x1-x5)	(y1-y5)	(z1-z5)
95	0.123	0.685	0.348	(x2-x4)	0.5+(y2+y4)	0.5+(z2-z4)
91	0.150	0.820	0.536	(x3-x4)	0.5+(y3+y4)	0.5+(z3-z4)
91	0.387	0.362	0.951	(x2+x3)	0.5+(y2-y3)	0.5+(z2+z3)
91	-0.430	0.859	0.440	(x1-x5)	0.5+(y1+y5)	0.5+(z1-z5)
90	0.165	0.308	0.319	(x1+x2)	(y1+y2)	(z1+z2)
90	0.001	0.500	0.855	2x1	0.5	0.5+2z1
90	0.426	0.360	0.418	(x1+x5)	(y1+y5)	(z1+z5)
89	-0.260	-0.054	-0.103	(x2-x5)	(y2-y5)	(z2-z5)
88	0.423	-0.421	0.916	(x1+x5)	0.5+(y1-y5)	0.5+(z1+z5)
87	0.274	0.318	0.599	(x3+x4)	(y3+y4)	(z3+z4)
87	-0.042	0.818	0.321	(x2-x3)	0.5+(y2+y3)	0.5+(z2-z3)
86	0.602	0.233	0.371	(x2+x5)	(y2+y5)	(z2+z5)

85	0.056	0.642	0.960	(x1+x4)	0.5+(y1-y4)	0.5+(z1+z4)
85	0.216	0.446	0.494	(x1+x3)	(y1+y3)	(z1+z3)
84	0.227	0.176	0.424	(x2+x4)	(y2+y4)	(z2+z4)
84	0.638	0.589	1.057	(x3+x5)	0.5+(y3-y5)	0.5+(z3+z5)
82	0.160	0.138	0.030	(x3-x4)	(y3-y4)	(z3-z4)
82	0.273	0.637	1.101	(x3+x4)	0.5+(y3-y4)	0.5+(z3+z4)
81	0.671	0.368	0.556	(x3+x5)	(y3+y5)	(z3+z5)
81	-0.175	0.128	0.046	(x1-x2)	(y1-y2)	(z1-z2)
81	0.602	0.449	0.874	(x2+x5)	0.5+(y2-y5)	0.5+(z2+z5)
80	-0.217	0.863	0.579	(x3-x5)	0.5+(y3+y5)	0.5+(z3-z5)
78	0.344	0.500	0.771	2x2	0.5	0.5+2z2
77	-0.056	0.126	-0.108	(x1-x4)	(y1-y4)	(z1-z4)
76	-0.062	0.810	0.398	(x1-x4)	0.5+(y1+y4)	0.5+(z1-z4)
76	0.000	0.218	0.500	0	0.5+2y5	0.5
76	0.000	0.782	0.500	0	0.5+2y2	0.5
				0	0.5+2y4	0.5
75	0.431	0.500	1.131	2x3	0.5	0.5+2z3
75	-0.175	0.807	0.544	(x1-x2)	0.5+(y1+y2)	0.5+(z1-z2)
75	0.174	0.628	0.813	(x1+x2)	0.5+(y1-y2)	0.5+(z1+z2)
73	-0.375	0.733	0.544	(x4-x5)	0.5+(y4+y5)	0.5+(z4-z5)
72	-0.259	0.727	0.401	(x2-x5)	0.5+(y2+y5)	0.5+(z2-z5)
72	0.386	0.327	0.450	(x2+x3)	(y2+y3)	(z3+z2)
71	0.487	0.451	1.015	(x4+x5)	0.5+(y4-y5)	0.5+(z4+z5)
69	0.500	0.450	0.000			
64	-0.375	-0.050	0.045	(x4-x5)	(y4-y5)	(z4-z5)
56	0.436	0.456	0.628	2x3	2y3	2z3
56	0.337	0.178	0.276	2x2	2y2	2z2
47	0.002	0.432	0.356	2x1	2y1	2z1
38	0.856	0.284	0.476	2x5	2y5	2z5

This gave the following fractional coordinates for the five ruthenium atoms:

Ru(1)	0.001	0.217	0.178
Ru(2)	0.172	0.090	0.136
Ru(3)	0.215	0.228	0.315
Ru(4)	0.058	0.093	0.284
Ru(5)	0.428	0.142	0.237

B.3 Patterson solution for $\text{HRu}_5\text{C}(\text{CO})_{13}(\text{C}_5\text{H}_4\text{N})(\text{C}_5\text{H}_5\text{N})$ (XR3)

R.H.	u	v	w	Vector assignment		
187	0.500	0.000	0.500	0.5	0.5+2y2	0.5
183	0.462	0.000	0.262	0.5+(x2-x4)	0.5+(y2+y4)	0.5+(z2-z4)
				0.5+(x5-x3)	0.5+(y5+y3)	0.5+(z5-z3)
167	0.307	0.500	-0.059	0.5+(x3+x2)	0.5+(y3-y2)	0.5+(z3+z2)
				0.5+2x1	0.5	0.5+2z1
				0.5+(x5+x4)	0.5+(y5-y4)	0.5+(z5+z4)
162	0.471	0.500	-0.128	0.5+2x4	0.5	0.5+2z4
				0.5+(x2+x4)	0.5+(y2-y4)	0.5+(z2+z4)
150	0.181	0.441	-0.460	(x3+x2)	(y3+y2)	(z3+z2)
				(x4+x5)	(y4+y5)	(z4+z5)
148	0.500	0.076	0.500	0.5	0.5+2y3	0.5
				0.5	0.5+2y4	0.5
				0.5	0.5+2y5	0.5
145	0.102	0.000	-0.314	(x3-x2)	(y3-y2)	(z3-z2)
144	0.358	0.037	-0.423	0.5+(x5-x2)	0.5+(y5+y2)	0.5+(z5-z2)
				0.5+(x3-x4)	0.5+(y3+y4)	0.5+(z3-z4)

133	0.324	0.500	0.464	(x3+x5)	(y3+y5)	(z3+z5)
130	0.018	0.500	-0.369	2x4	2y4	2z4
				(x2+x4)	(y2+y4)	(z2+z4)
114	0.051	0.000	0.263	(x2-x4)	(y2-y4)	(z2-z4)
106	0.107	0.216	0.079	(x5-x1)	(y5-y1)	(z5-z1)
102	0.182	0.062	0.166	(x5-x4)	(y5-y4)	(z5-z4)
98	0.136	0.074	-0.089	(x5-x2)	(y5-y2)	(z5-z2)
97	0.254	0.284	-0.106	0.5+(x5+x1)	0.5+(y5-y1)	0.5+(z5+z1)
94	0.024	0.134	-0.176	(x1-x2)	(y1-y2)	(z1-z2)
91	0.153	0.039	-0.061	(x3-x4)	(y3-y4)	(z3-z4)
91	0.065	0.340	0.444	(x1+x4)	(y1+y4)	(z1+z4)
90	0.222	0.469	-0.218	(x2+x5)	(y2+y5)	(z2+z5)
90	0.398	0.064	-0.185	0.5+(x3-x2)	0.5+(y3+y2)	0.5+(z3-z2)
89	0.318	0.053	0.336	0.5+(x5-x4)	0.5+(y5+y4)	0.5+(z5-z4)
89	0.141	0.457	0.300	(x3+x4)	(y3+y4)	(z3+z4)
89	0.359	0.463	0.199	0.5+(x3+x4)	0.5+(y3-y4)	0.5+(z3+z4)
89	0.283	0.382	0.113	0.5+(x1+x3)	0.5+(x1-x3)	0.5+(z1+z3)
88	0.115	0.316	-0.297	(x1+x2)	(y1+y2)	(z1+z2)
87	0.279	0.418	-0.283	0.5+(x5+x2)	0.5+(y5-y2)	0.5+(z5+z2)
86	0.177	0.402	0.036	0.5+(x5+x3)	0.5+(y5-y3)	0.5+(z5+z3)
85	0.076	0.155	0.085	(x1-x4)	(y1-y4)	(z1-z4)
85	0.216	0.303	0.386	(x1+x3)	(y1+y3)	(z1+z3)
85	0.146	0.500	-0.189	0.5+2x5	0.5	0.5+2z5
84	0.500	0.312	0.500	0.5	0.5+2y1	0.5
83	0.244	0.401	-0.392	(x1+x5)	(y1+y5)	(z1+z5)
83	0.028	0.099	0.222	(x5-x3)	(y5-y3)	(z5-z3)
83	0.424	0.196	-0.354	0.5+(x1-x3)	0.5+(y1+y3)	0.5+(z1-z3)
83	0.426	0.161	0.415	0.5+(x1-x4)	0.5+(y1+y4)	0.5+(z1-z4)
82	0.204	0.500	0.256	0.5+2x3	0.5	0.5+2z3
80	0.434	0.347	0.056	0.5+(x1+x4)	0.5+(y1-y4)	0.5+(z1+z4)
80	0.385	0.365	-0.202	0.5+(x1+x2)	0.5+(y1-y2)	0.5+(z1+z2)
78	0.471	0.183	-0.330	0.5+(x1-x2)	0.5+(y1+y2)	0.5+(z1-z2)
78	0.077	0.118	-0.145	(x1-x3)	(y1-y3)	(z1-z3)
76	0.392	0.101	0.419	0.5+(x5-x1)	0.5+(y5+y1)	0.5+(z5-z1)
75	0.410	0.500	-0.373	0.5+2x2	0.5	0.5+2z2
57	0.136	0.186	-0.473	2x1	2y1	2z1
53	0.354	0.387	-0.317	2x5	2y5	2z5
52	0.083	0.456	-0.120	2x2	2y2	2z2
42	0.293	0.420	0.246	2x3	2y3	2z3

This gave the following fractional coordinates for the five ruthenium atoms:

Ru(1)	0.069	0.094	0.265
Ru(2)	0.045	0.225	0.436
Ru(3)	0.147	0.210	0.122
Ru(4)	-0.004	0.246	0.180
Ru(5)	0.176	0.307	0.345

B.4 Patterson solution for $\text{Ru}_6\text{C}(\text{CO})_{15}(\text{C}_6\text{H}_8)$ (XR5).

The structure was originally solved by H. Curtis in the space group $P2_1$. However the two apparently independent molecules in the asymmetric unit were found to be related by a c-glide, at an arbitrary y value. The atomic coordinates were adjusted so that the two molecules were related by a c-glide at $y=1/4$ and one set of atoms was eliminated from the list leaving:

Ru(1)	0.760	0.587	0.839
Ru(2)	0.822	0.636	0.719
Ru(3)	0.645	0.622	0.688
Ru(4)	0.840	0.355	0.793
Ru(5)	0.660	0.359	0.745
Ru(6)	0.731	0.398	0.628

Part of the original problem had arisen because the c-glide systematic absences were violated by a number of reflections. Furthermore the Patterson synthesis contained a number of high peaks with near zero v coordinates making solution difficult. One of the major problems with solution was that the vectors of the type $0\ 1/2+2y\ 1/2$ were not resolved. Use of the new coordinates, after adjustment from the $P2_1$ solution allowed the following assignments to be made.

R.H.	u	v	w	Vector assignment		
402	0.483	0.000	0.461	(x1+x6)	(y1+y6)	(z1+z6)
				(x2+x5)	(y2+y5)	(z2+z5)
				(x3+x4)	(y3+y4)	(z3+z4)
308	0.180	0.000	0.049	(x2-x3)	(y2-y3)	(z2-z3)
				(x4-x5)	(y4-y5)	(z4-z5)
297	0.000	0.233	0.500	0	0.5+2y1	0.5
				0	0.5+2y2	0.5
				0	0.5+2y3	0.5
				0	0.5+2y4	0.5
				0	0.5+2y5	0.5
				0	0.5+2y6	0.5
271'	-0.019	0.500	0.422	(x2-x4)	0.5+(y2+y4)	0.5+(z2-z4)
				(x3-x5)	0.5+(y3+y5)	0.5+(z3-z5)
169	0.339	0.000	0.489	(x2+x4)	(y2+y4)	(z2+z4)
154	-0.180	0.227	0.450	(x2-x3)	0.5+(y2+y3)	0.5+(z2-z3)
				(x4-x5)	0.5+(y4+y5)	0.5+(z4-z5)
154	0.115	0.000	0.172	(x1-x3)	(y1-y3)	(z1-z3)
				(x4-x6)	(y4-y6)	(z4-z6)
149	0.162	0.500	0.472	(x2-x5)	0.5+(y2+y5)	0.5+(z2-z5)
142	-0.066	0.037	0.122	(x1-x2)	(y1-y2)	(z1-z2)
				(x5-x6)	(y5-y6)	(z5-z6)

142	-0.096	0.485	0.406	(x1-x5)	0.5+(y1+y5)	0.5+(z1-z5)
				(x2-x6)	0.5+(y2+y6)	0.5+(z2-z6)
140	-0.482	0.232	0.039	(x2+x5)	0.5+(y2-y5)	0.5+(z2+z5)
				(x3+x4)	0.5+(y3-y4)	0.5+(z3+z4)
140	0.086	0.500	0.456	(x1-x4)	0.5+(y1+y4)	0.5+(z1-z4)
				(x3-x6)	0.5+(y3+y6)	0.5+(z3-z6)
139	0.019	0.273	0.077	(x2-x4)	(y2-y4)	(z2-z4)
				(x3-x5)	(y3-y5)	(z3-z5)
137	0.096	0.233	0.095	(x1-x)	(y1-y5)	(z1-z5)
				(x2-6)	(y2-y6)	(z2-z6)
135	-0.084	0.231	0.045	(x1x4)	(y1-y4)	(z1-z4)
				(xx-x6)	(y3-y6)	(z3-z6)
134	-0.197	0.500	0.373	(x3-x4)	0.5+(y3+y4)	0.5+(z3-z4)
132	-0.499	0.500	0.038	(x4+x5)	0.5+(y4-y5)	0.5+(z4+z5)
131	0.065	0.269	0.378	(x1-x2)	0.5+(y1+y2)	0.5+(z1-z2)
				(x5-x6)	0.5+(y5+y6)	0.5+(z5-z6)
127	-0.463	0.500	0.116	(x2+x3)	0.5+(y2-y3)	0.5+(z2+z3)
125	0.378	0.000	0.299	(x3+x6)	(y3+y6)	(z3+z6)
123	0.302	0.000	0.414	(x3+x5)	(y3+y5)	(z3+z5)
121	-0.029	0.500	0.293	(x1-x6)	0.5+(y1+y6)	0.5+(z1-z6)
121	-0.114	0.273	0.328	(x1-x3)	0.5+(y1+y3)	0.5+(z1-z3)
				(x4-x6)	0.5+(y4+y6)	0.5+(z4-z6)
108	-0.444	0.000	0.350	(x2+x6)	(y2+y6)	(z2+z6)
88	-0.339	0.216	0.012	(x2+x4)	0.5+(y2-y4)	(z2+z4)
87	-0.317	0.500	0.087	2x4	0.5	0.5+2z4
85	-0.161	0.276	0.028	(x2-x5)	(y2-y5)	(z2-z5)
82	0.199	0.263	0.127	(x3-x4)	(y3-y4)	(z3-z4)
77	-0.301	0.232	0.085	(x3+x5)	0.5+(y3-y5)	0.5+(z3+z5)
77	-0.393	0.500	0.121	(x5+x6)	0.5+(y5-y6)	0.5+(z5-z6)
74	0.026	0.185	0.208	(x1-x6)	(y1-y6)	(z1-z6)
73	-0.401	0.265	0.132	(x1+x4)	0.5+(y1-y4)	(z1+z4)
71	0.498	0.289	0.460	(x4+x5)	(y4+y5)	(z4+z5)
69	0.401	0.500	0.003	(x1+x3)	0.5+(y1-y3)	(z1+z3)
69	-0.317	0.500	0.009	2x5	0.5	0.5+2z5
69	0.444	0.262	0.151	(x2+x6)	0.5+(y2-y6)	(z2+z6)
68	-0.427	0.248	0.423	(x4+x6)	(y4+y6)	(z4+z6)
67	-0.460	0.500	0.248	2x6	0.5	0.5+2z6
66	0.427	0.468	0.077	(x1+x2)	0.5+(y1-y2)	(z1+z2)
				(x4+x6)	0.5+(y4-y6)	(z4+z6)
66	0.353	0.500	0.065	2x2	0.5	0.5+2z2
65	0.418	0.272	0.084	(x1+x5)	0.5+(y1-y5)	(z1+z5)
65	-0.378	0.272	0.203	(x3+x6)	0.5+(y3-y6)	0.5+(z3+z6)
65	-0.418	0.054	0.415	(x1+x5)	(y1+y5)	(z1+z5)
64	-0.478	0.500	0.178	2x1	0.5	0.5+2z1
64	0.400	0.064	0.367	(x1+x4)	(y1+y4)	(z1+z4)
63	-0.292	0.500	0.158	2x3	0.5	0.5+2z3
61	0.467	0.258	0.386	(x2+x3)	(y2+y3)	(z2+z3)
60	0.417	0.223	0.443	(x1+x2)	(y1+y2)	(z1+z2)
60	0.390	0.243	0.367	(x5+x6)	(y5+y6)	(z5+z6)
57	-0.417	0.450	0.058			
55	0.401	0.210	-0.495	(x1+x3)	(y1+y3)	(z1+z3)
55	-0.401	0.210	0.495			
42	-0.358	0.265	0.433	2x2	2y2	2z2
42	0.319	0.286	0.494	2x5	2y5	2z5
41	0.316	0.289	0.411	2x4	2y4	2z4
38	0.461	0.198	0.253	2x6	2y6	2z6
33	-0.120	0.500	0.160			
33	0.289	0.246	0.336	2x3	2y3	2z3
32	0.476	0.173	0.324	2x1	2y1	2z1

B.5 Patterson solution for $\text{Ru}_6\text{C}(\text{CO})_{15}(\text{PhCCMe})$ (XR7)

Solution yielded the following fractional co-ordinates for the six ruthenium atoms defining the cluster octahedron:

Ru(1)	-0.3403	-0.1693	0.0634
Ru(2)	-0.1822	-0.0722	0.0775
Ru(3)	-0.2315	-0.1203	0.3307
Ru(4)	-0.2528	-0.3575	-0.1167
Ru(5)	-0.2998	-0.3983	0.1566
Ru(6)	-0.1405	-0.3011	0.1542

R.H.	u	v	w	Vector assignment		
451	0.483	0.473	-0.220	(x1+x6)	(y1+y6)	(z1+z6)
				(x2+x5)	(y2+y5)	(z2+z5)
				(x3+x4)	(y3+y4)	(z3+z4)
306	0.159	0.095	0.007	(x1-x2)	(y1-y2)	(z1-z2)
				(x5-x6)	(y5-y6)	(z5-z6)
306	0.159	0.095	0.007			
301	-0.090	0.185	0.177	(x1-x4)	(y1-y4)	(z1-z4)
				(x3-x6)	(y3-y6)	(z3-z6)
297	0.113	0.056	0.272	(x1-x3)	(y1-y3)	(z1-z3)
				(x4-x6)	(y4-y6)	(z4-z6)
295	0.069	0.281	0.185	(x2-x4)	(y2-y4)	(z2-z4)
				(x3-x5)	(y3-y5)	(z3-z5)
295	0.049	0.046	-0.264	(x2-x3)	(y2-y3)	(z2-z3)
				(x4-x5)	(y4-y5)	(z4-z5)
285	-0.040	0.231	-0.081	(x1-x5)	(y1-y5)	(z1-z5)
				(x2-x6)	(y2-y6)	(z2-z6)
161	0.020	0.235	0.447	(x3-x4)	(y3-y4)	(z3-z4)
161	0.118	0.325	-0.081	(x2-x5)	(y2-y5)	(z2-z5)
156	0.372	0.423	-0.487	(x3+x6)	(y3+y6)	(z3+z6)
155	0.359	0.434	0.224	(x1+x5)	(y1+y5)	(z1+z5)
155	-0.201	0.129	-0.097	(x1-x6)	(y1-y6)	(z1-z6)
152	0.414	0.195	-0.408	(x2+x3)	(y2+y3)	(z2+z3)
150	-0.429	0.288	-0.398	(x1+x3)	(y1+y3)	(z1+z3)
149	-0.479	0.242	-0.142	(x1+x2)	(y1+y2)	(z1+z2)
145	0.448	0.244	0.039	(x4+x5)	(y4+y5)	(z4+z5)
142	0.321	0.370	-0.231	(x2+x6)	(y2+y6)	(z2+z6)
141	0.468	0.479	0.486	(x3+x5)	(y3+y5)	(z3+z5)
140	-0.393	0.342	0.040	(x4+x6)	(y4+y6)	(z4+z6)
137	0.433	0.428	0.034	(x2+x4)	(y2+y4)	(z2+z4)
135	-0.439	0.303	0.311	(x5+x6)	(y5+y6)	(z5+z6)
135	0.404	0.468	-0.059	(x1+x4)	(y1+y4)	(z1+z4)
135	0.408	0.476	-0.050			
93	0.461	0.243	0.334	2x3	2y3	2z3
84	-0.281	0.402	0.316	2x6	2y6	2z6
82	0.402	0.207	0.310	2x5	2y5	2z5
82	-0.317	0.341	-0.127	2x1	2y1	2z1
77	0.361	0.142	-0.159	2x2	2y2	2z2
60	0.491	0.281	-0.231	2x4	2y4	2z4

B.6 Patterson solution for $\text{Ru}_6\text{C}(\text{CO})_{14}(\text{PhCCH})(\text{AuPet}_3)_2$ (XR8)

Solution yielded the fractional coordinates of the six ruthenium atoms and the two gold atoms of the fundamental polyhedron:

Au(1)	0.259	0.001	0.037
Au(2)	0.167	0.131	0.107
Ru(1)	0.218	-0.006	0.296
Ru(2)	0.316	0.050	0.184
Ru(3)	0.364	-0.108	0.272
Ru(4)	0.148	-0.054	0.147
Ru(5)	0.202	-0.208	0.239
Ru(6)	0.310	-0.153	0.129

R.H.	u	v	w	Vector assignment		
334	0.000	0.500	0.500	0	0.5+2y1	0.5
				0	0.5+2y3	0.5
201	0.472	0.000	0.334	(x1+x3)	(y1+y3)	(z1+z3)
				(x4+x6)	(y4+y6)	(z4+z6)
154	-0.040	0.000	0.259	(x1-x3)	(y1-y3)	(z1-z3)
153	0.000	0.214	0.500	0	0.5+2y2	0.5
				0	0.5+2y5	0.5
				0	0.5+2y8	0.5
153	0.000	0.214	0.500			
152	-0.151	0.500	0.474	(x2-x8)	0.5+(y2+y8)	(z2-z8)
				(x4-x6)	0.5+(y4+y6)	0.5+(z4-z6)
149	0.469	0.202	0.280	(x1+x7)	(y1+y7)	(z1+z7)
				(x2+x4)	(y2+y4)	(z2+z4)
				(x6+x8)	(y6+y8)	(z6+z8)
				(x2+x8)	0.5+(y2-y8)	0.5+(z2+z8)
147	0.041	0.500	0.241	(x1-x3)	0.5+(y1+y3)	0.5+(z1-z3)
140	-0.055	0.441	0.357	(x1-x4)	0.5+(y1+y4)	0.5+(z1-z4)
				(x2-x7)	0.5+(y2+y7)	0.5+(z2-z7)
				(x3-x6)	0.5+(y3+y6)	0.5+(z3-z6)
131	-0.482	0.000	0.075	2x1	2y1	2z1
130	0.099	0.354	0.433	(x1-x2)	0.5+(y1+y2)	0.5+(z1-z2)
129	-0.476	0.500	0.167	(x1+x3)	0.5+(y1-y3)	0.5+(z1+z3)
127	0.061	0.046	0.147	(x1-x4)	(y1-y4)	(z1-z4)
				(x3-x6)	(y3-y6)	(z3-z6)
				(x5-x8)	(y5-y8)	(z5-z8)
126	-0.107	0.055	0.111	(x1-x6)	(y1-y6)	(z1-z6)
				(x3-x4)	(y3-y4)	(z3-z4)
				(x7-x8)	(y7-y8)	(z7-z8)
124	0.481	0.500	0.425			
121	0.052	0.154	0.092	(x1-x8)	(y1-y8)	(z1-z8)
				(x6-x7)	(y6-y7)	(z6-z7)
121	-0.428	0.360	0.357	(x4-x5)	(y4-y5)	(z4-z5)
				(x1+x2)	0.5+(y1-y2)	0.5+(z1+z2)
				(x1+x2)	(y1+y2)	(z1+z2)
120	0.426	0.142	0.144			
119	-0.333	0.500	0.285			
116	0.479	0.000	0.236	(x2+x8)	(y2+y8)	(z2+z8)
113	-0.481	0.161	0.423	(x3+x8)	(y3+y8)	(z3+z8)
				(x4+x7)	(y4+y7)	(z4+z7)
				(x5+x6)	(y5+y6)	(z5+z6)
107	-0.092	0.142	0.071	(x1-x2)	(y1-y2)	(z1-z2)
99	-0.007	0.200	0.047	(x2-x6)	(y2-y6)	(z2-z6)

				(x_3-x_7)	(y_3-y_7)	(z_3-z_7)
				(x_4-x_8)	(y_4-y_8)	(z_4-z_8)
97	-0.374	0.105	0.312	(x_1+x_5)	(y_1+y_5)	(z_1+z_5)
				(x_4+x_8)	(y_4+y_8)	(z_4+z_8)
91	0.106	0.450	0.389	(x_1-x_6)	$0.5+(y_1+y_6)$	$0.5+(z_1-z_6)$
				(x_3-x_4)	$0.5+(y_3+y_4)$	$0.5+(z_3-z_4)$
78	-0.375	0.351	0.101	(x_2+x_3)	$0.5+(y_2-y_3)$	$0.5+(z_2+z_3)$
				(x_6+x_7)	$0.5+(y_6-y_7)$	$0.5+(z_6+z_7)$
				(x_6+x_7)	$0.5+(y_6-y_7)$	$0.5+(z_6+z_7)$
76	-0.474	0.407	0.211	(x_2+x_4)	$0.5+(y_2-y_4)$	$0.5+(z_2+z_4)$
				(x_6+x_8)	$0.5+(y_6-y_8)$	$0.5+(z_6+z_8)$
75	-0.376	0.150	0.157			
74	-0.463	0.007	0.383	(x_2+x_5)	(y_2+y_5)	(z_2+z_5)
74	0.407	0.052	0.183	(x_1+x_6)	(y_1+y_6)	(z_1+z_6)
73	-0.418	0.151	0.163			
73	0.424	0.454	0.279	(x_1+x_8)	(y_1+y_8)	(z_1+z_8)
				(x_1+x_4)	$0.5+(y_1-y_4)$	$0.5+(z_1+z_4)$
73	-0.316	0.304	0.244	(x_2+x_6)	$0.56+(y_2-y_6)$	$0.5+(z_2+z_6)$
70	0.166	0.103	0.042	(x_4-x_6)	(y_4-y_6)	(z_4-z_6)
69	0.014	0.410	0.464	(x_2-x_6)	$0.5+(y_2+y_6)$	$0.5+(z_2-z_6)$
69	-0.198	0.480	0.335	(x_2-x_5)	$0.5+(y_2+y_5)$	$0.5+(z_2-z_5)$
68	-0.150	0.309	0.422	(x_2-x_4)	$0.5+(y_2+y_4)$	$0.5+(z_2-z_4)$
68	-0.406	0.444	0.318	(x_1+x_6)	$0.5+(y_1-y_6)$	$0.5+(z_1+z_6)$
68	0.109	0.107	0.235	(x_1-x_5)	(y_1-y_5)	(z_1-z_5)
66	0.000	0.402	0.500	0	$0.5+2y_4$	0.5
				0	$0.5+2y_6$	0.5
66	-0.107	0.396	0.264	(x_1-x_5)	$0.5+(y_1+y_5)$	$0.5+(z_1-z_5)$
66	0.313	0.088	0.258	(x_2+x_6)	(y_2+y_6)	(z_2+z_6)
65	0.196	0.251	0.164	(x_2-x_5)	(y_2-y_5)	(z_2-z_5)
65	0.060	0.293	0.300	(x_1-x_7)	$0.5+(y_1+y_7)$	$0.5+(z_1-z_7)$
65	-0.423	0.049	0.220	(x_1+x_4)	(y_1+y_4)	(z_1+z_4)
64	0.383	0.136	0.403	(x_2+x_3)	(y_2+y_3)	(z_2+z_3)
64	0.432	0.348	0.334	(x_1+x_8)	$0.5+(y_1-y_8)$	$0.5+(z_1+z_8)$
63	0.373	0.392	0.190	(x_1+x_5)	$0.5+(y_1-y_5)$	$0.5+(z_1+z_5)$
61	-0.048	0.369	0.309	(x_1-x_7)	(y_1-y_7)	(z_1-z_7)
61	-0.056	0.211	0.202	(x_2-x_3)	$0.5+(y_2+y_3)$	$0.5+(z_2-z_3)$
60	-0.159	0.100	0.020	(x_3-x_5)	(y_3-y_5)	(z_3-z_5)
				(x_6-x_8)	(y_6-y_8)	(z_6-z_8)
59	0.150	0.092	0.072	(x_2-x_4)	(y_2-y_4)	(z_2-z_4)
				(x_5-x_7)	(y_5-y_7)	(z_5-z_7)
59	-0.459	0.289	0.223	(x_1+x_7)	$0.5+(y_1-y_7)$	$0.5+(z_1+z_7)$
57	0.369	0.068	0.348	(x_2+x_7)	(y_2+y_7)	(z_2+z_7)
57	0.049	0.150	0.189	(x_2-x_3)	(y_2-y_3)	(z_2-z_3)
56	0.143	0.295	0.022	(x_2-x_8)	(y_2-y_8)	(z_2-z_8)
56	0.038	0.350	0.133	(x_2-x_7)	(y_2-y_7)	(z_2-z_7)
55	0.470	0.249	0.115	(x_2+x_5)	$0.5+(y_2-y_5)$	$0.5+(z_2+z_5)$
				(x_4+x_7)	$0.5+(y_4-y_7)$	$0.5+(z_4-z_7)$
53	0.333	0.283	0.213	$2x_2$	$2y_2$	$2z_2$
52	-0.053	0.350	0.406	(x_1-x_8)	$0.5+(y_1+y_8)$	$0.5+(z_1-z_8)$
51	0.349	0.288	0.205			
49	-0.366	0.452	0.058	(x_3+x_6)	$0.5+(y_3-y_6)$	$0.5+(z_3-z_6)$
46	0.347	0.269	0.387	(x_6+x_7)	(y_6+y_7)	(z_6+z_7)
45	-0.319	0.064	0.459	(x_4+x_5)	(y_4+y_5)	(z_4+z_5)
44	0.366	0.061	0.443	(x_3+x_6)	(y_3+y_6)	(z_3+z_6)
44	0.219	0.052	0.123	(x_5-x_6)	(y_5-y_6)	(z_5-z_6)
42	-0.272	0.500	0.045			
42	-0.404	0.500	0.022			
42	0.000	0.078	0.500	0	$0.5+2y_7$	0.5
42	0.000	0.078	0.500			

42	0.317	0.336	0.042	(x4+x5)	0.5+(y4-y5)	0.5+(z4+z5)
39	0.322	0.459	0.101			
38	-0.214	0.332	0.378	(x5-x6)	0.5+(y5+y6)	0.5+(z5-z6)
37	0.370	0.500	0.131			
36	-0.329	0.258	0.401	(x5+x8)	(y5+y8)	(z5+z8)
35	-0.424	0.216	0.462	(x3+x7)	(y3+y7)	(z3+z7)
35	0.107	0.140	0.387	(x7-x8)	0.5+(y7+y8)	0.5+(z7-z8)
35	0.378	0.500	0.246			
34	-0.416	0.396	0.065	(x3+x5)	0.5+(y3-y5)	0.5+(z3+z5)
33	-0.114	0.261	0.056	(x4-x7)	(y4-y7)	(z4-z7)
32	0.433	0.500	0.094	(x5+x7)	(y5+y7)	(z5+z7)
32	-0.467	0.042	0.480			
32	0.435	0.319	0.485			
31	-0.295	0.500	0.207			
31	-0.164	0.181	0.466	(x5-x7)	0.5+(y5+y7)	0.5+(z5-z7)
31	0.468	0.438	0.015	(x3+x4)	0.5+(y3-y4)	0.5+(z3+z4)
30	0.474	0.352	0.075	(x3+x8)	0.5+(y3-y8)	0.5+(z3+z8)
29	-0.434	0.403	0.015	(x5+x7)	0.5+(y5-y7)	0.5+(z5+z7)
28	0.151	0.390	0.475	(x3-x5)	0.5+(y3+y5)	0.5+(z3-z5)
28	-0.319	0.500	0.095	(x5+x8)	0.5+(y5-y8)	0.5+(z5+z8)
27	0.420	0.297	0.036	(x3+x7)	0.5+(y3-y7)	0.5+(z3+z7)
27	0.040	0.000	0.261			
27	-0.093	0.147	0.167	(x3-x8)	(y3-y8)	(z3-z8)
27	-0.056	0.237	0.354	(x5-x8)	0.5+(y5+y8)	0.5+(z5-z8)

B.7 Patterson solution for $\text{Ru}_6\text{C}(\text{CO})_{14}(\text{C}_6\text{H}_3\text{Me})$ (XR9).

Solution yielded the following fractional atomic coordinates for the four unique ruthenium atoms of the octahedron:

Ru(1)	-0.263	0.340	-0.202
Ru(2)	-0.474	0.250	-0.432
Ru(4)	-0.281	0.340	-0.522
Ru(6)	-0.070	0.250	-0.300

R.H.	u	v	w	Vector assignment		
457	0.459	0.500	0.275	(x2+x6)	(y2+y6)	(z2+z6)
				(x1+x4)	0.5+(y1-y4)	(z1+z4)
				(x2+x6)	0.5+(y2-y6)	(z2+z6)
309	-0.191	0.091	0.094	(x1-x6)	(y1-y6)	(z1-z6)
				(x2-x4)	(y2-y4)	(z2-z4)
				(x1-x6)	0.5+(y1+y6)	(z1-z6)
				(x2-x4)	0.5+(y2+y4)	(z2-z4)
302	0.211	0.091	0.227	(x1-x2)	(y1-y2)	(z1-z2)
				(x4-x6)	(y4-y6)	(z4-z6)
				(x1-x2)	0.5+(y1+y2)	(z1-z2)
				(x4-x6)	0.5+(y4+y6)	(z4-z6)
293	0.000	0.180	0.000	0	0.5+2y1	0
				0	0.5+2y4	0
286	0.020	0.000	0.320	(x1-x4)	(y1-y4)	(z1-z4)
171	-0.351	0.410	0.183	(x4+x6)	(y4+y6)	(z4+z6)
				(x4+x6)	0.5+(y4-y6)	(z4+z6)
169	0.021	0.181	0.320	(x1-x4)	0.5+(y1+y4)	(z1-z4)
166	0.405	0.000	0.135	(x2-x6)	(y2-y6)	(z2-z6)

150	-0.331	0.410	-0.498	(x2-x6)	0.5+(y2+y6)	(z2-z6)
				(x1+x6)	(y1+y6)	(z1+z6)
148	0.241	0.410	0.046	(x1+x6)	0.5+(y1-y6)	(z1+z6)
				(x2+x4)	(y2+y4)	(z2+z4)
144	0.458	0.320	0.277	(x2+x4)	0.5+(y2-y4)	(z2+z4)
141	-0.438	0.500	0.042	(x1+x4)	(y1+y4)	(z1+z4)
135	-0.477	0.500	0.402	2x4	0.5	2z4
133	0.262	0.410	0.364	2x1	0.5	2z1
				(x1+x2)	(y1+y2)	(z1+z2)
91	-0.438	0.318	0.043	(x1+x2)	0.5+(y1-y2)	(z1+z2)
79	-0.140	0.500	0.408	2x4	2y4	2z4
				2x6	2y6	2z6
70	0.054	0.500	0.132	2x6	0.5	2z6
				2x2	2y2	2z2
67	-0.478	0.320	0.403	2x2	0.5	2z2
				2x1	2y1	2z1

B.8 Patterson solution for $\text{Ru}_6(\text{CO})_{15}(\text{C}_6\text{H}_3\text{Me}_3)$ (XR10).

This gave the following fractional coordinates for the six ruthenium atoms:

Ru(1)	-0.411	0.152	-0.108
Ru(2)	-0.034	0.186	-0.231
Ru(3)	-0.221	0.200	-0.142
Ru(4)	-0.366	0.246	-0.338
Ru(5)	-0.190	0.265	-0.393
Ru(6)	-0.258	0.433	-0.170

R.H.	u	v	w	Vector assignment		
315	0.183	0.019	-0.058	(x1-x3)	(y1-y3)	(z1-z3)
				(x2-x3)	(y2-y3)	(z2-z3)
				(x4-x5)	(y4-y5)	(z4-z5)
263	0.037	0.080	-0.242	(x1-x4)	(y1-y4)	(z1-z4)
				(x3-x5)	(y3-y5)	(z3-z5)
262	-0.151	0.063	-0.182	(x2-x5)	(y2-y5)	(z2-z5)
				(x3-x4)	(y3-y4)	(z3-z4)
236	0.408	0.433	-0.487	(x1+x5)	(y1+y5)	(z1+z5)
				(x3+x4)	(y3+y4)	(z3+z4)
228	-0.404	0.445	0.444	(x2+x4)	(y2+y4)	(z2+z4)
				(x3+x5)	(y3+y5)	(z3+z5)
162	0.446	-0.493	0.266	(x4+x5)	(y4+y5)	(z4+z5)
152	-0.333	0.062	-0.107	(x2-x4)	(y2-y4)	(z2-z4)
146	-0.254	0.385	-0.372	(x2+x3)	(y2+y3)	(z2+z3)
146	-0.224	0.449	0.372	(x2+x5)	(y2+y5)	(z2+z5)
146	-0.376	0.320	-0.491	(x4+x6)	(y4+y6)	(z4+z6)
145	0.224	0.398	-0.450	(x1+x4)	(y1+y4)	(z1+z4)
145	0.447	0.301	-0.435	(x5+x6)	(y5+y6)	(z5+z6)
141	0.221	0.114	-0.284	(x1-x5)	(y1-y5)	(z1-z5)
141	0.108	0.187	0.166	(x4-x6)	(y4-y6)	(z4-z6)
140	0.155	0.282	-0.061	(x1-x6)	(y1-y6)	(z1-z6)
139	0.378	0.034	-0.122	(x1-x2)	(y1-y2)	(z1-z2)
139	0.290	0.381	0.401	(x2+x6)	(y2+y6)	(z2+z6)
138	-0.223	0.248	0.064	(x2-x6)	(y2-y6)	(z2-z6)
138	-0.037	0.236	-0.028	(x3-x6)	(y3-y6)	(z3-z6)
137	0.478	0.366	0.312	(x3+x6)	(y3+y6)	(z3+z6)

134	-0.068	0.169	0.221	(x5-x6)	(y5-y6)	(z5-z6)
133	-0.331	0.415	0.278	(x1+x6)	(y1+y6)	(z1+z6)
132	0.369	0.355	-0.248	(x1+x3)	(y1+y3)	(z1+z3)
124	-0.444	0.343	-0.336	(x1+x2)	(y1+y2)	(z1+z2)
79	-0.484	0.135	0.347	2x6	2y6	2z6
76	-0.068	0.373	-0.464	2x2	2y2	2z2
73	0.377	0.472	-0.214	2x5	2y5	2z5
66	-0.398	0.218	0.267			
66	0.177	0.305	-0.223	2x1	2y1	2z1
56	-0.003	0.007	-0.197			
56	-0.003	0.007	-0.197			
56	0.003	-0.007	0.197			
56	0.003	-0.007	0.197			

B.9 Patterson solution for $\text{Os}_3(\text{CO})_{10}(\text{PhCCH}_2)(\text{AuPEt}_3)$ (XR13)

The above solution yielded the following metal atom co-ordinates

Os(1)	0.243	0.217	-0.211
Os(2)	0.043	0.183	-0.169
Os(3)	0.179	0.215	-0.053
Au(1)	0.266	0.400	-0.122

R.H.	u	v	w	Vector assignment		
281	0.000	0.072	0.500	0	0.5+2y1	0.5
				0	0.5+2y2	0.5
				0	0.5+2y3	0.5
247	0.064	0.000	-0.159	(x1-x3)	(y1-y3)	(z1-z3)
240	0.423	0.500	0.237	(x1+x3)	0.5+(y1-y3)	0.5+(z1-z3)
152	0.137	0.000	0.118	(x2-x3)	(y2-y3)	(z2-z3)
150	0.222	0.500	0.279	(x2+x3)	0.5+(y2-y3)	0.5+(z2+z3)
137	0.285	0.486	0.120	(x1+x2)	0.5+(y1-y2)	0.5+(z1+z3)
137	0.201	0.014	-0.043	(x1-x2)	(y1-y2)	(z1-z2)
136	0.358	0.500	0.396	2x3	0.5	0.5+2z3
128	0.000	0.303	0.500	0	0.5+2y4	0.5
125	0.220	0.398	-0.221	(x2+x3)	(y2+y3)	(z2+z3)
123	0.284	0.400	-0.380	(x1+x2)	(y1+y2)	(z1+z2)
120	0.485	0.500	0.078	2x1	0.5	0.5+2z1
120	0.137	0.103	-0.382	(x2-x3)	0.5+(x2+x3)	0.5+(x2-x3)
117	0.064	0.068	0.341	(x1-x3)	0.5+(x1+x3)	0.5+(x1-x3)
112	0.086	0.500	0.162	2x2	0.5	0.5+2z2
112	0.201	0.100	0.458	(x1-x2)	0.5+(y1+y2)	0.5+(z1-z2)
112	0.424	0.433	-0.262	(x1+x3)	(y1+y3)	(z1+z3)
111	0.447	0.313	0.327	(x3+x4)	0.5+(y3-y4)	0.5+(z3+z4)
111	0.224	0.084	-0.452	(x2+x4)	0.5+(y2-y4)	0.5+(z2+z4)
109	0.223	0.219	0.048	(x2-x4)	(y2-y4)	(z2-z4)
107	0.489	0.318	-0.168	(x1+x4)	0.5+(y1-y4)	0.4+(z1+z4)
107	0.447	0.383	-0.174	(x3+x4)	(y3+y4)	(z3+z4)
104	0.488	0.379	0.333	(x1+x4)	(y1+y4)	(z1+z4)
y04	0.086	0.187	-0.067	(x3-x4)	(y3-y4)	(z3-z4)
102	0.022	0.184	0.093	(x1-x4)	(y1-y4)	(z1-z4)
101	0.087	0.117	0.432	(x3-x4)	0.5+(y3+y4)	0.5+(z3-z4)
101	0.464	0.500	-0.259	2x4	0.5	0.5+2z4

101	0.307	0.281	0.210	(x2+x4)	0.5+(y2-y4)	0.5+(z2+z4)
96	0.310	0.416	-0.291	(x2+x4)	(y2+y4)	(z2+z4)
96	0.024	0.119	-0.409	(x1-x4)	0.5+(y1+y4)	0.5+(z1-z4)
68	0.357	0.432	-0.103	2x3	2y3	2z3
63	0.486	0.437	-0.425	2x1	2y1	2z1
62	0.085	0.365	-0.338	2x2	2y2	2z2
48	0.469	0.197	0.242	2x4	2y4	2z4

B.10 Patterson solution for $\text{HOs}_3(\text{CO})_9(\text{MeCCMe})(\text{AuPPH}_3)$ (XR14)

Solution yielded the following fractional coordinates:

Os(1)	0.211	0.348	0.015
Os(2)	0.390	0.263	0.034
Os(3)	0.232	0.055	-0.005
Au(1)	0.219	0.141	0.095

R.H.	u	v	w	Vector assignment		
225	0.434	0.500	0.117	(x3+y4)	(y3+y4)	(z3+z4)
219	0.000	0.206	0.500	2x3	0.5+2y3	0.5
				2x4	0.5+2y4	0.5
208	-0.007	0.000	0.421	(x3-x4)	0.5+(y3+y4)	0.5+(z3-z4)
162	0.000	0.000	0.500	0	0.5+2y2	0.5
131	0.401	0.383	-0.041	(x2+x3)	(y2+y3)	(z2+z3)
128	0.437	0.396	0.003	(x1+x3)	(y1+y3)	(z1+z3)
126	0.438	0.208	-0.493	(x1+x3)	0.5+(y1-y3)	0.5+(z1+z3)
125	0.013	0.301	0.400	(x1-x4)	0.5+(y1+y4)	0.5+(z1-z4)
124	0.161	0.179	-0.462	(x1-x2)	0.5+(y1+y2)	0.5+(z1-z2)
124	0.022	0.295	-0.020	(x1-x3)	(y1-y3)	(z1-z3)
122	0.178	0.117	-0.479	(x2-x3)	0.5+(y2+y3)	0.5+(z2-z3)
120	0.456	0.198	0.096	(x1+x4)	(y1+y4)	(z1+z4)
119	0.382	0.316	-0.027	(x1+x2)	(y1+y2)	(z1+z2)
116	0.443	0.500	-0.310	2x4	0.5	0.5+2x4
116	0.000	0.391	0.500	0	0.5+2y1	0.5
115	0.223	0.500	0.433	2x2	0.5	0.5+2x2
115	0.460	0.500	0.489	2x1	0.5	0.5+2x1
113	0.417	0.500	-0.471	2x3	0.5	0.5+2x3
112	0.174	0.098	0.441	(x2-x4)	0.5+(y2+x4)	0.5+(z2-z4)
111	0.172	0.121	-0.059	(x2-x4)	(y2-y4)	(z2-z4)
110	0.160	0.208	0.039	(x1-x2)	(y1-y2)	(z1-z2)
109	0.183	0.084	0.019	(x2-x3)	(y2-y3)	(z2-z3)
109	0.382	0.290	0.473	(x1+x2)	0.5+(y1-y2)	0.5+(z1+z2)
104	0.007	0.207	0.079	(x3-x4)	(y3-y4)	(z3-z4)
103	0.434	0.294	-0.383	(x3+x4)	0.5+(y3-y4)	0.5+(z3+z4)
102	0.020	0.097	0.482	(x1-x3)	0.5+(y1+y3)	0.5+(z1-z3)
99	0.403	0.416	0.452	(x2+x3)	0.5+(y2-y3)	0.5+(z2+z3)
98	0.457	0.413	-0.406	(x1+x4)	0.5+(y1-y4)	0.5+(z1+z4)
98	0.014	0.087	-0.098	(x1-x4)	(y1-y4)	(z1-z4)
96	0.221	0.500	-0.064	2x2	2y2	2z2
95	0.395	0.400	-0.124	(x2+x4)	(y2+y4)	(z2+z4)
95	0.395	0.376	0.375	(x2+x4)	0.5+(y2-y4)	0.5+(z2+z4)
59	0.441	0.282	0.196	2x4	2y4	2z4
57	0.459	0.104	-0.011	2x1	2y1	2z1

B.11 Patterson solution for $\text{Os}_7(\text{CO})_{14}(\text{MeCCMe})_3$ (XR15)

Solution yielded the following fractional coordinates:

Os(1)	0.112	-0.061	-0.055
Os(2)	0.107	0.055	-0.291
Os(3)	0.102	0.150	0.048
Os(4)	0.130	0.262	-0.148
Os(5)	0.176	0.079	-0.035
Os(6)	0.151	-0.158	-0.208
Os(7)	0.226	-0.100	-0.031

R.H.	u	v	w	Vector assignment		
220	0.440	0.500	0.484	$0.5+(x1-x5)$	$0.5+(y1+y5)$	$0.5+(z1-z5)$
				$0.5+(x5-x7)$	$0.5+(y5+y7)$	$0.5+(z5-z7)$
185	0.500	0.370	0.500	2x1	2y1	2z1
				2x2	2y2	2z2
				2x5	2y5	2z5
				2x7	2y7	2z7
153	0.220	0.000	-0.345	$(x1+x2)$	$(y1+y2)$	$(z1+z2)$
137	0.497	0.500	0.265	$0.5+(x1-x2)$	$0.5+(y1+y2)$	$0.5+(z1-z2)$
137	-0.497	0.500	-0.265			
122	0.282	0.000	-0.099	$(x1+x5)$	$(y1+y5)$	$(z1+z5)$
121	0.157	0.500	-0.419	$0.5+(x1+x7)$	$0.5+(y1-y7)$	$0.5+(z1+z7)$
				$0.5+2x5$	0.5	$0.5+2z5$
119	0.401	0.000	-0.066	$(x5+x7)$	$(y5+y7)$	$(z5+z7)$
118	0.022	0.223	0.154	$(x1-x3)$	$(y1-y3)$	$(z1-z3)$
117	0.281	0.120	-0.340	$(x2+x5)$	$(y2+y5)$	$(z2+z5)$
				$(x3+x5)$	$(y3+y5)$	$(z3+z5)$
				$(x4+x6)$	$(y4+y6)$	$(z4+z6)$
116	0.222	0.500	-0.174	$0.5+(x2+x5)$	$0.5+(y2-y5)$	$0.5+(z2+z5)$
				$0.5+2x4$	0.5	$0.5+2z4$
114	0.259	0.188	-0.296	$(x1+x4)$	$(y1+y4)$	$(z1+z4)$
				$(x3+x6)$	$(y3+y6)$	$(z3+z6)$
113	0.500	0.191	0.500	0.5	$0.5+2x3$	0.5
				0.5	$0.5+2x6$	0.5
112	0.041	0.198	0.101	$(x2-x6)$	$(y2-y6)$	$(z2-z6)$
				$(x4-x5)$	$(y4-y5)$	$(z4-z5)$
106	0.261	0.000	-0.148	$(x3+x6)$	$(y3+y6)$	$(z3+z6)$
98	0.039	0.102	-0.165	$(x1-x6)$	$(y1-y6)$	$(z1-z6)$
				$(x3-x4)$	$(y3-y4)$	$(z3-z4)$
98	0.500	0.000	0.500	0.5	$0.5+2x4$	0.5
97	0.452	0.500	-0.233	$0.5+(x3-x6)$	$0.5+(y3+y6)$	$0.5+(z3-z6)$
97	0.482	0.401	-0.426	$0.5+(x1-x3)$	$0.5+(y1+y3)$	$0.5+(z1-z3)$
				$0.5+(x4-x6)$	$0.5+(y4+y6)$	$0.5+(z4-z6)$
91	0.060	0.153	0.017	$(x1-x5)$	$(y1-y5)$	$(z1-z5)$
				$(x5-x7)$	$(y5-y7)$	$(z5-z7)$
90	0.342	0.161	-0.080	$(x1+x7)$	$(y1+y7)$	$(z1+z7)$
				2x5	2y5	2z5
82	0.069	0.000	0.252	$(x2-x5)$	$(y2-y5)$	$(z2-z5)$
79	0.283	0.383	-0.159	$0.5+(x1+x2)$	$0.5+(y1-y2)$	$0.5+(z1+z2)$
76	0.461	0.163	0.383	$0.5+(x2-x4)$	$0.5+(y2+y4)$	$0.5+(z2-z4)$
				$0.5+(x4-x5)$	$0.5+(y4+y5)$	$0.5+(z4-z5)$
75	0.283	0.500	0.079	$0.5+2x2$	0.5	$0.5+2z2$
74	0.460	0.280	-0.352	$0.5+(x1-x6)$	$0.5+(y1+y6)$	$0.5+(z1-z6)$
72	0.303	0.346	-0.187	$(x4+x5)$	$(y4+y5)$	$(z4+z5)$

71	0.243	0.286	-0.002	$0.5+(x_2+x_6)$	$0.5+(y_2-y_6)$	$0.5+(z_2+z_6)$
71	0.243	0.286	-0.002			
71	0.019	0.323	-0.095	(x_1-x_4)	(y_1-y_4)	(z_1-z_4)
				(x_2-x_4)	(y_2-y_4)	(z_2-z_4)
71	0.238	0.200	-0.207	(x_1+x_4)	(y_1+y_4)	(z_1+z_4)
				(x_1+x_6)	(y_1+y_6)	(z_1+z_6)
				(x_2+x_3)	(y_2+y_3)	(z_2+z_3)
71	0.220	0.095	-0.128	$0.5+(x_4+x_6)$	$0.5+(y_4-y_6)$	$0.5+(z_4+z_6)$
				$2x_1$	$2y_1$	$2z_1$
71	0.472	0.181	0.360			
70	0.279	0.500	-0.390	$0.5+2x_1$	0.5	$0.5+2z_1$
70	-0.001	0.117	0.236	(x_1-x_2)	(y_1-y_2)	(z_1-z_2)
70	0.001	0.117	-0.236			
70	0.099	0.322	-0.434	$0.5+(x_5+x_7)$	$0.5+(y_5-y_7)$	$0.5+(z_5+z_7)$
69	0.120	0.155	0.261	(x_2-x_7)	(y_2-y_7)	(z_2-z_7)
69	0.198	0.500	-0.082	$0.5+2x_6$	0.5	$0.5+2z_6$
67	0.279	0.229	0.017	$0.5+(x_2+x_4)$	$0.5+(y_2-y_4)$	$0.5+(z_2+z_4)$
66	0.237	0.318	-0.438	(x_2+x_4)	(y_2+y_4)	(z_2+z_4)
66	0.380	0.461	0.237	$0.5+(x_2-x_7)$	$0.5+(y_2+y_7)$	$0.5+(z_2-z_7)$
66	0.379	0.257	-0.236	(x_6+x_7)	(y_6+y_7)	(z_6+z_7)
65	0.099	0.364	0.121	(x_4-x_7)	(y_4-y_7)	(z_4-z_7)
65	0.259	0.102	0.500	(x_2+x_6)	(y_2+y_6)	(z_2+z_6)
65	0.423	0.270	-0.423			
65	0.121	0.249	-0.082	(x_3-x_7)	(y_3-y_7)	(z_3-z_7)
65	0.298	0.500	0.408	$0.5+2x_3$	0.5	$0.5+2z_3$
64	0.283	0.290	0.499	$0.5+(x_1+x_3)$	$0.5+(y_1-y_3)$	$0.5+(z_1+z_3)$
64	0.021	0.420	-0.060	(x_4-x_6)	(y_4-y_6)	(z_4-z_6)
64	0.477	0.300	-0.403	$0.5+(x_1-x_4)$	$0.5+(y_1+y_4)$	$0.5+(z_1-z_4)$
64	0.216	0.088	0.001	(x_1+x_3)	(y_1+y_3)	(z_1+z_3)
64	0.216	0.088	0.001			
63	-0.003	0.093	0.346	(x_2-x_3)	(y_2-y_3)	(z_2-z_3)
63	0.003	0.093	-0.346			
63	0.220	0.428	0.484			
63	0.141	0.140	-0.324	$0.5+(x_4+x_7)$	$0.5+(y_4-y_7)$	$0.5+(z_4+z_7)$
61	0.120	0.441	-0.264	$0.6+(x_6+x_7)$	$0.5+(y_6-y_7)$	$0.5+(z_6+z_7)$
60	0.196	0.315	-0.311	$0.5+(x_4+x_5)$	$0.5+(y_4-y_5)$	$0.5+(z_4+z_5)$
60	0.176	0.262	-0.253	$0.5+(x_5+x_6)$	$0.5+(y_5-y_6)$	$0.5+(z_5+z_6)$
59	0.498	0.295	-0.153	$0.5+(x_2-x_3)$	$0.5+(y_2+y_3)$	$0.5+(z_2-z_3)$
59	-0.498	0.295	0.153			
59	0.260	0.294	-0.059			
58	0.359	0.163	-0.177	(x_4+x_7)	(y_4+y_7)	(z_4+z_7)
58	0.239	0.402	-0.234	$0.5+(x_1+x_6)$	$0.5+(y_1-y_6)$	$0.5+(z_1+z_6)$
				$0.5+(x_3+x_5)$	$0.5+(y_3-y_5)$	$0.5+(z_3+z_5)$
				(x_1-x_7)	(y_1-y_7)	(z_1-z_7)
58	0.119	0.015	0.034			
58	0.433	0.367	0.248	$0.5+(x_2-x_5)$	$0.5+(y_2+y_5)$	$0.5+(z_2-z_5)$
57	0.217	0.354	-0.411	$0.5+(x_1+x_5)$	$0.5+(y_1-y_5)$	$0.5+(z_1+z_5)$
56	0.078	0.073	-0.076	(x_3-x_5)	(y_3-y_5)	(z_3-z_5)
56	0.401	0.336	0.377	$0.5+(x_4-x_7)$	$0.5+(y_4+y_7)$	$0.5+(z_4-z_7)$
56	0.175	0.248	0.489	$0.5+(x_3+x_7)$	$0.5+(y_3-y_7)$	$0.5+(z_3+z_7)$
56	0.297	0.398	-0.242	$0.5+(x_2+x_3)$	$0.5+(y_2-y_3)$	$0.5+(z_2+z_3)$
55	0.163	0.346	-0.183	$0.5+(x_2+x_7)$	$0.5+(y_2-y_7)$	$0.5+(z_2+z_7)$
55	0.204	0.208	-0.253			
55	0.382	0.339	0.469	$0.5+(x_1-x_7)$	$0.5+(y_1+y_7)$	$0.5+(z_1-z_7)$
54	0.474	0.085	-0.293	$0.5+(x_3-x_4)$	$0.5+(y_3+y_4)$	$0.5+(z_3-z_4)$
54	0.423	0.241	0.317	$0.5+(x_6-x_7)$	$0.5+(y_6+y_7)$	$0.5+(z_6-z_7)$
53	0.336	0.042	-0.318	(x_2+x_7)	(y_2+y_7)	(z_2+z_7)
52	0.481	0.420	0.330	$0.5+(x_5-x_6)$	$0.5+(y_5+y_6)$	$0.5+(z_5-z_6)$
52	0.458	0.395	0.421	$0.5+(x_2-x_6)$	$0.5+(y_2+y_6)$	$0.5+(z_2-z_6)$
51	0.324	0.082	-0.252	(x_5+x_6)	(y_5+y_6)	(z_5+z_6)

51	0.377	0.451	-0.414	$0.5+(x_3-x_7)$	$0.5+(y_3+y_7)$	$0.5+(z_3-z_7)$
50	0.323	0.046	0.005	(x_3+x_7)	(y_3+y_7)	(z_3+z_7)
50	0.323	0.046	0.005			
50	0.045	0.500	-0.445	$0.5+2x_7$	0.5	$0.5+2z_7$
47	0.048	0.310	-0.265	(x_3-x_6)	(y_3-y_6)	(z_3-z_6)
46	0.079	0.060	0.185	(x_6-x_7)	(y_6-y_7)	(z_6-z_7)
44	0.261	0.500	-0.304	$2x_4$	$2y_4$	$2z_4$
43	0.233	0.411	-0.092	(x_3+x_4)	(y_3+y_4)	(z_3+z_4)
41	0.202	0.299	0.095	$2x_3$	$2y_3$	$2z_3$
37	0.264	0.388	-0.411	$0.5+(x_3+x_4)$	$0.5+(y_3-y_4)$	$0.5+(z_3+z_4)$
33	0.217	0.110	0.418	$2x_2$	$2y_2$	$2z_2$
28	0.453	0.200	-0.056	$2x_7$	$2y_7$	$2z_7$

APPENDIX C

Publications arising from the
work described in this thesis.

IMAGING SERVICES NORTH

Boston Spa, Wetherby

West Yorkshire, LS23 7BQ

www.bl.uk

**SOME PAGES BOUND
INTO/CLOSE TO SPINE.**

Formation of Cationic Molybdenum η^2 -Vinyl Complexes; Structural Evidence for the Coupling of η^2 -Vinyl and Alkyne Ligands

Grainne C. Conole,^a Michael Green,^b Mary McPartlin,^a Carolyn Reeve,^b and Christopher M. Woolhouse^b

^a School of Chemistry, Polytechnic of North London, Holloway Road, London N7 8DB, U.K.

^b Department of Chemistry, King's College London, Strand, London WC2R 2LS, U.K.

Protonation (HBF₄·Et₂O) of [MoX(η^2 -MeC₂Me)₂L] (X = Cl, Br, I; L = η -C₅H₅ or η^5 -C₉H₇) affords the cations [XMo=C(Me)CHMe(η^2 -MeC₂Me)L] [BF₄], which react with LiX to give [X₂Mo=C(Me)CHMe(η^2 -MeC₂Me)L] or with PR₃ (R = Me, or OMe) to give the C-C coupled products [XMo=C(Me)- η^3 -(C(Me)C(Me)CHMe)(PR₃)(L)][BF₄], the latter being structurally identified by X-ray crystallography; carbon-carbon coupling also occurs on reduction of [Br₂Mo=C(Me)CHMe(η^2 -MeC₂Me)(η -C₅H₅)] with Mg/Hg in the presence of CO to form [MoBr(CO){ η^4 -CHMe=C(Me)-C(Me)=CHMe}(η -C₅H₅)], and treatment of the phosphine promoted coupled products with Li[N(SiMe₃)₂] leads to reversible deprotonation reactions affording [MoX{ η^4 -CHMe=C(Me)-C(Me)=C=CH₂}(PR₃)L].

The synthesis and structural characterisation of complexes containing $\eta^2(3e)$ -vinyl ligands¹⁻³ has interesting implications for catalysis, in that co-ordinatively unsaturated $\eta^1(1e)$ -vinyl species can in principle be stabilised, and in a sense stored, by an $\eta^1(1e)$ to $\eta^2(3e)$ transformation of the bonding mode of the

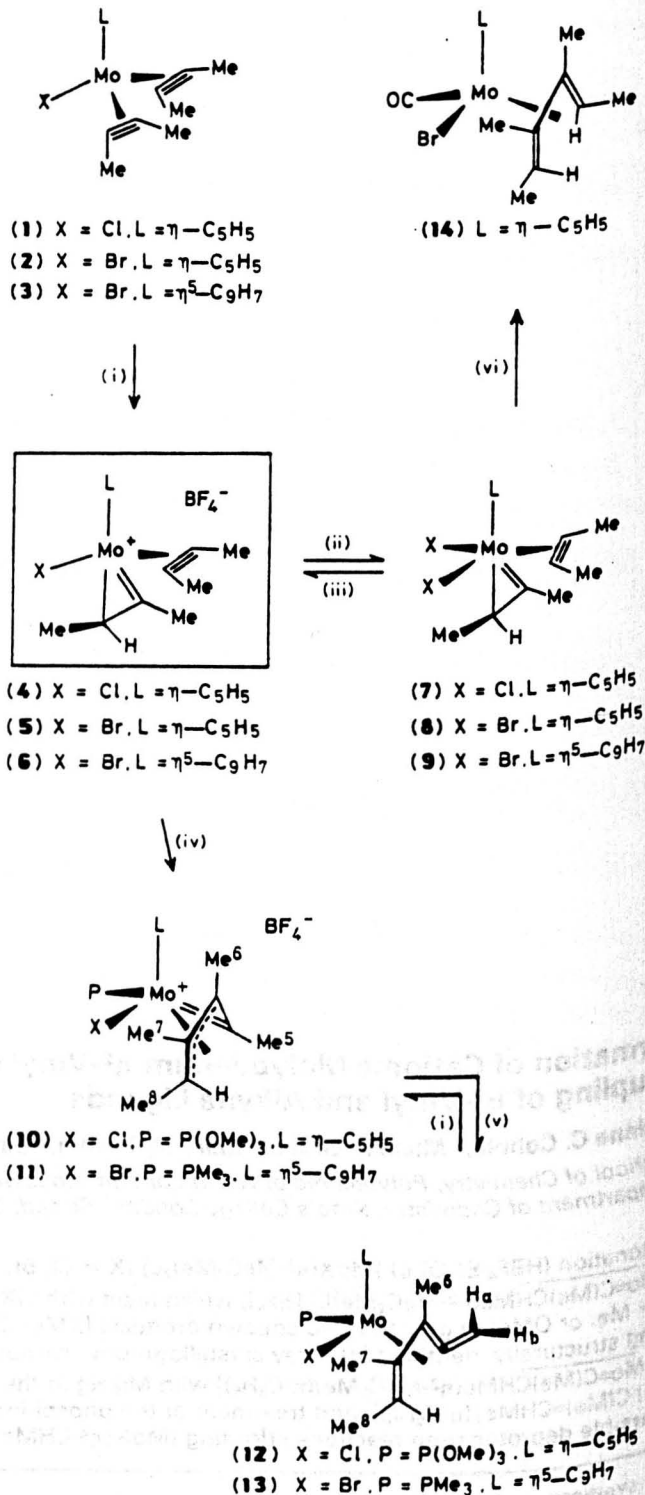
vinyl ligand. However, the development of this chemistry has so far been centred around the neutral η^2 -vinyl complexes prepared by nucleophilic attack on three- or four-electron donor alkyne complexes, and therefore has been restricted in its scope. In this paper we describe how protonation of neutral

bis(alkyne)molybdenum⁺ complexes provides access to reactive cationic η^2 -vinyl/alkyne species.

The neutral halogeno-complexes (1) to (3)[‡] containing three-electron donor alkyne ligands can be readily synthesised as yellow to orange crystalline materials by reaction (refluxing tetrahydrofuran, thf) of LiX with the cations $[\text{Mo}(\text{NCMe})(\eta^2\text{-MeC}_2\text{Me})_2(\eta\text{-C}_5\text{H}_5 \text{ or } \eta^5\text{-C}_9\text{H}_7)][\text{BF}_4]$.⁴ Protonation (-78°C , CH_2Cl_2) of (1), (2), and (3) with $\text{HBF}_4 \cdot \text{Et}_2\text{O}$ affords the orange to red crystalline cations (4), (5), and (6), characterised by ^1H and ^{13}C - $\{^1\text{H}\}$ n.m.r. spectroscopy[‡] as complexes containing $\eta^2(4e)$ -alkyne and $\eta^2(3e)$ -vinyl ligands. The ^{13}C - $\{^1\text{H}\}$ n.m.r. spectrum of, for example (5), showed a low-field resonance at 297.6 p.p.m. characteristic¹ of the α -carbon or carbene carbon of an η^2 -vinyl complex, and at room temperature there were resonances due to a non-rotating but-2-yne ligand. In view of the isolobal relationship^{1,3} between HC_2H and CHCH_2^- it is likely that these cations have a structure analogous to that found⁵ in $[\text{WCl}(\eta^2\text{-CF}_3\text{C}_2\text{CF}_3)_2(\eta\text{-C}_5\text{H}_5)]$ with the C-C vector of both the but-2-yne and $\text{C}(\text{Me})\text{CHMe}$ η^2 -vinyl fragments in (4)–(6) lying approximately parallel to the Mo–X axis.

Treatment of solutions of (4), (5), and (6) with lithium halides in $\text{CH}_2\text{Cl}_2/\text{thf}$ results in the formation of the neutral purple crystalline complexes (7), (8), and (9)[‡] (Scheme 1). These molecules show low-field ^{13}C resonances due to the η^2 -vinyl fragment; however, in contrast with the parent

cations the $\eta^2\text{-MeC}_2\text{Me}$ ligands donate only two electrons to the molybdenum, and it is interesting that relatively lower barriers to alkyne rotation are observed, as is illustrated by the coalescence of the MeC_2Me ^1H resonances [$\Delta G^\ddagger_{288\text{K}}$ 58.5



[‡] It is interesting that protonation (HX) of $[\text{Pt}(\eta^2\text{-RC}_2\text{R})(\text{PPh}_3)_2]$ affords *trans*- $[\text{PtX}(\eta^1\text{-C}(\text{R})=\text{CHR})(\text{PPh}_3)_2]$. See B. E. Mann, B. L. Shaw, and N. I. Tucker, *J. Chem. Soc. (A)*, 1971, 2667.

[‡] Selected spectroscopic data for (2): n.m.r. ^{13}C - $\{^1\text{H}\}$ (CD_2Cl_2), δ 180.3 (MeC \equiv), 165.4 (MeC \equiv), 101.3 (C $_5$ H $_5$), 20.2 (MeC), 15.7 (MeC). Compound (5): n.m.r. ^1H (CD_3NO_2), δ 6.0 (s, 5H, C $_5$ H $_5$), 2.8 (s, 3H, MeC \equiv), 2.4 (s, 3H, MeC \equiv), 2.15 (s, 3H, MeC \equiv), 2.0 [d, 3H, CHMe, $^3J(\text{HH})$ 6.0 Hz]; ^{13}C - $\{^1\text{H}\}$ (CD_3NO_2), δ 297.6 [Mo=C(Me)], 134.6 (br.s MeC \equiv), 104.0 (C $_5$ H $_5$), 73.6 (CHMe) [$^1J(\text{CH})$ 66.2 Hz from off-resonance spectrum of $\eta^2\text{-C}_9\text{H}_7$ analogue], 31.0 [Mo=C(Me)], 16.6 (MeC \equiv), 16.1 (CHMe), 12.2 (MeC \equiv). Compound (7): n.m.r. ^1H (CD_2Cl_2), δ 5.70 (s, 5H, C $_5$ H $_5$), 2.80 (s, 3H, MeC \equiv), 2.08 (s, 6H, MeC \equiv), 2.03 [d, 3H, CHMe, $^3J(\text{HH})$ 6.04 Hz], 1.90 [q, 1H, CHMe, $^3J(\text{HH})$ 6.07 Hz]; ^{13}C - $\{^1\text{H}\}$ (CD_2Cl_2), δ 291.3 [Mo=C(Me)], 134.2 (MeC \equiv), 113.6 (MeC \equiv), 102.6 (C $_5$ H $_5$), 70.0 (CHMe), 27.5 (Me), 16.8 (MeC \equiv), 16.4 (MeC \equiv), 11.1 (Me). Compound (11) (major isomer): ^1H n.m.r. (CD_2Cl_2), δ 7.7–7.35 (m, 4H, C $_5$ H $_4$), 6.15, 5.96, 5.55 (m, 3H, C $_5$ H $_4$), 2.89 [d, 3H, Me 5 , $^4J(\text{HP})$ 5.37 Hz], 2.36 [m, 1H, CHMe 6 , $J(\text{HH})$ 5.90 Hz], 2.32 (s, 3H, Me 7), 1.98 (s, 3H, Me 8), 1.56 [d, 9H, PMe $_3$, $^1J(\text{HP})$ 10.36 Hz], 1.18 [m, 3H, CHMe 6 , $^3J(\text{HH})$ 5.86 Hz]; ^{13}C - $\{^1\text{H}\}$ (CD_2Cl_2), δ 298.1 [d, Mo=C(Me)], $^3J(\text{CP})$ 16.9 Hz], 127.1 (MeC), 115.8 (MeC), 132.6, 131.7, 127.3, 127.0 (C $_9$ H $_7$), 117.1, 107.3 (C $_9$ H $_7$), 92.7, 92.4, 88.6 (C $_9$ H $_7$), 77.3 (CHMe), 30.3 (Me), 18.0 [d, PMe $_3$, $^1J(\text{CP})$ 33.0 Hz], 17.6 (Me), 15.5 (Me), 10.9 (Me); ^{31}P - $\{^1\text{H}\}$ (CD_2Cl_2) δ -0.17 p.p.m. Compound (12): n.m.r. ^1H (C $_6$ D $_6$), δ 5.39 [dd, 1H, CH a H, $^4J(\text{HP})$ 3.30, $^2J(\text{HH})$ 0.94 Hz], 4.55 [d, 5H, C $_5$ H $_4$, $^1J(\text{HP})$ 1.43 Hz], 3.69 [dd, 1H, CHH a , $^4J(\text{HP})$ 1.96, $^2J(\text{HH})$ 0.94], 3.33 [d, 9H, POMe, $^1J(\text{HP})$ 10.36 Hz], 2.39 [dd, 3H, Me 7 , $^4J(\text{HP})$ 1.6, $^3J(\text{HH})$ 1.01], 2.07 [dq, 1H, CHMe, CHMe 6 , $^3H(\text{HH})$ 6.05, $^3J(\text{HP})$ 2.5, $^4J(\text{HH})$ 1.0 Hz], 1.91 (s, 3H, Me 8), 1.86 [d, 3H, Me 6 , $J(\text{HP})$ 6.09 Hz]; ^{13}C - $\{^1\text{H}\}$ (C $_6$ D $_6$), δ 196.5 [d, CH $_2$ =C, $^3J(\text{CP})$ 10.5 Hz], 129.1 (MeC), 103.6 (MeC), 93.0 (C $_5$ H $_4$), 91.7 (CH $_2$), 65.2 (CHMe), 52.6 [d, POMe, $^3J(\text{CP})$ 6.1 Hz], 17.8 (Me 8), 15.9 (Me 6), 14.3 (Me 7); ^{31}P - $\{^1\text{H}\}$ (CD_2Cl_2), δ 168.6 p.p.m. Compound (14): ν_{CO} (Et_2O) 1945s cm^{-1} ; n.m.r. ^1H (CD_2Cl_2), δ 4.94 (s, 5H, C $_5$ H $_4$), 2.47 [q, 1H, CHMe, $^3J(\text{HH})$ 5.95 Hz], 2.41 (s, 3H, MeC), 1.99 (s, 3H, MeC), 1.70 [d, 3H, MeCH, $^3J(\text{HH})$ 5.95 Hz], 1.34 [d, 3H, MeCH, $^3J(\text{HH})$ 5.97 Hz], 0.84 [q, 1H, MeCH, $^3J(\text{HH})$ 6.00 Hz]; ^{13}C - $\{^1\text{H}\}$ (CD_2Cl_2), δ 244.6 (CO), 123.6 (MeC), 109.6 (MeC), 92.3 (C $_5$ H $_4$), 69.1 (CHMe), 59.4 (CHMe), 19.1 (MeC), 17.5 (MeC), 15.9 (MeCH), 15.6 p.p.m. (MeCH).

Scheme 1. Reagents and conditions: (i) + $\text{HBF}_4 \cdot \text{Et}_2\text{O}$, CH_2Cl_2 ; (ii) + LiX, $\text{CH}_2\text{Cl}_2/\text{thf}$ (1:1); (iii) + AgBF_4 , $-\text{AgX}$, CH_2Cl_2 ; (iv) + P, CH_2Cl_2 ; (v) + $\text{LiN}(\text{SiMe}_3)_2$, thf, -78°C ; (vi) Mg/Hg, + CO, thf.

(± 0.5 kJ mol⁻¹) in the dichloro-complex (7). It was confirmed that in the formation of (7)–(9) from (4)–(6), coupling of the $\eta^2(3e)$ -vinyl and η^2 -alkyne ligands had not occurred because when (7)–(9) were treated with AgBF₄, a precipitate of AgX was produced and the parent cations (4)–(6) were reformed in good yield.

In contrast, linking of the η^2 -vinyl and but-2-yne ligands does occur on treatment of, for example, (4) with trimethyl phosphite and (6) with trimethylphosphine. In both reactions orange crystalline products are formed, the reaction with P(OMe)₃ and (4) giving (10), and PMe₃ and (6) affording two isomeric complexes of (11) in the ratio of (6:1). These materials all showed low-field (≈ 300 p.p.m.) ¹³C resonances attributable to Mo=C. In addition there were ¹³C and ¹H signals present in the respective n.m.r. spectra consistent with the presence of $\eta^4(5e)$ -butadienyl,^{6,7,8} i.e. Mo=C(Me)- η^3 -(C(Me)C(Me)CHMe), ligands. This was confirmed by a single crystal X-ray crystallographic study with the major isomeric complex of (11).[§]

As is shown in Figure 1 the molecule contains a molybdenum atom to which are co-ordinated a slipped η^5 -indenyl, PMe₃ and Br ligands. In addition there is an η^4 -bonded four-carbon fragment C(11)·C(12)·C(13)·C(14) beginning with a molybdenum to carbon double bond to C(11) [1.91(1) Å], and terminating with a CHMe group [Mo–C(14)] at 2.32(1) Å from the molybdenum. The other two carbons C(12) and C(13) are also bonded to the metal with Mo–C(12) and Mo–C(13) distances of 2.36(2) and 2.48(1) Å respectively. Thus, twisting of the C₄ chain, reflected in the torsion angles (see Figure 1), allows η^4 -bonding. Interestingly, the C(11)–C(12) and C(13)–C(14) distances of 1.35(2) and 1.40(2) Å respectively suggest that the butadienyl fragment adopts an $\eta^3(3e)$ bonding mode.^{9,10} However, this is clearly inconsistent with the short Mo–C(11) distance and the presence of a low field ¹³C resonance. Whatever the precise details of the mode

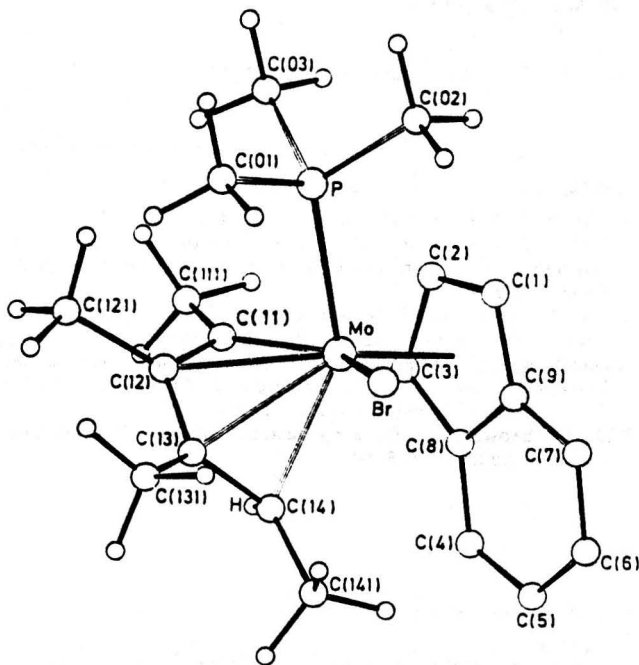


Figure 1. Molecular structure of cation in (11). Selected bond lengths (Å): Mo(1)–Br 2.641(1); Mo(1)–P 2.531(4); Mo(1)–C(11) 1.91(1); Mo(1)–C(12) 2.36(2); Mo(1)–C(13) 2.48(1); Mo(1)–C(14) 2.32(1); mean Mo(1)–C₆H₇ 2.36(2); P–C(01) 1.82(2); P–C(02) 1.79(2); P–C(03) 1.81(2); C(11)–C(12) 1.35(2); C(11)–C(111) 1.52(2); C(12)–C(13) 1.42(2); C(12)–C(121) 1.57(3); C(13)–C(14) 1.40(2); C(14)–C(141) 1.53(2).

of bonding of the C₄ fragment to the molybdenum it is clear that coupling of the η^2 -vinyl and but-2-yne ligands has occurred suggesting that the recently reported⁷ formation of an $\eta^4(5e)$ -C₄R₄H ligand by protonation of the bis(alkyne)di-thiocarbamate complexes [M(R¹C₂R²)₂(S₂CNR₂)] (M = Mo, W) might also involve a stepwise¹¹ process. As shown in Figure 1 the hydrogen substituent of the $\eta^4(5e)$ -butadienyl fragment, which has its origin in the proton source HBF₄·Et₂O, occupies an inside or pseudo-*anti* position.

It is interesting that whilst the carbon–carbon coupling reaction initiated by reaction with P(OMe)₃ is selective, the reaction with PMe₃ forms two isomers presumably *via* attack on either of the two XMOL faces.

These cationic $\eta^4(5e)$ -butadienyl complexes are reactive towards nucleophilic reagents, and of particular interest is their reaction with the sterically demanding reagent Li[N-(SiMe₃)₂]. Reaction at low temperature leads to a regioselective deprotonation of the methyl group, which is bonded to the carbenoid or α carbon atom, and formation in good yield of the neutral complexes (12) and (13).[‡] These molecules can be represented as $\eta^4(4e)$ -vinylallene complexes and it is interesting that (12) and (13) can be regioselectively reprotonated [HBF₄·Et₂O] on the 'allenic' methylene carbon to reform the cations (10) and (11) in quantitative yield. This suggests a possible general route to other $\eta^4(5e)$ -butadienyl complexes *via* protonation of species carrying η^4 -vinylallene ligands.

Finally, in exploring the reduction of the neutral η^2 -vinyl/alkyne complexes (7)–(9), it was found that treatment of, for example, (8) with magnesium amalgam suspended in thf in the presence of carbon monoxide (1 atm) leads to a novel carbon–carbon coupling reaction and the formation (43% yield) of the η^4 -1,3-diene complex (14).[‡]

[§] Crystal data: for [BrMo=C(Me)- η^3 -(C(Me)C(Me)CHMe)-(PMe₃)(C₆H₇)] [BF₄](0.5(CH₂Cl₂)) (11): *M* = 576.05, monoclinic, space group C2/c, *a* = 26.765(4), *b* = 13.310(2), *c* = 15.482(3) Å, β = 117.587(2)°, *U* = 4888.29 Å³, *F*(000) = 2424, μ (Mo-K α) = 22.71 cm⁻¹, *Z* = 8, *D*_c = 1.63 g cm⁻³. Data were collected on a Philips PW1100 diffractometer in the θ -range 3–25°, with a scan width of 0.70°, using the technique described previously.¹ Lorentz and polarisation corrections were applied,¹ and equivalent reflections were merged to give 3020 data with *I*/ σ (*I*) > 3.0. The co-ordinates of the molybdenum atom were deduced from a Patterson synthesis, and all remaining non-hydrogen atoms were located from subsequent difference Fourier syntheses. There appears to be some rotational disorder of the BF₄⁻ anion, shown by regions of extended electron density in the vicinity of three of the fluorine atoms, resulting in high anisotropic thermal parameters for these atoms. Half a dichloromethane solvent molecule is present per asymmetric unit, with the central carbon lying on a 2-fold axis (0, *y*, 0.25). The hydrogen atom H(1), attached to carbon atom C(14) of the organic fragment, was located in a difference Fourier synthesis using data with $\sin \theta < 0.35$. The parameters of this atom were included in the structure factor calculations but were not refined. The remaining hydrogen atoms were included in geometrically idealised positions and were constrained to 'ride' on the relevant carbon atoms with isotropic thermal parameters fixed at 0.80 Å². The molybdenum, phosphorus, and bromine atoms, and all five atoms of the counter ion were assigned anisotropic thermal parameters in the final cycles of full-matrix refinement which gave *R* 0.0639 and *R*' 0.0680, with weights of *w* = 1/ $\sigma^2 F_o$, assigned to the individual reflections. Atomic co-ordinates, bond lengths and angles, and thermal parameters have been deposited at the Cambridge Crystallographic Data Centre. See Notice to Authors, Issue No. 1.

We thank the Koninklijke-Shell Laboratorium and the S.E.R.C. for support.

Received, 31st May 1988; Com. 8/02153H

References

- 1 M. Green, N. C. Norman, and A. G. Orpen, *J. Am. Chem. Soc.*, 1981, **103**, 1267; S. R. Allen, R. G. Beevor, M. Green, N. C. Norman, A. G. Orpen, and I. D. Williams, *J. Chem. Soc., Dalton Trans.*, 1985, 435.
- 2 J. L. Davidson, W. F. Wilson, L. Manojlovic-Muir, and K. W. Muir, *J. Organomet. Chem.*, 1983, **254**, C6; L. Carlton, J. L. Davidson, J. C. Miller, and K. W. Muir, *J. Chem. Soc., Chem. Commun.*, 1984, 11; J. L. Davidson, *J. Chem. Soc., Dalton Trans.*, 1987, 5715; and references therein.
- 3 D. C. Brower, K. R. Birdwhistell, and J. L. Templeton, *Organometallics* 1986, **5**, 94.
- 4 S. R. Allen, P. K. Baker, S. G. Barnes, M. Green, L. Trollope, L. Manojlovic-Muir, and K. W. Muir, *J. Chem. Soc., Dalton Trans.*, 1981, 873.
- 5 J. L. Davidson, M. Green, D. W. A. Sharp, F. G. A. Stone, and A. J. Welch, *J. Chem. Soc., Chem. Commun.*, 1974, 706.
- 6 M. Crocker, M. Green, A. G. Orpen, H. P. Neumann, and C. Schaverien, *J. Chem. Soc., Chem. Commun.*, 1984, 1351.
- 7 J. R. Morrow, T. L. Tonker, and J. L. Templeton, *J. Am. Chem. Soc.*, 1985, **107**, 5004.
- 8 L. Carlton, J. L. Davidson, P. Ewing, L. Manojlovic-Muir, and K. W. Muir, *J. Chem. Soc., Chem. Commun.*, 1985, 1474.
- 9 T. Blackmore, M. I. Bruce, and F. G. A. Stone, *J. Chem. Soc. Dalton Trans.*, 1974, 106.
- 10 L. Brammer, M. Crocker, B. J. Dunne, M. Green, C. E. Morton, K. R. Nagle, and A. G. Orpen, *J. Chem. Soc., Chem. Commun.*, 1986, 1226.
- 11 It is also important to note that thermolysis or u.v. irradiation of $[\text{Mo}(\eta^3\text{-C}(\text{CF}_3)\text{C}(\text{CF}_3)\text{S}_2\text{CNR}_2)(\text{CF}_3\text{C}_2\text{CF}_3)(\eta\text{-C}_5\text{H}_5)]$ gives the coupled complex $[\text{Mo}(\eta^3\text{-C}(\text{CF}_3)\text{C}(\text{CF}_3)\text{C}(\text{CF}_3)=\text{C}(\text{CF}_3)\text{S})(\eta^2\text{-R}_2\text{NCS})(\eta\text{-C}_5\text{H}_5)]$, J. L. Davidson, *J. Chem. Soc., Dalton Trans.*, 1987, 2715.

CHEMISTRY OF PHOSPHIDO-BRIDGED DIMOLYBDENUM COMPLEXES. PART 2²¹:
THE REACTION OF $[(\eta\text{-C}_5\text{H}_5)_2\text{Mo}_2(\mu\text{-H})(\mu\text{-PMe}_2)(\text{CO})_4]$ WITH ALKYNES: X-RAY
CRYSTAL STRUCTURE OF $[(\eta\text{-C}_5\text{H}_5)_2\text{Mo}_2\{\mu\text{-}\sigma:\eta^2\text{-C}(\text{Me})=\text{CHMe}\}(\mu\text{-PMe}_2)(\text{CO})_3]$

Gráinne Conole, Kim Henrick and Mary McPartlin

Department of Chemistry, Polytechnic of North London, Holloway Road, London (N7 8DB).

Andrew D. Horton and Martin J. Mays

University Chemical Laboratory, Lensfield Road, Cambridge (CB2 1EW).

Received December 11, 1987, accepted January 28, 1988.

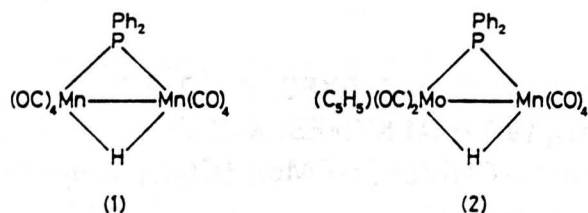
RÉSUMÉ. — Les réactions photolytiques de $[(\eta\text{-C}_5\text{H}_5)_2\text{Mo}_2(\mu\text{-H})(\mu\text{-PMe}_2)(\text{CO})_4]$ avec des alcynes ont été étudiées. Avec $\text{MeC}\equiv\text{CMe}$ le produit principal est le complexe μ -vinylique $[(\eta\text{-C}_5\text{H}_5)_2\text{Mo}_2\{\mu\text{-}\sigma:\eta^2\text{-C}(\text{CH}_3)=\text{CHCH}_3\}(\mu\text{-PMe}_2)(\text{CO})_3]$ qui a été caractérisé par diffraction des rayons X. Celle-ci montre que les groupes méthyle du ligand μ -vinylique adoptent une orientation mutuellement *trans*, la longueur moyenne prise sur deux molécules indépendantes de la liaison Mo-Mo est de 3,056 (1) Å. Les alcynes non symétriques $\text{RC}\equiv\text{CR}'$ [R=Me, R'=H ou R=Et, R'=H] donnent un mélange inséparable d'isomères constitué de $[(\eta\text{-C}_5\text{H}_5)_2\text{Mo}_2\{\mu\text{-}\sigma:\eta^2\text{-C}(\text{R})=\text{CHR}'\}(\mu\text{-PMe}_2)(\text{CO})_3]$ et de $[(\eta\text{-C}_5\text{H}_5)_2\text{Mo}_2\{\mu\text{-}\sigma:\eta^2\text{-C}(\text{R}')=\text{CHR}\}(\mu\text{-PMe}_2)(\text{CO})_3]$ mais $\text{HC}\equiv\text{CH}$ et $\text{PhC}\equiv\text{CPh}$ ne donnent pas de simples produits μ -vinyliques. Chacun des complexes μ -vinyliques ci-dessus est accompagné par une petite quantité du complexe oxo correspondant $[(\eta\text{-C}_5\text{H}_5)_2\text{Mo}_2(\text{O})(\mu\text{-vinyl})(\mu\text{-PMe}_2)(\text{CO})]$ et une faible quantité d'un complexe de ce genre est obtenu également dans la réaction avec l'acétylène lui-même. Les différences qui existent entre les réactions des alcynes avec $[(\eta\text{-C}_5\text{H}_5)_2\text{Mo}_2(\mu\text{-H})(\mu\text{-PMe}_2)(\text{CO})_4]$ et les réactions correspondantes avec $[\text{Mn}_2(\mu\text{-H})(\mu\text{-PPh}_2)(\text{CO})_8]$ et avec $[(\eta\text{-C}_5\text{H}_5)_2\text{MoMn}(\mu\text{-H})(\mu\text{-PPh}_2)(\text{CO})_6]$ sont discutées.

ABSTRACT. — The photolytic reactions of $[(\eta\text{-C}_5\text{H}_5)_2\text{Mo}_2(\mu\text{-H})(\mu\text{-PMe}_2)(\text{CO})_4]$ with alkynes have been studied. With $\text{MeC}\equiv\text{CMe}$ the major product is the μ -vinyl complex $[(\eta\text{-C}_5\text{H}_5)_2\text{Mo}_2\{\mu\text{-}\sigma:\eta^2\text{-C}(\text{CH}_3)=\text{CHCH}_3\}(\mu\text{-PMe}_2)(\text{CO})_3]$ which has been characterised by a single crystal X-ray diffraction study. This shows that the methyl groups on the μ -vinyl ligand adopt a mutually *trans* orientation; the Mo-Mo bond length is 3.056 (1) Å (mean for two independent molecules). The unsymmetrical alkynes $\text{RC}\equiv\text{CR}'$ [R=Me, R'=H or R=Et, R'=H] give inseparable isomeric mixtures of $[(\eta\text{-C}_5\text{H}_5)_2\text{Mo}_2\{\mu\text{-}\sigma:\eta^2\text{-C}(\text{R})=\text{CHR}'\}(\mu\text{-PMe}_2)(\text{CO})_3]$ and $[(\eta\text{-C}_5\text{H}_5)_2\text{Mo}_2\{\mu\text{-}\sigma:\eta^2\text{-C}(\text{R}')=\text{CHR}\}(\mu\text{-PMe}_2)(\text{CO})_3]$ but $\text{HC}\equiv\text{CH}$ and $\text{PhC}\equiv\text{CPh}$ do not give simple μ -vinyl products. Each of the above μ -vinyl complexes is accompanied by a minor yield of the corresponding oxo complex $[(\eta\text{-C}_5\text{H}_5)_2\text{Mo}_2(\text{O})(\mu\text{-vinyl})(\mu\text{-PMe}_2)(\text{CO})]$ and a low yield of such a complex is also obtained in the reaction with acetylene itself. Differences between the reactions of alkynes with $[(\eta\text{-C}_5\text{H}_5)_2\text{Mo}_2(\mu\text{-H})(\mu\text{-PMe}_2)(\text{CO})_4]$ and the corresponding reactions of alkynes with $[\text{Mn}_2(\mu\text{-H})(\mu\text{-PPh}_2)(\text{CO})_8]$ and with $[(\eta\text{-C}_5\text{H}_5)_2\text{MoMn}(\mu\text{-H})(\mu\text{-PPh}_2)(\text{CO})_6]$ are discussed.

Reactions of the dimanganese complex $[\text{Mn}_2(\mu\text{-H})(\mu\text{-PPh}_2)(\text{CO})_8]$ (1) with a wide range of alkynes under photolytic conditions invariably lead to complexes of the type $[\text{Mn}_2\{\mu\text{-}\sigma:\eta^2\text{-C}(\text{R})=\text{CHR}'\}(\mu\text{-PPh}_2)(\text{CO})_7]$ (R=alkyl, aryl or H)^{1,2}. In addition, when the alkyne substrate has at least one α -methyl or α -methylene substituent, η^3 -allyl complexes of the type $[\text{Mn}_2(\mu\text{-PPh}_2)(\eta^3\text{-allyl})(\text{CO})_7]$ are obtained, the formation of which involves a 1,2 hydrogen shift within the ligand². The heterodimetallic complex $[(\eta\text{-C}_5\text{H}_5)_2\text{MoMn}(\mu\text{-H})(\mu\text{-PPh}_2)(\text{CO})_6]$ (2)³ exhibits a dif-

ferent pattern of reactivity. With acetylene itself the major product is $[(\eta\text{-C}_3\text{H}_3)_2\text{MoMn}\{\mu\text{-}\sigma:\eta^4\text{-CHCHCH}_2\text{CHPPh}_2\}(\text{CO})_4]$, the formation of which involves the incorporation of two molecules of the alkyne³. With alkynes having α -methyl or α -methylene substituents (2) gives η^3 -allyl complexes in which the allyl ligand is exclusively bonded to the manganese atom but μ -vinyl complexes, which are formed as major products in the reactions of these alkynes with (1), are not obtained². A further difference between (1) and (2) is that whereas substituted allyl complexes obtained from (1)

are exclusively *syn*, those obtained from (2) exist as a mixture of *syn* and *anti* isomers².



These variations in the reactivity towards alkynes of the dimanganese and molybdenum-manganese complexes suggested that the study of a related dimolybdenum complex would be of interest. Such a complex, $[(\eta\text{-C}_5\text{H}_5)_2\text{Mo}_2(\mu\text{-H})(\mu\text{-PMe}_2)(\text{CO})_4]$ (3), has been synthesised previously⁴ and we now report the results of an investigation of the reaction of (3) with alkynes under photolytic conditions.

Results and discussion

Reactions of (3) with $\text{MeC}\equiv\text{CH}$, $\text{MeC}\equiv\text{CMe}$ and $\text{EtC}\equiv\text{CH}$ under photolysis give, as the major products, the orange μ -vinyl complexes $[(\eta\text{-C}_5\text{H}_5)_2\text{Mo}_2\{\mu\text{-}\sigma\text{:}\eta^2\text{-C}(\text{R}^1)=\text{CHR}^3\}(\mu\text{-PMe}_2)(\text{CO})_3]$ (4) the proposed structures of which are shown in the Scheme. The symmetrical alkyne $\text{MeC}\equiv\text{CMe}$ gives only one such complex, (4c), but the two unsymmetrical alkynes gives isomeric mixtures of products corresponding to the two alternative modes of insertion into the metal-hydrogen bond. In addition to the μ -vinyl complexes low yields of red products are obtained in each case. These have not been fully characterised but they have been identified from their spectroscopic properties as the oxo complexes $[(\eta\text{-C}_5\text{H}_5)_2\text{Mo}_2(\text{O})\{\mu\text{-}\sigma\text{:}\eta^2\text{-C}(\text{R}^1)=\text{CHR}^3\}(\text{CO})]$

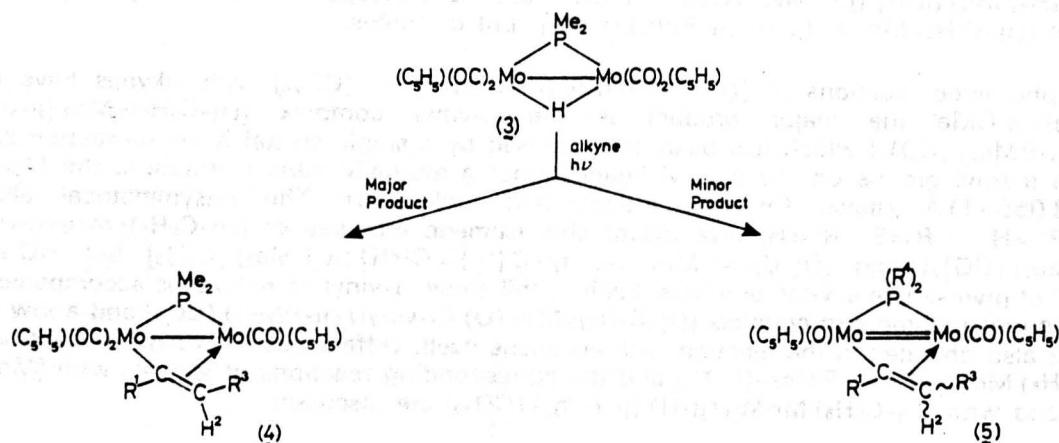
(5) (Scheme). The proposed structures for these complexes are based on that of an analogous complex (5f) ($\text{R}^1=\text{H}$, $\text{R}^3=\text{Ph}$; $\text{R}^4=\text{Ph}$) which is formed in very low yield on reaction of $[(\eta\text{-C}_5\text{H}_5)_2\text{Mo}_2(\text{CO})_4]$ with $\text{Ph}_3\text{P}=\text{CH}_2$ and has previously been characterised by an X-ray diffraction study⁵.

Reaction of C_2H_2 with (3) does not give a μ -vinyl complex analogous to that obtained with (1) or a double insertion product analogous to that obtained with the molybdenum-manganese complex, (2). Instead there is significant decomposition and only the oxo complex (5g) ($\text{R}^1=\text{R}^3=\text{H}$; $\text{R}^4=\text{Me}$) could be isolated from the reaction mixture, again in low yield. No significant reaction took place between $\text{PhC}\equiv\text{CPh}$ and (3); unreacted (3) was recovered in near quantitative yield after photolysis of the reaction mixture for 1.5 h.

The structure of the μ -vinyl complex (4c) has been determined by a single crystal X-ray diffraction study. The crystallographic unit cell contains two independent molecules (A) and (B). Equivalent views onto the Mo (1), Mo (2), P (1) plane of (A) and (B) are shown in Figures 1a and 1b respectively. Selected bond lengths are in Table Ia and inter-bond angles in Table Ib. Atomic coordinates are given in Table II.

The structures of molecules (A) and (B) are very similar, differing mainly in a slight rotation of the cyclopentadienyl ring bonded to Mo (1). The vinyl group in each molecule is linked to Mo (1) via a π -bond [mean Mo (1)–C (2) 2.088 (9) and mean Mo (1)–C (3) 2.328 (12) Å], and to Mo (2) via a σ -bond [means Mo (2)–C (2) 2.325 (9) Å].

The mean dihedral angle between the Mo(1)–Mo(2)–P(1) plane and the Mo(1)–Mo(2)–C(2) plane is 135.4° , which is considerably larger than the value of 124.7° found for the comparable angle in $[\text{Mn}_2\{\mu\text{-}\sigma\text{:}\eta^2\text{-CH}=\text{CH}_2\}(\mu\text{-PPh}_2)(\text{CO})_7]$ ¹. The μ -vinyl ligand is thus more nearly *trans*



Alkyne	Complex
$\text{MeC}\equiv\text{CH}$	(4a) $\text{R}^1 = \text{Me}, \text{R}^3 = \text{H}$
	(4b) $\text{R}^1 = \text{H}, \text{R}^3 = \text{Me}$
$\text{MeC}\equiv\text{CMe}$	(4c) $\text{R}^1 = \text{R}^3 = \text{Me}$
$\text{EtC}\equiv\text{CH}$	(4d) $\text{R}^1 = \text{Et}, \text{R}^3 = \text{H}$
	(4e) $\text{R}^1 = \text{H}, \text{R}^3 = \text{Et}$

[†] see ref 5 and text

Alkyne	Complex
$\text{MeC}\equiv\text{CH}$	(5a) $\text{R}^1 = \text{Me}, \text{R}^3 = \text{H}, \text{R}^4 = \text{Me}$
	(5b) $\text{R}^1 = \text{H}, \text{R}^3 = \text{Me}, \text{R}^4 = \text{Me}$
$\text{MeC}\equiv\text{CMe}$	(5c) $\text{R}^1 = \text{R}^3 = \text{Me}, \text{R}^4 = \text{Me}$
$\text{EtC}\equiv\text{CH}$	(5d) $\text{R}^1 = \text{CH}^a\text{H}^b\text{Me}^c, \text{R}^3 = \text{H}, \text{R}^4 = \text{Me}$
	(5e) $\text{R}^1 = \text{H}, \text{R}^3 = \text{CH}^a\text{H}^b\text{Me}^c, \text{R}^4 = \text{Me}$
—	(5f) $\text{R}^1 = \text{H}, \text{R}^3 = \text{Ph}, \text{R}^4 = \text{Ph}$
$\text{HC}\equiv\text{CH}$	(5g) $\text{R}^1 = \text{R}^3 = \text{H}, \text{R}^4 = \text{Me}$

Scheme 1

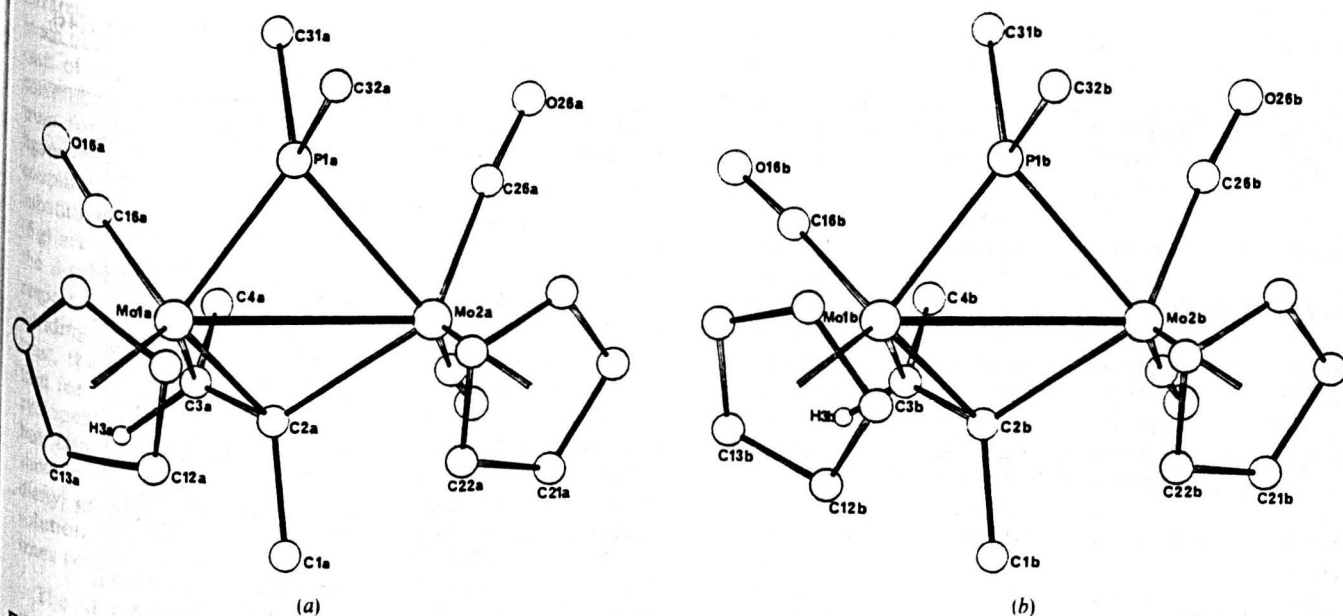


Figure 1. — Molecular structure of (4c) showing the atom numbering scheme for the two independent molecules (a) molecule (A), (b) molecule (B).

Table I (a). — Selected bond lengths (Å) for the two independent molecules of $[(\eta\text{-C}_5\text{H}_5)_2\text{Mo}_2\{\mu\text{-}\sigma\text{-}\eta^2\text{-C}(\text{Me})=\text{CHMe}\}(\mu\text{-PMe}_2)(\text{CO})_3]$ (4c)

	Molecule (A)	Molecule (B)
Mo (1)–Mo (2)	3.052 (1)	3.060 (1)
Mo (1)–P (1)	2.294 (3)	2.306 (3)
Mo (1)–C (2)	2.097 (9)	2.080 (9)
Mo (1)–C (3)	2.328 (12)	2.327 (11)
Mo (1)–C (16)	1.925 (13)	1.910 (11)
Mo (1)–Cp (mean)	2.344 (14)	2.34 (2)
Mo (2)–P (1)	2.509 (3)	2.521 (2)
Mo (2)–C (2a)	2.329 (9)	2.321 (10)
Mo (2)–C (26)	1.907 (12)	1.958 (11)
Mo (2)–C (27)	1.938 (12)	1.953 (10)
Mo (2)–Cp (mean)	2.358 (11)	2.365 (11)
P (1)–C (31)	1.86 (2)	1.839 (13)
P (1)–C (32)	1.87 (2)	1.85 (2)
C (1)–C (2)	1.59 (2)	1.54 (2)
C (2)–C (3)	1.37 (2)	1.388 (13)
C (3)–C (4)	1.48 (2)	1.493 (15)
C (16)–O (16)	1.17 (2)	1.159 (13)
C (26)–O (26)	1.191 (16)	1.131 (13)
C (27)–O (27)	1.172 (15)	1.149 (12)

Table I (b). — Selected bond angles for the two independent molecules of $[(\eta\text{-C}_5\text{H}_5)_2\text{Mo}_2\{\mu\text{-}\sigma\text{-}\eta^2\text{-C}(\text{Me})=\text{CHMe}\}(\mu\text{-PMe}_2)(\text{CO})_3]$ (4c).

	Molecule (A)	Molecule (B)
P (1)–Mo (1)–Mo (2)	53.7 (1)	53.8 (1)
C (2)–Mo (1)–Mo (29)	49.7 (2)	49.3 (3)
C (2)–Mo (1)–P (1)	97.6 (2)	97.8 (3)
C (3)–Mo (1)–C (2)	35.4 (4)	36.2 (3)
C (16)–Mo (1)–Mo (2)	111.8 (3)	114.9 (3)
C (16)–Mo (1)–P (1)	80.3 (4)	84.3 (4)
C (16)–Mo (1)–C (2)	102.5 (4)	103.5 (4)
C (16)–Mo (1)–C (3)	69.0 (5)	68.3 (4)
P (1)–Mo (2)–Mo (1)	47.5 (1)	47.6 (1)
C (2)–Mo (2)–Mo (1)	43.3 (2)	42.8 (2)
C (2)–Mo (2)–P (1)	86.1 (2)	86.1 (2)
C (26)–Mo (2)–Mo (1)	113.4 (4)	113.8 (3)
C (26)–Mo (2)–P (1)	73.8 (4)	73.1 (3)
C (26)–Mo (2)–C (2)	120.9 (5)	123.7 (4)
C (27)–Mo (2)–Mo (1)	105.1 (4)	123.0 (3)
C (27)–Mo (2)–P (1)	120.7 (4)	120.2 (3)
C (27)–Mo (2)–C (2)	67.0 (4)	68.1 (4)
C (27)–Mo (2)–C (26)	77.0 (5)	78.5 (4)
Mo (2)–P (1)–Mo (1)	78.8 (1)	78.5 (1)
C (31)–P (1)–Mo (1)	122.0 (6)	122.0 (6)
C (31)–P (1)–Mo (2)	120.8 (5)	121.2 (4)
C (32)–P (1)–Mo (1)	123.9 (4)	125.2 (5)
C (32)–P (1)–Mo (2)	111.1 (5)	108.8 (4)
C (32)–P (1)–C (31)	100.4 (8)	100.7 (7)
Mo (2)–C (2)–Mo (1)	87.0 (3)	88.0 (4)
C (1)–C (2)–Mo (1)	125.4 (6)	126.1 (7)
C (1)–C (2)–Mo (2)	113.6 (7)	114.8 (7)
C (3)–C (2)–Mo (1)	81.6 (6)	81.6 (6)
C (3)–C (2)–Mo (2)	126.2 (7)	124.0 (7)
C (3)–C (2)–C (1)	116. (1)	116 (1)
C (2)–C (3)–Mo (1)	63.0 (6)	62.2 (5)
C (4)–C (3)–Mo (1)	125 (1)	123.6 (8)
C (4)–C (3)–C (2)	128 (1)	129 (1)
O (16)–C (16)–Mo (1)	179 (1)	175.6 (9)
O (26)–C (26)–Mo (2)	175 (1)	175.1 (8)
O (27)–C (27)–Mo (2)	174 (1)	174.7 (8)

to the phosphido bridge in the Mo_2 complex than in the Mn_2 complex.

The vinyl bond lengths $\text{C}(2)\text{--}\text{C}(3)$ are equal within experimental error for the two independent molecules of (4c) and the mean value of 1.38 (2) Å is not significantly different from the value of 1.396 (4) Å observed in the neutron diffraction study of $[\text{Os}_3(\mu\text{-H})(\mu\text{-}\sigma\text{-}\eta^2\text{-CH}=\text{CH}_2)(\text{CO})_{10}]$.⁶ The methyl groups on the μ -vinyl ligand adopt a *trans* orientation, similar to that of the related bridging ligand in $[\text{Rh}_2(\mu\text{-H})(\mu\text{-}\sigma\text{-}\eta^2\text{-C}(\text{R})=\text{CHR})\{\text{P}(\text{O-}i\text{-C}_3\text{H}_7)_3\}_4]$ ($\text{R}=\text{C}_6\text{H}_4\text{-}p\text{-Me}$ or $\text{R}=\text{Me}$)⁷.

The relatively long mean $\text{Mo}\text{--}\text{Mo}$ bond distance of 3.056 (1) Å in (4c) is in the range observed for $\text{Mo}\text{--}\text{Mo}$ single bonds⁸, but it is ca. 0.2 Å shorter than that found in either the precursor molecule $[(\eta\text{-C}_5\text{H}_5)_2\text{Mo}_2(\mu\text{-H})(\mu\text{-PMe}_2)\text{-}$

Table II. — Fractional atomic coordinates and thermal parameters (\AA^2) for $[(\eta\text{-C}_5\text{H}_5)_2\text{Mo}_2\{\mu\text{-}\sigma\text{:}\eta^2\text{-C}(\text{Me})=\text{CHMe}\}(\mu\text{-PMe}_2)(\text{CO})_3]$ (4c).

Atom	x	y	z	Atom	x	y	z
Mo (1 a)	0.18568 (5)	0.23031 (6)	-0.02352 (5)	Mo (1 b)	0.67791 (5)	0.19047 (6)	0.44989 (5)
Mo (2 a)	0.09541 (5)	0.14707 (6)	-0.18799 (5)	Mo (2 b)	0.56323 (5)	0.18763 (5)	0.27688 (5)
P (1 a)	0.1497 (2)	0.3077 (2)	-0.1455 (2)	P (1 b)	0.7042 (1)	0.2588 (2)	0.3373 (2)
C (1 a)	0.1076 (8)	0.0205 (9)	-0.0240 (9)	C (1 b)	0.4920 (8)	0.1119 (9)	0.4257 (9)
C (2 a)	0.0950 (5)	0.1256 (6)	-0.0531 (5)	C (2 b)	0.5491 (5)	0.1881 (6)	0.4082 (5)
C (3 a)	0.0576 (7)	0.1821 (8)	-0.0093 (8)	C (3 b)	0.5575 (6)	0.2672 (7)	0.4566 (7)
C (4 a)	-0.0212 (9)	0.2343 (13)	-0.0382 (11)	C (4 b)	0.5390 (8)	0.3665 (7)	0.4319 (8)
C (31 a)	0.0788 (11)	0.4101 (11)	-0.1634 (11)	C (31 b)	0.7212 (9)	0.3851 (9)	0.3315 (10)
C (32 a)	0.2255 (9)	0.3453 (9)	-0.2014 (9)	C (32 b)	0.7767 (7)	0.2135 (10)	0.2824 (9)
C (16 a)	0.1255 (7)	0.3336 (9)	0.0050 (7)	C (16 b)	0.7012 (6)	0.3118 (8)	0.4967 (6)
O (16 a)	0.0899 (6)	0.3972 (6)	0.0216 (6)	O (16 b)	0.7187 (5)	0.3828 (6)	0.5294 (5)
C (26 a)	0.0201 (8)	0.2319 (9)	-0.2564 (8)	C (26 b)	0.5688 (6)	0.3010 (7)	0.2147 (6)
O (26 a)	-0.0290 (6)	0.2797 (7)	-0.3026 (6)	O (26 b)	0.5669 (5)	0.3645 (5)	0.1750 (5)
C (27 a)	-0.0114 (7)	0.1074 (8)	-0.1763 (7)	C (27 b)	0.4632 (6)	0.2533 (7)	0.2838 (6)
O (27 a)	-0.0763 (5)	0.0779 (6)	-0.1747 (6)	O (27 b)	0.4012 (4)	0.2887 (5)	0.2823 (5)
C (11 a)	0.3239 (8)	0.1941 (14)	-0.0177 (8)	C (11 b)	0.7290 (14)	0.0350 (10)	0.4565 (9)
C (12 a)	0.2960 (9)	0.1229 (9)	0.0221 (13)	C (12 b)	0.6793 (9)	0.0415 (12)	0.5087 (18)
C (13 a)	0.2793 (8)	0.1619 (16)	0.0894 (10)	C (13 b)	0.7204 (17)	0.1029 (16)	0.5662 (12)
C (14 a)	0.2984 (9)	0.2541 (14)	0.0899 (10)	C (14 b)	0.7898 (14)	0.1337 (12)	0.5505 (11)
C (15 a)	0.3237 (8)	0.2734 (10)	0.0259 (11)	C (15 b)	0.7945 (9)	0.0939 (14)	0.4836 (11)
C (21 a)	0.1229 (7)	-0.0041 (7)	-0.2261 (7)	C (21 b)	0.4841 (8)	0.0575 (8)	0.2208 (8)
C (22 a)	0.2002 (7)	0.0287 (7)	-0.1769 (7)	C (22 b)	0.5570 (8)	0.0189 (7)	0.2723 (8)
C (23 a)	0.2229 (6)	0.1057 (7)	-0.2167 (7)	C (23 b)	0.6243 (7)	0.0470 (7)	0.2427 (7)
C (24 a)	0.1641 (7)	0.1204 (7)	-0.2882 (7)	C (24 b)	0.5920 (7)	0.0998 (8)	0.1719 (7)
C (25 a)	0.0981 (6)	0.0525 (7)	-0.2964 (6)	C (25 b)	0.5032 (8)	0.1070 (8)	0.1580 (7)

(CO)₄] (3)⁸ or $[(\eta\text{-C}_5\text{H}_5)_2\text{Mo}_2(\mu\text{-H})(\mu\text{-PMe}_2)(\text{CO})_3\text{-P}(\text{OMe})_3]$ ⁹, where bridging hydride ligands are present. Although (4c) obeys the 18-electron rule overall, assuming a single, non-dative Mo—Mo bond, Mo (1) is electron poor and Mo (2) is electron rich. The electron imbalance is reflected in the asymmetric bridging of the Mo—Mo bond by the phosphido ligand. The Mo (1)—P distance is *ca.* 0.21 Å shorter than the Mo (2)—P distance, implying that the stronger bond is to the electron-poor metal atom. This compares with a difference in M—P bond distance of *ca.* 0.11 Å in $[\text{Mn}_2\{\mu\text{-}\sigma\text{:}\eta^2\text{-CH}=\text{CH}_2\}(\mu\text{-PPh}_2)(\text{CO})_7]$ ¹ and of only 0.02 Å in (3).

The cyclopentadienyl ligands in molecules (A) and (B) adopt a relative *cis* orientation with respect to the Mo—Mo axis. The mean Mo—C (cyclopentadienyl ligand) distances for Mo (1) and Mo (2) are equal within experimental error [mean for Mo (1) 2.34 (2) and for Mo (2) 2.36 (1) Å].

The Mo (2)—C (26) distance in molecule (A) of 1.907 (12) Å is shorter than the corresponding distance of 1.958 (11) Å in molecule (B). Although this difference is of low significance it may be related to the difference in the C (2)—Mo (2)—C (26) angles in the two molecules [120.9 (5)° for (A) and 123.7 (4)° for (B)]. The larger angle corresponds to the greater Mo (2)—C (26) distance, and is therefore connected with the known high *trans* influence of σ -bonded C-atoms. The carbonyl ligands in molecules (A) and (B) are all essentially linear.

¹H NMR spectra of the complexes (4) suggest that they all possess in solution the structure found for (4c) in the solid state. Thus the spectrum of (4c) exhibits a singlet resonance at δ 2.98 and a doublet at δ 0.48 which may be assigned to Me¹ and Me³ respectively on the μ -vinyl ligand. The doublet is coupled to a quartet at δ 3.23 which may therefore be assigned to H². The presence of two equal cyclopentadienyl resonances and two P-Me resonances indi-

cate the presence of only one isomer of (4c) in solution. In contrast, the ¹H NMR spectra of the major products from reaction of (3) with MeC \equiv CH and EtC \equiv CH show two sets of resonances due to the presence in solution of two isomers in each case *i.e.* (4a)/(4b) and (4d)/(4e) respectively (Scheme). In the spectrum of the product from MeC \equiv CH the more intense set of μ -vinyl resonances, a double doublet at δ 9.02 (H¹), a double quartet at δ 4.07 (H²) and a doublet of relative intensity 3 at δ 0.67 (Me³), may be assigned to complex (4b) with a methyl group on the β -vinyl carbon. The less intense set of resonances, singlets at δ 2.92 (H²) and δ 0.40 (H³) and a singlet of relative intensity 3 at δ 3.05 (Me¹) may be assigned to (4a), in which the methyl group is on the α -vinyl carbon. The ratio of the two isomers (4a):(4b) is *ca.* 2:5. In contrast, the analogous products from reaction of (3) with EtC \equiv CH, (4d) and (4e), are present in a ratio of *ca.* 5:1. The increase in the proportion of the isomer with the alkyl group (Me or Et) on the α -vinyl carbon, on going from R¹=Me to R¹=Et, may be due to the larger steric bulk of the ethyl group favouring the less crowded site on the α -vinyl carbon. Repeated recrystallisation of the isomeric mixture of (4d)+(4e) yielded pure (4d) which crystallised out preferentially, leaving (4e) in solution.

The ¹³CO-{¹H} NMR spectrum of (4a) at 243 K is also consistent with a solution structure for (4a) similar to the solid state structure of (4c). The spectrum, obtained on a sample of (4a) uncontaminated with (4b) [from the reaction of allene with (3)¹⁰ see experimental section], shows the expected three equal intensity carbonyl resonances. The two doublet resonances [²J(PC) 24.2, 23.3 Hz] and the singlet may be assigned respectively, on the basis of the study by Todd *et al.* of ³¹P-¹³C coupling constants in square pyramidal molybdenum complexes¹¹, to two *cis* (relative to PPh₂) and one *trans* carbonyl.

Each of the minor red products, (5a)-(5e) and (5g), obtained in the reactions of (3) with alkynes shows a single

infrared $\nu(\text{CO})$ absorption band, indicating the likely presence of one carbonyl group. Further, the mass spectrum of each of the complexes exhibits a parent molecular ion peak corresponding to the proposed formula. The $^1\text{H NMR}$ spectrum for each complex indicates the presence of a μ -vinyl ligand but it is not possible to determine from the $^1\text{H}-^1\text{H}$ coupling constants whether R^3 , when this group is an alkyl substituent, is *cis* or *trans* to R^1 . The fact that (5a)-(5e) and (5g) are formed on irradiation of the complexes (4) in which the β -substituent, if present, adopts a *trans* orientation with respect to R^1 suggests that the μ -vinyl groups in the corresponding oxo complexes have a similar orientation. In contrast, the X-ray study on (5f) revealed a relative *cis* orientation for R^1 and R^3 .⁵ The X-ray study also showed that the cyclopentadienyl groups in (5f) are *trans* in the solid state, but although the $^1\text{H NMR}$ spectra of (5a)-(5c) and (5g) show in each case only two resonances due to the cyclopentadienyl groups, indicating the presence of only one isomer in solution, it is impossible to deduce whether this has a *cis* or *trans* configuration.

The above results show that the pattern of reactivity of the dimolybdenum complex (3) towards alkynes differs in several respects from that of either the dimanganese complex (1) or the molybdenum-manganese complex (2). Thus whereas allyl complexes are the major products of the reactions of (1) and (2) with alkynes containing α -methyl or α -methylene substituents, such complexes are not found in the reactions of (3) with these alkynes. The mechanism which has been put forward to account for the formation of allyl products in reactions with (1) and (2) involves the oxidative addition of a C-H bond across one of the metal centres, with concomitant loss of a CO ligand, and this presumably takes place more easily at a manganese rather than at a molybdenum centre in this type of compound. Certainly (2) reacts readily under photolytic conditions with $\text{P}(\text{OMe})_3$ to give $[(\eta\text{-C}_5\text{H}_5)_2\text{MoMn}(\mu\text{-H})(\mu\text{-PPh}_2)(\text{CO})_5\text{P}(\text{OMe})_3]$, in which the organophosphite has been shown by an X-ray study to have displaced a CO ligand on the manganese rather than the molybdenum atom.¹² Complexes (1) and (3) [but not (2)] both give μ -vinyl complexes as major products of their reactions with various alkynes, but the stereochemistry of these products is sensitive to the metal combination employed. Thus an X-ray study on $[\text{Mn}_2\{\mu\text{-}\sigma\text{-}\eta^2\text{-C}(\text{Ph})=\text{CHPh}\}(\mu\text{-PPh}_2)(\text{CO})_6(\text{CNBu}^t)]$ shows that the two phenyl groups on the μ -vinyl ligand adopt a relative *cis* orientation, and further X-ray studies on the products of reaction of 2-electron donor ligands with $[\text{Mn}_2\{\mu\text{-C}(\text{Ph})=\text{CHPh}\}(\mu\text{-PPh}_2)(\text{CO})_7]$ indicate a similar stereochemistry for this latter compound.¹³ In contrast the methyl groups on the vinyl ligand in (4c) take up a *trans* configuration. This difference in stereochemistry may be related to greater steric crowding in the dimolybdenum system although it has been noted previously that, even in mononuclear vinyl complexes, *cis/trans* stereochemistry shows a delicate dependence on the identity of the metal, oxidation state, auxiliary ligands and the nature of the substituents on the alkyne.¹⁴ The factors involved in determining μ -vinyl stereochemistry in the dinuclear systems are expected to be even more complex.

The lack of reaction of (1) with $\text{PhC}\equiv\text{CPh}$ may be due to steric crowding in the insertion step but the same explanation cannot account for the failure to isolate a simple μ -vinyl product in the reaction of (1) with acetylene itself. Certainly a rapid reaction takes place and it seems likely that a μ -vinyl compound is formed in the first instance but that the facile

insertion of a second molecule of acetylene into the Mo-C σ -bond gives more complex products which are not stable under the conditions of the reaction. Such a double insertion has been observed in the reaction of acetylene with (2)¹⁵, and carbon-carbon bond forming reactions involving the coupling of alkynes at a dimolybdenum centre are well known.¹⁶ Similar double insertions have been observed for complexes of other metals.¹⁷

The formation of the red oxo products, (5a)-(5e) and (5g), in the reactions of (3) with alkynes probably arises via the decomposition of the initially formed μ -vinyl complexes (4). In accord with this suggestion (4a)-(4e) do decompose under UV irradiation to give low yields of (5a)-(5e). Traces of atmospheric oxygen are presumably the source of the oxo ligand. Indeed in a related study we have shown that $[(\eta\text{-C}_5\text{H}_5)_2\text{Mo}_2(\mu\text{-PPh}_2)_2(\text{CO})_2]$ is quantitatively oxidised by air to $[(\eta\text{-C}_5\text{H}_5)_2\text{Mo}_2(\mu\text{-PPh}_2)_2(\text{O})\text{CO}]$ ¹⁸.

Experimental

Details of experimental procedures and of the instrumentation used to obtain spectroscopic data have been given in Part I of this series.⁹ The complex $[(\eta\text{-C}_5\text{H}_5)_2\text{Mo}_2(\mu\text{-H})(\mu\text{-PMe}_2)(\text{CO})_4]$ (3) was prepared by the literature method.⁴ All other reagents were obtained from the usual commercial suppliers and used without further purification.

REACTIONS OF ALKYNES WITH (3)

a) With $\text{MeC}\equiv\text{CH}$. - Complex (3) (0.2 g, 0.4 mmol) was dissolved in 30:1 hexane:benzene (50 mL) and irradiated with UV light (Hanovia 125 w medium pressure lamp) for 1.25 h in the presence of $\text{MeC}\equiv\text{CH}$ (excess, bubbled slowly into solution). The solvent was removed on a rotary evaporator and the residue, after being dissolved in the minimum of CH_2Cl_2 , was applied to the base of t.l.c. plates. Elution with hexane:ethyl acetate (19:1) and evaporation of the solvent gave unreacted (3) (0.045 g, 23%), an inseparable mixture of orange $[(\eta\text{-C}_5\text{H}_5)_2\text{Mo}_2\{\mu\text{-}\sigma\text{-}\eta^2\text{-C}(\text{Me})=\text{CH}_2\}(\mu\text{-PMe}_2)(\text{CO})_3]$ (4a) and $[(\eta\text{-C}_5\text{H}_5)_2\text{Mo}_2\{\mu\text{-}\sigma\text{-}\eta^2\text{-CH}=\text{CHMe}\}(\mu\text{-PMe}_2)(\text{CO})_3]$ (4b) (combined yield 0.105 g, 52%), red $[(\eta\text{-C}_5\text{H}_5)_2\text{Mo}_2(\text{O})(\mu\text{-}\sigma\text{-}\eta^2\text{-C}(\text{Me})=\text{CH}_2)(\mu\text{-PMe}_2)(\text{CO})]$ (5a) (0.005 g) and red $[(\eta\text{-C}_5\text{H}_5)_2\text{Mo}_2(\text{O})(\mu\text{-}\sigma\text{-}\eta^2\text{-CH}=\text{CHMe})(\mu\text{-PMe}_2)(\text{CO})]$ (5b) (0.005 g) isomeric mixture of (4a) and (4b) mass spectrum m/e 508 (M^+), $M^+-n\text{CO}$ ($n=1-3$); $\nu_{\text{max}}(\text{CO})(n\text{-hexane})$ at 1954 s, 1949 s, 1884 s, 1874 s, 1868 s cm^{-1} . NMR (^1H , CDCl_3) (Ratio (4a):(4b), 2:5) (4a) δ 5.17 [s, 5H, C_5H_5], 5.11 [s, 5H, C_5H_5], 3.05 [s, 3H, Me^a], 2.92 [s, 1H, H^2], 1.98 [d, $^2\text{J}(\text{PH})$ 9.1, 3H, PMe^aMe^b], 1.80 [d, $^2\text{J}(\text{PH})$ 9.7, 3H, PMe^aMe^b], 0.40 [s, 1H, H^3]; (4b) δ 9.02 [dd, J_{12} 8.3, $^3\text{J}(\text{PH})$ 2.0, 1H, H^1], 5.20 [s, 5H, C_5H_5], 5.10 [s, 5H, C_5H_5], 4.07 [dq, J_{23} 5.9, $^3\text{J}(\text{PH})$ 1.0, 1H, H^2], 1.98 [d, $^2\text{J}(\text{PH})$ 9.0, 3H, PMe^aMe^b], 1.70 [d, $^2\text{J}(\text{PH})$ 9.8, 3H, PMe^aMe^b], 0.67 [d, 3H, Me^3]. Complex (5a): mass spectrum m/e 468 (M^+), $M^+-\text{CO}$; $\nu_{\text{max}}(\text{CO})(n\text{-hexane})$ at 1863 cm^{-1} . NMR (^1H , CDCl_3) δ 5.63 [d, $^3\text{J}(\text{PH})$ 0.7, 5H, C_5H_5], 4.85 [d, $^3\text{J}(\text{PH})$ 1.1, 5H, C_5H_5], 2.96 [s, 1H, H^2] 2.71 [s, 3H, Me^1], 2.24 [s, 1H, H^3], 2.05 [d, $^2\text{J}(\text{PH})$ 10.8, 3H, PMe^aMe^b], 1.80 [d, $^2\text{J}(\text{PH})$ 9.7, 3H, PMe^aMe^b]. Complex (5b): mass spectrum: m/e 468 (M^+), $M^+-\text{CO}$; $\nu_{\text{max}}(\text{CO})(n\text{-hexane})$ at 1878 cm^{-1} . NMR (^1H , CDCl_3) δ 8.13 [d, J_{12} 9.2, 1H, H^1], 5.49 [d, $^3\text{J}(\text{PH})$ 0.9, 5H, C_5H_5], 4.76 [d, $^3\text{J}(\text{PH})$ 1.2, 5H, C_5H_5], 3.17 [ddd, J_{23} 6.1, $^3\text{J}(\text{PH})$ 0.6, 1H, H^2], 2.07 [d, $^2\text{J}(\text{PH})$ 2.0, 3H, PMe^aMe^b], 1.94 [d, $^2\text{J}(\text{PH})$ 1.0, 3H, PMe^aMe^b], 1.80 [d, 3H, Me^3].

b) With $\text{MeC}\equiv\text{CMe}$. - In an analogous procedure to that in (a) above a solution of complex (3) (0.2 g, 0.4 mmol) in 30:1 hexane:benzene (50 mL) was photolysed with $\text{MeC}\equiv\text{CMe}$ (large excess). Separation by t.l.c. as in (a) gave unreacted (3) (0.04 g, 20%) orange crystalline (4c) (0.102 g, 49%) and red (5c) (0.005 g). Complex (4c) (Found: C, 43.0; H, 4.3; P, 5.1. $\text{C}_{19}\text{H}_{23}\text{Mo}_2\text{O}_3\text{P}$ requires C, 43.7; H, 4.4; P, 5.9%): mass spectrum 522 (M^+), $M^+-n\text{CO}$ ($n=1-3$); $\nu_{\text{max}}(\text{CO})(n\text{-hexane})$ at 1946 s, 1878 s, 1870 s.

NMR (^1H , CDCl_3) δ 5.23 [s, 5H, C_5H_5], 5.09 [s, 5H, C_5H_5], 3.23 [q, $J_{2,3}$ 6.1, 1H, H^2], 2.98 [s, 3H, Me^1], 1.94 [d, $^2J(\text{PH})$ 8.9, 3H, $\text{PMe}^{\wedge}\text{Me}^{\text{B}}$], 1.66 [d, $^2J(\text{PH})$ 9.7, 3H, $\text{PMe}^{\wedge}\text{Me}^{\text{B}}$], 0.48 [d, 3H, Me^3]. Complex (5c) mass spectrum: 482 (M^+), M^+-CO ; $\nu_{\text{max}}(\text{CO})(n\text{-hexane})$ at 1859 cm^{-1} . NMR (^1H , CDCl_3) δ 5.17 [d, $^3J(\text{PH})$ 0.6, 5H, C_5H_5], 4.92 [d, $^3J(\text{PH})$ 1.4, 5H, C_5H_5], 3.20 [d, $^4J(\text{PH})$ 0.9, 3H, Me^1], 2.10 [d, $^2J(\text{PH})$ 10.1, 3H, $\text{PMe}^{\wedge}\text{Me}^{\text{B}}$], 2.01 [d, $^2J(\text{PH})$ 10.8, 3H, $\text{PMe}^{\wedge}\text{Me}^{\text{B}}$], 1.84 [obscured, H^2], 1.74 [d, $J_{2,3}$ 6.3, 3H, Me^3].

c) With $\text{EtC}\equiv\text{CH}$. — In an analogous procedure to that in (a) above a solution of (3) (0.2 g, 0.4 mmol) was photolysed with $\text{EtC}\equiv\text{CH}$ (large excess). Separation by t.l.c. as in (a) gave unreacted (3) (0.06 g, 30%), an inseparable mixture of orange (4d) and (4e) (combined yield 0.085 g, 41%), red (5d) (0.002 g) and red (5e) (0.002 g). Isomeric mixture of (4d) and (4e) (Found: C, 43.2; H, 4.5; P, 6.5 $\text{C}_{19}\text{H}_{23}\text{Mo}_2\text{O}_3\text{P}$ requires C, 43.7; H, 4.4; P, 5.9%): mass spectrum m/e 522 (M^+), $\text{M}^+-n\text{CO}(n=1,2)$; $\nu_{\text{max}}(\text{CO})(n\text{-hexane})$ at 1953 s, 1950 s, 1884 s, 1882 s, 1873 s, 1865 s cm^{-1} . NMR (^1H , CDCl_3) (Ratio (4d):(4e), 5:1) (4d) δ 5.17 [s, 5H, C_5H_5], 5.09 [s, 5H, C_5H_5], 3.30 [dq, J_{ab} 14.0, J_{ac} 7.3, 1H, H^q], 3.05 [s, 1H, H^2], 2.82 [dq, J_{bc} 7.3, 1H, H^p], 1.98 [d, $^2J(\text{PH})$ 9.1, 3H, $\text{PMe}^{\wedge}\text{Me}^{\text{B}}$], 1.81 [d, $^2J(\text{PH})$ 9.6, 3H, $\text{PMe}^{\wedge}\text{Me}^{\text{B}}$], 1.66 [t, 3H, Me^r], 0.42 [s, 3H, H^3]; (4e) δ 9.30 [dd, J_{12} 8.3, $^3J(\text{PH})$ 2.2, 1H, H^1], 5.20 [s, 5H, C_5H_5], 5.09 [s, 5H, C_5H_5], 1.98 [d, 3H, $\text{PMe}^{\wedge}\text{Me}^{\text{B}}$], 1.81 [d, 3H, $\text{PMe}^{\wedge}\text{Me}^{\text{B}}$], 1.06 [t, J_{ac} 7.2, 3H, Me^r]. Complex (5d): mass spectrum m/e 482 (M^+), M^+-CO ; $\nu_{\text{max}}(\text{CO})(n\text{-hexane})$ at 1862 cm^{-1} . NMR (^1H , CDCl_3) δ 5.21 [d, $^3J(\text{PH})$ 0.7, 5H, C_5H_5], 4.94 [d, $^3J(\text{PH})$ 1.6, 5H, C_5H_5], 3.20 [dq, J_{ab} 18.9, J_{ac} 7.4, 1H, H^q], 3.15 [s, 1H, H^2], 2.53 [dq, J_{bc} 7.4, 1H, H^p], 2.14 [d, $^2J(\text{PH})$ 10.1, 3H, $\text{PMe}^{\wedge}\text{Me}^{\text{B}}$], 2.06 [d, $^2J(\text{PH})$ 10.5, 3H, $\text{PMe}^{\wedge}\text{Me}^{\text{B}}$], 2.00 [s, 1H, H^3], 1.90 [t, 3H, Me^r]. Complex (5e): mass spectrum m/e 482 (M^+), M^+-CO ; $\nu_{\text{max}}(\text{CO})$ at 1879 cm^{-1} . NMR (^1H , CDCl_3) δ 8.17 [d, J_{12} 9.1, 1H, H^1], 5.48 [d, $^3J(\text{PH})$ 0.8, 5H, C_5H_5], 4.74 [d, $^3J(\text{PH})$ 1.1, 5H, C_5H_5], 3.05 [dt, J_{2a} 6.6, J_{2b} 6.1, 1H, H^2], 2.11 [dq, J_{ab} 13.3, J_{ac} 7.3, 1H q], 2.02 [d, $^2J(\text{PH})$ 1.7, 3H, $\text{PMe}^{\wedge}\text{Me}^{\text{B}}$], 1.98 [s, 3H, $\text{PMe}^{\wedge}\text{Me}^{\text{B}}$], 1.66 [dq, J_{bc} 7.3, 1H, H^p], 1.22 [t, 3H, Me^r].

d) With C_2H_2 . — In an analogous procedure to that in (a) above a solution of (3) (0.2 g, 0.4 mmol) was photolysed with C_2H_2 (large excess bubbled through solution) to give a cloudy brown solution. The only product isolated in significant yield was (5g). Complex (5g): mass spectrum m/e 454 (M^+), M^+-CO ; $\nu_{\text{max}}(\text{CO})(n\text{-hexane})$ at 1863 cm^{-1} . NMR (^1H , CDCl_3) δ 9.04 [ddd, $J_{1,2}$ 9.9, $J_{1,3}$ 8.7, $^3J(\text{PH})$ 1.5, 1H, H^1], 5.19 [s, 5H, C_5H_5], 4.93 [d, $^3J(\text{PH})$ 1.5, 5H, C_5H_5], 3.48 [dd, $^3J(\text{PH})$ 1.0, 1H, H^2], 2.14 [d, $^2J(\text{PH})$ 10.1, 3H, $\text{PMe}^{\wedge}\text{Me}^{\text{B}}$], 2.03 [d, $^2J(\text{PH})$ 10.7, 3H, $\text{PMe}^{\wedge}\text{Me}^{\text{B}}$], 1.53 [d, 1H, H^3].

REACTION OF ALLENE WITH (3)

Complex (3) (0.2 g, 0.4 mmol) was dissolved in 1:1 hexane:benzene (60 mL) and a small excess (*ca.* x2) of allene was bubbled into the solution. After UV irradiation for 3 h. the solvent was removed on a rotary evaporator and the residue redissolved in the minimum of CH_2Cl_2 . Column chromatography (10 \times 1.5 cm) on Florisil (60-100 mesh) using 3:1 hexane: CH_2Cl_2 as eluant gave unreacted (3) (0.12 g, 60%). The remaining products were separated by t.l.c. using hexane:ethylacetate (9:1) as eluant to give (4a) (0.045 g, 22%) and red [(C_5H_5) $_2\text{Mo}_2(\mu\text{-PMe}_2)(\eta^3\text{-C}_3\text{H}_5)(\text{CO})_3$] 18 together with 0.005 g combined yield of at least three other products. Complex (4a) (Found: C, 42.1; H, 4.4. $\text{C}_{18}\text{H}_{21}\text{Mo}_2\text{O}_3\text{P}$ requires C, 42.5; H, 4.1%) $\nu_{\text{max}}(\text{CO})(n\text{-hexane})$ at 1949 s, 1884 s, 1874 cm^{-1} . NMR [^1H spectrum already given under (a) above]: $^{13}\text{C}(\text{CD}_2\text{Cl}_2, 243 \text{ K})$ δ 239.5 [s, 1CO(*trans*)], 238.6 [d, $^2J(\text{PC})$ 24.2 1CO(*cis*)], 236.8 [d, $^2J(\text{PC})$ 23.3, 1CO(*cis*)] 169.9 [d, $^2J(\text{PC})$ 8.9, C(Me) CH_2], 92.8 [s, C_5H_5], 92.4 [s, C_5H_5], 51.6 [s, C(Me) CH_2], 42.6 [s, C(Me) CH_2], 30.9 [d, $^1J(\text{PC})$ 15.2, $\text{PMe}^{\wedge}\text{Me}^{\text{B}}$], 24.6 [d, $^1J(\text{PC})$ 30.6, $\text{PMe}^{\wedge}\text{Me}^{\text{B}}$].

X-RAY SINGLE CRYSTAL STRUCTURE ANALYSIS OF (4c)

Crystals of (4c) were grown by slow evaporation of hexane/ CH_2Cl_2 solution.

Crystal data for [$\text{Mo}_2(\text{C}_4\text{H}_7)(\mu\text{-PMe}_2)(\text{CO})_3(\text{C}_5\text{H}_5)_2$] (4c) — $\text{C}_{19}\text{H}_{23}\text{Mo}_2\text{O}_3\text{P}$, $M=522.16$, Monoclinic, $a=16.742(3)^\circ$, $b=14.331(3)$, $c=17.100(3)^\circ$, $\beta=105.70(2)^\circ$ (by least squares refinement on diffractometer angles for 25 automatically centred reflections) 19 , $V=3949.75 \text{ \AA}^3$, space group $P2_1/C$ (No. 14), $Z=8$, $D_c=1.756 \text{ g cm}^{-3}$. A burgundy red crystal of size $0.17 \times 0.21 \times 0.23 \text{ mm}$, $\mu(\text{Mo-K}\alpha)=12.24 \text{ cm}^{-1}$, $F(000)=2080$. Blocked full matrix refinement of the atomic parameters, (anisotropic thermal parameter for all non-hydrogen atoms), using 4875 reflections with $I>3\sigma(I)$, $[3<\theta<25^\circ]$ lead to a satisfactory final value of $R=0.0591$ and $R_w=0.0606$.

Acknowledgment

We thank Dr. A. G. Kent for valuable discussion and the S.E.R.C. and BP Chemicals Limited for financial support.

REFERENCES

- 1 Iggo J. A., Mays M. J., Raithby P. R., Henrick K., *J. Chem. Soc., Dalton Trans.*, 1983, 205.
- 2 Horton A. D., Kemball A. C., Mays M. J., *J. Chem. Soc., Dalton Trans.* (submitted for publication).
- 3 Horton A. D., Mays M. J., Raithby P. R., *J. Chem. Soc., Chem. Commun.*, 1987, 247.
- 4 Hayter R. G., *J. Am. Chem. Soc.*, 1963, **85**, 3120.
- 5 Endrich K., Korswagen R., Zahn T., Ziegler M. L., *Angew. Chem., Int. Ed. Engl.*, 1982, **21**, 919.
- 6 Orpen A. G., Pippard D. A., Sheldrick G. M., Rouse K. D., *Acta Cryst.*, 1978, **B34**, 2466.
- 7 Burch R. R., Shusterman A. J., Muetterties E. L., Teller R. G., Williams J. M., *J. Am. Chem. Soc.*, 1983, **105**, 3546.
- 8 Petersen J. L., Stewart R. P., *Inorg. Chem.*, 1980, **19**, 186.
- 9 Horton A. D., Henrick K., Mays M. J., McPartlin M., *J. Chem. Soc., Dalton Trans.*, 1988, 1083.
- 10 Horton A. D., Mays M. J., Raithby P. R., *Polyhedron*, 1988 (in press).
- 11 Todd L. J., Wilkinson J. R., Hickley J. P., Beach D. L., Barnett K. W., *J. Organomet. Chem.*, 1978, **154**, 151.
- 12 Horton A. D., Mays M. J., Raithby P. R., *J. Chem. Soc., Dalton Trans.*, 1987, 1557.
- 13 Henrick K., McPartlin M., Iggo J. A., Kemball A. C., Mays M. J., Raithby P. R., *J. Chem. Soc., Dalton Trans.*, 1987, 2669.
- 14 Otsuka S., Nakamura A., *Adv. Organometal. Chem.*, 1976, **14**, 249.
- 15 Horton A. D., Mays M. J., Raithby P. R., *J. Chem. Soc., Chem. Commun.*, 1985, 247.
- 16 Knox S. A. R., Stansfield R. F. D., Stone F. G. A., Winter M. J., Woodward P., *J. Chem. Soc., Dalton Trans.*, 1982, 173.
- 17 Eshtiagh-Hosseini H., Nixon J. F., Poland J. S., *J. Organomet. Chem.*, 1979, **164**, 107.
- 18 Horton A. D., *Ph. D. Thesis*, Cambridge, 1985.
- 19 Cooper M. K., Guerny P. J., McPartlin M., *J. Chem. Soc., Dalton Trans.*, 1982, 757.
- 20 Sheldrick G. M., SHELX 76 program for crystal structure determination, University of Cambridge, 1976.
- 21 For Part 1, see ref. 9 .

Journal of Organometallic Chemistry, 379 (1989) C1–C4
 Elsevier Sequoia S.A., Lausanne – Printed in The Netherlands
 JOM 20472PC

Preliminary communication

Isomeric clusters differing only in the orientation of a bidentate ligand; synthesis and crystal structures of two isomers of $[\text{HRu}_5\text{C}(\text{CO})_{14}(\text{C}_5\text{H}_4\text{N})]$

Gráinne Conole, Mary McPartin *, and Harold R. Powell

School of Chemistry, The Polytechnic of North London, Holloway Road, London N7 8DB (U.K.)

Tom Dutton, Brian F.G. Johnson and Jack Lewis *

University Chemical Laboratories, Lensfield Road, Cambridge, CB2 1EW (U.K.)

(Received September 11th, 1989)

Abstract

An X-ray diffraction study has confirmed that reaction of $[\text{Ru}_5\text{C}(\text{CO})_{15}]$ (1) with an excess pyridine gives an equimolar mixture of two isomers of $[\text{HRu}_5\text{C}(\text{CO})_{14}(\text{C}_5\text{H}_4\text{N})]$ (2a and 2b) that differ only in the orientation of a bridging ligand, along with a third minor product $[\text{HRu}_5\text{C}(\text{CO})_{13}(\text{C}_5\text{H}_4\text{N})(\text{C}_5\text{H}_5\text{N})]$ (3); 2a and 2b undergo quantitative thermal decarbonylation to give the same unstable product $[\text{HRu}_5\text{C}(\text{CO})_{13}(\text{C}_5\text{H}_4\text{N})]$ (4), which can be recarbonylated quantitatively under mild conditions to regenerate equal proportions of the isomers 2a and 2b.

Metal cluster isomers are relatively rare in the solid state but several have now been structurally characterised. These have previously involved different sites for hydride or other monodentate ligands [1–3], alternative metal framework polyhedra [3], or isomerism of an organo ligand [4].

An X-ray structural study of $[\text{HRu}_5\text{C}(\text{CO})_{14}(\text{C}_5\text{H}_4\text{N})]$ (2) * shows cluster isomers differing only in the orientation of a bridging ligand (Fig. 1), and provides the

* Crystal data for 2a: $\text{C}_{20}\text{H}_5\text{NO}_{14}\text{Ru}_5$, $M = 988.06$, monoclinic, space group $P2_1/c$, a 8.864(2), b 17.962(5), c 17.200(5) Å, β 95.84(3)°, U 2724.29 Å³, $F(000) = 1856$, $\mu(\text{Mo-K}\alpha)$ 25.21 cm⁻¹, $Z = 4$, D_c 2.41 g cm⁻³, $R = 0.0281$ for 3995 reflections with $I/\sigma(I) > 3.0$.

Crystal data for 2b: $\text{C}_{20}\text{H}_5\text{NO}_{14}\text{Ru}_5$, $M = 988.06$, triclinic, space group $P\bar{1}$ (No. 2), a 19.095(5), b 17.870(5), c 9.479(3) Å, α 97.86(3), β 106.52(4), γ 63.02(2)°, U 2763.39 Å³, $F(000) = 1856$, $\mu(\text{Mo-K}\alpha)$ 24.86 cm⁻¹, $Z = 4$, D_c 2.37 g cm⁻³, $R = 0.0436$ for 4140 reflections with $I/\sigma(I) > 3.0$.

Data were collected for both compounds in the θ -range 3–25° with a scan width of 0.80°. The H ligands in isomer 2a and in both molecules of 2b were located directly by difference-Fourier syntheses ($\sin \theta < 0.35$), and evidence for their positions were also obtained from potential energy minimization calculations [8] and examination of computed space filling models. Confirmation of the N-atom sites in the two isomers was obtained by reversal of the assignment of the coordinated N-atom and C-atom in each structure, which gave unreasonable thermal parameters on refinement.

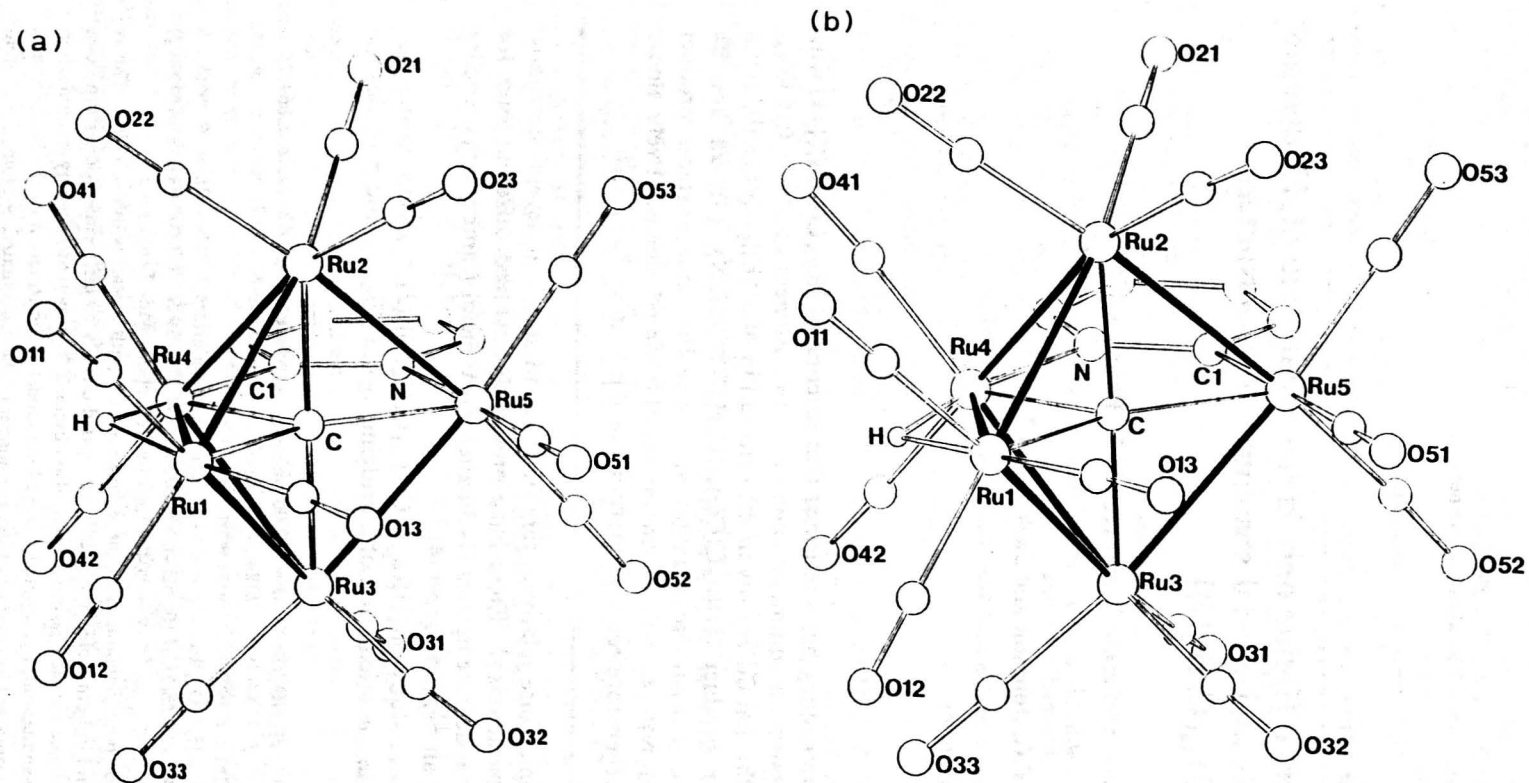


Fig. 1. Structures of the two isomers of $[\text{HRu}_5\text{C}(\text{CO})_{14}(\text{C}_5\text{H}_4\text{N})]$; (a) isomer **2a**; (b) one molecule of isomer **2b**. Principal bond lengths (\AA) for isomer **2a** with the corresponding mean values for the two independent molecules of isomer **2b** in parentheses: Ru(1)–Ru(2) 2.877(1) (2.860(2)), Ru(1)–Ru(3) 2.882(1) (2.858(2)), Ru(1)–Ru(4) 2.895(1) (2.833(2)), Ru(2)–Ru(4) 2.833(1) (2.819(2)), Ru(2)–Ru(5) 2.876(1) (2.896(2)), Ru(3)–Ru(4) 2.823(1) (2.809(1)), Ru(3)–Ru(5) 2.876(1) (2.899(2)), Ru–N 2.169(4) (2.134(12)), Ru–C(1) 2.080(5) (2.131(15)). Non-bonded contacts (\AA): Ru(1)–Ru(5) 4.05 (4.05), Ru(2)–Ru(3) 3.94 (3.95), Ru(4)–Ru(5) 3.57 (3.59).

first example of this type of isomerism in the solid state. The metal framework in each isomer may be described as a bridged 'butterfly' or as arachno-pentagonal bipyramidal, an expected structure for a 76 electron cluster ($S = 8$). [5] The hydride ligand bridges the Ru(1)–Ru(4) hinge bond in both compounds, and the Ru(4)...Ru(5) unbonded edge is bridged by the orthometallated pyridine via the nitrogen atom and the deprotonated carbon atom. Essentially, the two new ruthenium isomers differ only in the orientation of this aromatic ligand; in isomer **2a** the nitrogen atom is bonded to the bridging metal (Ru(5)–N 2.169(4) Å), whereas in isomer **2b** it is bonded to the hinge ruthenium atom (Ru(4)–N 2.134(12) Å). This difference has a large effect on the chemical shift of the hydride in the ^1H NMR spectrum* which in **2a** is approximately 5 ppm upfield from that in **2b**.

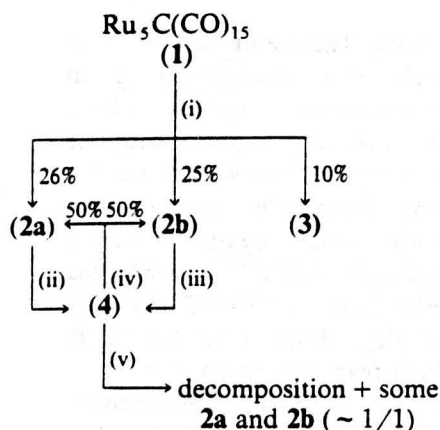
The structure of isomer **2a** is essentially similar to that reported for the osmium analogue $[\text{HO}_5\text{C}(\text{CO})_{14}(\text{C}_5\text{H}_4\text{N})]$, for which no evidence of a second isomer has been observed so far [6].

Lengthening of metal–metal bonds bridged by μ -hydride ligands is a feature of many cluster compounds [2,7,8]. This is observed in isomer **2a**, in which the hydrido-bridged bond (Ru(1)–Ru(4) 2.895(1) Å) is the longest in the structure. In contrast, in isomer **2b** the equivalent 'hinge' bond, which is also hydrido-bridged, is much shorter in both independent molecules (mean 2.833(2) Å), the longest Ru–Ru bonds in this structure being those from the 'wing-tip' spanning ruthenium atom (mean lengths Ru(5)–Ru(2) 2.896(2) and Ru(5)–Ru(3) 2.899(2) Å). Relatively short H-bridged M–M distances have been observed previously; for example the μ -H edge in $[\text{Os}_8\text{H}(\text{CO})_{22}]^-$ (Os–Os 2.848(1) Å) and the μ_3 -H face in $[\text{Os}_8\text{H}(\text{CO})_{22}]^-$ (mean Os–Os 2.787 Å) [9].

Both isomers **2a** and **2b** are converted quantitatively (as determined by IR) to $[\text{HRu}_5\text{C}(\text{CO})_{13}(\text{C}_5\text{H}_4\text{N})]$ (**4**) on prolonged heating in heptane (Scheme 1). However, the decarbonylation of **2a** is twice as fast as that of **2b**, indicating a greater kinetic stability for isomer **2b**. When kept at room temperature in heptane solution in air, **4** decomposes to give a mixture that includes small but equimolar amounts of **2a** and **2b**. Treatment of a hot solution of **4** for 10 min with CO regenerates **2a** and **2b** in equimolar proportions and no other detectable products, indicating that this reaction is kinetically controlled.

The reaction of pentanuclear clusters with pyridine and its derivatives provides interesting scope for further investigation. There are parallels to the types of

* Selected spectroscopic data (IR in hexane, NMR in CDCl_3 (**2a**) or CD_2Cl_2 (**2b**, **3**, **4**), coupling constants in Hz, all ^1H unless stated otherwise. Compound **2a**: IR: $\nu(\text{CO})$ 2099m, 2072s, 2055vs, 2029m, 2016s, 2006m, 1999m, 1991w, 1967m, 1937vw cm^{-1} ; ^1H NMR: –25.83 (s), 6.46 (dt, $^3J(\text{H}-\text{H})$ 5.8, $^4J(\text{H}-\text{H})$ 1.7), 6.87 (dt, $^3J(\text{H}-\text{H})$ 7.5, $^4J(\text{H}-\text{H})$ 1.7), 7.28 (dd, $^3J(\text{H}-\text{H})$ 7.5, $^4J(\text{H}-\text{H})$ 1.7), 8.42 (dd, $^3J(\text{H}-\text{H})$ 5.8, $^4J(\text{H}-\text{H})$ 1.7). Compound **2b**: IR: $\nu(\text{CO})$ 2099m, 2072s, 2055vs, 2029m, 2016s, 2006m, 1999m, 1991w, 1967m, 1937vw cm^{-1} ; ^1H NMR: –20.90 (s), 6.42 (dt, $^3J(\text{H}-\text{H})$ 5.7, $^4J(\text{H}-\text{H})$ 1.8), 6.83 (dt, $^3J(\text{H}-\text{H})$ 7.8, $^4J(\text{H}-\text{H})$ 1.8), 7.45 (dd, $^3J(\text{H}-\text{H})$ 7.8, $^4J(\text{H}-\text{H})$ 1.8), 8.22 (dd, $^3J(\text{H}-\text{H})$ 5.7, $^4J(\text{H}-\text{H})$ 1.8). For **2a**, peak intensity of 2016 > 2072 cm^{-1} and 2006 > 1999 cm^{-1} ; for **2b**, 2072 > 2016 cm^{-1} and 2006 > 1999 cm^{-1} . Compound **3**: IR: $\nu(\text{CO})$ 2092m, 2058s, 2039vs, 2021m, 2007m, 1996w, 1978vw, 1971w cm^{-1} ; ^1H NMR: –21.56 (br s), 7.06 (m), 7.49 (m, 2H), 8.20 (m). Compound **4**: IR: $\nu(\text{CO})$ 2087m, 2052s, 2044s, 2031s, 2010sh, 2000m, 1993m, 1969m, 1957w cm^{-1} ; ^1H NMR: –21.31 (s), 6.44 (dt, $^3J(\text{H}-\text{H})$ 5.8, $^4J(\text{H}-\text{H})$ 1.5), 6.85 (dt, $^3J(\text{H}-\text{H})$ 7.5, $^4J(\text{H}-\text{H})$ 1.5), 7.87 (dd, $^3J(\text{H}-\text{H})$ 5.8, $^4J(\text{H}-\text{H})$ 1.5), 8.84 (dd, $^3J(\text{H}-\text{H})$ 7.5, $^4J(\text{H}-\text{H})$ 1.5), 7.5–7.6 (m, 3H, $\text{C}_5\text{H}_5\text{N}$), 8.0–8.1 (m, 2H, $\text{C}_5\text{H}_5\text{N}$).



Scheme 1. Reactions of $[\text{Ru}_5\text{C}(\text{CO})_{15}]$ (1) with pyridine: (i) excess pyridine, CH_2Cl_2 , 40°C , 5 h; (ii) 98°C , heptane, 24 h; (iii) 98°C , heptane, 48 h; (iv) $\text{CO}(\text{g})$, heptane, 80°C , 10 min; (v) air, heptane, ambient temperature, several days.

bonding and reactivity observed in the reactions of trinuclear analogues, but the pentanuclear clusters have a greater flexibility in terms of metal core rearrangement.

References

- 1 M. McPartlin and W.J.H. Nelson, *J. Chem. Soc., Dalton Trans.*, (1986) 1557.
- 2 M. Green, D.R. Hankey, M. Murray, A.G. Orpen and F.G.A. Stone, *J. Chem. Soc., Chem. Commun.*, (1981) 689.
- 3 K. Henrick, B.F.G. Johnson, J. Lewis, J. Mace, M. McPartlin and J. Morris, *J. Chem. Soc., Chem. Commun.*, (1985) 1617.
- 4 E. Boyar, A.J. Deeming, M.S.B. Felix, S.E. Kabir, T. Adatia, R. Bhusate, M. McPartlin and H.R. Powell, *J. Chem. Soc., Dalton Trans.*, (1989) 5.
- 5 K. Wade, *Adv. Inorg. Chem. Radiochem.*, 18 (1976) 1; M. McPartlin, *Polyhedron*, 3 (1984) 1279.
- 6 P.F. Jackson, B.F.G. Johnson, J. Lewis, W.J.H. Nelson and M. McPartlin, *J. Chem. Soc., Dalton Trans.*, (1982) 2099.
- 7 For example, R.G. Teller and R. Bau, *Struct. Bonding (Berlin)*, 44 (1981) 1; M. McPartlin and W.J.H. Nelson, *J. Chem. Soc., Dalton Trans.*, (1986) 1557.
- 8 A.G. Orpen, *J. Chem. Soc., Dalton Trans.*, (1980) 2509.
- 9 B.F.G. Johnson, J. Lewis, W.J.H. Nelson, M.D. Vargas, D. Braga, K. Henrick and M. McPartlin, *J. Chem. Soc., Dalton Trans.*, (1984) 2151.

Mechanism of Protonation of Side-on Bonded Vinylidene Complexes; Structural Evidence for the Formation of a Cationic Di-molybdenum Complex containing an Asymmetrically Bridged Allyl Ligand

Grainne C. Conole,^a Simon F. T. Froom,^b Michael Green,^b and Mary McPartlin^a

^a School of Chemistry, The Polytechnic of North London, Holloway Road, London N7 8DB, U.K.

^b Department of Chemistry, King's College London, Strand, London WC2R 2LS, U.K.

α -Protonation of side-on bonded vinylidenes is indicated by the observations that reaction of $\text{CF}_3\text{CO}_2\text{D}$ with $[\text{Mo}_2\{\mu\text{-}\sigma\text{-}\eta^2(4e)\text{C}=\text{CH}_2\}(\text{CO})_4(\eta\text{-C}_5\text{H}_5)_2]$ affords $[\text{Mo}_2\{\sigma\text{-OC(O)CF}_3\}(\eta\text{-CD}=\text{CH}_2)(\text{CO})_4(\eta\text{-C}_5\text{H}_5)_2]$, whereas, $\text{CF}_3\text{CO}_2\text{H}$ and $[\text{Mo}_2\{\mu\text{-}\sigma\text{-}\eta^2(4e)\text{C}=\text{CD}_2\}(\text{CO})_4(\eta\text{-C}_5\text{H}_5)_2]$ gives $[\text{Mo}_2\{\sigma\text{-OC(O)CF}_3\}(\mu\text{-CH}=\text{CD}_2)(\text{CO})_4(\eta\text{-C}_5\text{H}_5)_2]$; in contrast, reaction of $\text{HBF}_4\cdot\text{Et}_2\text{O}$ with $[\text{Mo}_2\{\mu\text{-}\sigma\text{-}\eta^2(4e)\text{C}=\text{CMe}_2\}(\text{CO})_4(\eta\text{-C}_5\text{H}_5)_2]$ leads to loss of CO and formation of the Mo_2 triple bonded cation $[\text{Mo}_2(\mu\text{-}\eta^3\text{-2-MeC}_3\text{H}_4)(\text{CO})_3(\eta\text{-C}_5\text{H}_5)_2][\text{BF}_4]$, an asymmetrically bridged allyl complex which is also formed on protonation of $[\text{Mo}_2\{\mu\text{-}\sigma\text{-}\eta^3\text{-CHC(Me)CH}_2\}(\text{CO})_4(\eta\text{-C}_5\text{H}_5)_2]$.

It has been suggested¹⁻³ that surface bound vinylidenes might have a role in the Fischer-Tropsch reaction, and this has focused attention on the development of the chemistry of vinylidene ligands⁴ co-ordinated onto mono-, di-, and trinuclear centres. Recently,^{5,6} the side-on bonding mode, *i.e.*, $\mu\text{-}\sigma\text{-}\eta^2(4e)$, has been recognised for dinuclear vinylidene complexes and clearly it is important to understand and compare the reactivity of such species with that of conventional upright $[\mu\text{-}\sigma\text{-}\sigma(2e)]$ bonded vinylidenes.⁷ In establishing the regioselectivity of protonation reactions we have obtained structural evidence for the formation of an unusually bonded bridged allyl system.

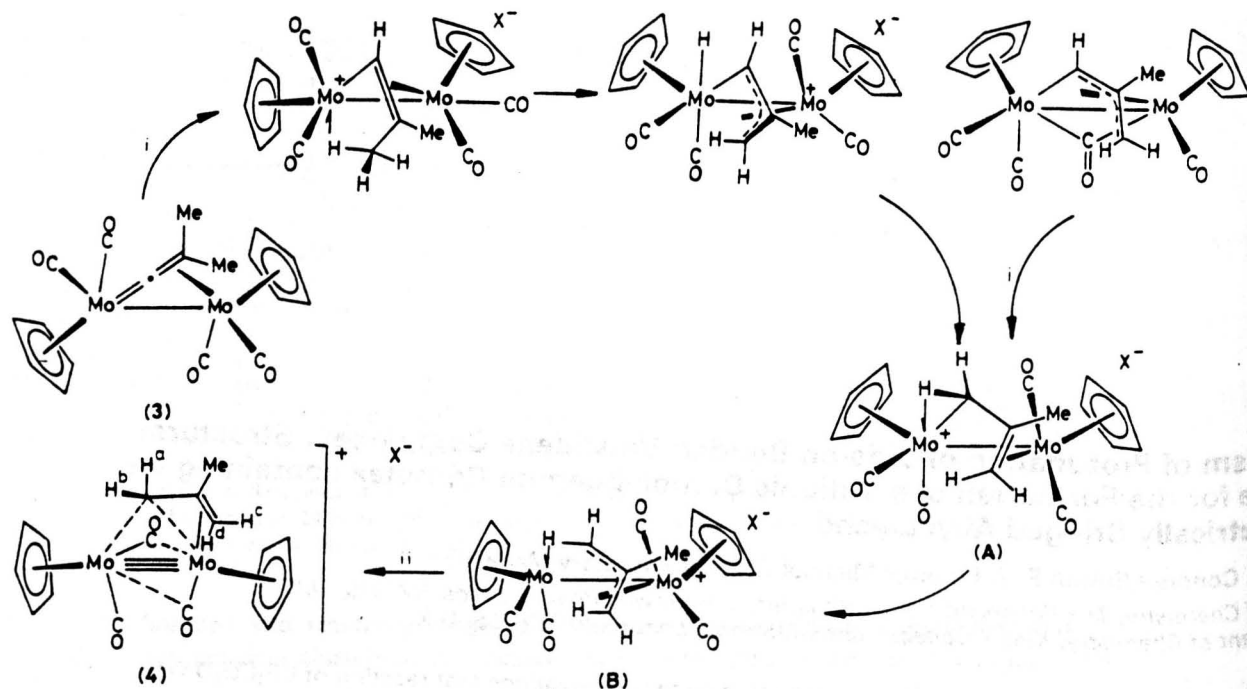
Protonation (-78°C , toluene) of $[\text{Mo}_2\{\mu\text{-}\sigma\text{-}\eta^2(4e)\text{C}=\text{CH}_2\}(\text{CO})_4(\eta\text{-C}_5\text{H}_5)_2]$ (1) with trifluoroacetic acid afforded† bright red crystals of the bridged vinyl complex $[\text{Mo}_2\{\sigma\text{-OC(O)CF}_3\}(\mu\text{-CH}=\text{CH}_2)(\text{CO})_4(\eta\text{-C}_5\text{H}_5)_2]$ (2). This reaction can be explained if a proton is delivered either directly or indirectly‡ to the α or carbenoid carbon of (1) followed by capture of the resulting unsaturated μ -vinyl cation with trifluoroacetate anion. There is, however, an alternative pathway from (1) to (2), which is suggested by recent studies with μ -carbyne Fe_2 ⁸ and Os_3 ⁹ complexes. This involves delivery of a proton to the β -carbon of the $\mu\text{-}\sigma\text{-}\eta^2(4e)\text{-C}=\text{CH}_2$ fragment of (1) resulting in the formation of a cationic bridged μ -carbyne complex $[\text{Mo}_2(\mu\text{-CCH}_3)(\text{CO})_4(\eta\text{-C}_5\text{H}_5)_2][\text{CF}_3\text{CO}_2]$, which then undergoes a 1,2-hydrogen shift from

the methyl carbon to the electron deficient carbyne carbon thus generating the μ -vinyl ligand. We have distinguished between these two pathways by deuterium labelling experiments. Protonation (-78°C , toluene) of (1) with $\text{CF}_3\text{CO}_2\text{D}$ afforded $[\text{Mo}_2\{\sigma\text{-OC(O)CF}_3\}(\mu\text{-CD}=\text{CH}_2)(\text{CO})_4(\eta\text{-C}_5\text{H}_5)_2]$.§ Secondly, reaction of $\text{CF}_3\text{CO}_2\text{H}$ with $[\text{Mo}_2\{\mu\text{-}\sigma\text{-}\eta^2(4e)\text{C}=\text{CD}_2\}(\text{CO})_4(\eta\text{-C}_5\text{H}_5)_2]$, which was synthesised by deprotonation⁶ [-78°C , Bu^nLi , tetrahydrofuran (thf)] of $[\text{Mo}_2(\mu\text{-DC}_2\text{D})(\text{CO})_4(\eta\text{-C}_5\text{H}_5)_2]$ followed by quenching (-78°C) with $\text{CF}_3\text{CO}_2\text{D}$, gave $[\text{Mo}_2\{\sigma\text{-OC(O)CF}_3\}$ -

§ Selected spectroscopic data for compound (1): n.m.r. ^1H (CDCl_3), δ 5.44 (s, 5H, C_5H_5), 5.30 (s, 5H, C_5H_5), 3.44 [d, 1H, =CHH, J (HH) 14.2 Hz], 2.83 [d, 1H, =CHH, 14.2 Hz]; ^{13}C - ^1H (CDCl_3), δ 329.5 (Mo=C), 241.8, 231.6, 231.0, 230.3 (CO), 94.6 (C_5H_5), 93.0 (C_5H_5), 40.0 (Mo=C=CH₂); ν_{CO} (hexane) 1976w, 1928s, 1905m, 1868w cm^{-1} . Compound (2-D): n.m.r. ^1H (CDCl_3), δ 9.05 (dd, CH=CH₂, J (H,H) 12, J (H,H) 8 Hz, 10%), 5.32 (s, 5H, C_5H_5), 5.16 (s, 5H, C_5H_5), 4.00 (bs, 1H, CD=CH₂), 3.30 (bs, 1H, CD=CH₂); ^2D (CH_2Cl_2), δ 9.05 p.p.m. (bs, 1D, CD=CH₂). Compound (2-D₂): n.m.r. ^1H (CDCl_3), δ 9.05 (bs, 1H, CH=CD₂), 5.32 (s, 5H, C_5H_5), 5.16 (s, 5H, C_5H_5), 4.00 [d, CH=CH₂, residual proton <5%, J (HH) 12 Hz], 3.30 [d, CH=CH₂, residual proton <5%, J (HH) 8 Hz]. Compound (4): n.m.r. ^1H (CD_2Cl_2 , room temperature), δ 5.66 (s, 5H, C_5H_5), 5.41 (s, 5H, C_5H_5), 3.05 (br. s, 2H), 2.56 (s, 3H, Me), 1.95 (br. s, 2H); ^1H (CD_2Cl_2 , -60°C), δ 5.72 (s, 5H, C_5H_5), 5.47 (s, 5H, C_5H_5), 3.59 [d, 1H, H^a, J (H^aH^c) 3.3 Hz] 2.56 (s, 3H, Me), 2.43 [dd, 1H, H^c, J (H^aH^c) 3.3, J (H^cH^d) 1.9 Hz], 2.36 [d, 1H, H^d, J (H^aH^c) 1.9 Hz], 1.53 (s, 1H, H^b); ^{13}C - ^1H (CD_2Cl_2 , -60°C), δ 233.4 (CO), 228.8 (CO), 228.1 (CO), 111.5 [CH₂C(Me)CH], 98.5 (C_5H_5), 95.3 (C_5H_5), 43.1 [at, CH₂, J (CH) 160 Hz], 25.0 [at, CH₂, J (CH) 150 Hz], 29.6 [Me, J (CH) 130 Hz]; ν_{CO} (CH_2Cl_2) 1999w, 1938m, 1920 sh cm^{-1} . Compound (5): n.m.r. ^1H (CDCl_3 , -40°C), δ 7.61—7.40 (m, 5H, Ph), 5.78 (s, 5H, C_5H_5), 5.07 (s, 5H, C_5H_5), 4.12 [d, 1H, H^a, J (H^aH^c) 3.9 Hz], 2.85 [dd, 1H, H^c, J (H^aH^c) 3.9, J (H^aH^d) 2.8 Hz], 2.37 [d, 1H, H^d, J (H^aH^d) 2.8 Hz], 1.83 (s, 1H, H^b).

† A similar reaction has been reported (ref. 5) between $[\text{Mo}_2\{\mu\text{-}\sigma\text{-}\eta^2(4e)\text{C}=\text{CH}_2\}(\text{CO})_4(\eta\text{-C}_5\text{Me}_5)_2]$ and $\text{CF}_3\text{CO}_2\text{H}$.

‡ Protonation of the molybdenum atom which carries the μ -vinylidene, *i.e.* $\text{Mo}=\text{C}=\text{CH}_2$, followed by migratory insertion of the hydrogen onto the α -carbon would also lead to the same regioselectivity. It is planned to carry out calculations which should help to distinguish between these two paths.



Scheme 1. X = BF₄⁻ or CF₃SO₃⁻; i. HBF₄·Et₂O, or CF₃SO₃H; ii. -CO.

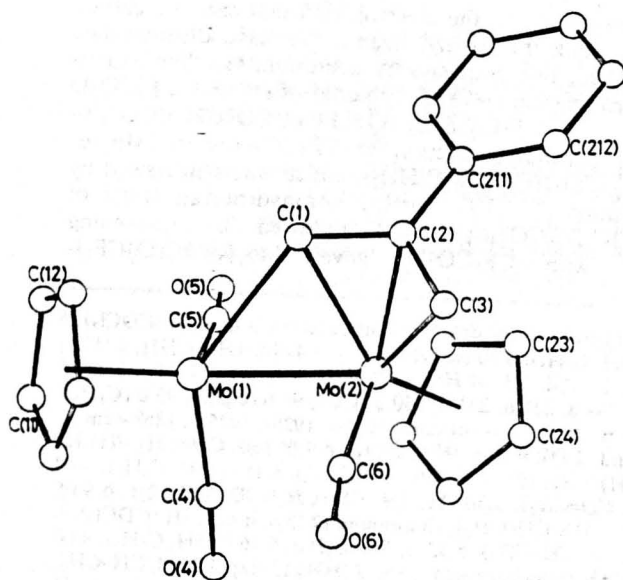


Figure 1. The structure of the novel asymmetrically bridging allyl complex [Mo₂{μ-σ:η³-CH₂C(Ph)CH₂}(CO)₄(η⁵-C₅H₅)₂][CF₃SO₃] (5). Principal bond lengths (Å) and angles (°): Mo(1)-Mo(2) 2.561(2), Mo(1)-C(1) 2.462(18), Mo(1)-C(4) 1.975(19), Mo(1)-C(5) 2.016(18), Mo(1)-C(6) 2.692(20), Mo(2)-C(1) 2.364(18), Mo(2)-C(2) 2.197(17), Mo(2)-C(3) 2.317(16), Mo(2)-C(6) 1.937(20), C(1)-C(2) 1.450(23), C(2)-C(3) 1.455(25), C(2)-C(21) 1.478(20); C(1)-Mo(1)-Mo(2) 56.1(4), C(1)-Mo(2)-Mo(1) 59.8(4), C(2)-Mo(2)-Mo(1) 96.1(4), C(2)-Mo(2)-C(1) 36.8(6), C(3)-Mo(2)-Mo(1) 107.8(4), C(3)-Mo(2)-C(1) 63.5(6), C(3)-Mo(2)-C(2) 37.5(6), C(3)-Mo(2)-C(1) 63.5(6), C(3)-Mo(2)-C(2) 37.5(6), Mo(2)-C(1)-Mo(1) 64.1(5), C(2)-C(1)-Mo(1) 128(1), C(2)-C(1)-Mo(2) 65.3(9), C(1)-C(2)-Mo(2) 78(1), C(3)-C(2)-Mo(2) 76(1), C(3)-C(2)-C(1) 116(1), C(2)-C(3)-Mo(2) 66.8(9).

(μ-CH=CD₂)(CO)₄(η-C₅H₅)₂] there being no evidence for deuterium leakage onto the α-carbon of the vinyl ligand. Thus, these observations strongly support the former mechanism, *i.e.*, α-protonation.

Additional insight into the reaction paths available in the protonation reaction came from a study of the related reactions of β,β'-disubstituted vinylidenes such as [Mo₂{μ-σ,η²(4e)C=CMe₂}(CO)₄(η-C₅H₅)₂] (3), which when protonated with CF₃CO₂H undergoes an analogous reaction leading to the formation of [Mo₂{σ-OC(O)CF₃}(μ-CH=CMe₂)(CO)₄(η-C₅H₅)₂]. However, protonation of (3) with HBF₄·Et₂O did not afford a stable μ-vinyl complex. Instead the ¹H and ¹³C-¹H n.m.r. spectra of the cationic product (4) showed the presence of only *one* methyl group and three terminal carbonyl ligands. Interestingly, the same cation was obtained on protonation[¶] (HBF₄·Et₂O or CF₃SO₃H) of the μ-allylidene complex [Mo₂{μ-σ:η³-CH-C(Me)CH₂}(CO)₄(η-C₅H₅)₂] formed on thermolysis^b (70°C, hexane, 4 h) of [Mo₂{μ-σ,η²(4e)C=CMe₂}(CO)₄(η-C₅H₅)₂]. An insight into the structural identity of (4) was gained from an X-ray diffraction study^{||} of the related cation (5), which was prepared by reaction (-78°C, CH₂Cl₂) of CF₃SO₃H with [Mo₂{μ-σ:η³-CHC(Ph)CH₂}(CO)₄(η-C₅H₅)₂].^b

[¶] Addition (-78°C) of K[BHBU₃] to a tetrahydrofuran (thf) suspension of (4) results in a deprotonation/disproportionation reaction and formation (30%) of [Mo₂{μ-σ:η³-CH-C(Me)CH₂}(CO)₄(η-C₅H₅)₂].

^b Recently a complex has been reported in which an η³-allyl group bonded to Mo is involved in an agostic interaction to a Mn atom. C. M. Hay, A. D. Horton, M. J. Mays, and P. R. Raithby. *Polyhedron*, 1988, 7, 897.

The structure** of the protonated product (5) is shown in Figure 1. The metal-metal bond length of 2.561(2) Å is comparable to that found for other formally triply bonded dimolybdenum structures.¹¹ This compound is the first structurally characterised cationic species with a μ -allyl ligand, which adopts a markedly different bridging role to that usually observed where the central C-atom bonds symmetrically to both metal atoms.¹² In (5), the unusual bonding may be envisaged as η^2 -co-ordination to Mo(2) only [Mo(2)-C(2) 2.197(17) and Mo(2)-C(3) 2.317(16) Å], and a 3c-2e interaction between the α -carbon and both metal atoms [Mo(1)-C(1) 2.462(18) and Mo(2)-C(1) 2.364(18) Å]. This type of three centred bonding is rare for alkyl ligands,^{13,14} and has not been previously observed for an allyl group. Variable temperature n.m.r. studies \S show that in solution there is a dynamic process which on the n.m.r. time scale equilibrates the two ends of the allyl ligand, *i.e.*, $H^a \rightleftharpoons H^c$, $H^b \rightleftharpoons H^d$.

It is reasonable to suggest that the formation of (4) involves α -protonation of the μ - σ , $\eta^2(4e)$ bonded vinylidene to form a co-ordinatively unsaturated vinyl species. Unlike the reaction with CF_3CO_2H , an agostic Mo(μ -H)C interaction with one of the β -methyl groups intervenes when the counteranion is BF_4^- . This sets things up for transfer, *via* the metal, of a hydrogen from one end of the C_3 chain to the other (see Scheme 1), thus allowing formation of the cation (A). This same cation is apparently accessed by α -protonation of the μ -allylidene complex $[Mo_2(\mu-\sigma:\eta^3-CHC(Me)CH_2)(CO)_4(\eta-C_5H_5)_2]$. This latter reaction relates to the formation¹⁵ of $[Mo_2(\mu-C_4Me_8)(\mu_{Mo-C-H})(\eta-C_5H_5)_2][BF_4]$ from the bis- μ -allylidene complex $[Mo_2(\mu-C_4Me_8)(\eta-C_5H_5)_2]$. However, in the carbonyl substituted system the reaction does not stop at either (A) or (B) (Scheme 1), instead carbon monoxide is lost and stability is achieved by formation of a metal-metal multiple bond. Examination of the i.r., ¹H and ¹³C n.m.r. spectra \S of (4) and (5) showed that there was no evidence for

an agostic Mo(μ -H)C interaction.¹⁶ This leads to the important conclusion that although in mononuclear systems unsaturation at a metal centre frequently leads to stabilisation by an agostic M(μ -H)C interaction, in dinuclear and perhaps in polynuclear systems alternative modes of achieving stability may over-ride M(μ -H)C interactions.

We thank the S.E.R.C. for support and a studentship (S. F. T. F.).

Received, 16th August 1988; Com. 8/03319F

References

- 1 W. Erley, P. H. McBreen, and H. Ibach, *J. Catal.*, 1983, **84**, 229.
- 2 L. E. McCandlish, *J. Catal.*, 1983, **83**, 362.
- 3 C. Zheng, Y. Apeloig, and R. Hoffmann, *J. Am. Chem. Soc.*, 1988, **110**, 749, and references therein.
- 4 M. I. Bruce and A. G. Swincer, *Adv. Organomet. Chem.*, 1983, **22**, 60.
- 5 N. M. Doherty, C. Elschenbroich, H.-J. Kneuper, and S. A. R. Knox, *J. Chem. Soc., Chem. Commun.*, 1985, 170.
- 6 R. J. Mercer, M. Green, and A. G. Orpen, *J. Chem. Soc., Chem. Commun.*, 1986, 567.
- 7 Protonation of upright dinuclear vinylidenes; Rh_2 : Y. N. Al-Obaidi, N. D. White, G. E. Taylor, and M. Green, *J. Chem. Soc., Dalton Trans.*, 1982, 319; Fe_2 : C. P. Casey, S. R. Marder, and P. J. Fagan, *J. Am. Chem. Soc.*, 1983, **105**, 7197.
- 8 C. P. Casey, P. J. Fagan, W. H. Miles, and S. R. Marder, *J. Mol. Catal.*, 1983, **21**, 173.
- 9 M. Green, A. G. Orpen, and C. J. Schaverien, *J. Chem. Soc., Chem. Commun.*, 1984, 37.
- 10 S. F. T. Froom, M. Green, R. J. Mercer, K. R. Nagle, A. G. Orpen, and S. Schwiegk, *J. Chem. Soc., Chem. Commun.*, 1986, 1666.
- 11 F. A. Cotton and R. A. Walton, in 'Multiple Bonds between Metal Atoms', John Wiley, New York, 1982, p. 183.
- 12 H. Werner and A. Kuhn, *Angew. Chem., Int. Ed. Engl.*, 1977, **16**, 412.
- 13 C. Krüger, J. C. Sekutowski, H. Berke, and R. Hoffmann, *Z. Naturforsch., Teil B.*, 1978, **33**, 1110.
- 14 More often one of the C-H bonds of the bridging alkyl also interacts with one of the metals forming a M(μ -H)C interaction: see R. B. Calvert and J. R. Shapley, *J. Am. Chem. Soc.*, 1978, **100**, 7726; G. M. Dawkins, M. Green, A. G. Orpen, and F. G. A. Stone, *J. Chem. Soc., Chem. Commun.*, 1982, 41; J. C. Jeffrey, A. G. Orpen, W. T. Robinson, F. G. A. Stone, and M. J. Went, *ibid.*, 1984, 396.
- 15 M. Green, N. C. Norman, A. G. Orpen, and C. J. Schaverien, *J. Chem. Soc., Dalton Trans.*, 1984, 2455.
- 16 M. Brookhart and M. L. H. Green, *J. Organomet. Chem.*, 1983, **250**, 395.

** Crystal data for (5): $C_{23}H_{19}Mo_2O_6S$, $M = 672.25$, orthorhombic, space group $Pbca$, $a = 20.665$ (4), $b = 20.274$ (4), $c = 11.446$ (2) Å, $U = 4795.44$ Å³, $Z = 8$, $D_c = 1.86$ g cm⁻³, $F(000) = 2656$, $\mu(Mo-K\alpha) = 10.70$ cm⁻¹. Data were collected on a Philips PW 1100 diffractometer in the θ -range 3–25°, with a scan width of 0.70°. Equivalent reflections were merged to give 1757 absorption corrected data with $I/\sigma(I) > 3.0$. $R = 0.0619$ and $R_w = 0.0582$ with weights of $w = 1/\sigma^2 F_o$ assigned to the individual reflections.

Atomic co-ordinates, bond lengths and angles, and thermal parameters have been deposited at the Cambridge Crystallographic Data Centre. See Notice to Authors, Issue No. 1.

The First Isolation of an Intermediate in the Formation of a Hexaruthenium Carbido-cluster from the Reaction of $[\text{Ru}_3(\text{CO})_{12}]$: X-Ray Structure Analyses of $[\text{Ru}_6(\eta^2-\mu_4\text{-CO})_2(\text{CO})_{13}(\eta^6\text{-C}_6\text{H}_3\text{Me}_3)]$ and $[\text{HRu}_6(\eta^2-\mu_4\text{-CO})(\text{CO})_{13}(\eta^7-\mu_2\text{-C}_6\text{H}_3\text{Me}_2\text{CH}_2)]$

Christopher E. Anson,^a Philip J. Bailey,^a Grainne Conole,^b Brian F. G. Johnson,^a Jack Lewis,^{a*} Mary McPartlin,^{b*} and Harold R. Powell^b

^a University Chemical Laboratory, Lensfield Road, Cambridge CB2 1EW, U.K.

^b School of Chemistry, The Polytechnic of North London, London N7 8DB, U.K.

Thermolysis of $[\text{Ru}_3(\text{CO})_{12}]$ (1) in hydrocarbons heated under reflux containing excess of 1,3,5-trimethylbenzene (mesitylene) has yielded $[\text{Ru}_6\text{C}(\text{CO})_{14}(\eta^6\text{-C}_6\text{H}_3\text{Me}_3)]$ (2a) and two new hexaruthenium compounds $[\text{Ru}_6(\eta^2-\mu_4\text{-CO})_2(\text{CO})_{13}(\eta^6\text{-C}_6\text{H}_3\text{Me}_3)]$ (3) and $[\text{HRu}_6(\eta^2-\mu_4\text{-CO})(\text{CO})_{13}(\eta^7-\mu_2\text{-C}_6\text{H}_3\text{Me}_2\text{CH}_2)]$ (4), shown by X-ray structure analyses to have metal frameworks previously unknown in ruthenium cluster chemistry; on further thermolysis the cluster (3) gives (2a) and is therefore the first intermediate in the well established conversion of triruthenium to hexaruthenium carbido-clusters to be identified.

The first ruthenium carbido-clusters to be characterised, $[\text{Ru}_n\text{C}(\text{CO})_{14}(\eta^6\text{-arene})]$ (2a—d),¹ were prepared by thermolysis of $[\text{Ru}_3(\text{CO})_{12}]$ (1) in the appropriate arene (Scheme 1). Studies on the sealed-tube pyrolysis of (1) established that the carbido-atom in the parent cluster $[\text{Ru}_n\text{C}(\text{CO})_{17}]$ originates via the cleavage of a co-ordinated carbonyl ligand.² We now report the first isolation of an intermediate in the formation of a hexaruthenium carbido-cluster from (1).

The reaction of (1) with mesitylene has been investigated at a range of temperatures by carrying out the thermolysis in a

number of different hydrocarbons, containing 10% (v/v) mesitylene (Scheme 1), and it is apparent that the yield is strongly dependent on temperature. At the highest temperatures, in refluxing n-nonane or n-octane, the reaction gave only $[\text{Ru}_6\text{C}(\text{CO})_{14}(\eta^6\text{-C}_6\text{H}_3\text{Me}_3)]$ (2a) in 15% yield, while in n-heptane it gave not only (2a) but also the new compounds $[\text{Ru}_6(\eta^2-\mu_4\text{-CO})_2(\text{CO})_{13}(\eta^6\text{-C}_6\text{H}_3\text{Me}_3)]$ (3) and $[\text{HRu}_6(\eta^2-\mu_4\text{-CO})(\text{CO})_{13}(\eta^7-\mu_2\text{-C}_6\text{H}_3\text{Me}_2\text{CH}_2)]$ (4) in approximately equal yield. At the lowest temperature studied, in n-hexane, the reaction gave a low yield of (3) only.

cm^{-1} ($\nu^{13}\text{CO}$ 1410 cm^{-1}), § in the solid state i.r. spectra. The stretching frequencies of the ^{13}C labelled analogues confirm these assignments. These stretching frequencies are similar to those reported for other ($\eta^2\text{-}\mu_4\text{-CO}$) ligands (ν_{CO} range 1340–1457 cm^{-1}).⁷

Significantly thermolysis of (3) in mesitylene gives (2a) and (4) in approximately equal yield (Scheme 1), thus confirming that (3) is an intermediate in the formation of the hexaruthenium carbido-cluster (2a) from $[\text{Ru}_3(\text{CO})_{12}]$ (1). Carbon-13 labelling experiments have established that the carbido-atom in (2a) is derived from a carbonyl ligand. It would therefore seem likely that the transformation of (3) into the carbido-cluster (2a) occurs *via* cleavage of one of the activated ($\eta^2\text{-}\mu_4\text{-CO}$) ligands. However, if this transformation involves ejection of CO_2 it cannot proceed *via* an intramolecular process as this would result in a cluster containing only 13 carbonyl ligands.

§ Spectroscopic data for $[\text{HRu}_6(\eta^2\text{-}\mu_4\text{-CO})(\text{CO})_{13}(\eta^7\text{-}\mu_2\text{-C}_6\text{H}_7\text{-Me}_2\text{CH}_2)]$ (4): i.r. (hexane solution); $\nu(\text{CO})$ 2087(s), 2051(s), 2031(s), 2010(s), 1989(m), 1978(m), 1943(m), 1865(w, br.), 1851(m, br.); i.r. (CsI disc, 130 K); $\nu(\eta^2\text{-}\mu_4\text{-CO})$ 1446 cm^{-1} ; $\nu(\eta^2\text{-}\mu_4\text{-}^{13}\text{CO})$ 1410 cm^{-1} ; ^1H n.m.r. (CD_2Cl_2 solution); δ 5.36 (s, 1H), 4.74 (s, 1H), 4.19 (s, 1H), 3.33 (d, J 6 Hz, 1H), 2.99 (d, J 6 Hz, 1H), 1.93 (s, 3H), 1.83 (s, 3H), -19.50 (s, 1H).

A mechanism for the formation of (3) from (1) is difficult to envisage and we are currently attempting to isolate an intermediate between these two clusters.

We thank the S.E.R.C. (P. J. B., G. C., and H. R. P.) and British Petroleum (P. J. B.) for financial support, and Johnson Matthey for generous loans of ruthenium trichloride.

Received, 10th October 1988; Com. 8 04042G

References

- 1 B. F. G. Johnson, R. D. Johnston, J. Lewis, and B. H. Robinson *Chem Commun.*, 1966, 851; B. F. G. Johnson, R. D. Johnston, and J. Lewis, *J. Chem. Soc. (A)*, 1968, 2856; R. Mason and W. R. Robinson, *Chem Commun.*, 1968, 468.
- 2 C. R. Eady, B. F. G. Johnson, and J. Lewis, *J. Chem. Soc., Dalton Trans.*, 1975, 2606.
- 3 M. McPartlin, *Polyhedron*, 1984, **3**, 1279.
- 4 A. G. Orpen, *J. Chem. Soc., Dalton Trans.*, 1980, 2509.
- 5 L. M. Bullock, J. S. Field, R. J. Haines, E. Minshall, D. N. Smit, and G. M. Sheldrick, *J. Organomet. Chem.*, 1986, **310**, C47.
- 6 N. R. Avery, *J. Chem. Soc., Chem. Commun.*, 1988, 153.
- 7 C. P. Horwitz, E. M. Holt, C. P. Brock, and D. F. Shriver, *J. Am. Chem. Soc.*, 1985, **107**, 8136; R. D. Adams, G. E. Babin, and M. Tasi, *Angew. Chem., Int. Ed. Engl.*, 1987, **26**, 685; C. P. Gibson and L. F. Dahl, *Organometallics*, 1988, **7**, 535.

Phosphorus–Carbon Bond Formation in Dimolybdenum Alkyne Complexes induced by Oxidative Addition of Chlorodiphenylphosphine

Gráinne Conole,^a Katherine A. Hill,^b Mary McPartlin,^a Martin J. Mays*^c and Michael J. Morris*^{b,c}

^a School of Chemistry, The Polytechnic of North London, Holloway Road, London N7 8DB, U.K.

^b Department of Chemistry, University of Manchester, Manchester M13 9PL, U.K.

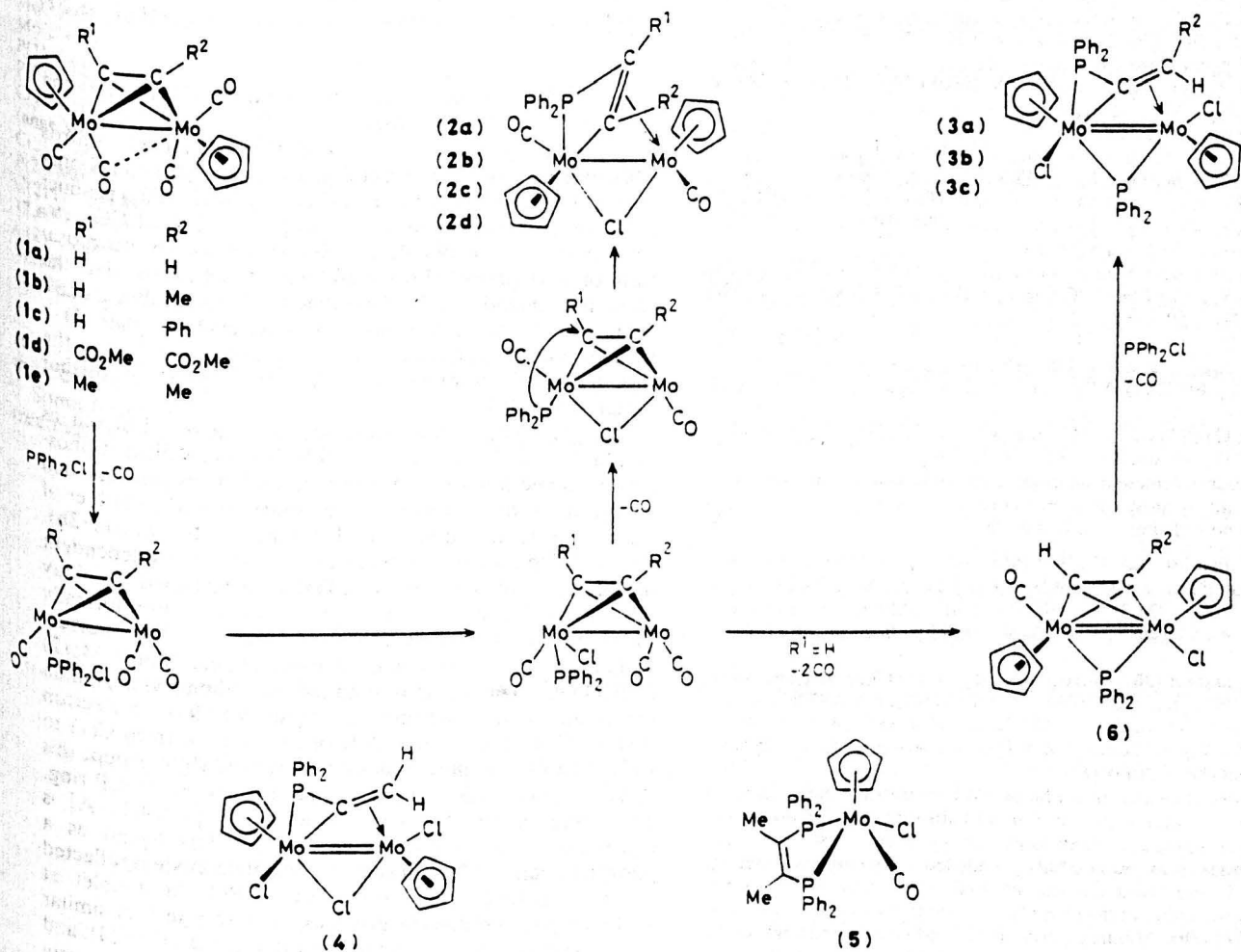
^c University Chemical Laboratory, Lensfield Road, Cambridge CB2 1EW, U.K.

The reaction of $[\text{Mo}_2(\text{CO})_4(\mu\text{-R}^1\text{C}_2\text{R}^2)(\eta\text{-C}_5\text{H}_5)_2]$ ($\text{R}^1, \text{R}^2 = \text{H}$, alkyl, or aryl) with PPh_2Cl proceeds via P–Cl bond cleavage and coupling of the diphenylphosphido group with the alkyne in one of three different ways depending on the nature of R^1 and R^2 ; two of the resulting complexes, $[\text{Mo}_2(\mu\text{-Cl})(\mu\text{-Ph}_2\text{PC}(\text{H})=\text{CH})(\text{CO})_2(\eta\text{-C}_5\text{H}_5)_2]$ and $[\text{Mo}_2\text{Cl}_2(\mu\text{-PPh}_2)(\mu\text{-Ph}_2\text{PC}=\text{CHMe})(\eta\text{-C}_5\text{H}_5)_2]$ have been characterised by X-ray analysis.

The cleavage of phosphorus–hydrogen, phosphorus–phosphorus, and phosphorus–carbon bonds at dimetallic centres are well known reactions which lead to a wide variety of dinuclear transition metal complexes.^{1–3} In contrast, the cleavage of phosphorus–halogen bonds remains relatively unexplored⁴ and has not been previously reported for dimetallic complexes containing bridging organic ligands. In this communication we report the reaction of chlorodiphenylphosphine with the dimolybdenum alkyne complexes $[\text{Mo}_2(\text{CO})_4(\mu\text{-R}^1\text{C}_2\text{R}^2)(\eta\text{-C}_5\text{H}_5)_2]$ (**1a–e**). These reactions, which involve novel examples of phosphorus–carbon bond formation and unprecedented transformations of the alkyne

ligands, suggest that a more general study of oxidative addition reactions of this type is warranted.

Treatment of $[\text{Mo}_2(\text{CO})_4(\mu\text{-R}^1\text{C}_2\text{R}^2)(\eta\text{-C}_5\text{H}_5)_2]$ ($\text{R}^1 = \text{H}$, $\text{R}^2 = \text{H}$, Me, Ph) (**1a–c**)⁵ with PPh_2Cl (1–2 equiv., refluxing toluene, 17 h) affords the chromatographically separable complexes $[\text{Mo}_2(\mu\text{-Cl})(\mu\text{-Ph}_2\text{PCR}^1\text{CR}^2)(\text{CO})_2(\eta\text{-C}_5\text{H}_5)_2]$ (**2a–c**) and $[\text{Mo}_2\text{Cl}_2(\mu\text{-PPh}_2)(\mu\text{-Ph}_2\text{PC}=\text{CR}^1\text{R}^2)(\eta\text{-C}_5\text{H}_5)_2]$ (**3a–c**) in low to moderate yields (see Scheme 1). In the reaction with (**1a**) a species related to (**3a**), $[\text{Mo}_2\text{Cl}_2(\mu\text{-Cl})(\mu\text{-Ph}_2\text{PC}=\text{CH}_2)(\eta\text{-C}_5\text{H}_5)_2]$ (**4**), is also obtained and is the major product. Similar reactions of the disubstituted alkyne complexes (**1d**) ($\text{R}^1 = \text{R}^2 = \text{CO}_2\text{Me}$) and (**1e**) ($\text{R}^1 = \text{R}^2 = \text{Me}$) with



Scheme 1. Structural formulae for the new complexes with some possible reaction pathways. For (**6**), only (**6c**) was isolated.

PPh_2Cl lead to (2d) and (5) respectively as the only isolable compounds. All new complexes were characterised by analysis and standard spectroscopic methods.⁷

The occurrence of phosphido-alkyne coupling in orange, crystalline, slightly air-sensitive (2a) was clearly shown by its n.m.r. spectra, and subsequently confirmed by an X-ray diffraction study, the results of which are summarised in Figure 1 and its caption.⁸ The Mo-Mo single bond [2.871(1) Å] is bridged by a chloride ligand and by a μ -vinyl ligand which is σ -bonded to Mo(1) [Mo(1)-C(2) 2.207(9) Å] and asymmetrically π -bonded to Mo(2) [Mo(2)-C(1) 2.212(8), Mo(2)-C(2) 2.074(8) Å]. One of the β -substituents of this vinyl ligand is the diphenylphosphido group which is itself co-ordinated to Mo(1) [Mo(1)-P(1) 2.467(2) Å], thus forming a four-membered MoCCP ring. Similar ligands have previously been formed by the insertion of alkynes into phosphido-bridged complexes,⁶ but this is the first example resulting from the insertion of a phosphido group into a μ -alkyne complex. The n.m.r. spectra of (2b) and (2c) reveal the presence of a single isomer of each, in which the phosphido group is joined

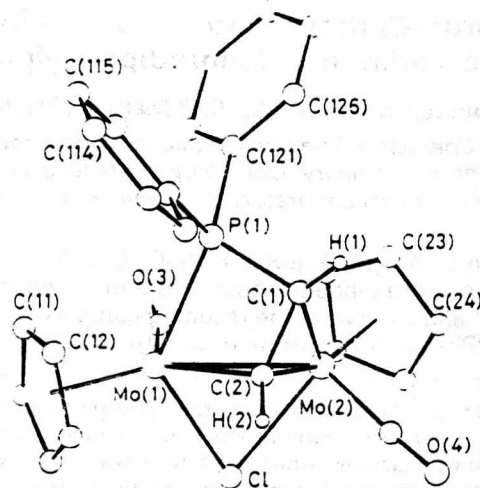


Figure 1. The structure of $[\text{Mo}_2(\mu\text{-Cl})(\mu\text{-Ph}_2\text{PC(H)C(H)})(\text{CO})_2(\eta^2\text{-C}_5\text{H}_5)_2]$ (2a). Principal bond lengths (Å) and angles ($^\circ$) are: Mo(1)-Mo(2) 2.871(1), Mo(1)-P(1) 2.467(2), Mo(1)-Cl 2.496(2), Mo(1)-C(2) 2.207(9), Mo(1)-C(3) 1.919(10), Mo(2)-C(1) 2.212(8), Mo(2)-C(2) 2.074(8), Mo(2)-C(4) 1.951(11), P(1)-C(1) 1.782(10), P(1)-C(11) 1.833(5), P(1)-C(12) 1.813(6), C(1)-C(2) 1.463(10), C(3)-O(3) 1.188(13), C(4)-O(4) 1.145(14); range Mo(1)-C(Cp) 2.303(11)-2.373(20), range Mo(2)-C(Cp) 2.273(10)-2.390(13), C(111)-P(1)-Mo(1) 118.1(2), C(111)-P(1)-C(1) 108.3(4), C(121)-P(1)-Mo(1) 127.9(2), C(121)-P(1)-C(1) 114.0(3), C(121)-P(1)-C(111) 100.4(3), P(1)-C(1)-Mo(2) 104.6(4), C(2)-C(1)-Mo(2) 65.0(4), C(2)-C(1)-P(1) 97.8(6), Mo(2)-C(2)-Mo(1) 84.2(3), C(1)-C(2)-Mo(1) 106.0(6), C(1)-C(2)-Mo(2) 75.2(5) (Cp = cyclopentadienyl).

⁷ Selected spectroscopic data [i.r. in CH_2Cl_2 , n.m.r. in CDCl_3 unless otherwise stated, coupling constants in Hz: ^{31}P n.m.r. shifts are relative to $\text{P}(\text{OMe})_3 = 0.0$ p.p.m.]:

(2a) $\nu(\text{CO})$ 1865 cm^{-1} ; ^1H n.m.r. δ 6.47 (dd, $J_{\text{HH}} 4.7$, $J_{\text{HP}} 10.1$), 3.85 (dd, $J_{\text{HH}} 4.7$, $J_{\text{HP}} 10.5$); ^{13}C n.m.r. 110.7 (d, $J_{\text{CP}} 28$, $\mu\text{-CH}$), 30.6 (d, $J_{\text{CP}} 42$, CH); ^{31}P n.m.r. -130.3 p.p.m.

(2b) $\nu(\text{CO})$ 1864 cm^{-1} ; ^1H n.m.r. δ 3.57 (d, $J_{\text{HP}} 6.8$, CH), 2.86 (d, $J_{\text{HP}} 5.5$, CMe); ^{31}P n.m.r. -132.7 p.p.m.

(2c) $\nu(\text{CO})$ 1875 cm^{-1} ; ^1H n.m.r. δ 4.16 (d, $J_{\text{HP}} 6.8$, CH); ^{13}C n.m.r. 122.8 (d, $J_{\text{CP}} 20$, CPh), 29.3 (d, $J_{\text{CP}} 40$, CH); ^{31}P n.m.r. -130.1 p.p.m.

(3a) ^1H n.m.r. δ 4.80 (td, $J_{\text{Hu-P}} 0.9$, $J_{\text{HH}} = J_{\text{HP}} = 3.8$, 1H of CH_2), 2.27 (ddd, $J_{\text{Hu-P}} 0.7$, $J_{\text{HP}} 8.5$, $J_{\text{HH}} 3.8$, 1H of CH_2); ^{31}P n.m.r. 38.9 (d, $J_{\text{PP}} 47$, $\mu\text{-P}$), -247.2 (d, $J_{\text{PP}} 47$) p.p.m.

(3b) ^1H n.m.r. δ 3.05 (dq, $J_{\text{HH}} 6.4$, $J_{\text{HP}} 10.6$, CH), 2.63 (d, $J_{\text{HH}} 6.4$, Me); ^{13}C n.m.r. 154.5 (d, $J_{\text{CP}} 16$, $\mu\text{-C}$), 73.3 (d, $J_{\text{CP}} 13$, CHMe); ^{31}P n.m.r. 42.5 (d, $J_{\text{PP}} 58$, $\mu\text{-P}$), -243.3 (d, $J_{\text{PP}} 58$) p.p.m.

(3c) ^1H n.m.r. δ 3.44 (d, $J_{\text{HP}} 10.3$, CHPh); ^{13}C n.m.r. (CD_2Cl_2) 134.2 (d, $J_{\text{CP}} 48$, $\mu\text{-C}$) 72.0 (d, $J_{\text{CP}} 13$, CHPh); ^{31}P n.m.r. 39.7 (d, $J_{\text{PP}} 54$, $\mu\text{-P}$), -227.3 (d, $J_{\text{PP}} 54$) p.p.m.

(4) ^1H n.m.r. δ 3.60 (dd, $J_{\text{HP}} 1.6$, $J_{\text{HH}} 5.0$, 1H of CH_2), 2.21 (dd, $J_{\text{HH}} 5.0$, $J_{\text{HP}} 6.8$, 1H of CH_2); ^{13}C n.m.r. (CD_2Cl_2) 149.2 (s, $\mu\text{-C}$), 40.4 (d, $J_{\text{CP}} 12$, CH_2); ^{31}P n.m.r. -249.1 p.p.m.

(5) $\nu(\text{CO})$ 1866 cm^{-1} ; ^1H n.m.r. δ 2.05 (dd, $J_{\text{HP}} 5.9$ and 1.1, Me), 1.79 (dd, $J_{\text{HP}} 7.1$ and 0.6, Me); ^{13}C n.m.r. 152.7 (t, $J_{\text{CP}} 37$, CMe), 152.5 (t, $J_{\text{CP}} 40$, CMe); ^{31}P n.m.r. -31.5 (d, $J_{\text{PP}} 34$), -44.9 (d, $J_{\text{PP}} 34$) p.p.m.

(6c) $\nu(\text{CO})$ 1970 cm^{-1} ; ^1H n.m.r. δ 9.13 (s, $\mu\text{-CH}$); ^{13}C n.m.r. 121.5 (s, CPh) 111.7 (s, $\mu\text{-CH}$); ^{31}P n.m.r. 12.2 p.p.m.

Satisfactory elemental analyses were obtained for all new compounds, and in most cases molecular ions were observed in their fast-atom bombardment mass spectra.

\dagger Crystal data for (2a): $\text{C}_{26}\text{H}_{22}\text{ClMo}_2\text{O}_2\text{P}$, $M = 624.68$, monoclinic, space group $\text{P}2_1/n$, $a = 17.735(3)$, $b = 10.023(2)$, $c = 14.790(3)$ Å, $\beta = 112.54(2)^\circ$, $U = 2428.25$ Å³, $F(000) = 1240$, $\mu(\text{Mo-K}\alpha) = 11.08$ cm^{-1} , $Z = 4$, $D_c = 1.71$ g cm^{-3} , $R = 0.0424$, for 2420 reflections with $I/I_0 > 3.0$.

Crystal data for (3b): $\text{C}_{17}\text{H}_{14}\text{Cl}_2\text{Mo}_2\text{P}_2$, $M = 803.33$, triclinic, space group $\text{P}\bar{1}$ (No. 2), $a = 21.263(4)$, $b = 17.675(3)$, $c = 9.970(2)$ Å, $\alpha = 110.02(2)^\circ$, $\beta = 106.22(2)^\circ$, $\gamma = 111.32(2)^\circ$, $U = 3345.36$ Å³, $F(000) = 1616$, $\mu(\text{Mo-K}\alpha) = 9.28$ cm^{-1} , $Z = 4$, $D_c = 1.60$ g cm^{-3} , $R = 0.0578$ for 6192 reflections with $I/I_0 > 3.0$.

Data were collected on a Philips PW1100 diffractometer in the θ range 3–25°. Lorentz-polarisation and absorption corrections were applied. One of the cyclopentadienyl ligands of (2a) is disordered, and this disorder was successfully modelled. Anisotropic thermal parameters were assigned to the non-hydrogen atoms of (2a), except for the carbon atoms of the phenyl rings, and to Mo, P, Cl, C(1), C(2), and C(02) of (3b). Atomic co-ordinates, bond lengths and angles, and thermal parameters have been deposited at the Cambridge Crystallographic Data Centre. See Notice to Authors, Issue No. 1.

to the CH terminus of the unsymmetrical alkyne, i.e. the coupling process is regioselective.

The disubstituted alkyne complex (1d) similarly affords (2d), but in contrast the but-2-yne complex (1e) yields only traces of the analogous product (2e); instead the main product is the mononuclear complex $[\text{MoCl}(\text{CO})(\text{cis-Ph}_2\text{PC}(\text{Me})=\text{C}(\text{Me})\text{PPh}_2)(\eta\text{-C}_5\text{H}_5)]$ (5), in which incorporation of two phosphido groups⁷ has occurred to give the chelating ligand *cis*-2,3-bis(diphenylphosphino)but-2-ene.⁸ Although at present we have no direct evidence that (5) is formed via the species (2e), this seems plausible despite the fact that the complexes (2a–d) appear inert to further reaction with PPh_2Cl .

The ^1H and ^{13}C n.m.r. spectra of (3a–c), isolated as air-stable, purple, crystalline solids, likewise indicated phosphido-alkyne linkage and also that a 1,2-hydrogen shift had occurred on the alkyne, e.g. the observation of a doublet of quartets (1H) and a doublet (3H) for the CHMe group in (3b). Figure 2 depicts the structure of one of the two independent molecules in the unit cell of (3b)⁸ as determined by X-ray diffraction. The two molybdenum atoms, now both formally Mo^{III} , are each ligated by a C_5H_5 ring and a terminal chloride, and are linked by a formal double bond [mean Mo(1)-Mo(2) 2.792(1) Å]. This bond is spanned by a diphenylphosphido bridge and an α -phosphino vinyl ligand which is a 5 electron donor. There has been a shift of the H-atom from C(1) to C(2), and C(1) is now bonded to a second PPh_2 group; this links to Mo(1) thus forming a three-membered MoCP ring. The rather short P(2)-C(1) bond length [1.724(12) Å] is consistent with an alternative view of this ligand as a phospho-allene.⁹ This unusual co-ordination mode is reflected in the high-field ^{31}P n.m.r. shift of P(2) [a doublet at -243.3 p.p.m. relative to $\text{P}(\text{OMe})_3 = 0.0$ p.p.m.]. A similar signal, a singlet, comprises the ^{31}P n.m.r. spectrum of (4), and elemental analysis indicates that this complex is directly

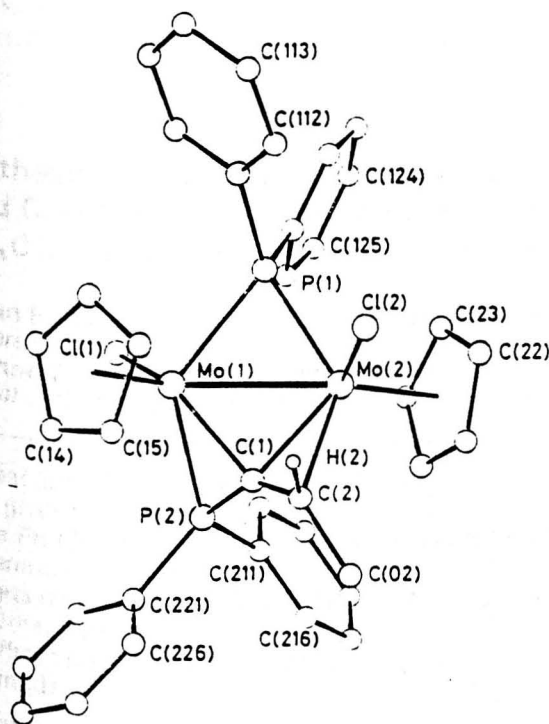


Figure 2. The structure of one of the two virtually identical independent molecules of $[\text{Mo}_2\text{Cl}_2(\mu\text{-PPh}_2)(\mu\text{-Ph}_2\text{PC=CHMe})(\eta^5\text{-C}_5\text{H}_5)_2]$ (**3b**). Mean principal bond lengths (Å) and angles ($^\circ$) are: Mo(1)–Mo(2) 2.792(1), Mo(1)–P(1) 2.428(3), Mo(1)–P(2) 2.441(3), Mo(1)–Cl(1) 2.450(5), Mo(1)–C(1) 2.140(10), Mo(2)–P(1) 2.385(3), Mo(2)–Cl(2) 2.472(4), Mo(2)–C(1) 2.124(9), Mo(2)–C(2) 2.304(10), P(1)–C(111) 1.836(7), P(1)–C(121) 1.853(9), P(2)–C(1) 1.724(12), P(2)–C(211) 1.814(10), P(2)–C(221) 1.816(6), C(1)–C(2) 1.409(18), C(2)–C(02) 1.502(15); range Mo(1)–C(Cp) 2.293(15)–2.410(14), range Mo(2)–C(Cp) 2.281(14)–2.408(14), C(1)–P(2)–Mo(1) 58.8(3), C(211)–P(2)–Mo(1) 132.1(3), C(211)–P(2)–C(1) 120.0(5), C(221)–P(2)–Mo(1) 120.0(3), C(221)–P(2)–C(1) 113.1(5), C(221)–P(2)–C(211) 104.4(4), Mo(2)–C(1)–Mo(1) 81.8(3), P(2)–C(1)–Mo(1) 77.6(5), P(2)–C(1)–Mo(2) 125.0(6), C(2)–C(1)–Mo(1) 132.1(8), C(2)–C(1)–Mo(2) 78.6(6), C(2)–C(1)–P(2) 147.5(7), C(1)–C(2)–Mo(2) 64.6(5), C(02)–C(2)–Mo(2) 124.9(9), C(02)–C(2)–C(1) 121.9(9).

related to (**3a**) by the replacement of the $\mu\text{-PPh}_2$ group by a third chloride ligand.

Some insight into the formation of (**3**) can be gained by treatment of (**1c**) with one equivalent of PPh_2Cl (refluxing

toluene, 6 h, relatively dilute conditions) which allows the isolation of an intermediate complex (**6c**).[†] On heating with further PPh_2Cl , (**6c**) is rapidly converted into (**3c**). This process is evidently facile since only traces of an analogous complex can be isolated from (**1b**): even with one equivalent of PPh_2Cl , (**3b**) is the major product.

A plausible mechanism for the reaction is shown in Scheme 1. We propose that the key step is oxidative addition of PPh_2Cl followed by migration to a bridging position of either the chloride ligand [leading to (**2**)] or the phosphido group [leading to (**6**) and ultimately (**3**)].

No evidence for P–C bond formation was found in the reactions of (**1**) with PPh_3 ,¹⁰ PPh_2H ,¹⁰ or P_2Ph_4 .¹¹ Its occurrence in the products (**2**)–(**5**) attests to the markedly different reactivity obtained with PPh_2Cl .

We thank the S.E.R.C. and the University of Manchester for support, and Miss G. Acum for assistance in characterisation of (**3a**).

Received, 10th February 1989; Com. 9/00663J

References

- 1 F. Iwasaki, M. J. Mays, P. R. Raithby, P. L. Taylor, and P. J. Wheatley, *J. Organomet. Chem.*, 1981, **213**, 185; J. A. Iggo, M. J. Mays, P. R. Raithby, and K. Henrick, *J. Chem. Soc., Dalton Trans.*, 1983, 205; A. D. Horton, M. J. Mays, P. R. Raithby, and K. Henrick, *ibid.*, 1988, 1083.
- 2 R. G. Hayter, in 'Preparative Inorganic Reactions,' ed. W. L. Jolly, Wiley, New York, 1965, vol. 2, p. 211.
- 3 A. J. Carty, *Pure Appl. Chem.*, 1982, **54**, 113.
- 4 K. Evertz and G. Huttner, *Chem. Ber.*, 1987, **120**, 937.
- 5 W. I. Bailey, M. H. Chisholm, F. A. Cotton, and L. A. Rankel, *J. Am. Chem. Soc.*, 1978, **100**, 5764.
- 6 R. Regragui, P. H. Dixneuf, N. J. Taylor, and A. J. Carty, *Organometallics*, 1984, **3**, 814; H. Werner and R. Zolk, *Chem. Ber.*, 1987, **120**, 1003; K. Yasafuku and H. Yamazaki, *J. Organomet. Chem.*, 1972, **35**, 367; K. Yasafuku, K. Aoki and H. Yamazaki, *ibid.*, 1975, **84**, C28; B. L. Barnett and C. Kruger, *Cryst. Struct. Commun.*, 1973, **2**, 347.
- 7 B. Klingert, A. L. Rheingold, and H. Werner, *Inorg. Chem.*, 1988, **27**, 673.
- 8 H. Kumabayashi, H. Taketomi, and S. Akutagawa, Jpn. Kokai, Tokkyo Koho 8002627, 8002628 (*Chem. Abstr.* 1980, **93**, P26588t, P26589u).
- 9 N. J. Grist, G. Hogarth, S. A. R. Knox, B. R. Lloyd, D. A. V. Morton, and A. G. Orpen, *J. Chem. Soc., Chem. Commun.*, 1988, 673.
- 10 G. R. Doel, N. D. Feasey, S. A. R. Knox, A. G. Orpen, and J. Webster, *J. Chem. Soc., Chem. Commun.*, 1986, 542.
- 11 G. Conole, M. McPartlin, M. J. Mays, and M. J. Morris, unpublished work.

Synthesis of a Series of Hexanuclear Ruthenium Carbido Cluster Alkynes under Mild Conditions: X-Ray Structure Analyses of the Complexes

$[\text{Ru}_6\text{C}(\text{CO})_{15}(\mu_3\text{-}\eta^2\text{-PhCCH})]$ and $[\text{Ru}_6\text{C}(\text{CO})_{15}(\mu_3\text{-}\eta^2\text{-PhCCMe})]^{\dagger}$

Simon R. Drake, Brian F. G. Johnson, and Jack Lewis*

University Chemical Laboratory, Lensfield Road Cambridge CB2 1EW

Gráinne Conole and Mary McPartlin*

School of Chemistry, The Polytechnic of North London, Holloway Road, London N7 8DB

The reaction of $[\text{Ru}_6\text{C}(\text{CO})_{16}]^{2-}$ (1) with alkynes in the presence of $[\text{Fe}(\text{cp})_2]\text{BF}_4$ ($\text{cp} = \eta^5\text{-C}_5\text{H}_5$) or FeCl_3 gives the alkyne cluster derivatives $[\text{Ru}_6\text{C}(\text{CO})_{15}(\mu_3\text{-}\eta^2\text{-RCCR}')] [R = R' = \text{H}$ (2), Me (3), Et (4), or Ph (5); $R \neq R'$, H and Ph (6), Me and Ph (7)] as the respective major products at room temperature. Prolonged heating of the cluster $[\text{Ru}_6\text{C}(\text{CO})_{15}(\mu_3\text{-}\eta^2\text{-PhCCH})]$ (6) in toluene over 3 d converts it into $[\text{Ru}_6\text{C}(\text{CO})_{15}(\mu\text{-H})(\text{CCPh})]$ (8), with hydride migration from the organo-fragment to a ruthenium metal centre. The structure of complexes (6) and (7) have been established by X-ray diffraction studies which show the alkyne ligands bonding to triangular ruthenium faces in a $\mu_3\text{-}\eta^2$ mode.

The analogy between the chemistry of alkyne- or alkene-substituted cluster complexes and the chemisorption of such organic molecules on a metal surface is well known.¹ An understanding of the interaction of an alkyne with a transition metal cluster may provide some insight into the nature of the interaction occurring between an unsaturated organic molecule and a metal surface. The chemistry of alkyne derivatives of M_3 and M_4 ($\text{M} = \text{Fe}, \text{Ru}, \text{or Os}$) clusters is now well established,^{2,3} and for trinuclear ruthenium clusters the use of the activated cluster $[\text{Ru}_3(\text{CO})_{12-n}(\text{NCMe})_n]$ ($n = 1$ or 2)⁴ containing the labile acetonitrile ligand has considerably simplified the production of specific cluster complexes under mild reaction conditions.⁵

Progress in the area of organo higher-nuclearity clusters has until recently been restricted due to the forcing conditions required, and many early Ru_6 organo complexes were products of $[\text{Ru}_3(\text{CO})_{12}]$ aggregation reactions.⁶ Ansell and Bradley⁷ were able to isolate $[\text{Ru}_6\text{C}(\text{CO})_{14}(\text{C}_{14}\text{H}_{14})]$ in high yield by the direct reaction of $[\text{Ru}_6\text{C}(\text{CO})_{16}]^{2-}$ (1) and tropylium bromide $[\text{C}_7\text{H}_7]^+\text{Br}^-$. The incoming ligand bitropyl ($\text{C}_{14}\text{H}_{14}$) is a product of the simple redox reaction between $[\text{Ru}_6\text{C}(\text{CO})_{16}]^{2-}$ (1) and tropylium. More recently Hayward and Shapley⁸ have shown that the oxidation of (1) under CO to $[\text{Ru}_6\text{C}(\text{CO})_{17}]$ occurs in high yield. It has now been found that this approach is widely applicable for the synthesis of a range of substituted complexes of (1).⁹

Results and Discussion

We have previously shown that the electrochemical two-electron oxidation of $[\text{Ru}_6\text{C}(\text{CO})_{16}]^{2-}$ (1) under a carbon monoxide atmosphere at a platinum electrode occurs at +0.5 V (vs. Ag-AgCl) and on the same scale the couples $[\text{Fe}(\text{cp})_2]/[\text{Fe}(\text{cp})_2]\text{BF}_4$ ($\text{cp} = \eta^5\text{-C}_5\text{H}_5$) and $\text{FeCl}_2\text{-FeCl}_3$ occur at similar values of +0.53 V.¹⁰ This provides the basis for an

alternative method of synthesis using either chemical or electrochemical oxidation of ruthenium cluster dianions in the presence of the ligand at room temperature, which results in a higher and more selective yield of the product desired.

The reactions of $[\text{Ru}_6\text{C}(\text{CO})_{16}]^{2-}$ (1) with alkynes in the presence of 2 equivalents of either of the oxidants $[\text{Fe}(\text{cp})_2]\text{BF}_4$ or FeCl_3 results in the formation of products of general formula $[\text{Ru}_6\text{C}(\text{CO})_{15}(\text{RCCR}')]$. All of the products were isolated from the reaction mixtures in high yield, by the use of chromatography. The clusters (2)–(7) have been characterised by i.r., ¹H n.m.r., electron-impact mass spectrometry (Table 1), and satisfactory microanalysis. The derivatives all had clear molecular ions consistent with the formulation $[\text{Ru}_6\text{C}(\text{CO})_{15}(\text{RCCR}')]$, and the mass spectra showed the stepwise loss of 15 carbonyl groups. The i.r. spectra (Table 1) indicated the presence of only terminal carbonyl ligands, and no resonances in the metal hydride region were observed in the ¹H n.m.r. spectra. The nature of the bonding of the organic fragments and the overall molecular geometries of (6) and (7) were established by single-crystal X-ray structure analysis. Selected bond lengths and angles are in Table 2.

In the structures of (6) and (7) shown in Figures 1 and 2 the six ruthenium atoms adopt a slightly distorted octahedral geometry [Ru-Ru 2.764–2.980(2) for (6) and 2.782–2.991(1) for (7)], with the interstitial carbon atom lying close to the geometric centre in each [Ru-C 2.015(14)–2.073(15) for (6) and 1.992(13)–2.098(11) Å for (7)] and mean $\text{Ru-C}(\text{carbido})$ distances of 2.045(25) in (6) and 2.045(42) in (7), which are shorter than that in $[\text{Ru}_6\text{C}(\text{CO})_{16}]^{2-}$ (1).¹¹ The organo ligand is bonded to the triangular face $\text{Ru}(1), \text{Ru}(2), \text{Ru}(3)$, the coordination of each metal being completed by carbonyl ligands, with three carbonyls on each of the three remaining ruthenium atoms.

In structures (6) and (7) both carbon atoms of the alkyne group bond to $\text{Ru}(3)$ [$\text{Ru}(3)\text{-C}(1)$ 2.264(11) (6) and 2.181(11) (7), $\text{Ru}(3)\text{-C}(2)$ 2.174(11) (6) and 2.201(11) (7)], in addition each bonds to one other ruthenium atom of the triangular face [$\text{Ru}(1)\text{-C}(1)$ 2.095(13) (6) and 2.069(8) (7); $\text{Ru}(2)\text{-C}(2)$ 2.076(13) (6) and 2.078(9) Å (7)].

The alkyne $\text{C}(1)\text{-C}(2)$ bond lies nearly parallel to the $\text{Ru}(1)\text{-Ru}(2)$ edge of the two clusters (Figures 1 and 2), and in both cases a reduction in the formal C–C bond order upon co-

* μ_3 -Carbido-1,1,2,2,3,3,3,4,4,5,5,6,6,6-pentadecacarbonyl- μ_3 -[phenylvinylene- $\text{C}^1(\text{Ru}^{1,4})\text{C}^2(\text{Ru}^{1,5})$]- and - μ_3 -[methyl(phenyl)vinylene- $\text{C}^1(\text{Ru}^{1,4})\text{C}^2(\text{Ru}^{1,5})$]-octahedro-hexaruthenium.

Supplementary data available: see Instructions for Authors, *J. Chem. Soc., Dalton Trans.*, 1990, Issue 1, pp. xix–xxii.

Table 1. Selected spectroscopic data for complexes (2)—(8)

Complex	I.r. ^a $\nu(\text{CO})/\text{cm}^{-1}$	m/z^b	¹ H N.m.r. ^c (δ)
(2)	2 089w, 2 046vs, 2 039s, 2 025m, 2 018m, 1 995w, 1 987w, 1 973vw	1 070	9.09 (s, 2 H)
(3)	2 087w, 2 042vs, 2 035s (sh), 2 020m, 2 011m, 1 988w, 1 960w (sh)	1 098	3.02 (s, 6 H)
(4)	2 088w, 2 043vs, 2 036s (sh), 2 019m, 2 010m, 1 982w (sh), 1 963vw (sh)	1 126	3.12 (q, 3 H), 1.57 (t, 2 H)
(5)	2 088w, 2 045vs, 2 038s (sh), 2 018m (sh), 2 014m, 1 986w, 1 962vw (sh)	1 222	7.42 (m, Ph)
(6)	2 088w, 2 044vs, 2 039s (sh), 2 019m (sh), 2 014m, 1 988w, 1 963vw (sh)	1 146	10.17 (s, 1 H), 7.41 (m, Ph)
(7)	2 088w, 2 046vs, 2 037s (sh), 2 022m, 2 015m (sh), 1 982w, 1 964vw	1 160	7.38 (m, Ph), 3.40 (s, 3 H)
(8)	2 096w, 2 051vs, 2 039s (sh), 2 028m, 2 016m, 1 994w (sh)	1 146	7.36 (m, Ph), -17.04 (s, Ru-H-Ru)

^a In CH_2Cl_2 . ^b Using ¹⁰²Ru. ^c In CD_2Cl_2 , J in Hz.

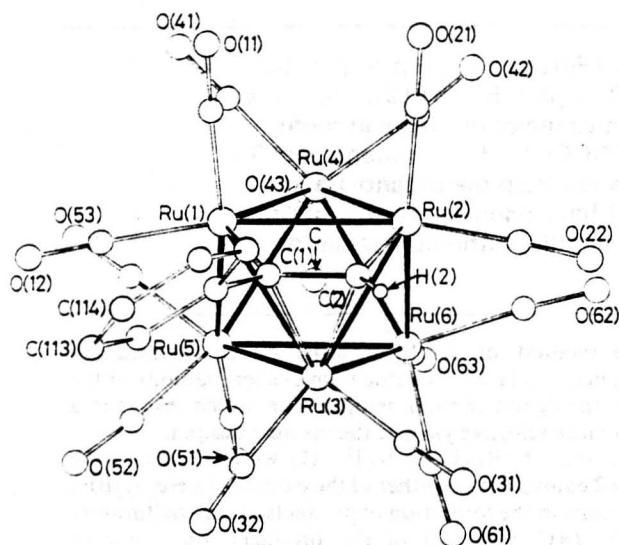


Figure 1. The structure of $[\text{Ru}_6\text{C}(\text{CO})_{15}(\mu_3\text{-}\eta^2\text{-PhCCH})]$ (6). The carbonyl carbon atoms have the same number as the corresponding oxygen atoms

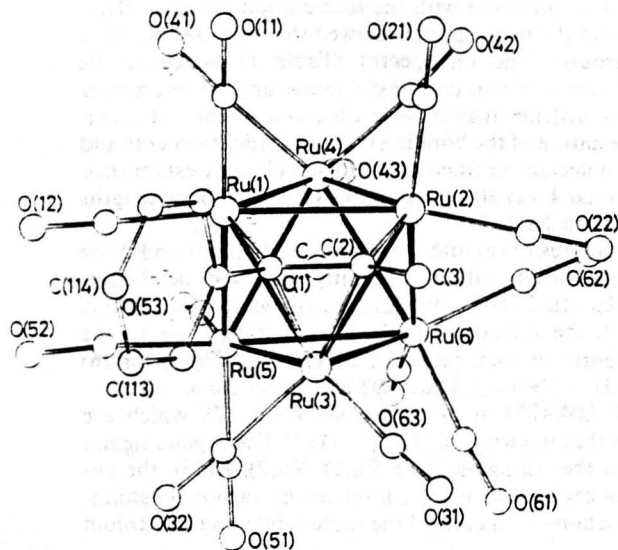


Figure 2. The structure of $[\text{Ru}_6\text{C}(\text{CO})_{15}(\mu_3\text{-}\eta^2\text{-PhCCMe})]$ (7). The carbonyl carbon atoms have the same number as the corresponding oxygen atoms

ordination of the alkyne is indicated by the C(1)–C(2) bond lengths of 1.365(17) in (6) and 1.395(13) in (7). The interaction of the alkyne with metal atoms Ru(1) and Ru(2) in both structures may be formally described as σ bonding in character, with that

to Ru(3) being π bonding (Figures 1 and 2). This 'parallel' $\mu_3\text{-}\eta^2$ mode of bonding is more widely observed in clusters containing alkyne ligands than the alternative perpendicular $\mu_3\text{-}\eta^2$ mode.¹² Formally in (6) and (7) the alkyne ligand is contributing a total of four electrons to the overall polyhedral count of the cluster giving a total of 86 electrons, as expected for octahedral clusters.

The alkyne clusters (2)—(5) and (7) were found to be stable to extremes of heat, e.g. (3) was heated under reflux in toluene for 4 d and recovered in near-quantitative yield. In contrast the cluster $[\text{Ru}_6\text{C}(\text{CO})_{15}(\mu_3\text{-}\eta^2\text{-PhCCH})]$ (6) on heating in toluene at 60 °C for 3 d is converted into the new cluster $[\text{Ru}_6\text{C}(\text{CO})_{15}(\mu\text{-H})(\text{CPh})]$ (8). The mass spectrum shows a clear molecular ion and the ¹H n.m.r. spectrum of (8) in CD_2Cl_2 is consistent with the presence of a metal hydride. It appears that there has been a transfer of a hydrogen atom from the organo fragment to the metal core. We attribute this thermal stability to the presence of the interstitial carbido atom in these hexanuclear ruthenium clusters. The corresponding Os₆ and Os₇ alkyne-based clusters have been found to undergo major skeletal rearrangements on prolonged heating.^{13,14}

Experimental

All reactions were carried out under nitrogen using dry degassed solvents. Infrared spectra were recorded on a Perkin-Elmer PE 983 spectrometer. ¹H n.m.r. spectra on Bruker WM 250 and WH 400 instruments using CD_2Cl_2 as the internal reference. Electron-impact mass spectroscopy was performed on a N.E.I. MS 12 spectrometer using tris(perfluoroheptyl)-s-triazine as calibrant. Microanalyses were performed in the University Chemical Laboratory, Cambridge. Thin-layer chromatography plates (20 × 20 cm) were bought from Merck and were coated with a 0.25-mm layer of silica gel. The cluster $[\text{N}(\text{PPh}_3)_2]_2[\text{Ru}_6\text{C}(\text{CO})_{16}]$ was prepared by the literature method.¹¹

Preparations.— $[\text{Ru}_6\text{C}(\text{CO})_{15}(\text{HCCH})]$ (2). The salt $[\text{N}(\text{PPh}_3)_2]_2[\text{Ru}_6\text{C}(\text{CO})_{16}]$ (100 mg, 0.0467 mmol) was dissolved in CH_2Cl_2 (freeze-thaw degassed) (15 cm³) and HCCH bubbled through the solution for 10 min. The oxidant $[\text{Fe}(\text{cp})_2]\text{BF}_4$ (30 mg, 0.111 mmol) was then added as a solid and the reaction monitored by i.r. spectroscopy. It was complete after 15 min with a change in colour from red to black. The reaction mixture was then filtered through a sintered funnel and reduced in volume. The resulting solution was then separated on thin silica plates using 20% CH_2Cl_2 –80% hexane to yield a yellow band at r.f. 0.1 (ferrocene) and the alkyne cluster $[\text{Ru}_6\text{C}(\text{CO})_{15}(\text{HCCH})]$ (2) as a brown band at r.f. 0.4. Black crystals of (2) were obtained by slow diffusion of a layered CH_2Cl_2 –hexane solution under N_2 over 24 h at 0 °C (yield 16 mg, 27%), and were characterised by i.r. ¹H n.m.r., mass spectroscopy (Table 1), and microanalysis (Found: C, 20.35; H, 0.20. Calc. for $\text{C}_{18}\text{H}_2\text{O}_{15}\text{Ru}_6$: C, 20.20; H, 0.20%).

Table 2. Selected bond lengths (Å) and angles (°) for complexes (6) and (7)

	(6)	(7)		(6)	(7)
Ru(1)-Ru(2)	2.837(2)	2.815(1)	Ru(3)-C(2)	2.174(11)	2.201(11)
Ru(1)-Ru(3)	2.815(2)	2.791(1)	Ru(4)-Ru(5)	2.874(2)	2.915(1)
Ru(1)-Ru(4)	2.980(2)	2.989(1)	Ru(4)-Ru(6)	2.857(2)	2.836(1)
Ru(1)-Ru(5)	2.863(1)	2.952(1)	Ru(4)-C(41)	1.946(20)	1.916(11)
Ru(1)-C(11)	1.894(15)	1.883(13)	Ru(4)-C(42)	1.925(16)	1.894(12)
Ru(1)-C(12)	1.895(15)	1.882(12)	Ru(4)-C(43)	1.930(16)	1.908(17)
Ru(1)-C(1)	2.095(13)	2.069(8)	Ru(5)-Ru(6)	2.912(2)	2.870(1)
Ru(2)-Ru(3)	2.764(2)	2.782(1)	Ru(5)-C(51)	1.902(14)	1.910(13)
Ru(2)-Ru(4)	2.963(2)	2.991(1)	Ru(5)-C(52)	1.908(19)	1.876(17)
Ru(2)-Ru(6)	2.934(1)	2.885(1)	Ru(5)-C(53)	1.880(18)	1.902(11)
Ru(2)-C(21)	1.892(16)	1.904(13)	Ru(6)-C(61)	1.913(19)	1.929(12)
Ru(2)-C(22)	1.871(17)	1.888(10)	Ru(6)-C(62)	1.893(16)	1.890(13)
Ru(2)-C(2)	2.076(13)	2.078(9)	Ru(6)-C(63)	1.862(21)	1.880(14)
Ru(3)-Ru(5)	2.969(2)	2.880(1)	C(1)-C(2)	1.365(17)	1.395(13)
Ru(3)-Ru(6)	2.930(2)	2.974(1)	C(1)-C(111)	1.475(13)	1.504(12)
Ru(3)-C(31)	1.864(17)	1.906(9)	C(2)-C(3)		1.519(13)
Ru(3)-C(32)	1.915(15)	1.902(12)	Cl(1)-C(S)		1.61(6)
Ru(3)-C(1)	2.264(11)	2.181(11)	Cl(2)-C(S)		1.97(6)
Ru-Carbide	2.015-2.073	1.992-2.098			
Ru(3)-Ru(1)-Ru(2)	58.6(1)	59.5(1)	C(32)-Ru(3)-Ru(1)	110.5(5)	102.1(3)
Ru(4)-Ru(1)-Ru(2)	61.2(1)	62.0(1)	C(32)-Ru(3)-Ru(2)	165.8(4)	162.7(3)
Ru(4)-Ru(1)-Ru(3)	90.1(1)	90.7(1)	C(32)-Ru(3)-Ru(5)	94.3(4)	81.1(3)
Ru(5)-Ru(1)-Ru(2)	91.3(1)	89.6(1)	C(32)-Ru(3)-Ru(6)	131.6(4)	126.4(3)
Ru(5)-Ru(1)-Ru(3)	63.0(1)	60.1(1)	C(41)-Ru(4)-Ru(1)	73.9(5)	76.1(3)
Ru(5)-Ru(1)-Ru(4)	58.9(1)	58.8(1)	C(41)-Ru(4)-Ru(2)	113.0(5)	117.7(3)
Ru(3)-Ru(2)-Ru(1)	60.3(1)	59.8(1)	C(41)-Ru(4)-Ru(5)	102.7(5)	102.6(4)
Ru(4)-Ru(2)-Ru(1)	61.8(1)	61.9(1)	C(41)-Ru(4)-Ru(6)	161.3(5)	161.5(4)
Ru(4)-Ru(2)-Ru(3)	91.5(1)	90.9(1)	C(42)-Ru(4)-Ru(1)	121.3(5)	109.5(4)
Ru(6)-Ru(2)-Ru(1)	90.1(1)	91.5(1)	C(42)-Ru(4)-Ru(2)	75.4(6)	68.7(3)
Ru(6)-Ru(2)-Ru(3)	61.8(1)	63.3(1)	C(42)-Ru(4)-Ru(5)	157.1(6)	154.1(3)
Ru(6)-Ru(2)-Ru(4)	58.0(1)	57.7(1)	C(42)-Ru(4)-Ru(6)	96.4(6)	98.4(3)
Ru(2)-Ru(3)-Ru(1)	61.1(1)	60.7(1)	C(43)-Ru(4)-Ru(1)	144.5(4)	157.9(5)
Ru(5)-Ru(3)-Ru(1)	59.3(1)	62.7(1)	C(43)-Ru(4)-Ru(2)	152.1(5)	143.4(4)
Ru(5)-Ru(3)-Ru(2)	90.6(1)	91.7(1)	C(43)-Ru(4)-Ru(5)	93.8(5)	104.4(6)
Ru(6)-Ru(3)-Ru(1)	90.6(1)	90.1(1)	C(43)-Ru(4)-Ru(6)	96.7(6)	96.2(5)
Ru(6)-Ru(3)-Ru(2)	61.9(1)	60.1(1)	C(51)-Ru(5)-Ru(1)	171.2(5)	143.2(3)
Ru(6)-Ru(3)-Ru(5)	59.2(1)	58.7(1)	C(51)-Ru(5)-Ru(3)	119.5(6)	90.4(3)
Ru(2)-Ru(4)-Ru(1)	57.0(1)	56.2(1)	C(51)-Ru(5)-Ru(4)	110.1(5)	143.7(4)
Ru(5)-Ru(4)-Ru(1)	58.5(1)	60.0(1)	C(51)-Ru(5)-Ru(6)	81.8(5)	90.1(4)
Ru(5)-Ru(4)-Ru(2)	88.6(1)	86.9(1)	C(52)-Ru(5)-Ru(1)	97.5(4)	81.0(6)
Ru(6)-Ru(4)-Ru(1)	88.8(1)	88.9(1)	C(52)-Ru(5)-Ru(3)	85.4(5)	106.1(4)
Ru(6)-Ru(4)-Ru(2)	60.5(1)	59.3(1)	C(52)-Ru(5)-Ru(4)	158.7(5)	120.8(5)
Ru(6)-Ru(4)-Ru(5)	61.1(1)	59.8(1)	C(52)-Ru(5)-Ru(6)	132.6(6)	167.8(5)
Ru(3)-Ru(5)-Ru(1)	57.7(1)	57.2(1)	C(53)-Ru(5)-Ru(1)	88.3(4)	121.9(4)
Ru(4)-Ru(5)-Ru(1)	62.6(1)	61.3(1)	C(53)-Ru(5)-Ru(3)	145.1(4)	161.1(4)
Ru(4)-Ru(5)-Ru(3)	89.2(1)	90.5(1)	C(53)-Ru(5)-Ru(4)	80.7(5)	74.8(4)
Ru(6)-Ru(5)-Ru(1)	90.1(1)	89.0(1)	C(53)-Ru(5)-Ru(6)	135.0(5)	99.4(4)
Ru(6)-Ru(5)-Ru(3)	59.7(1)	62.3(1)	C(61)-Ru(6)-Ru(2)	120.2(4)	107.4(4)
Ru(6)-Ru(5)-Ru(4)	59.2(1)	58.7(1)	C(61)-Ru(6)-Ru(3)	78.2(5)	76.5(4)
Ru(3)-Ru(6)-Ru(2)	56.3(1)	56.7(1)	C(61)-Ru(6)-Ru(4)	162.1(5)	166.6(4)
Ru(4)-Ru(6)-Ru(2)	61.5(1)	63.0(1)	C(61)-Ru(6)-Ru(5)	102.4(5)	111.2(4)
Ru(4)-Ru(6)-Ru(3)	90.3(1)	90.2(1)	C(62)-Ru(6)-Ru(2)	76.9(4)	85.1(4)
Ru(5)-Ru(6)-Ru(2)	88.5(1)	89.8(1)	C(62)-Ru(6)-Ru(3)	117.1(5)	132.9(4)
Ru(5)-Ru(6)-Ru(3)	61.1(1)	59.0(1)	C(62)-Ru(6)-Ru(4)	102.7(6)	96.0(4)
Ru(5)-Ru(6)-Ru(4)	59.7(1)	61.4(1)	C(62)-Ru(6)-Ru(5)	161.4(5)	156.4(3)
C(11)-Ru(1)-Ru(2)	95.7(5)	90.6(3)	C(63)-Ru(6)-Ru(2)	142.6(8)	156.0(4)
C(11)-Ru(1)-Ru(3)	140.7(6)	140.0(3)	C(63)-Ru(6)-Ru(3)	151.7(6)	134.0(4)
C(11)-Ru(1)-Ru(4)	103.1(5)	98.0(4)	C(63)-Ru(6)-Ru(4)	87.8(8)	93.6(3)
C(11)-Ru(1)-Ru(5)	153.9(6)	153.0(3)	C(63)-Ru(6)-Ru(5)	94.1(7)	83.1(3)
C(12)-Ru(1)-Ru(2)	168.0(6)	164.2(3)	Ru(3)-C(1)-Ru(1)	80.4(4)	82.0(4)
C(12)-Ru(1)-Ru(3)	111.3(5)	112.5(3)	C(2)-C(1)-Ru(1)	108.2(9)	110.2(6)
C(12)-Ru(1)-Ru(4)	128.1(4)	133.7(3)	C(2)-C(1)-Ru(3)	68.5(7)	72.2(6)
C(12)-Ru(1)-Ru(5)	88.7(4)	97.8(4)	C(111)-C(1)-Ru(1)	125.3(8)	124.1(6)
C(21)-Ru(2)-Ru(1)	94.3(5)	96.4(3)	C(111)-C(1)-Ru(3)	127.9(8)	130.7(7)
C(21)-Ru(2)-Ru(3)	143.8(5)	141.3(3)	C(111)-C(1)-C(2)	125(1)	121.8(7)
C(21)-Ru(2)-Ru(4)	98.6(6)	104.6(3)	Ru(3)-C(2)-Ru(2)	81.1(4)	81.0(3)
C(21)-Ru(2)-Ru(6)	150.0(5)	153.7(3)	C(1)-C(2)-Ru(2)	113(1)	109.8(6)

Table 2 (continued)

	(6)	(7)		(6)	(7)
C(22)-Ru(2)-Ru(1)	158.8(5)	165.4(3)	C(1)-C(2)-Ru(3)	75.7(7)	70.7(6)
C(22)-Ru(2)-Ru(3)	105.5(5)	107.4(3)	C(3)-C(2)-Ru(2)		123.6(7)
C(22)-Ru(2)-Ru(4)	138.0(5)	128.9(3)	C(3)-C(2)-Ru(3)		128.7(7)
C(22)-Ru(2)-Ru(6)	96.6(4)	88.3(4)	C(3)-C(2)-C(1)		124.4(9)
C(31)-Ru(3)-Ru(1)	155.4(4)	155.3(4)	C(112)-C(111)-C(1)	123.4(7)	122.1(8)
C(31)-Ru(3)-Ru(2)	99.7(4)	106.8(4)	C(116)-C(111)-C(1)	116.6(7)	117.9(8)
C(31)-Ru(3)-Ru(5)	141.2(4)	141.9(4)	Cl(2)-C(S)-Cl(1)		106(3)
C(31)-Ru(3)-Ru(6)	93.1(4)	101.9(4)			

Table 3. Fractional atomic co-ordinates for complexes (6) and (7)

Atom	(6)			(7)		
	x	y	z	x	y	z
Ru(1)	-0.347 80(12)	0.317 26(6)	0.049 07(6)	-0.340 26(4)	-0.169 29(8)	0.063 42(8)
Ru(2)	-0.319 18(12)	0.162 52(6)	-0.000 65(6)	-0.182 20(4)	-0.072 17(8)	0.077 53(8)
Ru(3)	-0.111 41(12)	0.275 84(6)	0.007 83(6)	-0.231 52(4)	-0.120 32(8)	0.330 74(8)
Ru(4)	-0.273 23(12)	0.184 85(7)	0.158 68(6)	-0.252 76(5)	-0.357 48(8)	-0.116 74(8)
Ru(5)	-0.065 82(12)	0.307 21(6)	0.166 20(6)	-0.299 79(5)	-0.398 29(8)	0.156 63(8)
Ru(6)	-0.029 55(12)	0.148 02(6)	0.118 14(6)	-0.140 53(4)	-0.301 12(8)	0.154 24(8)
C(11)	-0.554 8(16)	0.317 6(10)	0.010 6(9)	-0.368 5(6)	-0.086 0(11)	-0.083 6(11)
O(11)	-0.678 4(12)	0.315 5(7)	-0.012 7(8)	-0.385 7(5)	-0.033 1(9)	-0.170 0(9)
C(12)	-0.348 6(17)	0.427 1(9)	0.068 1(8)	-0.442 6(6)	-0.188 2(11)	0.096 5(12)
O(12)	-0.345 5(13)	0.492 0(6)	0.079 1(6)	-0.504 9(5)	-0.195 4(11)	0.115 7(12)
C(21)	-0.522 4(17)	0.141 8(9)	-0.037 8(9)	-0.197 5(6)	0.031 6(11)	-0.056 3(12)
O(21)	-0.643 5(12)	0.130 4(8)	-0.056 1(7)	-0.208 5(5)	0.094 5(9)	-0.137 3(10)
C(22)	-0.293 8(17)	0.082 8(9)	-0.061 9(8)	-0.076 6(6)	0.014 3(10)	0.140 0(11)
O(22)	-0.271 5(13)	0.034 3(7)	-0.100 1(7)	-0.012 9(4)	0.069 5(9)	0.180 8(10)
C(31)	-0.021 7(16)	0.227 6(8)	-0.050 9(7)	-0.155 4(6)	-0.011 2(11)	0.506 3(11)
O(31)	0.028 7(13)	0.196 0(6)	-0.088 1(6)	-0.109 2(5)	0.055 5(9)	0.606 6(9)
C(32)	-0.008 5(15)	0.368 5(8)	-0.002 3(7)	-0.294 9(6)	-0.161 2(10)	0.466 0(11)
O(32)	0.052 8(12)	0.420 2(6)	-0.012 1(6)	-0.334 1(5)	-0.186 7(9)	0.542 8(10)
C(41)	-0.431 1(20)	0.243 0(8)	0.173 1(9)	-0.350 1(6)	-0.389 8(10)	-0.252 8(12)
O(41)	-0.516 5(13)	0.272 1(7)	0.188 6(7)	-0.405 8(5)	-0.416 9(8)	-0.342 5(10)
C(42)	-0.367 5(18)	0.083 4(9)	0.133 2(10)	-0.192 2(6)	-0.266 4(11)	-0.222 1(11)
O(42)	-0.425 6(15)	0.026 6(7)	0.122 4(7)	-0.159 6(5)	-0.230 8(9)	-0.304 9(8)
C(43)	-0.181 1(18)	0.157 9(8)	0.262 9(9)	-0.228 8(9)	-0.525 5(17)	-0.223 1(18)
O(43)	-0.124 6(13)	0.145 6(7)	0.323 3(6)	-0.213 6(7)	-0.628 3(14)	-0.279 4(15)
C(51)	0.118 0(17)	0.283 5(9)	0.242 1(9)	-0.268 3(7)	-0.452 1(11)	0.330 8(12)
O(51)	0.224 6(14)	0.271 5(9)	0.288 7(8)	-0.249 1(6)	-0.487 1(8)	0.430 9(9)
C(52)	0.005 9(19)	0.407 8(11)	0.150 6(9)	-0.404 5(9)	-0.422 7(16)	0.172 8(17)
O(52)	0.044 6(16)	0.470 6(7)	0.145 6(7)	-0.467 6(8)	-0.447 6(13)	0.188 4(15)
C(53)	-0.148 6(17)	0.350 5(10)	0.231 2(8)	-0.315 3(6)	-0.574 8(12)	0.013 5(12)
O(53)	-0.195 3(14)	0.378 5(8)	0.271 9(7)	-0.325 9(6)	-0.686 3(8)	-0.056 6(10)
C(61)	0.142 9(18)	0.158 1(9)	0.095 5(9)	-0.078 7(7)	-0.233 6(12)	0.358 8(14)
O(61)	0.249 5(12)	0.156 7(7)	0.085 0(7)	-0.037 5(5)	-0.202 6(10)	0.473 4(9)
C(62)	-0.071 0(17)	0.043 4(9)	0.081 6(9)	-0.053 2(6)	-0.268 1(13)	0.066 2(14)
O(62)	-0.084 3(15)	-0.022 0(6)	0.064 0(8)	-0.000 5(5)	-0.255 1(11)	0.013 8(13)
C(63)	0.065 8(24)	0.110 6(12)	0.214 8(12)	-0.135 0(6)	-0.483 6(13)	0.118 9(14)
O(63)	0.126 5(19)	0.082 0(10)	0.271 2(10)	-0.129 8(6)	-0.594 6(9)	0.097 7(12)
C	-0.194 4(16)	0.232 1(8)	0.084 2(8)	-0.242 2(7)	-0.237 7(12)	0.101 3(13)
C(1)	-0.338 5(13)	0.322 5(7)	-0.057 5(6)	-0.299 5(5)	0.007 3(9)	0.246 1(10)
C(2)	-0.321 0(14)	0.247 4(7)	-0.078 7(7)	-0.221 6(5)	0.057 5(9)	0.251 7(10)
C(111)	-0.379 3(9)	0.391 6(4)	-0.107 6(4)	-0.350 5(4)	0.096 5(7)	0.321 5(8)
C(112)	-0.318 6(9)	0.466 6(4)	-0.087 2(4)	-0.366 5(4)	0.101 3(7)	0.465 3(8)
C(113)	-0.364 3(9)	0.529 2(4)	-0.137 6(4)	-0.416 0(4)	0.182 5(7)	0.528 6(8)
C(114)	-0.470 7(9)	0.516 9(4)	-0.208 3(4)	-0.449 6(4)	0.259 0(7)	0.448 1(8)
C(115)	-0.531 4(9)	0.441 9(4)	-0.228 7(4)	-0.433 6(4)	0.254 2(7)	0.304 4(8)
C(116)	-0.485 7(9)	0.379 2(4)	-0.178 4(4)	-0.384 1(4)	0.172 9(7)	0.241 1(8)
C(3)				-0.179 4(6)	0.202 1(11)	0.338 8(12)
C(S)				-0.020 1(31)	-0.429 3(52)	-0.359 3(59)
Cl(1)				-0.054 6(5)	-0.552 8(10)	-0.303 2(13)
Cl(2)				0.023 1(8)	-0.509 3(13)	-0.540 8(16)

[Ru₆C(CO)₁₅(MeCCMe)] (3). The salt [N(PPh₃)₂]₂[Ru₆-C(CO)₁₆] (100 mg, 0.0467 mmol) was dissolved in CH₂Cl₂ (freeze-thaw degassed) (15 cm³) and MeCCMe (5 μl, 0.060 mmol) added at 0 °C to the solution. The oxidant [Fe(cp)₂]₂BF₄

(38 mg, 0.111 mmol) was then added as a solid and the reaction monitored by i.r. spectroscopy. It was complete after 15 min with a change in colour from red to black. The reaction mixture was then filtered through a sintered funnel and reduced in

volume. The resulting solution was separated on thin silica plates using 20% CH₂Cl₂-80% hexane to yield a yellow band at *R_f* 0.1 (ferrocene) and the alkyne cluster [Ru₆C(CO)₁₅(MeCCMe)] (3) as a brown band at *R_f* 0.4. Black crystals of (3) were obtained by slow diffusion of a layered CH₂Cl₂-hexane solution under N₂ over 24 h at 0 °C (yield 45 mg, 89%), and were characterised by i.r., ¹H n.m.r., mass spectroscopy (Table 1), and microanalysis (Found: C, 22.20; H, 0.65. Calc for C₂₀H₆O₁₅Ru₆: C, 21.85; H, 0.55%).

[Ru₆C(CO)₁₅(EtCCEt)] (4). The salt [N(PPh₃)₂]₂[Ru₆C(CO)₁₅]₂ (100 mg, 0.0467 mmol) was dissolved in CH₂Cl₂ (freeze-thaw degassed) (15 cm³) and EtCCEt (5 μl, 0.061 mmol) added at 0 °C to the solution. The oxidant [Fe(cp)₂]₂BF₄ (30 mg, 0.111 mmol) was then added as a solid and the reaction monitored by i.r. spectroscopy. It was complete after 15 min with a change in colour from red to black. The reaction mixture was then filtered through a sintered funnel and reduced in volume. The resulting solution was separated on thin silica plates using 20% CH₂Cl₂-80% hexane to yield a yellow band at *R_f* 0.1 (ferrocene) and the alkyne cluster [Ru₆C(CO)₁₅(EtCCEt)] (4) as a brown band at *R_f* 0.4. Black crystals of (4) were obtained by slow diffusion of a layered CH₂Cl₂-hexane solution under N₂ over 24 h at 0 °C (yield 48 mg, 90%), and were characterised by i.r., ¹H n.m.r., mass spectroscopy (Table 1), and microanalysis (Found: C, 23.50; H, 1.00. Calc. for C₂₂H₁₀O₁₅Ru₆: C, 23.45; H, 0.90%).

[Ru₆C(CO)₁₅(PhCCPh)] (5). The salt [N(PPh₃)₂]₂[Ru₆C(CO)₁₅]₂ (100 mg, 0.0467 mmol) was dissolved in CH₂Cl₂ (freeze-thaw degassed) (15 cm³) and PhCCPh (10 mg, 0.0562 mmol) added at 0 °C to the solution. The oxidant [Fe(cp)₂]₂BF₄ (30 mg, 0.111 mmol) was then added as a solid and the reaction monitored by i.r. spectroscopy. It was complete after 15 min with a change in colour from red to black. The reaction mixture was then filtered through a sintered funnel and reduced in volume. The resulting solution was separated on thin silica plates using 20% CH₂Cl₂-80% hexane to yield a yellow band at *R_f* 0.1 (ferrocene) and the alkyne cluster [Ru₆C(CO)₁₅(PhCCPh)] (5) as a brown band at *R_f* 0.4. Black crystals of (5) were obtained by slow diffusion of a layered CH₂Cl₂-hexane solution under N₂ over 24 h at 0 °C (yield 54 mg, 94%), and were characterised by i.r., ¹H n.m.r., mass spectroscopy (Table 1), and microanalysis (Found: C, 29.65; H, 0.95. Calc. for C₃₀H₁₀O₁₅Ru₆: C, 29.45; H, 0.80%).

[Ru₆C(CO)₁₅(PhCCH)] (6). The salt [N(PPh₃)₂]₂[Ru₆C(CO)₁₅]₂ (100 mg, 0.0467 mmol) was dissolved in CH₂Cl₂ (freeze-thaw degassed) (15 cm³) and PhCCH (7 μl, 0.060 mmol) added at 0 °C to the solution. The oxidant [Fe(cp)₂]₂BF₄ (30 mg, 0.111 mmol) was then added as a solid and the reaction monitored by i.r. spectroscopy. It was complete after 15 min with a change in colour from red to black. The reaction mixture was then filtered through a sintered funnel and reduced in volume. The resulting solution was then separated on thin silica plates using 20% CH₂Cl₂-80% hexane to yield a yellow band at *R_f* 0.1 (ferrocene) and the alkyne cluster [Ru₆C(CO)₁₅(PhCCH)] (6) as a brown band at *R_f* 0.4. Black crystals of (6) were obtained by slow diffusion of a layered CH₂Cl₂-hexane solution under N₂ over 24 h at 0 °C (yield 50 mg, 92%), and were characterised by i.r., ¹H n.m.r., mass spectroscopy (Table 1), and microanalysis (Found: C, 25.25; H, 0.70. Calc. for C₂₄H₆O₁₅Ru₆: C, 25.15; H, 0.55%).

[Ru₆C(CO)₁₅(PhCCMe)] (7). The salt [N(PPh₃)₂]₂[Ru₆C(CO)₁₅]₂ (100 mg, 0.0467 mmol) was dissolved in CH₂Cl₂ (freeze-thaw degassed) (15 cm³) and PhCCMe (7 μl, 0.0604 mmol) added at 0 °C to the solution. The oxidant [Fe(cp)₂]₂BF₄ (30 mg, 0.111 mmol) was then added as a solid and the reaction monitored by i.r. spectroscopy. It was complete after 15 min with a change in colour from red to black. The reaction mixture was then filtered through a sintered funnel and reduced in

volume. The resulting solution was separated on thin silica plates using 20% CH₂Cl₂-80% hexane to yield a yellow band at *R_f* 0.1 (ferrocene) and the alkyne cluster [Ru₆C(CO)₁₅(PhCCMe)] (7) as a brown band at *R_f* 0.4. Black crystals of (7) were obtained by slow diffusion of a layered CH₂Cl₂-hexane solution under N₂ over 24 h at 0 °C (yield 50 mg, 91%), and were characterised by i.r., ¹H n.m.r., mass spectroscopy (Table 1), and microanalysis (Found: C, 26.05; H, 0.85. Calc. for C₂₅H₈O₁₅Ru₆: C, 25.85; H, 0.70%).

[Ru₆C(CO)₁₅(μ-H)(CCPh)] (8). The cluster [Ru₆C(CO)₁₅(PhCCH)] (100 mg, 0.0873 mmol) was dissolved in toluene (freeze-thaw degassed) (15 cm³) and heated at 60 °C for 3 d. The reaction was monitored by i.r. spectroscopy and was complete after this time with a change in colour from brown to black. The reaction mixture was then filtered through a sintered funnel and reduced in volume. The resulting solution was separated on thin silica plates using 40% CH₂Cl₂-60% hexane to yield a red-brown band of [Ru₆C(CO)₁₅(μ-H)(CCPh)] (8) at *R_f* 0.5. Black crystals of (8) were obtained by slow diffusion of a layered CH₂Cl₂-hexane solution under N₂ over 24 h at 0 °C (yield 82 mg, 82%), and were characterised by i.r., ¹H n.m.r., mass spectroscopy (Table 1), and microanalysis (Found: C, 25.40; H, 0.75. Calc. for C₂₄H₆O₁₅Ru₆: C, 25.15; H, 0.55%).

X-Ray Structure Analyses.—Crystal data for complex (6), C₂₄H₆O₁₅Ru₆, *M* = 1 140.30, monoclinic, space group *P*2₁/*c*, *a* = 9.853(2), *b* = 16.911(3), *c* = 19.312(4) Å, β = 111.79(2)°, *U* = 2 987.93 Å³, *Z* = 4, *D_c* = 2.534 g cm⁻³, *F*(000) = 2 136, μ(Mo-K_α) = 27.51 cm⁻¹.

Crystal data for complex (7)·0.5 CH₂Cl₂, C_{25.5}H₉Cl₂O₁₅Ru₆, *M* = 1 197, triclinic, space group *P*1̄ (no. 2), *a* = 17.809(3), *b* = 10.567(2), *c* = 9.310(2) Å, α = 106.99(2), β = 98.135(2), γ = 98.824(2)°, *U* = 1 623.23 Å³, *Z* = 2, *D_c* = 2.449 g cm⁻³, *F*(000) = 1 126, μ(Mo-K_α) = 28.2 cm⁻¹.

Data collection. Crystals of sizes 0.38 × 0.26 × 0.18 mm for (6) and 0.25 × 0.20 × 0.18 mm for (7) were used for data collection using a Philips PW1100 diffractometer in the θ range 3–25°, as described previously,¹⁵ with scan widths of 0.80° for (6) and 0.90° for (7). Equivalent reflections for (6) and for (7) were merged to give 3 033 and 4 037 data respectively with *I*/σ(*I*) ≥ 3.0.

*Structure solution and refinement.*¹⁶ The co-ordinates of the six ruthenium atoms in each structure were deduced from a Patterson synthesis, and the remaining non-hydrogen atoms were located from subsequent difference Fourier syntheses. Absorption corrections were applied to the data using the method of Walker and Stuart.¹⁷ For both structures the metal atoms and the atoms of the carbonyl ligands were assigned anisotropic thermal parameters in the final cycles of full-matrix refinement, in which weights of *w* = 1/σ²(*F_o*) were assigned to the individual reflections. Refinement converged at *R* = 0.0487 and *R'* = 0.0483 for (6) and *R* = 0.0460 and *R'* = 0.0469 for (7).

Additional material available from the Cambridge Crystallographic Data Centre comprises H-atom co-ordinates, thermal parameters, and remaining bond lengths and angles.

Acknowledgements

We thank the S.E.R.C. for a studentship to G. C. and St. John's College, Cambridge, for the award of a Research Fellowship (to S. R. D.).

References

- 1 R. C. Brady and R. Pettit, *J. Am. Chem. Soc.*, 1981, **103**, 1287.
- 2 G. A. Somorjai, *Chem. Rev.*, 1984, 321.
- 3 E. L. Muetterties, *Pure Appl. Chem.*, 1982, **54**, 83.
- 4 G. A. Foulds, B. F. G. Johnson, and J. Lewis, *J. Organomet. Chem.*, 1985, **296**, 147.

- 5 G. A. Foulds, B. F. G. Johnson, and J. Lewis, *J. Organomet. Chem.*, 1985, **294**, 123.
- 6 B. F. G. Johnson, R. D. Johnson, and J. Lewis, *Chem. Commun.*, 1967, 1057; R. Mason and W. R. Robinson, *ibid.*, 1968, 468.
- 7 G. B. Ansell and J. S. Bradley, *Acta Crystallogr., Sect. B*, 1980, **36**, 1930.
- 8 C.-M. T. Hayward and J. R. Shapley, *Inorg. Chem.*, 1982, **21**, 3816.
- 9 S. R. Drake, B. F. G. Johnson, and J. Lewis, *J. Chem. Soc., Chem. Commun.*, 1988, 1033.
- 10 S. R. Drake, B. F. G. Johnson, and J. Lewis, *J. Chem. Soc., Dalton Trans.*, 1989, 505.
- 11 B. F. G. Johnson, J. Lewis, S. W. Sankey, K. Wong, M. McPartlin, and W. J. H. Nelson, *J. Organomet. Chem.*, 1980, **191**, C3.
- 12 E. Sappa, A. Tiripicchio, and P. Braunstein, *Chem. Rev.*, 1983, **83**, 203.
- 13 M. P. Gomez-Sal, B. F. G. Johnson, R. A. Kamarudin, J. Lewis, and P. R. Raithby, *J. Chem. Soc., Chem. Commun.*, 1985, 1622.
- 14 D. Braga, B. F. G. Johnson, J. Lewis, and J. Lunniss, *J. Chem. Soc., Chem. Commun.*, 1988, 972.
- 15 M. K. Cooper, P. J. Guerney, and M. McPartlin, *J. Chem. Soc., Dalton Trans.*, 1982, 757.
- 16 G. M. Sheldrick, SHELX 76 program for crystal structure determination. University of Cambridge, 1976.
- 17 N. Walker and D. Stuart, *Acta Crystallogr., Sect. A*, 1983, **39**, 158.

Received 30th November 1988; Paper 8/04741C

Chemistry of Phosphido-bridged Dimolybdenum Complexes. Part 5.¹ Synthesis and Protonation of a Phosphido-bridged Dimolybdenum Complex containing a Terminal Alkyne Ligand: X-Ray Crystal Structures of $[\text{Mo}_2(\mu\text{-PPh}_2)_2(\text{CO})(\eta\text{-C}_2\text{Me}_2)(\eta\text{-C}_5\text{H}_5)_2]$ and $[\text{Mo}_2(\mu\text{-CO})(\mu\text{-PPh}_2)\{\mu\text{-Ph}_2\text{PC}(\text{Me})=\text{CHMe}\}(\eta\text{-C}_5\text{H}_5)_2][\text{BF}_4]^+$

Gráinne Conole and Mary McPartlin

School of Chemistry, The Polytechnic of North London, Holloway Road, London N7 8DB

Martin J. Mays* and Michael J. Morris

University Chemical Laboratory, Lensfield Road, Cambridge CB2 1EW

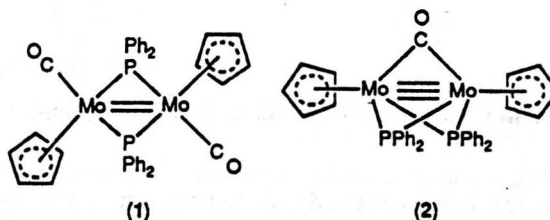
The reaction between the alkyne complex $[\text{Mo}_2(\mu\text{-C}_2\text{Me}_2)(\text{CO})_4(\eta\text{-C}_5\text{H}_5)_2]$ and P_2Ph_4 in refluxing toluene affords a 42% yield of $[\text{Mo}_2(\mu\text{-PPh}_2)_2(\text{CO})(\eta\text{-C}_2\text{Me}_2)(\eta\text{-C}_5\text{H}_5)_2]$. An X-ray diffraction study has revealed that the but-2-yne ligand is co-ordinated to only one molybdenum atom, and that the molecule contains a planar $\text{Mo}_2(\mu\text{-PPh}_2)_2$ unit with a formal Mo–Mo double bond of length 2.865(1) Å. Several other minor products are discussed in relation to the proposed mechanism of the reaction. Reaction of the terminal alkyne complex with $\text{HBF}_4\cdot\text{OEt}_2$ causes a structural rearrangement in which the protonated but-2-yne is inserted into one of the Mo–P bonds to give a bridging $\text{Ph}_2\text{PC}(\text{Me})=\text{CHMe}$ vinylphosphine ligand; the structure of the product has been confirmed by X-ray diffraction.

The organic chemistry of dimolybdenum complexes derived from $[\text{Mo}_2(\text{CO})_6(\eta\text{-C}_5\text{H}_5)_2]$ and $[\text{Mo}_2(\text{CO})_4(\eta\text{-C}_5\text{H}_5)_2]$ is extensive, and has been recently reviewed.² As part of our current effort to develop a similar range of chemistry for phosphido-bridged dimolybdenum systems^{3,4} we have recently reported that the thermal reaction of $[\text{Mo}_2(\text{CO})_6(\eta\text{-C}_5\text{H}_5)_2]$ with tetraphenyldiphosphane produces $[\text{Mo}_2(\mu\text{-PPh}_2)_2(\text{CO})_2(\eta\text{-C}_5\text{H}_5)_2]$ (1), which on further photochemical decarbonylation gives $[\text{Mo}_2(\mu\text{-CO})(\mu\text{-PPh}_2)_2(\eta\text{-C}_5\text{H}_5)_2]$ (2).⁵ Despite their formally unsaturated nature, however, neither (1) nor (2) reacted with alkynes either thermally or under u.v. irradiation, a fact we attribute to steric hindrance by the bulky diphenylphosphido groups. To circumvent this problem we decided to explore an alternative synthetic strategy, in which the alkyne ligand is introduced into the dimolybdenum complex prior to the incorporation of the phosphido groups. In this paper we describe the reaction of P_2Ph_4 with the complex $[\text{Mo}_2(\mu\text{-C}_2\text{Me}_2)(\text{CO})_4(\eta\text{-C}_5\text{H}_5)_2]$ (3), containing a transversely bound but-2-yne ligand, and the protonation of the resulting product.

Results and Discussion

(a) *Synthesis of $[\text{Mo}_2(\mu\text{-PPh}_2)_2(\text{CO})(\eta\text{-C}_2\text{Me}_2)(\eta\text{-C}_5\text{H}_5)_2]$.*—Heating $[\text{Mo}_2(\mu\text{-C}_2\text{Me}_2)(\text{CO})_4(\eta\text{-C}_5\text{H}_5)_2]$ with 1 equivalent of P_2Ph_4 in refluxing toluene for 96 h resulted in the consumption of most of the starting material according to spot t.l.c. monitoring. Subsequent chromatographic work-up provided $[\text{Mo}_2(\mu\text{-PPh}_2)_2(\text{CO})(\eta\text{-C}_2\text{Me}_2)(\eta\text{-C}_5\text{H}_5)_2]$ (4) as an air-stable, red-purple crystalline solid in 42% yield, as well as several other minor products which are described in detail below.

The i.r. spectrum of (4) showed a single peak at $1\ 826\ \text{cm}^{-1}$. As well as two cyclopentadienyl resonances (one split into a triplet), the ^1H n.m.r. spectrum showed phenyl and methyl protons in a ratio of 20:6, indicating the incorporation of two PPh_2 groups into the dinuclear molecule with retention of the alkyne ligand. The $^{31}\text{P}\text{-}\{^1\text{H}\}$ spectrum consisted of a single peak in the region expected for bridging phosphido ligands [$\delta\ 30.2$ p.p.m. relative

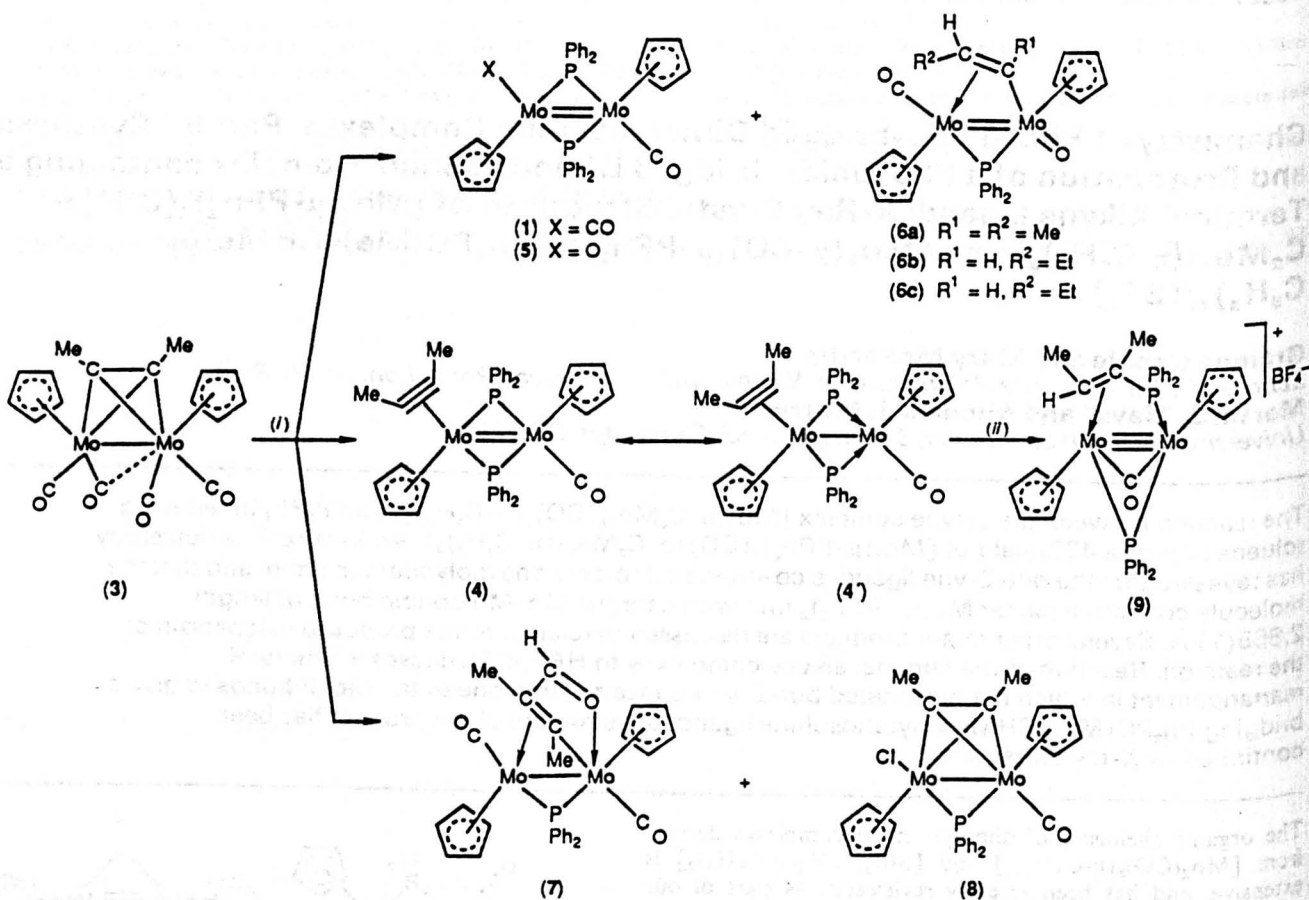


to $\text{P}(\text{OMe})_3 = 0.0$ p.p.m.], and a molecular ion was observed in the mass spectrum at $m/z\ 774$ (^{96}Mo) with one carbonyl loss peak at $m/z\ 746$. Peaks corresponding to a single terminal carbonyl ligand and two inequivalent C_5H_5 rings were observed in the ^{13}C n.m.r. spectrum, with the resonance due to the internal carbons of the alkyne appearing at 155.8 p.p.m. The general similarity of the spectroscopic data to those of the oxo complex *trans*- $[\text{Mo}_2\text{O}(\mu\text{-PPh}_2)_2(\text{CO})(\eta\text{-C}_5\text{H}_5)_2]$ (5)⁵ indicated a similar structure with the alkyne acting as a two-electron ligand terminally bound to one molybdenum atom. No evidence was found for the existence of a *cis* isomer of (4).

It has previously been shown by Templeton and Ward⁶ that for mononuclear molybdenum(II) alkyne complexes there is an experimental correlation between the number of electrons formally donated by an alkyne ligand and its ^{13}C n.m.r. chemical shift. The value observed for (4) lies to somewhat lower field than might be expected for a two-electron donor alkyne, and an alternative canonical form, (4'), can be envisaged in which the but-2-yne ligand is donating four electrons and the metal atoms are joined by a single bond (see Scheme 1). An X-ray

† $[1(\eta^5\text{-But-2-yne})\text{carbonyl-}2\kappa\text{C-bis}[1,2(\eta^5\text{-cyclopentadienyl})\text{bis}(\mu\text{-diphenylphosphido})\text{-dimolybdenum (2 Mo-Mo) and } \mu\text{-carbonyl-bis}[1,2(\eta^5\text{-cyclopentadienyl})\text{-}\mu\text{-diphenylphosphido-}\mu\text{-[2-(diphenylphosphino-}2\kappa\text{P)but-2-ene-1}\kappa^2\text{C}^{2,3}]\text{-dimolybdenum (3 Mo-Mo) tetrafluoroborate.}$

Supplementary data available: see Instructions for Authors, *J. Chem. Soc., Dalton Trans.*, 1990, Issue 1, pp. xix–xxii.



Scheme 1. Products from the reaction of $[\text{Mo}_2(\mu\text{-C}_2\text{Me}_2)(\text{CO})_4(\eta\text{-C}_5\text{H}_5)_2]$ with tetraphenyldiphosphane. (i) P_2Ph_4 ; (ii) $\text{HBF}_4 \cdot \text{OEt}_2$, -78°C

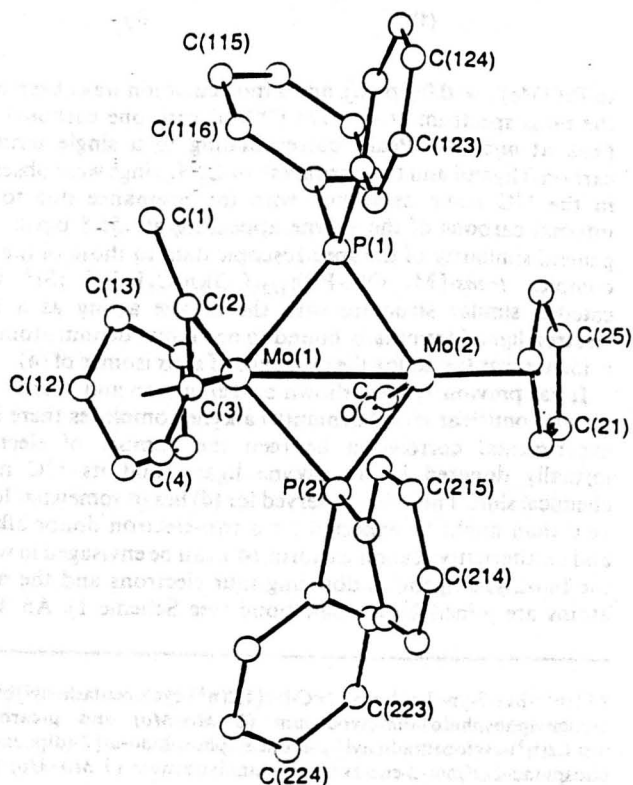


Figure 1. Molecular structure of $[\text{Mo}_2(\mu\text{-PPh}_2)_2(\text{CO})(\eta\text{-C}_2\text{Me}_2)(\eta\text{-C}_5\text{H}_5)_2]$ (4) including the atom numbering scheme

diffraction study was therefore carried out on a suitable crystal of (4) in order to compare the structural parameters with those of other $\text{Mo}_2(\mu\text{-PPh}_2)_2$ complexes.

Figure 1 shows the molecular structure of complex (4) in the crystal, with selected bond lengths and angles collected in Table 1. The structure consists of discrete dinuclear molecules with no unusually short intermolecular contacts.

As deduced from the spectra, the but-2-yne ligand is solely bonded to Mo(1). This is unusual for dinuclear complexes, where alkynes tend to adopt bridging modes of co-ordination. As in (1) and (5) the Mo_2P_2 unit is virtually planar (maximum deviation 0.14 Å) with the C(2)–C(3) bond of the alkyne ligand almost parallel to it. The C(2)–C(3) bond is of length 1.271(10) Å, and the two methyl groups are bent back at angles of 144.5(6)° [C(1)–C(2)–C(3)] and 143.6(6)° [C(4)–C(3)–C(2)], these values being typical for non-bridging but-2-yne ligands bonded to molybdenum.⁸

The Mo(1)–Mo(2) bond length of 2.865(1) Å lies between that of 2.716(1) Å in (1) and that of 2.942(1) Å in (5),⁵ and is close to that of 2.885(1) Å found in $[\text{Mo}_2\text{O}(\mu\text{-CH=CHPh})(\mu\text{-PPh}_2)_2(\text{CO})(\eta\text{-C}_5\text{H}_5)_2]$ ⁹ (see below), all of which may be considered as having Mo–Mo double bonds. In the first canonical form (4) a formal double bond is required purely on the basis of the 18-electron rule if the alkyne ligand acts as a two-electron donor. The alternative description of the bonding, (4'), in which the alkyne ligand acts as a four-electron donor with a formal Mo–Mo bond order of one, could account for the asymmetry observed in the phosphido bridges [Mo(1)–P(1) 2.420(2), Mo(2)–P(1) 2.346(2), Mo(1)–P(2) 2.419(2), and Mo(2)–P(2) 2.348(2) Å].

The other products obtained from the reaction of $[\text{Mo}_2(\mu\text{-C}_2\text{Me}_2)(\text{CO})_4(\eta\text{-C}_5\text{H}_5)_2]$ (3) with P_2Ph_4 can be divided into

Table 1. Selected bond lengths (Å) and angles (°) for complexes (4) and (9) *

(4)		(9)	
Mo(1)–Mo(2)	2.865(1)	Mo(1)–Mo(2)	2.593(2)
Mo(1)–P(1)	2.420(2)	Mo(1)–P(2)	2.367(3)
Mo(1)–P(2)	2.419(2)	Mo(1)–C	2.373(12)
Mo(1)–C(2)	2.094(6)	Mo(1)–C(2)	2.249(12)
Mo(1)–C(3)	2.100(6)	Mo(1)–C(3)	2.340(12)
Mo(2)–P(1)	2.346(2)	Mo(2)–P(1)	2.428(4)
Mo(2)–P(2)	2.348(2)	Mo(2)–P(2)	2.387(3)
Mo(2)–C	1.930(6)	Mo(2)–C	1.947(12)
C(1)–C(2)	1.487(10)	P(1)–C(2)	1.810(13)
C(2)–C(3)	1.271(10)	C(1)–C(2)	1.535(20)
C(3)–C(4)	1.498(11)	C(2)–C(3)	1.416(16)
C(3)–C(4)	1.498(11)	C(3)–C(4)	1.518(18)
Range Mo(1)–Cp	2.350(7)–2.415(9)	Range Mo(1)–Cp	2.325(15)–2.376(16)
Range Mo(2)–Cp	2.341(10)–2.377(9)	Range Mo(2)–Cp	2.343(18)–2.378(17)
Mo(2)–P(1)–Mo(1)	73.9(1)	—	—
Mo(2)–P(2)–Mo(1)	73.9(1)	C(2)–P(1)–Mo(2)	111.6(4)
C(1)–C(2)–Mo(1)	141.3(5)	Mo(2)–P(2)–Mo(1)	66.1(1)
C(3)–C(2)–Mo(1)	72.6(4)	P(1)–C(2)–Mo(1)	86.3(5)
C(3)–C(2)–C(1)	144.5(6)	C(1)–C(2)–Mo(1)	125.7(8)
C(2)–C(3)–Mo(1)	72.1(4)	C(1)–C(2)–P(1)	120.7(8)
C(4)–C(3)–Mo(1)	142.7(5)	C(3)–C(2)–Mo(1)	75.6(7)
C(4)–C(3)–C(2)	143.6(6)	C(3)–C(2)–P(1)	111(1)
—	—	C(3)–C(2)–C(1)	124(1)
—	—	C(2)–C(3)–Mo(1)	68.6(7)
O–C–Mo(2)	175.0(5)	C(4)–C(3)–Mo(1)	127.4(9)
—	—	C(4)–C(3)–C(2)	122(1)
—	—	Mo(2)–C–Mo(1)	73.0(4)
—	—	O–C–Mo(1)	129(1)
—	—	O–C–Mo(2)	158(1)

* Cp = Cyclopentadienyl ring carbon atoms.

three groups in order of their subsequent elution from the chromatography column. First, the green complex $[\text{Mo}_2(\mu\text{-PPh}_2)_2(\text{CO})_2(\eta\text{-C}_5\text{H}_5)_2]$ (1) was obtained in 7–25% yield, accompanied by a small amount of the oxo complex (5), which we have previously shown to be derived from (1) by oxidation in air³ [complex (4) cannot also be a source of (5) since it appears to be completely air-stable].

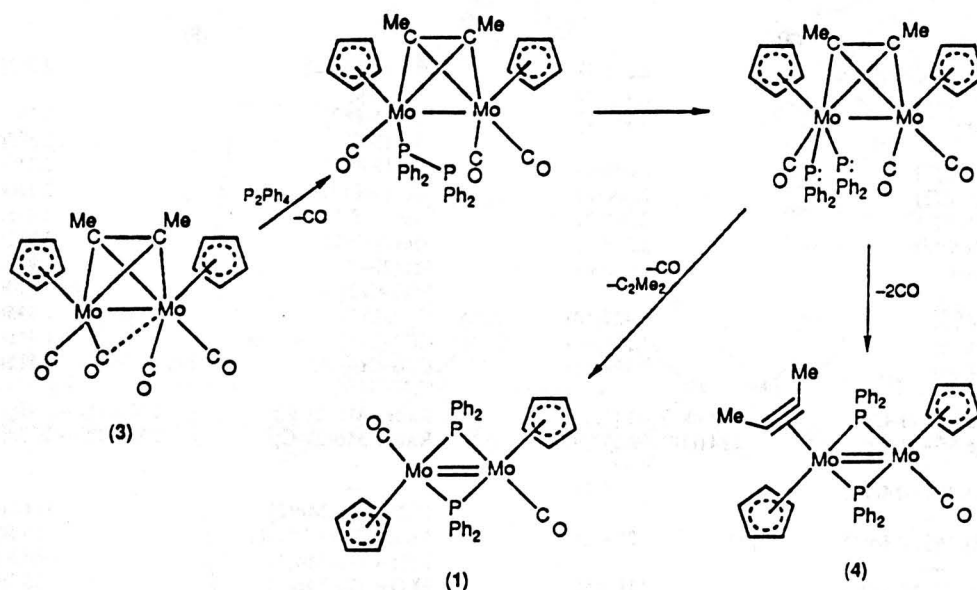
The following zone was purple, and was shown to contain the two isomeric complexes $[\text{Mo}_2\text{O}(\mu\text{-CMe=CHMe})(\mu\text{-PPh}_2)_2(\text{CO})(\eta\text{-C}_5\text{H}_5)_2]$ (6a) and $[\text{Mo}_2\text{O}(\mu\text{-CH=CHEt})(\mu\text{-PPh}_2)_2(\text{CO})(\eta\text{-C}_5\text{H}_5)_2]$ (6b). These proved extremely difficult to separate: (6b) could be obtained pure but (6a), which is also obtained from the reaction of $[\text{Mo}_2(\mu\text{-H})(\mu\text{-PPh}_2)(\text{CO})_4(\eta\text{-C}_5\text{H}_5)_2]$ with buta-1,3-diene,¹ was characterised as a mixture. In related reactions of other dimolybdenum μ -alkyne complexes with P_2Ph_4 we have prepared a number of such complexes differing only in the substituents on the μ -vinyl ligand, all of which display similar n.m.r. spectra: in particular their ³¹P chemical shifts all lie in the range 34–44 p.p.m. As mentioned above, one of these, $[\text{Mo}_2\text{O}(\mu\text{-CH=CHPh})(\mu\text{-PPh}_2)(\text{CO})(\eta\text{-C}_5\text{H}_5)_2]$, was originally prepared and structurally characterised by Ziegler and co-workers.⁹ The structures of (6a) and (6b) are probably similar, with a *trans* orientation of the cyclopentadienyl groups and with the vinyl ligand σ -bound to the molybdenum atom bearing the oxo group. However, as pointed out previously,⁴ the stereochemistry of the substituents on the vinyl ligand is difficult to assign unambiguously from the spectroscopic data.

On some occasions, in addition to (6a) and (6b), a further complex of this type, (6c), was obtained from the reaction of (3) with P_2Ph_4 . According to its ¹H n.m.r. spectrum, (6c), which was eluted as a separate purple band during chromatography,

contains a $\mu\text{-CH=CHEt}$ ligand and we therefore assume it to be another isomer similar to (6b), though it is not possible to say whether this isomerism involves the *cis/trans* orientation of the C_5H_5 rings, the orientation of the vinyl ligand, or simply the arrangement of the substituents on the vinyl ligand.

Further elution of the chromatography column provided another red-purple zone, again containing two compounds. These could readily be separated by fractional crystallisation into the less-soluble red complex $[\text{Mo}_2\{\mu\text{-CMe=C(Me)CHO}\}(\mu\text{-PPh}_2)(\text{CO})_2(\eta\text{-C}_5\text{H}_5)_2]$ (7) and a purple compound which we identify as $[\text{Mo}_2(\mu\text{-C}_2\text{Me}_2)(\mu\text{-PPh}_2)\text{Cl}(\text{CO})(\eta\text{-C}_5\text{H}_5)_2]$ (8).

We have previously prepared several complexes analogous to (7) from related reactions; again all have similar spectroscopic characteristics *e.g.* their ³¹P n.m.r. chemical shifts lie in the range $\delta +5$ to -5 p.p.m. Such complexes have also been prepared by Knox and co-workers¹⁰ who found that thermolysis of the phosphine-substituted compound $[\text{Mo}_2(\mu\text{-C}_2\text{H}_2)(\text{CO})_3(\text{PPh}_3)(\eta\text{-C}_5\text{H}_5)_2]$ led to phosphorus-carbon bond cleavage and phenyl migration to give $[\text{Mo}_2\{\mu\text{-CH=CHC(Ph)O}\}(\mu\text{-PPh}_2)(\text{CO})_2(\eta\text{-C}_5\text{H}_5)_2]$. A range of alkyne complexes and phosphines was explored; if the phosphine involved was PPh_2H , P–H bond cleavage occurred preferentially, and we concluded from their results that (7) might alternatively be prepared from $[\text{Mo}_2(\mu\text{-C}_2\text{Me}_2)(\text{CO})_4(\eta\text{-C}_5\text{H}_5)_2]$ and diphenylphosphine. In order to confirm this point a separate reaction of (3) with PPh_2H was undertaken, and (7) indeed proved the major product (20% yield); the vinyl complexes (6a) and (6b) (combined yield 11.5%) and (6c) (8%) were also formed. It is therefore likely that the presence of small quantities of diphenylphosphine remaining from the *in situ* synthesis of P_2Ph_4 (from PPh_2H and PPh_2Cl ¹¹) is responsible for the production of at least some proportion of these four compounds in the original reaction.



Scheme 2. Proposed mechanism for the reaction of complex (3) with P_2Ph_4

In a similar manner, (8) is probably formed through the presence of small amounts of residual PPh_2Cl , and we have recently shown that the reaction of PPh_2Cl with alkyne-bridged dimolybdenum¹² and ditungsten¹³ complexes does give rise to similar compounds under conditions of comparatively high dilution. The relatively high value of $\nu(CO)$ for these compounds [1959 cm^{-1} for (8)] compared to the other complexes discussed provides a convenient method for their identification. Despite several attempts, however, we have so far failed to produce (8) by the direct reaction of (3) with PPh_2Cl ; in each case, even with 0.5 equivalents of the chlorophosphine, the only isolated product has been the mononuclear chelate complex $[MoCl(CO)\{cis\text{-}PPh_2PC(Me)=C(Me)PPh_2\}(\eta\text{-}C_5H_5)]$, which contains two diphenylphosphido groups coupled to the but-2-yne ligand.¹² However we feel that this does not exclude the formation of (8) by this route in the original reaction, considering the very small amounts of PPh_2Cl which are likely to be present.

The mechanism of the reaction between complex (3) and P_2Ph_4 is uncertain, but a plausible proposal (Scheme 2) consists of initial substitution of a CO ligand of (3) by a P_2Ph_4 molecule, followed by cleavage of the P-P bond (effectively oxidative addition of the P_2Ph_4 to one molybdenum centre). Similar oxidative-cleavage processes of P-C, P-H, and P-Cl bonds have previously been postulated in reactions of dimolybdenum complexes analogous to (3) with phosphines¹⁰ and chlorophosphines.¹² Migration of both PPh_2 groups to bridging positions could then occur with concomitant displacement of either two CO ligands to give (4) or of one CO and the alkyne ligand to give (1).

The reaction of complex (3) with PPh_2H can be rationalised in a similar manner (Scheme 3). Initial substitution is followed by oxidative addition of the P-H bond to give terminal PPh_2 and H ligands. Migration of the diphenylphosphido group to a bridging position is accompanied by migration of the hydride ligand either to a carbonyl group, as previously described by Knox and co-workers,¹⁰ to give (7) (by subsequent migration of the resulting formyl to the alkyne) or to the alkyne, leading eventually to (6a), (6b), and (6c). Clearly a hydrogen-shift process is involved in the production of (6b) and (6c); one possibility might involve the formation of an intermediate containing a $\mu\text{-}CH_2=C=CHMe$ allene ligand, as shown.

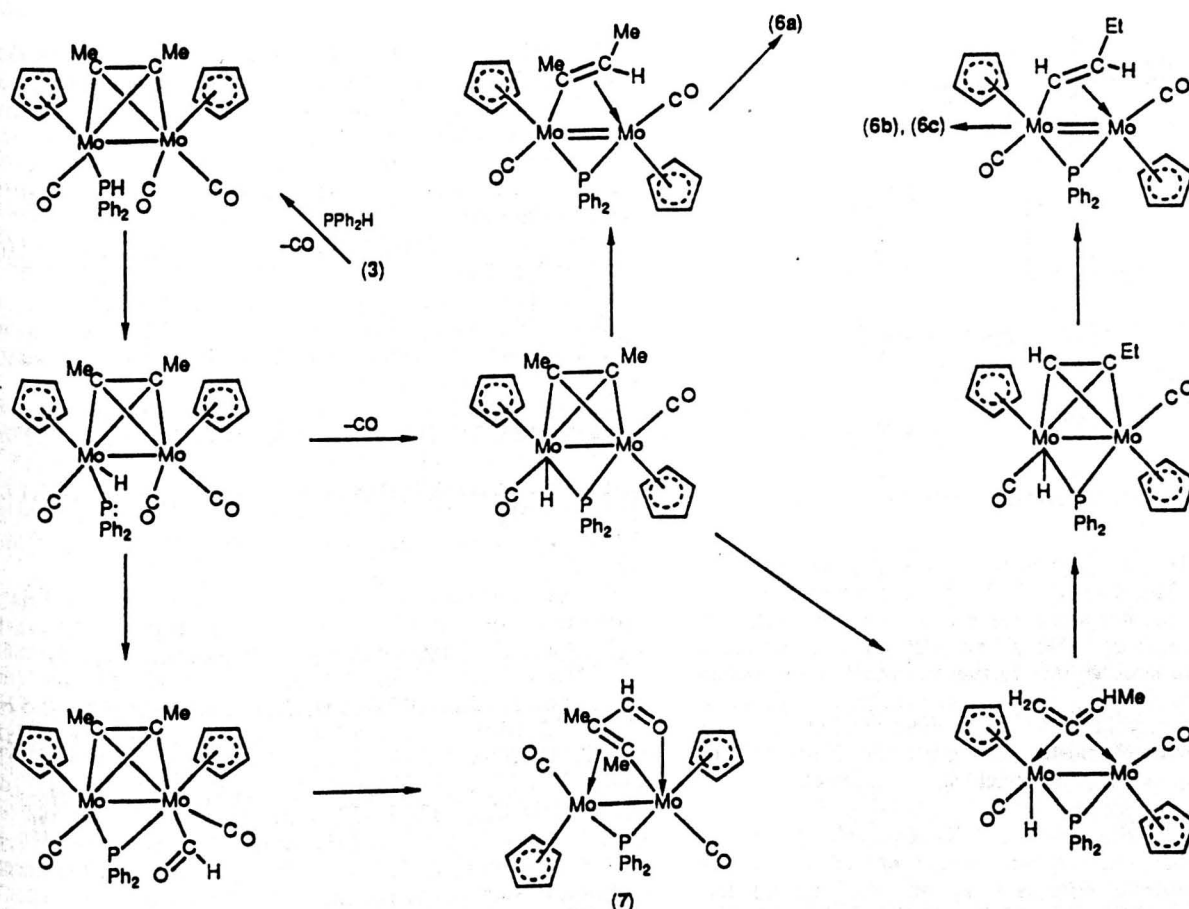
(b) Protonation of $[Mo_2(\mu\text{-}PPh_2)_2(CO)(\eta\text{-}C_2Me_2)(\eta\text{-}$

$C_5H_5)_2]$.—We have previously shown that protonation of complex (1) occurs at the metal-metal bond to give $[Mo_2(\mu\text{-}H)(\mu\text{-}PPh_2)_2(CO)_2(\eta\text{-}C_5H_5)_2][BF_4]$.⁵ Addition of an excess of $HBF_4\cdot OEt_2$ to a dichloromethane solution of (4) at $-78^\circ C$ caused an immediate colour change to bright purple. We have so far been unable to isolate or characterise this initial product, but on warming a further colour change to dark green occurred, and work-up afforded a quantitative yield of $[Mo_2(\mu\text{-}CO)(\mu\text{-}PPh_2)\{\mu\text{-}Ph_2PC(Me)=CHMe\}(\eta\text{-}C_5H_5)_2][BF_4]$ (9) (Scheme 1).

The i.r. spectrum now showed a peak at 1798 cm^{-1} , which, taking into account the shift to higher wavenumber expected for a cationic complex, implied that the CO ligand had migrated to a bridging position. Extensive structural reorganisation was also indicated by the n.m.r. spectra; hence in the ^{31}P spectrum the two phosphorus atoms were no longer equivalent, one appearing at $\delta 105.1\text{ p.p.m.}$ and the other at -110.7 p.p.m. , this latter being characteristic of a terminally bound phosphine ligand. The coupling pattern observed in the 1H and ^{13}C n.m.r. spectra showed that the proton was attached to the but-2-yne ligand, and moreover that this had inserted into one of the Mo-P bonds to form a bridging vinylphosphine ligand. Hence the proton of the CHMe group appears as a doublet of doublet of quartets through coupling to the methyl protons and both phosphorus atoms, with one small $J(HP)$ and one large.

Confirmation of this formulation was obtained by an X-ray diffraction study of complex (9). The structure of the dinuclear organometallic cation is shown in Figure 2, with relevant bond lengths and angles collected in Table 1.

The Mo-Mo distance of $2.593(2)\text{ \AA}$ in (9) is comparable to that of $2.515(1)\text{ \AA}$ observed in (2),⁵ and is thus consistent with the presence of the metal-metal triple bond required for each molybdenum atom to attain an 18-electron configuration. The bond is bridged almost symmetrically by the remaining $\mu\text{-}PPh_2$ unit [Mo(1)-P(2) $2.367(3)$, Mo(2)-P(2) $2.387(3)\text{ \AA}$] and asymmetrically by the semibridging CO ligand [Mo(1)-C $2.373(12)$, Mo(2)-C $1.947(12)\text{ \AA}$]. The linking of the second phosphido group to the protonated alkyne has produced a bridging vinylphosphine ligand, $Ph_2PC(Me)=CHMe$, which is coordinated to Mo(2) through the phosphorus atom [Mo(2)-P(1) $2.428(4)\text{ \AA}$] and to Mo(1) by the double bond of the vinyl group [Mo(1)-C(2) $2.249(12)$, Mo(1)-C(3) $2.340(12)\text{ \AA}$]. As expected, the two methyl substituents adopt a *cis* arrangement, and the

Scheme 3. Proposed mechanism for the reaction of complex (3) with PPh₂H

C(2)–C(3) distance of 1.416(16) Å is longer than the corresponding length of 1.271(10) Å in (4).

Comparison of the structures of complexes (4) and (9) reveals that comparatively little movement of the alkyne ligand is required to effect P–C bond formation during the protonation reaction. In terms of mechanism, if protonation occurs at the organic centre (or at the metal centre with subsequent transfer to the organic ligand) this would produce a σ,π -bound vinyl group (*i.e.* a metallacyclopropene) which could then insert into the Mo–P bond. Insertion of alkynes into bridging phosphido groups has been observed previously by several groups, but the most closely related reaction is that reported by Werner and Zolk;¹⁴ protonation with HPF₆ of the dicobalt complex [Co₂(μ -HC₂CO₂Me)(μ -PMe₂)₂(η -C₅H₅)₂] (10), containing an alkyne bound in the two-electron 'parallel' mode, results in a similar coupling with one of the μ -PMe₂ groups to give the bridging vinylphosphine complex [Co₂(μ -PMe₂)(μ -Me₂PCH=CHCO₂Me)(η -C₅H₅)₂][PF₆] (11). We have also previously observed the coupling of divinyl ligands with μ -PPh₂ groups to give similar ligands in dimanganese complexes.¹⁵

It is interesting that in the reaction of [Mo₂(μ -C₂Me₂)(CO)₄(η -C₅H₅)₂] with P₂Ph₄ no products are isolated in which phosphorus–carbon bond formation has taken place, yet on protonation of (4) facile coupling of the organic ligand with the phosphido group occurs at low temperature. Further studies of the factors influencing such processes are in progress.

Experimental

General techniques and instrumentation were as described in Part 1 of this Series.³ The complex [Mo₂(μ -C₂Me₂)(CO)₄(η -C₅H₅)₂] (3) was prepared by the literature method.¹⁶ Exam-

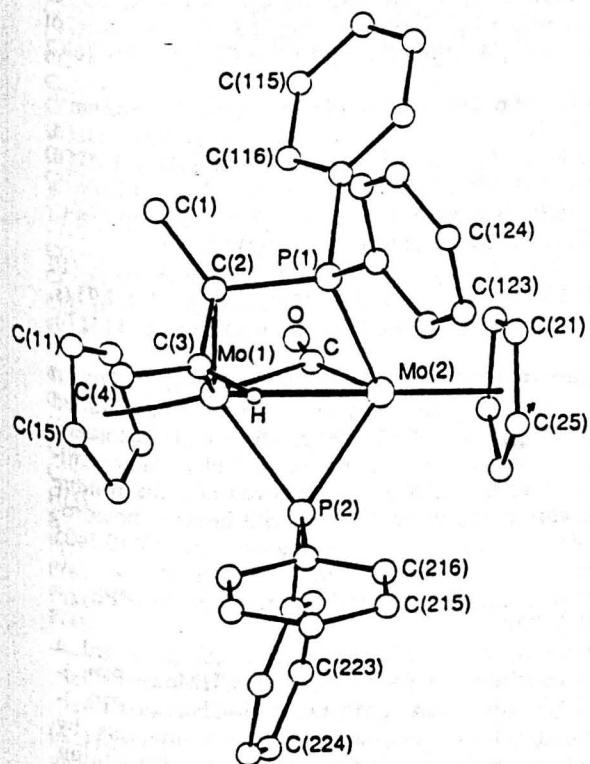
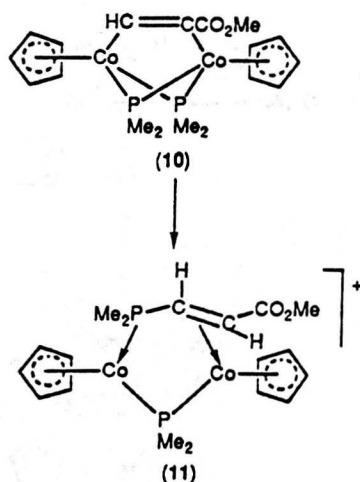


Figure 2. Molecular structure of [Mo₂(μ -CO)(μ -PPh₂)](μ -Ph₂PC(Me)CHMe)(η -C₅H₅)₂][BF₄] (9) including the atom numbering scheme



ation of the ^1H n.m.r. spectrum of (3) showed that contamination by $[\text{Mo}_2(\text{CO})_6(\eta\text{-C}_5\text{H}_5)_2]$ was negligible (*ca.* 1–2%). Tetraphenyldiphosphane was prepared by the method of Küchen and Buchwald;¹¹ PPh_2Cl and PPh_2H were purchased from Aldrich and used without further purification. I.r. spectra were recorded in CH_2Cl_2 . Unless otherwise stated, all n.m.r. spectra were recorded in CDCl_3 , with chemical shifts in p.p.m. on the δ scale relative to SiMe_4 (0.0 p.p.m.) (for ^1H and ^{13}C) or $\text{P}(\text{OMe})_3$ (0.0 p.p.m.) for ^{31}P (upfield shifts negative).

(i) *Reaction of $[\text{Mo}_2(\mu\text{-C}_2\text{Me}_2)(\text{CO})_4(\eta\text{-C}_5\text{H}_5)_2]$ (3) with P_2Ph_4 .*—Tetraphenyldiphosphane was prepared *in situ* by refluxing a mixture of PPh_2H (1.10 cm³, 6.32 mmol) and PPh_2Cl (1.14 cm³, 6.35 mmol) in heptane (175 cm³) for 3 h. The solvent was removed *in vacuo*, and $[\text{Mo}_2(\mu\text{-C}_2\text{Me}_2)(\text{CO})_4(\eta\text{-C}_5\text{H}_5)_2]$ (2.5024 g, 5.27 mmol) was added, followed by toluene (175 cm³). The resulting solution was refluxed for 96 h, monitoring the reaction by spot t.l.c. until virtually all of the starting material had disappeared. After addition of silica (5 g) the solvent was removed and the residue loaded onto a silica chromatography column.

Elution with hexane–dichloromethane (4:1) produced a red band of the starting complex (3) contaminated with excess of phosphine (623.6 mg), followed by a further red band containing $[\text{Mo}_2(\mu\text{-PPh}_2)_2(\text{CO})(\eta\text{-C}_2\text{Me}_2)(\eta\text{-C}_5\text{H}_5)_2]$ (4) (1.7142 g, 42%), m.p. 260–264 °C, $\nu(\text{CO})$ 1 826 cm⁻¹. N.m.r.: ^1H , δ 8.48–6.30 (m, 20 H, Ph), 4.64 [t, $J(\text{HP})$ 0.8, 5 H, C_5H_5], 4.02 (s, 5 H, C_5H_5), and 2.20 (s, 6 H, Me); ^{13}C , δ 237.0 [t, $J(\text{CP})$ 8.5, CO], 155.8 (s, CMe), 151.5 [d, $J(\text{CP})$ 28.2, C_{ipso}], 142.5 [d, $J(\text{CP})$ 37.2 Hz, C_{ipso}], 135.6–126.1 (m, Ph), 96.1 (s, C_5H_5), 87.6 (s, C_5H_5), and 21.4 p.p.m. (s, Me) (Found: C, 60.60; H, 4.65; P, 7.60. $\text{C}_{39}\text{H}_{36}\text{Mo}_2\text{OP}_2$ requires C, 60.45; H, 4.65; P, 8.00%).

Owing to the relative insolubility of $[\text{Mo}_2(\mu\text{-PPh}_2)_2(\text{CO})_2(\eta\text{-C}_5\text{H}_5)_2]$ (1), which tends to contaminate all the following bands, we adopted the following procedure to separate the remaining compounds. The eluting solvent was changed to CH_2Cl_2 and then to CH_2Cl_2 –acetone (9:1) until no further bands descended. After removal of solvent from the eluate, it was washed with acetone to yield (1) (282.7 mg) as an insoluble green powder. A small amount of silica was added to the acetone washings, the solvent was removed *in vacuo*, and the residue loaded onto a second chromatography column. Elution with hexane–dichloromethane (1:1) produced small further amounts of complexes (4) (8.6 mg) and (1) (14.2 mg, total yield 7.2%), followed by a red band due to the oxo complex *trans*- $[\text{Mo}_2\text{O}(\mu\text{-PPh}_2)_2(\text{CO})(\eta\text{-C}_5\text{H}_5)_2]$ (5) (17.2 mg, 0.4% after further purification by t.l.c. as previously described).⁵

A stronger red-purple band was eluted using hexane– CH_2Cl_2 (1:1), and shown to consist of a mixture of $[\text{Mo}_2\text{O}(\mu\text{-CMe=CHMe})(\mu\text{-PPh}_2)_2(\text{CO})(\eta\text{-C}_5\text{H}_5)_2]$ (6a) and $[\text{Mo}_2\text{O}(\mu\text{-CH=CHEt})(\mu\text{-PPh}_2)_2(\text{CO})(\eta\text{-C}_5\text{H}_5)_2]$ (6b) (combined yield 78.5 mg, 2.5%). Further purification by exhaustive t.l.c. (eluting solvent hexane–dichloromethane, first 3:7 and then 4:6) provided more mobile (6b) as a pure compound. Complex (6a) was characterised as a mixture with (6b) in *ca.* 3:1 ratio by ^1H n.m.r. integration.

Complex (6a). $\nu(\text{CO})$ 1 839 cm⁻¹. N.m.r.: ^1H , δ 8.02–7.17 (m, 10 H, Ph), 5.09 (s, 5 H, C_5H_5), 4.73 [d, $J(\text{HP})$ 1.3, 5 H, C_5H_5], 3.19 [d, $J(\text{HP})$ 0.6, 3 H, CMe], 2.79 [q, $J(\text{HH})$ 6.3, 1 H, CH], and 1.83 [d, $J(\text{HH})$ 6.3 Hz, 3 H, CHMe]; ^{31}P , δ 38.4 p.p.m. (Found: C, 53.55; H, 4.65; P, 4.95. $\text{C}_{27}\text{H}_{27}\text{Mo}_2\text{O}_2\text{P}$ requires C, 53.45; H, 4.45; P, 5.10%), m/z 606 (M^+).

Complex (6b). M.p. 208–210 °C, $\nu(\text{CO})$ 1 839 cm⁻¹. N.m.r.: ^1H , δ 9.06 [dd, $J(\text{HH})$ 9.5, $J(\text{HP})$ 1.8, 1 H, $\mu\text{-CH}$], 8.02–7.17 (m, 10 H, Ph), 5.03 (s, 5 H, C_5H_5), 4.66 [d, $J(\text{HP})$ 1.3, 5 H, C_5H_5], 2.78 (m, 1 H, CHEt), 1.97 (m, 2 H, CH₂), and 1.37 [t, $J(\text{HH})$ 7.3 Hz, 3 H, CH₃]; ^{31}P , δ 34.6 p.p.m. (Found: C, 53.55; H, 4.65; P, 5.13. $\text{C}_{27}\text{H}_{27}\text{Mo}_2\text{O}_2\text{P}$ requires C, 53.45; H, 4.45; P, 5.10%), m/z 606 (M^+).

Complex (6b). M.p. 208–210 °C, $\nu(\text{CO})$ 1 839 cm⁻¹. N.m.r.: ^1H , δ 9.06 [dd, $J(\text{HH})$ 9.5, $J(\text{HP})$ 1.8, 1 H, $\mu\text{-CH}$], 8.02–7.17 (m, 10 H, Ph), 5.03 (s, 5 H, C_5H_5), 4.66 [d, $J(\text{HP})$ 1.3, 5 H, C_5H_5], 2.78 (m, 1 H, CHEt), 1.97 (m, 2 H, CH₂), and 1.37 [t, $J(\text{HH})$ 7.3 Hz, 3 H, CH₃]; ^{31}P , δ 34.6 p.p.m. (Found: C, 53.55; H, 4.65; P, 5.13. $\text{C}_{27}\text{H}_{27}\text{Mo}_2\text{O}_2\text{P}$ requires C, 53.45; H, 4.45; P, 5.10%), m/z 606 (M^+).

Elution with hexane–dichloromethane (1:4) produced a bright purple band containing $[\text{Mo}_2\text{O}(\mu\text{-CH=CHEt})(\mu\text{-PPh}_2)_2(\text{CO})(\eta\text{-C}_5\text{H}_5)_2]$ (6c) (27.7 mg, 0.9%), m.p. (92 °C, decomp.), $\nu(\text{CO})$ 1 865 cm⁻¹. N.m.r.: ^1H , δ 8.48 [d, $J(\text{HP})$ 9.4, 1 H, $\mu\text{-CH}$], 7.81–6.97 (m, 10 H, Ph), 5.35 [d, $J(\text{HP})$ 0.8, 5 H, C_5H_5], 5.00 [d, $J(\text{HP})$ 1.0, 5 H, C_5H_5], 3.21 [d of t, $J(\text{HH})$ 6.5, 9.4, 1 H, CHEt], 2.00 (m, 2 H, CH₂), and 1.25 [t, $J(\text{HH})$ 7.3, 3 H, CH₃]; ^{13}C , δ 235.1 [d, $J(\text{CP})$ 15, CO], 154.7 [d, $J(\text{CP})$ 2, $\mu\text{-CH}$], 147.0 [d, $J(\text{CP})$ 26, C_{ipso}], 141.0 [d, $J(\text{CP})$ 45 Hz, C_{ipso}], 134.3–127.4 (m, Ph), 99.7 (s, C_5H_5), 88.0 (s, C_5H_5), 71.7 (s, CH), 34.9 (s, CH₂), and 17.1 p.p.m. (s, Me); ^{31}P , δ 23.9 p.p.m. (Found: C, 53.85; H, 4.76. $\text{C}_{27}\text{H}_{27}\text{Mo}_2\text{O}_2\text{P}$ requires C, 53.45; H, 4.45%), m/z 606 (M^+).

Further elution of the chromatography column with dichloromethane–acetone (9:1) provided another red-purple band. Fractional crystallisation from CH_2Cl_2 –hexane gave small amounts of first red $[\text{Mo}_2\{\mu\text{-CMe=C(Me)CHO}\}(\mu\text{-PPh}_2)_2(\text{CO})_2(\eta\text{-C}_5\text{H}_5)_2]$ (7) (43.3 mg, 1.3%), and then of purple $[\text{Mo}_2(\mu\text{-C}_2\text{Me}_2)(\mu\text{-PPh}_2)\text{Cl}(\text{CO})(\eta\text{-C}_5\text{H}_5)_2]$ (8) (69.2 mg, 2.1%).

Complex (7). M.p. 237–238 °C (decomp.), $\nu(\text{CO})$ 1 862 cm⁻¹. N.m.r.: ^1H , δ 8.66 (s, 1 H, CHO), 7.62–7.08 (10 H, Ph), 5.16 [d, $J(\text{HP})$ 1.5, 5 H, C_5H_5], 4.84 [d, $J(\text{HP})$ 1.0, 5 H, C_5H_5], 2.70 [d, $J(\text{HP})$ 1.4 Hz, 3 H, Me], and 1.58 (s, 3 H, Me); ^{31}P , δ 4.9 p.p.m. (Found: C, 53.85; H, 4.30; P, 4.50. $\text{C}_{29}\text{H}_{27}\text{Mo}_2\text{O}_3\text{P}$ requires C, 53.85; H, 4.20; P, 4.80%), m/z 618 ($M - \text{CO}$).

Complex (8). $\nu(\text{CO})$ 1 959 cm⁻¹. N.m.r.: ^1H , δ 8.09–6.40 (10 H, Ph), 5.36 (s, 5 H, C_5H_5), 4.83 [d, $J(\text{HP})$ 0.8 Hz, C_5H_5], 2.95 (s, 3 H, Me), and 2.81 (s, 3 H, Me); ^{31}P , δ 6.5 p.p.m. m/z 624 (M^+).

(ii) *Reaction of $[\text{Mo}_2(\mu\text{-C}_2\text{Me}_2)(\text{CO})_4(\eta\text{-C}_5\text{H}_5)_2]$ (3) with PPh_2H .*—Diphenylphosphine (0.8 cm³, 4.60 mmol) was added to a solution of complex (3) (2.2500 g, 4.61 mmol) in toluene (175 cm³), and the mixture was refluxed for 19 h. After addition of silica (5 g) the solvent was removed and the residue subjected to chromatography. Elution with hexane–dichloromethane (6:4) gave a red zone containing unreacted (3) (0.2405 g, 10.7% recovery), followed by minor bands of $[\text{Mo}_2(\mu\text{-PPh}_2)_2(\text{CO})_2(\eta\text{-C}_5\text{H}_5)_2]$ (1) and *trans*- $[\text{Mo}_2\text{O}(\mu\text{-PPh}_2)_2(\text{CO})(\eta\text{-C}_5\text{H}_5)_2]$ (5).

Elution with hexane–dichloromethane (1:1) produced a purple band consisting of $[\text{Mo}_2\text{O}(\mu\text{-CMe=CHMe})(\mu\text{-PPh}_2)_2(\text{CO})(\eta\text{-C}_5\text{H}_5)_2]$ (6a) and $[\text{Mo}_2\text{O}(\mu\text{-CH=CHEt})(\mu\text{-PPh}_2)_2(\text{CO})(\eta\text{-C}_5\text{H}_5)_2]$ (6b) in approximately equal amounts by n.m.r. integration (total yield 321.8 mg, 11.5%). Further elution with CH_2Cl_2 provided the second isomer of $[\text{Mo}_2\text{O}(\mu\text{-CH=CHEt})(\mu\text{-PPh}_2)_2(\text{CO})(\eta\text{-C}_5\text{H}_5)_2]$ (6c) (224.4 mg, 8%) as a separate purple band.

The major product, $[\text{Mo}_2\{\mu\text{-CMe=C(Me)CHO}\}(\mu\text{-PPh}_2)_2(\text{CO})_2(\eta\text{-C}_5\text{H}_5)_2]$ (7), was obtained as a red-purple band.

Table 2. Fractional atomic co-ordinates

Atom	(4)			(9)		
	x	y	z	x	y	z
Mo(1)	0.239 25(4)	-0.066 26(5)	-0.137 21(2)	0.275 63(9)	-0.143 97(6)	0.063 50(5)
Mo(2)	0.200 67(4)	-0.329 90(5)	-0.151 44(2)	0.119 77(8)	-0.238 39(6)	0.102 61(5)
P(1)	0.355 03(12)	-0.225 54(15)	-0.161 92(6)	0.215 1(3)	-0.309 7(2)	0.024 5(1)
P(2)	0.105 18(13)	-0.190 50(15)	-0.106 56(7)	0.284 1(3)	-0.174 7(2)	0.175 0(2)
C(1)	0.477 8(6)	0.030 6(7)	-0.072 4(3)	0.364 7(12)	-0.244 5(9)	-0.060 6(6)
C(2)	0.366 1(5)	-0.007 9(6)	-0.078 5(2)	0.340 6(10)	-0.250 1(7)	0.008 7(6)
C(3)	0.284 3(5)	-0.001 3(6)	-0.057 3(3)	0.429 9(10)	-0.241 1(8)	0.066 0(7)
C(4)	0.241 6(7)	0.050 7(8)	-0.010 2(3)	0.558 6(11)	-0.222 2(9)	0.064 1(8)
C	0.131 6(5)	-0.275 0(6)	-0.222 3(3)	0.065 1(10)	-0.142 2(8)	0.046 5(6)
O	0.089 3(4)	-0.251 0(5)	-0.266 4(2)	-0.002 8(7)	-0.096 8(6)	0.014 1(5)
C(11)	0.124 6(7)	0.108 7(8)	-0.162 6(3)	0.366 8(13)	-0.056 5(10)	-0.004 0(8)
C(12)	0.230 6(7)	0.156 2(9)	-0.155 9(4)	0.246 7(13)	-0.024 3(10)	-0.006 2(8)
C(13)	0.282 9(7)	0.096 2(8)	-0.195 1(3)	0.236 1(13)	0.000 4(10)	0.059 9(8)
C(14)	0.208 4(6)	0.010 6(7)	-0.226 8(3)	0.351 6(13)	-0.013 2(10)	0.101 7(8)
C(15)	0.112 2(6)	0.019 0(7)	-0.206 5(3)	0.433 4(13)	-0.046 8(10)	0.064 5(8)
C(21)	0.112 9(8)	-0.522 7(9)	-0.161 9(4)	0.009 9(14)	-0.365 4(11)	0.103 5(8)
C(22)	0.135 6(7)	-0.495 5(8)	-0.104 9(4)	-0.072 3(14)	-0.296 6(11)	0.073 1(8)
C(23)	0.247 6(7)	-0.492 5(8)	-0.086 7(4)	-0.072 4(14)	-0.233 4(11)	0.125 9(8)
C(24)	0.296 0(8)	-0.518 4(9)	-0.134 7(4)	0.009 4(14)	-0.261 6(11)	0.183 4(8)
C(25)	0.211 1(8)	-0.537 1(10)	-0.181 2(4)	0.059 8(14)	-0.341 1(11)	0.170 4(8)
C(111)	0.399 0(3)	-0.203 2(4)	-0.227 1(1)	0.107 0(6)	-0.319 0(5)	-0.053 2(3)
C(112)	0.362 2(3)	-0.238 0(4)	-0.270 5(1)	0.056 0(6)	-0.397 0(5)	-0.073 5(3)
C(113)	0.393 6(3)	-0.264 8(4)	-0.320 3(1)	-0.029 2(6)	-0.402 9(5)	-0.131 4(3)
C(114)	0.461 7(3)	-0.166 9(4)	-0.326 7(1)	-0.063 4(6)	-0.330 9(5)	-0.168 9(3)
C(115)	0.498 5(3)	-0.087 2(4)	-0.283 3(1)	-0.012 5(6)	-0.252 9(5)	-0.148 5(3)
C(116)	0.467 1(3)	-0.105 4(4)	-0.233 5(1)	0.072 7(6)	-0.247 0(5)	-0.090 7(3)
C(121)	0.478 4(3)	-0.275 1(4)	-0.117 4(1)	0.277 3(6)	-0.414 1(4)	0.045 2(4)
C(122)	0.475 7(3)	-0.290 4(4)	-0.062 4(1)	0.291 3(6)	-0.444 3(4)	0.108 9(4)
C(123)	0.563 2(3)	-0.377 6(4)	-0.027 5(1)	0.339 3(6)	-0.524 3(4)	0.124 8(4)
C(124)	0.653 3(3)	-0.369 5(4)	-0.047 5(1)	0.373 5(6)	-0.574 2(4)	0.076 9(4)
C(125)	0.656 0(3)	-0.354 3(4)	-0.102 5(1)	0.359 5(6)	-0.544 1(4)	0.013 2(4)
C(126)	0.568 5(3)	-0.307 0(4)	-0.137 5(1)	0.311 5(6)	-0.464 1(4)	-0.002 7(4)
C(211)	0.102 9(3)	-0.229 0(4)	-0.034 6(1)	0.407 1(6)	-0.229 9(5)	0.226 1(4)
C(212)	0.009 6(3)	-0.243 6(4)	-0.015 0(1)	0.523 1(6)	-0.202 6(5)	0.227 7(4)
C(213)	0.011 8(3)	-0.287 5(4)	0.037 6(1)	0.618 8(6)	-0.244 8(5)	0.266 3(4)
C(214)	0.107 3(3)	-0.316 8(4)	0.070 6(1)	0.598 6(6)	-0.314 4(5)	0.303 4(4)
C(215)	0.200 7(3)	-0.302 2(4)	0.051 0(1)	0.482 7(6)	-0.341 7(5)	0.301 9(4)
C(216)	0.198 5(3)	-0.258 3(4)	-0.001 6(1)	0.386 9(6)	-0.299 5(5)	0.263 2(4)
C(221)	-0.032 1(2)	-0.146 1(4)	-0.131 2(2)	0.256 8(7)	-0.087 6(4)	0.228 1(4)
C(222)	-0.094 7(2)	-0.218 6(4)	-0.170 7(2)	0.147 6(7)	-0.046 0(4)	0.213 8(4)
C(223)	-0.199 0(2)	-0.185 1(4)	-0.189 3(2)	0.127 7(7)	0.024 2(4)	0.250 4(4)
C(224)	-0.240 7(2)	-0.079 1(4)	-0.168 5(2)	0.217 2(7)	0.052 7(4)	0.301 4(4)
C(225)	-0.178 1(2)	-0.006 6(4)	-0.129 0(2)	0.326 5(7)	0.011 1(4)	0.315 7(4)
C(226)	-0.073 8(2)	-0.040 0(4)	-0.110 3(2)	0.346 3(7)	-0.059 1(4)	0.279 1(4)
C(11a)	0.100 4(13)	0.063 1(21)	-0.184 9(9)	0.425 7(23)	-0.050 8(21)	0.039 0(17)
C(12a)	0.174 6(13)	0.144 3(21)	-0.153 6(9)	0.323 3(23)	-0.045 4(21)	-0.012 1(17)
C(13a)	0.269 9(13)	0.135 3(21)	-0.173 7(9)	0.228 6(23)	-0.012 7(21)	0.014 6(17)
C(14a)	0.254 6(13)	0.048 6(21)	-0.217 4(9)	0.272 4(23)	0.002 0(21)	0.082 1(17)
C(15a)	0.149 8(13)	0.004 0(21)	-0.224 3(9)	0.394 3(23)	-0.021 5(21)	0.097 2(17)
C(21a)	0.146 8(7)	-0.535 3(10)	-0.183 1(3)	0.050 3(21)	-0.361 4(13)	0.150 6(13)
C(22a)	0.102 7(7)	-0.511 0(10)	-0.136 3(3)	-0.026 5(21)	-0.344 7(13)	0.089 6(13)
C(23a)	0.186 3(7)	-0.496 5(10)	-0.091 5(3)	-0.082 9(21)	-0.265 8(13)	0.094 3(13)
C(24a)	0.282 1(7)	-0.512 0(10)	-0.110 7(3)	-0.040 9(21)	-0.233 8(13)	0.158 2(13)
C(25a)	0.257 7(7)	-0.535 9(10)	-0.167 3(3)	0.041 4(21)	-0.292 9(13)	0.193 0(13)
H(3)				0.427(10)	-0.284(10)	0.106(10)
B				0.229 3(18)	0.492 9(12)	0.312 0(9)
F(1)				0.209 1(10)	0.503 7(7)	0.248 8(5)
F(2)				0.337 1(11)	0.478 4(11)	0.338 1(7)
F(3)				0.160 2(13)	0.440 8(9)	0.330 4(7)
F(4)				0.210 7(15)	0.567 6(8)	0.336 1(6)

(CO)₂(η-C₅H₅)₂] (7), was then eluted as a bright red band using dichloromethane-acetone (9:1) (yield 603.8 mg, 20.3%).

(iii) Protonation of [Mo₂(μ-PPH₂)₂(CO)(η-C₂Me₂)(η-C₅H₅)₂] (4).—Complex (4) (341.5 mg, 0.44 mmol) was dissolved in

dichloromethane (15 cm³) and the solution was cooled to -78 °C (2-propanol-solid CO₂ bath). An excess of HBF₄·OEt₂ (0.5 cm³) was added, causing an immediate colour change to bright purple. On warming to room temperature a further change occurred, to give a dark green solution. The CH₂Cl₂ was

removed *in vacuo*, and the salt $[\text{Mo}_2(\mu\text{-CO})(\mu\text{-PPh}_2)\{\mu\text{-Ph}_2\text{-PC}(\text{Me})\text{=CHMe}\}(\eta\text{-C}_5\text{H}_5)_2][\text{BF}_4]$ (9) was isolated in essentially quantitative yield by washing with diethyl ether: m.p. 230–233 °C, $\nu(\text{CO})$ 1798 cm^{-1} . N.m.r.: ^1H (CD_2Cl_2), δ 7.74–7.00 (m, 20 H, Ph), 5.50 [d, $J(\text{HP})$ 1.2, 5 H, C_5H_5], 5.29 (s, 5 H, C_5H_5), 3.31 [ddq, $J(\text{HP})$ 27.5 and 9.3, $J(\text{HH})$ 6.4, 1 H, CHMe], 2.16 [d, $J(\text{HP})$ 9.4, 3 H, CMe], and 1.64 [dd, $J(\text{HH})$ 6.4, $J(\text{HP})$ 0.6 Hz, CHMe]; ^{13}C , δ 268.9 [dd, $J(\text{CP})$ 10.4 and 6.6, CO], 149.2 [d, $J(\text{CP})$ 38.3, C_{ipso}], 135.2 [d, $J(\text{CP})$ 43.0, C_{ipso}], 134.0–128.9 (m, Ph), 126.0 [d, $J(\text{CP})$ 33.2, C_{ipso}], 99.4 (s, C_5H_5), 95.6 (s, C_5H_5), 66.0 [d, $J(\text{CP})$ 16.2, CHMe], 49.6 [d, $J(\text{CP})$ 30.1, CMe], 20.2 (s, CHMe), and 19.5 p.p.m. [d, $J(\text{CP})$ 12.8 Hz, CMe]; ^{31}P , δ 105.1 (s, $\mu\text{-PPh}_2$) and -110.7 p.p.m. (s, PPh_2) (Found: C, 54.50; H, 4.55; P, 6.40. $\text{C}_{39}\text{H}_{37}\text{BF}_4\text{Mo}_2\text{OP}_2$ requires C, 54.30; H, 4.30; P, 7.20%). Fast atom bombardment mass spectrum: m/z 775 (M^+ for cation).

(iv) *Crystal Structure Determinations.*—Crystal data for complex (4). $\text{C}_{39}\text{H}_{36}\text{Mo}_2\text{OP}_2$, $M = 774.50$, monoclinic, space group $P2_1/c$, $a = 12.965(3)$, $b = 10.659(2)$, $c = 25.072(5)$ Å, $\beta = 100.44(2)^\circ$, $Z = 4$, $U = 3407.44$ Å³, $\mu(\text{Mo-K}_\alpha) = 7.66$ cm^{-1} , $D_c = 1.51$ g cm^{-3} , $F(000) = 1568$. A red-purple crystal of size $0.40 \times 0.27 \times 0.32$ mm, grown by diffusion of hexane into a dichloromethane solution, was used in the data collection.

Crystal data for complex (9). $\text{C}_{39}\text{H}_{37}\text{BF}_4\text{Mo}_2\text{OP}_2$, $M = 862.27$, monoclinic, space group $P2_1/c$, $a = 11.494(2)$, $b = 15.836(3)$, $c = 20.944(4)$ Å, $\beta = 101.93(2)^\circ$, $Z = 4$, $U = 3729.86$ Å³, $\mu(\text{Mo-K}_\alpha) = 7.17$ cm^{-1} , $D_c = 1.54$ g cm^{-3} , $F(000) = 1736$. A green crystal of size $0.16 \times 0.20 \times 0.32$ mm, grown from dichloromethane–diethyl ether solution, was used in the data collection.

Data collection. Data for both structures were collected in the range θ 3–25°, with a scan width of 0.90° for complex (4) and 0.74° for (9), using the technique described previously.¹⁷ For both structures Lorentz and polarisation corrections were applied. The total number of independent reflections was 4389 for (4) and 3145 for (9). Equivalent reflections were merged to give 4168 data for (4) and 2959 for (9), with $I/\sigma(I) > 3.0$.

*Structure solution and refinement.*¹⁸ The co-ordinates of the metal atoms in the structures of complexes (4) and (9) were deduced from Patterson syntheses, and the remaining non-hydrogen atoms were located from subsequent Fourier-difference syntheses. The hydrogen atom attached to C(3) in compound (9) was located in a Fourier-difference synthesis calculated using data with $\sin \theta < 0.35$. This was included in the structure-factor calculations with a thermal parameter of 0.08 Å² but its parameters were not refined. The remaining hydrogen atoms in both structures were included in geometrically idealised positions and were constrained to ride on the relevant carbon atoms with fixed isotropic thermal parameters of 0.08 Å². The phenyl groups in both structures were refined as rigid hexagons. Regions of high electron density around each of the cyclopentadienyl ligands in both structures indicated that these ligands were disordered. Refinement with fixed thermal parameters of 0.05 Å² led to a fractional occupancy of 0.80 for the major component of atoms C(11)—C(15) in (4) and to 0.70 for the equivalent atoms in compound (9). Similarly for the second cyclopentadienyl ligands,

C(21)—C(25), fractional values of 0.60 and 0.65 were found for (4) and (9) respectively. There also appears to be rotational disorder of the BF_4^- anion in (9), shown by regions of extended electron density in the vicinity of the fluorine atoms, which could not be resolved and therefore resulted in high anisotropic thermal parameters for these atoms.

Full-matrix refinement was carried out for both structures, with anisotropic thermal parameters assigned for all non-hydrogen atoms (except the carbon atoms of the phenyl and cyclopentadienyl rings) in the final stages of refinement. For both complexes (4) and (9) weights of $w = 1/\sigma^2 F_o$ were assigned to individual reflections. Refinement converged at R 0.0449 and R' 0.0470 for (4) and at R 0.0558 and R' 0.0554 for (9).¹⁷ The fractional atomic co-ordinates for (4) and (9) are collected in Table 2.

Additional material available from the Cambridge Crystallographic Data Centre comprises H-atom co-ordinates, thermal parameters, and remaining bond lengths and angles.

Acknowledgements

We thank the S.E.R.C. for financial support.

References

- 1 Part 4, A. D. Horton and M. J. Mays, *J. Chem. Soc., Dalton Trans.*, 1990, 155.
- 2 M. D. Curtis, *Polyhedron*, 1987, 6, 759.
- 3 K. Henrick, M. McPartlin, A. D. Horton, and M. J. Mays, *J. Chem. Soc., Dalton Trans.*, 1988, 1083.
- 4 G. Conole, K. Henrick, M. McPartlin, A. D. Horton, and M. J. Mays, *Nouv. J. Chim.*, 1988, 12, 559.
- 5 T. Adatia, M. J. Mays, M. McPartlin, M. J. Morris, and P. R. Raithby, *J. Chem. Soc., Dalton Trans.*, 1989, 1555.
- 6 J. L. Templeton and B. C. Ward, *J. Am. Chem. Soc.*, 1980, 102, 3288.
- 7 G. A. Carriedo, J. A. K. Howard, D. B. Lewis, G. E. Lewis, and F. G. A. Stone, *J. Chem. Soc., Dalton Trans.*, 1983, 271; J. S. Drage, M. Tilset, K. P. C. Vollhardt, and T. W. Weidman, *Organometallics*, 1984, 3, 812.
- 8 K. A. Mead, H. Morgan, and P. Woodward, *J. Chem. Soc., Dalton Trans.*, 1983, 271.
- 9 K. Endrich, R. Korswagen, T. Zahn, and M. L. Ziegler, *Angew. Chem., Int. Ed. Engl.*, 1982, 21, 919; *Angew. Chem. Suppl.*, 1982, 1906.
- 10 G. R. Doel, N. D. Feasey, S. A. R. Knox, A. G. Orpen, and J. Webster, *J. Chem. Soc., Chem. Commun.*, 1986, 542; N. D. Feasey, Ph.D. Thesis, University of Bristol, 1984.
- 11 W. Küchen and H. Buchwald, *Chem. Ber.*, 1958, 91, 2871.
- 12 G. Conole, K. A. Hill, M. McPartlin, M. J. Mays, and M. J. Morris, *J. Chem. Soc., Chem. Commun.*, 1989, 688.
- 13 M. J. Mays, M. J. Morris, P. F. Reinisch, M. McPartlin, and H. R. Powell, *Polyhedron*, 1989, 8, 1807.
- 14 H. Werner and R. Zolk, *Chem. Ber.*, 1987, 120, 1003.
- 15 K. Henrick, M. McPartlin, J. A. Iggo, A. C. Kemball, M. J. Mays, and P. R. Raithby, *J. Chem. Soc., Dalton Trans.*, 1987, 2669.
- 16 W. I. Bailey, M. H. Chisholm, F. A. Cotton, and L. A. Rankel, *J. Am. Chem. Soc.*, 1978, 100, 5764.
- 17 M. K. Cooper, P. J. Guernsey, and M. McPartlin, *J. Chem. Soc., Dalton Trans.*, 1982, 757.
- 18 G. M. Sheldrick, SHELX 76 program for crystal structure determination, University of Cambridge, 1976.

Received 15th January 1990; Paper 0/00199F

Chemistry of Phosphido-bridged Dimolybdenum Complexes. Part 6.¹ The Insertion of Allene into Co-ordinated μ -Vinyl and η^3 -Allyl Ligands; X-Ray Crystal Structures of $[\text{Mo}_2(\eta\text{-C}_5\text{H}_5)_2(\mu\text{-PMe}_2)\{\eta^3\text{-CH}_2\text{C}(\text{CH}_2)\text{C}(\text{Me})=\text{CH}_2\}(\text{CO})_3]$ and $[\text{Mo}_2(\eta\text{-C}_5\text{H}_5)_2\{\mu\text{-}\eta^5\text{-CH}_2\text{C}(\text{CH}_2)\text{C}(\text{Me})=\text{CH}_2\}(\mu\text{-PMe}_2)(\text{CO})_2]$ †

Gráinne Conole,* Kim Henrick, and Mary McPartlin

School of Chemistry, The Polytechnic of North London, Holloway Road, London N7 8DB

Andrew D. Horton and Martin J. Mays*

University Chemical Laboratory, Lensfield Road, Cambridge CB2 1EW

Enrico Sappa

Dipartimento di Chimica Inorganica, Chimica, Fisica e Chimica dei Materiali, Università di Torino, Via P. Giuria 7, 10125 Torino, Italy

Prolonged photolysis of $[\text{Mo}_2(\eta\text{-C}_5\text{H}_5)_2(\mu\text{-H})(\mu\text{-PMe}_2)(\text{CO})_4]$ in the presence of allene gives the new complexes $[\text{Mo}_2(\eta\text{-C}_5\text{H}_5)_2\{\mu\text{-}\eta^5\text{-CH}_2\text{C}(\text{CH}_2)\text{C}(\text{Me})=\text{CH}_2\}(\mu\text{-PMe}_2)(\text{CO})_2]$ and $[\text{Mo}_2(\eta\text{-C}_5\text{H}_5)_2(\mu\text{-PMe}_2)\{\eta^3\text{-CH}_2\text{C}(\text{CH}_2)\text{C}(\text{Me})=\text{CH}_2\}(\text{CO})_3]$ the structures of which in the solid state have been determined by single-crystal X-ray analyses. The former of these new complexes is also obtained in the reaction of the μ -vinyl complex $[\text{Mo}_2(\eta\text{-C}_5\text{H}_5)_2\{\mu\text{-}\sigma\text{:}\eta^2\text{-C}(\text{Me})=\text{CH}_2\}(\mu\text{-PMe}_2)(\text{CO})_3]$ with allene but not in the reaction of the isomeric η^3 -allyl complex $[\text{Mo}_2(\eta\text{-C}_5\text{H}_5)_2(\mu\text{-PMe}_2)(\eta^3\text{-C}_3\text{H}_5)(\text{CO})_3]$ with allene. On the other hand the *syn*-methylallyl complex $[\text{Mo}(\eta\text{-C}_5\text{H}_5)_2(\mu\text{-PMe}_2)(\eta^3\text{-syn-MeCHCH}_2\text{CH}_2)(\text{CO})_3]$ does react with allene to give a *ca.* 1:2 inseparable mixture of $[\text{Mo}_2(\eta\text{-C}_5\text{H}_5)_2\{\mu\text{-}\eta^5\text{-CH}_2\text{C}(\text{CH}_2)\text{C}(\text{Me})=\text{CHMe}\}(\mu\text{-PMe}_2)(\text{CO})_2]$ and $[\text{Mo}_2(\eta\text{-C}_5\text{H}_5)_2\{\mu\text{-}\sigma\text{:}\eta^5\text{-CH}_2\text{C}(\text{CH}_2)\text{C}(\text{Et})=\text{CH}_2\}(\mu\text{-PMe}_2)(\text{CO})_2]$. These complexes may be obtained separately from reactions of the appropriate μ -vinyl complexes with allene. The mechanism of formation of the new complexes is discussed in the light of the above experimental results.

In previous papers we have described the reactions of $[\text{Mo}_2(\eta\text{-C}_5\text{H}_5)_2(\mu\text{-H})(\mu\text{-PR}_2)(\text{CO})_4]$ (1)^{2,3} [R = Me, (1a); Ph, (1b)] with alkynes⁴ and dienes⁵ which lead to the synthesis of a number of dinuclear μ -vinyl and η^3 -allyl complexes of molybdenum of the type $[\text{Mo}_2(\eta\text{-C}_5\text{H}_5)_2(\mu\text{-vinyl})(\mu\text{-PR}_2)(\text{CO})_3]$ (2)^{4,5} and $[\text{Mo}_2(\eta\text{-C}_5\text{H}_5)_2(\mu\text{-PR}_2)(\eta^3\text{-allyl})(\text{CO})_3]$ (3)⁵ (R = Me or Ph). The proposed structures of these complexes are shown in Figure 1, the structure for a complex of type (2) [μ -vinyl = $\mu\text{-C}(\text{Me})=\text{CHMe}$, R = Me] having been confirmed by X-ray analysis.⁴ We now find that, on prolonged photolysis in the presence of excess of allene, the mixture of complexes $[\text{Mo}_2(\eta\text{-C}_5\text{H}_5)_2\{\mu\text{-}\sigma\text{:}\eta^2\text{-C}(\text{Me})=\text{CH}_2\}(\mu\text{-PMe}_2)(\text{CO})_3]$ (2a) and $[\text{Mo}_2(\eta\text{-C}_5\text{H}_5)_2(\mu\text{-PMe}_2)(\eta^3\text{-C}_3\text{H}_5)(\text{CO})_3]$ (3a) obtained in the initial reaction of $[\text{Mo}_2(\eta\text{-C}_5\text{H}_5)_2(\mu\text{-H})(\mu\text{-PMe}_2)(\text{CO})_4]$ (1a) with allene reacts further to give new products. In this paper we report the characterisation of these new products and our studies on the reactions of complexes of types (2) and (3) with allene, which we have undertaken in order to explore the mechanism of formation of the new species.

Results and Discussion

Prolonged Photolysis of Complex (1a) with Excess of Allene.—

Reaction of complex (1a) with a *ca.* two-fold excess of allene for 4 h under photolysis (Hanovia 125-W medium-pressure immersion lamp) gave (2a) (22), (3a) (12), unreacted (1a) (60%), and traces of at least three other products.⁵ We now find that prolonged photolysis of (1a) with a large excess of allene (saturated solution in benzene–hexane, 1:1) for 3 d results in a reduction in the yields of (2a) (7), (3a) (10), and unreacted (1a) (20%) and the appearance of two new orange complexes in 45 and 7% yield. These new major and minor products have been characterised on the basis of i.r. and ¹H n.m.r. spectroscopy, mass spectrometry, microanalysis, and X-ray structural studies

(see below) as, respectively, $[\text{Mo}_2(\eta\text{-C}_5\text{H}_5)_2\{\mu\text{-}\eta^5\text{-CH}_2\text{C}(\text{CH}_2)\text{C}(\text{Me})=\text{CH}_2\}(\mu\text{-PMe}_2)(\text{CO})_2]$ (4a) and $[\text{Mo}_2(\eta\text{-C}_5\text{H}_5)_2(\mu\text{-PMe}_2)\{\eta^3\text{-CH}_2\text{C}(\text{CH}_2)\text{C}(\text{Me})=\text{CH}_2\}(\text{CO})_3]$ (5a) (Figure 1).

Crystals of (4a) and (5a) suitable for the X-ray studies were grown by slow evaporation of hexane–CH₂Cl₂ (1:1) solutions at 0 °C. The molecular structure of the minor product, (5a), is shown in Figure 2. Table 1 lists the atomic co-ordinates; selected bond lengths and interbond angles are given in Table 2. Complex (5a) crystallizes with the η^3 -allyl ligand in the *exo* conformation relative to the cyclopentadienyl ligand on Mo(2). If the Mo–Mo bond is ignored, the ligands on Mo(2) adopt a similar geometry to that found in the mononuclear complex $[\text{Mo}(\eta\text{-C}_5\text{H}_5)(\eta^3\text{-C}_3\text{H}_5)(\text{CO})_2]$.⁶ Thus the four atoms P(1), C(21), and the two terminal allyl carbons C(1) and C(3) form the irregular base of an approximate square-pyramidal geometry. The Mo–C (terminal, allyl) bond distances of 2.315(8) and 2.309(7) Å are identical within error limits, hence implying that the bonding of the η^3 -allyl ligand is normal and not of the σ - π type observed for the ligand in the asymmetric electronic environment of $[\text{Mo}(\eta\text{-C}_5\text{H}_5)(\eta^3\text{-C}_3\text{H}_5)(\text{NO})]$.⁶ As in $[\text{Mo}(\eta\text{-C}_5\text{H}_5)(\eta^3\text{-C}_3\text{H}_5)(\text{CO})_2]$,⁶ the average Mo–C (terminal, allyl) bond length is significantly greater than the Mo–C (central, allyl) bond length of 2.261(7) Å, although the difference is less than in the mononuclear complex. The structure of the $\eta^3\text{-C}_6\text{H}_9$ ligand may be compared to that of the $\eta^3\text{-C}_6\text{H}_9\text{Cl}$ ligand in $[\{\text{Pd}(\eta^3\text{-C}_6\text{H}_9\text{Cl})\}_2]$,⁷ which differs formally only in

† μ -Carbonyl-1,1-dicarbonyl-1,2-bis(η -cyclopentadienyl)- μ -dimethylphosphido-2-(2'-isopropenylallyl)-C^{1'-3'}dimolybdenum (*Mo-Mo*) and μ -dimethylphosphido- μ -[2'-(isopropenyl-2 κ^2 C^{1'-2'}allyl)-1 $\kappa(\eta^3)$]-bis-[carbonyl(η -cyclopentadienyl)molybdenum] (*Mo-Mo*).

Supplementary data available: see Instructions for Authors, *J. Chem. Soc., Dalton Trans.*, 1990, Issue 1, pp. xix–xxii.

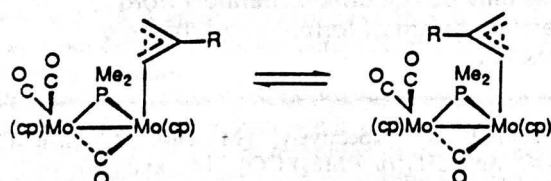
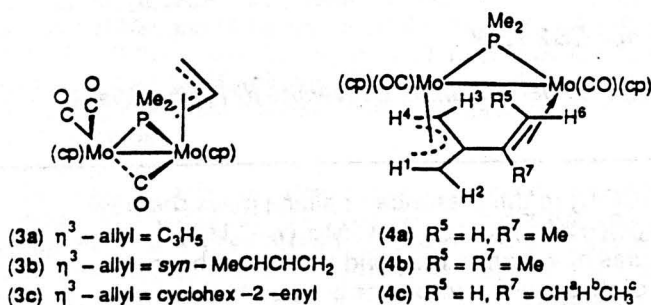
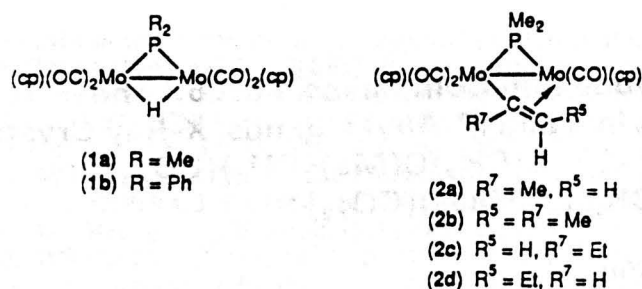


Figure 1. Structures of the dimolybdenum complexes (cp = η⁵-C₅H₅)

the replacement of one of the ethyl hydrogens by chlorine. The dihedral angle between the planes containing C(1)–C(2)–C(3) and C(5)–C(4)–C(6) is *ca.* 8° in (5a) compared to 27° in the palladium compound, implying a greater element of electron delocalization over the two parts of the ligand in the former complex. The C=C double bond length in (5a), 1.336(14) Å, is, however, equal within error limits to the 1.38(6) Å for the corresponding bond in the palladium complex.

Complex (5a) has a semi-bridging carbonyl, CO(21), as evidenced by the Mo(2)–C(21)–O(21) interbond angle of 155.9(6)° and Mo–CO(21) distances of 1.963(7) and 2.629(7) Å for Mo(2) and Mo(1) respectively. The slightly shorter Mo(2)–P bond length of 2.408(2) Å, compared to 2.426(2) Å for Mo(1)–P,

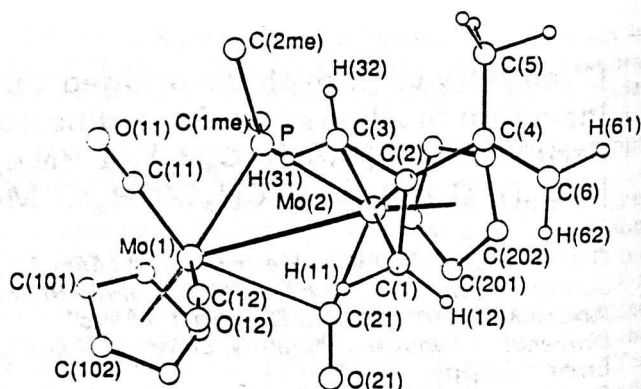


Figure 2. Molecular structure of [Mo₂(η-C₃H₅)₂(μ-PMe₂){η³-CH₂C(CH₃)C(Me)=CH₂}(CO)₃] (5a) showing the crystallographic numbering

may reflect the reduced π-acid character of the η³-allyl group compared to a carbonyl ligand, this then increasing the electron density available to Mo(2) for π-back bonding to phosphorus. The Mo–Mo bond length of 3.285(1) Å is slightly greater than that in [Mo₂(η-C₃H₅)₂(μ-H)(μ-PMe₂)(CO)₄] (1a)⁸ [3.267(1) Å] but is within the range normally observed for Mo–Mo single bonds.⁹ The shorter Mo–P bonds and longer Mo–Mo bond in (5a) compared to complex (1a) result in a slightly larger bite angle at phosphorus of 85.6(1) compared to 84.8(1)°. The geometry of the ligands at Mo(1) is similar in both complexes except that in (5a) a μ-CO group replaces the μ-H group in (1a). In contrast to (1a), the two cyclopentadienyl ligands in (5a) adopt a relative *cis* orientation with respect to the Mo–Mo vector.

The i.r. [ν(CO)] spectrum of complex (5a) is similar to those of other η³-allyl complexes of type (3)⁵ with two terminal carbonyl absorptions and a semi-bridging carbonyl absorption at 1798 cm⁻¹ as expected on the basis of the crystal structure. However, the ¹H n.m.r. spectrum of (5a) in CDCl₃ at 238 K indicates the presence in solution of two isomers in a ratio of *ca.* 1.1:1. Thus four cyclopentadienyl resonances are observed in addition to twelve resonances with relative intensity corresponding to one hydrogen each and two resonances corresponding to methyl groups. On the basis of a series of selective-decoupling experiments the resonances have been assigned to specific hydrogens in the C₆H₉ ligand in each of the two isomers. For each isomer, four resonances in the region δ 3.0 to –0.9 correspond to the *syn* and *anti* allyl hydrogens and two resonances in the range δ 5.3–4.6 correspond to the alkene hydrogens. The assignments are given in the Experimental section and the numbering scheme for the ligand hydrogen atoms is shown in Figure 1. Presumably one isomer corresponds to an *exo* configuration for the allyl ligand and the other to an *endo* configuration (Figure 1). It is not, however, possible to determine from the ¹H n.m.r. data which set of resonances corresponds to the *exo* isomer and which to the *endo*. Similar isomerism has been observed in other η³-allyl complexes of type (3).⁵

The molecular structure of the major product (4a), from the reaction of (1a) with excess of allene is shown in Figure 3. Table 3 lists the atomic co-ordinates; selected bond lengths and interbond angles are given in Table 4. The C₆H₉ ligand bridges the Mo–Mo bond *via* coordination of the η³-allyl group to Mo(2) and of the η²-alkene group to Mo(1). The non-coplanarity of the η³-allyl and the η²-alkene groups, the dihedral angle between the two planes being 52.35°, contrasts strongly with the structure of the ligand in (5a) in which the corresponding angle is *ca.* 8°. However the similarity in C–C 'backbone' bond distances in the C₆H₉ ligand in (4a), 1.498(6) Å, and (5a), 1.494(12) Å, argues against any significant

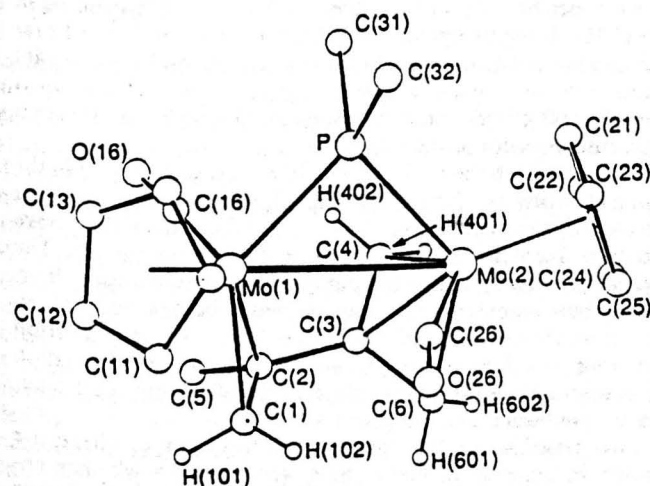
Table 1. Fractional atomic co-ordinates for complex (5a)

Atom	x	y	z	Atom	x	y	z
Mo(1)	0.158 93(3)	0.290 53(7)	0.128 69(8)	O(21)	0.244 2(2)	0.069 0(6)	0.008 6(7)
Mo(2)	0.132 68(2)	-0.027 25(6)	0.058 76(7)	C(101)	0.185 0(4)	0.461 1(11)	0.300 7(13)
P	0.090 4(1)	0.141 7(2)	0.217 4(3)	C(102)	0.220 7(4)	0.453 6(10)	0.184 6(15)
C(1)	0.150 7(3)	-0.023 7(10)	-0.209 9(9)	C(103)	0.244 8(4)	0.332 3(10)	0.192 8(15)
C(2)	0.097 8(3)	-0.047 4(8)	-0.186 5(8)	C(104)	0.225 1(4)	0.257 3(11)	0.316 6(14)
C(3)	0.070 8(3)	0.057 1(8)	-0.113 5(9)	C(105)	0.186 1(5)	0.342 8(13)	0.389 7(11)
C(4)	0.072 4(3)	-0.176 9(9)	-0.231 3(10)	C(201)	0.188 2(3)	-0.187 9(8)	0.165 1(11)
C(5)	0.016 9(4)	-0.191 5(13)	-0.183 1(13)	C(202)	0.155 8(3)	-0.254 0(7)	0.057 1(12)
C(6)	0.095 3(4)	-0.270 1(11)	-0.321 5(13)	C(203)	0.105 8(3)	-0.246 0(8)	0.114 5(10)
C(11)	0.098 6(3)	0.392 4(8)	0.067 3(13)	C(204)	0.105 6(3)	-0.175 8(8)	0.257 6(9)
O(11)	0.063 6(3)	0.456 1(7)	0.026 5(12)	C(205)	0.157 9(3)	-0.137 6(8)	0.291 2(10)
C(12)	0.167 8(4)	0.307 0(10)	-0.102 4(13)	C(1me)	0.088 6(4)	0.115 3(12)	0.434 6(11)
O(12)	0.173 6(4)	0.326 4(10)	-0.232 2(9)	C(2me)	0.022 6(3)	0.186 1(11)	0.194 3(13)
C(21)	0.199 7(3)	0.062 7(7)	0.031 4(9)				

Table 2. Selected bond lengths (Å) and angles (°) for complex (5a)*

Mo(1)-Mo(2)	3.285(1)	Mo(2)-P-Mo(1)	85.6(1)
Mo(1)-P	2.426(2)	C(2me)-P-C(1me)	96.7(5)
Mo(1)-C(11)	1.930(9)	C(2)-C(1)-Mo(2)	70.3(4)
Mo(1)-C(12)	1.965(11)	C(1)-C(2)-Mo(2)	74.0(4)
Mo(1)-C(21)	2.629(7)	C(3)-C(2)-Mo(2)	74.4(4)
Mo(2)-P	2.408(2)	C(3)-C(2)-C(1)	115.1(7)
Mo(2)-C(1)	2.309(7)	C(4)-C(2)-Mo(2)	118.8(5)
Mo(2)-C(2)	2.261(7)	C(4)-C(2)-C(1)	122.6(7)
Mo(2)-C(3)	2.315(8)	C(4)-C(2)-C(3)	122.3(7)
Mo(2)-C(21)	1.963(7)	C(2)-C(3)-Mo(2)	70.2(4)
P-C(1me)	1.847(10)	C(5)-C(4)-C(2)	115.9(8)
P-C(2me)	1.817(9)	C(6)-C(4)-C(2)	123.1(8)
C(1)-C(2)	1.402(10)	C(6)-C(4)-C(5)	120.7(9)
C(2)-C(3)	1.394(11)	O(11)-C(11)-Mo(1)	177.4(9)
C(2)-C(4)	1.494(12)	O(12)-C(12)-Mo(2)	175(1)
C(4)-C(5)	1.496(13)	Mo(2)-C(21)-Mo(1)	90.2(3)
C(4)-C(6)	1.336(14)	O(21)-C(21)-Mo(1)	113.6(5)
C(11)-O(11)	1.157(12)	O(21)-C(21)-Mo(2)	155.9(6)
C(12)-O(12)	1.119(13)		
C(21)-O(21)	1.167(8)		
Range Mo(1)-Cp	2.320(10)-		
	2.363(10)		
Range Mo(2)-Cp	2.326(8)-		
	2.339(8)		

* Cp = Cyclopentadienyl ring carbon atoms.

Figure 3. Molecular structure of $[\text{Mo}_2(\eta\text{-C}_5\text{H}_5)_2]\mu\text{-}\eta^5\text{-CH}_2\text{C}(\text{CH}_2)\text{C}(\text{Me})=\text{CH}_2(\mu\text{-PMMe}_2)(\text{CO})_2$ (4a) showing the crystallographic numbering

difference in electron delocalisation between the allyl and alkene groups in the two complexes. Co-ordination of the alkene to

Mo(1) results in an increase in the C=C double bond distance from 1.336(14) Å in (5a) to 1.384(6) Å in (4a) which may be rationalised on the basis of metal back bonding into the alkene π^* antibonding orbitals. Although the mean Mo-C (allyl, terminal) bond distance is only slightly reduced, at 2.296(5) Å in (4a) compared to 2.312(8) Å in (5a), the corresponding bond to the central allyl carbon is significantly longer in (4a), at 2.315(4) compared to 2.261(7) Å in (5a). The η^3 -allyl group in (4a) is constrained, by the co-ordination of the alkene to the adjacent molybdenum centre, to adopt an *endo* conformation relative to the cyclopentadienyl group on Mo(2). The large separation of the central allyl carbon and Mo(2) may thus reflect the requirement of the alkene group to be in reasonable proximity to Mo(1).

Although overall the complex obeys the effective atomic number (e.a.n.) rule, Mo(1) is electron poor and Mo(2) is electron rich. The electron deficiency at Mo(1) may be partially compensated by the reduced Mo(1)-P bond distance of 2.392(1) Å compared to Mo(2)-P 2.421(1) Å. The lack of a significant semi-bridging carbonyl interaction in (4a) in comparison to (5a) may reflect the replacement of a carbonyl by an η^2 -alkene on Mo(1) which, due to the reduced π -acid character of the alkene, results in an increase in the electron density at Mo(1). However, at least equally important in hindering a semi-bridging carbonyl interaction is the steric crowding at Mo(1). The non-linearity of CO(26) [Mo(2)-C(26)-O(26) interbond angle 167.1(4)°] may reflect the steric crowding in the molecule; the large Mo(1)-CO(26) separation of 3.00 Å indicates that there is no significant bonding interaction. The two cyclopentadienyl ligands adopt an approximate relative *cis* orientation with respect to the Mo-Mo vector.

The Mo-Mo bond distance, 3.333(1) Å in (4a) is significantly longer than in (5a), 3.285(1) Å, although it is still consistent with the presence of a Mo-Mo single bond. The longer Mo-Mo bond may reflect an attempt to reduce the steric crowding in the molecule. The slightly reduced average Mo-P bond distance, together with the increased Mo-Mo distance, result in an increased bite angle at phosphorus of 87.7(1) compared to 85.6(1) in (5a).

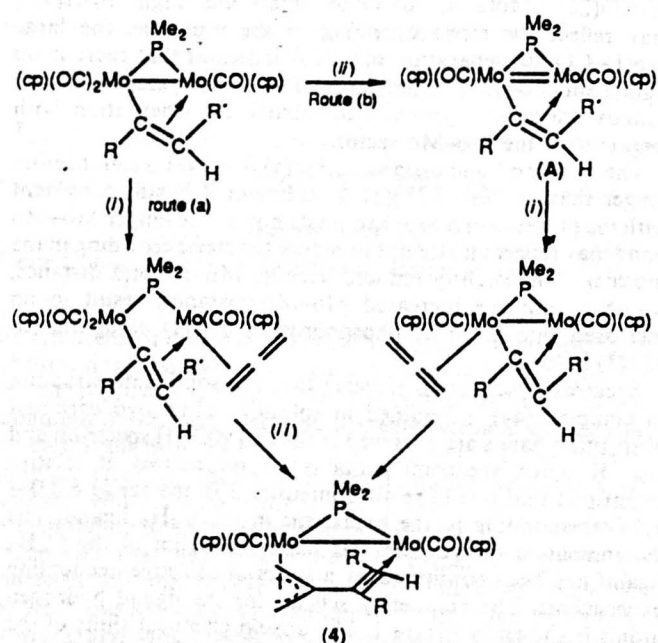
Spectroscopic studies indicate that the solid-state structure of complex (4a) is retained in solution. Thus two carbonyl absorption bands are observed in the i.r. [$\nu(\text{CO})$] spectrum and the ^1H n.m.r. spectrum contains six resonances of relative intensity 1 and one of relative intensity 3 in the range δ 3.0-1.0 corresponding to the hydrogens in the C_6H_9 ligand. The assignment of the complex ^1H n.m.r. spectrum of the C_6H_9 ligand has been confirmed by a series of selective-decoupling experiments. The numbering scheme for the ligand hydrogen atoms is shown in Figure 1. The upfield chemical shifts of the two alkene hydrogens, δ 1.84 (H^5) and 1.73 (H^6), imply that the

Table 3. Fractional atomic co-ordinates for complex (4a)

Atom	x	y	z	Atom	x	y	z
Mo(1)	0.337 28(3)	0.146 51(2)	0.184 06(2)	C(26)	0.281 7(5)	0.077 8(2)	0.393 8(3)
Mo(2)	0.169 59(3)	0.005 30(2)	0.297 59(2)	O(26)	0.345 2(4)	0.111 4(2)	0.466 6(2)
P	0.370 26(11)	0.011 64(5)	0.188 91(8)	C(11)	0.465 3(5)	0.246 4(3)	0.277 8(4)
C(1)	0.150 4(5)	0.213 0(3)	0.241 8(4)	C(12)	0.453 9(5)	0.260 4(2)	0.166 6(4)
C(2)	0.077 3(4)	0.166 0(2)	0.163 1(3)	C(13)	0.537 2(5)	0.205 6(3)	0.121 1(4)
C(3)	0.016 9(4)	0.091 7(2)	0.196 2(3)	C(14)	0.599 8(5)	0.157 1(3)	0.201 5(5)
C(4)	0.021 4(5)	0.025 4(3)	0.135 5(3)	C(15)	0.557 4(5)	0.181 7(3)	0.298 8(4)
C(31)	0.354 7(6)	-0.049 1(3)	0.068 1(4)	C(21)	0.229 5(5)	-0.124 0(2)	0.304 2(4)
C(32)	0.547 2(5)	-0.025 1(3)	0.258 4(5)	C(22)	0.074 6(6)	-0.120 4(3)	0.286 0(4)
C(6)	-0.033 1(5)	0.082 6(3)	0.297 2(4)	C(23)	0.278 9(6)	-0.090 2(3)	0.404 5(4)
C(5)	-0.009 1(6)	0.199 7(3)	0.061 7(4)	C(24)	0.025 0(6)	-0.084 8(3)	0.374 0(5)
C(36)	0.266 5(4)	0.132 2(2)	0.034 5(3)	C(25)	0.150 5(7)	-0.065 6(3)	0.447 8(4)
O(16)	0.236 1(3)	0.127 7(2)	-0.058 9(2)				

Table 4. Selected bond lengths (Å) and angles (°) for complex (4a)

Mo(1)–Mo(2)	3.333(1)	Mo(2)–P–Mo(1)	87.7(1)
Mo(1)–P	2.392(1)	C(32)–P–C(31)	98.6(3)
Mo(1)–C(16)	1.913(4)	C(2)–C(1)–Mo(1)	76.6(3)
Mo(1)–C(1)	2.258(5)	C(1)–C(2)–Mo(1)	68.6(2)
Mo(1)–C(2)	2.360(4)	C(3)–C(2)–Mo(1)	103.9(2)
Mo(2)–P	2.421(1)	C(3)–C(2)–C(1)	118.8(4)
Mo(2)–C(3)	2.315(4)	C(5)–C(2)–Mo(1)	122.8(3)
Mo(2)–C(4)	2.303(4)	C(5)–C(2)–C(1)	120.3(4)
Mo(2)–C(6)	2.285(5)	C(5)–C(2)–C(3)	114.0(3)
Mo(2)–C(26)	1.943(4)	C(2)–C(3)–Mo(2)	120.7(2)
P–C(31)	1.843(5)	C(4)–C(3)–Mo(2)	71.9(2)
P–C(32)	1.834(5)	C(4)–C(3)–C(2)	122.6(4)
C(1)–C(2)	1.384(6)	C(6)–C(3)–Mo(2)	71.0(2)
C(2)–C(3)	1.498(6)	C(6)–C(3)–C(2)	121.5(4)
C(3)–C(4)	1.396(6)	C(6)–C(3)–C(4)	115.5(4)
C(3)–C(6)	1.412(6)	C(3)–C(4)–Mo(2)	72.9(2)
C(16)–O(16)	1.169(5)	C(3)–C(6)–Mo(2)	73.3(2)
C(26)–O(26)	1.170(5)	O(16)–C(16)–Mo(1)	172.9(3)
Range Mo(1)–Cp	2.290(4)– 2.375(5)	O(26)–C(26)–Mo(2)	167.1(4)
Range Mo(2)–Cp	2.286(5)– 2.371(5)		

Scheme 1. Possible mechanism for the insertion of allene into the μ -vinyl complexes (2): (i) allene; (ii) $h\nu$, -CO

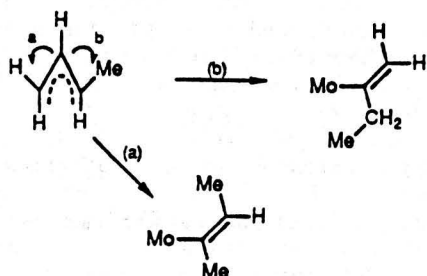
alkene remains co-ordinated to the Mo in solution. The ^{13}C n.m.r. spectrum of (4a) which contains six resonances in the range δ 100–20 due to the C_6H_9 ligand, assigned on the basis of ^{13}C - ^1H coupling constants, is also consistent with the retention of the solid-state structure in solution.

The formation of (4a) and (5a) from the reaction of (1a) with excess of allene could proceed either *via* the μ -vinyl complex (2a) or *via* the allyl complex (3a), which are both formed initially. In order to determine the reaction pathway which is followed we have investigated separately the reactions of the μ -vinyl complexes (2) and the allyl complexes (3) with allene.

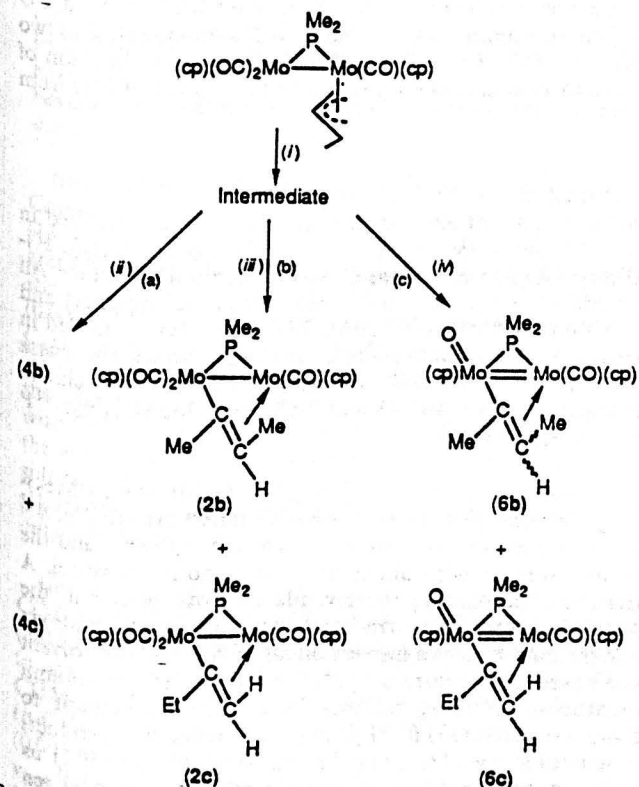
Reaction of the Vinyl Complexes (2) with Allene.—Photolysis of an allene-saturated hexane solution of complex (2a) for 1.5 h gave (4a) in high yield (68%) as the only significant product. Photolysis of the dimolybdenum μ -vinyl complexes $[\text{Mo}_2(\eta\text{-C}_5\text{H}_9)_2\{\mu\text{-}\sigma\text{-}\eta^2\text{-C}(\text{R}^7)\text{=CHR}^5\}(\mu\text{-PMe}_2)(\text{CO})_3]$ $[\text{R}^5 = \text{R}^7 = \text{Me}$, (2b); $\text{R}^5 = \text{H}$, $\text{R}^7 = \text{Et}$, (2c)] with allene similarly gave $[\text{Mo}_2(\eta\text{-C}_5\text{H}_9)_2\{\mu\text{-}\sigma\text{-}\eta^2\text{-CH}_2\text{C}(\text{CH}_2)\text{C}(\text{R}^7)\text{-CHR}^5\}(\mu\text{-PMe}_2)(\text{CO})_2]$ $[\text{R}^5 = \text{R}^7 = \text{Me}$, (4b); $\text{R}^5 = \text{H}$, $\text{R}^7 = \text{Et}$, (4c)]. The proposed structures of (4a)–(4c) (Figure 1) are based on i.r. and ^1H n.m.r. spectroscopy, mass spectrometry, and, in the case of (4a) and (4c), microanalysis. Complex (4b) is always obtained contaminated with other unidentified products and it has not proved possible to identify resonances in the ^1H n.m.r. spectrum of (4b) associated with all of the hydrogens in the C_7H_{11} bridging ligand. It has been assumed in Figure 1 that the two methyl groups on the alkene part of the ligand in (4b) adopt the same relative *trans* orientation as in the μ -vinyl complex, (2b), from which it is derived, although the ^1H n.m.r. spectrum does not prove this.

It is clear, from the positioning of the alkyl substituents in the complexes (4b) and (4c), that the η^2 -alkene part of the bridging organic ligand in the complexes (4) is derived in the above reaction from the μ -vinyl ligand in the complexes (2). The overall process by which the complexes (4) are obtained from the μ -vinyl complexes (2) may therefore be described as an insertion of allene into the Mo-C σ bond. Related insertion reactions of allene in which carbon-carbon bond formation involving the central carbon atom of the allene molecule takes place have been described previously.^{10,11}

Two possible mechanisms for the insertion of allene are shown in Scheme 1. These differ according to whether co-ordination of allene takes place before [route (a)] or after [route (b)] the loss of CO induced by u.v. irradiation. Stirring a hexane solution of complex (2a) with allene in the dark results in no change in the i.r. spectrum. There is therefore no evidence for the formation of an adduct as proposed for route (a). However, u.v. irradiation of a solution of (2a) in the absence of allene results in a rapid colour change from orange to orange-green. Subsequent



Scheme 2. 1,2-Hydrogen shift in the allyl ligand in complex (3b) required to give (a) (2b) and (b) (2c)



Scheme 3. Reactions of the intermediate obtained on irradiation of the η^3 -allyl complex (3b): (i) $h\nu$; (ii) allene; (iii) CO; (iv) no CO or allene

stirring of the irradiated solution in the dark with allene gives (4a) in ca. 20% yield. If no allene is added the only product isolated from the irradiated solution is a trace of the red μ -vinyl oxo complex $[\text{Mo}_2\text{O}(\eta\text{-C}_5\text{H}_5)_2\{\mu\text{-}\sigma\text{:}\eta^2\text{-C}(\text{Me})\text{=CH}_2\}(\mu\text{-PMe}_2)(\text{CO})]$ (6a).⁴ The structure proposed for intermediate (A) in Scheme 1, route (b), is closely related to that of $[\text{Mo}_2(\eta\text{-C}_5\text{H}_5)_2(\mu\text{-PPh}_2)_2(\text{CO})_2]$,^{12a} which also contains an Mo-Mo double bond. We cannot, however, exclude the possibility that CO loss from (2a) is accompanied by co-ordination of a solvent molecule rather than an increase in the metal-metal bond order. The fact that (A) reacts rapidly with allene suggests that it is the likely intermediate. Further evidence that the intermediate is an unsaturated complex formed by loss of CO is provided by the fact that stirring of the irradiated solution with CO enables some (2a) to be recovered which is not the case if CO is absent. It thus appears that the loss of CO from (2a) on irradiation may be reversible. Once allene has reacted with (A) insertion presumably occurs rapidly as no simple allene adduct may be isolated.

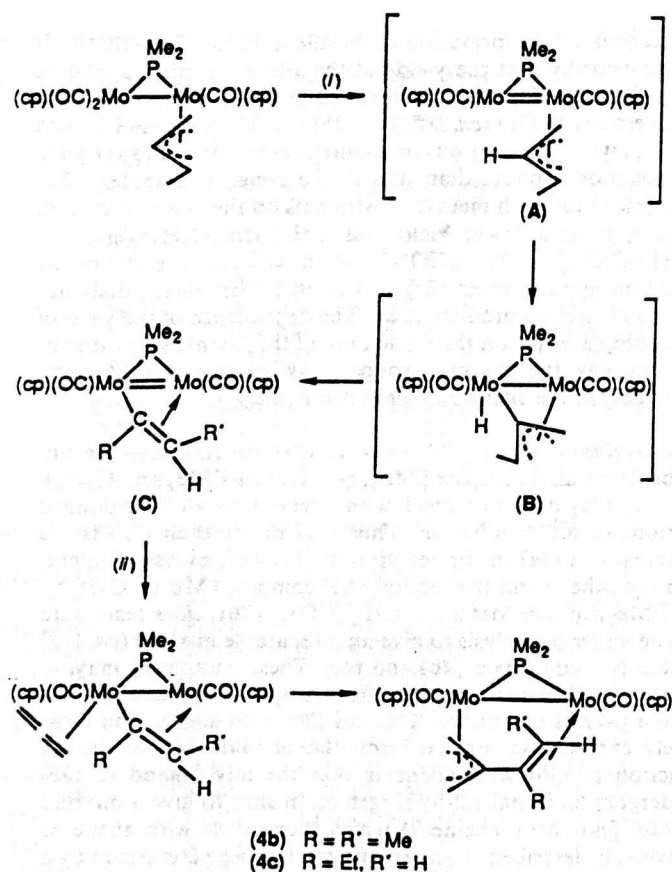
Nubel and Brown^{12b} have shown that the first step in the insertion reaction of ethene with the μ -vinyl complex $[\text{Re}_2(\mu\text{-H})\{\mu\text{-}\sigma\text{:}\eta^2\text{-C}(\text{H})\text{=CH}_2\}(\text{CO})_n]$, involves photochemical loss of CO and formation of an ethene adduct. There is therefore some

precedent for the formation of the allene adduct in route (b). It is noteworthy that the yields of the allene insertion products, (4) decrease for the μ -vinyl complexes, (2a), (ca. 70% conversion) > (2c) (ca. 50%) > (2b) (ca. 30%). Thus (2c), with an α -ethyl substituent on the μ -vinyl ligand, gives a lower yield of insertion product than that of the α -methyl complex, (2a). Complex (2b), with methyl substituents on the α - and β -carbon atoms, gives a lower yield still and $[\text{Mo}_2(\text{C}_5\text{H}_5)_2\{\mu\text{-}\sigma\text{:}\eta^2\text{-C}(\text{H})\text{=CHEt}\}(\mu\text{-PMe}_2)(\text{CO})_3]$, which was also present in the reaction mixture when (2c) was treated with allene, does not give an insertion product at all. The dependence of the yield of the complexes (4) on the steric bulk of the μ -vinyl substituents, particularly the β -alkyl groups, may be a result of steric crowding in the allene adduct in route (b).

Reaction of the Allyl Complexes (3) with Allene.—The unsubstituted allyl complex $[\text{Mo}_2(\eta\text{-C}_5\text{H}_5)_2(\mu\text{-PMe}_2)(\eta^3\text{-C}_3\text{H}_5)(\text{CO})_3]$ (3a) does not react with allene even after prolonged periods of u.v. irradiation. Thus (2a) rather than (3a) is the precursor of (4a) in the reaction of (1a) with excess of allene. On the other hand the methyl allyl complex $[\text{Mo}_2(\eta\text{-C}_5\text{H}_5)_2(\mu\text{-PMe}_2)(\eta^3\text{-syn-MeCHCHCH}_2)(\text{CO})_3]$ (3b)⁵ does react with allene under photolysis to give an inseparable mixture (ca. 1:2) of the two complexes (4b) and (4c). These complexes may, of course, be obtained separately from, respectively, the reactions of the μ -vinyl complexes (2b) and (2c) with allene. The most likely explanation for the formation of (4b) and (4c) in the reaction of (3b) with allene is that the allyl ligand in (3b) undergoes an initial 1,2-hydrogen atom shift to give a mixture of (2b) and (2c) (Scheme 2) which then reacts with allene as previously described. This explanation has been confirmed by a number of experiments. Thus u.v. irradiation of a solution of complex (3b) results in a colour change from red to red-green. On stirring the irradiated solution with allene in the dark a mixture of (4b) and (4c) is formed in ca. 50% yield. Similar treatment of the irradiated solution with CO for 1 h, followed by stirring with allene, gives the μ -vinyl complexes (2b) and (2c) in ca. 30% combined yield with only traces of (4b), (4c), and other unidentified products. Under similar conditions, but using N_2 rather than CO, (2b) and (2c) are formed with a lower combined yield (ca. 10%); in addition the complexes $[\text{Mo}_2\text{O}(\eta\text{-C}_5\text{H}_5)_2\{\mu\text{-C}(\text{R}^7)\text{=CHR}^5\}(\mu\text{-PMe}_2)(\text{CO})]$ ⁴ [$\text{R}^5 = \text{R}^7 = \text{Me}$, (6b); $\text{R}^7 = \text{Et}$, $\text{R}^5 = \text{H}$, (6c)] (ca. 20% combined yield) and traces of other unidentified species are obtained. From these results it is clear that u.v. irradiation of (3b) gives an unstable intermediate which may participate in three competing reactions (Scheme 3): (a) with allene to give (4b) and (4c); (b) with CO to give (2b) and (2c); and (c) with air in the absence of allene or CO, to give (6b) and (6c).

Any mechanism proposed to explain the reaction of complex (3b) with allene must account for the overall 1,2-hydrogen atom shift and the C-C bond formation in the reaction. The latter may occur *via* insertion of allene into a Mo-C σ bond as proposed for the reaction of allene with the μ -vinyl complexes. It is proposed (Scheme 4) that u.v. irradiation of (3b) induces CO loss from the molybdenum atom adjacent to the one to which the allyl ligand is co-ordinated giving a co-ordinatively unsaturated intermediate (A). Carbon-hydrogen bond cleavage, perhaps *via* an initial CHMo agostic interaction, gives (B) and readdition of the hydride to one or other of the two terminal allyl carbon atoms then gives two isomers of an unsaturated μ -vinyl intermediate, (C), similar to that proposed to be formed on u.v. irradiation of the μ -vinyl complexes (2). Addition of allene and insertion into the Mo-C σ -bond then proceeds as previously described.

Hydrogen-shift processes similar to the one described here have been observed previously in the rearrangement of μ -allylidyne to μ -alkyne ligands at a dimolybdenum centre, and a



Scheme 4. Possible mechanism for the formation of complexes (4b) and (4c) from the η^3 -allyl complex (3b); (i) $h\nu$, $-\text{CO}$; (ii) allene

similar mechanism was postulated to account for the phenomenon.¹³ In addition, the bridging $\sigma:\eta^3$ -allyl ligand in the co-ordinatively unsaturated intermediate, (B), in Scheme 4 has been previously observed in stable di-iron complexes such as $[\text{Fe}_2(\mu-\sigma:\eta^3\text{-C}_3\text{H}_4)(\text{CO})_7]$.¹⁴ Finally, intramolecular attack of a metal hydride on an η^3 -allyl ligand has been previously postulated to account for the variable-temperature ^1H n.m.r. behaviour of $[\text{Mo}(\eta^3\text{-C}_3\text{H}_5)(\text{Ph}_2\text{PCH}_2\text{CH}_2\text{PPh}_2)_2\text{H}]$.¹⁵

An alternative route to complexes (4b) and (4c) to that shown in Scheme 4 is the insertion of allene into the Mo-C σ bond in intermediate (B) prior to readdition of the hydride ligand. We cannot exclude this possibility but the formation of the unsaturated μ -vinyl intermediate (C), which is also proposed as an intermediate in the reaction of the μ -vinyl complexes (2) with allene, is perhaps in this case also the most likely route to (4).

The conversion of a σ -vinyl ligand into an η^3 -allyl ligand has been proposed previously as part of the mechanism by⁹ which attack of H^- on a cationic molybdenum alkyne complex affords an allyl species.^{16,17} That the reverse reaction, as observed in the dimolybdenum system described here, has not been previously documented can be ascribed to the fact that most known allyl complexes are mononuclear. Presumably the isomerisation of an allyl to a vinyl ligand requires the driving force provided by the presence of a second metal centre, which then enables the vinyl ligand to co-ordinate in a bridging σ,π mode. Why this isomerisation takes place for the $\eta^3\text{-C}_6\text{H}_7$ ligand in (3b) [and for the $\eta^3\text{-C}_6\text{H}_9$ (cyclohex-2-enyl) ligand in (3c),⁴ see Experimental section] but not for the $\eta^3\text{-C}_3\text{H}_5$ ligand in (3a) remains to be resolved.

Interconversion of Complexes (4a) and (5a). The mechanism of formation of complex (4a) from (2a) (Scheme 1) assumes

that (5a), which contains an extra molecule of CO in place of the co-ordinated double bond in (4a), is not the initial product of the reaction. Although (5a) may be converted into (4a) on u.v. irradiation, the low conversion factor for this reaction is incompatible with it being on the primary route to (4a), since this latter complex is generated in *ca.* 70% conversion on reaction of (2a) with allene. Furthermore no (5a) is formed on reaction of (2a) with allene. However, although no reaction is observed between complex (4a) and CO under pressure [60 atm (*ca.* 6×10^6 Pa), room temperature (r.t.)], u.v. irradiation of a solution of (4a) under CO rapidly gives an equilibrium mixture of (4a) and (5a) in the ratio *ca.* 1:4. The most likely explanation of the formation of (5a) on reaction of (1a) with allene is therefore *via* the reaction of (4a) with scavenged CO under u.v. irradiation. The formation of (4a) involves loss of two molecules of CO from (1a) and the solution concentration of CO is clearly sufficient to give a significant yield of (5a) from (4a).

Experimental

General techniques and instrumentation were as described in Part 1 of this series.³ The complex $[\text{Mo}_2(\eta\text{-C}_5\text{H}_5)_2(\mu\text{-H})(\mu\text{-PMe}_2)(\text{CO})_4]$ was prepared by the literature method.² All other chemicals were obtained from commercial suppliers and used without further purification. I.r. spectra were recorded in *n*-hexane and all n.m.r. spectra in CDCl_3 unless otherwise stated. N.m.r. chemical shifts are in p.p.m. on the δ scale relative to SiMe_4 (0 p.p.m.) (for ^1H and ^{13}C) or to $\text{P}(\text{OMe})_3$ for ^{31}P (upfield shifts negative).

(i) **Prolonged Photolysis of $[\text{Mo}_2(\eta\text{-C}_5\text{H}_5)_2(\mu\text{-H})(\mu\text{-PMe}_2)(\text{CO})_4]$ (1a) with Excess of Allene.**—Complex (1a) (0.2 g, 0.4 mmol) was dissolved in hexane–benzene (1:1, 60 cm^3) and the solution saturated with allene in a glass photolysis vessel. A quartz vessel containing the u.v. filament was placed in the vessel and the solution irradiated with u.v. light (Hanovia 125-W medium-pressure immersion lamp) for 3 d. The solvent was removed on a rotary evaporator and the residue column chromatographed using hexane– CH_2Cl_2 (1:1) as eluant to separate unreacted (1a) (0.04 g, 20%). The remaining products were separated by t.l.c. using hexane–ethyl acetate (9:1) as eluant to give (in order of elution, decreasing R_f values) red $[\text{Mo}_2(\eta\text{-C}_5\text{H}_5)_2\{\mu\text{-}\eta^3\text{-CH}_2\text{C}(\text{CH}_2)\text{C}(\text{Me})=\text{CH}_2\}\{\mu\text{-PMe}_2\}(\text{CO})_2]$ (4a) (0.095 g, 45%), orange $[\text{Mo}_2(\eta\text{-C}_5\text{H}_5)_2(\mu\text{-PMe}_2)\{\eta^3\text{-CH}_2\text{C}(\text{CH}_2)\text{C}(\text{Me})=\text{CH}_2\}(\text{CO})_3]$ (5a) (0.015 g, 7%), (2a) (0.015 g, 7%),⁵ and (3a) (0.02 g, 10%).⁵

Complex (4a) (Found: C, 46.4; H, 4.9; P, 5.2. $\text{C}_{20}\text{H}_{25}\text{Mo}_2\text{O}_2\text{P}$ requires C, 46.2; H, 4.8; P, 6.0%); m/z 520 (M^+), $M^+ - n\text{CO}$ ($n = 0-2$); $\nu_{\text{max}}(\text{CO})$ at 1 854s and 1 829s cm^{-1} . N.m.r.: ^1H (303 K), δ 4.93 (s, 5 H, C_5H_5), 4.78 (s, 5 H, C_5H_5), 2.48 [m, $J(\text{H}^1\text{H}^3)$ 0.5, H^3], 2.37 (s, 3 H, Me⁷), 1.84 [dd, $^3J(\text{PH})$ 14, $J(\text{H}^5\text{H}^6)$ 3.7, 1 H, H^5], 1.80 [d, $^2J(\text{PH})$ 9.2, 3 H, $\text{PMe}^{\text{A}}\text{Me}^{\text{B}}$], 1.73 (d, 1 H, H^6), 1.58 [d, $^2J(\text{PH})$ 9.2, 3 H, $\text{PMe}^{\text{A}}\text{Me}^{\text{B}}$], 1.44 [m, J_{12} 1.7, J_{24} 0.5, 1 H, H^2], 1.41 [m, $^3J(\text{PH})$ 3.9, 1 H, H^1], 0.99 [dd, $^3J(\text{PH})$ 2.6, 1 H, H^4]; ^{13}C (243 K, ^1H gated decoupled), δ 250.2 [d, $^2J(\text{PC})$ 15.5, 1 CO], 244.4 [d, $^2J(\text{PC})$ 9.0, 1 CO], 99.9, 73.9 [s, $\text{CH}_2\text{C}(\text{CH}_2)\text{C}(\text{Me})\text{CH}_2$], 92.7 [d, $J(\text{CH})$ 176.7, C_5H_5], 89.1 [d, $J(\text{CH})$ 177.0, C_5H_5], 45.4 [t, $J(\text{CH})$ 152.2, $\text{CH}_2\text{C}(\text{CH}_2)\text{C}(\text{Me})\text{CH}_2$ or $\text{CH}_2\text{C}(\text{CH}_2)\text{C}(\text{Me})\text{CH}_2$], 37.6 [t, $J(\text{CH})$ 154.6, $\text{CH}_2\text{C}(\text{CH}_2)\text{C}(\text{Me})\text{CH}_2$ or $\text{CH}_2\text{C}(\text{CH}_2)\text{C}(\text{Me})\text{CH}_2$], 31.8 [q, $J(\text{CH})$ 128.2, $\text{CH}_2\text{C}(\text{CH}_2)\text{C}(\text{Me})\text{CH}_2$], 28.6 [qd, $J(\text{CH})$ 128.2, $^2J(\text{PC})$ 21.9, $\text{PMe}^{\text{A}}\text{Me}^{\text{B}}$], 23.6 [t, $J(\text{CH})$ 160.9, $\text{CH}_2\text{C}(\text{CH}_2)\text{C}(\text{Me})\text{CH}_2$], and 21.7 p.p.m. [qd, $J(\text{CH})$ 127.6, $^2J(\text{PC})$ 19.1 Hz, $\text{PMe}^{\text{A}}\text{Me}^{\text{B}}$]; ^{31}P (263 K), δ -25.2 (s, $\mu\text{-PPh}_2$).

Complex (5a): m/z 548 (M^+), $M^+ - n\text{CO}$ ($n = 0-3$); $\nu_{\text{max}}(\text{CO})$ at 1 935s, 1 865s, and 1 798 cm^{-1} . ^1H N.m.r. (238 K): rotamer 1 (52%), δ 5.25 [m, $J(\text{H}^5\text{H}^6)$ 1.6, 1 H, H^5], 5.09 (s,

5 H, C₅H₅), 4.68 [m, *J*(H⁶H⁷) 0.5, 1 H, H⁶], 4.56 (s, 5 H, C₅H₅), 3.01 [m, *J*(H¹H²) 4.5, *J*(H²H³) 2.5, 1 H, H²], 2.25 [dd, ³*J*(PH) 10.8, 1 H, H¹], 2.1–1.9 (m, 6 H, PMe₂), 1.78 (m, 3 H, Me^c), 0.91 (m, 1 H, H³), and –0.68 [m, ³*J*(PH) 5, 1 H, H⁴]; rotamer ² (48%), 5.20 (s, 5 H, C₅H₅), 5.09 [m, *J*(H⁵H⁶) 1.6, *J*(H⁵H⁷) 0.5, 1 H, H⁵], 4.70 [m, *J*(H⁶H⁷) 0.5, 1 H, H⁶], 4.69 (s, 5 H, C₅H₅), 2.88 [m, *J*(H¹H²) 3.4, *J*(H²H³) 2.8, 1 H, H²], 2.1–1.9 (m, 6 H, PMe₂), 2.01 (obscured, H¹), 1.67 (m, 3 H, Me^c), 1.16 (m, 1 H, H³), and –0.89 [d, ³*J*(PH) 10.3 Hz, 1 H, H⁴].

(ii) *Reaction of the Vinyl Complex (2a) with Allene.*—The complex [Mo₂(η-C₅H₅)₂{μ-σ:η²-C(Me)=CH₂}(μ-PMe₂)(CO)₃] (2a)³ (0.02 g, 0.039 mmol) was dissolved in hexane (30 cm³) and the solution saturated with allene. After u.v. irradiation for 1.5 h the solvent was removed on a rotary evaporator and the residue separated by t.l.c. Elution with hexane–ethyl acetate (9:1) gave (4a) (0.014 g, 68%) as the only significant product.

(iii) *Photolysis of Complex (2a) followed by Allene Addition.*—Complex (2a) (0.01 g, 0.02 mmol) was dissolved in hexane (15 cm³) and irradiated with u.v. light for 1.5 h to give an orange-green solution. The solution was then saturated with allene and stirred in the dark for 1.5 h to give, after t.l.c. separation, (4a) (0.002 g, 19%) and a trace of the vinyl oxo complex [Mo₂O(η-C₅H₅)₂{μ-σ:η²-C(Me)=CH₂}(μ-PMe₂)(CO)] (6a)⁴ (identified by mass spectrometry and i.r. spectroscopy). In a variation of the above reaction the same irradiated solution was treated with CO instead of allene, to give (2a) (0.002 g) and a trace of the vinyl oxo complex. In another reaction the same irradiated solution was stirred under N₂ for 1.5 h to give, after t.l.c. separation, a trace of the vinyl oxo complex (0.001 g) as the only significant product.

(iv) *Reaction of the Vinyl Complex [Mo₂(η-C₅H₅)₂{μ-σ:η²-C(Me)=CHMe}(μ-PMe₂)(CO)₃] (2b) with Allene.*—Complex (2b) (0.01 g, 0.02 mmol) and allene were treated as in (ii) above to give orange [Mo₂(η-C₅H₅)₂{μ-σ:η²-CH₂C(CH₃)C(Me)=CHMe}(μ-PMe₂)(CO)₂] (4b) (0.003 g, 30%) and [Mo₂O(η-C₅H₅)₂{μ-σ:η²-C(Me)=CHMe}(μ-PMe₂)(CO)] (6b)⁴ (0.001 g). Complex (4b): *m/z* 534 (*M*⁺), *M*⁺ – *n*CO (*n* = 0–2); *v*_{max}(CO) 1 851s and 1 829s cm⁻¹. ¹H N.m.r. (303 K): δ 4.79 (m, 10 H, C₅H₅), 2.98 [q, *J*(H⁵H⁶) 6.4, 1 H, H⁶], 2.66 (s, 1 H, H³), 2.30 (s, 3 H, Me^c), 1.77 [d, ²*J*(PH) 9.2, 3 H, PMe^AMe^B], 1.55 [d, ²*J*(PH) 9.0 Hz, 3 H, PMe^AMe^B], and 1.33 (d, 3 H, Me^c).

(v) *Reaction of the Vinyl Complex [Mo₂(η-C₅H₅)₂{μ-σ:η²-C(Et)=CH₂}(μ-PMe₂)(CO)₃] (2c) with Allene.*—Complex (2c) was only available as a 5:1 mixture with [Mo₂(η-C₅H₅)₂{μ-σ:η²-C(H)=CHEt}(μ-PMe₂)(CO)₃] (2d).⁴ A solution of (2c)/(2d) (0.02 g, 0.04 mmol) in hexane (30 cm³) was treated with allene as in (ii) above to give (4c) (0.008 g, 40%) and unreacted (2d) (0.002 g). Irradiation of 0.01 g of the mixture of (2c) and (2d) in the absence of allene gave, on t.l.c. separation, (2d) (0.001 g) and [Mo₂O(η-C₅H₅)₂{μ-σ:η²-C(Et)=CH₂}(μ-PMe₂)(CO)] (6c)⁴ (0.001 g) as the only products. Complex (4c) (Found: C, 47.4; H, 5.2. C₂₁H₂₇Mo₂O₂P requires C, 47.3; H, 4.9%); *m/z* 534 (*M*⁺), *M*⁺ – *n*CO (*n* = 0–2); *v*_{max}(CO) at 1 854s and 1 829s cm⁻¹. ¹H N.m.r. (303 K): δ 4.92 (s, 5 H, C₅H₅), 4.78 [d, ³*J*(PH) 0.5, 5 H, C₅H₅], 3.01 (dq, *J*_{ab} 13.8, *J*_{ac} 7.3, 1 H^a), 2.43 [m, *J*(H³H⁴) 0.5, 1 H, H³], 1.95 (dq, *J*_{bc} 7.3, 1 H, H^b), 1.83 [dd, ³*J*(PH) 11.1, *J*₅₆ 3.6, 1 H, H⁶], 1.81 [d, ²*J*(PH) 9.2, 3 H, PMe^AMe^B], 1.72 (d, 1 H, H⁵), 1.59 [d, ²*J*(PH) 9.2, 3 H, PMe^AMe^B], 1.43 (s, 1 H, H²), 1.42 [d, ³*J*(PH) 3.2, 1 H, H¹], 1.28 (t, 3 H, Me^c), and 1.02 [d, ³*J*(PH) 2.7, 1 H, H⁴].

(vi) *Reaction of the η³-Allyl Complex [Mo₂(η-C₅H₅)₂(μ-PMe₂)(η³-C₃H₅)(CO)₃] (3a) with Allene.*—Complex (3a)

(0.005 g, 0.01 mmol) was dissolved in hexane–benzene (10 cm³: 2 cm³) and the solution saturated with allene. Irradiation with u.v. light for 1 h gave (3a) (0.003 g) as the only significant product on t.l.c. separation.

(vii) *Reaction of the η³-Allyl Complex [Mo₂(η-C₅H₅)₂(μ-PMe₂)(η³-syn-MeCHCHCH₂)(CO)₃] (3b) with Allene.*—Complex (3b) (0.02 g, 0.04 mmol) was dissolved in hexane–benzene (10 cm³: 10 cm³) and the solution saturated with allene. The mixture was irradiated with u.v. light for 1 h at 2 °C and then stirred for 1 h in the dark at 15 °C. The solvent was removed on a rotary evaporator and the products separated by t.l.c. using hexane–ethyl acetate (9:1) as eluant to give (4b) and (4c) (0.012 g, 55%) as an inseparable mixture in ca. 1:2 ratio, unreacted (3b) (0.002 g), and [Mo₂O(η-C₅H₅)₂{μ-σ:η²-C(Et)=CH₂}(μ-PMe₂)(CO)]⁴ (0.001 g).

(viii) *Reaction of the Cyclohex-2-enyl Complex [Mo₂(η-C₅H₅)₂(μ-PMe₂)(η³-C₆H₉)(CO)₃] (3c)⁵ with Allene.*—Complex (3c) (0.025 g, 0.045 mmol) was treated with allene as in (vii) to give [Mo₂(η-C₅H₅)₂{μ-η⁵-CH₂C(CH₃)(C₆H₉)}(μ-PMe₂)(CO)₂] (0.008 g, 30%) (4d) and unreacted (3c) (0.003 g). Complex (4d): *m/z* 560 (*M*⁺), *M*⁺ – *n*CO (*n* = 0 or 2); *v*_{max}(CO) at 1 854s and 1 829s cm⁻¹. ¹H N.m.r. (303 K): δ 5.44 [m, *J*(H⁶H⁷) 15.0, 1 H, H⁷], 5.22 [m, *J*(H⁵H⁶) 10.1, 1 H, H⁶], 4.82 (s, 5 H, C₅H₅), 4.60 (s, 5 H, C₅H₅), 3.53 (d, 1 H, H⁵), 2.39 (s, 2 H, H¹², H¹³), 2.37 (s, 1 H, H⁵), 1.9–1.5 (m, 4 H, H⁸, H⁹, H¹⁰, H¹¹), 1.74 [d, ²*J*(PH) 9.1, 3 H, PMe^AMe^B], 1.56 [m, ²*J*(PH) 9.3, 3 H, PMe^AMe^B], 1.47 (m, 2 H, H¹, H²), and 0.93 [d, ³*J*(PH) 2.4, 1 H, H⁴].

Crystallography.—*Crystal data for [Mo₂(C₅H₅)₂{μ-η⁵-CH₂C(CH₃)C(Me)=CH₂}(μ-PMe₂)(CO)₂] (4a)* C₂₀H₂₅Mo₂O₂P, *M* = 519.88, monoclinic, space group *P*2₁/*c* (no. 14), *a* = 9.064(2), *b* = 17.595(4), *c* = 12.540(3), β = 97.93(3)°, *U* = 1 980.77 Å³ (by least-squares refinement on diffractometer angles for 25 automatically centred reflections, λ = 0.710 69 Å), *Z* = 4, *D*_c = 1.740 g cm⁻³. 2 816 Unique absorption-corrected data [*I* > 3σ(*I*), 3 < θ < 25°, Mo-K_α radiation]. A burgundy red crystal of size 0.15 × 0.21 × 0.24 mm, μ(Mo-K_α) = 12.20 cm⁻¹, was used in the data collection; *F*(000) = 992.

Crystal data for [Mo₂(η-C₅H₅)₂(μ-PMe₂){η³-CH₂C(CH₃)-C(Me)=CH₂}(CO)₃] (5a) C₂₁H₂₇Mo₂O₂P, *M* = 548.28, orthorhombic, space group *P*2₁2₁2₁, *a* = 25.839(4), *b* = 9.943(3), *c* = 8.415(3) Å, *U* = 2 161.96 Å³, *Z* = 4, *F*(000) = 1 096, μ(Mo-K_α) = 11.26 cm⁻¹, *D*_c = 1.684 g cm⁻³. 1 915 Unique absorption-corrected data. [*I* > 3σ(*I*), 3 < θ < 25°, Mo-K_α radiation]. A deep orange crystal of size 0.18 × 0.15 × 0.10 mm was used in the data collection.

Data collection. Data for both structures were collected in the range θ 3–25°, with a scan width of 0.84° for (4a) and 0.86° for (5a), using the technique described previously.¹⁸ For both structures Lorentz and polarisation corrections were applied. Equivalent reflections were merged to give 2 816 data for (4a) and 1 915 for (5a) with *I*/σ(*I*) > 3.0.

*Structure solution and refinement.*¹⁹ The co-ordinates of both metal atoms in structures (4a) and (5a) were deduced from a Patterson synthesis, and the remaining non-hydrogen atoms were located from subsequent Fourier difference syntheses. The hydrogen atoms of both organic fragments were located in a Fourier difference synthesis calculated using data with sin θ < 0.35. All remaining hydrogen atoms, in both structures, were included in geometrically idealised positions and were constrained to 'ride' on the relevant carbon atoms. Full-matrix refinement was carried out for both structures, with anisotropic thermal parameters assigned to all non-hydrogen atoms in the final stages of refinement. For both (4a) and (5a) weights of *w* = 1/σ²*F*_o were assigned to individual reflections. Refinement

converged at R 0.0251 and R' 0.0269 for (4a) and R 0.0306 and R' 0.0312 for (5a).

Additional material available from the Cambridge Crystallographic Data Centre comprises H-atom co-ordinates, thermal parameters, and remaining bond lengths and angles.

Acknowledgements

We thank Dr. A. G. Kent for valuable discussion and the S.E.R.C. and BP Chemicals Limited (Hull Division) for financial support.

References

- 1 Part 5, G. Conole, M. McPartlin, M. J. Mays, and M. J. Morris, preceding paper.
- 2 R. G. Hayter, *Inorg. Chem.*, 1963, 2, 1031.
- 3 K. Henrick, M. McPartlin, A. D. Horton, and M. J. Mays, *J. Chem. Soc., Dalton Trans.*, 1988, 1083.
- 4 G. Conole, K. Henrick, M. McPartlin, A. D. Horton, and M. J. Mays, *New J. Chem.*, 1988, 12, 559.
- 5 A. D. Horton and M. J. Mays, *J. Chem. Soc., Dalton Trans.*, 1990, 155.
- 6 J. W. Faller, C-C. Chen, M. J. Mattina, and A. Jakubowski, *J. Organomet. Chem.*, 1973, 52, 361.
- 7 T. A. Broadbent and C. E. Pringle, *J. Inorg. Nucl. Chem.*, 1971, 33, 2009.
- 8 R. J. Doedens and L. F. Dahl, *J. Am. Chem. Soc.*, 1965, 87, 2576; J. L. Petersen, L. F. Dahl, and J. M. Williams, *ibid.*, 1974, 96, 6610.
- 9 J. L. Petersen and R. P. Stewart, *Inorg. Chem.*, 1980, 19, 186.
- 10 M. H. Chisholm, K. Folting, J. A. Heppert, and W. E. Streib, *J. Chem. Soc., Chem. Commun.*, 1985, 1755; N. D. Feasey, S. A. R. Knox, A. G. Orpen, and M. J. Winter, *New J. Chem.*, 1988, 12, 581; T. Okamoto, *Bull. Chem. Soc. Jpn.*, 1971, 44, 1353.
- 11 R. D. Adams and S. Wang, *Organometallics*, 1987, 6, 45; R. Aumann and H. J. Weidenhaupt, *Chem. Ber.*, 1987, 120, 23; S. Otsuka, A. Nakamura, and K. Tani, *J. Chem. Soc. A*, 1971, 154.
- 12 (a) T. Adatia, M. McPartlin, M. J. Mays, M. J. Morris, and P. R. Raithby, *J. Chem. Soc., Dalton Trans.*, 1989, 1555; (b) P. O. Nubel and T. L. Brown, *J. Am. Chem. Soc.*, 1984, 106, 3474.
- 13 W. E. Carroll, M. Green, A. G. Orpen, C. J. Schaverien, I. D. Williams, and A. J. Welch, *J. Chem. Soc., Dalton Trans.*, 1986, 1021.
- 14 R. Ben-Shoshan and R. Pettit, *Chem. Commun.*, 1968, 247; R. E. Davis, *ibid.*, p. 248.
- 15 J. W. Byrne, H. U. Blaser, and J. A. Osborn, *J. Am. Chem. Soc.*, 1975, 97, 3871.
- 16 J. Schwartz, D. W. Hart, and B. McGiffert, *J. Am. Chem. Soc.*, 1974, 96, 5613.
- 17 S. R. Allen, P. K. Baker, S. G. Barnes, M. Bottrill, M. Green, A. G. Orpen, I. D. Williams, and A. J. Welch, *J. Chem. Soc., Dalton Trans.*, 1983, 927.
- 18 M. K. Cooper, P. J. Guerney, and M. McPartlin, *J. Chem. Soc., Dalton Trans.*, 1982, 757.
- 19 G. M. Sheldrick, SHELX 76 program for crystal structure determination, University of Cambridge, 1976.

Received 23rd November 1989; Paper 9/05025F

Journal of Organometallic Chemistry, 383 (1990) 441–461
 Elsevier Sequoia S.A., Lausanne – Printed in The Netherlands
 JOM 20436

Carbide forming and cluster build-up reactions in ruthenium carbonyl cluster chemistry

Philip J. Bailey, M.J. Duer, Brian F.G. Johnson, Jack Lewis *,
 University Chemical Laboratory, Lensfield Road, Cambridge, CB2 1EW (U.K.)

Grainne Conole, Mary McPartlin *, Harold R. Powell,
 School of Chemistry, The Polytechnic of North London, London, N7 8DB (U.K.)

and Christopher E. Anson

School of Chemical Sciences, University of East Anglia, Norwich, NR4 7TJ (U.K.)
 (Received May 3rd, 1989)

Abstract

The reinvestigation of an early synthesis of hexaruthenium carbido clusters has led to the isolation of a number of new clusters which have been fully characterised by spectroscopic and crystallographic techniques. The thermolysis of $\text{Ru}_3(\text{CO})_{12}$ in the presence of mesitylene (1,3,5-trimethylbenzene) at moderate temperatures yields two new clusters, $[\text{Ru}_6(\mu_4\text{-}\eta^2\text{-CO})_2(\text{CO})_{13}(\eta^6\text{-C}_6\text{H}_3\text{Me}_3)]$ (I) and $[\text{HRu}_6(\mu_4\text{-}\eta^2\text{-CO})(\text{CO})_{13}(\mu_2\text{-}\eta^7\text{-C}_6\text{H}_3\text{Me}_2\text{CH}_2)]$ (II), the structures and reactivity of which indicate the origin and mechanism of formation of the carbido-carbon in the hexaruthenium carbido clusters $[\text{Ru}_6\text{C}(\text{CO})_{14}(\eta^6\text{-C}_6\text{H}_3\text{Me}_3)]$ (III) and $[\text{Ru}_6\text{C}(\text{CO})_{17}]$ (IV). A further product of the reaction is the decaruthenium carbido cluster dianion $[\text{Ru}_{10}\text{C}(\text{CO})_{24}]^{2-}$ (V) which has the tetracapped octahedral geometry. The monohydrido-cluster anion $[\text{HRu}_{10}\text{C}(\text{CO})_{24}]^-$ (VI) may be synthesised quantitatively from V by protonation. The nature of the hydrido-ligand in VI has been investigated in the solid state by NMR spectroscopy and it has been found to be fluxional, its location being temperature dependent. The decanuclear dianion V has been found to react with mercury salts to yield the 21 metal atom cluster dianion $[\text{Ru}_{18}\text{Hg}_3\text{C}_2(\text{CO})_{42}]^{2-}$ (VII) which consists of two tricapped octahedral nonaruthenium "subclusters" fused by a bi-facecapping $(\text{Hg}_3)^{2+}$ unit.

The reaction of $\text{Ru}_3(\text{CO})_{12}$ with mesitylene was first reported in 1967 to yield $[\text{Ru}_6\text{C}(\text{CO})_{14}(\eta^6\text{-C}_6\text{H}_3\text{Me}_3)]$ (III) and $\text{Ru}_6\text{C}(\text{CO})_{17}$ (IV), and at that time these were the only examples of clusters containing completely encapsulated carbon

atoms [1]. Carbido-transition metal carbonyl clusters of many metals have now been characterised [2]. The origin of the carbide atom in these clusters has been the subject of some conjecture. Labelling experiments with ^{13}C have established its origin in some cases however; the carbido atom in $[\text{Rh}_6\text{C}(\text{CO})_{15}]^{2-}$ has been shown to be derived from solvent CHCl_3 for example [3], whilst preparation of some ruthenium or osmium carbido clusters from ^{13}C enriched precursors has shown that it is the result of the cleavage of coordinated carbon monoxide [4]. In early work the sealed tube pyrolysis of $\text{Ru}_3(\text{CO})_{12}$ was shown to give a low yield of IV and CO_2 was detected in the gases evolved during the reaction; thus establishing that in this reaction the carbido atom is the result of the disproportionation of two molecules of carbon monoxide [5] (eq. 1). In contrast, in the pyrolysis of

$$2\text{CO} \rightarrow \text{CO}_2 + \text{C} \quad (1)$$

$[\text{Ru}_5(\text{CO})_{15}(\text{NCBu}^t)(\mu_5\text{-NCBu}^t)]$ to give $[\text{Ru}_6\text{C}(\text{CO})_{16}(\text{NCBu}^t)]$, labelling of the NCBu^t ligands with ^{13}C has established that the carbido atom originates from the cyano-carbon. [6]

The mechanism of carbonyl disproportionation has received much attention as the cleavage of the C–O bond of carbon monoxide is of fundamental importance to many homogeneous and heterogeneous catalytic processes. The initial process in Fischer–Tropsch chemistry is thought to involve such a process on the catalyst surface prior to hydrogenation and polymerisation of the resulting hydrocarbyl species. Many studies of the Fischer–Tropsch related chemistry of several transition metals under heterogeneous conditions confirm that disproportionation of CO results in surface carbide species, moreover such pretreated metals produce hydrogenated products more rapidly under pressures of CO/H_2 mixtures than the “clean” metal [7].

The chemistry of larger carbido clusters has developed in recent years to constitute a distinct field of cluster chemistry. For the iron triad the clusters are exclusively based on the octahedral geometry; the tetra- and penta-nuclear clusters being regarded as *arachno* and *nido* derivatives of this basic metal framework, and the higher nuclearity systems being capped octahedra [2]. The tetracapped octahedral geometry is now well established for a number of decanuclear osmium clusters, the metal which has dominated the field of high nuclearity iron triad carbonyl clusters. The reason for the paucity of high nuclearity clusters of ruthenium remains unclear; the isolation of the decaruthenium carbido cluster dianion $[\text{Ru}_{10}\text{C}(\text{CO})_{24}]^{2-}$ (V) suggests however that this chemistry of ruthenium may develop to parallel that for osmium. Remarkably since our discovery of V, its synthesis by a different route, and structure has been reported by another group [8].

A tetrahedral site for a hydrido ligand was first deduced from the X-ray structure analysis of the tetracapped octahedral decaosmium monohydride anion $[\text{HOs}_{10}\text{C}(\text{CO})_{24}]^-$ (VIII) where the undistorted close packing of the carbonyl ligands precluded a surface location for the hydrido ligand, and it was proposed that it was located inside one of the Os_4 caps, since the octahedral cavity was occupied by the carbide ligand [9]. This type of site symmetry for a hydrido ligand is still very rare. The hexaruthenium monoanion $[\text{HRu}_6(\text{CO})_{18}]^-$ provided the first example of an interstitial hydrido ligand ever reported in a carbonyl cluster, although this was octahedrally sited [10]. There has been no example of a hydrido ligand inside a tetrahedron of ruthenium atoms until now.

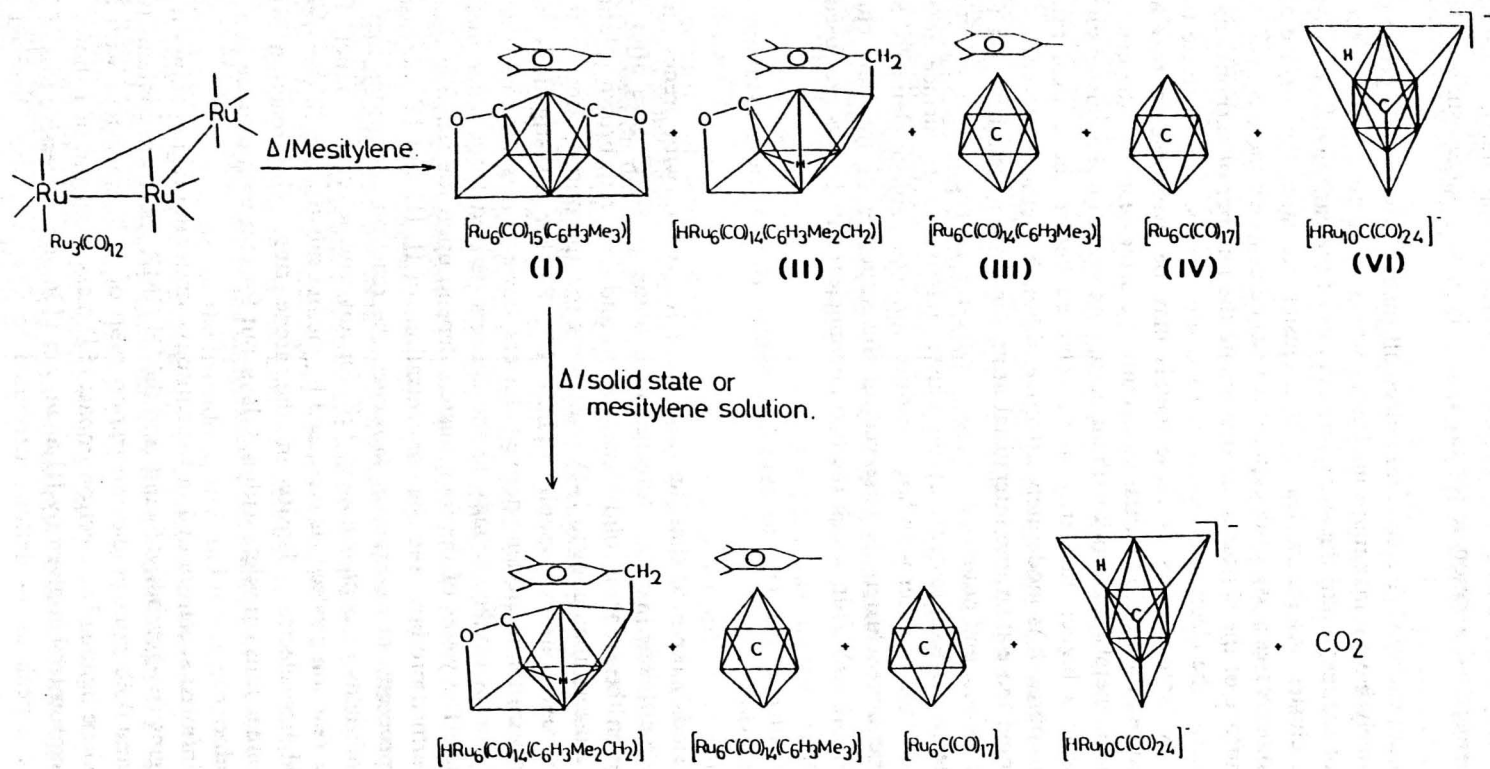
The synthesis and characterisation of the osmium cluster dianion reported as $[\text{Os}_{20}\text{HgC}_2(\text{CO})_{48}]^{2-}$ (IX) was a significant breakthrough in osmium cluster chemistry since, not only is it the largest ever cluster reported for this metal, its formation and structure suggested a rationale for the synthesis of very large osmium clusters [11].

Binary osmium carbonyl clusters, and indeed all such relatively early group metal clusters, effectively have a maximum nuclearity which is dictated by the electronic requirements of the metal and the steric interactions of the carbonyl ligands on the surface of the cluster. As the nuclearity of a cluster increases the surface area/nuclearity ratio decreases and a critical point is reached at which there is insufficient room on the surface of the cluster to accommodate the number of carbonyl ligands necessary to satisfy the electronic requirements of the metals. This obstacle to the synthesis of very large clusters of these metals may be overcome in two ways. Firstly, the incorporation of interstitial atoms into a cluster decreases the electronic requirement of the metal framework without occupying space on the cluster surface, therefore allowing a higher nuclearity to be achieved before the critical ratio is exceeded. This approach is moderately effective although methods of synthesising clusters containing more than one interstitial atom for these metals have yet to be developed. The second, and potentially far more effective, procedure is to effectively "dilute" the electronic requirements of the cluster relative to its surface area by fusing subcluster units together with late transition, or even *p*-block elements. Such a route to these large clusters is observed in the structure of the new cluster $[\text{Ru}_{18}\text{Hg}_3\text{C}_2(\text{CO})_{42}]^{2-}$ (VII) in which the two nonanuclear subclusters are fused by a Hg_3 triangle.

Results and discussion

We have previously reported that the reaction of $\text{Ru}_3(\text{CO})_{12}$ with arenes (hexamethylbenzene, mesitylene, xylenes, toluene) in heptane at 97°C gave after 3–5 days (depending on the arene) a solid black deposit and deep red/brown solutions from which the clusters analogous to I–IV containing the appropriate arene may be isolated by thin layer chromatography (TLC) [12]. Further investigations were carried out mainly on the mesitylene-derived clusters, however it is apparent that in principle the chemistry applies equally to the clusters derived from other methyl substituted arenes. The yields of the four clusters depend upon the reaction time, I being the first formed product, and the concentrations of II, III and IV increasing as the reaction proceeds, at its expense. However, the reaction conditions may be optimised to give yields of approximately 15% for any one selected product. The rate at which the reaction proceeds is increased by methyl substitution of the arene, and thus by higher electron density in the arene ring. The reaction with hexamethylbenzene is thus complete within 3 days, but for that with toluene at least 5 days is required.

The solution infrared spectrum of I in the carbonyl stretching region shows it to contain one bridging (μ_2 -) carbonyl ligand, and the ^1H NMR spectrum contains two singlets at 4.90 and 1.66 ppm in the integration ratio of 1/3, consistent with an η^6 -bonded mesitylene ligand. The electron impact (EI) mass spectrum of I shows an identical molecular ion to that given by III at $m/z = 1136$ and successive loss of 14 carbonyl ligands; a peak at 44 daltons attributed to CO_2 was also observed to



Scheme 1.

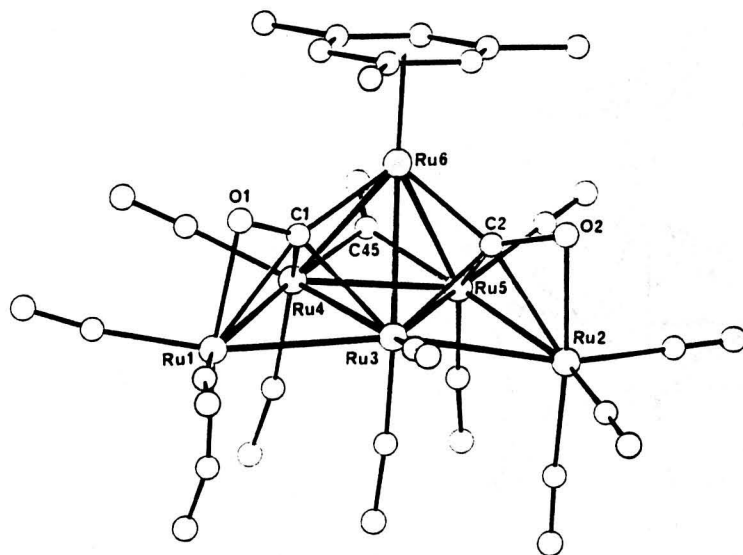


Fig. 1. The molecular structure of $[\text{Ru}_6(\mu_4\text{-}\eta^2\text{-CO})_2(\text{CO})_{13}(\eta^6\text{-C}_6\text{H}_3\text{Me}_3)]$ (I).

increase in intensity relative to that due to O_2 (32 daltons) during the experiment, showing that I is converting into III and CO_2 inside the spectrometer.

In order to elucidate the structure of I a single crystal X-ray structure determination was carried out [12]. The determination confirms the formulation of I as $[\text{Ru}_6(\mu_4\text{-}\eta^2\text{-CO})_2(\text{CO})_{13}(\eta^6\text{-C}_6\text{H}_3\text{Me}_3)]$, and establishes that the metal framework consists of a tetrahedral Ru_4 arrangement with two edge bridging Ru atoms, the first example of this polyhedron for ruthenium (Fig. 1). There are two, 4 electron donating, π -bonded ($\mu_4\text{-}\eta^2$ -) carbonyl ligands situated in the two Ru_4 'butterflies' created by the two bridging Ru atoms and the faces of the metal tetrahedron, and there is a symmetrically bridging (μ_2 -) carbonyl ligand spanning the unique basal edge of the central Ru tetrahedron. The mesitylene ligand is η^6 -bonded to the apical Ru(6) atom, and is planar. The methyl groups of this ligand are staggered with respect to the vectors of the π -bonded carbonyl ligands in the solid state. However, the ^1H NMR spectrum shows all methyl hydrogens to be equivalent in solution at room temperature, as are the methine hydrogens, indicating that the cluster has C_s symmetry on the NMR timescale, with spinning of the mesitylene ring.

Clusters containing η^2 -bonded carbonyl ligands are relatively rare [13], and to our knowledge the only other cluster containing two such ligands is $[\text{Ru}_5\text{Mo}_2(\mu_4\text{-}\eta^2\text{-CO})_2(\text{CO})_{14}(\mu_4\text{-S})(\eta^5\text{-C}_5\text{H}_5)]$ [14]. The C-O bond lengths of the η^2 -bonded carbonyl ligands in I are equal within experimental error with a mean value of 1.255(10) Å, and are therefore considerably lengthened relative to the terminally coordinated ligands (mean 1.138(18) Å). This may be attributed to electron donation from the C-O π -bond, and increased electron density in the C-O π^* orbital due to the $d_\pi\text{-}p_\pi$ bonding from three metals. These two carbonyl ligands may therefore be regarded as "activated" (vide infra).

The solution infrared spectrum of II in the carbonyl stretching region indicates that it contains two bridging carbonyl ligands; its EI mass spectrum shows a strong isotopic envelope centred at $m/ = 1122$ and successive loss of 14 carbonyl ligands. The ^1H NMR spectrum can be interpreted if we suppose that it arises from the

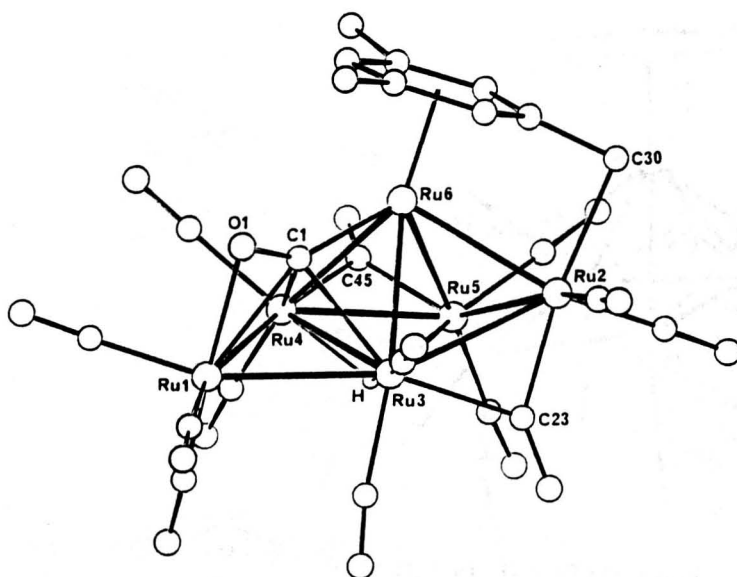


Fig. 2. The molecular structure of $[\text{HRu}_6(\mu_4\text{-}\eta^2\text{-CO})(\text{CO})_{13}(\mu_2\text{-}\eta^7\text{-C}_6\text{H}_3\text{Me}_3)]$ (II).

mesitylene ligand losing a methyl hydrogen to the metal framework and the resulting hydride ligand giving a singlet resonance at -19.5 ppm (1H); the remaining methylene group thus created is bonded to the cluster giving rise to two doublets at 3.33 and 2.99 ppm (J 6 Hz). Other resonances in the spectrum are consistent with a $(\mu_2\text{-}\eta^7\text{-})$ coordination mode for the mesityl ligand. This coordination mode anchors the ligand to the asymmetric cluster and prevents it from spinning, and so causes the inequivalence of the methine, methylene and the methyl group hydrogens in the ligand.

A single crystal X-ray study of $[\text{HRu}_6(\mu_4\text{-}\eta^2\text{-CO})(\text{CO})_{13}(\mu_2\text{-}\eta^7\text{-C}_6\text{H}_3\text{Me}_2\text{CH}_2)]$ (II) shows the cluster to be closely related to I, having just one less carbonyl ligand than this cluster [12]. The metal framework of II may be described as a trigonal bipyramidal Ru_5 arrangement with a Ru atom bridging an apical-equatorial edge (Fig. 2). There are two bridging $(\mu_2\text{-})$ carbonyl ligands spanning the edges Ru(2)–Ru(3) and Ru(4)–Ru(5), and a face capping $(\mu_3\text{-})$ hydride ligand is located beneath the basal plane, Ru(3)–Ru(4)–Ru(5), of the central Ru tetrahedron. The position of this hydrido ligand was determined by potential energy minimisation calculations [15]. There is one $(\mu_4\text{-}\eta^2\text{-CO})$ π -bonded carbonyl ligand coordinated in a similar position to those in $[\text{Ru}_6(\mu_4\text{-}\eta^2\text{-CO})_2(\text{CO})_{13}(\eta^6\text{-C}_6\text{H}_3\text{Me}_3)]$ (I) which shows an equivalent lengthening of the C–O bond relative to the terminal carbonyls. The organic ligand is η^6 -bonded to the apical Ru(6) atom and is also bonded via the methylene carbon to Ru(2) (C(30)–Ru(2) 2.25 Å), giving an overall $(\mu_2\text{-}\eta^7\text{-})$ bonding mode for the ligand of the type indicated by the ^1H NMR spectrum. This coordination is similar to that found for the benzyl ligand in $[\text{Ru}_8(\mu_8\text{-P})(\mu_2\text{-}\eta^7\text{-C}_6\text{H}_5\text{CH}_2)(\text{CO})_{19}]$ [16].

Infrared spectroscopy of I, II and III

Infrared spectra of I, II and III and their ^{13}C enriched analogues in CsI discs were measured at 113 K. The spectra of the unenriched clusters over the frequency

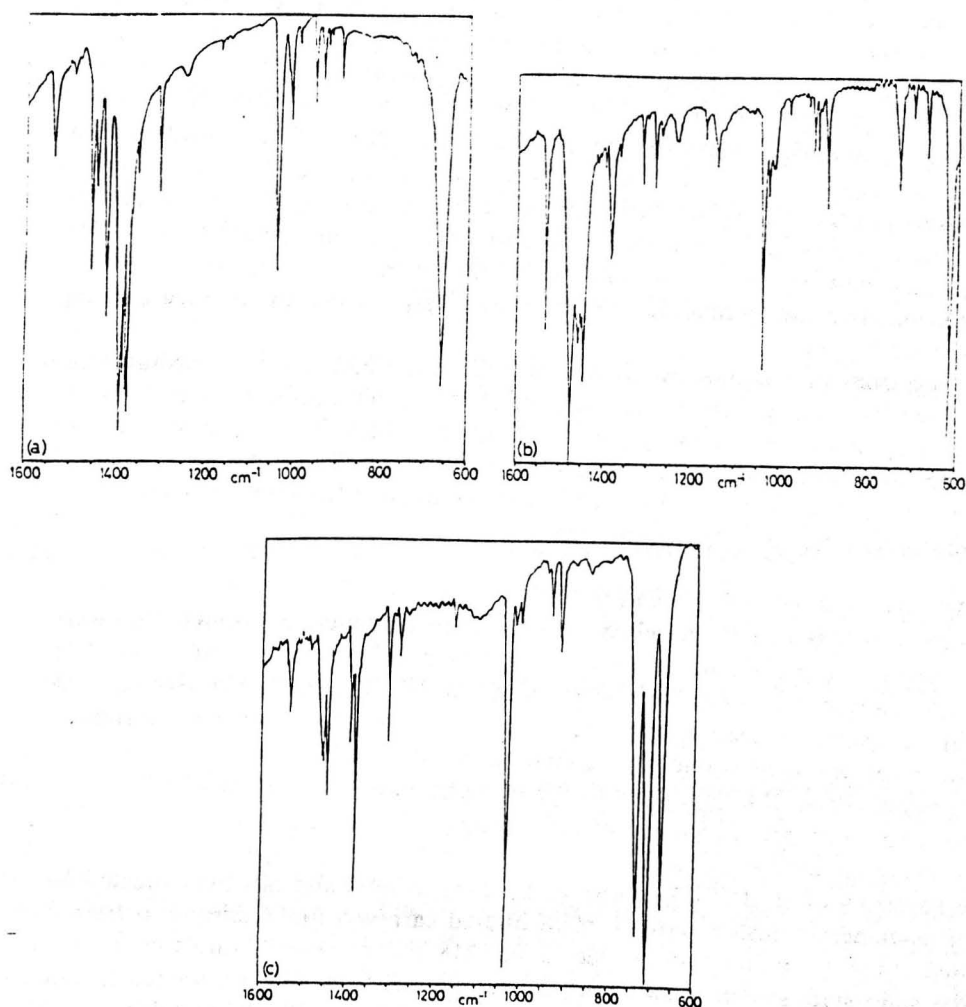


Fig. 3. The infrared spectra of (a) $[\text{Ru}_6(\mu_4\text{-}\eta^2\text{-CO})_2(\text{CO})_{13}(\eta^6\text{-C}_6\text{H}_3\text{Me}_3)]$ (I), (b) $[\text{HRu}_6(\mu_4\text{-}\eta^2\text{-CO})(\text{CO})_{13}(\mu_2\text{-}\eta^7\text{-C}_6\text{H}_3\text{Me}_3)]$ (II) and (c) $[\text{Ru}_6\text{C}(\text{CO})_{14}(\eta^6\text{-C}_6\text{H}_3\text{Me}_3)]$ (III) in the region $1600\text{--}600\text{ cm}^{-1}$, recorded in CsI discs at 113 K.

range $1600\text{--}600\text{ cm}^{-1}$ are shown in Fig. 3. The simplest spectrum is that of III, which is dominated by a triplet of very strong bands at 735 , 709 and 674 cm^{-1} , which is characteristic of a carbide ligand inside an octahedral Ru_6 cluster [17]. These bands are reduced in intensity on ^{13}C enrichment, with three new bands appearing in the spectrum at 707 , 682 and 651 cm^{-1} . The triplet of bands due to the carbide ligand show shifts very close to the expected $(12/13)^{1/2}$ and are replaced by bands of comparable sharpness, confirming their assignment to a single, vibrationally isolated carbide ligand, and also the derivation of this ligand from a coordinated carbonyl ligand in $[\text{Ru}_3(\text{CO})_{12}]$. The remaining bands in this region of the spectrum can be assigned as modes of the mesitylene ligand.

In the spectrum of II, a strong band at 1446 cm^{-1} loses intensity and a new band appears at 1410 cm^{-1} on ^{13}C enrichment, and is assigned to the $\nu(\text{CO})$ mode of the $(\mu_4\text{-}\eta^2\text{-CO})$ ligand in this cluster. Similar frequencies have been observed for such

ligands in other clusters [13]. A weak band at 912 cm^{-1} and a very strong band at 618 cm^{-1} are likewise shifted on enrichment, to 893 and 606 cm^{-1} respectively. The isotope shifts (0.974 and 0.979) are both indicative of modes in which the carbonyl ligand as a whole vibrates against the tetrametal butterfly framework in which it is located. If the carbonyl is formally considered as μ_3 -bridging over three of the metal atoms and π -bonded to the fourth, then the most likely assignment of the 917 cm^{-1} band is to a mode which involves deformation of the " Ru_3CO " unit with simultaneous stretching of the Ru-CO π -bond. This mode can most readily be visualised as a "frustrated rotation" of the carbonyl ligand in the plane defined by the two wingtip metal atoms, the ligand itself and the mid-point of the "hinge". Two bands at 1233 and 694 cm^{-1} which sharpen markedly on cooling, can be assigned to the antisymmetric and symmetric $\nu(\text{RuH})$ modes respectively, of the face capping (μ_3 -) hydride ligand.

The spectrum of I shows two bands at 1423 and 1392 cm^{-1} of medium and strong intensities respectively, which are assigned to the antisymmetric and symmetric stretching modes of the two (μ_4 - η^2 -CO) carbonyl ligands. On enrichment two new bands at 1394 and 1357 cm^{-1} result from cluster molecules in which two such carbonyls have been replaced by ^{13}CO , and bands at 1413 and 1364 cm^{-1} are assigned to the (^{12}CO)(^{13}CO) isotopomer.

^{13}C NMR spectroscopy of I, II and III

The clusters I, II and III enriched with ^{13}C (approximately 50 atom% ^{13}C) were prepared from ^{13}CO enriched $\text{Ru}_3(\text{CO})_{12}$, and their variable temperature ^{13}C - $\{^1\text{H}\}$ NMR spectra were recorded. The spectrum of I at 291 K is entirely consistent with its solid state structure assuming C_s symmetry on the NMR timescale (vide supra); it shows seven resonances due to terminal carbonyl ligands between 206 and 187 ppm, a resonance at 224.7 ppm due to the bridging carbonyl and one at 292.1 ppm from the two symmetry related η^2 -bonded CO ligands. No changes were observed in this spectrum on cooling to 220 K.

The spectrum of II at 291 K shows only 11 resonances and not the expected 14 for this asymmetric cluster, some form of limited carbonyl fluxionality is therefore proposed at this temperature. The spectrum at 218 K is however, entirely consistent with the solid state structure and contains resonances from one η^2 -bonded (279.0 ppm), two bridging (225.0 and 220.6 ppm) and 11 terminal (205–182 ppm) carbonyl ligands. Three of the resonances due to terminal carbonyl ligands are doublets ($J(\text{CH})$ 11 Hz) and this confirms the position of the hydride ligand as (μ_3 -) facecapping, vide supra, as in this position it would be expected to couple to three *trans*-carbonyl carbons.

The spectrum of III at 291 K indicates that there is a total carbonyl fluxionality on the NMR timescale since only a single, broad resonance is observed at 203.2 ppm in the terminal carbonyl region of the spectrum. The carbido resonance appears at 442.8 ppm and its intensity shows that it is ^{13}C enriched, and must therefore have originated from a coordinated carbonyl ligand. On cooling to 243 K a second, less intense, resonance develops at 194.2 ppm and the major resonance is further broadened. At the lowest temperature achieved, 170 K in $\text{CD}_2\text{Cl}_2/\text{CCl}_2\text{F}_2$, a number of shoulders develop on the major resonance, and the resonance at 194.2 ppm sharpens considerably, but no further peaks can be resolved. From these data, it is possible to deduce that there are at least two fluxional processes involving the

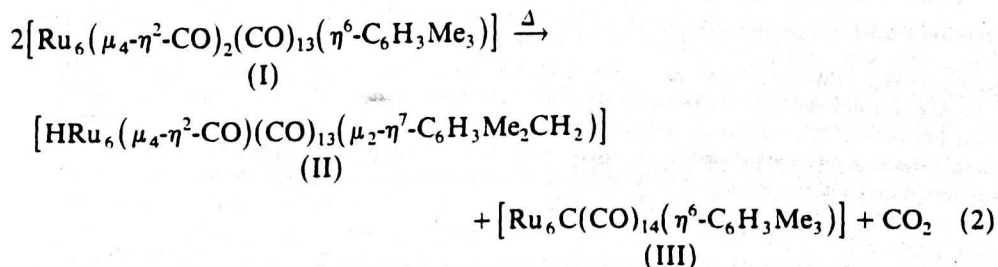
carbonyl ligands occurring in this cluster, and that both involve the bridging carbonyl ligand, since no resonance is observed from this ligand at any temperature.

The formation of the carbido atom in III and IV

The ^{13}C NMR and infrared evidence shows that the carbido atom in III, and by inference that in IV, is derived from a coordinated carbonyl ligand, however the mechanism of the C–O bond cleavage is not apparent from the above arguments. It was found that the thermolysis of I in mesitylene solution or in the solid state gave hexaruthenium carbido clusters. In order to provide evidence indicating the mechanism of the formation of the carbido clusters the thermolyses were carried out in an infrared gas cell and the gaseous products were identified by their infrared spectra in situ.

In the case of solution thermolysis the infrared spectrum of the gaseous products, after freezing out the mesitylene solvent, showed strong absorptions at 2360 and 2344 cm^{-1} characteristic of CO_2 . Separation of the products remaining in solution by TLC showed that clusters II and III had been formed in equal yield. The thermolysis in the solid state also gave CO_2 , but in addition the gaseous infrared spectrum showed the characteristic absorptions of CO at 2175 and 2116 cm^{-1} suggesting cluster decomposition. The solid residue consisted mainly of ruthenium metal, however TLC showed that the soluble fraction contained III, IV and unreacted I. The observation of CO_2 in the reaction products confirms that the carbido atoms are the result of the disproportionation of two molecules of CO (eq. 1). Significantly, reaction of I with CO in solution at 20°C and 1 atm. resulted in complete decomposition to $\text{Ru}_3(\text{CO})_{12}$.

Evidence that the coordination of a carbonyl ligand in the $(\mu_4-\eta^2-)$ mode weakens the C–O bond is given by the bond length, infrared stretching frequencies and, to a certain extent, the ^{13}C NMR chemical shift of such a ligand, *vide supra*, and it is reasonable to conclude that the C–O bond is considerably activated towards cleavage in this situation. The cluster I contains two such activated carbonyl ligands, and it seems probable that the carbido atom contained in III, generated during the thermolysis of I, is derived from one of these ligands. The reaction (eq. 2) is known to generate CO_2 , two carbonyl ligands must therefore be involved in the carbido-forming reaction however, an intramolecular process may be ruled out on the grounds of carbon stoichiometry in that the carbido-containing product $[\text{Ru}_6\text{C}(\text{CO})_{14}(\eta^6\text{-C}_6\text{H}_3\text{Me}_3)]$ (III) has an equal number of non-aryl carbon atoms to that of the reactant molecule $[\text{Ru}_6(\mu_4-\eta^2\text{-CO})_2(\text{CO})_{13}(\eta^6\text{-C}_6\text{H}_3\text{Me}_3)]$ (I). Significantly, the other product of the thermolysis of I, $[\text{HRu}_6(\mu_4-\eta^2\text{-CO})(\text{CO})_{13}(\mu_2-\eta^7\text{-C}_6\text{H}_3\text{Me}_2\text{CH}_2)]$ (II), produced in equal molecular amounts to III, has one less carbonyl ligand than III (Scheme 1).



The following process may therefore be envisaged: two activated carbonyl ligands, one on each of two molecules of cluster I, undergo an intermolecular electronic rearrangement such that a molecule of CO₂ is formed and liberated, leaving a carbido atom coordinated to one of the cluster molecules. This intermediate, therefore has the formula [Ru₆C(CO)₁₄(C₆H₃Me₃)], and rearranges to the most stable structure, which is that observed for cluster III. The other half of the reacting pair, having lost a η²-bonded carbonyl ligand, is coordinatively unsaturated, and this facilitates formation of a Ru–Ru bond across the cavity where the carbonyl ligand was located, and metallation at one of the methyl groups on the mesitylene ligand, with a hydride ligand migrating to the metal framework. This process results in the formation of the observed structure of cluster II.

The fact that both unreacted cluster I and ruthenium metal along with III and IV are found in the solid residues of the solid state thermolysis of I, and that carbon monoxide is present in the gaseous products, is indicative of non-uniform heating of the reactant, a problem frequently associated with solid state reactions. It may also be associated with the need to disrupt the lattice structure of the crystalline material in order for the reacting molecules to adopt the correct reaction geometry. The reaction therefore proceeds in an atmosphere of carbon monoxide due to this unavoidable decomposition. As a result not only is III formed, by a similar process to that described for the solution reaction, but IV is also formed by ejection of the mesitylene ligand from III, or from an intermediate at some earlier stage in the reaction, in favour of coordination of carbon monoxide.

This is the first observation indicating the mechanism of cleavage of carbon monoxide by its interaction with a metal cluster substrate alone, although the mechanism of cleavage on an Fe₄ cluster by successive protonation has been elucidated by isolation of intermediates [18]. It is possible that if the metal substrate were a metal surface, which would have greater structural stability, instead of a molecular species, the rearrangement of the metal framework surrounding the carbide atom to encapsulate it would be restricted, and it would remain coordinated to a tetrametal site. Such a surface-bound carbide atom has long been postulated as the pivotal intermediate in many heterogeneous catalytic reactions of carbon monoxide.

The isolation and characterisation of [Ru₁₀C(CO)₂₄]²⁻ (V) and [HRu₁₀C(CO)₂₄]⁻ (VI)

Investigation of the solid residues from the reaction of Ru₃(CO)₁₂ with mesitylene has led to the isolation of the decaruthenium carbido-cluster anions [Ru₁₀C(CO)₂₄]²⁻ (V) * and [HRu₁₀C(CO)₂₄]⁻ (IV) **, in 35% yield (based on

* Crystal data for [PPN]₂[Ru₁₀C(CO)₂₄]²⁻ (V): C₉₇H₆₀N₂O₂₄P₄Ru₁₀·C₆H₁₄, *M* = 2858.63, monoclinic, space group *C2/c*, *a* 17.349(5), *b* 27.443(6), *c* 21.570(6) Å, β 92.74(1)°, *U* 10257.82 Å³, *F*(000) = 5592, μ(Mo-K_α) 14.09 cm⁻¹, *Z* = 4, *D_c* 1.85 g cm⁻³. In the space group *C2*, location of three phenyl rings and the hexane molecule could not be achieved satisfactorily because of pseudo symmetry (a 'c-glide') relating the two independent molecules, each of exact *C2* symmetry. Consequently the structure was refined in the space group *C2/c* resulting in an apparent disorder of the counterion and solvent. Present *R* = 0.1455 and *R'* = 0.1471 for 2549 reflections with *I*/σ(*I*) > 3.

** Crystal data for [PPN][HRu₁₀C(CO)₂₄]⁻ (VI): C₆₁H₃₁NP₂Ru₁₀·CH₂Cl₂, *M* = 2341.39, monoclinic, space group *P2₁/c*, *a* 11.777(2), *b* 17.805(4), *c* 35.365(5) Å, β 94.03(1)°, *U* 7397.33 Å³, *F*(000) 4476, μ(Mo-K_α) 19.45 cm⁻¹, *Z* = 4, *D_c* = 2.10 g cm⁻³. Final *R* = 0.0725 and *R'* = 0.0650 for 3555 reflections with *I*/σ(*I*) > 3.

$\text{Ru}_3(\text{CO})_{12}$) [19]. X-ray structure analysis shows that they are isostructural with their respective osmium analogues $[\text{Os}_{10}\text{C}(\text{CO})_{24}]^{2-}$ (X) and $[\text{HOs}_{10}\text{C}(\text{CO})_{24}]^-$ (VIII) [20,9], both having the giant tetrahedral metal framework, well known for a range of decaosmium clusters. For some years, such species have eluded detection in studies of ruthenium clusters by many workers [20].

The ^1H NMR spectrum of V shows no resonances other than those due to the $[\text{N}(\text{PPh}_3)_2]^+$ counterion, whilst that of VI has an additional singlet at -13.5 ppm corresponding to a hydrido ligand. The negative ion fast atom bombardment (FAB) mass spectrum of VI shows a strong molecular ion at $m/z = 1695$, successive loss of 24 carbonyl ligands and a weak isotopic envelope at $m/z = 1032$ corresponding to the Ru_{10}C metal core. Treatment of VI with base results in complete conversion to V; this reaction can be reversed quantitatively by protonation of VI.

Significantly the structure of the non-hydrido dianion V is indistinguishable from that of the hydrido cluster VI (Fig. 4). In the structure of VI, as in its osmium analogue (VIII), the entire surface of the cluster is covered with close-packed carbonyl ligands (Fig. 5), and there is no space to accommodate an external hydrido ligand: this is consistent with the location of the H-ligand in one of the tetrahedral caps of the cluster.

As the solution infrared spectrum of VI has two absorptions in the carbonyl stretching region and V has three, the structure of V might have been expected to have lower symmetry than VI. Since a cluster $[\text{M}_{10}\text{C}(\text{CO})_{24}]^{2-}$ of T_d symmetry has four IR active $\nu(\text{CO})$ modes, it would appear that accidental coincidence of IR absorptions is occurring, and that this, rather than small perturbations in the cluster symmetry, governs the number of bands resolved in the spectra.

The variable temperature (VT) ^{13}C NMR spectra of the clusters V and VI were recorded from ^{13}C enriched samples. The spectra of both anions are temperature dependent, and stacked plots of the spectra obtained are shown in Fig. 6. The spectrum of I at 290 K shows a broad singlet at 204.4 ppm, which on cooling broadens further and separates into two singlets. On further cooling to 200 K two sharp resonances of equal intensity at 213.7 and 192.7 ppm are obtained, the carbido resonance is observed at 362 ppm in this cluster. These spectra are entirely consistent with the solid state structure of V since there are only two carbonyl environments viz. four apical " $\text{Ru}(\text{CO})_3$ " caps and six " $\text{Ru}(\text{CO})_2$ " fragments at the apices of the central octahedron. It is clear from the spectra that at 290 K all carbonyl ligands are fluxional, but as the temperature decreases the speed of carbonyl motion is reduced, until at 200 K the structure is static on the NMR timescale.

The VT spectra of the anion VI are somewhat more complex due to the asymmetry introduced into the structure by the hydrido ligand. The spectrum at 290 K shows four broad resonances at 189.9, 206.7, 209.5 and 211.3 ppm, and a shoulder on the high field side of the resonance at 189.9 ppm. As the temperature is decreased the resonances sharpen, but no new resonances are observed, except that the shoulder is resolved into a sharp singlet. The spectrum observed at 210 K thus shows five resonances at 188.1, 189.2, 206.4, 209.1, and 211.2 ppm in the intensity ratio 1/3/2/1/1, the carbido resonance in this anion is observed at 374.5 ppm. This spectrum is consistent with the structural formulation in which the hydrido ligand is located in one of the interstitial tetrahedral sites provided by the " $\text{Ru}(\text{CO})_3$ " fragments capping the central octahedron, resulting in a structure of C_{3v} symmetry.

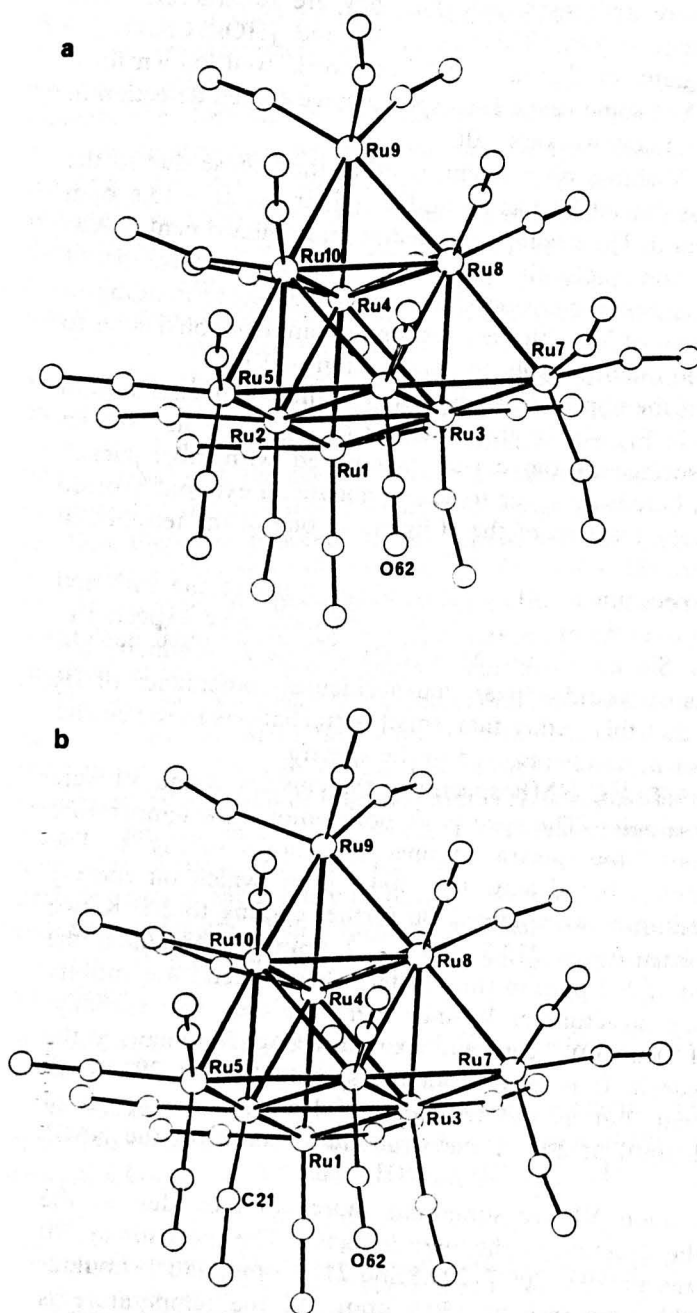


Fig. 4. The molecular structures of the anions (a) $[\text{Ru}_{10}\text{C}(\text{CO})_{24}]^{2-}$ (V) and (b) $[\text{HRu}_{10}\text{C}(\text{CO})_{24}]^{-}$ (VI) showing the similarity of the carbonyl ligand distribution between the two clusters.

The five carbonyl environments may be identified as follows: (i) a unique apical $\text{Ru}(\text{CO})_3$ fragment of the cap containing the hydride ligand, (ii) three equivalent apical $\text{Ru}(\text{CO})_3$ fragments at the corners of the basal Ru_6 plane relative to the cap containing the hydride, (iii) six equivalent carbonyls situated equatorially around

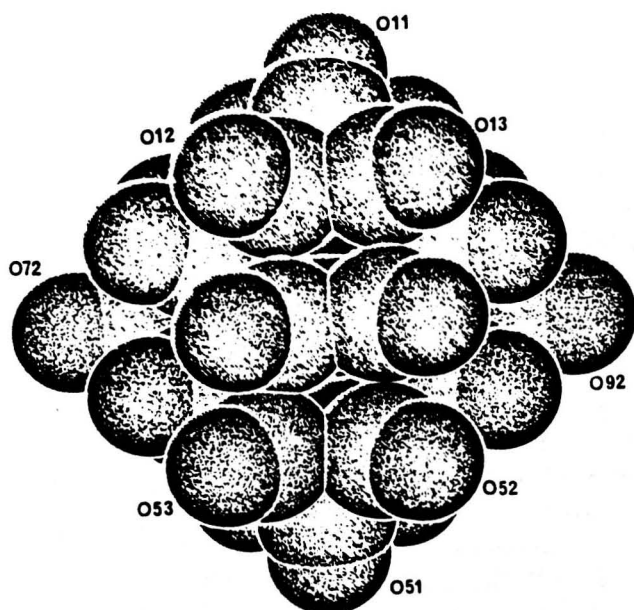


Fig. 5. Computed space filling model for $[\text{HRu}_{10}\text{C}(\text{CO})_{24}]^-$ (VI) showing the closed packed carbonyl array precluding a surface location for the hydrido ligand.

the base of the tetrahedron containing the hydride ligand. (iv) three equatorial carbonyls on the $\text{Ru}(\text{CO})_2$ fragments of the central triangle of the basal Ru_6 plane and (v) three axial carbonyls on the same $\text{Ru}(\text{CO})_2$ fragments. It is clear that the broadening of the resonances as the temperature increases indicates some form of fluxional behaviour within the cluster. However, whether this is due solely to motion of the carbonyls, or whether the hydride ligand is also fluxional is unclear from these data. These interpretations of the ^{13}C NMR spectra assume that the carbonyls of the capping $\text{Ru}(\text{CO})_3$ fragments are equivalent by virtue of rapid equilibration between the three environments relative to the rest of the cluster, which has proved to be valid for the spectroscopic investigations of other cluster carbonyl systems.

To further characterise the nature of the hydrido ligand in VI variable temperature (VT) ^1H NMR and infrared studies on static powder samples were undertaken [22]. The ^1H NMR spectra obtained are shown in Fig. 7, and are characterised by: (i) at 300 K, a single, relatively sharp, resonance is observed at +0.2 ppm relative to TMS; (ii) as the temperature decreases below 300 K the resonance at +0.2 ppm broadens and features being to appear around -24 ppm with a shoulder at -35 ppm (iii) at 140 K, a spectrum is acquired which has two features centred at approximately -5 and -35 ppm.

Interstitial hydrido ligands in transition metal clusters have previously been observed with low field resonances [10,23]; and the high temperature spectrum is assigned to an a hydrido ligand inside a Ru cap of the tetracapped octahedral structure (δ +0.2 ppm). The sharpness of the resonance is due to very high frequency "hopping" between the four equivalent cap sites. The 140 K spectrum is compatible with the powder spectrum of a hydride with effective axial symmetry. However, the very high field shift of this resonance (the isotropic chemical shift of

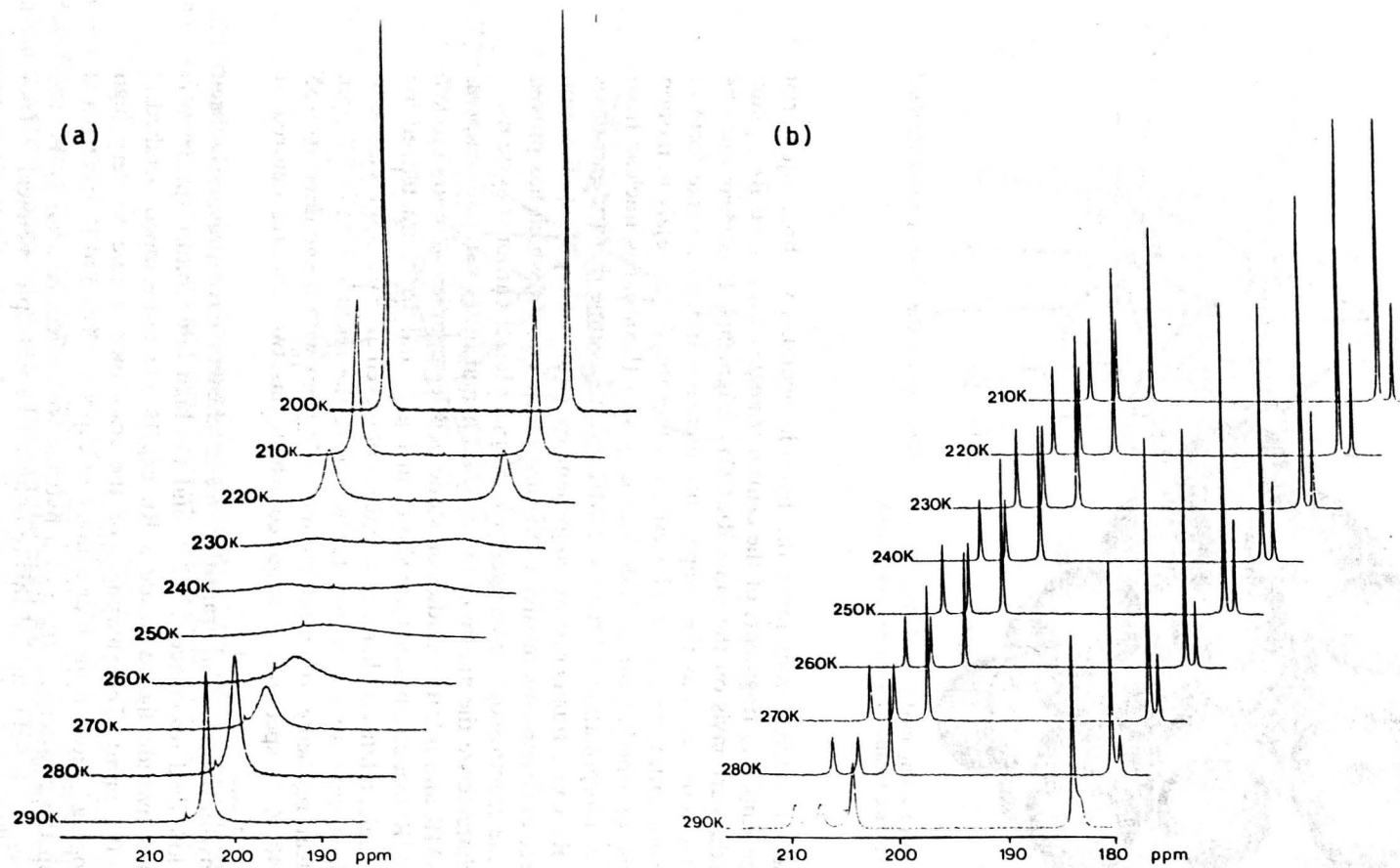


Fig. 6. Variable temperature ^{13}C NMR spectra of the anions (a) $[\text{Ru}_{10}\text{C}(\text{CO})_{24}]^{2-}$ (V) and (b) $[\text{HRu}_{10}\text{C}(\text{CO})_{24}]^{-}$ (VI).

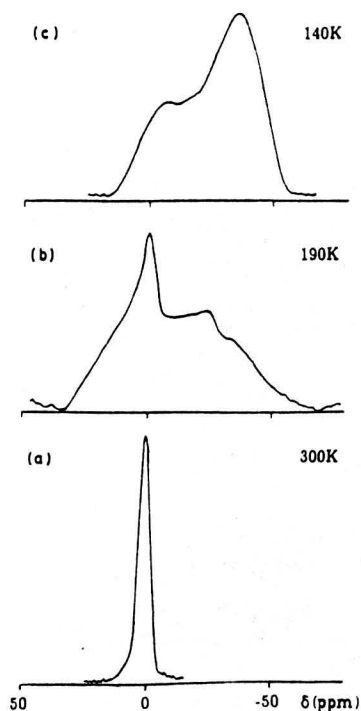


Fig. 7. The VT ^1H NMR spectra of a static powder sample of $[\text{HRu}_{10}\text{C}(\text{CO})_{24}]^-$ (VI) at (a) 300 K, (b) 190 K and (c) 140 K.

the resonance is -24 ppm) causes us to assign it to an externally bound hydrido ligand. The features in the 190 K spectrum arise from this hydride hopping relatively slowly over equivalent sites on the exterior of the metal framework.

In solution the hydride resonance is observed at -13.5 ppm; this is consistent with the ligand migrating rapidly (on the NMR timescale) between internal and external sites. In the solid state, the isotropic chemical shift for an external site is -24 ppm, while that for an interstitial site is $+0.2$ ppm, giving a mean chemical shift of -12 ppm which is certainly compatible with resonance observed in the solution spectrum. Furthermore we suppose that the external site to which hydride migrates at low temperatures is a face of a tetrahedral Ru_4 cap, then the cluster retains its C_{3v} symmetry on the NMR timescale, and this is the symmetry demanded by the ^{13}C NMR results.

The infrared spectrum of the $[\text{Bu}^+\text{N}]$ salt of $[\text{HRu}_{10}\text{C}(\text{CO})_{24}]^-$ (VI) was recorded in a CsI disc, and the spectra in the region $600\text{--}800\text{ cm}^{-1}$ at 293 and 113 K are shown in Fig. 8. The strong bands in this region of the spectrum may be assigned to the vibrational modes of the carbide atom. The carbide ligand in these decanuclear clusters is well isolated from adjacent molecules within the unit cell by virtue of its location within the central octahedral cavity. As a result the vibrational modes of the carbide ligand may be regarded, to a good approximation, as reflecting the symmetry of its local environment. It is well established that the width of infrared absorption bands decreases as the temperature of the sample is lowered due mainly to the dampening of the librational modes of the crystal lattice. It is thus often the case that additional bands to those observed at ambient temperature may be resolved by cooling the sample.

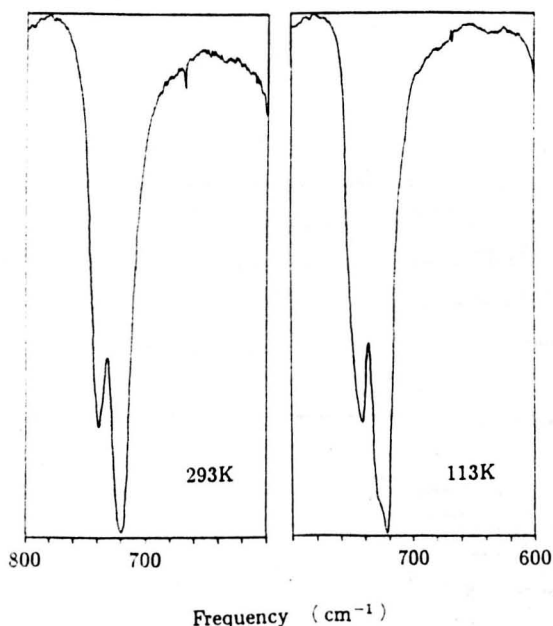


Fig. 8. The infrared spectrum of $[\text{HRu}_{10}\text{C}(\text{CO})_{24}]^-$ (VI) at (a) 300 K and (b) 113 K in a CsI disc.

If the hydrido ligand in VI is located in one of the tetrahedral caps the cluster would have C_{3v} symmetry and the carbide ligand would have an A and a degenerate E vibrational mode. The observed spectrum at 293 K is entirely consistent with this structural formulation; and shows a band at 738 cm^{-1} and a more intense band at 720 cm^{-1} which may be assigned to the A and E modes respectively. The spectrum at 113 K however, shows the lower frequency band to have split to give a distinct shoulder at 728 cm^{-1} . This band can be unequivocally assigned as a new band, and not simply a result of the higher resolution achieved at low temperatures, since the new band has resulted in an increase of the width of the absorption assigned to the degenerate E mode at ambient temperature, and not a narrowing which would be expected if the shoulder was a result of enhanced resolution. This low temperature spectrum is consistent with a cluster of C_{2v} symmetry or lower, since for point groups lower than C_{3v} the degeneracy of the E modes is lifted whilst the A mode remains unchanged.

This is therefore further evidence that the hydride ligand is being expelled from the interior of the cluster at low temperature, as its location on one of the triangular faces of one of the capping tetrahedra would result in a structure of C_{2v} symmetry. Such a process would therefore fully explain the observed infrared spectra.

The synthesis and characterisation of $[\text{Ru}_{18}\text{C}_2\text{Hg}_3(\text{CO})_{42}]^{2-}$ (VII)

The dianion V has been found to react with mercury(II) trifluoroacetate to give a larger cluster dianion together with a small quantity of an uncharacterised precipitate. An X-ray structure determination of this new compound shows it to be the fused cluster dianion $[\text{Ru}_{18}\text{C}_2\text{Hg}_3(\text{CO})_{42}]^{2-}$ (VII) (Fig. 9) [24], in which two decaruthenium clusters have each lost a capping $\text{Ru}(\text{CO})_3$ fragment, and the

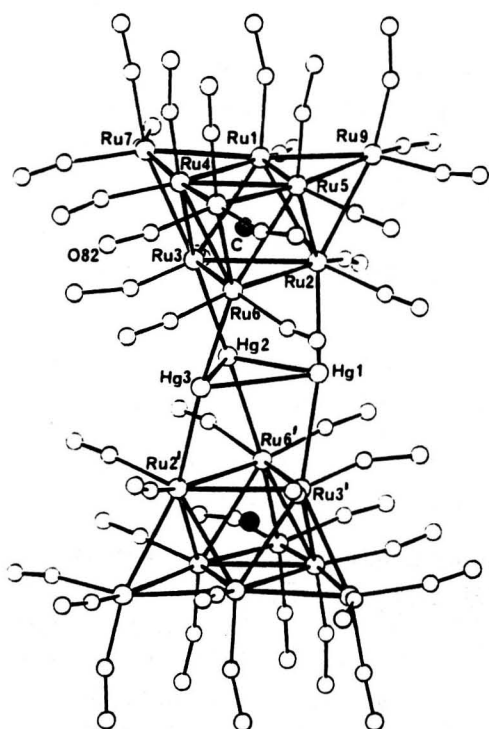


Fig. 9. The molecular structure of the dianion $[\text{Ru}_{18}\text{Hg}_3\text{C}_2(\text{CO})_{42}]^{2-}$ (VII).

resulting nonaruthenium species are fused by a bi-facecapping $(\eta^3\text{-}\mu_6\text{-Hg}_3)^{2+}$ unit*. The ruthenium atom 'sub-clusters' have a tricapped octahedral framework, an expected geometry for a 120 electron species; however this has not been reported previously for any cluster of the iron triad metals. Mercury has been noted previously for its ability to bridge between small metal aggregates to form larger clusters; as in $[\text{Ru}_7\text{Hg}_2(\text{CO})_{22}(\mu_3\text{-C}_2\text{Bu}^1)_2]$ [25] and $[\text{Os}_3(\text{CO})_{11}\text{Hg}]_3$ [26] for example.

In the solid state the cluster VII has virtual C_3 symmetry, the mean twist angle of 30° between the central Hg_3 triangle and the two adjacent Ru_3 triangles (which together form a central 'spiral' linking unit) results in the two faces $\text{Ru}_2\text{-Ru}_3\text{-Ru}_6$ and $\text{Ru}_2'\text{-Ru}_3'\text{-Ru}_6'$ of the Ru_9 units being exactly staggered with respect to each other, with a total twist angle of 60° . The simple infrared spectrum in the CO stretching region in solution is consistent with the C_3 symmetry of the dianion. The ^{13}C NMR spectrum shows only four sharp resonances in the region 211–190 ppm in the intensity ratio 1/1/2/3 which is consistent with the solid state structure, the resonance due to the carbide ligands in this cluster is observed at 371.4 ppm (Fig. 10). The resonance at 203.7 ppm, of relative intensity two, is considerably broad-

* Crystal data for $[\text{PPN}]_2[\text{Ru}_{18}\text{Hg}_3(\text{C})_2(\text{CO})_{42}]$ (VII): $\text{C}_{116}\text{H}_{60}\text{N}_2\text{O}_{42}\text{P}_4\text{Ru}_{18}\text{Hg}_3\cdot\text{CH}_2\text{Cl}_2$, $M = 4697.12$ (4782.05), space group $P\bar{1}$ (No. 2), a 19.042(4), b 15.729(3), c 15.197(3) Å, α 115.59(2), β 68.51(2), γ 115.46(2)°, U 2983.18 Å³, D_c 2.66 g cm⁻³, $F(000) = 2240$, $\mu(\text{Mo-K}\alpha)$ 48.48 cm⁻¹, a black crystal of size 0.19 × 0.14 × 0.16 mm was used in the data collection on a Phillips PW1100 diffractometer in the θ range 3–25°, with a scan width of 0.8°, final $R = 0.0720$ and $R_w = 0.0720$ for 2761 reflections with $I/\sigma(I) > 3$.

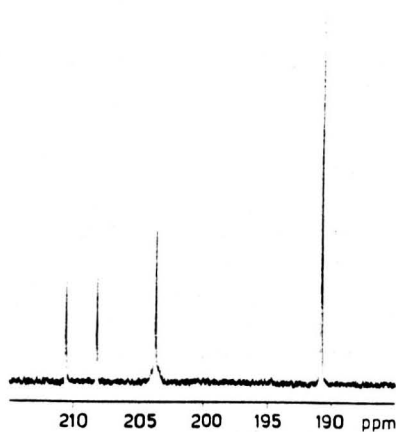


Fig. 10. The ^{13}C NMR spectrum of $[\text{Ru}_{18}\text{C}_2\text{Hg}_3(\text{CO})_{42}]^{2-}$ (VII) in CD_2Cl_2 solution showing the significant broadening at the base of the resonance at 203.7 ppm, assigned to the carbonyl ligands of the ruthenium atoms adjacent to the mercury atoms, due to $^2J(\text{Hg}-\text{C})$ coupling to ^{199}Hg .

ened at its base; this broadening may be attributed to the presence of weak satellite resonances due to 2J coupling to ^{199}Hg (16.8% natural abundance), since this resonance may be assigned to the 12 carbonyl ligands equatorially disposed above and below the Hg_3 plane. There is evidence from the crystal structure analysis that there is an interaction between the mercury atoms and these carbonyl carbon atoms (mean $\text{Hg}\cdots\text{C}$ (carbonyl) 2.64(9) Å), and the molecule VII is consequently extremely congested about the central Hg_3 triangle; the carbonyl ligands on each nonaruthenium unit are displaced toward the other sub-cluster.

Conclusions

It is clear that, contrary to expectations, ruthenium exhibits a wide and diverse higher nuclearity chemistry. So far, this chemistry has been based on species containing interstitial carbido atoms which may be essential in the stabilisation of aggregates of more than six ruthenium atoms. This, of course remains to be seen and our efforts are also directed towards an investigation of higher clusters which do not contain interstitial carbon. In this work we have also established that for the lower nuclearity species, containing six or less metal atoms, the chemistry differs from that of osmium in that, as mentioned above, it tends to be dominated by carbido derivatives. This is presumably due to mechanistic requirements, and here we have presented data which clearly provide a probable source and route for carbide formation. Nevertheless, it is interesting to note that a clear relationship between the chemistry of Ru_6 and Os_6 exists and further steps are underway to more fully appreciate the factors which govern the mechanistic pathway adopted.

Experimental

(i) General

All reactions were performed using freshly distilled solvents and under an atmosphere of dry nitrogen. Thin layer chromatography (TLC) was performed using Merck silica gel 60 F-254 plates. Infrared spectra were recorded on a Perkin-Elmer 1710 Fourier transform spectrometer, the low temperature spectra were obtained using a liquid nitrogen cooled, evacuable apparatus supplied by Specac Ltd. ^1H NMR spectra were obtained on a Bruker WH 250 spectrometer, whilst ^{13}C NMR spectra were recorded on a Bruker AM 400 instrument. For the ^{13}C spectra chromium(III) trisacetylacetonate was routinely added to the sample as a relaxation agent.

(ii) Thermolyses of $\text{Ru}_3(\text{CO})_{12}$ in arene-containing hydrocarbon solutions

In a typical experiment 1 g (1.565 mmol) of $\text{Ru}_3(\text{CO})_{12}$ was dissolved in 250 cm^3 of a 10% v/v solution of the arene (hexamethylbenzene, mesitylene, xylenes or toluene) in the hydrocarbon. The solution was heated under reflux until TLC (hexane/dichloromethane, 4/1) showed that a reasonable balance between consumption of $\text{Ru}_3(\text{CO})_{12}$ and deposition as a black material had been achieved. A delicate balance between reaction time, temperature, arene and product yields and distribution was observed, however reflux for approximately 3 d at 97°C in heptane/mesitylene gave a reasonable yield of clusters (I-IV). Reflux in hexane/arene solutions (68°C) favoured I in a very slow reaction, whilst refluxing octane or nonane solutions (125, 150°C) favoured the carbido-clusters III and IV. The resulting solution was filtered and the solvent removed from the dark red/brown filtrate in vacuo. The residue was dissolved in the minimum of dichloromethane and separated by TLC (hexane/dichloromethane, 4/1) to give orange IV (R_F 0.9), green II (R_F 0.55), brown III (R_F 0.45) and purple I (R_F 0.35); the maximum yield for each product, achieved after optimisation of the reaction conditions, was 15%.

(iii) Thermolysis of I in mesitylene

10 mg (0.008 mmol) of I was placed in the bulb in the floor of an infrared gas cell with NaCl windows and path length 10 cm, along with 1 cm^3 of mesitylene. The cell was evacuated whilst the mesitylene was frozen down with liquid nitrogen. The cell was then placed in the IR spectrometer and a background spectrum recorded. The bulb of the cell containing the reactants was then heated to approximately 100°C for 5 min, taking care not to completely evaporate the mesitylene, the mesitylene was again frozen out and the spectrum of the gaseous products obtained. Although strong bands due to the hydrocarbon modes were present in the spectrum, the characteristic *P* and *R* bands of the $\nu(\text{CO})$ mode of gaseous CO_2 could clearly be seen centred at 2352 cm^{-1} , and further thermolysis resulted in an increase in intensity of these bands. The thermolysis products remaining in solution were identified by TLC separation (hexane/dichloromethane, 4/1), followed by solution IR spectroscopy, as a small amount of unreacted I, and approximately equal yields of II and III.

(iv) Solid state pyrolysis of I

A similar procedure to that in (iii) above was adopted, without the necessity of

freezing out the mesitylene. After 2 min of pyrolysis at approximately 150°C a ruthenium mirror had been deposited on the inside of the bulb containing the reactant. The IR spectrum of the gaseous products showed clearly that CO₂ had been evolved as above, but additionally the characteristic *P* and *R* bands of the $\nu(\text{CO})$ mode of gaseous CO were present in the spectrum centred at 2143 cm⁻¹. Dissolution of the solid residues in dichloromethane followed by tlc. showed that the products of the pyrolysis were Ru metal, II, III, and a small amount of unreacted I.

(v) *Synthesis of [PPN][HRu₁₀C(CO)₂₄] (VI) and [PPN]₂[Ru₁₀(CO)₂₄] (V)*

In a typical experiment 1 g (1.565 mmol) of Ru₃(CO)₁₂ was heated to reflux in 50 cm³ of a 10% solution of mesitylene in n-heptane. The thermolysis was continued for 4–5 days and resulted in a solution containing mostly III and IV along with a finely divided black deposit. The black material was filtered off and dissolved in 50 cm³ of an acetone/methanol mixture containing an excess (0.50 g, 0.87 mmol) of [PPN]Cl resulting in a dark green solution of [PPN][HRu₁₀C(CO)₂₄] (VI). Slow evaporation of the solution at this stage resulted in the deposition of black microcrystals of the salt (377 mg, 0.168 mmol, 36% from Ru₃(CO)₁₂) which was washed with cold methanol followed by ether and dried in vacuo. If the acetone/methanol solution of the crude product was heated to reflux for 1 h, quantitative deprotonation of VI resulted yielding [PPN]₂[Ru₁₀C(CO)₂₄] (V) (450 mg, 0.162 mmol, 35% from Ru₃(CO)₁₂) which may be isolated in a similar manner. Crystals of V and VI suitable for X-ray examination were obtained from CH₂Cl₂/hexane solution. Spectroscopic data for [PPN]₂[Ru₁₀C(CO)₂₄] (V): IR (CH₂Cl₂): $\nu(\text{CO})$ 2027vs, 2000m, 1983s cm⁻¹; ¹H NMR (CD₂Cl₂): δ 7.70 ppm (multiplet). Spectroscopic data for [PPN][HRu₁₀C(CO)₂₄] (VI): IR (CH₂Cl₂): $\nu(\text{CO})$ 2053vs, 2009s cm⁻¹; ¹H NMR (CD₂Cl₂): δ 7.70 ppm (multiplet, 30H), -13.5 ppm (s, 1H).

(vi) *Synthesis of [PPN]₂[Ru₁₈Hg₃(C)₂(CO)₄₂] (VII)*

40 mg (0.0144 mmol) of [PPN]₂[Ru₁₀C(CO)₂₄] (V) was dissolved in 40 cm³ of CH₂Cl₂ and 6.2 mg (0.0146 mmol) of freshly sublimed Hg(CF₃CO₂)₂ was added in 5 cm³ of CH₂Cl₂. The solution immediately changed colour from green to brown. After a period of 4 d the product was precipitated from solution as brown microcrystals by addition of ether (11 mg, 0.0023 mmol, 18%). Crystals for X-ray examination were obtained from CH₂Cl₂/hexane solution. Spectroscopic data for [PPN]₂[Ru₁₈Hg₃(C)₂(CO)₄₂] (VII): IR (CH₂Cl₂): $\nu(\text{CO})$ 2065s, 2055vs, 2002s, cm⁻¹; ¹H NMR (CD₂Cl₂): δ 7.70 ppm (multiplet); ¹³C NMR (CD₂Cl₂): δ 210.6, 208.2, 203.7, 190.6 ppm; Negative ion fast atom bombardment mass spectrum $M^+ = 3623$.

Acknowledgements

We thank SERC (P.J.B. and H.R.P.) and British Petroleum plc (P.J.B.) for financial support, and Johnson Matthey plc for generous loans of ruthenium trichloride.

References

- 1 B.F.G. Johnson, R.D. Johnston, J. Lewis, *J. Chem. Soc., Chem. Commun.*, (1967) 1057; B.F.G. Johnson, R.D. Johnston, J. Lewis, *J. Chem. Soc. A*, (1968) 2865; R. Mason, W.R. Robinson, *J. Chem. Soc., Chem. Commun.*, (1968) 468.
- 2 J.S. Bradley, *Adv. Organometallic Chem.*, 22 (1982) 1; B.F.G. Johnson, J. Lewis, W.H.J. Nelson, J.N. Nicholls, M.D. Vargas, *J. Organomet. Chem.*, 249 (1983) 255; V.G. Albano, D. Braga, S. Martinengo, *J. Chem. Soc., Dalton Trans.*, (1986) 981; and refs. cited therein.
- 3 V.G. Albano, M. Sansoni, P. Chini, S. Martinengo, *J. Chem. Soc. Dalton Trans.*, (1973) 651.
- 4 E.C. Constable, B.F.G. Johnson, J. Lewis, G.N. Pain, M.J. Taylor, *J. Chem. Soc., Chem. Commun.*, (1982) 754.
- 5 C.R. Eady, B.F.G. Johnson, J. Lewis, *J. Chem. Soc. Dalton Trans.*, (1975) 2606.
- 6 R.D. Adams, P. Mathur, B.E. Segmüller, *Organometallics*, 2 (1983) 1258.
- 7 W.A. Herrmann, *Angew. Chem. Int. Eng. Ed.*, 21 (1982) 117; E.L. Muetterties, *J. Stein. Chem. Rev.*, 79 (1979) 479; M. Araki, V. Ponec, *J. Catal.*, 44 (1976) 439; P. Biloen, J.N. Helle, W.M.H. Satchler, *ibid* 58 (1979) 95; N.W. Cant, A.T. Bell, *ibid.*, 73 (1982) 257; J.W.A. Satchler, J.M. Kool, V. Ponec, *ibid.*, 56 (1979) 284.
- 8 T. Chihara, R. Komoto, K. Kobayashi, H. Yamazaki, Y. Matsura, *Inorg. Chem.*, 28 (1989) 964.
- 9 P.F. Jackson, B.F.G. Johnson, J. Lewis, M. McPartlin, W.J.H. Nelson, *J. Chem. Soc. Chem. Commun.*, (1982) 49.
- 10 C.R. Eady, B.F.G. Johnson, J. Lewis, M.C. Malatesta, P. Machin, M. McPartlin, *J. Chem. Soc. Chem. Commun.*, (1976) 945; P.F. Jackson, B.F.G. Johnson, J. Lewis, P.R. Raithby, M. McPartlin, W.J.H. Nelson, K.D. Rouse, J. Allibon, S.A. Mason, *ibid.*, (1980) 295.
- 11 S.R. Drake, K. Henrick, B.F.G. Johnson, J. Lewis, M. McPartlin, J. Morris, *J. Chem. Soc. Chem. Commun.*, (1986) 928.
- 12 C.E. Anson, P.J. Bailey, G. Conole, B.F.G. Johnson, J. Lewis, M. McPartlin, H.R. Powell, *J. Chem. Soc., Chem. Commun.*, (1989) 442.
- 13 C.P. Horwitz, D.F. Shriver, *Adv. Organomet. Chem.*, 23 (1983) 219.
- 14 R.D. Adams, G.E. Babin, M. Tasi, *Angew. Chem. Int. Eng. Ed.*, 26 (1987) 685.
- 15 A.G. Orpen, *J. Chem. Soc. Dalton Trans.*, (1980) 2509.
- 16 L.M. Bullock, J.S. Field, R.J. Haines, E. Minsal, D.N. Smit, G.M. Sheldrick, *J. Organomet. Chem.*, 310 (1986) C47.
- 17 C.E. Anson, PhD. Thesis, University of East Anglia, Norwich, 1987.
- 18 K. Whitmire, D.F. Shriver, *J. Am. Chem. Soc.*, 102 (1980) 1456.
- 19 P.J. Bailey, B.F.G. Johnson, J. Lewis, M. McPartlin, H.R. Powell, *J. Organomet. Chem.*, 377 (1989) C17.
- 20 P.F. Jackson, B.F.G. Johnson, J. Lewis, M. McPartlin, W.J.H. Nelson, *J. Chem. Soc. Chem. Commun.*, (1980) 224; P.F. Jackson, B.F.G. Johnson, J. Lewis, M. McPartlin, W.J.H. Nelson, *J. Chem. Soc. Dalton Trans.*, (1982) 2099.
- 21 J.N. Nicholls, M.D. Vargas, *Adv. Inorg. Radiochem.*, (1986) 123.
- 22 P.J. Bailey, M.J. Duer, *J. Chem. Soc. Chem. Commun.*, (1989) 1139.
- 23 D.W. Hart, R.G. Teller, C-Y. Wei, R. Bau, G. Longoni, S. Campanella, P. Chini, T.F. Koetzle, *Angew. Chem. Int. Ed. Engl.*, 18 (1979) 80.
- 24 P.J. Bailey, B.F.G. Johnson, J. Lewis, M. McPartlin, H.R. Powell, *J. Chem. Soc. Chem. Commun.*, (1989) 1513.
- 25 E. Rosenberg, D. Ryckman, I-Nan Hsu, R.W. Gellert, *Inorg. Chem.*, 25 (1986) 194.
- 26 M. Fajardo, H.D. Holden, B.F.G. Johnson, J. Lewis, P.R. Raithby, *J. Chem. Soc. Chem. Commun.*, (1984) 24; see also J.M. Ragosta, J.M. Burlitch, *ibid.*, (1985) 1187; L.J. Farrugia, *ibid.*, (1987) 147.